

**Multiple strategies targeting  
c-Jun N-terminal kinases: synthesis of  
novel inhibitors and development of a new  
binding assay methodology**

**Dissertation**

Der Mathematisch-Naturwissenschaftlichen Fakultät  
der Eberhard Karls Universität Tübingen  
zur Erlangung des Grades eines  
Doktors der Naturwissenschaften  
(Dr. rer. nat.)

Vorgelegt von

**Francesco Ansideri**

aus Umbertide/Italien

Tübingen

2018

The research described in this thesis was conducted at the Department of Pharmaceutical and Medicinal Chemistry, Institute of Pharmaceutical Sciences, Eberhard Karls Universität Tübingen in the period between 17.06.2014 and 31.03.2018 under the supervision of Professor Dr. Pierre Koch and Professor Dr. Stefan A. Laufer.

Gedruckt mit Genehmigung der Mathematisch-Naturwissenschaftlichen Fakultät der Eberhard Karls Universität Tübingen.

Tag der mündlichen Qualifikation	03/05/2018
Dekan	Professor Dr. Wolfgang Rosenstiel
1. Berichterstatter	Professor Dr. Pierre Koch
2. Berichterstatter	Professor Dr. Stefan A. Laufer

*To my Family*

*"Faber est suae quisque fortunae"*

Each man is the smith of his own fortune





# Table of Contents

<b>FOREWORD.....</b>	<b>III</b>
Acknowledgments .....	III
Summary of the thesis .....	VI
Zusammenfassung der Dissertation.....	VII
<b>ABBREVIATIONS LIST .....</b>	<b>1</b>
<b>LIST OF PUBLICATIONS.....</b>	<b>3</b>
<b>AUTHOR CONTRIBUTIONS.....</b>	<b>5</b>
<b>1. INTRODUCTION .....</b>	<b>13</b>
1.1. Protein Kinases .....	13
1.1.1. <i>Structure of protein kinases</i> .....	15
1.1.2. <i>Protein kinases as drug targets</i> .....	18
1.2. MAPKs.....	26
1.2.1. <i>JNKs</i> .....	27
1.2.2. <i>JNK inhibition</i> .....	32
1.2.3. <i>Fluorescence Polarization (FP)</i> .....	36
<b>2. OBJECTIVE OF THE THESIS WORK .....</b>	<b>39</b>
<b>3. RESULTS AND DISCUSSION.....</b>	<b>41</b>
3.1. Development and optimization of an FP-based competition binding assay for JNK1, 2, and 3, and p38 $\alpha$ MAPK.....	41
3.1.1. <i>Design and synthesis of a new FP probe</i> .....	41
3.1.2. <i>Probes characterization</i> .....	45
3.1.3. <i>Assay conditions optimization</i> .....	48
3.1.4. <i>Assay validation</i> .....	49
3.1.5. <i>Applicability to the HTS format</i> .....	53
3.1.6. <i>Extension of the developed assay to the JNK1 and JNK2</i> .....	55
3.2. Optimization of a pyridinylimidazole scaffold aimed at achieving selectivity on JNK.....	58
3.2.1. <i>Selection of a suitable lead compound</i> .....	58
3.2.2. <i>Exploration of the substitution at the HR I</i> .....	60
3.2.3. <i>Modifications on the five-membered core</i> .....	66
3.2.4. <i>Evaluation of the binding mode of compounds 42 and 66</i> .....	72

---

3.2.5. <i>Modification of the substituent at the HR II</i> .....	74
3.2.6. <i>Further characterization of compound 66</i> .....	79
3.2.7. <i>Application of a covalent inhibition strategy on compound 66</i> .....	80
<b>EXPERIMENTAL SECTION</b> .....	<b>83</b>
<b>BIBLIOGRAPHY</b> .....	<b>91</b>
<b>APPENDIX</b> .....	<b>105</b>
Publication I.....	105
Publication II.....	131
Publication III.....	141
Publication IV.....	159
Publication V.....	207
Publication VI.....	227
Publication VII.....	242
<b>LIST OF SYNTHESIZED COMPOUNDS</b> .....	<b>303</b>

# Foreword

## Acknowledgments

My greatest thanks go to Professor Dr. Pierre Koch for supervising me throughout all the years spent as a Ph.D. student, for being always available and helpful for any question or necessity, for trusting in me and for encouraging and guiding me with care and patience.

I am as much thankful to my second supervisor Professor Dr. Stefan A. Laufer for making this whole experience possible, for his valuable advice and for providing me all the support I needed to carry out my studies abroad.

My gratitude also goes to Professor Dr. Frank M. Boeckler who enabled part of my work to take place by allowing the access to his laboratory equipment and who accepted to collaborate in different research projects, always dispensing constructive suggestions.

Additionally, I want to thank both Professor Dr. Frank M. Boeckler and Prof. Dr. Harald Groß for accepting to take part as examiners in my thesis defense.

A huge thanks goes to Dr. Ahmed El-Gokha who represented for me a “big and stable” anchor in many situations and who became a real friend with whom sharing both personal- and work-related subjects.

A special mention goes also to Fabian Heider for being an always reliable colleague, for his constant help, his encouragements, and most of all for the constructive scientific discussions typically ending with: “I think it should work...” (and it never did, in the end).

In addition, I would like to express my sincere gratitude to all current and former members of the “small-but-great” AK Koch with whom I had the luck to work in these years for the extremely pleasant working environment, for the laughter and the reciprocal support. Thanks to Catharina Sessler for her assistance with both the FP and ADP-Glo assays and for the coffee break “ritual” that we started unfortunately too late, thanks to Stanislav Andreev for his always friendly help and advice in many circumstances, and thanks to Michael Eitel for being a great lab and office mate who provided me a great moral support (together with a lot of chocolate).

I would also like to thank Dr. Annette Kuhn for her precious help with the synthesis of several intermediates and for her collaboration in the project of tetrasubstituted derivatives.

Many thanks to the members of the AK Boeckler, in particular Christoph Ernst, Johannes Heidrich, Erdem Veyisoglu, Dr. Tamer Ibrahim, and Dr. Markus Zimmermann for contributing to the nice working atmosphere in the 8<sup>th</sup> floor. My appreciation also goes to Susanne Hennig for her assistance in the laboratory. Furthermore, I would like to thank Markus Cieslik for being a nice laboratory mate who helped me and cheered me up numerous times during the first period of my Ph.D. studies. Within the AK Boeckler, I also owe a special acknowledgment to Dr. Andreas Lange and to Marcel Dammann for their collaboration in the JNK project.

My appreciation goes to the present colleagues and alumni/ae of the AK Laufer, whose work was in several cases inspiring for me and who many times assisted me with the use of the laboratory equipment (in this regard, I am really grateful to Eva Döring for her patience with the use of the TLC-MS device). Among all, I would like to thank Dr. Fernando Rodrigues De Sá Alves for the nice time spent together, Dr. Ida D'Orazio for being my Italian chatting partner in the institute, and Mark Kudolo, for the always interesting conversations upon scientific and non-scientific subjects. A special acknowledgement goes to Dr. Silke Bauer who was always extremely kind and helpful, and with whom I could have very constructive discussions regarding the development of the FP assay.

I am very grateful to my friend and colleague Joana Tavares Macedo from the AK Stehle for her collaboration in the JNK project with the performance of the crystallographic studies. Many thanks also to Dr. Bärbel S. Blaum for her supervision and her constructive suggestions during the preparation of the article manuscript.

I gratefully acknowledge Katharina Bauer, Daniela Müller, Jens Strobach, and Mark Kudolo for testing my substances in the ELISA assay. Furthermore, as her "Sekretario" I must thank in particular Katharina Bauer for the funny talks, for pushing me to speak more German, and in general for making me feel welcome every time I joined the second floor.

I also want to thank Marion Boos for her assistance in the learning process of the ADP-Glo assay method and Melanie Henning for helpful discussions in the optimization of the same assay.

Many thanks to Dr. Raimund Nieß for taking care of many bureaucratic matters and for all the organization work.

I am also grateful to Karin Ward for her helpful and friendly assistance in solving different administrative issues.

Furthermore, my deep appreciation goes to Gerd Helms for his kindness and his valuable support with the NMR measurements.

I would like to thank the students I co-supervised during these years for their contribution in the laboratory work, for the passion and dedication they showed during the time spent here, and for giving me the opportunity to face the challenging task of being a guide.

My gratitude goes to all the friends and colleagues who proofread my thesis giving me valuable suggestions to improve my work. Many thanks also to Dr. Christoph Raisch who helped me with the translation of the Summary and who represented a great support in the non-easy challenge of learning the German language.

I am extremely grateful to all the wonderful people I had the chance to meet in this experience, words are not enough to describe how much you improved the time I spent here and how much you contributed to my personal growth. In particular, I am very happy to have known Prateek and Diana, who without exaggerating have become my family here in Tübingen.

Thanks to Giulia, because without her I would have never found the strength to go that far in this experience.

A special dedication goes to my lifelong friends back in Italy, who despite the distance never forgot to support me with their thoughts, and who always welcomed me in a special way every time I came back home.

Finally, I devote my deepest gratitude to my family, in particular to my parents and my sister, who encouraged me in pursuing my interests, who gave me help, comforted me in bad periods, and made me feel all the love and appreciation a person would need.

## Summary of the thesis

In the field of drug discovery protein kinases have emerged as extremely promising therapeutic targets, as witnessed by the increasing amount of FDA-approved kinase inhibitors in the last decade. In particular, this thesis focuses on the c-Jun N-terminal kinases (JNKs), a group of enzymes belonging to the family of mitogen-activated protein kinases (MAPKs) which regulate the cell response to a variety of extracellular stress stimuli. The dysregulated activity of JNKs has been connected to diverse pathological states ranging from neurodegenerative disorders to cancer and inflammatory or metabolic diseases. However, despite the intense endeavor devoted to the research of novel inhibitors, no clinical candidate has reached approval in therapy to date. For this reason, the presented work pursued the targeting of JNKs by means of diverse strategies such as alternative biological assay methodologies and synthesis of small-molecule inhibitors.

In the first part of the thesis a fluorescence polarization (FP)-based competition binding assay was developed as a tool to efficiently evaluate the affinity of novel inhibitors for the different JNK isoforms (JNK1, 2, and 3), as well as for the closely-related p38 $\alpha$  MAPK. Such assay required the synthesis of a fluorescently-labeled probe based on a pyridinylimidazole scaffold which displayed  $K_d$  values in the low nM range for all the target enzymes. After optimizing the procedure conditions, the new FP assay was validated by employing known inhibitors and comparing the measured affinities with results from different methods. Finally, the suitability for the high throughput screening format was confirmed, highlighting the developed FP assay as a fast and relatively inexpensive methodology for the rapid screening of novel inhibitors.

The second part of this thesis work consisted instead in the optimization of a dual JNK3/p38 $\alpha$  MAPK pyridinylimidazole-based lead compound aimed at shifting the selectivity towards the JNK3. In detail, the substitution at different key positions of the scaffold, as well as the nature of the five-membered core were alternatively modified. Among the different attempts, the presence of a simple methyl group at the imidazole-C4 position, together with a 2-methylsulfonyl moiety permitted to abolish the activity on the p38 $\alpha$  MAPK while maintaining the inhibition on the JNK3. The best inhibitor of the series inhibited the JNK3 in the low triple digit nanomolar range, with a > 27-fold selectivity over the p38 $\alpha$  MAPK. The achieved information concerning the structure-activity relationship (SAR) together with the crystal structure determination of the best inhibitor in complex with the JNK3 might aid the design of future optimization strategies.

## Zusammenfassung der Dissertation

Auf dem Gebiet der Wirkstoffforschung wurden Proteinkinasen als sehr vielversprechende therapeutische Ziele identifiziert. Dies lässt sich insbesondere an der stetig steigenden Anzahl an von der FDA zugelassenen Kinaseinhibitoren in den letzten fünfzehn Jahren erkennen. Die vorliegende Arbeit konzentriert sich im Speziellen auf c-Jun N-terminale Kinasen (JNKs), eine Gruppe von Enzymen aus der Familie der mitogenaktivierten Proteinkinasen (MAPKs), die die Zellantwort auf eine ganze Reihe extrazellulärer Stressreize regulieren. Störungen der Aktivität der JNKs wird mit zahlreichen Krankheiten wie neurodegenerativen Prozessen, Krebserkrankungen, Entzündungen oder Stoffwechselstörungen in Verbindung gebracht. Trotz intensiver Forschung an neuartigen Inhibitoren wurde bis heute aber kein Wirkstoff zugelassen. Die vorliegende Arbeit verfolgt daher das Ziel, die JNKs zum einen mittels alternativer biologischer Assays zu charakterisieren und zum anderen mittels der Synthese geeigneter Moleküle zu inhibieren.

Der erste Teil der Arbeit behandelt die Entwicklung eines kompetitiven Bindungsassays auf Basis der Fluoreszenzpolarisationsmessung. Er dient als Werkzeug zur Bestimmung der Affinität der neuartigen Inhibitoren zu den drei verschiedenen Isoformen von JNK (JNK1, 2 und 3) sowie der damit engverwandten p38 $\alpha$  MAPK. Der Assay erforderte die Synthese einer fluoreszenzmarkierten Verbindung auf Basis eines Pyridinylimidazolgerüsts, welche  $K_d$ -Werte im niedrigen nanomolaren Bereich für alle Zielenzyme aufweist. Nach der Optimierung der Bedingungen wurde der neue FP-Assay validiert, indem bekannte Inhibitoren getestet wurden und deren gemessene Affinitäten mit Ergebnissen aus anderen Methoden verglichen wurden. Schließlich wurde die Eignung des Assays zum schnellen und relativ kostengünstigen Hochdurchsatzscreening zur Identifizierung von neuartigen Inhibitoren bestätigt.

Der zweite Teil der Arbeit befasst sich mit der Optimierung einer pyridinylimidazolbasierten Testverbindung zur Hemmung von JNK3 und p38 $\alpha$  MAPK mit dem Ziel die Selektivität hin zu JNK3 zu verschieben. Dazu wurden sowohl der zentrale Fünfring als auch die Substituenten variiert. So konnte gezeigt werden, dass eine einfache Methylgruppe an der Imidazol-C4-Position in Verbindung mit einer 2-Methylsulfanylgruppe die Inhibition der p38 $\alpha$  MAPK unterbindet während die JNK3 weiterhin gehemmt wird. Die beste Verbindung dieser Serie inhibierte die JNK3 im niedrigen dreistelligen nanomolaren Bereich bei einer mehr als 27-fachen Selektivität gegenüber p38 $\alpha$  MAPK.

Die im Rahmen dieser Arbeit gewonnen Erkenntnisse hinsichtlich der Struktur-Wirkungs-Beziehung (SAR), in Verbindung mit der erlangten Kristallstruktur des besten gefundenen JNK3-Inhibitors bilden die Grundlage für weitere Optimierungsansätze in der Zukunft.





# Abbreviations List

A $\beta$	B-Amyloid
AD	Alzheimer's disease
AMP-PCP	$\beta$ , $\gamma$ -methyleneadenosine 5'-triphosphate
AP	Activation protein
APP	Amyloid precursor protein
ATF	Activating transcription factor
ATP	Adenosine triphosphate
CDK	Cyclin dependent kinases
CV	Coefficient of variation
CYP450	Cytochrome P450
DAD	Diode array detector
DFG	Asp-Phe-Gly conserved tripeptide
EGFR	Epidermal growth factor receptor
ELISA	Enzyme-linked immunosorbent assay
ERK	Extracellular signal-regulated kinase
ESI-MS	Electrospray ionization mass spectrometry
FA	Fluorescence anisotropy
FDA	Food and drug administration
FITC	Fluorescein isothiocyanate
FP	Fluorescence polarization
GPCR	G-Protein coupled receptor
hERG	Human ether-à-go-go related gene
HLM	Human liver microsomes
HR	Hydrophobic region
HPLC	High performance liquid chromatography
HRD	His-Arg-Asp conserved tripeptide

---

HTS	High throughput screening
IC <sub>50</sub>	Concentration producing 50% of inhibition
IL	Interleukin
ITC	Isothermal titration calorimetry
JIP	JNK-interacting protein
JNK	c-Jun N-terminal kinase
K <sub>d</sub>	Dissociation constant
K <sub>i</sub>	Inhibition constant
LC-MS	Liquid chromatography mass spectrometry
MAPK	Mitogen activated protein kinase
MAPKK, MEK, MKK	MAPK kinase
MAPKKK, MEKK	MAPKK/MEK kinase
MMP	Matrix metalloproteinase
MPTP	1-Methyl-4-phenyl-1,2,3,6-tetrahydropyridine
mP	Millipolarization
NaHMDS	Sodium bis(trimethylsilyl)amide
NCBI	National center for biotechnology information
PD	Parkinson's disease
PDB	Protein data bank
PK	Pharmacokinetic
PAIN	Pan Assay interference compound
RA	Reumathoid arthritis
SD	Standard deviation
SEM	Standard error of the mean
Sn <sub>Ar</sub>	Aromatic nucleophilic substitution
SAPK	Stress activated protein kinase
TCI	Targeted covalent inhibitor
TNF	Tumor necrosis factor
YRD	Tyr-Arg-Asp conserved tripeptide

# List of Publications

## Publication I

Ansideri, F.; Lange, A.; El-Gokha, A.; Boeckler, F. M.; Koch, P. Fluorescence polarization-based assays for detecting compounds binding to inactive c-Jun N-terminal kinase 3 and p38 alpha mitogen-activated protein kinase. *Anal. Biochem.* **2016**, *503*, 28-40.

## Publication II

Ansideri, F.; Dammann, M.; Boeckler, F. M.; Koch, P. Fluorescence polarization-based competition binding assay for c-Jun N-terminal kinases 1 and 2. *Anal. Biochem.* **2017**, *532*, 26-28.

## Publication III

Koch, P.; Ansideri, F. 2-Alkylsufanyl-4(5)-aryl-5(4)-heteroarylimidazoles: An Overview on Synthetic Strategies and Biological Activity. *Arch. Pharm.* **2017**, *350*, e1700258.

## Publication IV

Muth, F.; El-Gokha, A.; Ansideri, F.; Eitel, M.; Döring, E.; Sievers-Engler, A.; Lange, A.; Boeckler, F. M.; Lämmerhofer, M.; Koch, P.; Laufer, S. A. Tri- and Tetrasubstituted Pyridinylimidazoles as Covalent Inhibitors of c-Jun N-Terminal Kinase 3. *J. Med. Chem.* **2017**, *60*, 594-607.

## Publication V

Ansideri, F.; Andreev, S.; Kuhn, A.; Albrecht, W.; Laufer, S. A.; Koch, P. A Diverse and Versatile Regiospecific Synthesis of Tetrasubstituted Alkylsulfanylimidazoles as p38 $\alpha$  Mitogen-Activated Protein Kinase Inhibitors. *Molecules* **2018**, *23*, 221.

## Publication VI

Ansideri, F.; Schollmeyer, D.; Koch, P. 1-(3',6'-Dihydroxy-3-oxo-3H-spiro[isobenzofuran-1,9'-xanthen]-5-yl)-3-[4-({4-[1-(4-fluorophenyl)-1H-imidazol-5-yl]pyridin-2-yl}amino)phenyl]thiourea methanol monosolvate. *IUCrData* **2016**, *1*, x160840.

**Publication VII**

Ansideri, F.; Macedo, T. J.; Eitel, M.; El-Gokha, A.; Zinad, D. S.; Scarpellini, C.; Kudolo, M.; Schollmeyer, D.; Boeckler, F. M.; Blaum, B. S.; Laufer, S. A.; Koch, P. Structural Optimization of a Pyridinylimidazole Scaffold: Shifting the Selectivity from p38 $\alpha$  Mitogen-Activated Protein Kinase to c-Jun N-terminal Kinase 3. *ACS Omega* **2018**, 3, 7809-7831.

# Author Contributions

## Publication I

*Fluorescence polarization-based assays for detecting compounds binding to inactive c-Jun N-terminal kinase 3 and p38 alpha mitogen-activated protein kinase*

## Author Contributions

### Francesco Ansideri:

- Design and synthesis of the fluorescent probes
- Planning of the experiments
- Performance of titration experiments as well as experiments relative to assay optimization and validation
- Data analysis and interpretation
- Writing of the manuscript and of most of supplementary information

### **Dr. Andreas Lange:**

- Expression and purification of JNK3 and p38 $\alpha$  MAPK
- Assistance with the Fluorescence Polarization measurements
- Docking experiments
- Performance of the Isothermal Titration Calorimetry experiments

### **Dr. Ahmed El-Gokha:**

- Preparation of the probe 5 precursor
- Optimization of the synthetic strategy

### **Professor Dr. Frank M. Boeckler:**

- Preliminary idea of the project
- Supply of the facilities for the assay performance

### **Professor Dr. Pierre Koch:**

- Generation and coordination of the project
- Writing of the manuscript
- Final approval of the manuscript

## Publication II

*Fluorescence polarization-based competition binding assay for c-Jun N-terminal kinases 1 and 2*

### Author Contributions

#### Francesco Ansideri:

- Planning and performance of the experiments
- Processing, analysis, and interpretation of the raw data
- Writing of the manuscript and of supporting information

#### **Marcel Dammann:**

- Expression and purification of the JNK1 and JNK2 isoforms

#### **Professor Dr. Frank M. Boeckler:**

- Supply of the facilities for the assay performance
- Supervision of the protein expression procedure

#### **Professor Dr. Pierre Koch:**

- Generation, coordination, and financing of the project
- Writing of the manuscript
- Final approval of the manuscript

## Publication III

*2-Alkylsufanyl-4(5)-aryl-5(4)-heteroarylimidazoles: An Overview on Synthetic Strategies and Biological Activity*

### Author Contributions

#### **Professor Dr. Pierre Koch:**

- Literature search
- Writing of the manuscript

#### Francesco Ansideri:

- Writing of the manuscript

## Publication IV

*Tri- and Tetrasubstituted Pyridinylimidazoles as Covalent Inhibitors of c-Jun N-Terminal Kinase 3*

### Authors Contributions

#### Dr. Felix Muth:

- Synthesis of the majority of the compounds (70%) and interpretation of the biological data
- Writing of the manuscript and supporting information

#### Dr. Ahmed El-Gokha:

- Synthesis of covalent trisubstituted imidazole derivatives and interpretation of the biological data

#### Francesco Ansideri:

- Synthesis of the saturated analogs of the trisubstituted imidazole derivatives and interpretation of the biological data
- Proofreading of the manuscript
- Assistance in the revision process

#### Michael Eitel:

- Optimization of the synthesis route towards trisubstituted imidazole derivatives
- Preparation of intermediates for the synthesis of trisubstituted imidazole derivatives

#### Eva Döring:

- Performance of the experiments with Glutathione to estimate the non-specific activity of covalent inhibitors
- Execution of the *in-vitro* metabolic stability experiments with human liver microsomes

#### Adrian Sievers-Engler:

- Realization of the mass spectrometry experiments for the detection of the covalent binding
- Processing, analysis, and interpretation of the raw data

**Dr. Andreas Lange:**

- Expression and purification of the JNK3 wild-type and C154A mutant forms to be used in the mass experiments

**Professor Dr. Frank M. Boeckler:**

- Supervision of wild-type protein expression and purification as well as of single-point mutation experiments

**Professor Dr. Michael Lämmerhofer:**

- Planning and supervision of the mass spectrometry experiments

**Professor Dr. Pierre Koch:**

- Preliminary conception of the project strategy
- Generation and coordination of the project
- Planning of the synthesis route for the trisubstituted imidazole derivatives
- Analysis of data
- Writing of the manuscript
- Final approval of the manuscript

**Professor Dr. Stefan A. Laufer:**

- Generation and coordination of the project
- Analysis of data
- Final approval of the manuscript

**Publication V**

*A Diverse and Versatile Regiospecific Synthesis of Tetrasubstituted Alkylsulfanylimidazoles as p38 $\alpha$  Mitogen-Activated Protein Kinase Inhibitors*

**Author Contributions****Francesco Ansideri:**

- Planning of the synthesis route
- Synthesis of test compounds
- Analysis and interpretation of biological data
- Writing of the manuscript



**Stanislav Andreev:**

- Design of the experiments
- Optimization of three steps of the synthesis route
- Assistance in the preparation of synthesis intermediates and in the collection of analytical data
- Writing of the manuscript

**Dr. Annette Kuhn:**

- Assistance in the preparation of synthesis intermediates and in the collection of analytical data

**Dr. Wolfgang Albrecht:**

- Conceiving of the project
- Analysis of data

**Professor Dr. Stefan A. Laufer:**

- Conceiving of the project
- Analysis of data
- Supervision of the biological assay performance

**Juniorprofessor Dr. Pierre Koch:**

- Conceiving, generation, and coordination of the project
- Analysis of data
- Writing of the manuscript
- Final approval of the manuscript

**Publication VI**

*1-(3',6'-Dihydroxy-3-oxo-3H-spiro[isobenzofuran-1,9'-xanthen]-5-yl)-3-[4-({4-[1-(4-fluorophenyl)-1H-imidazol-5-yl]pyridin-2-yl}amino)phenyl]thiourea*      *methanol monosolvate*

**Author Contributions****Francesco Ansideri:**

- Synthesis and crystallization of the compound
- Writing of the manuscript

**Dr. Dieter Schollmeyer:**

- Collection and interpretation of the diffraction data
- Writing of the manuscript

**Professor Dr. Pierre Koch**

- Generation and coordination of the project
- Writing of the manuscript
- Final approval of the manuscript

**Publication VII**

*Structural Optimization of a Pyridinylimidazole Scaffold: Shifting the Selectivity from p38 $\alpha$  Mitogen-Activated Protein Kinase to c-Jun N-terminal Kinase 3*

**Author Contributions****Francesco Ansideri:**

- Design and synthesis of majority of the reported compounds (>50%)
- Co-supervision of master student Camilla Scarpellini in the preparation of other compounds
- Interpretation of the biological data
- Writing of the majority of the manuscript and supporting information

**Joana T. Macedo:**

- Crystallization of the JNK3 and preparation of the protein-ligand complexes
- Collection and interpretation of the diffraction data
- Preparation of the figures concerning the protein-ligand structure
- Minor contribution to the manuscript writing

**Michael Eitel:**

- Development of the synthesis route for a class of presented inhibitors
- Preparation of some of the presented compounds (10%)
- Crystallization of a tetrasubstituted intermediate for structure determination experiments

**Dr. Ahmed El-Gokha:**

- Preparation of some of the presented compounds (10%)

**Dr. Dhafer Zinad:**

- Preparation of some of the presented compounds (5%)

**Camilla Scarpellini:**

- Preparation of several of the presented compounds (20%)

**Mark Kudolo:**

- Realization of the *in vitro* metabolic stability experiments

**Dr. Dieter Schollmeyer:**

- Collection and interpretation of diffraction data for the tetrasubstituted imidazole derivative

**Professor Dr. Frank M. Boeckler:**

- Expression and purification of JNK3 used in crystallization studies

**Dr. Bärbel S. Blaum:**

- Supervision of the experiments of the structural determination of JNK3-inhibitor complexes
- Proofreading of the manuscript

**Professor Dr. Stefan A. Laufer:**

- Scientific support of the project
- Supervision of the biological assay performance

**Professor Dr. Pierre Koch:**

- Generation and coordination of the project
- Analysis of data
- Writing of the manuscript
- Final approval of the manuscript



# 1. Introduction

## 1.1. Protein Kinases

The family of protein kinases is constituted by enzymes catalyzing the reaction of phosphorylation, namely the covalent transfer of the  $\gamma$ -phosphate group from a nucleoside triphosphate (generally adenosine triphosphate (ATP)) to the free hydroxyl group of an amino acid side chain (Ser, Thr, and Tyr).<sup>1-3</sup> In detail, depending on the targeted amino acid, these enzymes can be divided into Ser/Thr kinases, Tyr kinases, and dual-specificity Ser/Thr/Tyr kinases.<sup>2</sup> The action of protein kinases is counterbalanced by corresponding protein phosphatases, which are able to reverse the process by cleaving the phosphoester bond.<sup>4</sup>

Phosphorylation represents the most widespread and well-studied post-translational modification in eukaryotic organisms,<sup>5,6</sup> with an estimation of more than 200,000 phosphorylation sites within the human proteome.<sup>7</sup> Kinases are able to recognize one or more substrates in an exceptionally specific fashion based both on local features, such as a determined consensus sequence surrounding the phosphorylation site, as well as spatially-separated docking motifs, favoring the recruitment and the right positioning of the targets.<sup>8,9</sup> Additionally, some kinases can associate with adaptors known as scaffold proteins forming supramolecular complexes which ease the identification and phosphorylation of the desired substrate.<sup>8,10</sup> The introduction of a negatively-charged phosphoryl group produces a conformational modification of the targeted protein which can affect its functionality in a multitude of ways, like modulating its activation state, altering the interaction with molecular partners, and influencing its stability or cellular localization.<sup>11</sup>

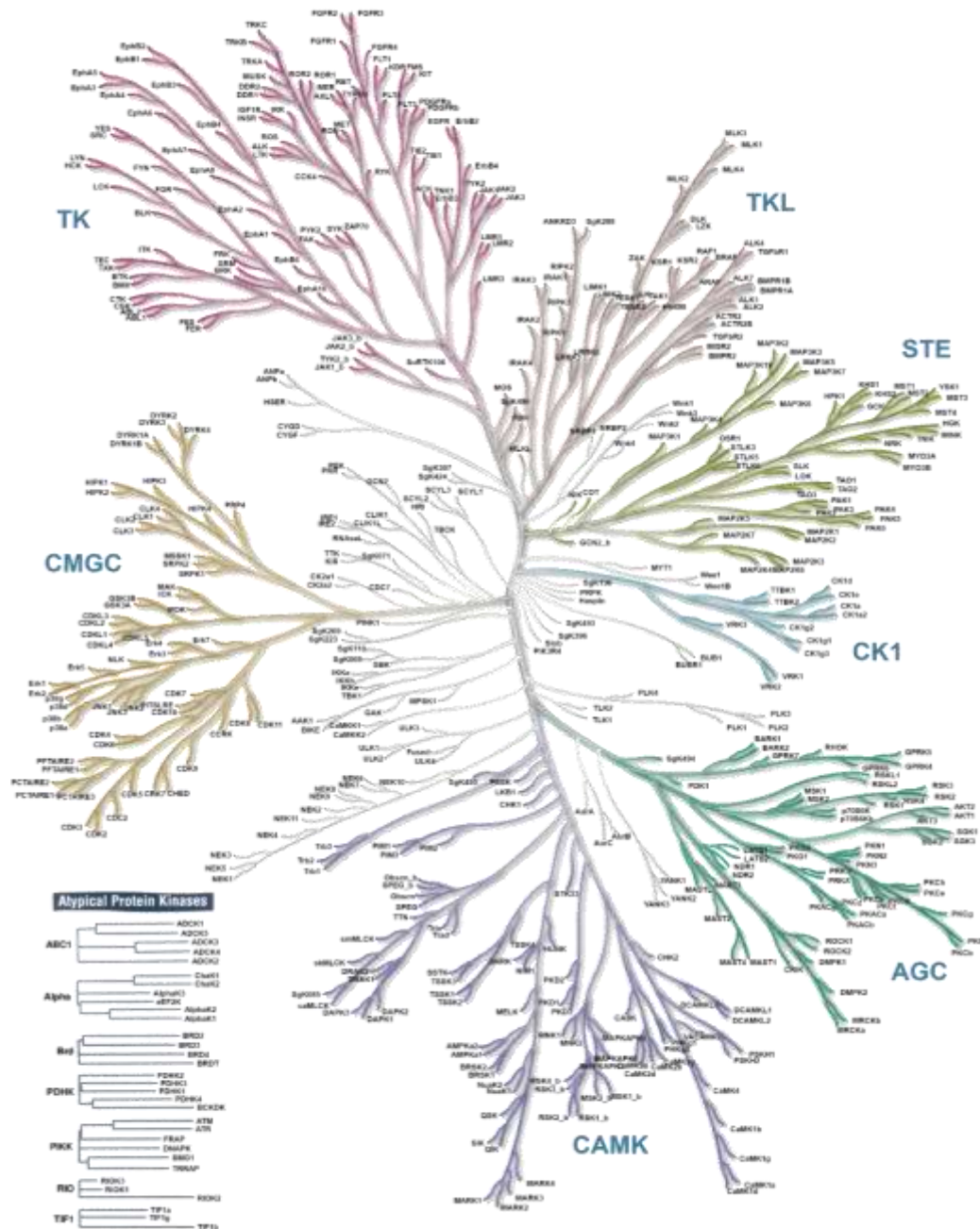
Protein kinases are among the major actors in signal transduction pathways, wherein various phosphorylation events represent key steps of signaling cascades which regulate nearly every basic cellular activity including proliferation, differentiation, apoptosis, immunity, and metabolism.<sup>11-14</sup> The potential of different kinases to phosphorylate multiple sites on the same target<sup>15</sup> as well as the coordinated activity of protein kinases and phosphatases<sup>4</sup> allow the fine tuning of this biochemical process, thus confirming its pivotal role in the regulation of biological events. As a direct consequence, however, dysregulation

in the activity of protein kinases is strongly connected with several pathological states, causing these enzymes to emerge as potential drug targets in different therapeutic approaches.<sup>16,17</sup>

Sequence alignment of eukaryotic protein kinases has allowed the detection of conserved features within their catalytic domains.<sup>18</sup> Subsequent advancements in the human genome sequencing have then permitted to progressively broaden the number of genes belonging to this superfamily and to deduce their phylogeny.<sup>18-22</sup> To date 518 genes have been included in the superfamily of protein kinases, accounting for approximately the 1.7% of the whole human genome and therefore acquiring the common denomination of “kinome”. The possibility of alternative splicing leads to an estimation of more than 1,000 members, making kinases one of the widest protein families in the human organism.<sup>21</sup> Based on their sequence similarity and evolutionary relationships, human protein kinases have been classified into seven different groups as depicted in Figure 1.1:

- AGC group: mainly contains kinases activated by second messengers like PKA, PKG, and PKC
- CAMK group: includes kinases dependent on the Ca<sup>2+</sup>/calmodulin system
- CMGC group: contains different classes of kinases generally activated by phosphorylation like cyclin-dependent kinases (CDKs) and mitogen-activated protein kinases (MAPKs)
- TK group: composed of Tyr specific kinases often representing intracellular catalytic domains of membrane receptors
- TKL group: a heterogeneous group including diverse kinases structurally related to Tyr kinases
- STE group: includes upstream activators of MAPKs
- CK1 group: mostly constituted by the casein kinase 1 family

In addition, this classification includes a group of 40 atypical protein kinases exhibiting biochemical activity although lacking sequence similarity with the conserved kinase domain.



**Figure 1.1** Representation of the human kinome phylogenetic tree as described by Manning *et al.*<sup>21</sup> The figure was obtained through the web-based tool KinMap;<sup>23</sup> illustration reproduced courtesy of Cell Signaling Technology, Inc. ([www.cellsignal.com](http://www.cellsignal.com)).

### 1.1.1. Structure of protein kinases

As previously mentioned, comparison of primary sequences of several kinase catalytic domains has led to the identification of conserved features, which have been therefore considered fundamental for the phosphotransfer activity. In particular, 12 conserved subdomains have been detected, separated by amino acid stretches which instead diverge

between the different classes of protein kinases.<sup>22</sup> These identified subdomains mainly consist of sequences possessing a defined secondary structure and are involved in the formation of the active site and in the catalytic activity.<sup>4,18</sup>

The high primary structure similarity reflects on a common folding shared by the majority of kinases. The catalytic domain of protein kinases, typically constituted by 250-300 amino acids, is characterized by a two-lobed structure comprising a small N-terminal lobe and a larger C-terminal domain, tethered by a flexible loop termed "hinge region". The ATP is accommodated in a cleft at the interface between the two lobes, where the adenine group forms a bidentate hydrogen bond with the hinge region (Figure 1.2).<sup>2,3,24</sup>

The N-terminal lobe, or N-lobe, is composed by a five-stranded antiparallel  $\beta$ -sheet motif and generally a single  $\alpha$ -helix (the  $\alpha$ C-helix) which represents an important regulatory element for the catalytic activity.<sup>24</sup> A Lys residue in the N-lobe, belonging to a highly conserved motif Ala-Xxx-Lys, coordinates the  $\alpha$  and  $\beta$  phosphate groups of ATP, and interacts with an almost invariable Glu residue of the  $\alpha$ C-helix through the formation of a salt bridge, assumed to be crucial for the kinase activity. The flexible loop connecting  $\beta$ 1 and  $\beta$ 2 strands, known as the Gly-rich loop, comprises a conserved motif Gly-Xxx-Gly-Xxx-Xxx-Gly which coordinates the  $\beta$  and  $\gamma$  phosphates and was described to fold as a lid over the bound ATP in the kinase active form.<sup>3,22,24-27</sup>

Oppositely to the N-lobe, the C-terminal domain is prevalently composed of  $\alpha$ -helices and additionally contains four  $\beta$ -sheet strands ( $\beta$ 6- $\beta$ 9). The latter constitute the bottom of the nucleotide binding cleft and comprise residues which are essential for the catalytic activity.<sup>3,24</sup> The catalytic loop, connecting  $\beta$ 6 and  $\beta$ 7 strands, contains most of the kinase catalytic machinery including the conserved motif His/Tyr-Arg-Asp (HRD/YRD motif). The Asp residue of this tripeptide takes part in the catalytic mechanism by extracting a proton from the hydroxyl group of the substrate while a nearly invariable Asn within the same loop binds a  $Mg^{2+}$  ion that interacts with the  $\alpha$  and  $\gamma$  phosphates.<sup>24,28,29</sup> Of primary importance for the regulation of the kinase catalytic activity is the activation loop, or A-loop, which consists of a segment in the C-lobe whose length and composition vary depending on the kinase. This sequence typically comprises one or more phosphorylation sites which allow the activation of the enzyme by upstream kinases.<sup>29,30</sup> The N-terminal end of the A-loop, often named Mg binding loop, contains the highly conserved Asp-Phe-Gly (DFG) motif in which the Asp residue points toward the ATP binding pocket and chelates a second  $Mg^{2+}$  ion coordinating the  $\beta$  and  $\gamma$  phosphate groups. The Phe side chain of the DFG tripeptide makes hydrophobic interactions with two residues of the  $\alpha$ C-helix (N-lobe) and contributes to its correct positioning.<sup>27,30</sup>

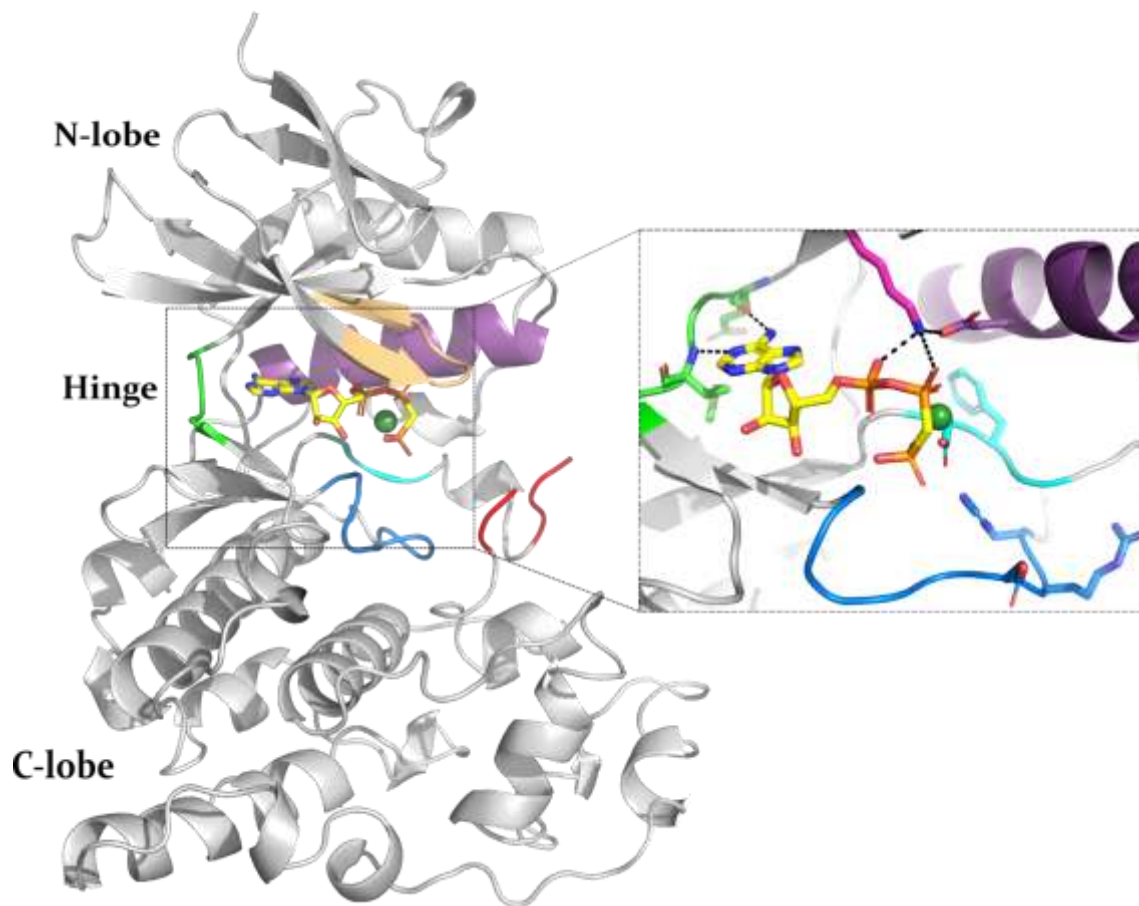
Analysis of the protein kinase folding also resulted in the identification of hydrophobic spines, namely series of non-continuous amino acid residues which are aligned and



interconnected in the kinase active form, thus forming skeletons that stabilize the two lobes. Although these structures are present in all kinases, the amino acid residues constituting them are not always conserved and are not detectable in primary structure. The regulatory spine, or R-spine, is composed of four residues, two in the N-lobe (of which one in the  $\alpha$ C-helix), and two in the C-lobe (the His/Tyr of the HRD/YRD motif in the catalytic loop and the Phe of the DFG motif). The catalytic spine is instead consisting of eight non-conserved hydrophobic residues belonging to both lobes and is completed by the adenine ring of the bound ATP.<sup>31,32</sup> Both spines are anchored to the  $\alpha$ F-helix, an extended  $\alpha$ -helix sequence in core of the C-lobe.<sup>33</sup>

Phosphorylation at one or multiple sites on the A-loop generally stabilizes the kinase in the active conformation. In this state, the DFG motif is described to be in an “in” conformation where the Asp points towards the ATP binding site and the Phe interacts with hydrophobic residues of the  $\alpha$ C-helix. The  $\alpha$ C-helix also assumes an “in” conformation and is rotated toward the catalytic site where the conserved Glu residue forms the aforementioned salt bridge with the Lys side chain of the Ala-Xxx-Lys sequence. In addition, both the R-spine and the catalytic spine are assembled.<sup>27-29,34</sup> Conversely, inactive, non-phosphorylated kinases tend to adopt a “DFG-out” conformation where the positions of Asp and Phe residues are switched due to a flip of the tripeptide of about 180°. As a result, the Asp side chain points away from the ATP binding site, no longer stabilizing the phosphate groups through the Mg<sup>2+</sup> ion. At the same time, the bulky side chain of Phe is shifted away from the  $\alpha$ C-helix and faces the ATP pocket, in some cases sterically blocking the binding of the nucleotide. The inactive conformation is also characterized by a torsional movement of the  $\alpha$ C-helix away from the binding site, preventing the formation of the catalytic salt bridge. The change of position of both  $\alpha$ C-helix and the DFG-Phe causes the disruption of the R-spine which results in a misalignment of the two lobes for the catalytic activity.

Finally, other structural elements can characterize the kinase “off-state” such as a particular folding of the A-loop or the distortion of the Gly-rich loop.<sup>27-29,35-37</sup> In any case, whereas kinases share very similar conformations in their catalytically active state, several structural differences can exist in their inactive forms and an univocal definition of the common features characterizing the kinase “off-state” is extremely challenging.<sup>29,34</sup>



**Figure 1.2.** Crystal structure of c-Jun N-terminal kinase (JNK) 3 in complex with  $\beta,\gamma$ -methyleneadenosine 5'-triphosphate (AMP-PCP, yellow), PDB entry: 6EQ9. The protein backbone is displayed in gray while the diverse kinase structural elements mentioned in section 1.1.1. are highlighted with different colors: light green: hinge region; purple:  $\alpha$ C-helix; salmon: Gly-rich loop; cyan: DFG motif; blue: catalytic loop; red: activation loop; magenta: conserved Lys (Lys93 in JNK3); Mg ion is displayed as a dark green sphere while polar interaction are shown as black dashed lines; due to high flexibility, most of the electron density for the activation loop was missing; protein structure on the left shows the typical bilobal folding of protein kinases whereas the close-up view shown on the right highlights the ATP cleft, wherein the side chains of key amino acids are displayed as sticks and some segments, including the Gly-rich loop, have been omitted for the sake of clarity; in the enlargement it is possible to observe the bidentate hydrogen bond of the AMP-PCP with the backbone atoms of Met149 and Glu147, as well as the interactions of Lys93 with the  $\alpha$  and  $\beta$  phosphates and the salt bridge with Glu111; furthermore, the side chains of the conserved DFG and HRD motifs are also shown.

### 1.1.2. Protein kinases as drug targets

As previously mentioned, a deregulated activity of several kinases has been recognized having a causal role in the pathogenesis of different diseases.<sup>16</sup> In the first instance, a strong evidence has connected aberrant phosphorylation with various forms of cancer, as kinases often constitute a switch in many signaling pathways regulating cell growth and

proliferation.<sup>38,39</sup> Additionally, abnormal phosphotransfer activity has also been considered responsible for other complex pathological conditions as inflammatory, autoimmune and neurodegenerative diseases.<sup>40,41</sup> The major role played by kinases in relevant diseases, along with their druggability,<sup>42</sup> has prompted a remarkable endeavor in the discovery of protein kinase inhibitors.<sup>17</sup> Since the FDA approval of the first small molecule kinase inhibitor Imatinib in 2001, more than 35 new small molecules have been approved at a constantly increasing rate.<sup>43,44</sup> Although nearly the totality of molecules have been released as therapeutic agents for various forms of malignancies, the introduction of Tofacitinib<sup>45</sup> (Xeljanz®) in 2012 as an immunomodulating agent has proven the possibility to broaden the field of applicability of kinase inhibitors.

In the research of kinase inhibitors directed at the ATP binding site, two primary challenges need to be faced. Firstly, due to the similar structural features characterizing the members of the kinome especially with regard to the ATP cleft, it is particularly difficult to achieve molecules selectively inhibiting the target kinase. Moreover, inhibitors need to display a high potency in order to be able to compete with high intracellular ATP concentrations, typically ranging between 2 and 10 mM. Nevertheless, many kinase inhibitors have succeeded in overcoming these complications and can be classified according to their specific binding mode. A first criterion is based on the reversibility of the binding and permits to distinguish between covalent and non-covalent inhibitors. Additionally, non-covalent/reversible inhibitors can be divided into five different subgroups (Type I, II, I<sup>1/2</sup>, III, IV) according to the targeted areas of the kinase (a graphical representation of the different classes of kinase inhibitors is outlined in Figure 1.4 at the end of this section).

### Type I inhibitors

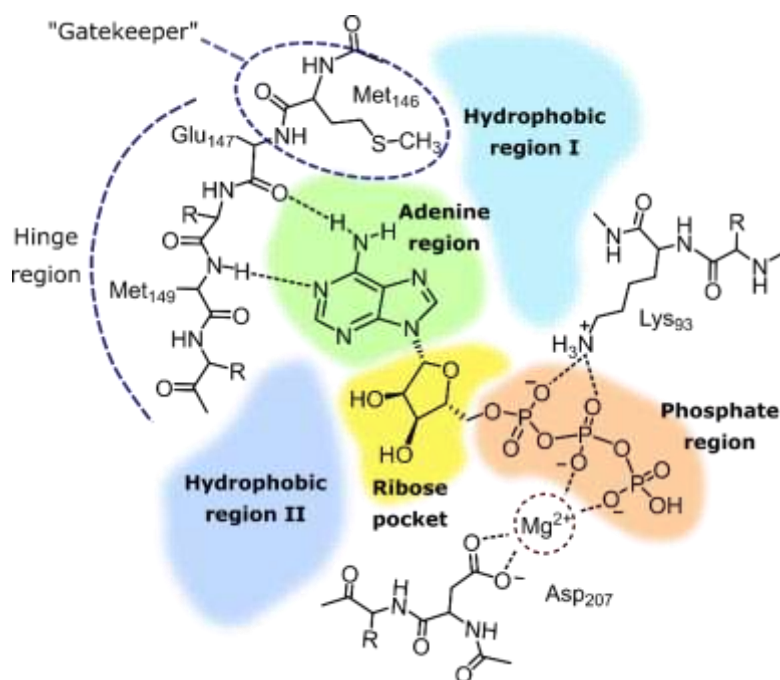
Type I inhibitors generally bind to the ATP cleft of the kinase in its active, DFG-in,  $\alpha$ C-helix-in conformation, wherein the Phe side chain of the DFG motif is buried in a hydrophobic area of the protein close to the  $\alpha$ C-helix. Since this conformation of the kinase allows the binding with ATP, members of the type I class are considered fully ATP competitive.<sup>2,46,47</sup> A more correct description for the binding of type I inhibitors is that they can bind the ATP pocket regardless of the kinase activation state, thus not requiring a particular conformation of determined structural elements.<sup>48</sup>

Given the close resemblance of the ATP binding pocket in the active kinases, a satisfactory selectivity was originally believed not to be achievable by targeting this conformation. However, the high success in therapy of type I inhibitors has demonstrated the possibility of reaching a clean selectivity profile by exploiting non-conserved features of specific kinases.

ATP competitive inhibitors typically follow a pharmacophore model developed by Traxler and coworkers<sup>49</sup> which identifies five different subsites within the ATP binding pocket (Figure 1.3):

- Adenine region: in an analogous fashion as for ATP, this hydrophobic area allows the formation of hydrogen bonds between the inhibitor and the backbone amino acids of the hinge region. All type I inhibitors form at least one H-bond interaction in this area
- Sugar/Ribose pocket: this region, accommodating the ribose of the ATP, presents mostly a hydrophilic character and offers the possibility of hydrogen bond formation which can improve the binding affinity
- Phosphate region: this area is opened to the solvent and has a highly hydrophilic character. It is generally not addressed to increase the binding affinity but polar substituents occupying this area can be useful to improve the inhibitor solubility and pharmacokinetic (PK) properties
- Hydrophobic region I: (HR I) also known as hydrophobic back pocket or selectivity pocket, this area opens in the N-terminal lobe and is not addressed by ATP. The access to this region is controlled by a specific amino acid residue of the N-lobe named “gatekeeper”. Since the gatekeeper and other residues surrounding this pocket are not highly conserved, this region can be targeted in order to achieve both selectivity for a specific kinase and increase in binding affinity
- Hydrophobic region II: (HR II) this section consists in a solvent-exposed area which is not occupied by ATP when bound to the enzyme. As the amino acid composition is not conserved within the kinome it can be targeted by both hydrophobic and hydrophilic substituents to gain potency and selectivity

Many of the FDA-approved kinase inhibitors belong to the type I class, such as the EGFR inhibitors Gefitinib (Iressa®) and Erlotinib (Tarceva®).<sup>26,43</sup>



**Figure 1.3.** Representation of the Traxler's pharmacophore model; the figure illustrates the endogenous substrate ATP in the binding site of JNK3.

### Type II inhibitors

Inhibitors belonging to this category bind preferentially at the ATP pocket of the kinase in the inactive DFG-out conformation, resulting in its stabilization.<sup>50</sup> As previously mentioned, this form occurs when the kinase is not phosphorylated at the A-loop and is characterized by a flip of the DFG-motif where the Phe side chain is shifted approximately 10 Å away from the  $\alpha$ C-helix. This results in the exposure of a hydrophobic cleft often named "deep pocket" or "allosteric site" which is absent in the ATP-bound kinase.<sup>50</sup> Type II inhibitors typically form hydrogen bond contacts with the hinge region and target the deep pocket with a hydrophobic substituent. A hydrogen bond donor-acceptor pair (generally an amide or a urea) is also present immediately before this hydrophobic substituent and contributes to the positioning of the latter in the deep pocket by interacting with the  $\alpha$ C-helix-Glu side chain and the DFG-Asp backbone.<sup>48</sup>

Since the amino acid composition of the deep pocket is not conserved, type II inhibitors are considered to have a higher potential to achieve a clean selectivity profile. Moreover, not all the members of the kinase family are supposed to assume the DFG-out conformation, thus reducing the possible off-targets of this class of molecules.<sup>51</sup> Nevertheless, despite an overall higher selectivity profile of this category, some type II inhibitors also showed a certain promiscuity within the kinome, and the original dogma claiming the elevated selectivity of this category of inhibitors had to be revised.<sup>52</sup>

As mentioned, type II inhibitors interact with some of the regions occupied by ATP and can be theoretically classified as ATP competitive. However, the inactive DFG-out conformation is known to have a significantly lower affinity for the endogenous substrate compared to the active form, thus reducing the ATP competition with the inhibitors.<sup>50</sup> Moreover, when analyzing the binding kinetics, it can be observed that type II inhibitors present a low association rate ( $k_{on}$ ), and a very low dissociation rate ( $k_{off}$ ), which increase the residence time on the target.<sup>53</sup> Finally, studies analyzing the DFG-in and DFG-out forms of the p38 $\alpha$  MAPK have highlighted how in the latter the conformation of the A-loop places the phosphorylation sites in a hidden position, probably preventing the activation by upstream kinases.<sup>54</sup>

Various type II inhibitors can be found among the FDA approved kinase inhibitors as the aforementioned Abl-inhibitor Imatinib (Gleevec®) and the VEGFR/PDGFR inhibitor Sorafenib (Nexavar®).<sup>26,43</sup>

### Type I<sup>1/2</sup> inhibitors

This recent class of inhibitors was first described by Zuccotto *et al.* when observing the binding mode of certain published inhibitors.<sup>55</sup> Such compounds, still addressing the ATP cleft, bind the kinase in an inactive DFG-in form wherein the  $\alpha$ C-helix is shifted outwards from the ATP binding site. Despite adopting a DFG-in conformation, such state is catalytically non-competent, as the crucial Lys-Glu salt bridge is broken and the R-spine is disassembled. The movement of the  $\alpha$ C-helix results as well in the formation of a hydrophobic cavity akin to the deep pocket of the DFG-out conformation, which can be addressed to improve selectivity. Type I<sup>1/2</sup> inhibitors generally interact with the hinge via hydrogen bonds and point towards the back cavity, in some cases also addressing other areas defined by the Traxler's pharmacophore (Figure 1.3). Some inhibitors of this class have been described not to reach the back pocket but instead forming hydrogen bonds with the  $\alpha$ C-helix-Glu side chain and the DFG-Asp backbone, thus stabilizing the  $\alpha$ C-helix-out conformation.<sup>56,57</sup> The name attributed to this class suggests, therefore, the ability of these "hybrid" inhibitors to target the DFG-in conformation of the kinase by forming interactions analogous to the type II class. As in the case of type II inhibitors, the lower conservation of the back cavity has been hypothesized to represent a determining factor in the achievement of a higher selectivity. Furthermore, induction/selection of a particular conformation of the kinase is responsible for the slow binding kinetics of these compounds, significantly increasing the target residence time. As a result, the activity of these inhibitors is scarcely influenced by the ATP concentration, despite their classification as ATP competitive due to the occupancy of the nucleotide cleft.

Among the FDA approved inhibitors, examples for this class are represented by the EGFR inhibitor Lapatinib (Tykerb®) and by the Raf inhibitor Vemurafenib (Zelboraf®).<sup>26,43</sup>

#### Type III inhibitors

The definition of this class of inhibitors is particularly challenging and often not univocal, due to the heterogeneity of compounds composing it. Type III inhibitors are generally described to bind the kinase in an allosteric pocket adjacent to the ATP cleft and are therefore non ATP competitive, as a simultaneous binding of the inhibitor and the nucleotide is theoretically admitted.<sup>43</sup> In some cases, these compounds can bind the deep pocket of DFG-out conformations without interacting with the hinge. Otherwise, these inhibitors can interact with the phosphoacceptor substrate binding site or exploit a novel binding site of specific kinases.<sup>58</sup> These features provide the potential of an exquisite selectivity of action, accompanied by a lack of competition with the endogenous nucleotide substrate. However, inhibitors belonging to this class can hardly be rationally designed and, especially when aiming at the peptidic substrate binding site, this modality of inhibition is rarely achievable through small molecules. To date, only one FDA approved inhibitor can be included in this class, namely the MEK1/2 inhibitor Trametinib (Mekinist®).

When referring to the substrate binding site it is worth to mention that this area can be targeted by bivalent inhibitors which are presented in some classifications as type V inhibitors.<sup>59</sup> These molecules consist of a classical small-molecule scaffold addressing the ATP pocket that is connected through a linker to a peptide portion, occupying the substrate binding site. To date, no molecule belonging to this class has been released.

#### Type IV inhibitors

The last class of reversible inhibitors includes those molecules binding the kinase in an allosteric site remote from the ATP binding cleft. Multiple binding modes are possible as each kinase possesses unique features when moving away from the catalytic site. Although the high potential of these molecules in terms of selectivity, it is rather uncommon to reach this modality of inhibition with small molecules due to the scarce presence of druggable pockets in this region of the protein. Examples of type IV approved inhibitors can be represented by the macrolide-based compounds Sirolimus/Rapamicine (Rapamune®) and Everolimus (Certican®), both targeting mTOR.

### Covalent inhibitors

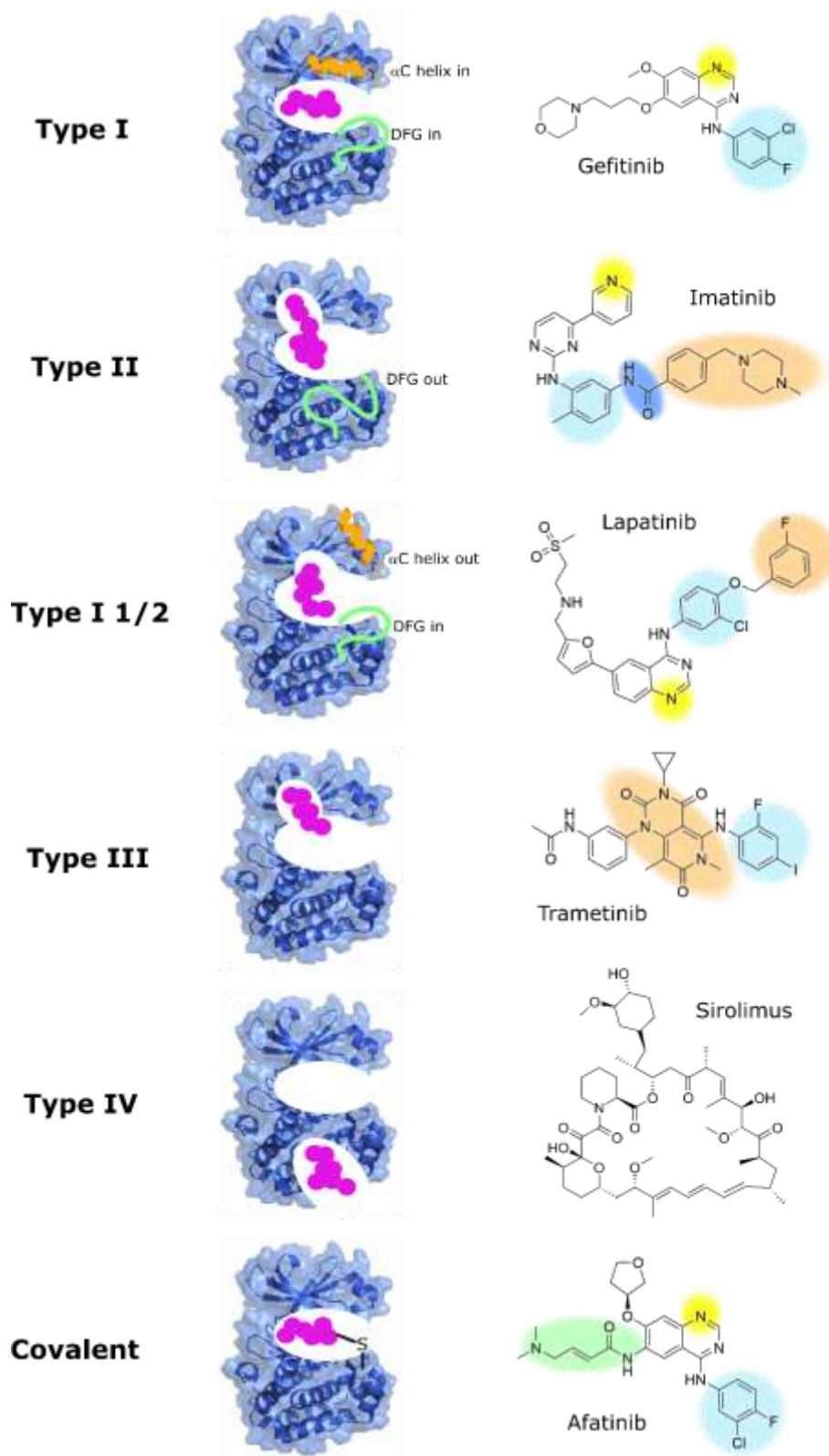
Differently from reversible inhibitors, the compounds belonging to this category are able to covalently modify the target enzyme leading to a long-lasting inactivation, since the catalytic functionality can only be restored through *ex novo* synthesis of the protein.<sup>60</sup> Despite the existence of different classes of covalent inhibitors, targeted covalent inhibitors (TCIs) are the only ones which can be employed in the realm of kinases.<sup>61</sup> Such molecules consist of a core scaffold binding the ATP cleft and a weakly electrophilic moiety which forms the covalent bond with a specific nucleophilic amino acid. The generic mechanism of action of these inhibitors entails an initial noncovalent binding which allows the positioning of the tempered “warhead” in proximity of the target residue, followed by the formation of the covalent bond. For this reason, the activity of irreversible inhibitors depends both on their affinity for the enzyme (described by the  $K_i$  parameter) and on the rate of covalent bond formation (indicated by the  $k_{\text{inact}}$  value).<sup>60,62</sup>

The most commonly targeted residue in protein kinases is represented by Cys,<sup>63,64</sup> although a few examples of inhibitors covalently modifying a Lys side chain have been reported.<sup>65,66</sup> Cys is the sole amino acid possessing a highly nucleophilic thiol group and is therefore prone to react with the weakly electrophilic warheads of TCIs. In addition, such amino acid is not involved in the catalytic mechanism of kinases, hence not conserved in the active site, offering the potential for a high degree of selectivity.<sup>64</sup>

The electrophilic warhead has to be positioned at optimal distance and orientation with regard to the targeted Cys, and needs to possess a mild reactivity in order to not modify off-target nucleophiles. The covalent tag is most commonly represented by an  $\alpha,\beta$ -unsaturated carbonyl group which can react as a Michael’s acceptor in the conjugate addition of nucleophiles. However, other alkylating agents as  $\alpha$ -haloketones or epoxides can be employed as well.<sup>61,67</sup>

The interest on kinase covalent inhibitors has been increasingly rising during the last decade, as this class presents several advantages compared to classical reversible inhibitors.<sup>68</sup> Firstly, the irreversible inactivation of the enzyme allows to uncouple the pharmacodynamic effect from the PK properties, conferring a high potency even at low concentrations and ensuring an extended duration of action which persists even after the drug has been cleared from the organism. This results in the possibility of administering lower inhibitor doses and with lower frequency. Moreover, as mentioned before, targeting an opportune non catalytic Cys residue allows to achieve a high level of selectivity, due to the low conservation of those areas not involved in the phosphorylation reaction.<sup>60-62</sup>





**Figure 1.4.** Schematic overview of the diverse types of kinase inhibitors. Each type is structurally exemplified by a FDA-approved inhibitor wherein the key structural features are highlighted using different colors; hinge-binding atoms are highlighted in yellow; for moieties occupying the HR I and the deep pocket cyan and salmon were used, respectively; hydrogen bond donor-acceptor pair is highlighted in blue while green was used for the covalent warhead; figure modified from Wu *et al.*<sup>43</sup>

A major concern in the development of covalent inhibitors regards the possibility of severe side effects deriving from the indiscriminate reactivity with off-targets. In particular, a primary risk consists of idiosyncratic adverse reactions which can be triggered by the formation of immunogenic protein-inhibitor adducts, a phenomenon known as haptization.<sup>67</sup> Nevertheless, the therapeutic success of FDA-approved covalent inhibitors like Afatinib (Giotrif®) and Osimertinib (Tagrisso®), targeting the epidermal growth factor receptor (EGFR), demonstrate the efficacy and tolerability of this class of inhibitors.

## 1.2. MAPKs

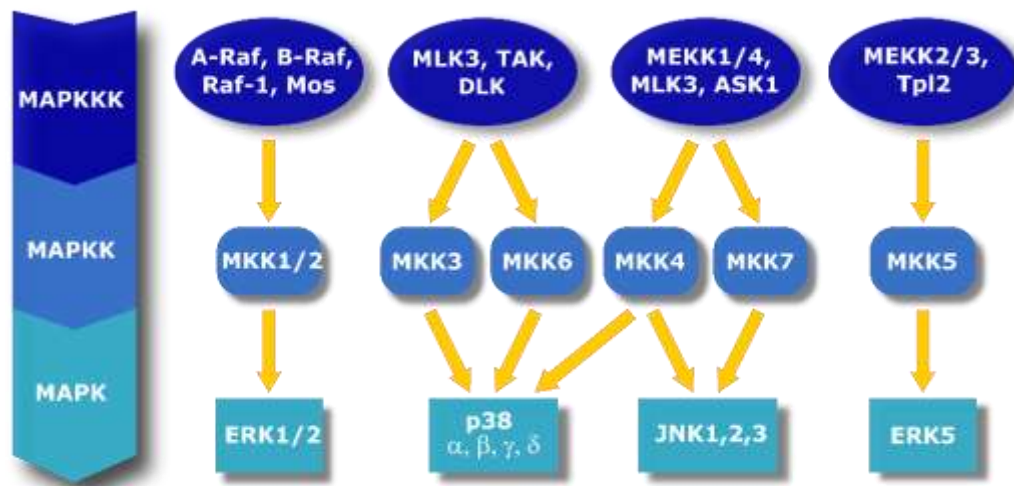
MAPKs are a family of Ser/Thr kinases belonging to the CMGC group and constitute a key element of signal transduction pathways mediating the cellular response to a broad variety of extracellular stimuli. Based on sequence homology and functionality four subgroups have been observed within this family: the extracellular signal-regulated kinases (ERKs) 1 and 2, the c-Jun N-terminal kinases (JNKs) 1, 2, and 3, the p38 MAPKs  $\alpha$ ,  $\beta$ ,  $\gamma$ , and  $\delta$ , and the ERK5.<sup>69</sup> Each member is characterized by an overall specific activation mechanism and by distinct biological functions, although possibilities of cross-talk between different pathways have also been described.<sup>70</sup>

All components of the MAPK family are activated through a phosphorylation cascade comprising the activation in series of at least two upstream kinases. This multistep mechanism offers the double advantage of amplifying the signal and allowing the integration of diverse signaling pathways.<sup>71</sup> The transition of MAPKs to a catalytically active form is promoted by the double phosphorylation of a Thr and Tyr residues within a Thr-Xxx-Tyr motif, carried out by a substrate-specific MAPK kinase (MAPKK, MKK or MEK). MAPKKs are in turn activated via Ser/Thr phosphorylation by upstream kinases referred as MAPKK kinases (MAPKKKs) or MEK kinases (MEKKs). Activation of MAPKKKs/MEKKs can be triggered by a plethora of different stimuli which range from environmental stress stimuli (such as heat or osmotic shock, UV radiation or ischemic hypoxia) to the interaction of extracellular ligands (hormones, growth factors, cytokines, lipopolysaccharide) with specific receptors, generally represented by Tyr kinase receptors or G-protein coupled receptors (GPCRs). Each of these stimuli results in a distinct activation profile which can involve one or more MAPKs to a different extent.<sup>69-73</sup> Figure 1.5 provides an overview of the different activation pathways of the MAPK family members.

Once activated, each member of the MAPK family can phosphorylate a variety of different substrates resulting in the mediation of complex mechanisms as cell survival, proliferation, and differentiation. The vast majority of MAPK substrates is represented by transcription factors which upon phosphorylation can regulate the expression of specific genes; besides,

MAPK-mediated signaling can also involve the phosphorylation of cytoplasmic targets. Each MAPK presents specificity for a distinct subset of downstream targets although in some cases two different MAPKs can act on the same substrate.<sup>69,72,73</sup> This substrate selectivity is reached not only by the recognition of a particular sequence surrounding the phosphorylation site (all MAPKs generally phosphorylate Ser or Thr residues followed by a Pro amino acid), but mostly thanks to docking motifs which confer complementarity between the MAPK and its specific substrates.<sup>72</sup>

An additional important method in the regulation of the MAPK-mediated signaling pathways is the presence of scaffold proteins which coordinate the sequential activation within a MAPK module. In detail, such multi domain proteins can bind the different components of a phosphorylation cascade (MAPKKK, MAPKK, and MAPK) thereby promoting their spatial contiguity. The formation of this multi-enzyme complex increases the efficiency of the signal propagation compared to diffusion-based signaling and reduces the cross-talk between different pathways.<sup>74,75</sup>



**Figure 1.5.** Schematic representation of MAPKs activation pathways. Figure was modified from Margutti *et al.*<sup>76</sup>

### 1.2.1. JNKs

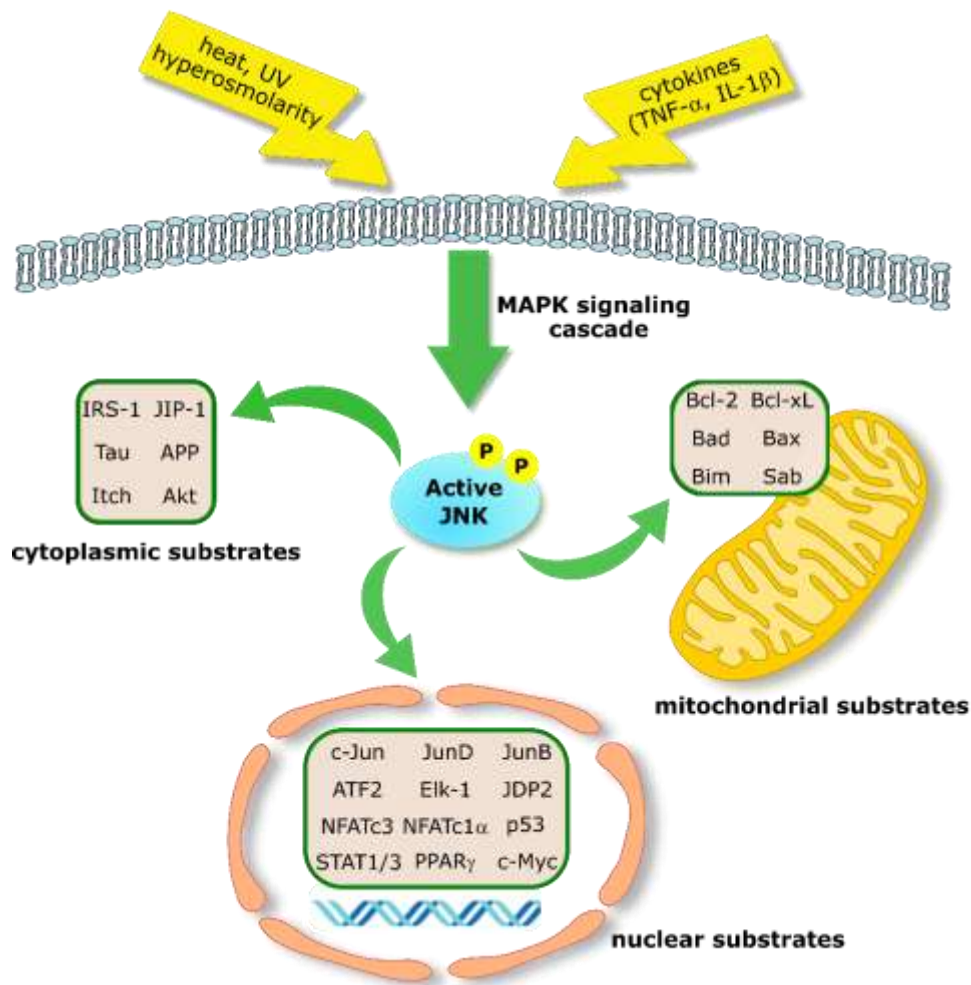
As already mentioned in the previous section, JNKs are Ser/Thr kinases constituting one of the four subgroups of the MAPK family.<sup>76</sup> The first members of this subfamily were discovered in the 1990s and originally termed stress-activated protein kinases (SAPKs). The name JNKs was instead later given after the c-Jun transcription factor, which represents the first downstream target identified for these enzymes.<sup>77</sup> Three different isoforms have been classified within this group, namely JNK1 (also known as SAPK- $\gamma$ /MAPK8), JNK2 (SAPK-

$\alpha$ /MAPK9) and JNK3 (SAPK- $\beta$ /MAPK10), encoded by the three distinct genes *jnk1*, *jnk2*, and *jnk3*. Each gene can then undergo alternative splicing, giving rise to a total of 10 JNK isoforms (four isoforms for both JNK1 and JNK2 and two for JNK3).<sup>78-80</sup> Despite sharing a high structural similarity, the JNK isoforms exhibit different tissue distribution since the JNK1 and JNK2 are ubiquitously expressed, whereas the JNK3 is mostly restricted to the brain, heart and testes. Moreover, the different isoforms are characterized by a distinct substrate specificity, suggesting dissimilarities in their physiological functions.<sup>79,80</sup>

In conformity with other members of the MAPK family, activation of JNKs is organized in signaling modules comprising tandem phosphorylation of three protein kinases (Figure 1.5). More closely, activation of JNKs results from a concomitant phosphorylation of a Thr and a Tyr residues within a Thr-Pro-Tyr motif in the activation loop carried out by the two MAPKK MKK4 and MKK7.<sup>76,81</sup> While MKK7 is specific for JNKs, MKK4 can also phosphorylate p38 MAPK members, albeit not being the main activator of these enzymes *in vivo*. The two upstream kinases MKK4 and MKK7 have proven to function in a synergistic manner so that both are required for the achievement of full JNK activation.<sup>82,83</sup> The MAPKK enzymes MKK4 and MKK7 can be phosphorylated by a multiplicity of upstream MAPKKK which in turn are triggered by a variety of stress stimuli including heat or osmotic shock, UV radiation, ischemia/reperfusion, and pro-inflammatory cytokines.<sup>81</sup> An additional level of regulation of the JNK activation pattern is constituted by scaffolding protein which, as previously mentioned, are able to bind the different elements of a phosphorylation cascade, thus favoring the signal transmission.<sup>74</sup> Up to date, four different isoforms of the JNK-interacting protein (JIP) have been identified.<sup>81,84</sup>

Activated JNK can phosphorylate a broad subset of downstream targets including both transcription factors and non-nuclear substrates.<sup>85</sup> Phosphorylation of c-Jun, which takes part in the formation of the activation protein (AP)-1, increases the transcriptional activity of this complex. An analogous effect derives from the phosphorylation of the activating transcription factor (ATF)2 which modifies gene expression through the formation of dimers with members of the Jun family.<sup>86</sup> Besides these two well-characterized pathways, JNKs can also act on additional nuclear targets, thereby modulating their effects on gene transcription (Figure 1.6). Furthermore, JNKs have demonstrated to phosphorylate cytosolic and mitochondrial substrates resulting in a modification of their functionality or in the regulation of their stability.<sup>85</sup>

By means of diverse downstream targets, members of the JNK family are involved in various physiological functions. Firstly, these kinases are implicated in the regulation of cell survival/apoptosis in response to external stimuli. The role of JNKs in cell death has been described as bivalent, since it depends on the entity of the stimulus and on the signal integration with additional pathways.



**Figure 1.6.** Representation of the different substrates of JNK. The figure was realized using the information from Bogoyevitch and Kobe.<sup>85</sup>

In general, a transient activation of JNKs seems to promote cell survival whereas a prolonged stimulation results in triggering the apoptotic process.<sup>82,87</sup> Another significant role of the JNK proteins consists in the modulation of inflammatory response and immune system.<sup>88</sup> In particular, mostly by promoting AP-1/ATF2-mediated gene expression, such enzymes contribute to the production of pro-inflammatory cytokines as tumor necrosis factor (TNF)- $\alpha$  and modulate the differentiation and activation of T-cells.<sup>89,90</sup> Finally, as mostly shown in *Drosophila*, some members of the JNK family seem to be crucial in embryonal morphogenesis,<sup>88</sup> this presumably explaining the non-viability of double *jnk1/jnk2* knockout mice due to premature embryonal death.<sup>91</sup>

Due to their involvement in important physiological processes, a dysregulation of the functionality of JNKs has been regarded as critical in diverse pathologic conditions.<sup>92</sup> Since the JNK isoforms display dissimilarities regarding localization and substrate specificity,

each isoform can differently contribute to a particular disease as it could be pointed out by the selective silencing of one or more codifying genes.<sup>79</sup>

### Neurodegenerative diseases

Within the last decades, a considerable evidence has connected the abnormal activity of the JNK family members with diverse neurodegenerative diseases such as Alzheimer's disease (AD), Parkinson's disease (PD), Huntington's disease, and multiple sclerosis, as well with neuronal death following ischemic episodes.<sup>93,94</sup>

Increased expression of phosphorylated JNK has been observed in post-mortem brains as well as in biopsy samples of AD patients.<sup>95</sup> Additionally, activated JNK is able to phosphorylate the amyloid precursor protein (APP) at Thr668 promoting its amyloidogenic cleavage into the  $\beta$ -amyloid (A $\beta$ ) peptide 42, which is considered the major responsible factor in the formation of A $\beta$  plaques. The Tau protein can also be phosphorylated by the JNKs leading to the formation of neurofibrillary tangles representing, together with A $\beta$  plaques, the principal histological hallmarks of AD.<sup>92,94,96</sup> Finally, activation of the JNK pathway is also associated with neuroinflammation and apoptosis, thereby resulting in neuronal loss.<sup>96</sup>

Analogously to AD, specimens of post-mortem brains from PD patients revealed an increased activation of the JNK-c-Jun pathway.<sup>93,94</sup> In addition, mice knockout experiments permitted to observe a neuroprotective effect of JNK-deficiency against 1-methyl-4-phenyl-1,2,3,6-tetrahydropyridine (MPTP)-induced neurotoxicity, representing a typical animal model for PD. More closely, whereas *jnk1* knockout mice showed similar results in comparison to the wild-type ones, single *jnk2* or *jnk3* deletion proved to significantly reduce cell loss after MPTP treatment. The neuroprotective effect was further enhanced following double *jnk2/jnk3* knockout, hence confirming the pivotal role of these two isoforms in the progressive neurodegeneration characterizing PD.<sup>97</sup> As previously mentioned, effects arising from the double *jnk1/jnk2* knockout could not be observed due to non-viability of mice carrying this genetic deletion.<sup>91</sup>

The recovery of blood circulation after a stroke/ischemia event can be associated to an extended tissue damage along with neuronal death in a "penumbra area" surrounding the site directly affected by the lack of oxygen supply. Such phenomenon is known as ischemia/reperfusion injury and is caused by different factors including inflammatory reaction and excitotoxicity.<sup>98</sup> JNK3 deficiency has been demonstrated to protect neurons against hypoxia-driven excitotoxicity, as observed by the treatment of the cells with the Glu receptor agonist kainic acid or by simulating hypoxia in mice models.<sup>92-94,99</sup> A similar effect

was instead not registered in case of single *jnk2* or *jnk1* knockout,<sup>99</sup> suggesting a specific function of the JNK3 isoform in the response to excitotoxic insult.

### Cancer

As mentioned before in this section, the JNK signaling pathway plays a bivalent role in the cellular life cycle, on one hand mediating cell survival and proliferation and on the other promoting stress-induced apoptosis. This dual behavior translates into a still unclear function of the JNK family members in cancer development.<sup>92,100</sup>

The evidence of a pro-oncogenic role of JNKs has been provided by several studies demonstrating that these kinases take part in the Ras-mediated transformation by phosphorylating c-Jun, responsible for blocking the expression of the tumor suppressor p53.<sup>81,92,101,102</sup> Members of the JNK family can also promote tumor survival, development, and dissemination by means of diverse mechanisms including cytokines production and angiogenesis.<sup>103</sup> In addition, increased JNK1 or JNK2 activity has been observed in diverse cancer cell lines<sup>88</sup> and a selective deletion of *jnk1* or *jnk2* in animal models has proven to reduce the development of certain types of malignancies.<sup>100-102</sup>

At the same time, a significant number of experiments suggested a tumor suppressor activity of the JNKs, as it would also be expected from their well-characterized pro-apoptotic function. As an example, selective isoform knockout in mice models led to an increased neoplastic proliferation<sup>104</sup> or to a major susceptibility to develop tumors following exposure to carcinogens.<sup>105</sup> In any case, the different behavior of JNKs as tumor suppressor or as tumor promoter seems to depend on the cell/tissue involved, as well as on the kinase isoform.<sup>100-102</sup>

### Metabolic diseases

An association of JNK isoforms with obesity, insulin resistance, and type 2 diabetes has been highlighted in both *in vitro* and *in vivo* assays. In general, it can be observed that obesity and type 2 diabetes are associated with a chronic inflammatory condition of the adipose and liver tissues, wherein the cytokines and the free fatty acids produced may activate the JNK pathway.<sup>106</sup> A first observation hinting the implication of JNKs in these metabolic pathologies is the increased activity of these enzymes in both dietary and genetically obese mice. In addition, selective ablation of *jnk1* resulted in a reduced weight gain and lower adiposity of mice on a high-fat diet, along with lower plasma levels of glucose and insulin. Similar results could be detected on JNK1-deficient genetically obese mice, hence clarifying a role of this isoform in the obesity-induced insulin resistance.<sup>79,106</sup> In

this pathological condition the molecular target of JNK1 was discovered to be the insulin receptor substrate 1, whose phosphorylation on Ser307 prevents the interaction with the insulin receptor.<sup>106,107</sup> Analogous outcomes could not be reproduced by *jnk2* knockout mice, which behaved analogously to the control. Such isoform might instead assume a role in the non-obese type 1 diabetes, as deletion of *jnk2* seemed to reduce the immune response towards pancreatic islets and to decrease the apoptotic response of  $\beta$ -pancreatic cells.<sup>79,108</sup>

### Inflammatory diseases

As already mentioned, JNKs are implicated in modulation of the inflammatory response and contribute to the regulation of the immune system by influencing the activity of T-lymphocytes, macrophages, and mast-cells.<sup>92</sup> These effects are mainly mediated by increasing the transcriptional activity of the AP-1 complex and of the ATF2. These factors can in turn increase the expression of pro-inflammatory cytokines as TNF- $\alpha$  and interleukin (IL)-2 and of other mediators of the inflammatory response as matrix metalloproteinases (MMPs).<sup>88,92</sup> These aspects have suggested a participation of the JNK signaling in chronic inflammatory diseases which was confirmed by diverse studies.<sup>109-112</sup> In particular, activation of the JNK pathway was observed in synovial cells and chondrocytes from patients affected by rheumatoid arthritis (RA) and osteoarthritis, respectively.<sup>109,110</sup> Additionally, treatment of synovial cells from RA patients with JNK inhibitors reduced the expression of MMPs involved in the degradation of joint cartilage, one of the symptoms characterizing this autoimmune disease.<sup>111</sup>

Use of JNK inhibitors in an acute asthma mice model determined a decrease of immune cells in the peribronchial area and a reduced production of pro-inflammatory cytokines and immunoglobulin E compared to control, thereby suggesting an implication of the JNK pathway in this inflammatory pathology.<sup>112</sup>

### **1.2.2. JNK inhibition**

The key role assumed by the JNK pathway in several pathologic conditions has made these enzymes emerge as attractive drug targets, prompting an intense endeavor in the pursue of therapeutic inhibitors.<sup>113-115</sup> Nevertheless, to date no JNK inhibitor has been introduced in therapy and only a scarce number of candidates has reached clinical phase (Table 1.1). While Tanzisertib, Bentamapimod, and CC-401 are classical type I inhibitors, binding reversibly to the ATP binding site, the retro-inverso peptide inhibitor XG-102 is able to occupy the docking site of the JIP scaffold protein, representing a less conventional strategy for JNK inhibition.



Table 1.1. JNK inhibitors in clinical trials

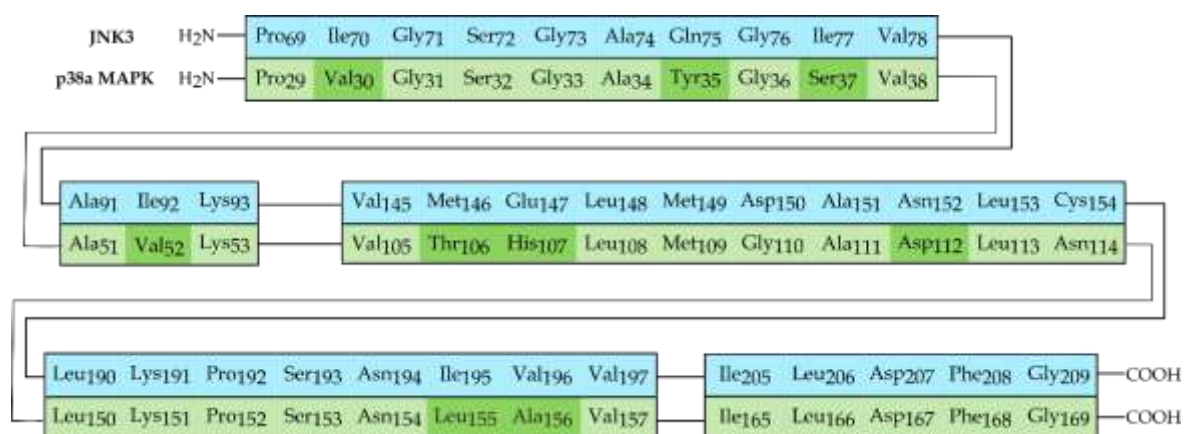
Name(s)	Structure	Indication, phase, status <sup>a</sup>
CC-930		Pulmonary fibrosis, Phase II, Terminated <sup>116</sup>
Tanzisertib		Discoid lupus erythematosus, Phase II, Terminated <sup>117</sup>
XG-102		Post cataract surgery inflammation, Phase III, Completed <sup>118</sup>
D-JNKI-1		Post cataract surgery inflammation and pain, Phase III, Completed <sup>119</sup>
AM-111		Acute inner ear hearing loss, Phase III, Completed <sup>120</sup>
Bentamapimod		Acute sudden sensorineural hearing loss, Phase III, Completed <sup>121</sup>
AS602801		Inflammatory endometriosis, Phase II, Completed <sup>122</sup>
PGL5001		
CC-401		Refractory acute myelogenous leukemia, Phase I, Terminated <sup>123</sup>
CC-90001	Undisclosed	Idiopathic pulmonary fibrosis, Phase II, Ongoing/Recruiting <sup>124</sup>

<sup>a</sup>For each candidate only the clinical trials at the most advanced phase have been reported.

The limited number of inhibitors reaching clinical phase underlines the necessity of new compounds targeting the JNKs. As already mentioned in section 1.1.2., the principal hurdle to overcome in the development of new kinase inhibitors consists in achieving high potency along with selectivity within the kinome. In particular, when aiming at JNK inhibition, a first challenge is represented by the achievement of selectivity of action over the structurally-related p38 $\alpha$  MAPK.<sup>125</sup> This well-known enzyme, belonging to the same family as JNKs, is analogously involved in signal transduction pathways triggered by stress

stimuli and has also demonstrated a clear involvement in inflammatory and neurodegenerative diseases, as well as in some types of malignancies.<sup>102,126,127</sup> Due to the contribution of JNKs and p38 $\alpha$  MAPK to akin pathological conditions, some studies pursued the dual inhibition of these targets as a potential strategy for the treatment of these disturbs.<sup>128</sup> Nevertheless, the research of JNK selective inhibitors would still be desirable due to different reasons. In a first instance, the achievement of JNK specific inhibition would facilitate a better understanding of the role of these kinases in the diverse diseases and would help in assessing the therapeutic utility of selectively blocking this signaling pathway. Additionally, as suggested by the failure of some preclinical and clinical candidates targeting this enzyme, inhibition of p38 $\alpha$  MAPK can potentially lead to additional side effects, mostly consisting in hepatic or central nervous system (CNS) toxicity, thus representing a risk for the safety profile of new compounds.<sup>129,130</sup>

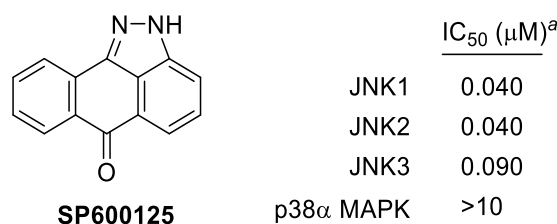
The two members of the MAPK family share a high sequence similarity at the ATP binding cleft, as outlined in Figure 1.7. JNK selective inhibitors need therefore to exploit the few structural differences in the amino acids composing the active site of the two enzymes.



**Figure 1.7.** Comparison of JNK3 (light blue) vs p38 $\alpha$  MAPK (green) sequences. Only amino acid residues located at the ATP binding site are displayed. Residues differing between the two sequences are highlighted in dark green. Sequence alignment was generated using EMBOSS-Needle tool from European Molecular Biology Laboratory (EMBL-EBI, Wellcome Genome Campus, Hinxton, Cambridgeshire, CB10 1SD, UK).

A major difference between the JNK and p38 $\alpha$  MAPK active sites lies in the “gatekeeper” residue which, as explained in section 1.1.2., is an amino acid limiting the access of inhibitors to the HR I. While the JNK gatekeeper consists of a Met residue which is conserved throughout the JNK isoforms (Met146 in JNK3), a smaller Thr residue occupies the same position in the p38 $\alpha$  MAPK (Thr106), therefore delineating a wider cavity in the

latter enzyme. In addition, some of the amino acids circumscribing the JNK binding site, e.g. Ile<sub>70</sub>, Ile<sub>92</sub>, and Val<sub>196</sub> (JNK3 numbering), are replaced by smaller residues in the p38 $\alpha$  MAPK, thereby resulting in the formation of a narrower binding cleft of the former kinase. As an example, features like small size, planarity and hydrophobicity are considered the determinant for the selectivity of the early JNK inhibitor SP600125 over the p38 $\alpha$  MAPK (Figure 1.8).<sup>131</sup> However, despite reaching *intra*-MAPK selectivity, such anthrapyrazolone derivative has been described to possess a poor selectivity within the kinome,<sup>132</sup> thus underlining the need of more specific interactions besides the aforementioned features.



**Figure 1.8.** Structure and biological activities of SP600126. <sup>a</sup>Data reported by Bennet *et al.*<sup>131</sup>

As already mentioned in the previous paragraph, the three JNK isoforms diverge in substrate specificity, hence differently contributing to the onset and progression of pathological conditions. However, the involvement of each member of the JNK family could only be assessed so far by selective gene knockout, a method which does not fully allow to evaluate the effects resulting by the inhibition of these pathways in wild type organisms, e.g. impossibility to observe effects of double *jnk1/jnk2* knockout. Consequently, the development of isoform-selective JNK inhibitors would provide a pharmacological tool to clearly identify the different involvement of the JNK isoforms in diseases, thus enabling the selection of the optimal therapeutic target within this subfamily. Unfortunately, JNK1, JNK2, and JNK3 share more than 80% sequence similarity and selectivity of action could not be reached so far.

In the vast majority of cases, kinase inhibitors are evaluated through the use of activity assays, namely experiments which evaluate the influence of the inhibitor on the kinase phosphotransfer activity by comparison with an uninhibited positive control. In particular, an in-house enzyme-linked immunosorbent assay (ELISA), previously developed in the group of Prof. Laufer, was successfully employed to measure the inhibitory activity of compounds on JNK3 and p38 $\alpha$  MAPK.<sup>133,134</sup> This assay format allows to quantify the phosphorylation of the common target ATF2 due to the use of a horseradish peroxidase-conjugated antibody that specifically binds the phosphorylated substrate. Such method has

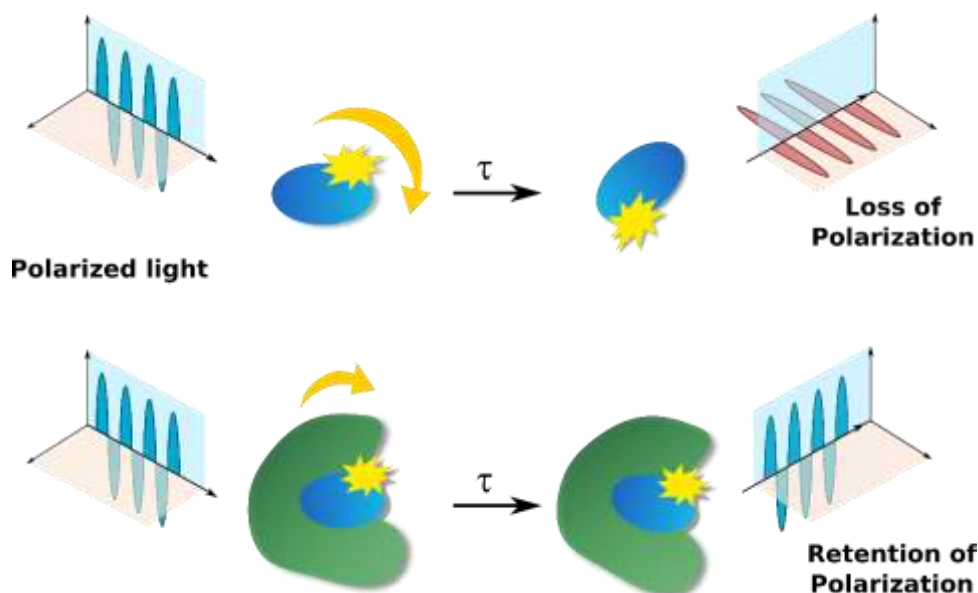
the clear advantage of providing a reliable and exhaustive assessment of the inhibitory activity in presence of the endogenous cofactor ATP and is still routinely employed, as it can be seen in the second part of this thesis, for the screening of newly synthesized compounds. Nevertheless, factors as low cost efficiency, non-easy handling, and long assay time limit the applicability of this procedure. Moreover, repeated separation and washing steps are comprised in this assay procedure (non-homogenous assay), hence preventing its applicability in high throughput screening (HTS) of compound libraries. Finally, the aforementioned ELISA-based assay has only been established for the p38 $\alpha$  MAPK and for the JNK3, and currently no protocol has been developed for the JNK1 and JNK2 isoforms. Alternatively, biological activity of candidate inhibitors can also be assessed through binding assays measuring the stability of the enzyme-inhibitor complex. Although binding parameters do not necessarily imply inhibitory activity, a correlation between binding and inhibition can be assumed for those classes of inhibitors occupying the ATP cleft of the enzyme, as they prevent the interaction with the endogenous cofactor and thus the phosphotransfer reaction.

### **1.2.3. Fluorescence Polarization (FP)**

FP is a fluorescence-based technique which can be applied to diverse assay formats and thanks to its advantageous features like easy handling, cost efficiency, and amenability for HTS is being widely used in the field of drug discovery.<sup>135-137</sup>

The theoretical basis of this method starts from the observation that the excitation of a fluorophore by plane-polarized light yields a polarized emission, by virtue of a phenomenon named photoselection. Considering a group of randomly-oriented fluorophores irradiated by polarized light, the photoselection derives from the increased probability of absorption of those molecules whose dipole is nearly parallel to the plane of the exciting radiation. In this way it is possible to “select” a population of excited fluorophores which, in case such molecules were immobilized, would emit light with a polarization analogous to the one of the source.<sup>138</sup> However, molecules in solution are susceptible to Brownian motions, representing casual, non-ordered movements which determine an extremely rapid tumbling of the fluorophores. Since the rotational relaxation time  $\rho$  (time required by the molecule to rotate by an angle of 68.42°) has a much lower order of magnitude than the fluorophore lifetime  $\tau$  (time window between absorption and emission), free fluorotracers in solution are unable to conserve the polarization achieved through photoselection. Conversely, when a fluorescently labeled molecule binds to a macromolecule, e.g., a protein, the whole complex has a longer rotational relaxation time

by virtue of the higher molecular weight, hence retaining the acquired polarization (Figure 1.9).<sup>138-141</sup>



**Figure 1.9.** Graphic explanation of the FP principle.  $\tau$  represents the fluorophore lifetime, namely the time required for the excited fluorophore to emit the radiation.

Upon excitation by plane-polarized light, the emitted radiation is split and directed into two detectors, which measure the intensities of the emission parallel and perpendicular to the plane of the source ( $I_{\parallel}$  and  $I_{\perp}$ , respectively).<sup>141</sup> These two parameters are then used to calculate FP and/or fluorescence anisotropy (FA) through the equations 1.1 and 1.2, respectively. FA is a parameter having the same meaning as FP, although the latter finds wider use in biological applications.

$$\text{(Eq. 1.1)} \quad FP = \frac{I_{\parallel} - I_{\perp}}{I_{\parallel} + I_{\perp}} \quad \text{(Eq. 1.2)} \quad FA = \frac{I_{\parallel} - I_{\perp}}{I_{\parallel} + 2I_{\perp}}$$

One of the multiple purposes of the FP principle is the use in competition binding assays. Such method consists in following the displacement of a fluorescently labeled probe by the candidate inhibitor through the measurement of the progressive FP signal decrease. Such method presents several advantages over the traditionally-employed radioligand-based binding assays such as improved safety and easy handling, not requiring separation and washing steps.<sup>142</sup> The establishment of a FP-based binding assay requires several considerations concerning the probe design, the choice of the fluorophore, and the different assay parameters.<sup>139,140</sup>

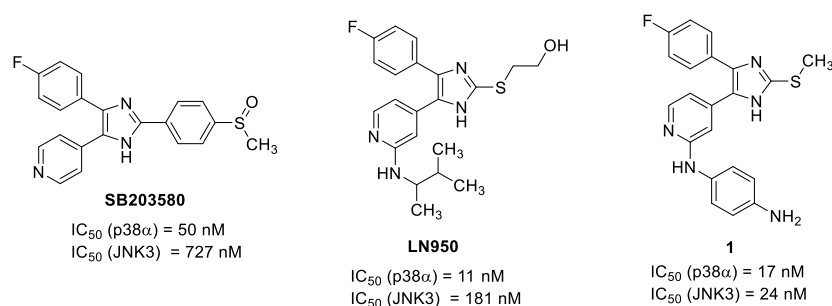


## 2. Objective of the Thesis Work

The implication of JNKs in diverse pathological states has raised the interest toward the development of JNK selective inhibitors. Such molecules might be useful both as tools for better understanding the effective role of these enzymes in diseases, and as therapeutic agents for the treatment of JNK-related disturbs. Although several selective inhibitors for JNK have been reported, the scarce number of clinical candidates and the current absence of approved inhibitors highlight the need for new molecules targeting these enzymes.

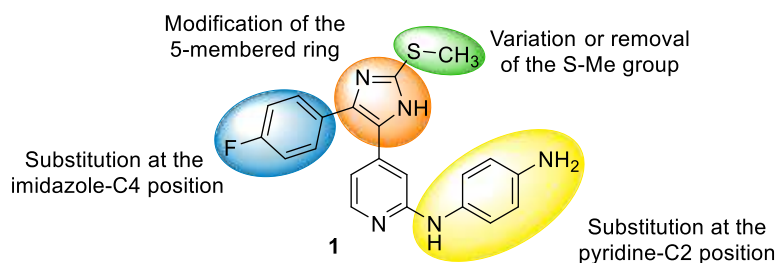
In a first instance, as an aid for the research of novel selective JNK inhibitors, a new competition binding assay was developed in order to ease the evaluation of the binding affinity of potential inhibitors of JNK3. Such assay is based on the technique of FP and required the design and the synthesis of a suitable fluorescently-labelled probe based on the pyridinylimidazole scaffold. After optimization, such assay was then extended to the other members of the JNK family, JNK1 and JNK2, as well as to the closely related p38 $\alpha$  MAPK in order to provide a tool for a fast assessment of *intra*-MAPK and *intra*-JNK selectivity. The findings resulting from this part of the thesis work are included in **Publications I** and **II**.

In the second part, different attempts were carried out to achieve selective inhibitors of JNK starting from a pyridinylimidazole-based lead. Numerous examples of molecules belonging to this class have been reported as potent inhibitors of the p38 $\alpha$  MAPK and were obtained by optimization of the precursor **SB203580** from SmithKline (Figure 2.1). An exhaustive summary on the synthesis routes and biological activity of this class of compounds is presented in **Publication III**.



**Figure 2.1.** Examples of pyridinylimidazole derivatives as MAPK inhibitors. Data taken from Goettert *et al.*,<sup>133,134</sup> Koch *et al.*,<sup>143</sup> and Ansideri *et al.*<sup>144</sup> (**Publication I**).

Besides p38 $\alpha$  MAPK, pyridinylimidazole-based compounds are also able to inhibit members of the closely related JNK family and, as visible from Figure 2.1, alteration of the substitution pattern can result in a different selectivity profile of these derivatives. For this reason, a series of structural modifications was performed on compound **1** both by altering the core scaffold and the substitution pattern (Figure 2.2), aimed at shifting the selectivity of this dual inhibitor towards the JNK (in particular, the focus was initially maintained on the JNK3, whereas the evaluation of *intra*-JNK selectivity was addressed only at a late stage). The broad set of performed structural modifications required the development of diverse synthesis strategies and is presented in **Publications V** and **VII**.



**Figure 2.2.** Structural modifications of lead compound **1** involving different regions of the pyridinylimidazole scaffold.

An alternative strategy which was pursued in order to obtain JNK selective inhibitors was the transformation of the reversible inhibitor **1** into a TCI by modification of the substituent at the pyridine-C2 position. Such approach aims at the formation of a covalent bond with the non-catalytic Cys154 (JNK3 numbering) which, as depicted in Figure 1.7, is not conserved in the p38 $\alpha$  MAPK. This second strategy was prevalently carried out by Dr. Felix Muth and Dr. Ahmed El-Gokha and the outcomes are collected in **Publication IV**.



## 3. Results and Discussion

### 3.1. Development and optimization of an FP-based competition binding assay for JNK1, 2, and 3, and p38 $\alpha$ MAPK

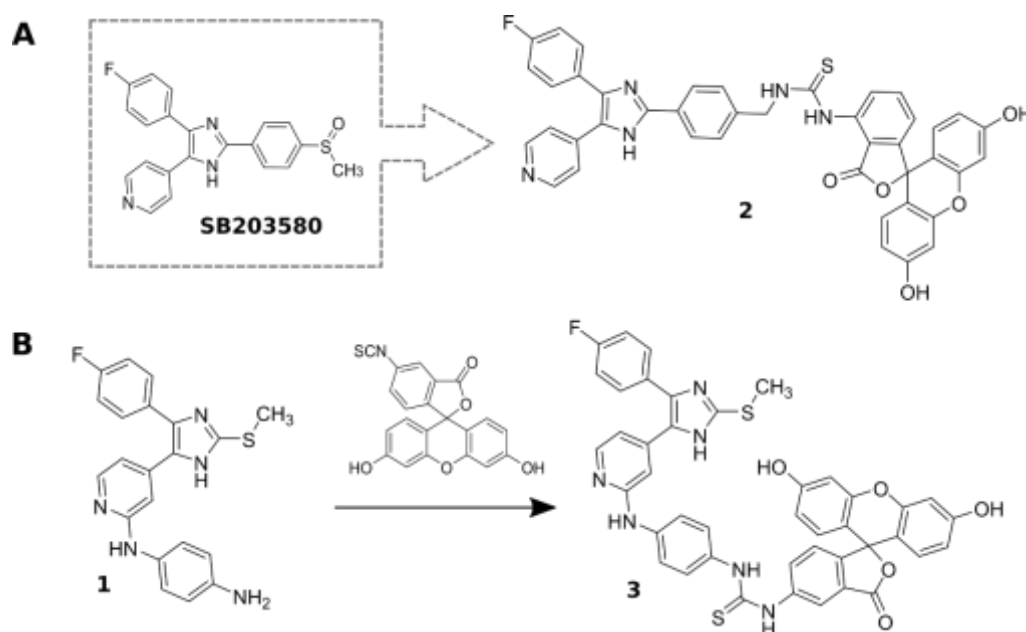
#### 3.1.1. Design and synthesis of a new FP probe

The first step in the establishment of a new FP-based competition binding assay consisted in the design of a suitable fluorescent probe for the target enzymes. Compound **1** (Figure 2.1 and 3.1B) was discovered in a previous in-house study as a potent dual JNK3/p38 $\alpha$  MAPK inhibitor, with IC<sub>50</sub> values in the low nM range on both enzymes and was therefore selected as a potential precursor for the FP fluorophore.

An extremely important aspect in projecting an FP-probe consists in the position of the labelling as the introduction of a bulky fluorescent tag might result in a loss of affinity of the probe for its targets. Munoz *et al.* reported in 2010 an FP probe for the p38 $\alpha$  MAPK derived from the pyridinylimidazole-based reference compound **SB203580**.<sup>145</sup> In such molecule, the fluorescent tag, represented by a fluorescein moiety, was linked at the imidazole-C2 position of the scaffold (compound **2**, Figure 3.1A). Nevertheless, when planning a new probe suitable for both JNK3 and p38 $\alpha$  MAPK, the aniline moiety at the pyridine-C2 position of compound **1** was assumed to be optimal for the installation of the fluorescent label. The reason for this lies in the well-known binding mode of pyridinylimidazole molecules, wherein the substituent at the pyridine-C2 position is located in the solvent-exposed HR II (a more detailed explanation of the binding mode of pyridinylimidazole-base inhibitors will be provided in section 3.2.1). Due to its opening on the outside of the protein, this area is presumably more prone to tolerate the large fluorescent group without substantial effects on the binding

A second crucial setting concerns the choice of the fluorophore and the method of labeling. Fluorescein was selected as a fluorophore due to the affordable cost and to the availability of a broad range of derivatives, allowing the labeling of diverse functional groups.

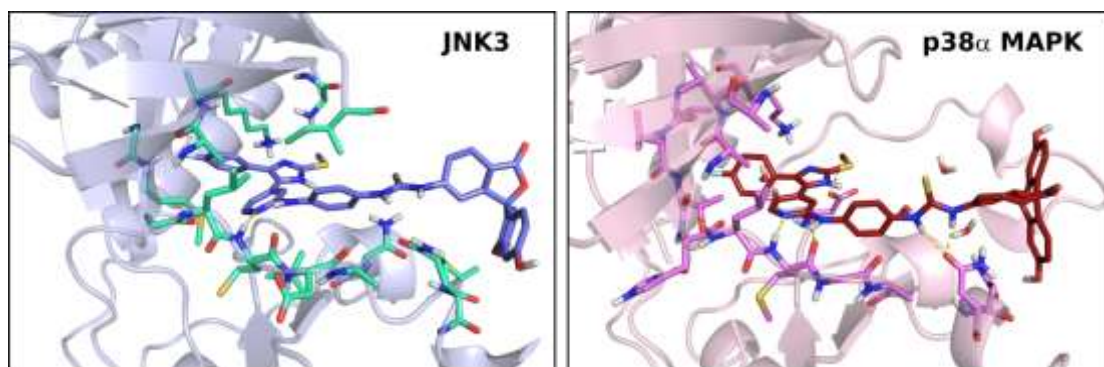
Furthermore, virtually all plate readers are provided with the excitation/emission filters necessary for this fluorophore (approximately 490/525 nm). Finally, the short lifetime  $\tau$  of this fluorescent marker ( $\approx 4$  ns) is well-suited for the analysis of small ligands interacting with proteins heavier than 10 kDa.<sup>140</sup> These features made fluorescein the first choice fluorescent dye employed in FP assays, as also recently reviewed by Hall and coworkers.<sup>135</sup> In particular, the selected dye was the fluorescein isothiocyanate (FITC) isomer 5', which would easily react with the terminal aniline of compound **1** through the formation of a thiourea bridge (Figure 3.1B).



**Figure 3.1.** Design of FP probes; A) probe **2** reported from Munoz *et al.*<sup>145</sup> derived from standard inhibitor SB203580; B) probe **3** designed for a new FP-based competition binding assay derived from compound **1**.

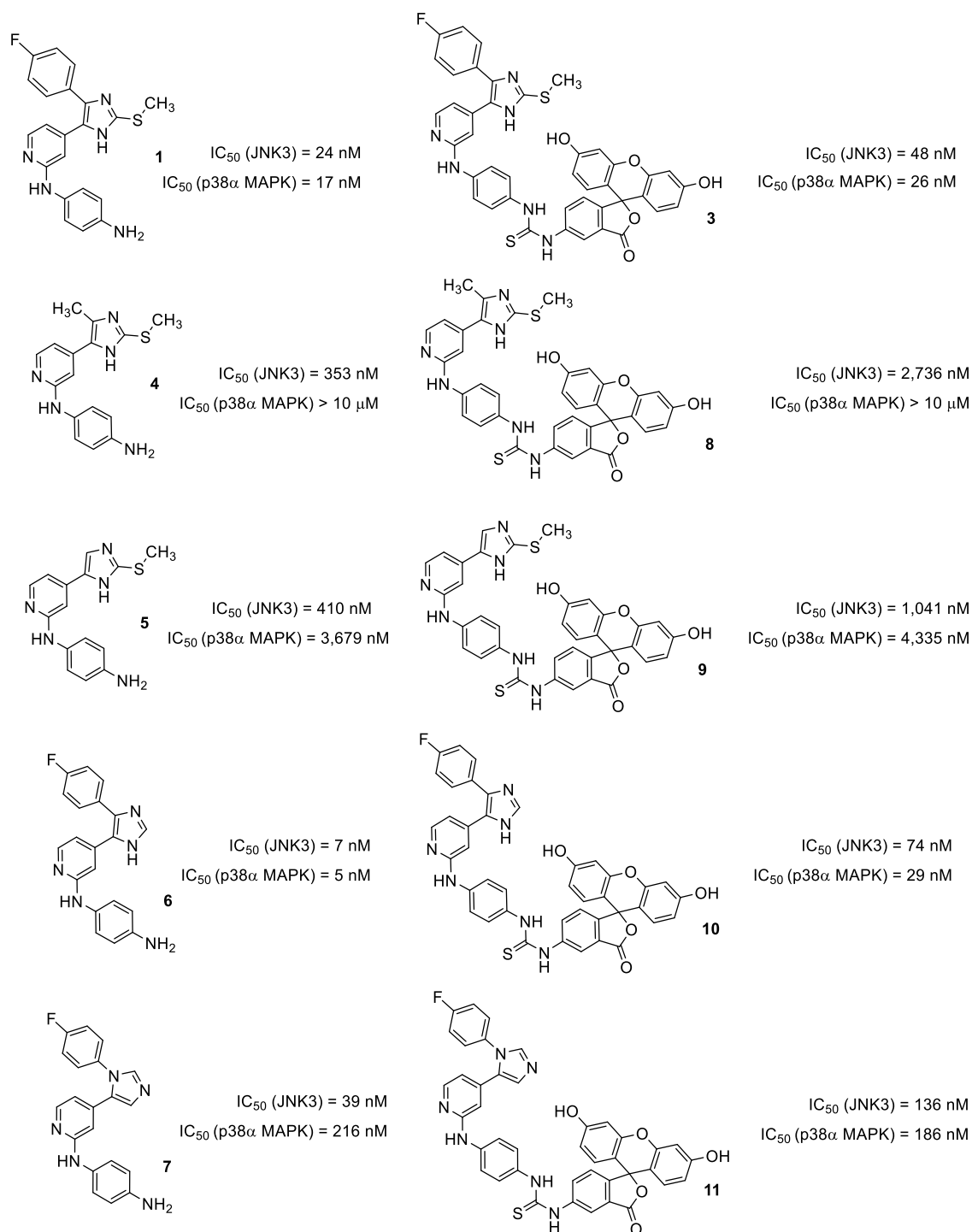
An initial choice made consisted in avoiding the introduction of a spacer between the core scaffold and the fluorescent moiety, which was therefore directly linked to the terminal amino group of compound **1**. The rationale behind this decision lies in the fact that although a spacer might increase the flexibility and reduce the impact of the bulky fluorophore on the binding interactions, it could also determine the rotational freedom of the fluorescent tag even when the probe is bound to the target. This phenomenon is named “propeller effect” and can have detrimental outcomes on the FP measurement as it reduces the signal window between bound and unbound ligand.<sup>139,140</sup>

Before synthesis, the suitability of the designed probe **3** was confirmed by docking studies (Figure 3.2). Both in the case of JNK3 and p38 $\alpha$  MAPK reasonable poses were generated wherein the fluorescent marker was positioned outside of the binding site, therefore seeming not to hinder the interactions of the core scaffold.



**Figure 3.2.** Docking poses of probe **3** with JNK3 (left, PDB entry: 3FI3) and p38 $\alpha$  MAPK (right, PDB entry: 1OUK).

Besides the preparation of probe **3**, four additional scaffolds and corresponding fluorescent probes were synthesized varying the substitution pattern around the imidazole ring (probes **3** and **8-11**, Figure 3.3). This was carried out in order to broaden the subset of potential probes and therefore select the one displaying the best features in terms of applicability. All probes were tested in the aforementioned ELISA activity assay on both JNK3 and p38 $\alpha$  MAPK and the results were compared with their precursors, aimed at observing the influence of the labelling on the inhibition potency (Figure 3.3). Among all the synthesized probes, compounds **3** and **10** seemed to display optimal features to serve as FP probes as they showed a high potency on the two enzymes which appeared to be only negligibly affected by the installation of the fluorescent dye. For this reason, such compounds were selected as candidates for the following assay optimization steps and the introduction of a spacer was not considered necessary. On the other hand, probes **8** and **9** are characterized by a lower potency on JNK3 and by scarce or no inhibition of p38 $\alpha$  MAPK and are therefore not suitable to be employed as dual probes. Moreover, in case of these two compounds the labelling with fluorescein seemed to have a considerable effect on the inhibitory activity, which decreased significantly on both kinases. Analogously to its precursor, probe **11** showed instead a moderate inhibition of both enzymes, with IC<sub>50</sub> values in the triple-digit nM range.



**Figure 3.3.** Structures and biological activity of the synthesized probe candidates (compounds 3 and 8-11) and their precursors (compounds 1 and 4-7). The synthetic schemes of compounds 1 and 4-7 will be discussed in the second part of the thesis, section 3.2 and detailed procedures as well as analytical data can be found in **Publication I** (compounds 1 and 6), **Publication IV** (compound 4), or in the experimental section of this thesis (compounds 5 and 7); experimental procedures for the preparation of the fluorescent probes together with analytical data can be found in **Publication I** (probes 3 and 10), **Publication VI** (probe 11) or in the experimental section of this thesis (probes 8 and 9).

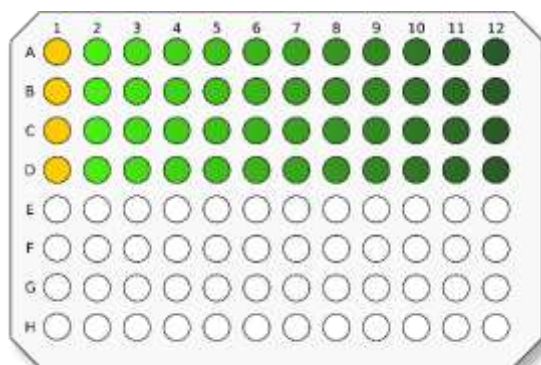
### 3.1.2. Probes characterization

The second step performed in the development of an FP-based competition binding assay consisted of measuring the binding affinity of the synthesized probes to the selected targets JNK3 and p38 $\alpha$  MAPK. In classical binding assays, e.g., radioligand-based assays, the  $K_d$  of a molecule is measured through saturation experiments wherein a fixed concentration of protein is titrated against increasing concentrations of ligand. This can be performed because by means of separation and washing steps the unbound ligand is removed before the reading and only the bound probe can be detected. Conversely, in the homogeneous FP-based binding assays, both bound and unbound species are present in the sample at the time of measurement and take part in the generation of the FP signal. Although the bound species has a much higher contribution on the observed polarization, increasing concentrations of free probe would result in a progressive reduction of the FP signal, thus hampering a correct  $K_d$  determination. This can be circumvented by modifying the assay settings through the titration of a fixed amount of fluoroprobe against increasing concentrations of protein.<sup>146</sup> Unfortunately, this strategy requires high concentrations of protein in order to reach the saturation conditions which might represent a limitation in case of expensive targets.

As discussed, the  $K_d$  of the synthesized probe was determined by titrating a 10 nM solution of probe with increasing concentrations of protein as schematized in Figure 3.4 (the range of concentrations was adapted for each probe in order to reach a full saturation curve). A well containing only fluoroprobe in assay buffer was also included as a negative control, establishing the signal baseline.

Particularly important to mention is the use, for this assay, of an inactive form of both JNK3 and p38 $\alpha$  MAPK. Probe **3** represents a classical type I inhibitor which, as explained in section 1.1.2., can bind to the ATP site of the protein regardless of its activation state as the flexible DFG motif can assume both the in and out conformations. On the other hand, the use of a catalytically inactive kinase might represent an advantage, as it would allow the identification of other inhibitor classes binding preferentially this form, as type II and type I $\frac{1}{2}$  (type III inhibitors are presumably excluded since they do not directly occupy the ATP cleft and therefore might not be able to displace the probe).

In case of probes **3** and **10**, which had been selected for following optimization, FP signal was measured after 15, 30, and 60 min of incubation in order to obtain additional information regarding time of binding equilibrium onset and signal stability (Figure 3.5).

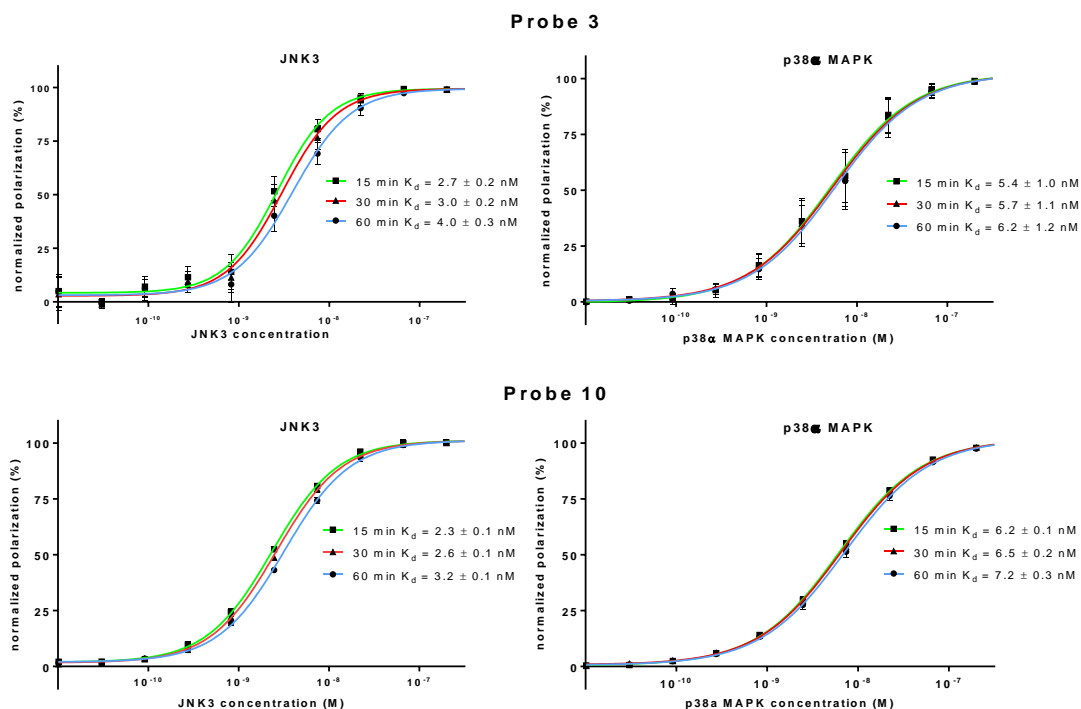


**Figure 3.4.** Microplate scheme for  $K_d$  determination of synthesized probes; experiment was performed three times in quadruplicate; in column 1 (light orange) a negative control containing 10 nM solution of probe in assay buffer was used, representing the baseline of the FP signal; the green gradient in columns 2-12 represents the probe with increasing concentrations of protein;

Both probes showed high binding affinity for the two tested enzymes with  $K_d$  values in the single digit nM range. Moreover, both compounds were characterized by a rapid binding equilibrium onset and the measured  $K_d$  values appeared to be stable over time, with only a negligible variation after 60 min incubation. An incubation time of 30 min and its corresponding probe  $K_d$  values were selected for the further development of the assay.

In order to confirm the binding profile of probes **3** and **10** on JNK3 and p38 $\alpha$  MAPK, an independent binding assay was performed through isothermal titration calorimetry (ITC). The two probes showed again high affinity for their targets with  $K_d$  values in the low double-digit nM range (**3**:  $K_{d(\text{JNK3})} = 25$  nM,  $K_{d(\text{p38}\alpha \text{ MAPK})} = 35$  nM; **10**:  $K_{d(\text{JNK3})} = 20$  nM,  $K_{d(\text{p38}\alpha \text{ MAPK})} = 33$  nM). The slight differences in the  $K_d$  absolute value in comparison with values reported in Figure 3.5 can be attributed to intrinsic differences of the two assay methods as well as to dissimilarities in the protocols used. Nevertheless, the high affinity and the similar binding features of probes **3** and **10** were confirmed.

Given the nearly identical inhibition profile of the two probes, and needing to promote only one fluoroprobe to the following steps, compound **10** was discarded only based on a lower yield of its synthesis route and the optimization was carried out exclusively on probe **3**.



**Figure 3.5.** Titration curves and corresponding  $K_d$  values of probes **3** and **10** on JNK3 and p38 $\alpha$  MAPK measured at different incubation times. Each experiment was performed 3 times in quadruplicate; data points represent mean value  $\pm$  SD; this and other graphs henceforth were obtained using the software GraphPad Prism version 7.3 for Windows (GraphPad Software, La Jolla California USA, www.graphpad.com).

Although not being chosen for further optimization, the  $K_d$  values of the other synthesized probes (compounds **8**, **9** and **11**) on JNK3 were also determined in order to achieve the characterization of all the prepared fluorotracers. For the titration experiments an incubation time of 30 min was selected and results are presented in Table 3.1.

**Table 3.1.**  $K_d$  values of compounds **8**, **9**, and **11** on JNK3.

Cpd n.	$K_d$ on JNK3 (nM) (mean value $\pm$ SD)
<b>8</b>	$188.0 \pm 3.0$
<b>9</b>	$44.6 \pm 6.9$
<b>11</b>	$11.4 \pm 6.6$

Experiments were performed three times in quadruplicate

### 3.1.3. Assay conditions optimization

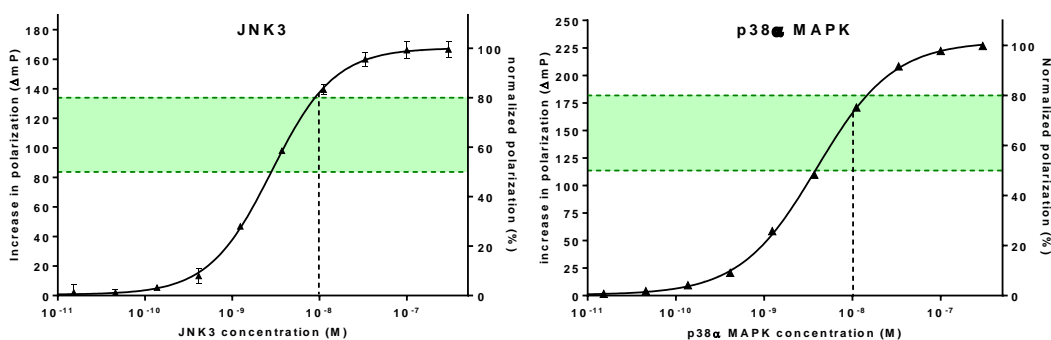
After determining the binding affinity of the selected probe **3** for JNK3 and p38 $\alpha$  MAPK an additional experiment was carried out in order to choose the final settings which would improve the performance of the assay. In detail, given for probe **3** the values of  $K_{d(\text{JNK3})} = 3.0 \pm 0.2$  nM and  $K_{d(\text{p38}\alpha \text{ MAPK})} = 5.7 \pm 1.1$  nM, a 5 nM concentration of compound **3** was chosen to be employed in the competition binding assay. This is in line with practical considerations in the development of an FP-based binding assay, suggesting to reduce the fluoroprobe concentration as much as possible, not exceeding twice the  $K_d$  value.<sup>140</sup>

A second crucial parameter in defining the assay efficiency is represented by the protein concentration. Performing the competition assay at saturation conditions, where all the fluoroprobe molecules are bound to the target, would obviously allow to obtain the maximum signal window. However, these stoichiometric conditions would imply high levels of unbound protein which would decrease the responsivity of the system to the addition of competitors, thus reducing the sensitivity of the assay.<sup>147</sup> In order to determine the optimal protein concentration a titration experiment analogous to the previous one was performed using a 5 nM concentration of probe **3** and 30 min of incubation time (Figure 3.6). As suggested in FP-assay development guidelines,<sup>140</sup> the optimal protein concentration should produce, at the probe concentration selected for the assay, an increase in polarization lying approximately between 50 and 80% of the titration curve. This range is sufficiently away from the saturation conditions to provide sensitivity to the assay, being at the same time able to yield an appropriate signal window (dynamic range). The titration experiments displayed in Figure 3.6 permitted to identify 10 nM as the optimal concentration of both JNK3 and p38 $\alpha$  MAPK to be used in the competition assay. Such concentration yielded for both enzymes an increase in polarization close to 80%, with the satisfactory signal windows of approximately 140 and 160 mP for JNK3 and p38 $\alpha$  MAPK, respectively (it is important to mention that although FP is a dimensionless parameter, millipolarization units or mP are commonly used to define its value).

To sum up, the parameters which were selected to be employed in the FP-based competition binding assay were:

- 5 nM concentration of probe **3**
- 10 nM concentration of protein
- 30 min incubation time

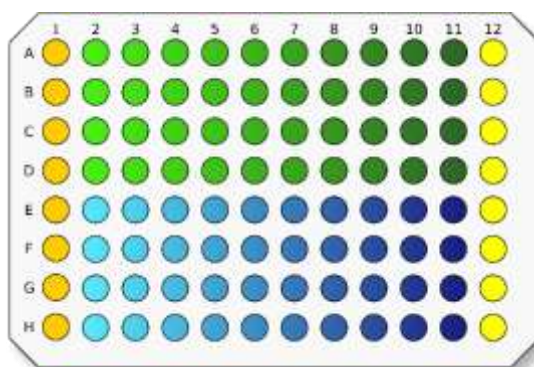




**Figure 3.6.** Titration experiments for determining the optimal protein concentration; both assays were performed using 5 nM concentration of probe **3**. The green band represents the optimal protein concentration range while the vertical dashed line indicates the selected protein concentration of 10 nM.

### 3.1.4. Assay validation

After setting the different parameters aimed at optimizing the assay performance, the competition binding assay was run using the precursor of probe **3** (compound **1**) to displace the fluorotracer. The use of the unlabeled probe generally represents the “gold standard” for the validation of this assay format as the interactions of the target with the labeled and unlabeled compounds should be analogous.<sup>140</sup> The assay was performed as depicted in Figure 3.7 by titrating a fixed concentration of probe **3** (5 nM) and JNK3 or p38α MAPK (10 nM) with increasing concentrations of the tested compound. For each compound tested a well containing probe and protein and a well containing probe in assay buffer were also added as positive and negative control, respectively.



**Figure 3.7.** Plate scheme for the competition binding assay; each compound was tested in quadruplicate; column 1 (light orange) represents a positive control consisting in probe and protein while a negative control containing only probe in assay buffer is placed in column 12 (yellow). The green and blue gradients in columns 2-11 represent increasing concentrations of two different compounds.

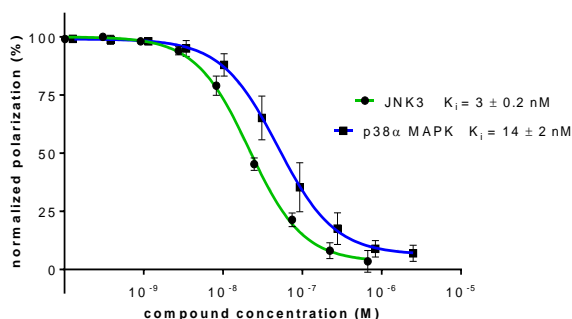
Compound **1** succeeded in displacing probe **3** in a dose-dependent manner both on JNK3 and p38 $\alpha$  MAPK (Figure 3.8), in both cases resulting in IC<sub>50</sub> values in the double-digit nM range (IC<sub>50</sub>(JNK3)= 20 nM; IC<sub>50</sub>(p38 $\alpha$  MAPK)= 51 nM). As the IC<sub>50</sub> value is strictly dependent on the assay conditions e.g, probe affinity or concentration of probe and protein, a common practice consists in the conversion of IC<sub>50</sub> values into the inhibition constant (K<sub>i</sub>). A well-known tool for transforming IC<sub>50</sub> values into K<sub>i</sub> is represented by the Cheng-Prusoff equation<sup>148</sup> (Eq. 3.1). This formula was developed for competitive inhibitors of Michaelis-Menten enzymes and was subsequently adapted to be applied to competition binding assays as well (Eq. 3.2) with the terms [L] and K<sub>d</sub> referring to concentration and affinity of the labeled ligand, respectively.

$$\text{(Eq. 3.1)} \quad K_i = \frac{IC_{50}}{1 + \frac{[S]}{K_m}} \quad \text{(Eq. 3.2)} \quad K_i = \frac{IC_{50}}{1 + \frac{[L]}{K_d}}$$

However, the aforementioned equations are not suitable to be directly applied to FP-based competitive binding assay, due to an incompatibility with the assumptions on which they are based. For this reason, a modified Cheng-Prusoff equation suitable for FP binding assays was developed by Nikolovska-Coleska *et al.*<sup>149</sup> (Eq. 3.3) with the parameters [I]<sub>50</sub>, [L]<sub>50</sub>, and [P]<sub>0</sub> indicating the concentration of free inhibitor at 50% inhibition, concentration of unbound labeled ligand at 50% inhibition, and concentration of free protein at 0% inhibition, respectively.

$$\text{(Eq. 3.3)} \quad K_i = \frac{[I]_{50}}{\frac{[L]_{50}}{K_d} + \frac{[P]_0}{K_d} + 1}$$

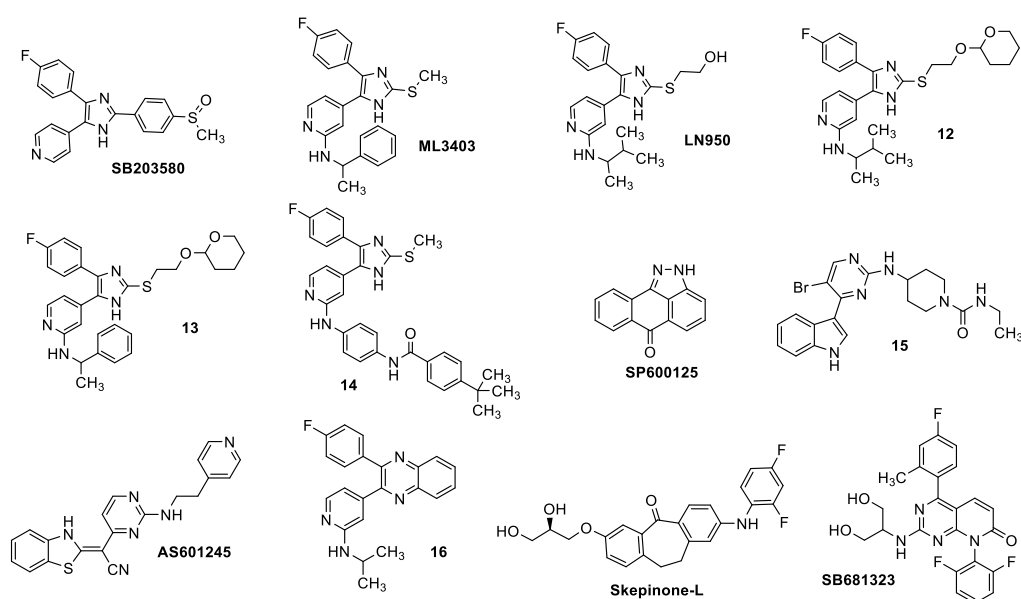
Such equation was also implemented in a web-based tool allowing an easy conversion of the IC<sub>50</sub> values into K<sub>i</sub> by simple input of the assay settings.<sup>150</sup>



**Figure 3.8.** Competition binding assay and K<sub>i</sub> values of compound **1** on JNK3 and p38 $\alpha$  MAPK; each experiment was performed three times in quadruplicate; data points represent mean values  $\pm$  SD; K<sub>i</sub> values indicate mean value  $\pm$  SEM.

The  $K_i$  values obtained by the assay of the probe precursor **1** on JNK3 and p38 $\alpha$  MAPK (Figure 3.8) proved to be extremely close to the  $K_d$  values of probe **3** on the same enzymes (Figure 3.5), demonstrating the low impact of the fluorescent tag on binding interactions.

An additional method for validating the developed assay consisted of screening a small library of compounds and comparing the obtained binding data with the results deriving from a different assay. In particular, given the availability of an in-house ELISA activity assay for both JNK3 and p38 $\alpha$  MAPK (already mentioned in section 1.2.2.), this method was chosen for comparison. The set of compounds was selected in order to achieve a broad structural diversity alongside with different potency on the two target enzymes (Figure 3.9). This consisted therefore of a series of pyridinylimidazole-based inhibitors, including the reference compounds **SB203580** and **ML3403**, and non-pyridinylimidazole derivatives, such as pyridinylquinoxaline **16**. In addition, reference compound **SP600125**, aminopyrimidine **15**, and clinical candidate **AS601245** were chosen to be tested uniquely on JNK3, whereas high quality probe **Skepinone-L** and clinical candidate **SB681323** were selected for the p38 $\alpha$  MAPK assay. An initial screening on the selected compound set consisted in analyzing their autofluorescence at the excitation and emission wavelengths used for the fluorescein (480 and 530 nm, respectively). Emission of fluorescence at the aforementioned wavelengths would indeed create interference with the FP signal measurement and would hamper the correct performance of the assay. Compounds showing fluorescence cannot therefore be tested with the developed assay. Fluorescence of compounds was measured and compared with the positive and negative controls containing a 5 nM probe concentration and only DMSO, respectively.



**Figure 3.9.** Set of compounds selected for the assay validation

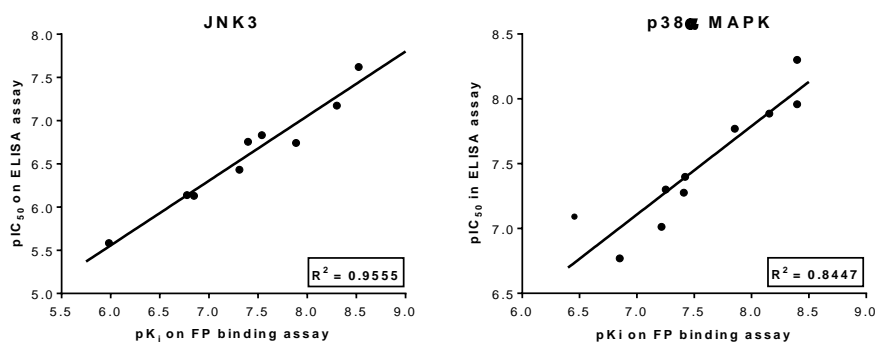
Although most of the compounds revealed to be suitable for the following assay, derivatives **SP600125** and **AS601245** emitted a significantly higher fluorescence than the negative control, thus needing to be excluded from the FP assay. Remaining compounds were tested on the two enzymes and  $IC_{50}$  values were converted to  $K_i$  using the aforementioned modified Cheng-Prusoff equation (Eq. 3.3). Results of the screening on the set of compounds are reported in Table 3.2, together with the  $IC_{50}$  values of the same compounds in the in house ELISA assay. As expected, given the high difference in the assay formats, an equivalence in the numeric value of inhibition data could not be observed.

**Table 3.2.** Biological activities of selected compounds measured in the FP assay

Cpd.	JNK3		p38 $\alpha$ MAPK	
	ELISA assay	FP assay	ELISA assay	FP assay
	$IC_{50} \pm SEM^a$ [nM]	$K_i \pm SEM^a$ [nM]	$IC_{50} \pm SEM^a$ [nM]	$K_i \pm SEM^a$ [nM]
<b>SB203580</b>	$727 \pm 28^b$	$167 \pm 10$	$50 \pm 0.4^c$	$56 \pm 1$
<b>1</b>	$24 \pm 1$	$3 \pm 0.2$	$17 \pm 0.4$	$14 \pm 2$
<b>ML3403</b>	$176 \pm 2$	$40 \pm 6$	$40 \pm 5^d$	$38 \pm 1$
<b>LN950</b>	$181 \pm 4$	$13 \pm 1$	$11 \pm 0.9^e$	$4 \pm 1$
<b>12</b>	$370 \pm 13$	$49 \pm 2$	$53 \pm 4$	$39 \pm 9$
<b>13</b>	$742 \pm 12$	$142 \pm 18$	$170 \pm 10$	$141 \pm 10$
<b>14</b>	$67 \pm 2$	$5 \pm 1$	$97 \pm 8$	$61 \pm 7$
<b>15</b>	$147 \pm 5$	$29 \pm 2$	n.t. <sup>f</sup>	n.t.
<b>16</b>	$3,950 \pm 200^g$	$1,041 \pm 32$	$81 \pm 5^g$	$350 \pm 10$
<b>Skepinone-L</b>	n.t.	n.t.	$5 \pm 2^h$	$4.2 \pm 0.4$
<b>SB681323</b>	n.t.	n.t.	$13 \pm 0.1$	$7 \pm 0.1$

<sup>a</sup>n = 3. <sup>b</sup>data previously reported by Goettert *et al.*<sup>134</sup>; <sup>c</sup>data previously reported by Goettert *et al.*<sup>133</sup>; <sup>d</sup>data previously reported by Laufer *et al.*<sup>151</sup>; <sup>e</sup>data previously reported by Koch *et al.*<sup>143</sup>; <sup>f</sup>n.t., not tested; <sup>g</sup>data previously reported by Koch *et al.*<sup>152</sup>; <sup>h</sup>data previously reported by Fischer *et al.*<sup>153</sup>.

Nevertheless, aimed at assessing a correlation between the results of the two different assay systems, the inhibition data reported in Table 3.2 were analyzed by linear regression. Results depicted in Figure 3.10 demonstrate that, despite the use of kinases in a different activation state, the two assay formats show a high correlation, with  $R^2$  values of 0.9555 and 0.8447 for JNK3 and p38 $\alpha$  MAPK, respectively.



**Figure 3.10.** Linear regression analysis of inhibition values reported in Table 3.2.

Besides confirming the validity of the developed assay, this observed correlation suggests a potential use of the FP-based competitive binding assay as a fast and relatively inexpensive pre-screening method for novel compounds, permitting to advance only most promising compounds to the activity assay. In this regard, it is worth to mention that the developed assay was employed to assess the influence of halogen bonding on JNK3 inhibition, this representing the first example of an FP-based binding assay on this enzyme.<sup>154</sup>

### 3.1.5. Applicability to the HTS format

As mentioned in the end of the previous section, the correlation between the developed assay and the in-house ELISA assay could be utilized for the fast estimation of the inhibitory activity of large compound libraries, hence allowing to discard inactive compounds at an early stage. For this reason, the applicability of the developed binding assay in an HTS format was evaluated. This is also possible thanks to the homogeneity of the FP-assay which allows its performance by simple addition of reactants (mix and measure), thus avoiding separation and washing steps. For the validation a procedure reported in an assay guidance manual from the national center for biotechnology information (NCBI) was used.<sup>155</sup> In particular, experiments were performed following the interleaved plate protocol on a 96-well plate. This consists of analyzing the *intra*- and *inter*-plate stability of three different kinds of signals:

- “Max”: highest FP signal; well containing 5 nM probe and 10 nM protein in assay buffer
- “Min”: lowest FP signal; well containing 5 nM probe, 10 nM protein, and a concentration of a reference compound (in this case the probe precursor **1**) at a concentration known to completely displace the probe

- “Mid”: intermediate signal; well containing 5 nM probe, 10 nM protein and a concentration of compound **1** close to the IC<sub>50</sub> value on the corresponding enzyme

The assay on each enzyme must be performed in three independent runs on different days, each time following a different pipetting pattern described in the manual so that each signal is measured in all possible plate positions after three repetitions.

The aim of HTS validation is to assess whether the assay presents a sufficient reproducibility of results and an adequate signal window width in order to avoid or reduce the occurrence of false positives or false negatives in an HTS screening. The acceptance criteria are in a first instance based on the conformity of calculated parameters within defined threshold values:

- Coefficient of variation (CV)  $\leq$  20% for each of the three signals in every plate
- Z factor  $>$  0.4 for every plate
- SD for the normalized %inhibition of the Mid value  $\leq$  20% in every plate
- Normalized %inhibition for Mid value between 30 and 70% within three days
- No difference  $>$ 15% in the normalized %inhibition of two different days

JNK3								
day	Max		Min		Mid		%inhibition (mean $\pm$ SD)	Z-factor
	FP value (mP) (mean $\pm$ SD)	CV	FP value (mP) (mean $\pm$ SD)	CV	FP value (mP) (mean $\pm$ SD)	CV		
1	300.3 $\pm$ 2.2	0.7%	161.7 $\pm$ 2.8	1.7%	220.8 $\pm$ 4.0	1.8%	57.4% $\pm$ 2.9%	0.89
2	300.5 $\pm$ 3.8	1.2%	151.3 $\pm$ 3.3	2.2%	210.7 $\pm$ 5.3	2.5%	60.2% $\pm$ 3.5%	0.86
3	298.0 $\pm$ 3.8	1.2%	143.1 $\pm$ 3.2	2.2%	195.1 $\pm$ 5.0	2.5%	66.5% $\pm$ 3.2%	0.86

p38 $\alpha$ MAPK								
day	Max		Min		Mid		%inhibition (mean $\pm$ SD)	Z-factor
	FP value (mP) (mean $\pm$ SD)	CV	FP value (mP) (mean $\pm$ SD)	CV	FP value (mP) (mean $\pm$ SD)	CV		
1	296.1 $\pm$ 2.7	0.9%	122.4 $\pm$ 4.3	3.5%	256.9 $\pm$ 3.4	1.3%	22.6% $\pm$ 2.0%	0.88
2	304.9 $\pm$ 4.1	1.3%	134.9 $\pm$ 3.5	2.6%	226.9 $\pm$ 2.9	1.3%	45.9% $\pm$ 1.7%	0.86
3	291.9 $\pm$ 6.9	2.3%	124.9 $\pm$ 4.6	3.6%	214.6 $\pm$ 4.7	2.2%	46.3% $\pm$ 2.8%	0.79

**Table 3.3.** Summary of HTS validation experiments

The results of the HTS validation experiments on both enzymes, displayed in Table 3.3, demonstrate that nearly all the acceptance criteria are satisfied. The unique slight deviation is represented by the day 1 experiment on p38 $\alpha$  MAPK wherein the measured value of %inhibition was lower than 30%, causing therefore a difference >15% with the results of the following days. However, the requirement of a Mid value lying within 30 and 70% is described more as an ideal than as a compulsory criterion and the suitability of the developed assays for the HTS format appears in any case to be clear from the other calculated parameters. In this regard, worth to mention is the very high Z-factor registered in all assay runs, indicating a broad signal window and a small *intra*-plate variability of results.

The assessment of the suitability for the HTS assay was then completed by a visual observation of the graphs resulting from the different experiments. In detail, data points were plotted following the two different patterns “by row, then by column” and “by column, then by row” and neither drift nor edge effect could be detected, thus confirming the applicability of the developed assay for the HTS format.

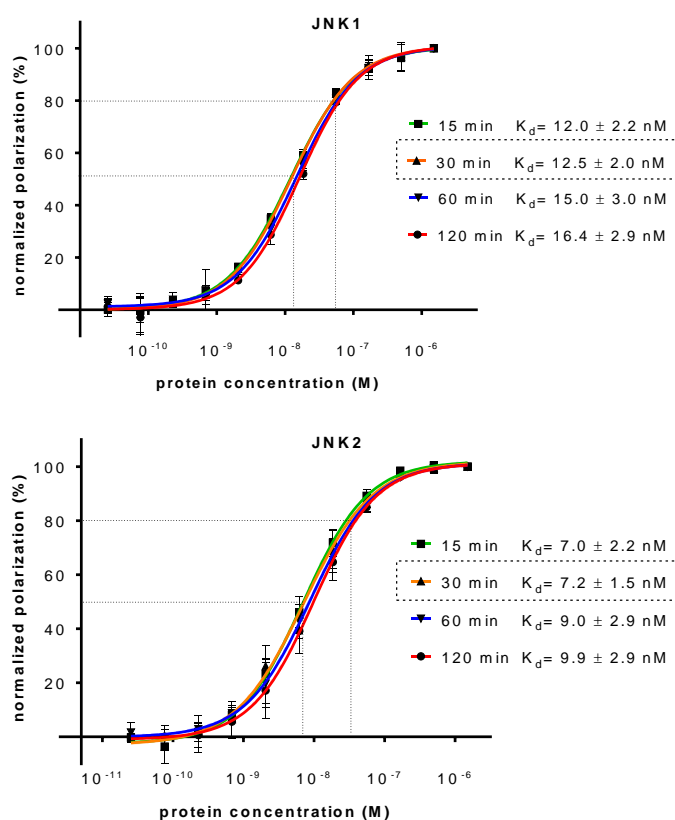
### 3.1.6. Extension of the developed assay to the JNK1 and JNK2

As discussed in section 1.2.2., *intra*-JNK selectivity of new inhibitors is still representing an unsatisfied need as only compounds displaying a slight preference for one of the three JNK isoforms have been reported to date.<sup>114</sup> In order to easily evaluate the selectivity of novel inhibitors within the JNK family, the FP-based competition binding assay previously developed for the JNK3 and p38 $\alpha$  MAPK was extended to the remaining isoforms of the JNK subgroup. This was possible thanks to the poor selectivity of the synthesized probe **3**, a feature which resulted beneficial in broadening its versatility of use.

#### Probe $K_d$ determination and optimization of assay parameters

In an analogous fashion as for the JNK3 and the p38 $\alpha$  MAPK (section 3.1.2), the affinity of probe **3** for JNK1 and JNK2 was determined by titrating a fixed concentration of fluoroprobe with increasing concentrations of protein. In order to evaluate time-dependence of the results, the FP signal was measured after incubation times of 15, 30, 60, and 120 min (Figure 3.11). In order to maintain similar settings between the assay protocols on different isoforms, a probe concentration of 5 nM was used in the titration experiments. As it is possible to observe from Figure 3.11, probe **3** seems to have a lower affinity for JNK1 and 2 in comparison with JNK3. Measurements conducted at different time points permitted to assess an overall stability of the  $K_d$  signal over time, with a negligible increase

at incubation times higher than 60 min. As in the case of the aforementioned assay, the  $K_d$  value measured after 30 min incubation was selected for both enzymes. The titration experiments were then directly used for the determination of the optimal protein concentration, as previously discussed. This led to select kinase concentrations of 50 and 30 nM for JNK1 and JNK2, respectively, both yielding an increase in polarization of approximately 80%.



**Figure 3.11.** Titration of probe **3** with JNK1 and JNK2. Experiments were performed three times in quadruplicate; data points and resulting  $K_d$  values are reported as mean value  $\pm$  SD; dashed lines represent the range of protein concentrations producing an increase in polarization between 50 and 80%.

### Assay validation

The first experiment to assess the validity of the assays consisted, as previously, in testing the probe precursor **1** in a competitive binding assay using the selected settings. Conversion of the resulting  $IC_{50}$  values through the aforementioned modified Cheng-Prusoff equation yielded  $K_i$  values in the low double-digit nM range (**1**,  $K_{i(JNK1)} = 19$  nM;  $K_{i(JNK2)} = 12$  nM), very close to the  $K_d$  of probe **3** for the same enzymes. However, unlike in the case of JNK3



and p38 $\alpha$  MAPK, the in-house ELISA assay was not developed for the JNK1 and JNK2 and a direct comparison of the results was therefore not possible. For this reason, the validation of the FP assay on JNK1 and JNK2 required this time the comparison of the binding results with literature values of reference compounds tested on the same enzymes. For this purpose four different ATP-competitive JNK standard inhibitors were selected (**IQ-1S**,<sup>156</sup> **JNK inhibitor VIII**,<sup>157</sup> **SR-3576**,<sup>158</sup> and **SR-3306**<sup>159</sup>). As in the previous case the selection was aimed at maximizing the chemical diversity. Moreover, additional factors had to be taken in account such as the commercial availability and the existence of inhibition data for both JNK isoforms on the same assay format. As these compounds did not show intrinsic fluorescence at the wavelengths used in the assay readout, they all were tested in the competition binding assay on the two enzymes (Table 3.4).

**Table 3.4.**  $K_i$  values resulting from the FP-assay in comparison with literature data

Compound	JNK1		JNK2	
	$K_i$ FP assay (nM) (mean $\pm$ SD <sup>a</sup> )	Literature data (nM)	$K_i$ FP assay (nM) (mean $\pm$ SD <sup>a</sup> )	Literature data (nM)
<b>1</b>	19 $\pm$ 4	n.r. <sup>b</sup>	12 $\pm$ 1	n.r.
<b>IQ-1S</b>	311 $\pm$ 43	390 ( $K_d$ ) <sup>c</sup>	390 $\pm$ 38	360 ( $K_d$ ) <sup>c</sup>
<b>JNK inhibitor VIII</b>	48 $\pm$ 12	2 ( $K_i$ ) <sup>d</sup>	35 $\pm$ 5	4 ( $K_i$ ) <sup>d</sup>
<b>SR3576</b>	40 $\pm$ 6	170 ( $IC_{50}$ ) <sup>e</sup>	8 $\pm$ 2	n.r.
<b>SR3306</b>	79 $\pm$ 12	67 $\pm$ 19 ( $IC_{50}$ ) <sup>f</sup>	215 $\pm$ 57	283 $\pm$ 3 ( $IC_{50}$ ) <sup>f</sup>

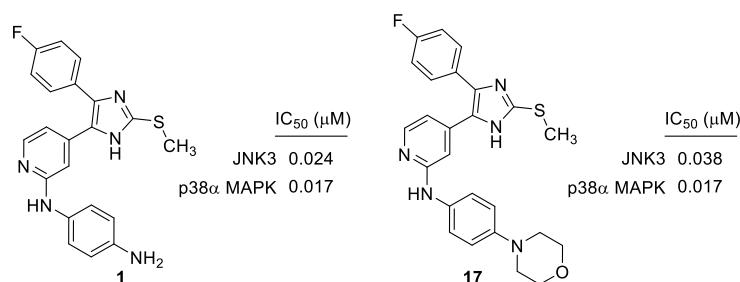
<sup>a</sup> n = 3; <sup>b</sup>n.r., data not reported in literature; <sup>c</sup>data reported by Schepetkin *et al.*<sup>156</sup>, SD not reported; <sup>d</sup>data reported by Szczepankiewicz *et al.*<sup>157</sup>, SD not reported; <sup>e</sup>data reported by Kamenecka *et al.*<sup>158</sup>, SD not reported; <sup>f</sup>data reported by Chambers *et al.*<sup>160</sup>.

Although in most cases the obtained  $K_i$  values seem to correspond to reported results of JNK standard inhibitors, the diversity of assay formats employed, type of the reported inhibition data ( $K_i$ ,  $K_d$ ,  $IC_{50}$ ), and activation state of the protein used do not allow a direct comparison of the results' absolute values. Nevertheless, it can be stated that, when inhibition data were reported for both JNK isoforms, the results obtained by the FP-based binding assay follow an analogous trend as the published ones. However, due to the different assay layouts of the published results and to the scarceness of tested inhibitors, a linear regression analysis could not be performed to support the correlation between the assays.

## 3.2. Optimization of a pyridinylimidazole scaffold aimed at achieving selectivity on JNK

### 3.2.1. Selection of a suitable lead compound

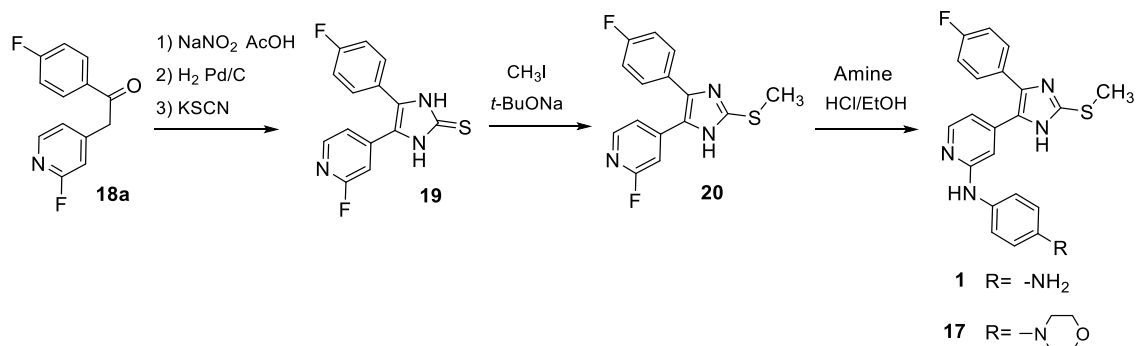
With the objective of reaching a selective inhibition of the JNKs, compound **1** ( $IC_{50(JNK3)} = 24$  nM;  $IC_{50(p38\alpha\ MAPK)} = 17$  nM) was selected as a starting point for subsequent modifications. However, this derivative cannot represent a lead compound “as such” due to the presence of the free terminal aniline group. This moiety is recognized by the ZINC15 pattern tool<sup>161</sup> as a potential responsible for compound aggregation and might therefore convert the compound into a so-called “pan assay interference compound” (PAIN). The latter represent a category of compounds which by means of their chemical/physical properties are able to interfere with common assay formats or to react non-specifically with the target, thereby displaying a misleading biological activity.<sup>162,163</sup> Since aggregation constitutes one of the most common causes of assay interference<sup>163</sup> the *p*-phenyldiamino group located at the pyridine-C2 position of compound **1** was replaced with a 4-morpholinoaniline moiety (compound **17**, Figure 3.12) which has been previously reported as a suitable substituent in this position.<sup>164</sup> The akin potency of the new derivative **17** seemed in any case to confirm the absence of an interference mechanism of the free terminal aniline substituent, thus validating the inhibitory activity of **1** on the tested enzymes. Nevertheless, the new 4-morpholinoaniline group was maintained constant when modifying other regions of the scaffold in order to rule out aggregation-driven interference which might arise from the combination of the *p*-phenyldiamino substituent with other moieties.



**Figure 3.12.** Replacement of the *p*-phenyldiamino group of compound **1** with the 4-morpholinoaniline moiety, affording compound **17**.  $IC_{50}$  values shown henceforth derive from the biological evaluation of compounds using the aforementioned ELISA activity assays.<sup>133,134</sup>

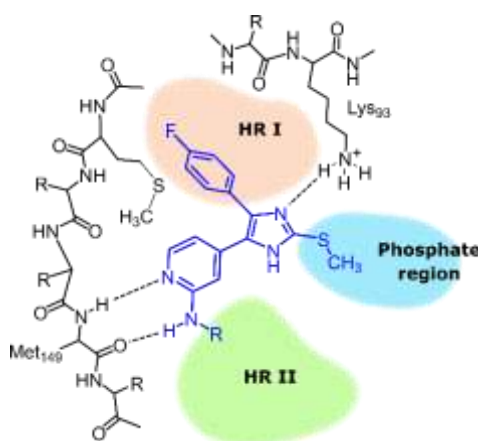
From the synthetic point of view, derivatives **1** and **17** could be prepared following a procedure described by Laufer and coworkers<sup>165</sup> wherein the construction of the 2-

sulfanylimidazole is based on the Marckwald imidazole synthesis<sup>166</sup> (Scheme 3.1). Introduction of the aromatic amine was then carried out by acid-catalyzed nucleophilic aromatic substitution ( $S_{\text{N}}\text{Ar}$ ).



**Scheme 3.1.** Synthesis route of compounds 1 and 17

Several studies on pyridinylimidazole-based inhibitors, also supported by X-ray crystallography, have provided a wide knowledge regarding the binding mode of this class of molecules to both p38 $\alpha$  MAPK and JNK3 (Figure 3.13). In particular, these molecules are known to form a bidentate hydrogen bond interaction with the backbone amino acid of the hinge region through the 2-aminopyridine donor/acceptor pair. In addition, the aromatic substituent at the imidazole-C4(5) position is known to be accommodated in the hydrophobic back pocket or HR I (see section 1.1.2) while the substituent at the pyridine-C2 position occupies the solvent exposed HR II. Moreover, the imidazole N atom distal to the pyridine ring forms a direct or  $\text{H}_2\text{O}$  mediated hydrogen bond with the conserved lysine side chain of the N lobe. Finally, the 2-methylsulfanyl moiety stretches towards the phosphate region.

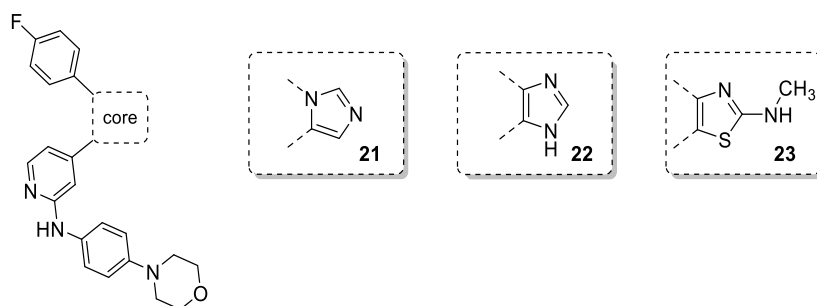


**Figure 3.13.** Binding mode of pyridinylimidazole-based inhibitors in the binding site of JNK3. Figure was modified from Laufer *et al.*<sup>151</sup>

### 3.2.2. Exploration of the substitution at the HR I

The first attempts aimed at increasing the selectivity towards the JNK3 consisted in modifying the substitution at the imidazole-C4 position of compound **1**. As resulting from the well-known binding mode of the class of pyridinylimidazoles, the group in this position is accommodated in the HR I, an area of the protein which is crucial in determining the inhibitor selectivity.

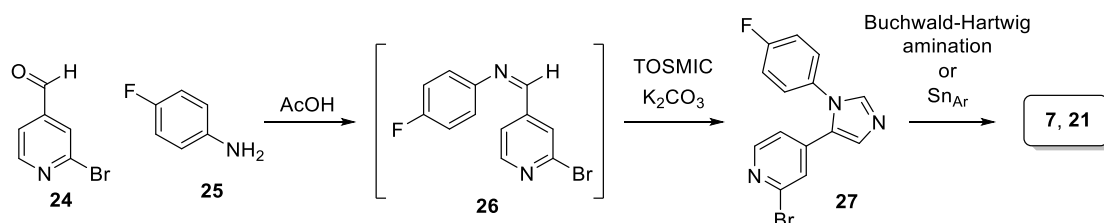
Prior to synthesize derivatives carrying different substituents at the imidazole-C4 position, a small set of modifications were conducted on the 5-membered core ring (Figure 3.14). These changes were aimed at observing the effect of a different substituents arrangement around the imidazole ring (such as 1,5- or 4,5-disubstituted imidazoles **21** and **22**, respectively), along with a change of the core to 2-amino-thiazole (compound **23**).



**Figure 3.14.** Core modifications of the lead compound **17**.

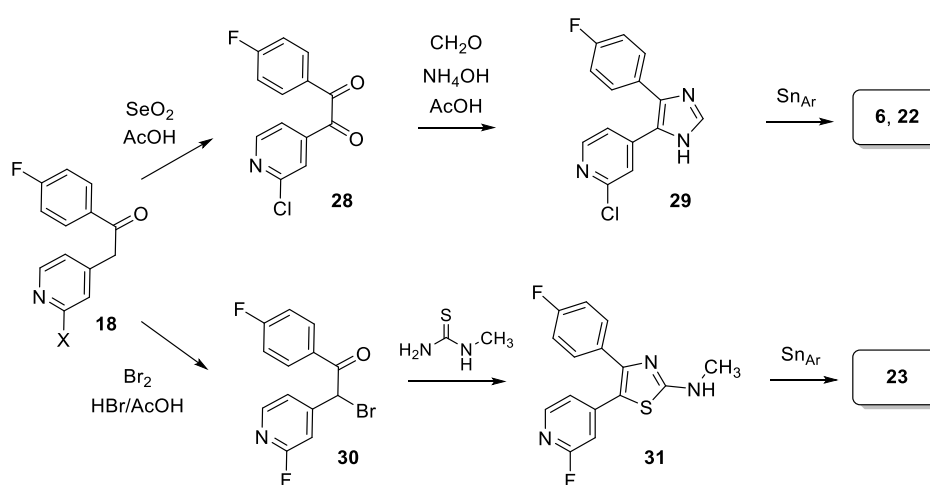
Moreover, these structural modifications resulted in an overall simplification of the scaffold, alongside with more convenient synthetic procedures.

The scaffold of compound **21** could be easily obtained through a multistep one-pot reaction starting from the 2-bromoisonicotinaldehyde and 4-fluoroaniline, and achieving the ring closure through Van Leusen reaction with *p*-toluenesulfonylisocyanide (Scheme 3.2). The same scaffold could be used for the preparation of compound **7** (precursor of probe **11**, Figure 3.3).



**Scheme 3.2.** Synthesis route for the preparation of compounds **7** and **21a**.

Both compounds **22** and **23** could instead be obtained starting from the ethanone derivatives **18** (Scheme 3.3). In case of the 4,5-disubstituted imidazole **22** the ethanone was reacted in a Riley oxidation giving the corresponding diketone and then cyclized under Debus-Radzizewski conditions. The strategy employed for the synthesis of **22** was also followed for the preparation of compound **6**, precursor of probe **10** (Figure 3.3). Worth to mention, the use of a 2-chloro-pyridine derivative instead of the corresponding 2-fluoro analog permitted to remarkably increase the yield of both steps, as it significantly reduced the substitution of the halogen by a molecule of water. On the other hand,  $\alpha$ -bromination of ethanone intermediate followed by cyclization with methylthiourea afforded compound **23**.



**Scheme 3.3.** Procedures for the preparation of compounds **6**, **22**, and **23**.

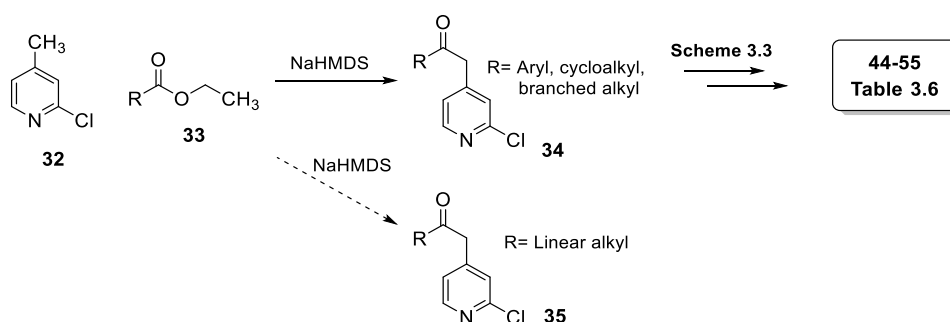
Table 3.5 shows the biological activity of the synthesized compounds on both JNK3 and p38 $\alpha$  MAPK in comparison with  $\text{IC}_{50}$  values of derivative **17**. The different arrangement of substituents around the imidazole ring characterizing compound **21** produced a decrease in activity of one order of magnitude. Conversely, removal of the *S*-methyl group or replacement of the core with a 2-methylamino-imidazole ring were well tolerated and gave rise to compounds potently inhibiting both enzymes. In particular, 4,5-disubstituted imidazole **22** displayed extremely similar inhibition values compared to the lead compound **17**, leading to the assumption that the 2-methylsulfanyl substituent doesn't exert an additional influence on the activity. Moreover, likewise its trisubstituted analog **17**, compound **22** is also characterized by a balanced activity on both kinases (in contrast to thiazole derivative **23**, showing preference towards the p38 $\alpha$  MAPK). These features in combination with an easier synthesis route suggested to conduct the following modifications on the disubstituted imidazole core rather than on the trisubstituted ring.

**Table 3.5.** Biological activity of compounds derived from modification of the central core

Cpd	IC <sub>50</sub> ± SD [μM] <sup>a</sup>	
	JNK3	p38α MAPK
17	0.038 ± 0.002	0.017 ± 0.001
21	0.276 ± 0.010	0.323 ± 0.014
22	0.031 ± 0.002	0.021 ± 0.001
23	0.015 ± 0.003	0.002 ± 0.000

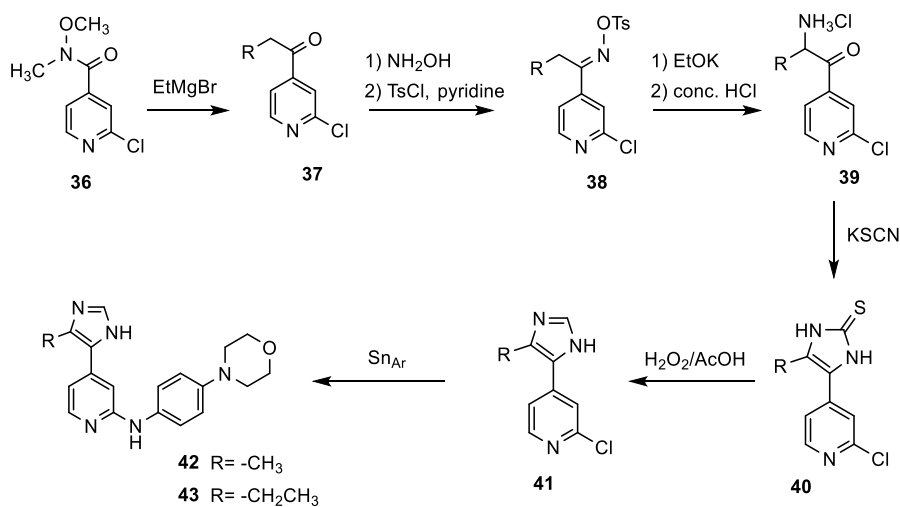
<sup>a</sup>Values represent the mean of three experiments

As outlined in Scheme 3.4 the 2-chloro-4-methylpyridine was first deprotonated by sodium bis(trimethylsilyl)amide (NaHMDS) and then condensed with the appropriate ester obtaining a series of ethanone derivatives carrying different aryl, cycloalkyl, and branched alkyl substituents (compounds **34**). These intermediates were then converted to the final 4,5-disubstituted imidazoles using the same procedure reported in Scheme 3.3.

**Scheme 3.4.** Synthesis of compounds 44-55.

Such synthetic strategy was unfortunately not applicable to the synthesis of derivatives carrying linear alkyl chains (compounds **35**), due to the impossibility to condense the 2-chloro-4-methylpyridine (**28**) with the corresponding ethyl esters. This could derive from the extraction of a proton at the αC of the ester by the deprotonated pyridine, thus preventing the nucleophilic attack. The success on the NaHMDS condensation reaction on cyclic or branched alkyl moieties, also having a proton in α position to the carbonyl group, might be explained by the higher hindrance of their substituents. The synthesis of methyl- and ethyl-substituted derivatives **42** and **43**, respectively, required therefore a different strategy (Scheme 3.5). Ketone derivatives **37** were transformed into the corresponding oximes and subsequently tosylated. α-Aminoketones **39** were then obtained by Neber rearrangement of tosyloximes **38** followed by hydrolysis of the resulting azirine intermediate. Finally, after ring closure with KSCN, the imidazolin-2-thione ring of

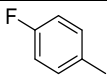
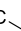
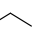
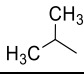
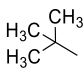


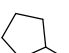
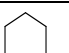
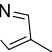
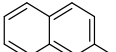
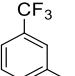
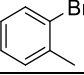
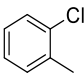
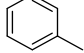
derivatives **40** was desulfurized in oxidative conditions and the 4-morpholinoaniline moiety was successively installed.



**Scheme 3.5.** Synthetic strategy towards 4,5-disubstituted imidazoles **42** and **43** bearing a linear alkyl substituent.

Table 3.6 illustrates the biological activities of compounds featuring different substituents at the imidazole-C4(5) position (compounds **42-55**) in comparison to the 4-fluorophenyl derivative **22**. As it can be observed, modification of the substitution pattern around the phenyl ring seemed not to influence the activity on the two enzymes, giving rise in most of cases to dual JNK3/p38 $\alpha$  MAPK inhibitors with IC<sub>50</sub> values in the double-digit nM range. The lack of selectivity of these derivatives can be explained through the observations of previous studies from Scapin and coworkers based on the structural determination of JNK3 in complex with different inhibitors, including a pyridinylimidazole-based compound.<sup>167</sup> Although the gatekeeper amino acid of JNK3 (Met146) differs from the corresponding residue on p38 $\alpha$  MAPK (Thr106) the aforementioned studies permitted to observe a shift of the Met149 side chain of approximately 3 Å in order to accommodate the aromatic substituent on the imidazole core. By affecting the gatekeeper amino acid, this induced fit significantly reduces the size difference between the two binding sites, hence not allowing the achievement of a selectivity of action. Size increase of the substituent was still well-tolerated in both cases as exemplified by the high potency of naphthyl derivative **51**, whereas the substitution with a heteroaromatic 5-membered ring (compound **50**) caused a loss of activity more prominent on the p38 $\alpha$  MAPK.

**Table 3.6** Structure and biological activity of analogs of compound **22** bearing a different substituent at the imidazole-C4 position.

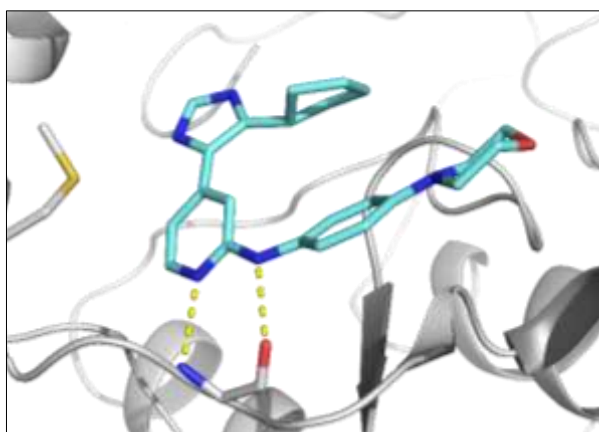
Cpd	R	IC <sub>50</sub> ± SD [μM] <sup>a</sup>	
		JNK3	p38α MAPK
<b>22</b>		0.031 ± 0.002	0.021 ± 0.001
<b>42</b>	H <sub>3</sub> C- 	0.833 ± 0.139	>10 (41%) <sup>b</sup>
<b>43</b>	H <sub>3</sub> C- 	1.198 ± 0.193	>10 (34%) <sup>b</sup>
<b>44<sup>c</sup></b>		2.833 ± 0.046	≈10 (50%) <sup>b</sup>
<b>45<sup>c</sup></b>		>10 (32%) <sup>c</sup>	>10 (41%) <sup>b</sup>
<b>46</b>		1.080 ± 0.165	4.023 ± 0.193
<b>47<sup>c</sup></b>		1.757 ± 0.133	2.265 ± 0.177
<b>48<sup>c</sup></b>		2.189 ± 0.136	1.716 ± 0.081
<b>48<sup>c</sup></b>		1.724 ± 0.179	0.726 ± 0.021
<b>50</b>	H <sub>3</sub> C-N- 	0.758 ± 0.049	3.259 ± 0.181
<b>51</b>		0.031 ± 0.003	0.016 ± 0.003
<b>52<sup>c</sup></b>		0.143 ± 0.012	0.022 ± 0.003
<b>53<sup>c</sup></b>		0.131 ± 0.021	0.061 ± 0.002
<b>54<sup>c</sup></b>		0.060 ± 0.008	0.038 ± 0.002
<b>55<sup>c</sup></b>		0.037 ± 0.003	0.024 ± 0.003

<sup>a</sup>IC<sub>50</sub> values are the mean of three experiments; <sup>b</sup>percent inhibition at indicated concentration; <sup>c</sup>compounds synthesized by master student Camilla Scarpellini under my co-supervision.



A different effect could be detected by substituting the 4-fluorophenyl moiety with cyclic or branched aliphatic groups. In case of p38 $\alpha$  MAPK, the activity decreased along with the reduction of the ring size, probably due to the progressive inability to occupy the larger HR I of this enzyme. On the other hand, excluding the cyclopropyl derivative **46**, the inhibitory activity on JNK3 seemed not to be affected by the ring size.

A possible explanation for this behavior is that the cycloaliphatic moieties are not able to induce the shift of the Met146 due to their higher flexibility. As a result, the small size of the JNK3 HR I might force the inhibitor to adopt a different conformation wherein the imidazole core is flipped of approximately 180° respect to the pyridine ring. Being located in the wider phosphate region the cycloalkyl moiety does not contribute to the binding, thus explaining the akin inhibitory activity of compounds **47-49**. The hypothesis of the central core flip can be supported by analogous findings reported by Wytiak and coworkers for similar molecules<sup>168</sup> and can also be observed by docking these inhibitors in the binding site of JNK3, using the crystal structure with PDB entry 3V6S.<sup>169</sup> Since the inhibitor crystallized in this structure does not target the HR I, the position of the Met146 reflects the natural orientation of the JNK3 gatekeeper residue, hence representing the original size of this pocket. As exemplified by Figure 3.15, representing the cyclopentyl derivative **48**, several poses were generated wherein the cycloalkyl substituent pointed away from the HR I, thus resulting in a flip of the imidazole ring. It is worth to mention that also poses displaying the classical conformation of the imidazole ring were possible, requiring however a different orientation of the whole scaffold in order to fit the cyclic substituent in the narrower HR I.



**Figure 3.15.** Docking pose of compound **48** (PDB entry: 3V6S). Docking was performed using the software Schrödinger Maestro v11.03.016.

Regarding the introduction of branched aliphatic substituents, the isopropyl group determined a severe drop of the inhibitory activity on p38 $\alpha$  MAPK yet producing  $\mu\text{M}$  IC<sub>50</sub>

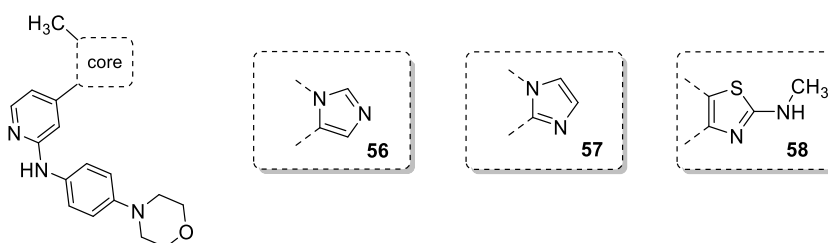
values on JNK3. Substitution with a bulkier *tert*-butyl moiety was instead not tolerated by both enzymes.

A further decrease in the substituent size, consisting in the introduction of a methyl or an ethyl group, resulted in a total loss of inhibitory activity on p38 $\alpha$  MAPK (compounds **42** and **43**, respectively). Interestingly, the same substituents managed to conserve the activity on the JNK3, with the methyl derivative **42** representing the only example of the series reaching an IC<sub>50</sub> value in the submicromolar range. This outcome seems to be in line with the previous assumptions regarding the effect of cycloalkyl substituents. More closely, the methyl group of compound **42** possesses the right size to fit in the narrow HR I of the JNK3 with the gatekeeper amino acid in its natural conformation, thus not requiring the 180° flip of the imidazole ring. Because of the advantageous inhibition profile of compound **42**, the methyl group at the imidazole-C4(5) position was maintained stable when modifying other areas of the scaffold.

### 3.2.3. Modifications on the five-membered core

Once the methyl substituent was selected as a suitable substituent at the imidazole-C4(5) position, further structural changes were performed on the central core.

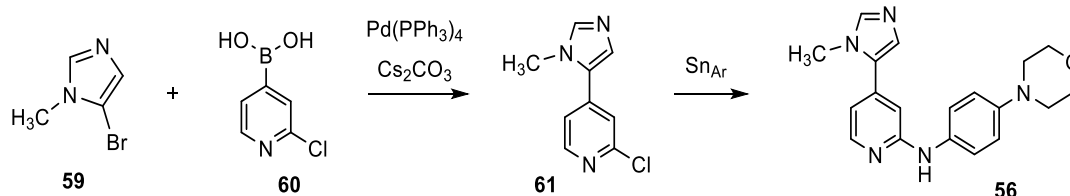
At a first instance, similar modifications to the ones described in the previous section were carried out, aimed at modifying the arrangement of substituents around the imidazole core (compounds **56** and **57**, Figure 3.16). Alternatively, the imidazole core was replaced by a 2-aminothiazole ring (compound **58**).



**Figure 3.16.** Modifications at the imidazole core maintaining the methyl substituent at the imidazole-C4(5) position.

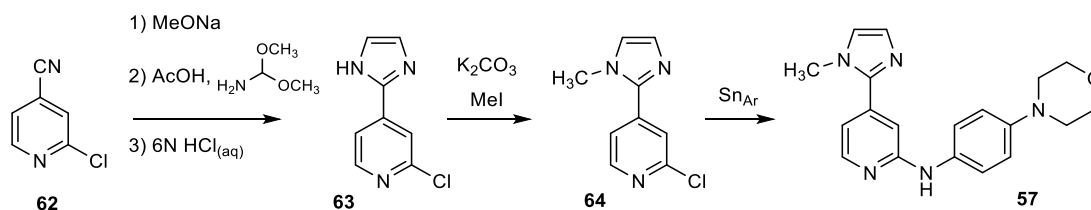
For the preparation of the three scaffolds depicted in Figure 3.16 diverse strategies were required. In case of inhibitor **56** the procedure reported in Scheme 3.2, based on Van Leusen cyclization reaction, was not applicable due to the instability of the corresponding methyl-imine intermediate. For this reason, the commercially available 5-bromo-*N*-methylimidazole (**59**) was coupled to the (2-chloropyridin-4-yl)boronic acid (**60**) through a

Pd-catalyzed Suzuki-Miyaura coupling reaction (Scheme 3.6). As in the previous examples, the 4-morpholinoaniline moiety could be then introduced by nucleophilic aromatic substitution.



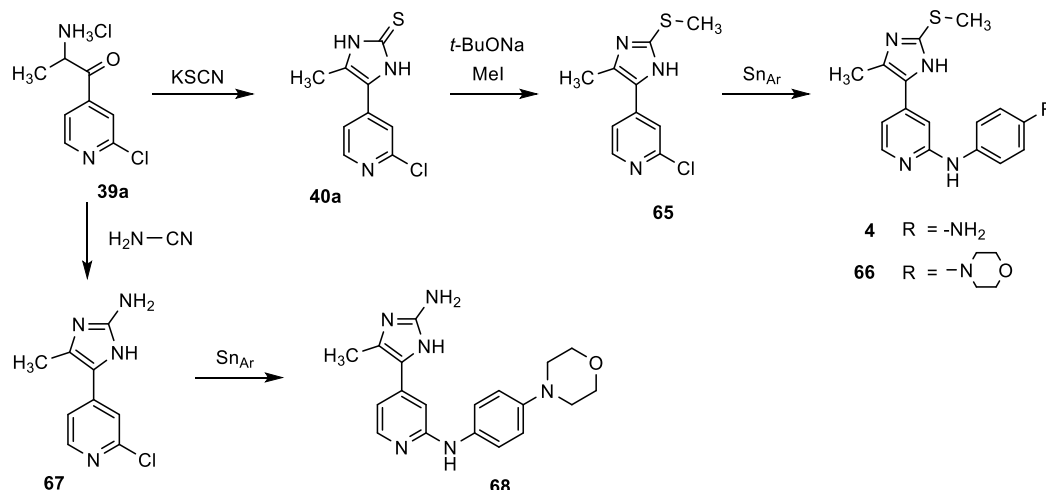
**Scheme 3.6.** Synthesis strategy for the preparation of compound **56**.

For the 1,2-disubstituted imidazole scaffold of compound **57** a one-pot reaction starting from the 2-chloro-isonicotinonitrile (**62**) was instead employed, following the procedure described by Voss *et al.*<sup>170</sup> (Scheme 3.7). Finally, the 2-methylaminothiazole core could be obtained according to the Hantzsch method, namely by cyclizing an  $\alpha$ -halogen carbonyl compound with *N*-methylthiourea. This procedure was analog to the one used for the synthesis of the 4-aryl-5-pyridinyl thiazole **23**. However, due to the inaccessibility of the corresponding ketone derivative (Scheme 3.4), the  $\alpha$ -halogenation was conducted on its regioisomer **36**, thus leading to the 5-methyl-4-pyridinyl thiazole **58**.



**Scheme 3.7.** Synthesis route towards 1,2-disubstituted imidazole **57**.

Other modifications on the central core consisted instead in altering the substitution pattern at the C2 position of the imidazole ring. Firstly, the 2-methylsulfanyl group was reintroduced in order to evaluate its possible influence in combination with the 4-methyl group (compound **66**). Additionally, a 2-amino group was also installed in this position in order to observe the effect of an electron donating group (compound **68**). From the synthetic point of view compound **66** was accessed by alkylating intermediate **40a** with methyl iodide and proceeding with the nucleophilic aromatic substitution (Scheme 3.8). The same procedure allowed to obtain compound **4**, the precursor of probe **8** (Figure 3.3). The 2-aminoimidazole core could instead be obtained by reacting the  $\alpha$ -aminoketone **39a** with cyanamide (Scheme 3.8).



**Scheme 3.8.** Synthesis of derivatives carrying different substituents at the imidazole-C2 position

The first feature emerging from biological results of compounds **56-58**, **66**, and **68** (Table 3.7) is the complete loss of activity on the p38 $\alpha$  MAPK which can be mostly attributed to the replacement of the 4-fluorophenyl ring with a methyl substituent.

**Table 3.7.** Biological activities derivatives resulting from modifications at the central core

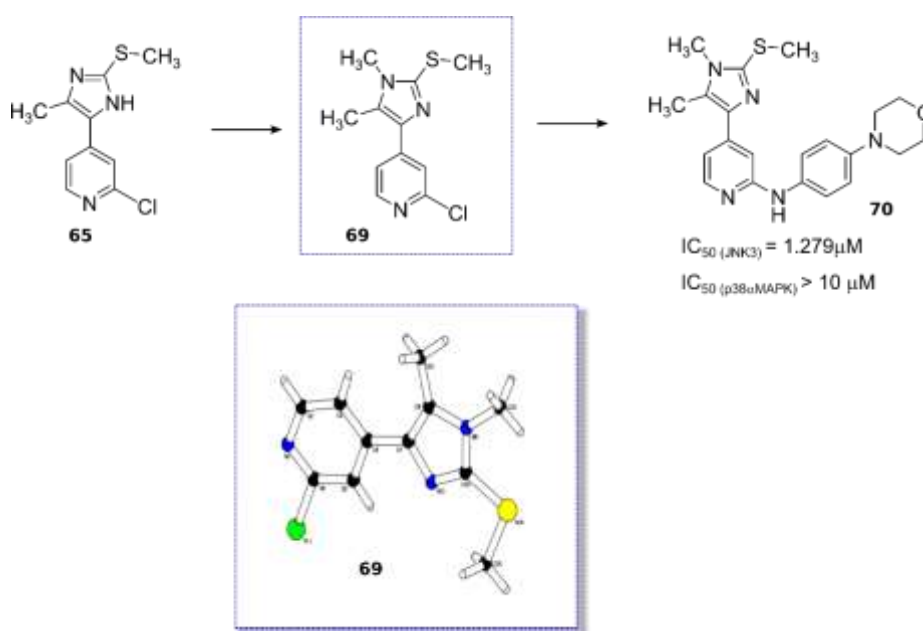
Cpd	IC <sub>50</sub> $\pm$ SD [ $\mu$ M] <sup>a</sup>	
	JNK3	p38 $\alpha$ MAPK
<b>56</b>	0.714 $\pm$ 0.021	>10 (32%) <sup>b</sup>
<b>57</b>	>10 (42%) <sup>b</sup>	>10 (15%) <sup>b</sup>
<b>58</b>	2.500 $\pm$ 0.092	>10 (9%) <sup>b</sup>
<b>66</b>	0.363 $\pm$ 0.034	>10 (48%) <sup>b</sup>
<b>68</b>	1.395 $\pm$ 0.230	>10 (43%) <sup>b</sup>

<sup>a</sup>IC<sub>50</sub> values are the mean of three independent experiments; <sup>b</sup>percent inhibition at 10  $\mu$ M concentration.

In addition, it can be observed that the replacement of the core to a 1,5-disubstituted imidazole (**56**) was still tolerated whereas the 1,2-disubstitution (**57**) resulted in a dramatic drop in activity. Analogously, a significantly higher IC<sub>50</sub> value could be observed when the central imidazole core was transformed into a 2-methylaminothiazole (**58**). The presence of the free amino group at the imidazole-C2 position exerted a counterproductive effect on the inhibitory activity, producing an IC<sub>50</sub> value in the  $\mu$ M range (**68**). On the other hand, reintroduction of the 2-alkylsulfanyl group (**66**) determined a twofold increase in the inhibitory activity. This outcome was surprising since the results displayed in Table 3.5 hinted a scarce influence of the *S*-methyl group on the activity of derivatives bearing a 4-fluorophenyl substituent on the imidazole ring. Conversely, an evident contribution of the 2-alkylsulfanyl moiety could be observed on the 4-methyl substituted derivatives (a more

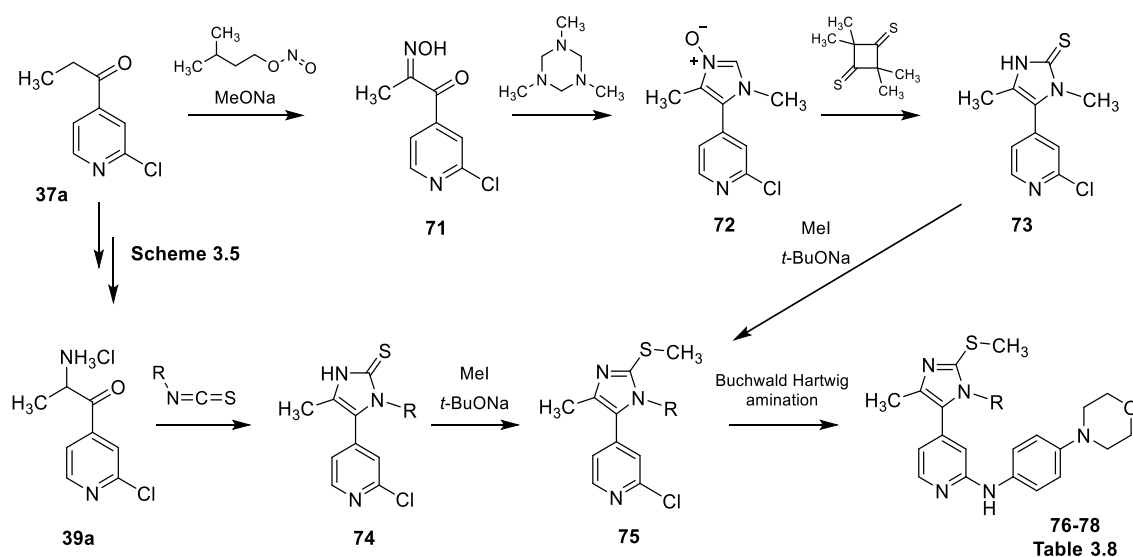
detailed elucidation of the influence of the *S*-methyl moiety will be provided in the following section).

After understanding the importance of the *S*-methyl moiety, a further series of pyridinylimidazole derivatives was synthesized wherein an alkyl group was introduced on the imidazole N atom while maintaining both the 4-methyl and the 2-alkylsulfanyl substituents. Tetrasubstituted imidazoles are present in the core of several p38 $\alpha$  MAPK and dual JNK3/p38 $\alpha$  MAPK potent inhibitors<sup>128,151,171</sup> and this strategy was therefore applied to the methyl-substituted scaffold as well. When synthesizing tetrasubstituted imidazole derivatives as kinase inhibitors a special attention should be given to regioisomery. As it is possible to understand from Figure 3.13, the position of the substituted imidazole N atom is crucial for the formation of the essential binding interactions. In particular, substitution on the imidazole N atom distal to the pyridine ring would hinder the formation of the hydrogen bond with Lys93, hence reducing the binding affinity. As a proof of this, the tetrasubstituted derivative **70** carrying a methyl group on the imidazole N atom away from the pyridine ring was synthesized by reaction of compound **65** with methyl iodide, followed by Buchwald-Hartwig amination on intermediate **69**. Previous studies have demonstrated that the nucleophilic substitution on pyridinylimidazoles tends to occur regioselectively on this N atom when a 4-fluorophenyl ring is installed at the imidazole-C4 position.<sup>172</sup> The same reaction carried out on the 4-methyl derivative **65** showed analogous regioselectivity, affording compound **69** as the major product as it could be assessed by X-ray crystallography (Figure 3.17).



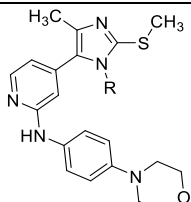
**Figure 3.17.** Synthesis and structure determination of tetrasubstituted derivative **70**.

The significant drop in inhibitory activity of compound **70** confirmed the previous assumptions and prompted the regioselective synthesis of analogs carrying the substitution on the imidazole N atom adjacent to the pyridine ring. Such molecules can normally be obtained through a route previously reported by Laufer and coworkers entailing the cyclization of an  $\alpha$ -ketoxime derivative with a trialkyl triazinane in order to introduce the substituent in the desired position (Scheme 3.9).<sup>173</sup> Nevertheless, the application of this strategy starting from compound **37a** was only successful in the case of the *N*-methyl-substituted imidazole **76**, yet being characterized by low yields and long reaction times. For this reason, an alternative procedure was developed for the regioselective preparation of tetrasubstituted imidazoles (Scheme 3.9). Such route slightly modifies a strategy previously published by Xi *et al.*<sup>174</sup> and is based on the reaction of the  $\alpha$ -aminoketone derivative **39a** with an opportune alkylisothiocyanate. Diverging from the reported route, the imidazolin-2-thione intermediates **74** were reacted in a nucleophilic substitution in order to introduce the alkyl group on the S atom.



**Scheme 3.9.** Synthetic strategies for the preparation of tetrasubstituted imidazoles.

The route reported in the lower part of Scheme 3.9 was also applied as an alternative and versatile strategy for the preparation of previously discovered tetrasubstituted derivatives as potent p38 $\alpha$  MAPK inhibitors (**Publication V**).

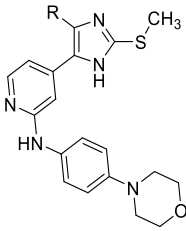
**Table 3.8.** Biological activity of tetrasubstituted derivatives **76-78**.


Cpd	R	IC <sub>50</sub> ± SD [μM] <sup>a</sup>	
		JNK3	p38α MAPK
76	—CH <sub>3</sub>	2.514 ± 0.312	> 10 (10%) <sup>b</sup>
77	—CH <sub>2</sub> CH <sub>3</sub>	2.091 ± 0.108	> 10 (21%) <sup>b</sup>
78	—Cyclopropyl	6.509 ± 1.326	> 10 (40%) <sup>b</sup>

<sup>a</sup>IC<sub>50</sub> values are the mean of three independent experiments; <sup>b</sup>percent inhibition at 10 μM concentration.

Results displayed in Table 3.8 show that substitution of the imidazole N atom adjacent to the pyridine had a detrimental effect on the inhibitory activity. In particular, *N*-methyl derivative **78** showed a drop in inhibitory potency of nearly one order of magnitude compared to the *N*-unsubstituted compound **66**. Furthermore, the same compound resulted even less active than the supposedly “wrong” regioisomer **70**, suggesting that substitution in such position might hinder crucial binding interactions.

After observing the beneficial effect of the 2-alkylsulfanyl group on the imidazole ring, analogs of compound **66** bearing an ethyl chain or being unsubstituted at the imidazole-C4 position were synthesized (compounds **79** and **80**, respectively). This detailed evaluation was performed in order to estimate the optimal length of the substituent in this position in combination with the *S*-methyl moiety. Compounds **79** and **80** could be obtained through the same procedure used for compound **66** (Schemes 3.5 and 3.8) starting from 1-(2-chloropyridin-4-yl)butan-1-one and 1-(2-chloropyridin-4-yl)ethan-1-one, respectively. As it can be observed from the results in Table 3.9 derivative **66** emerged once more as the best inhibitor of the series, thereby confirming the methyl group as the substituent possessing the optimal length to address the HR I.

**Table 3.9.** Assessment of the optimal length of the alkyl substituent at the imidazole-C4(5) position.


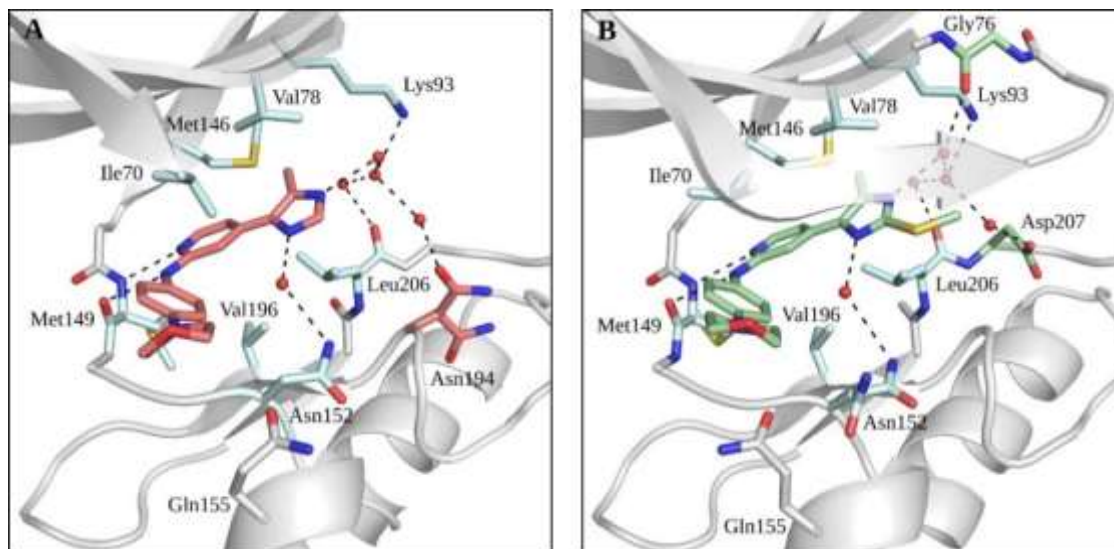
Cpd	R	IC <sub>50</sub> ± SD [μM] <sup>a</sup>	
		JNK3	p38α MAPK
66	—CH <sub>3</sub>	0.363 ± 0.034	>10 (48%) <sup>b</sup>
79	—CH <sub>2</sub> CH <sub>3</sub>	1.095 ± 0.064	>10 (38%) <sup>b</sup>
80	—H	0.562 ± 0.021	>10 (43%) <sup>b</sup>

<sup>a</sup>IC<sub>50</sub> values are the mean of three independent experiments; <sup>b</sup>percent inhibition at 10 μM concentration.

### 3.2.4. Evaluation of the binding mode of compounds 42 and 66

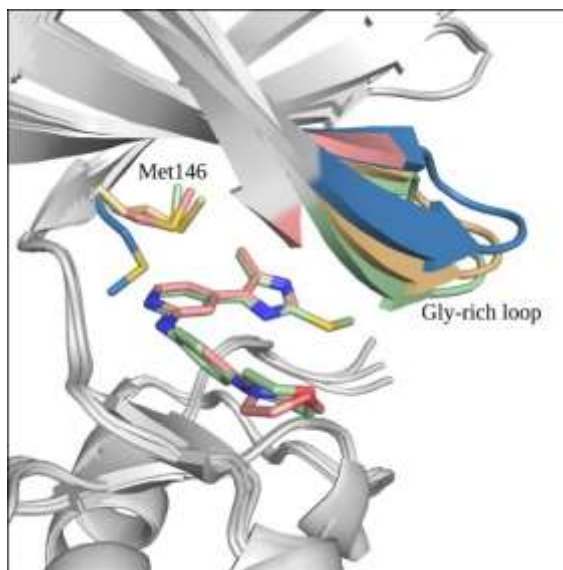
In order to understand the influence of the 2-alkylsulfanyl moiety in derivative **66** and to explain its significantly higher inhibitory activity in comparison to the 2-unsubstituted analog **42**, the structure of JNK3 in complex with the two derivatives was determined by X-ray crystallography. A preliminary assumption consisted in the capability of the *S*-methyl group of inhibitor **66** to prevent the potential 180° flip of the imidazole ring which can instead occur in derivative **42**, as already hypothesized for aforementioned compounds (Section 3.2.2. and Figure 3.15). This conformational change might be responsible for the twofold drop in inhibitory activity of compound **42**. Nevertheless, as noticeable from the two crystal structures depicted in Figure 3.18, both inhibitors assumed the “classical” conformation with the 4-methyl substituent pointing towards the HIR I of the enzyme, and the imidazole N atom interacting with the conserved Lys93 via a double water-mediated hydrogen bond. These findings seem therefore to rule out the hypothesis of the imidazole flip.





**Figure 3.18.** Crystal structures of inhibitors **42** (A, PDB entry: 6EMH) and **66** (B, PDB entry: 6EKD) soaked in JNK3. Only the JNK3 active site is displayed. The protein backbone is displayed in gray. The compounds and interacting amino acids are highlighted as sticks. Active site residues with common orientations and interactions are shown in light blue, while the residues that differ between both complexes are highlighted in the same color as the respective inhibitor. Side chains for which multiple orientations are observed (Asn194 in complex with **42** and Asn152 in complex with **66**) are shown in both orientations. Water molecules are represented as red spheres and hydrogen bonds are shown as black dashed lines.

General observations which can be done for both inhibitors are the bidentate hydrogen bond interaction with the Met149 and the formation of a water-mediated hydrogen bond between the imidazole N atom adjacent to the pyridine ring and the Asn152. The latter finding might explain the detrimental effect of alkyl substituents in this region (Table 3.8) (a more detailed description of the binding mode of the two inhibitors is presented in **Publication VII**). A major feature distinguishing the two crystal structures is the position of the conserved Gly-rich loop (see Section 1.1.1). In the case of the unsubstituted derivative **42** this region is lacking electron density due to high flexibility. Conversely, inhibitor **66** seems to stabilize this segment thanks to both hydrophobic and polar interactions, positioning it in a downward conformation. A closer analysis of this behavior based on the superposition of different crystal structures (Figure 3.19) revealed that inhibitor **66** induces a collapse of the Gly-rich loop akin to the one visible in the JNK3-AMP-PCP complex (PDB entry: 6EQ9), thus determining a compression of the ATP binding site. This effect which is driven by the *S*-methyl moiety seems therefore to be the responsible for the higher inhibitory potency of compound **66** in comparison with derivative **42**.



**Figure 3.19.** Comparison of gatekeeper Met146 orientation and the Gly-rich loop positioning upon JNK3 inhibitor binding with other ligand-bound JNK3 structures. Overlay of the JNK3-**66** complex structure (light green), the JNK3-**42** complex structure (light red), the AMP-PCP bound JNK3 structure (light orange), and the 1PMN structure reported by Scapin, *et al.*<sup>167</sup> (blue). The superposition was performed using the “align” function in PyMOL. The side chain of the gatekeeper Met146 and the Gly-rich loop are highlighted. Only compounds **42** and **66** are shown for the sake of clarity.

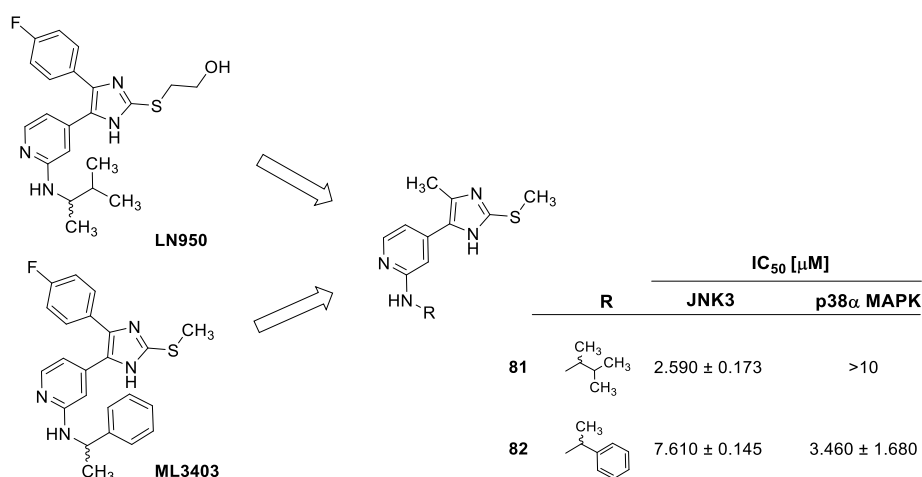
Other considerations on the inhibitors binding mode regard the positioning of the Met146 side chain, representing the gatekeeper of the enzyme. As expected, in both complexes with the 4-methyl substituted inhibitors **42** and **66** the gatekeeper is in a “natural” conformation, resembling the one of the JNK3-AMP-PCP complex. On the other side, as already mentioned in section 3.2.2., aryl substituents in this position can induce a shift in of the Met146 side chain, thus increasing the size of this hydrophobic pocket, as also visible in Figure 3.19 for the 1PMN crystal structure (blue). By binding to the enzyme with the gatekeeper in its natural conformation 4-methyl substituted derivatives present the optimal length to occupy the narrow HR I of the JNK3 while being too small to interact with the wider pocket in p38 $\alpha$  MAPK. This explanation might therefore provide a rationale for the high selectivity of compounds **42** and **66** towards the JNK3.

### 3.2.5. Modification of the substituent at the HR II

The last series of modifications consisted in the replacement of the 4-morpholinoaniline substituent of compound **66** with different aliphatic and aromatic substituents. Such

derivatives could be easily synthesized by nucleophilic aromatic substitution starting from intermediate **65** (Scheme 3.8).

The first attempt consisted in introducing moieties which have been previously reported in potent pyridinylimidazole-base inhibitors of the p38 $\alpha$  MAPK. In detail, the 3-methylbut-2-ylamine and the 1-phenylethyl-1-amine, which can be found in the structure of the LN950<sup>143</sup> and ML3403,<sup>151</sup> respectively, were installed at this position giving rise to derivatives **81** and **82**, respectively (Figure 3.20).



**Figure 3.20.** Design and biological activities of compounds **81** and **82**.

The purpose of this strategy was to increase the potency on the JNK3 by inserting groups which resulted beneficial for the closely-related p38 $\alpha$  MAPK while maintaining the selectivity of action provided by the methyl substituent on the imidazole core. Nevertheless, results displayed in Figure 3.20 revealed that this approach is counterproductive, as besides a dramatic loss in activity on JNK3 for both compounds **81** and **82**, the substituent of compound **82** could even restore the inhibitory activity on the p38 $\alpha$  MAPK. The effect of the two branched alkyl/arylalkyl substituents of p38 $\alpha$  MAPK standard inhibitors LN950 and ML3403 was further evaluated on different cores and compared with the corresponding derivatives bearing the aromatic 4-morpholinoaniline/*p*-phenyldiamine groups (Figure 3.21). In accordance with the results observed for compounds **81** and **82**, the 3-methylbut-2-ylamine and the 1-phenylethyl-1-amine were scarcely tolerated at the pyridine-C2 position also when combined with other cores. This demonstrates that, despite their high similarity, the JNK3 and the p38 $\alpha$  MAPK present different requirements when targeting this area of the protein.

	R	IC <sub>50</sub> [μM]	
		JNK3	p38α MAPK
5		0.562 ± 0.021	>10
80		3.263 ± 0.000	>10
83 <sup>a</sup>		1.941 ± 0.000	>10
84 <sup>a</sup>		6.346 ± 0.000	>10

	R	IC <sub>50</sub> [μM]	
		JNK3	p38α MAPK
7		0.276 ± 0.010	0.323 ± 0.014
21 <sup>b</sup>		0.216 ± 0.000	0.039 ± 0.000
85		0.253 ± 0.000	0.148 ± 0.000
86 <sup>b</sup>		1.408 ± 0.000	0.028 ± 0.000

	R	IC <sub>50</sub> [μM]	
		JNK3	p38α MAPK
57		>10	>10
87		>10	>10
88		>10	>10
89		>10	>10

	R	IC <sub>50</sub> [μM]	
		JNK3	p38α MAPK
6		0.031 ± 0.002	0.021 ± 0.001
22		0.007 ± 0.000	0.005 ± 0.000
90		0.125 ± 0.000	0.024 ± 0.000

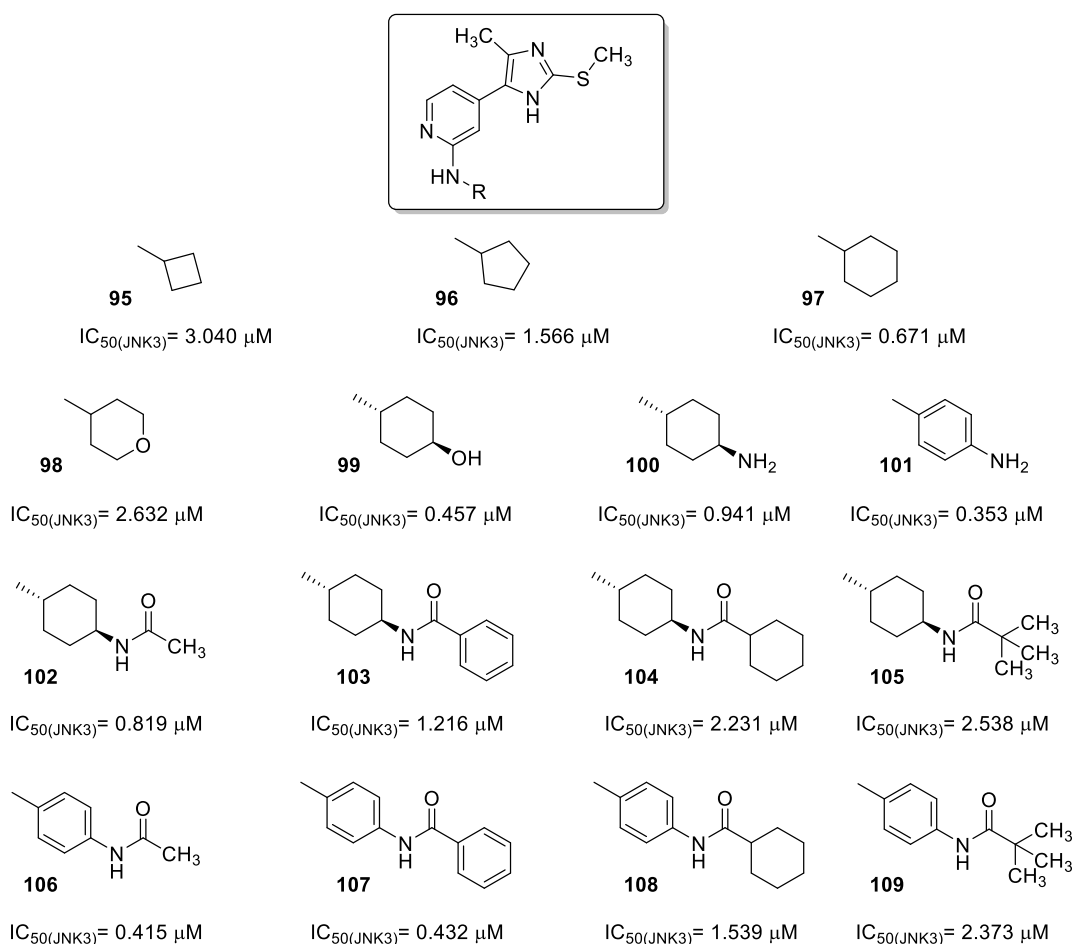
	R	IC <sub>50</sub> [μM]	
		JNK3	p38α MAPK
23		0.015 ± 0.003	0.002
91 <sup>c</sup>		0.027 ± 0.000	0.011 ± 0.000
92 <sup>c</sup>		0.102 ± 0.000	0.017 ± 0.000

	R	IC <sub>50</sub> [μM]	
		JNK3	p38α MAPK
58		3.263 ± 0.000	>10
93		2.501 ± 0.000	>10
94		>10	>10

**Figure 3.21.** Effect of substituents at the pyridine-C2 position in combination with different cores; <sup>a</sup>Eitel, M.; Koch, P., unpublished results; <sup>b</sup>compound reported in the diploma thesis from Philipp Krause; <sup>c</sup>El-Gokha, A.; Koch, P.; unpublished results;

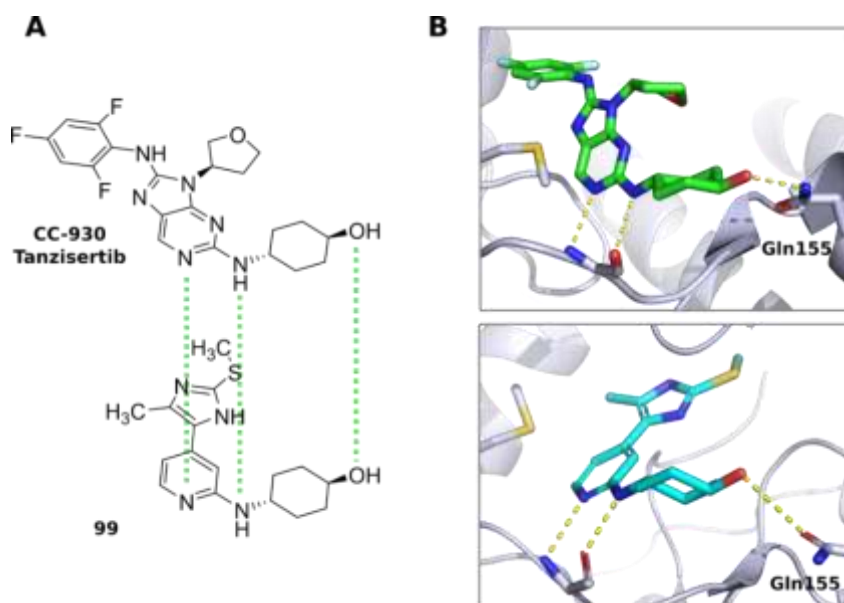
In addition, the substitution at the pyridine-C2 position was further explored through the insertion of different cycloalkyl moieties (Figure 3.22). Despite not producing any improvement on JNK3 inhibition, cycloaliphatic substituents showed an increase in activity alongside with the size of the cycle thus underlining the importance of hydrophobic interactions in this area.



**Figure 3.22.** Structure and biological activity of derivatives bearing different substituents at the pyridine-C2-N position; all compounds showed  $IC_{50}(p38\alpha_{MAPK}) > 10 \mu M$ .

As noticeable in the crystal structure of derivative **66** in complex with JNK3 (Figure 3.18), a potential chance to increase the inhibitory activity is represented by the targeting of Gln155, a residue located in the HR II of the enzyme and only 4 Å away from the N atom of the morpholine moiety. In order to achieve a sufficient flexibility to reach the Gln155, a *trans*-4-aminocyclohexanol and a *trans*-cyclohexane-1,4-diamine groups were installed at the pyridine-C2 position (compounds **99** and **100**, respectively). The former group was previously reported in potent p38 $\alpha$  MAPK inhibitors<sup>151</sup> and is present in the JNK clinical

candidate **CC-930/Tanzisertib** (Table 1.1) wherein its capability to target the Gln155 was confirmed by crystal structure (Figure 3.23). Due to the similarity between **Tanzisertib** and compound **99** at the hinge binding motif, the introduction of the same substituent was supposed to enable the formation of a hydrogen bond with the side chain of Gln155, as also predicted by docking studies (Figure 3.23).



**Figure 3.23.** Possible analogies in the binding mode of **CC-930/Tanzisertib** and compound **99**; A) structural similarity between **Tanzisertib** and compound **99**; B) comparison between crystal structure of **Tanzisertib** (green) in complex with JNK3 (PDB entry: 3TTI) and compound **99** (cyan) docked in the same enzyme (PDB entry: 6EKD); analogously to the **Tanzisertib**, compound **99** shows the possibility to target the Gln155 through the formation of a hydrogen bond.

Nevertheless, lower inhibitory activity of compound **99** in comparison with derivative **66** hints that an additional interaction might not be formed by the new substituent. Alternatively, the decreased inhibition might suggest once more the necessity of a phenyl ring in this region, rather than alkyl moieties. In order to increase the length of the substituent and improve its capability to target the side chain of Gln155, a series of amides was prepared starting both from compound **100** as well as from its aromatic analog **101** (Figure 3.22). In this way it would be possible to introduce a group able to act as both hydrogen donor and acceptor and to seek for additional interactions within the HR II. Unfortunately, none of the derivatives of this series were able to overcome the inhibitory activity of compound **66**, resulting in most cases even weaker than their amine precursors. An overall analysis of the biological activity within this series permits once again to assess the better suitability of the aromatic derivatives over their cycloaliphatic counterparts; furthermore, increasing the size of the substituent at this position was not beneficial, as the

small acetamido derivatives **102** and **106** represented the most active compounds of the group.

### 3.2.6. Further characterization of compound **66**

Since compound **66** represented the most potent and selective derivative synthesized in this work, a further characterization was carried out. At a first instance the *intra*-JNK selectivity was evaluated in order to understand whether such scaffold might possess selectivity towards one of the members of the JNK family. Results displayed in Table 3.10 only highlighted a slight selectivity of derivative **66** over the JNK2 isoform, although the three kinases showed similar IC<sub>50</sub> values.

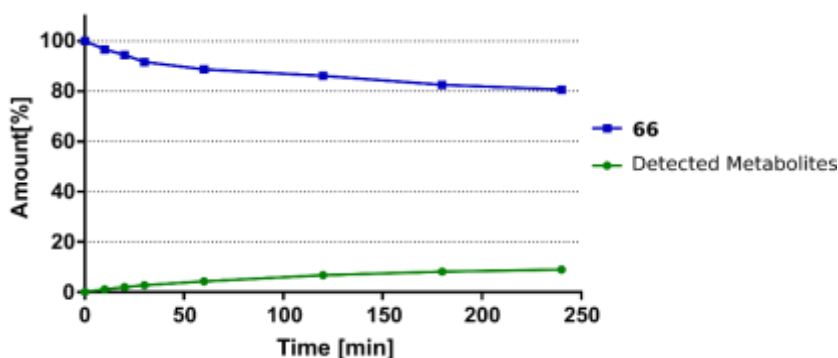
**Table 3.10.** Inhibitory activity of compound **66** on the three JNK isoforms

IC <sub>50</sub> [nM]		
JNK1	JNK2	JNK3
119	468	184

Compounds were tested by Reaction Biology corporation (Malvern, PA, USA) using a radiometric assay.

In order to spot potential liabilities to be addressed in a following optimization process compound **66** was also evaluated for its metabolic stability as well for non-specific interactions with potential off-targets.

Initially, the metabolic stability was evaluated in *in vitro* experiments performed by incubating the compound with human liver microsomes (HLM). A major drawback of 2-alkylsulfanyl derivatives is represented by their intense metabolism, mostly consisting in the oxidation of the thioether group to the corresponding sulfoxide moiety.<sup>175</sup>



**Figure 3.23.** Plotted results of metabolic stability assays on HLM.

Experiments performed on compound **66** revealed instead a relative stability, leaving approximately 80% of the unmodified product after 4 h incubation (Figure 3.24).

Compound **66** was additionally tested for its capability to interact with cytochrome P450 (CYP450) enzymes as well with human ether-à-go-go related gene (hERG) channels, both representing common non-specific off-targets of different drugs. In particular, CYP450 inhibition constitutes a prevalent liability of pyridinylimidazole scaffolds, mainly depending on their aptitude to coordinate the prosthetic haem iron of these enzymes.<sup>165,176</sup>

Table 3.11. inhibition of hERG channels and CYP450 enzymes by compound **66**

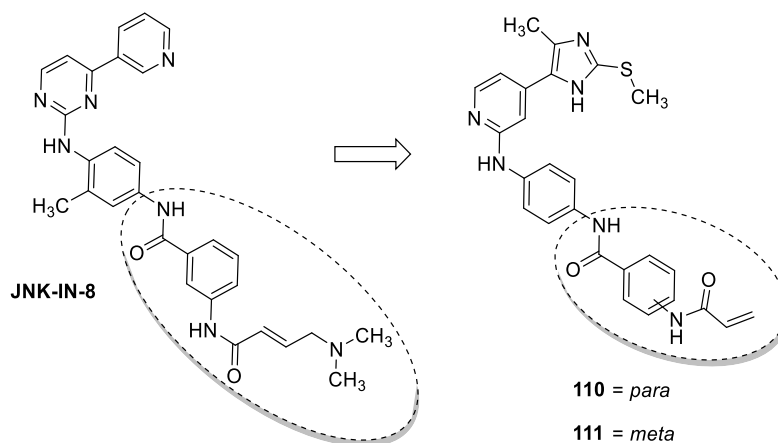
hERG inhibition [% inhibition at 10 $\mu$ M]	CYP450 inhibition [% inhibition at 10 $\mu$ M]				
	1A9	2C9	2C19	2D6	3A4
38.8	51.5	53.9	35.6	19.0	75.1

Data presented in Table 3.11 seem to display a reduced inhibition of four out of five tested isoenzymes. Nevertheless, the elevated inhibition of the most prominent isoform 3A4 represents a non-negligible shortcoming which would need to be resolved in following optimization strategies. On the other side, compound **66** displayed low interaction with the hERG channels, with less than 40% inhibition at 10  $\mu$ M.

### 3.2.7. Application of a covalent inhibition strategy on compound **66**

Due to the high selectivity of derivative **66** over the p38 $\alpha$  MAPK, the 4-methyl-substituted imidazole scaffold was selected as a starting point for the synthesis of irreversible inhibitors. As already mentioned in section 1.1.2. such inhibitors are composed by a core structure binding reversibly to the ATP cleft and by a mildly electrophilic moiety targeting a non-conserved Cys residue in the proximity of the binding site. In particular, as noticeable from the sequence alignment illustrated in Figure 1.7, a Cys residue located in the JNK3 HR II (Cys154, JNK3 numbering) is not conserved in the binding site of p38 $\alpha$  MAPK thus resulting suitable to be addressed by the electrophilic warhead. A similar strategy was previously adopted by Zhang and coworkers on a 2-amino-4-pyridinylpyrimidine scaffold giving rise to the potent high quality kinase probe **JNK-IN-8**<sup>169</sup> (Figure 3.24). In such approach an acrylamide-based warhead was linked to the main scaffold through a spacer represented by two aromatic rings connected by an amide bond.





**Figure 3.24.** Covalent inhibition strategy on the pyridinylimidazole scaffold based on high quality probe JNK-IN-8.

Due to the resemblance between the binding mode of **JNK-IN-8** and compound **66**, mainly centered on the bidentate hydrogen bond with the backbone of Met149, an analogous combination of spacer/warhead was installed on the pyridinylimidazole scaffold of the latter inhibitor. Since the linker needs to comprise the optimal length in order to position the reactive moiety in proximity of the targeted Cys residue, both the *meta*- and *para*-substituted derivatives were synthesized (compounds **110** and **111**, respectively).

**Table 3.12.** Structure and biological activities of compounds **110-112**.

Cpd	R	IC <sub>50</sub> ± SD [μM] <sup>a</sup>		
		JNK3 <sup>b</sup>	p38α MAPK <sup>c</sup>	
<b>110<sup>d</sup></b>	<i>meta</i>		0.002 ± 0.0003	1.952 ± 0.062
<b>110<sup>d</sup></b>	<i>para</i>		0.200 ± 0.021	5.920 ± 0.107
<b>112</b>	<i>meta</i>		0.253 ± 0.015	>10

<sup>a</sup>IC<sub>50</sub> values are the mean of three independent experiments; <sup>b</sup>incubation time 50 min; <sup>c</sup>incubation time 60 min; <sup>d</sup>compound synthesized by Dr. Ahmed El-Gokha.

Results displayed in Table 3.12 demonstrate the success of the covalent inhibition strategy transferred to the pyridinylimidazole scaffold. More closely, the insertion of the covalent warhead at the *meta* position of the phenyl ring (compound **110**) permitted to reach an  $IC_{50}$  value in the low single digit nM range while maintaining the selectivity over the p38 $\alpha$  MAPK. Such inhibitory activity was more than 100-fold higher than the one exhibited by the *para*-substituted derivative **111**, proving the latter substitution pattern not to be optimal to target the Cys154. In addition, the significantly higher  $IC_{50}$  value of compound **112**, representing the saturated analog of inhibitor **110**, permitted to attribute the high inhibitory activity of the latter to the formation of the covalent bond. A further demonstration of the irreversible targeting of Cys154 could be provided by mass shifts experiments performed by liquid chromatography-mass spectroscopy (LC-MS) analysis of the JNK3 after incubation with the inhibitor. Prior to the measurement, a declustering potential was applied to the sample in order to disrupt weak electrostatic interactions. In case of compound **110** a mass shift corresponding to the molecular weight of the inhibitor could be detected. Conversely, the same result was not obtained when performing the LC-MS experiment on the saturated analog **112**, once more confirming the covalent mechanism of action of derivative **110**. Additionally, the Cys154 was identified as the amino acid targeted by the irreversible inhibitor, since incubation of compound **110** with a JNK3 mutant wherein Cys154 was replaced by Ala did not result in an increase in molecular weight.

# Experimental section

The following section includes the detailed procedures for the preparation of those compounds presented in the thesis work which were not included in any of the accepted publications or in the submitted manuscript.

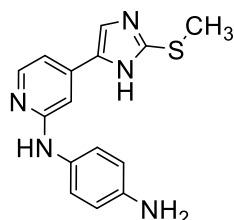
## General

All reagents and solvents were of commercial quality and utilized without further purification. Yields were calculated on the pure product and were not optimized. Thin layer chromatography (TLC) reaction controls were performed for all reactions using fluorescent silica gel 60 F<sub>254</sub> plates (Merck) and visualized under natural light and UV illumination at 254 and 366 nm. The purity of all tested compounds are > 95% as determined via reverse phase high performance liquid chromatography (HPLC) using one of the 2 following methods. For Method A the instrument used was a Hewlett Packard HP 1090 Series II LC equipped with a UV diode array detector (DAD, detection at 230 nm and 254 nm). The chromatographic separation was performed on a Phenomenex Luna 5u C8 column (150 mm x 4.6 mm, 5 μm) at 35 °C oven temperature. The injection volume was 5 μL and the flow 1.5 mL / min using the following gradient: 0.01 M KH<sub>2</sub>PO<sub>4</sub>, pH 2.3 (solvent A), MeOH (solvent B), 40% B to 85% B in 8 min; 85% B for 5 min; 85% to 40% B in 1 min; 40% B for 2 min; stop time 16 min. Alternatively, for Method B, Agilent 1100 Series HPLC system was used, equipped with a UV DAD (detection at 218 nm, 254 nm and 280 nm). The chromatographic separation was performed on a XBridge™ C18 column (150 mm x 4.6 mm, 5 μm) at 30 °C oven temperature. The injection volume was 10 μL and the flow 1.5 mL / min using the following gradient: 0.01 M KH<sub>2</sub>PO<sub>4</sub>, pH 2.3 (solvent A), MeOH (solvent B), 45% B to 85% B in 9 min; 85% B for 6 min; stop time 16 min. Column chromatography was performed on Davisil LC60A 20 - 45 μm silica from Grace Davison and Geduran Si60 63-200 μm silica from Merck for the pre-column using an Interchim PuriFlash 430 automated flash chromatography system. Nuclear magnetic resonance (NMR) spectra were measured on a Bruker ARX NMR spectrometer at 250 MHz or on a Bruker Avance III HD NMR spectrometer at 300 MHz in the Organic Chemistry Institute, Eberhard Karls Universität Tübingen or on a Bruker Avance NMR spectrometer at 400 MHz in the Institute of

Pharmaceutical Sciences, Eberhard Karls Universität Tübingen. Chemical shifts are reported in parts per million (ppm) relative to tetramethylsilane. All spectra were calibrated against the (residual proton) peak of the deuterated solvent used. Mass spectra were performed on an Advion Expression S electrospray ionization mass spectrometer (ESI-MS) with TLC interface in the Institute of Pharmaceutical Sciences, Eberhard Karls Universität Tübingen.

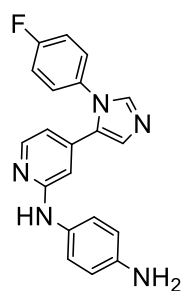
## Detailed procedures

### *N*<sup>1</sup>-(4-(2-(Methylthio)-1*H*-imidazol-5-yl)pyridin-2-yl)benzene-1,4-diamine (5)



In a pressure vial 2-chloro-4-(2-(methylthio)-1*H*-imidazol-5-yl)pyridine (248 mg, 1.1 mmol, for the synthesis of 2-chloro-4-(2-(methylthio)-1*H*-imidazol-5-yl)pyridine see **Publication VII**) and *p*-phenyldiamine (154 mg, 1.5 mmol) were dissolved in *n*-butanol and after that 1.25 M HCl in EtOH (880  $\mu$ L, 1.1 mmol) was added in one portion. The vial was tightly closed and the reaction was heated at 180 °C and stirred for 12 h. The solvent was evaporated at reduced pressure and the residue was purified twice by flash column chromatography (SiO<sub>2</sub>, DCM/EtOH gradient elution from 97:03 to 50:50) and (SiO<sub>2</sub>, DCM/EtOH 85:15) obtaining 165 mg of the desired product (50% yield); <sup>1</sup>H NMR (400 MHz, DMSO-*d*<sub>6</sub>)  $\delta$  2.58 (s, 3H), 4.75 (br. s, 2H), 6.55 (d, *J* = 8.3 Hz, 2H), 6.90 (d, *J* = 4.5 Hz, 1H), 7.08 (br. s, 1H), 7.25 (d, *J* = 7.8 Hz, 2H), 7.72 (br. s, 1H), 7.97 (d, *J* = 5.1 Hz, 1H), 8.43 (s, 1H), 12.46 (br. s, 1H); <sup>13</sup>C NMR (101 MHz, DMSO-*d*<sub>6</sub>)  $\delta$  15.3, 103.2, 108.9, 114.3, 115.1, 116.7, 121.5, 131.0, 139.4, 142.0, 143.2, 147.5, 157.6; ESI-MS: (*m/z*) 296.2 [M-H]<sup>-</sup>, 298.2 [M+H]<sup>+</sup>; HPLC (B): *t*<sub>r</sub> = 1.860 min.

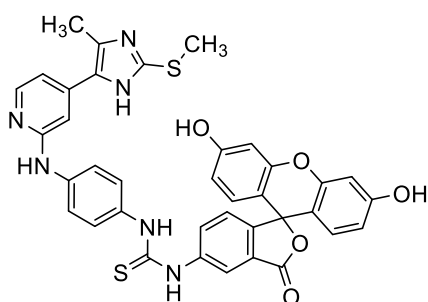
### *N*<sup>1</sup>-(4-(1-(4-Fluorophenyl)-1*H*-imidazol-5-yl)pyridin-2-yl)benzene-1,4-diamine (7)



In a pressure vial 2-bromo-4-(1-(4-fluorophenyl)-1*H*-imidazol-5-yl)pyridine (**27**, 300 mg, 0.94 mmol, for the synthesis of compound **27** see **Publication VII**) and *p*-phenyldiamine (509 mg, 4.71 mmol) were suspended in *n*-butanol (3 mL) and after that 1.25 M HCl in EtOH was added (752  $\mu$ L, 0.94 mmol). After tightly closing the vial the reaction was heated at 180 °C and stirred overnight (18 h); After evaporating the solvent at reduced pressure the residue was purified by flash column chromatography (SiO<sub>2</sub>, DCM/EtOH gradient elution from 100:0 to 95:05) giving 260 mg of the desired product (80% yield); <sup>1</sup>H NMR (250 MHz, DMSO-*d*<sub>6</sub>)  $\delta$  4.78 (br. s, 2H), 6.27 (s,

1H), 6.37 (dd,  $J = 5.4, 1.2$  Hz, 1H), 6.45 (d,  $J = 8.5$  Hz, 2H), 6.90 (d,  $J = 8.5$  Hz, 2H), 7.31 - 7.48 (m, 5H), 7.93 (d,  $J = 5.1$  Hz, 1H), 7.96 (d,  $J = 1.7$  Hz, 1H), 8.35 (s, 1H);  $^{13}\text{C}$  NMR (101 MHz, DMSO- $d_6$ )  $\delta$  105.4, 111.2, 114.2, 116.5 (d,  $J = 21.9$  Hz), 122.0, 127.8 (d,  $J = 8.8$  Hz), 129.7, 129.8, 130.7, 132.5, 137.2, 140.7, 143.9, 148.0, 157.3, 161.5 (d,  $J = 245.9$  Hz); ESI-MS: ( $m/z$ ) 344.2 [M-H] $^-$ , 346.1 [M+H] $^+$ ; HPLC (A):  $t_r = 2.487$  min.

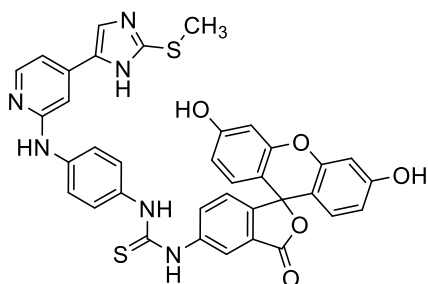
**1-(3',6'-Dihydroxy-3-oxo-3H-spiro[isobenzofuran-1,9'-xanthen]-5-yl)-3-((4-(4-methyl-2-(methylthio)-1H-imidazol-5-yl)pyridin-2-yl)amino)phenyl)thiourea (8)**



Compound **4** (100 mg, 0.32 mmol, for the synthesis of compound **4** see **Publication IV**) was dissolved in acetone ( $\approx 20$  mL) and after that fluorescein-isothiocyanate isomer 5'(6') (188 mg, 0.48 mmol) was added and the mixture was stirred for 24 h protected from light. After removing the solvent at reduced pressure the residue was purified twice by flash column

chromatography (SiO $_2$ , DCM/MeOH gradient elution from 95:05 to 90:10) and (SiO $_2$ , DCM/EtOH gradient elution from 95:05 to 50:50) obtaining 101 mg of the desired product (45% yield);  $^1\text{H}$  NMR (250 MHz, DMSO- $d_6$ )  $\delta$  2.43 (s, 3H), 2.56 (s, 3H), 6.55 - 6.74 (m, 6H), 7.00 (d,  $J = 4.6$  Hz, 1H), 7.12 - 7.26 (m, 2H), 7.38 (d,  $J = 8.3$  Hz, 2H), 7.71 (d,  $J = 8.5$  Hz, 2H), 7.91 (d,  $J = 8.1$  Hz, 1H), 8.09 (d,  $J = 5.4$  Hz, 1H), 8.39 (s, 1H), 9.14 (br. s., 1H), 10.25 (br. s., 2H), 10.49 (br. s., 1H), 10.86 (br. s., 1H), 12.41 (br. s., 1H);  $^{13}\text{C}$  NMR (75 MHz, DMSO- $d_6$ )  $\delta$  11.5, 15.5, 52.1, 102.3, 106.2, 109.8, 111.3, 112.9, 116.9, 117.7, 124.0, 124.6, 127.4, 129.1, 129.6, 131.4, 134.0, 135.6, 139.2, 139.4, 141.7, 143.2, 147.2, 152.0, 156.3, 160.0, 168.7, 179.3; ESI-MS: ( $m/z$ ) 699.3 [M-H] $^-$ ; HPLC (B):  $t_r = 7.514$  min.

**1-(3',6'-Dihydroxy-3-oxo-3H-spiro[isobenzofuran-1,9'-xanthen]-5-yl)-3-((4-(2-(methylthio)-1H-imidazol-5-yl)pyridin-2-yl)amino)phenyl)thiourea (9)**

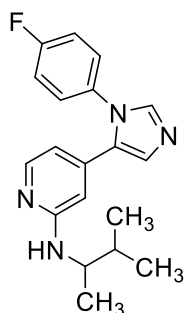


The title compound was synthesized following the same procedure as compound **8** starting from compound **5** (60 mg, 0.20 mmol) and fluorescein-isothiocyanate isomer 5'(6') (118 mg, 0.30 mmol) (8 h). The crude product was purified by flash column chromatography (DCM/EtOH gradient elution from 95:05 to 70:30) obtaining 102 mg of the desired product;

$^1\text{H}$  NMR (250 MHz, DMSO- $d_6$ )  $\delta$  2.59 (s, 3H), 6.55 - 6.73 (m, 6H), 7.04 (d,  $J = 5.1$  Hz, 1H), 7.19 (d,  $J = 8.3$  Hz, 1H), 7.27 (br. s, 1H), 7.34 (d,  $J = 8.8$  Hz, 2H), 7.70 (d,  $J = 8.7$  Hz, 2H), 7.80

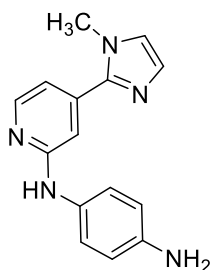
(br. s, 1H), 7.86 (dd,  $J = 8.1, 1.8$  Hz, 1H), 8.07 (d,  $J = 5.3$  Hz, 1H), 8.29 (d,  $J = 1.4$  Hz, 1H), 9.13 (s, 1H), 10.00 - 10.45 (m, 4H), 12.51 (br. s, 1H);  $^{13}\text{C}$  NMR (75 MHz,  $\text{DMSO-}d_6$ )  $\delta$  15.2, 48.6, 102.3, 105.0, 109.8, 110.3, 112.8, 117.0, 117.3, 117.9, 124.0, 124.8, 126.6, 129.1, 130.0, 131.3, 139.1, 139.4, 141.6, 142.2, 147.3, 152.0, 156.5, 159.8, 168.6, 179.4; ESI-MS: ( $m/z$ ) 685.3 [M-H] $^-$ ; HPLC (B):  $t_r = 7.292$  min.

#### 4-(1-(4-Fluorophenyl)-1H-imidazol-5-yl)-N-(3-methylbutan-2-yl)pyridin-2-amine (85)



In a pressure vial 2-bromo-4-(1-(4-fluorophenyl)-1H-imidazol-5-yl)pyridine (**27**, 100 mg, 0.31 mmol, for the synthesis of compound **27** see **Publication VII**) was suspended in 3-methylbutan-2-amine (700  $\mu\text{L}$ , 6.2 mmol) and after closing the vial the reaction mixture was heated at 180  $^\circ\text{C}$  for 96 h;  $\text{H}_2\text{O}$  was added and the aqueous layer was then extracted three times with EtOAc. The combined organic layers were then washed with  $\text{H}_2\text{O}$  and NaCl saturated solution, dried over anhydrous  $\text{Na}_2\text{SO}_4$  and concentrated at reduced pressure. The residue was then purified by flash column chromatography ( $\text{SiO}_2$ , DCM/EtOH gradient elution from 100:0 to 95:05) giving 42 mg of the desired product (42% yield);  $^1\text{H}$  NMR (250 MHz,  $\text{DMSO-}d_6$ )  $\delta$  0.81 (t,  $J = 6.3$  Hz, 6H), 0.95 (d,  $J = 6.6$  Hz, 3H), 1.56 - 1.75 (m, 1H), 3.56 - 3.64 (m, 1H, partially overlapping with the  $\text{H}_2\text{O}$  signal), 6.11 (d,  $J = 5.1$  Hz, 1H), 6.18 (s, 1H), 6.26 (d,  $J = 8.3$  Hz, 1H), 7.25 - 7.48 (m, 5H), 7.79 (d,  $J = 5.1$  Hz, 1H), 7.95 (s, 1H);  $^{13}\text{C}$  NMR (101 MHz,  $\text{DMSO-}d_6$ )  $\delta$  16.4, 17.7, 19.2, 31.8, 50.7, 105.3, 109.5, 116.4 (d,  $J = 22.7$  Hz), 127.9 (d,  $J = 8.8$  Hz), 129.4, 131.0, 132.6, 136.8, 140.5, 147.8, 158.7, 161.5 (d,  $J = 245.9$  Hz); ESI-MS: ( $m/z$ ) 323.2 [M-H] $^-$ , 325.4 [M+H] $^+$ ; HPLC (A):  $t_r = 4.975$  min.

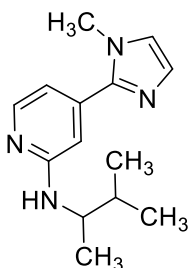
#### *N*-(4-(1-Methyl-1H-imidazol-2-yl)pyridin-2-yl)benzene-1,4-diamine (87)



In a pressure vial 2-chloro-4-(1-methyl-1H-imidazol-2-yl)pyridine (**64**, 200 mg, 1.0 mmol, for the synthesis of compound **64** see **Publication VII**) and *p*-phenylenediamine (168 mg, 1.5 mmol) were suspended in *n*-butanol and then 1.25 M HCl in EtOH (826  $\mu\text{L}$ , 1.0 mmol) was added and the close vial was heated at 180  $^\circ\text{C}$  and stirred for 17 h. After evaporating the solvent at reduced pressure the crude residue was purified by flash column chromatography ( $\text{SiO}_2$ , DCM/EtOH gradient elution from 100:0 to 80:20) obtaining 66 mg of the desired product (24% yield);  $^1\text{H}$  NMR (400 MHz,  $\text{DMSO-}d_6$ )  $\delta$  3.79 (s, 3H), 4.81 (br. s, 2H), 6.54 (d,  $J = 8.3$  Hz, 2H), 6.91 (d,  $J = 4.5$  Hz, 1H), 7.00 (s, 1H), 6.97 (s, 1H), 7.22 (d,  $J = 8.3$  Hz, 2H), 7.29 (s, 1H), 8.09 (d,  $J = 5.3$  Hz, 1H), 8.56 (s, 1H);  $^{13}\text{C}$  NMR (101 MHz,  $\text{DMSO-}$

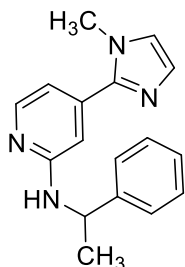
$d_6$ )  $\delta$  34.6, 107.1, 111.3, 114.6, 121.6, 124.4, 127.8, 130.8, 138.3, 142.8, 144.5, 147.6, 157.3; FAB-MS ( $m/z$ ) 266.3 [M+H]<sup>+</sup>; HPLC (B):  $t_r$  = 1.067 min.

#### 4-(1-Methyl-1H-imidazol-2-yl)-N-(3-methylbutan-2-yl)pyridin-2-amine (88)



The title compound was synthesized following the same procedure used for compound **85** starting from 2-chloro-4-(1-methyl-1H-imidazol-2-yl)pyridine (**64**, 65 mg, 0.33 mmol, for the synthesis of compound **64** see **Publication VII**) and 3-methylbutan-2-amine (773  $\mu$ L, 6.71 mmol) (48 h). After the work up the residue was purified by flash column chromatography (SiO<sub>2</sub>, DCM/EtOH 97:03) giving 40 mg of the desired product (48% yield); <sup>1</sup>H NMR (400 MHz, DMSO-*d*<sub>6</sub>)  $\delta$  0.91 (d,  $J$  = 6.8 Hz, 3H), 0.88 (d,  $J$  = 6.8 Hz, 3H), 1.05 (d,  $J$  = 6.6 Hz, 3H), 1.72 - 1.87 (m, 1H), 3.77 (s, 3H), 3.82 - 3.93 (m, 1H), 6.41 (d,  $J$  = 8.1 Hz, 1H), 6.73 (d,  $J$  = 5.3 Hz, 1H), 6.81 (s, 1H), 6.98 (s, 1H), 7.26 (s, 1H), 7.99 (d,  $J$  = 5.3 Hz, 1H); <sup>13</sup>C NMR (101 MHz, DMSO-*d*<sub>6</sub>)  $\delta$  16.7, 18.0, 19.2, 32.0, 34.5, 50.4, 106.8, 109.8, 124.1, 127.8, 138.1, 144.9, 147.7, 158.9; FAB-MS ( $m/z$ ) 245.3 [M+H]<sup>+</sup>; HPLC (A):  $t_r$  = 2.534 min.

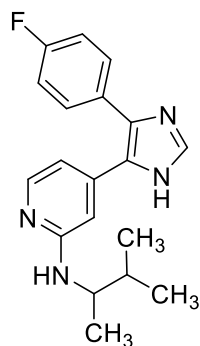
#### 4-(1-Methyl-1H-imidazol-2-yl)-N-(1-phenylethyl)pyridin-2-amine (89)



The title compound was synthesized following the same procedure used for compound **85** starting from 2-chloro-4-(1-methyl-1H-imidazol-2-yl)pyridine (**64**, 200 mg, 1.0 mmol, for the synthesis of compound **64** see **Publication VII**) and 1-phenylethan-1-amine (2.63 mL, 20.65 mmol) (72 h). After the work up the residue was purified by flash column chromatography (SiO<sub>2</sub>, DCM/EtOH 97:03) giving 130 mg of the desired product (45% yield); <sup>1</sup>H NMR (400 MHz, DMSO-*d*<sub>6</sub>)  $\delta$  1.45 (d,  $J$  = 6.8 Hz, 3H), 3.70 (s, 3H), 4.96 - 5.12 (m, 1H), 6.68 - 6.85 (m, 2H), 6.99 (s, 1H), 7.08 - 7.22 (m, 2H), 7.23 - 7.34 (m, 3H), 7.35 - 7.45 (m, 2H), 7.91 - 8.04 (m, 1H); <sup>13</sup>C NMR (101 MHz, DMSO-*d*<sub>6</sub>)  $\delta$  23.6, 34.4, 49.8, 106.5, 110.5, 124.2, 125.9, 126.3, 127.8, 128.1, 138.2, 144.6, 145.9, 147.8, 158.3; FAB-MS ( $m/z$ ) 279.3 [M+H]<sup>+</sup>; HPLC (A):  $t_r$  = 3.293 min.

#### 4-(4-(4-Fluorophenyl)-1H-imidazol-5-yl)-N-(3-methylbutan-2-yl)pyridin-2-amine (90)

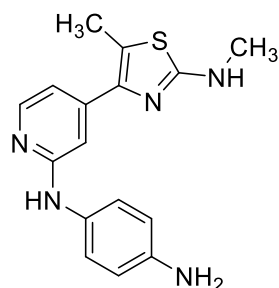
The title compound was synthesized following the same procedure used for compound **85** starting from 2-fluoro-4-(4-(4-fluorophenyl)-1H-imidazol-5-yl)pyridine (70 mg, 0.27 mmol, for the synthesis of 2-fluoro-4-(4-(4-fluorophenyl)-1H-imidazol-5-yl)pyridine see



3.376 min.

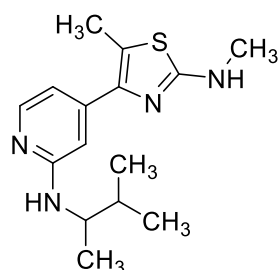
**Publication I**) and 3-methylbutan-2-amine (626  $\mu\text{L}$ , 5.44 mmol) (48 h). After the work up, the residue was purified by flash column chromatography ( $\text{SiO}_2$ , DCM/EtOH gradient elution from 95:05 to 85:15) giving 47 mg of the desired product (40% yield);  $^1\text{H}$  NMR (250 MHz,  $\text{DMSO}-d_6$ )  $\delta$  0.89 - 1.14 (m, 6H), 1.20 (d,  $J = 6.6$  Hz, 3H), 1.80 - 2.03 (m, 1H), 2.70 (s, 3H), 3.88 (d,  $J = 6.3$  Hz, 1H), 6.48 (br. s, 1H), 6.61 (d,  $J = 5.1$  Hz, 1H), 6.78 (br. s, 1H), 7.29 - 7.54 (m, 2H), 7.61 - 7.79 (m, 2H), 7.91 - 8.13 (m, 2H), 12.77 (br. s, 1H); ESI-MS: ( $m/z$ ) 323.3  $[\text{M}-\text{H}]^-$ , 325.3  $[\text{M}+\text{H}]^+$ ; HPLC (A):  $t_r =$

### *N*<sup>1</sup>-(4-(5-Methyl-2-(methylamino)thiazol-4-yl)pyridin-2-yl)benzene-1,4-diamine (93)



The title compound was synthesized following the same procedure of compound **7** starting from 4-(2-chloropyridin-4-yl)-*N*,5-dimethylthiazol-2-amine (200 mg, 0.83 mmol, synthesis of 4-(2-chloropyridin-4-yl)-*N*,5-dimethylthiazol-2-amine can be found in **Publication VII**), *p*-phenyldiamine (451 mg, 4.17 mmol), and 1.25 M HCl in EtOH (664  $\mu\text{L}$ , 0.83 mmol) (18 h). After evaporating the solvent at reduced pressure the residue was purified by flash column chromatography ( $\text{SiO}_2$ , DCM/EtOH gradient elution from 100:0 to 90:10) giving 95 mg of the desired product (27% yield);  $^1\text{H}$  NMR (250 MHz,  $\text{DMSO}-d_6$ )  $\delta$  2.37 (s, 3H), 2.80 (d,  $J = 4.6$  Hz, 3H), 4.73 (br. s, 2H), 6.53 (d,  $J = 8.8$  Hz, 2H), 6.80 (dd,  $J = 5.4, 1.2$  Hz, 1H), 6.90 (s, 1H), 7.22 (d,  $J = 8.5$  Hz, 2H), 7.33 (q,  $J = 4.7$  Hz, 1H), 8.02 (d,  $J = 5.4$  Hz, 1H), 8.43 (s, 1H);  $^{13}\text{C}$  NMR (101 MHz,  $\text{DMSO}-d_6$ )  $\delta$  12.2, 30.7, 107.1, 112.0, 114.2, 117.1, 121.5, 130.8, 143.2, 143.4, 143.5, 147.3, 157.4, 165.4; ESI-MS: ( $m/z$ ) 310.2  $[\text{M}-\text{H}]^-$ , 312.2  $[\text{M}+\text{H}]^+$ ; HPLC (A):  $t_r = 2.625$  min.

### *N*,5-Dimethyl-4-(2-((3-methylbutan-2-yl)amino)pyridin-4-yl)thiazol-2-amine (94)



The title compound was synthesized following the same procedure used for compound **85** starting from 4-(2-chloropyridin-4-yl)-*N*,5-dimethylthiazol-2-amine (135 mg, 0.56 mmol, the synthesis of 4-(2-chloropyridin-4-yl)-*N*,5-dimethylthiazol-2-amine can be found in **Publication I**) and 3-methylbutan-2-amine (1.29 mL, 11.3 mmol) (42 h). After the work up the residue was purified by flash column chromatography ( $\text{SiO}_2$ , DCM/EtOH gradient elution from 100:0 to 90:10) giving 47 mg of the desired product (30% yield);  $^1\text{H}$  NMR (250 MHz,  $\text{DMSO}-d_6$ )  $\delta$  0.91 - 1.04 (m, 6H), 1.12 (d,  $J = 6.6$  Hz, 3H), 1.78 - 1.96 (m, 1H), 2.44 (s, 3H), 2.89 (d,  $J = 4.9$  Hz, 3H), 3.82 - 4.03 (m,



1H), 6.38 (d,  $J = 8.3$  Hz, 1H), 6.71 (dd,  $J = 5.4, 1.2$  Hz, 1H), 6.81 (br. s, 1H), 7.37 (q,  $J = 4.6$  Hz, 1H), 7.99 (d,  $J = 5.4$  Hz, 1H);  $^{13}\text{C}$  NMR (101 MHz, DMSO- $d_6$ )  $\delta$  12.2, 16.7, 17.9, 19.2, 30.6, 32.0, 50.3, 107.0, 110.4, 116.6, 142.8, 143.8, 147.1, 158.9, 165.2; ESI-MS: ( $m/z$ ) 289.2  $[\text{M-H}]^-$ , 291.2  $[\text{M+H}]^+$ ; HPLC (B):  $t_r = 4.423$  min.



# Bibliography

1. Cohen, P. The origins of protein phosphorylation. *Nat. Cell. Biol.* **2002**, *4*, E127-30.
2. Fabbro, D.; Cowan-Jacob, S. W.; Moebitz, H. Ten things you should know about protein kinases: IUPHAR Review 14. *Br. J. Pharmacol.* **2015**, *172*, 2675-700.
3. Roskoski, R., Jr. A historical overview of protein kinases and their targeted small molecule inhibitors. *Pharmacol. Res.* **2015**, *100*, 1-23.
4. Hunter, T. Protein-Kinases and Phosphatases - the Yin and Yang of Protein-Phosphorylation and Signaling. *Cell* **1995**, *80*, 225-236.
5. Walsh, C. T.; Garneau-Tsodikova, S.; Gatto, G. J., Jr. Protein posttranslational modifications: the chemistry of proteome diversifications. *Angew. Chem. Int. Ed. Engl.* **2005**, *44*, 7342-72.
6. Khoury, G. A.; Baliban, R. C.; Floudas, C. A. Proteome-wide post-translational modification statistics: frequency analysis and curation of the swiss-prot database. *Sci. Rep.* **2011**, *1*, 90.
7. Vlastaridis, P.; Kyriakidou, P.; Chaliotis, A.; Van de Peer, Y.; Oliver, S. G.; Amoutzias, G. D. Estimating the total number of phosphoproteins and phosphorylation sites in eukaryotic proteomes. *Gigascience* **2017**, *6*, 1-11.
8. Ubersax, J. A.; Ferrell, J. E., Jr. Mechanisms of specificity in protein phosphorylation. *Nat. Rev. Mol. Cell Biol.* **2007**, *8*, 530-41.
9. Adams, J. A. Kinetic and catalytic mechanisms of protein kinases. *Chem. Rev.* **2001**, *101*, 2271-90.
10. Ferrell, J. E., Jr. What do scaffold proteins really do? *Sci. STKE* **2000**, *2000*, pe1.
11. Day, E. K.; Sosale, N. G.; Lazzara, M. J. Cell signaling regulation by protein phosphorylation: a multivariate, heterogeneous, and context-dependent process. *Curr. Opin. Biotechnol.* **2016**, *40*, 185-192.
12. Hunter, T. Signaling - 2000 and beyond. *Cell* **2000**, *100*, 113-127.
13. Manning, G.; Plowman, G. D.; Hunter, T.; Sudarsanam, S. Evolution of protein kinase signaling from yeast to man. *Trends Biochem. Sci.* **2002**, *27*, 514-20.
14. Schenk, P. W.; Snaar-Jagalska, B. E. Signal perception and transduction: the role of protein kinases. *Biochim. Biophys. Acta, Mol. Cell Res.* **1999**, *1449*, 1-24.
15. Cohen, P. The regulation of protein function by multisite phosphorylation - a 25 year update. *Trends Biochem. Sci.* **2000**, *25*, 596-601.

16. Cohen, P. The role of protein phosphorylation in human health and disease. The Sir Hans Krebs Medal Lecture. *Eur. J. Biochem.* **2001**, *268*, 5001-10.
17. Cohen, P. Protein kinases--the major drug targets of the twenty-first century? *Nat. Rev. Drug Discov.* **2002**, *1*, 309-15.
18. Hanks, S. K.; Hunter, T. Protein kinases 6. The eukaryotic protein kinase superfamily: kinase (catalytic) domain structure and classification. *FASEB J.* **1995**, *9*, 576-96.
19. Hanks, S. K. Genomic analysis of the eukaryotic protein kinase superfamily: a perspective. *Genome Biol.* **2003**, *4*, 111.
20. Kostich, M.; English, J.; Madison, V.; Gheyas, F.; Wang, L. Q.; Qiu, P.; Greene, J.; Laz, T. M. Human members of the eukaryotic protein kinase family. *Genome Biol.* **2002**, *3*.
21. Manning, G.; Whyte, D. B.; Martinez, R.; Hunter, T.; Sudarsanam, S. The protein kinase complement of the human genome. *Science* **2002**, *298*, 1912-+.
22. Hanks, S. K.; Quinn, A. M.; Hunter, T. The Protein-Kinase Family - Conserved Features and Deduced Phylogeny of the Catalytic Domains. *Science* **1988**, *241*, 42-52.
23. Eid, S.; Turk, S.; Volkamer, A.; Rippmann, F.; Fulle, S. KinMap: a web-based tool for interactive navigation through human kinome data. *Bmc Bioinformatics* **2017**, *18*.
24. Bossemeyer, D. Protein-Kinases - Structure and Function. *Febs Lett.* **1995**, *369*, 57-61.
25. Cowan-Jacob, S. W. Structural biology of protein tyrosine kinases. *Cell. Mol. Life Sci.* **2006**, *63*, 2608-2625.
26. Roskoski, R., Jr. Classification of small molecule protein kinase inhibitors based upon the structures of their drug-enzyme complexes. *Pharmacol. Res.* **2016**, *103*, 26-48.
27. Taylor, S. S.; Kornev, A. P. Protein kinases: evolution of dynamic regulatory proteins. *Trends Biochem. Sci.* **2011**, *36*, 65-77.
28. Johnson, L. N.; Lowe, E. D.; Noble, M. E. M.; Owen, D. J. The structural basis for substrate recognition and control by protein kinases. *Febs Lett.* **1998**, *430*, 1-11.
29. Johnson, L. N.; Noble, M. E. M.; Owen, D. J. Active and inactive protein kinases: Structural basis for regulation. *Cell* **1996**, *85*, 149-158.
30. Nolen, B.; Taylor, S.; Ghosh, G. Regulation of protein kinases: Controlling activity through activation segment conformation. *Molecular Cell* **2004**, *15*, 661-675.
31. Meharena, H. S.; Chang, P.; Keshwani, M. M.; Oruganty, K.; Nene, A. K.; Kannan, N.; Taylor, S. S.; Kornev, A. P. Deciphering the Structural Basis of Eukaryotic Protein Kinase Regulation. *Plos Biology* **2013**, *11*.
32. Taylor, S. S.; Keshwani, M. M.; Steichen, J. M.; Kornev, A. P. Evolution of the eukaryotic protein kinases as dynamic molecular switches. *Philos. Trans. R. Soc., B* **2012**, *367*, 2517-2528.

33. Kornev, A. P.; Taylor, S. S.; Ten Eyck, L. F. A helix scaffold for the assembly of active protein kinases. *Proc. Natl. Acad. Sci. U.S.A.* **2008**, *105*, 14377-14382.
34. Huse, M.; Kuriyan, J. The conformational plasticity of protein kinases. *Cell* **2002**, *109*, 275-282.
35. Palmieri, L.; Rastelli, G. alpha C helix displacement as a general approach for allosteric modulation of protein kinases. *Drug Discov. Today* **2013**, *18*, 407-414.
36. Vijayan, R. S. K.; He, P.; Modi, V.; Duong-Ly, K. C.; Ma, H. C.; Peterson, J. R.; Dunbrack, R. L.; Levy, R. M. Conformational Analysis of the DFG-Out Kinase Motif and Biochemical Profiling of Structurally Validated Type II Inhibitors. *J. Med. Chem.* **2015**, *58*, 466-479.
37. Engh, R. A.; Bossemeyer, D. Structural aspects of protein kinase control - role of conformational flexibility. *Pharmacol. Ther.* **2002**, *93*, 99-111.
38. Blume-Jensen, P.; Hunter, T. Oncogenic kinase signalling. *Nature* **2001**, *411*, 355-365.
39. Gross, S.; Rahal, R.; Stransky, N.; Lengauer, C.; Hoefflich, K. P. Targeting cancer with kinase inhibitors. *J. Clin. Invest.* **2015**, *125*, 1780-1789.
40. Patterson, H.; Nibbs, R.; McInnes, I.; Siebert, S. Protein kinase inhibitors in the treatment of inflammatory and autoimmune diseases. *Clin. Exp. Immunol.* **2014**, *176*, 1-10.
41. Chico, L. K.; Van Eldik, L. J.; Watterson, D. M. Targeting protein kinases in central nervous system disorders. *Nat. Rev. Drug Discov.* **2009**, *8*, 892-909.
42. Hopkins, A. L.; Groom, C. R. The druggable genome. *Nat. Rev. Drug Discov.* **2002**, *1*, 727-730.
43. Wu, P.; Nielsen, T. E.; Clausen, M. H. FDA-approved small-molecule kinase inhibitors. *Trends Pharmacol. Sci.* **2015**, *36*, 422-439.
44. Southan, C.; Sharman, J. L.; Benson, H. E.; Faccenda, E.; Pawson, A. J.; Alexander, S. P.; Buneman, O. P.; Davenport, A. P.; McGrath, J. C.; Peters, J. A.; Spedding, M.; Catterall, W. A.; Fabbro, D.; Davies, J. A.; Nc, I. The IUPHAR/BPS Guide to PHARMACOLOGY in 2016: towards curated quantitative interactions between 1300 protein targets and 6000 ligands. *Nucleic Acids Res.* **2016**, *44*, D1054-68.
45. Cutolo, M.; Meroni, M. Clinical utility of the oral JAK inhibitor tofacitinib in the treatment of rheumatoid arthritis. *J. Inflamm. Res.* **2013**, *6*, 129-37.
46. Fabbro, D. 25 years of small molecular weight kinase inhibitors: potentials and limitations. *Mol. Pharmacol.* **2015**, *87*, 766-75.
47. Backes, A.; Zech, B.; Felber, B.; Klebl, B.; Müller, G. Small-molecule inhibitors binding to protein kinases. Part I: exceptions from the traditional pharmacophore approach of type I inhibition. *Expert Opin. Drug Discov.* **2008**, *3*, 1409-25.

48. Liu, Y.; Gray, N. S. Rational design of inhibitors that bind to inactive kinase conformations. *Nat. Chem. Biol.* **2006**, *2*, 358-64.
49. Traxler, P.; Furet, P. Strategies toward the design of novel and selective protein tyrosine kinase inhibitors. *Pharmacol. Ther.* **1999**, *82*, 195-206.
50. Backes, A.; Zech, B.; Felber, B.; Klebl, B.; Müller, G. Small-molecule inhibitors binding to protein kinase. Part II: the novel pharmacophore approach of type II and type III inhibition. *Expert Opin. Drug Discov.* **2008**, *3*, 1427-49.
51. Zhao, Z.; Wu, H.; Wang, L.; Liu, Y.; Knapp, S.; Liu, Q.; Gray, N. S. Exploration of type II binding mode: A privileged approach for kinase inhibitor focused drug discovery? *ACS Chem Biol* **2014**, *9*, 1230-41.
52. Davis, M. I.; Hunt, J. P.; Herrgard, S.; Ciceri, P.; Wodicka, L. M.; Pallares, G.; Hocker, M.; Treiber, D. K.; Zarrinkar, P. P. Comprehensive analysis of kinase inhibitor selectivity. *Nat. Biotechnol.* **2011**, *29*, 1046-51.
53. Vogtherr, M.; Saxena, K.; Hoelder, S.; Grimme, S.; Betz, M.; Schieborr, U.; Pescatore, B.; Robin, M.; Delarbre, L.; Langer, T.; Wendt, K. U.; Schwalbe, H. NMR characterization of kinase p38 dynamics in free and ligand-bound forms. *Angew. Chem., Int. Ed.* **2006**, *45*, 993-997.
54. Sullivan, J. E.; Holdgate, G. A.; Campbell, D.; Timms, D.; Gerhardt, S.; Breed, J.; Breeze, A. L.; Bermingham, A.; Pauptit, R. A.; Norman, R. A.; Embrey, K. J.; Read, J.; VanScyoc, W. S.; Ward, W. H. J. Prevention of MKK6-dependent activation by binding to p38 alpha MAP kinase. *Biochemistry* **2005**, *44*, 16475-16490.
55. Zuccotto, F.; Ardini, E.; Casale, E.; Angiolini, M. Through the "gatekeeper door": exploiting the active kinase conformation. *J. Med. Chem.* **2010**, *53*, 2681-94.
56. Dong, J.; Zhao, H.; Zhou, T.; Spiliotopoulos, D.; Rajendran, C.; Li, X. D.; Huang, D.; Caflisch, A. Structural Analysis of the Binding of Type I, I1/2, and II Inhibitors to Eph Tyrosine Kinases. *ACS Med. Chem. Lett.* **2015**, *6*, 79-83.
57. Wentsch, H. K.; Walter, N. M.; Bührmann, M.; Mayer-Wrangowski, S.; Rauh, D.; Zaman, G. J. R.; Willemsen-Seegers, N.; Buijsman, R. C.; Henning, M.; Dauch, D.; Zender, L.; Laufer, S. Optimized Target Residence Time: Type I1/2 Inhibitors for p38alpha MAP Kinase with Improved Binding Kinetics through Direct Interaction with the R-Spine. *Angew. Chem. Int. Ed. Engl.* **2017**, *56*, 5363-5367.
58. Ohren, J. F.; Chen, H.; Pavlovsky, A.; Whitehead, C.; Zhang, E.; Kuffa, P.; Yan, C.; McConnell, P.; Spessard, C.; Banotai, C.; Mueller, W. T.; Delaney, A.; Omer, C.; Sebolt-Leopold, J.; Dudley, D. T.; Leung, I. K.; Flamme, C.; Warmus, J.; Kaufman, M.; Barrett, S.; Tecle, H.; Hasemann, C. A. Structures of human MAP kinase kinase 1 (MEK1) and MEK2 describe novel noncompetitive kinase inhibition. *Nat. Struct. Mol. Biol.* **2004**, *11*, 1192-7.
59. Lamba, V.; Ghosh, I. New directions in targeting protein kinases: focusing upon true allosteric and bivalent inhibitors. *Curr. Pharm. Des.* **2012**, *18*, 2936-45.

60. Singh, J.; Petter, R. C.; Baillie, T. A.; Whitty, A. The resurgence of covalent drugs. *Nat. Rev. Drug Discov.* **2011**, *10*, 307-17.
61. Baillie, T. A. Targeted Covalent Inhibitors for Drug Design. *Angew. Chem. Int. Ed. Engl.* **2016**, *55*, 13408-13421.
62. Mah, R.; Thomas, J. R.; Shafer, C. M. Drug discovery considerations in the development of covalent inhibitors. *Bioorg. Med. Chem. Lett.* **2014**, *24*, 33-9.
63. Chaikuad, A.; Koch, P.; Laufer, S.; Knapp, S. Targeting the Protein Kinases Cysteine. *Angew. Chem. Int. Ed. Engl.* **2017**.
64. Liu, Q.; Sabnis, Y.; Zhao, Z.; Zhang, T.; Buhrlage, S. J.; Jones, L. H.; Gray, N. S. Developing irreversible inhibitors of the protein kinase cysteine. *Chem. Biol.* **2013**, *20*, 146-59.
65. Coxon, C. R.; Anscombe, E.; Harnor, S. J.; Martin, M. P.; Carbain, B.; Golding, B. T.; Hardcastle, I. R.; Harlow, L. K.; Korolchuk, S.; Matheson, C. J.; Newell, D. R.; Noble, M. E.; Sivaprakasam, M.; Tudhope, S. J.; Turner, D. M.; Wang, L. Z.; Wedge, S. R.; Wong, C.; Griffin, R. J.; Endicott, J. A.; Cano, C. Cyclin-Dependent Kinase (CDK) Inhibitors: Structure-Activity Relationships and Insights into the CDK-2 Selectivity of 6-Substituted 2-Arylamino-purines. *J. Med. Chem.* **2017**, *60*, 1746-1767.
66. Pettinger, J.; Jones, K.; Cheeseman, M. D. Lysine-Targeting Covalent Inhibitors. *Angew. Chem. Int. Ed. Engl.* **2017**.
67. Kalgutkar, A. S.; Dalvie, D. K. Drug discovery for a new generation of covalent drugs. *Expert Opin. Drug Discov.* **2012**, *7*, 561-81.
68. Sanderson, K. Irreversible kinase inhibitors gain traction. *Nat. Rev. Drug. Discov.* **2013**, *12*, 649-51.
69. Chen, Z.; Gibson, T. B.; Robinson, F.; Silvestro, L.; Pearson, G.; Xu, B.; Wright, A.; Vanderbilt, C.; Cobb, M. H. MAP kinases. *Chem. Rev.* **2001**, *101*, 2449-76.
70. Hommes, D. W.; Peppelenbosch, M. P.; van Deventer, S. J. Mitogen activated protein (MAP) kinase signal transduction pathways and novel anti-inflammatory targets. *Gut* **2003**, *52*, 144-51.
71. Pearson, G.; Robinson, F.; Beers Gibson, T.; Xu, B. E.; Karandikar, M.; Berman, K.; Cobb, M. H. Mitogen-activated protein (MAP) kinase pathways: regulation and physiological functions. *Endocr. Rev.* **2001**, *22*, 153-83.
72. Chang, L.; Karin, M. Mammalian MAP kinase signalling cascades. *Nature* **2001**, *410*, 37-40.
73. Kyriakis, J. M.; Avruch, J. Mammalian mitogen-activated protein kinase signal transduction pathways activated by stress and inflammation. *Physiol. Rev.* **2001**, *81*, 807-69.

74. Brown, M. D.; Sacks, D. B. Protein scaffolds in MAP kinase signalling. *Cell. Signalling* **2009**, *21*, 462-9.
75. Meister, M.; Tomasovic, A.; Banning, A.; Tikkanen, R. Mitogen-Activated Protein (MAP) Kinase Scaffolding Proteins: A Recount. *Int. J. Mol. Sci.* **2013**, *14*, 4854-84.
76. Margutti, S.; Laufer, S. A. Are MAP kinases drug targets? Yes, but difficult ones. *ChemMedChem* **2007**, *2*, 1116-40.
77. Kyriakis, J. M.; Banerjee, P.; Nikolakaki, E.; Dai, T. A.; Rubie, E. A.; Ahmad, M. F.; Avruch, J.; Woodgett, J. R. The Stress-Activated Protein-Kinase Subfamily of C-Jun Kinases. *Nature* **1994**, *369*, 156-160.
78. Barr, R. K.; Bogoyevitch, M. A. The c-Jun N-terminal protein kinase family of mitogen-activated protein kinases (JNK MAPKs). *Int. J. Biochem. Cell Biol.* **2001**, *33*, 1047-1063.
79. Bogoyevitch, M. A. The isoform-specific functions of the c-Jun N-terminal kinases (JNKs): differences revealed by gene targeting. *BioEssays* **2006**, *28*, 923-934.
80. Gupta, S.; Barrett, T.; Whitmarsh, A. J.; Cavanagh, J.; Sluss, H. K.; Derijard, B.; Davis, R. J. Selective interaction of JNK protein kinase isoforms with transcription factors. *Embo J.* **1996**, *15*, 2760-2770.
81. Davis, R. J. Signal transduction by the JNK group of MAP kinases. *Cell* **2000**, *103*, 239-52.
82. Davies, C.; Tournier, C. Exploring the function of the JNK (c-Jun N-terminal kinase) signalling pathway in physiological and pathological processes to design novel therapeutic strategies. *Biochem. Soc. Trans.* **2012**, *40*, 85-89.
83. Lisnock, J.; Griffin, P.; Calaycay, J.; Frantz, B.; Parsons, J.; O'Keefe, S. J.; LoGrasso, P. Activation of JNK3 alpha 1 requires both MKK4 and MKK7: Kinetic characterization of in vitro phosphorylated JNK3 alpha 1. *Biochemistry* **2000**, *39*, 3141-3148.
84. Whitmarsh, A. J. The JIP family of MAPK scaffold proteins. *Biochem. Soc. Trans.* **2006**, *34*, 828-832.
85. Bogoyevitch, M. A.; Kobe, B. Uses for JNK: the many and varied substrates of the c-Jun N-terminal kinases. *Microbiol. Mol. Biol. Rev.* **2006**, *70*, 1061-+.
86. Hess, J.; Angel, P.; Schorpp-Kistner, M. AP-1 subunits: quarrel and harmony among siblings. *J. Cell Sci.* **2004**, *117*, 5965-5973.
87. Liu, J.; Lin, A. N. Role of JNK activation in apoptosis: A double-edged sword. *Cell Res.* **2005**, *15*, 36-42.
88. Ip, Y. T.; Davis, R. J. Signal transduction by the c-Jun N-terminal kinase (JNK) - from inflammation to development. *Curr. Opin. Cell Biol.* **1998**, *10*, 205-219.



89. Rincon, M.; Pedraza-Alva, G. JNK and p38 MAP kinases in CD4(+) and CD8(+) T cells. *Immunol. Rev.* **2003**, *192*, 131-142.
90. Swantek, J. L.; Cobb, M. H.; Geppert, T. D. Jun N-terminal kinase stress-activated protein kinase (JNK/SAPK) is required for lipopolysaccharide stimulation of tumor necrosis factor alpha (TNF-alpha) translation: Glucocorticoids inhibit TNF-alpha translation by blocking JNK/SAPK. *Mol. Cell. Biol.* **1997**, *17*, 6274-6282.
91. Sabapathy, K.; Jochum, W.; Hochedlinger, K.; Chang, L. F.; Karin, M.; Wagner, E. F. Defective neural tube morphogenesis and altered apoptosis in the absence of both JNK1 and JNK2. *Mech. Dev.* **1999**, *89*, 115-124.
92. Manning, A. M.; Davis, R. J. Targeting JNK for therapeutic benefit: from junk to gold? *Nat. Rev. Drug Discov.* **2003**, *2*, 554-65.
93. Mehan, S.; Meena, H.; Sharma, D.; Sankhla, R. JNK: a stress-activated protein kinase therapeutic strategies and involvement in Alzheimer's and various neurodegenerative abnormalities. *J. Mol. Neurosci.* **2011**, *43*, 376-90.
94. Resnick, L.; Fennell, M. Targeting JNK3 for the treatment of neurodegenerative disorders. *Drug Discov. Today* **2004**, *9*, 932-9.
95. Zhu, X.; Raina, A. K.; Rottkamp, C. A.; Aliev, G.; Perry, G.; Boux, H.; Smith, M. A. Activation and redistribution of c-jun N-terminal kinase/stress activated protein kinase in degenerating neurons in Alzheimer's disease. *J Neurochem* **2001**, *76*, 435-41.
96. Yarza, R.; Vela, S.; Solas, M.; Ramirez, M. J. c-Jun N-terminal Kinase (JNK) Signaling as a Therapeutic Target for Alzheimer's Disease. *Front. Pharmacol.* **2015**, *6*, 321.
97. Hunot, S.; Vila, M.; Teismann, P.; Davis, R. J.; Hirsch, E. C.; Przedborski, S.; Rakic, P.; Flavell, R. A. JNK-mediated induction of cyclooxygenase 2 is required for neurodegeneration in a mouse model of Parkinson's disease. *Proc. Natl. Acad. Sci. U. S. A.* **2004**, *101*, 665-70.
98. Dorweiler, B.; Pruefer, D.; Andradi, T. B.; Maksan, S. M.; Schmiedt, W.; Neufang, A.; Vahl, C. F. Ischemia-Reperfusion Injury : Pathophysiology and Clinical Implications. *Eur. J. Trauma Emerg. Surg.* **2007**, *33*, 600-12.
99. Kuan, C. Y.; Whitmarsh, A. J.; Yang, D. D.; Liao, G. H.; Schloemer, A. J.; Dong, C.; Bao, J.; Banasiak, K. J.; Haddad, G. G.; Flavell, R. A.; Davis, R. J.; Rakic, P. A critical role of neural-specific JNK3 for ischemic apoptosis. *Proc. Natl. Acad. Sci. U.S.A.* **2003**, *100*, 15184-15189.
100. Tournier, C. The 2 Faces of JNK Signaling in Cancer. *Genes Cancer* **2013**, *4*, 397-400.
101. Bubici, C.; Papa, S. JNK signalling in cancer: in need of new, smarter therapeutic targets. *Br. J. Pharmacol.* **2014**, *171*, 24-37.
102. Wagner, E. F.; Nebreda, A. R. Signal integration by JNK and p38 MAPK pathways in cancer development. *Nat. Rev. Cancer* **2009**, *9*, 537-549.

103. Ebelt, N. D.; Cantrell, M. A.; Van Den Berg, C. L. c-Jun N-Terminal Kinases Mediate a Wide Range of Targets in the Metastatic Cascade. *Genes Cancer* **2013**, *4*, 378-87.
104. She, Q. B.; Chen, N. Y.; Bode, A. M.; Flavell, R. A.; Dong, Z. G. Deficiency of c-Jun-NH2-terminal kinase-1 in mice enhances skin tumor development by 12-O-tetradecanoylphorbol-13-acetate. *Cancer Res.* **2002**, *62*, 1343-1348.
105. Gao, Y. F.; Tao, J.; Li, M. O.; Zhang, D. Q.; Chi, H. B.; Henegariu, O.; Kaech, S. M.; Davis, R. J.; Flavell, R. A.; Yin, Z. N. JNK1 is essential for CD8(+) T cell-mediated tumor immune surveillance. *J. Immunol.* **2005**, *175*, 5783-5789.
106. Hirosumi, J.; Tuncman, G.; Chang, L.; Gorgun, C. Z.; Uysal, K. T.; Maeda, K.; Karin, M.; Hotamisligil, G. S. A central role for JNK in obesity and insulin resistance. *Nature* **2002**, *420*, 333-6.
107. Aguirre, V.; Uchida, T.; Yenush, L.; Davis, R.; White, M. F. The c-Jun NH(2)-terminal kinase promotes insulin resistance during association with insulin receptor substrate-1 and phosphorylation of Ser(307). *J. Biol. Chem.* **2000**, *275*, 9047-54.
108. Jaeschke, A.; Rincon, M.; Doran, B.; Reilly, J.; Neuberger, D.; Greiner, D. L.; Shultz, L. D.; Rossini, A. A.; Flavell, R. A.; Davis, R. J. Disruption of the Jnk2 (Mapk9) gene reduces destructive insulinitis and diabetes in a mouse model of type I diabetes. *Proc. Natl. Acad. Sci. U. S. A.* **2005**, *102*, 6931-5.
109. Clancy, R.; Rediske, J.; Koehne, C.; Stoyanovsky, D.; Amin, A.; Attur, M.; Iyama, K.; Abramson, S. B. Activation of stress-activated protein kinase in osteoarthritic cartilage: evidence for nitric oxide dependence. *Osteoarthritis Cartilage* **2001**, *9*, 294-9.
110. Han, Z. N.; Boyle, D. L.; Aupperle, K. R.; Bennett, B.; Manning, A. M.; Firestein, G. S. Jun N-terminal kinase in rheumatoid arthritis. *J. Pharmacol. Exp. Ther.* **1999**, *291*, 124-130.
111. Han, Z. N.; Boyle, D. L.; Chang, L. F.; Bennett, B.; Karin, M.; Yang, L.; Manning, A. M.; Firestein, G. S. C-Jun N-terminal kinase is required for metalloproteinase expression, and joint destruction in inflammatory arthritis. *J. Clin. Invest.* **2001**, *108*, 73-81.
112. Wu, H. M.; Fang, L.; Shen, Q. Y.; Liu, R. Y. SP600125 promotes resolution of allergic airway inflammation via TLR9 in an OVA-induced murine acute asthma model. *Mol. Immunol.* **2015**, *67*, 311-316.
113. Gehringer, M.; Muth, F.; Koch, P.; Laufer, S. A. c-Jun N-terminal kinase inhibitors: a patent review (2010 - 2014). *Expert Opin. Ther. Pat.* **2015**, *25*, 849-72.
114. Koch, P.; Gehringer, M.; Laufer, S. A. Inhibitors of c-Jun N-terminal kinases: an update. *J. Med. Chem.* **2015**, *58*, 72-95.
115. Siddiqui, M. A.; Reddy, P. A. Small Molecule JNK (c-Jun N-Terminal Kinase) Inhibitors. *J. Med. Chem.* **2010**, *53*, 3005-3012.

116. A Study to Characterize the Safety, PK and Biological Activity of CC-930 in Idiopathic Pulmonary Fibrosis (IPF). <https://clinicaltrials.gov/ct2/show/NCT01203943> (18/12/2017).
117. A Research Study to Assess if CC-930 is Safe in Treating Subjects With Discoid Lupus Erythematosus. <https://clinicaltrials.gov/ct2/show/NCT01466725> (18/12/2017).
118. Efficacy and Safety of XG-102 in Reduction of Post-cataract Surgery Intraocular Inflammation. <https://clinicaltrials.gov/show/NCT02235272> (18/12/2017).
119. Efficacy and Safety of XG-102 in Reduction of Post-cataract Surgery Intraocular Inflammation and Pain. <https://clinicaltrials.gov/show/NCT02508337> (18/12/2017).
120. AM-111 in the Treatment of Acute Inner Ear Hearing Loss (HEALOS). <https://clinicaltrials.gov/show/NCT02561091> (18/12/2017).
121. Efficacy and Safety of AM-111 as Acute Sudden Sensorineural Hearing Loss Treatment (ASSENT). <https://clinicaltrials.gov/show/NCT02809118> (18/12/2017).
122. PGL5001 Proof of Concept Study in Inflammatory Endometriosis (JADE). <https://clinicaltrials.gov/show/NCT01630252> (18/12/2017).
123. Study to Determine the Optimal Biologic Dose of CC-401 in Subjects With High-Risk Myeloid Leukemia. <https://clinicaltrials.gov/ct2/show/NCT00126893?term=cc-401&rank=1> (27/02/2017).
124. A Study to Evaluate the Efficacy and Safety of CC-90001 in Subjects With Idiopathic Pulmonary Fibrosis. <https://clinicaltrials.gov/ct2/show/NCT03142191> (18/12/2017).
125. Cuenda, A.; Rousseau, S. p38 MAP-kinases pathway regulation, function and role in human diseases. *Biochim. Biophys. Acta* **2007**, *1773*, 1358-75.
126. Kumar, S.; Boehm, J.; Lee, J. C. p38 MAP kinases: key signalling molecules as therapeutic targets for inflammatory diseases. *Nat. Rev. Drug Discov.* **2003**, *2*, 717-26.
127. Munoz, L.; Ammit, A. J. Targeting p38 MAPK pathway for the treatment of Alzheimer's disease. *Neuropharmacology* **2010**, *58*, 561-8.
128. Muth, F.; Günther, M.; Bauer, S. M.; Döring, E.; Fischer, S.; Maier, J.; Drückes, P.; Köppler, J.; Trappe, J.; Rothbauer, U.; Koch, P.; Laufer, S. A. Tetra-Substituted Pyridinylimidazoles As Dual Inhibitors of p38 alpha Mitogen-Activated Protein Kinase and c-Jun N-Terminal Kinase 3 for Potential Treatment of Neurodegenerative Diseases. *J. Med. Chem.* **2015**, *58*, 443-456.
129. Dambach, D. M. Potential adverse effects associated with inhibition of p38 alpha/beta MAP kinases. *Curr. Top. Med. Chem.* **2005**, *5*, 929-939.
130. Genovese, M. C. Inhibition of p38: Has the Fat Lady Sung. *Arthritis Rheum.* **2009**, *60*, 317-320.

131. Bennett, B. L.; Sasaki, D. T.; Murray, B. W.; O'Leary, E. C.; Sakata, S. T.; Xu, W.; Leisten, J. C.; Motiwala, A.; Pierce, S.; Satoh, Y.; Bhagwat, S. S.; Manning, A. M.; Anderson, D. W. SP600125, an anthrapyrazolone inhibitor of Jun N-terminal kinase. *Proc. Natl. Acad. Sci. U. S. A.* **2001**, *98*, 13681-6.
132. Karaman, M. W.; Herrgard, S.; Treiber, D. K.; Gallant, P.; Atteridge, C. E.; Campbell, B. T.; Chan, K. W.; Ciceri, P.; Davis, M. I.; Edeen, P. T.; Faraoni, R.; Floyd, M.; Hunt, J. P.; Lockhart, D. J.; Milanov, Z. V.; Morrison, M. J.; Pallares, G.; Patel, H. K.; Pritchard, S.; Wodicka, L. M.; Zarrinkar, P. P. A quantitative analysis of kinase inhibitor selectivity. *Nat. Biotechnol.* **2008**, *26*, 127-132.
133. Goettert, M.; Graeser, R.; Laufer, S. A. Optimization of a nonradioactive immunosorbent assay for p38alpha mitogen-activated protein kinase activity. *Anal. Biochem.* **2010**, *406*, 233-4.
134. Goettert, M.; Luik, S.; Graeser, R.; Laufer, S. A. A direct ELISA assay for quantitative determination of the inhibitory potency of small molecules inhibitors for JNK3. *J. Pharm. Biomed. Anal.* **2011**, *55*, 236-40.
135. Hall, M. D.; Yasgar, A.; Peryea, T.; Braisted, J. C.; Jadhav, A.; Simeonov, A.; Coussens, N. P. Fluorescence polarization assays in high-throughput screening and drug discovery: a review. *Methods Appl. Fluoresc.* **2016**, *4*, 022001.
136. Jameson, D. M.; Croney, J. C. Fluorescence polarization: past, present and future. *Comb. Chem. High Throughput Screen.* **2003**, *6*, 167-73.
137. Burke, T. J.; Loniello, K. R.; Beebe, J. A.; Ervin, K. M. Development and application of fluorescence polarization assays in drug discovery. *Comb. Chem. High Throughput Screen.* **2003**, *6*, 183-94.
138. Lakowicz, J. R. Principles of Fluorescence Spectroscopy. In Third ed.; Springer: 2006; pp 353-380.
139. Lea, W. A.; Simeonov, A. Fluorescence polarization assays in small molecule screening. *Expert Opin. Drug Discov.* **2011**, *6*, 17-32.
140. Moerke, N. J. Fluorescence Polarization (FP) Assays for Monitoring Peptide-Protein or Nucleic Acid-Protein Binding. *Curr. Protoc. Chem. Biol.* **2009**, *1*, 1-15.
141. Rossi, A. M.; Taylor, C. W. Analysis of protein-ligand interactions by fluorescence polarization. *Nat. Protoc.* **2011**, *6*, 365-87.
142. Allen, M.; Reeves, J.; Mellor, G. High throughput fluorescence polarization: a homogeneous alternative to radioligand binding for cell surface receptors. *J. Biomol. Screen.* **2000**, *5*, 63-9.
143. Koch, P.; Bäuerlein, C.; Jank, H.; Laufer, S. Targeting the ribose and phosphate binding site of p38 mitogen-activated protein (MAP) kinase: Synthesis and biological testing of 2-alkylsulfanyl-, 4(5)-aryl-, 5(4)-heteroaryl-substituted imidazoles. *J. Med. Chem.* **2008**, *51*, 5630-5640.

144. Ansideri, F.; Lange, A.; El-Gokha, A.; Boeckler, F. M.; Koch, P. Fluorescence polarization-based assays for detecting compounds binding to inactive c-Jun N-terminal kinase 3 and p38 alpha mitogen-activated protein kinase. *Anal. Biochem.* **2016**, *503*, 28-40.
145. Munoz, L.; Selig, R.; Yeung, Y. T.; Peifer, C.; Hauser, D.; Laufer, S. Fluorescence polarization binding assay to develop inhibitors of inactive p38alpha mitogen-activated protein kinase. *Anal. Biochem.* **2010**, *401*, 125-33.
146. Prystay, L.; Gosselin, M.; Banks, P. Determination of equilibrium dissociation constants in fluorescence polarization. *J. Biomol. Screen.* **2001**, *6*, 141-150.
147. Huang, X. Fluorescence polarization competition assay: the range of resolvable inhibitor potency is limited by the affinity of the fluorescent ligand. *J. Biomol. Screen.* **2003**, *8*, 34-8.
148. Cheng, Y.; Prusoff, W. H. Relationship between Inhibition Constant ( $K_i$ ) and Concentration of Inhibitor Which Causes 50 Per Cent Inhibition ( $I_{50}$ ) of an Enzymatic-Reaction. *Biochem. Pharmacol.* **1973**, *22*, 3099-3108.
149. Nikolovska-Coleska, Z.; Wang, R.; Fang, X.; Pan, H.; Tomita, Y.; Li, P.; Roller, P. P.; Krajewski, K.; Saito, N. G.; Stuckey, J. A.; Wang, S. Development and optimization of a binding assay for the XIAP BIR3 domain using fluorescence polarization. *Anal. Biochem.* **2004**, *332*, 261-73.
150. The  $K_i$  calculator for Fluorescence-Based Competitive Binding Assays. [http://sw16.im.med.umich.edu/software/calc\\_ki/](http://sw16.im.med.umich.edu/software/calc_ki/) (19/01/2018).
151. Laufer, S. A.; Hauser, D. R.; Domeyer, D. M.; Kinkel, K.; Liedtke, A. J. Design, synthesis, and biological evaluation of novel Tri- and tetrasubstituted imidazoles as highly potent and specific ATP-mimetic inhibitors of p38 MAP kinase: focus on optimized interactions with the enzyme's surface-exposed front region. *J. Med. Chem.* **2008**, *51*, 4122-49.
152. Koch, P.; Jahns, H.; Schattel, V.; Goettert, M.; Laufer, S. Pyridinylquinoxalines and pyridinylpyridopyrazines as lead compounds for novel p38 alpha mitogen-activated protein kinase inhibitors. *J. Med. Chem.* **2010**, *53*, 1128-37.
153. Fischer, S.; Wentsch, H. K.; Mayer-Wrangowski, S. C.; Zimmermann, M.; Bauer, S. M.; Storch, K.; Niess, R.; Koeberle, S. C.; Grütter, C.; Boeckler, F. M.; Rauh, D.; Laufer, S. A. Dibenzosuberones as p38 mitogen-activated protein kinase inhibitors with low ATP competitiveness and outstanding whole blood activity. *J. Med. Chem.* **2013**, *56*, 241-53.
154. Lange, A.; Günther, M.; Michael Büttner, F.; Zimmermann, M. O.; Heidrich, J.; Hennig, S.; Zahn, S.; Schall, C.; Sievers-Engler, A.; Ansideri, F.; Koch, P.; Laemmerhofer, M.; Stehle, T.; Laufer, S. A.; Boeckler, F. M. Targeting the Gatekeeper MET146 of C-Jun N-Terminal Kinase 3 Induces a Bivalent Halogen/Chalcogen Bond. *J. Am. Chem. Soc.* **2015**, *137*, 14640-52.
155. Iversen, P. W.; Beck, B.; Chen, Y. F.; Dere, W.; Devanarayan, V.; Eastwood, B. J.; Farmen, M. W.; Iturria, S. J.; Montrose, C.; Moore, R. A.; Weidner, J. R.; Sittampalam, G. S. HTS Assay Validation. In *Assay Guidance Manual*, Sittampalam, G. S.; Coussens, N. P.; Nelson, H.;

Arkin, M.; Auld, D.; Austin, C.; Bejcek, B.; Glicksman, M.; Inglese, J.; Iversen, P. W.; Li, Z.; McGee, J.; McManus, O.; Minor, L.; Napper, A.; Peltier, J. M.; Riss, T.; Trask, O. J., Jr.; Weidner, J., Eds. Bethesda (MD), 2004.

156. Schepetkin, I. A.; Kirpotina, L. N.; Khlebnikov, A. I.; Hanks, T. S.; Kochetkova, I.; Pascual, D. W.; Jutila, M. A.; Quinn, M. T. Identification and Characterization of a Novel Class of c-Jun N-terminal Kinase Inhibitors. *Mol. Pharmacol.* **2012**, *81*, 832-845.

157. Szczepankiewicz, B. G.; Kosogof, C.; Nelson, L. T. J.; Liu, G.; Liu, B.; Zhao, H. Y.; Serby, M. D.; Xin, Z. L.; Liu, M.; Gum, R. J.; Haasch, D. L.; Wang, S. Y.; Clampit, J. E.; Johnson, E. F.; Lubben, T. H.; Stashko, M. A.; Olejniczak, E. T.; Sun, C. H.; Dorwin, S. A.; Haskins, K.; Abad-Zapatero, C.; Fry, E. H.; Hutchins, C. W.; Sham, H. L.; Rondinone, C. M.; Trevillyan, J. M. Aminopyridine-based c-Jun N-terminal kinase inhibitors with cellular activity and minimal cross-kinase activity. *J. Med. Chem.* **2006**, *49*, 3563-3580.

158. Kamenecka, T.; Habel, J.; Duckett, D.; Chen, W.; Ling, Y. Y.; Frackowiak, B.; Jiang, R.; Shin, Y.; Song, X.; LoGrasso, P. Structure-activity relationships and X-ray structures describing the selectivity of aminopyrazole inhibitors for c-Jun N-terminal kinase 3 (JNK3) over p38. *J. Biol. Chem.* **2009**, *284*, 12853-61.

159. Chambers, J. W.; Pachori, A.; Howard, S.; Ganno, M.; Hansen, D.; Kamenecka, T.; Song, X. Y.; Duckett, D.; Chen, W. M.; Ling, Y. Y.; Cherry, L.; Cameron, M. D.; Lin, L.; Ruiz, C. H.; LoGrasso, P. Small Molecule c-jun-N-Terminal Kinase Inhibitors Protect Dopaminergic Neurons in a Model of Parkinson's Disease. *ACS Chem. Neurosci.* **2011**, *2*, 198-206.

160. Chambers, J. W.; Pachori, A.; Howard, S.; Ganno, M.; Hansen, D.; Kamenecka, T.; Song, X. Y.; Duckett, D.; Chen, W. M.; Ling, Y. Y.; Cherry, L.; Cameron, M. D.; Lin, L.; Ruiz, C. H.; LoGrasso, P. Small Molecule c-jun-N-Terminal Kinase Inhibitors Protect Dopaminergic Neurons in a Model of Parkinson's Disease. *ACS Chemical Neuroscience* **2011**, *2*, 198-206.

161. ZINC15 Patterns. <http://zinc15.docking.org/patterns/home/> (30/01/2018).

162. Baell, J. B.; Holloway, G. A. New substructure filters for removal of pan assay interference compounds (PAINS) from screening libraries and for their exclusion in bioassays. *J. Med. Chem.* **2010**, *53*, 2719-40.

163. Dahlin, J. L.; Nissink, J. W. M.; Strasser, J. M.; Francis, S.; Higgins, L.; Zhou, H.; Zhang, Z. G.; Walters, M. A. PAINS in the Assay: Chemical Mechanisms of Assay Interference and Promiscuous Enzymatic Inhibition Observed during a Sulfhydryl-Scavenging HTS. *J. Med. Chem.* **2015**, *58*, 2091-2113.

164. He, Y. J.; Duckett, D.; Chen, W. M.; Ling, Y. Y.; Cameron, M. D.; Lin, L.; Ruiz, C. H.; LoGrasso, P. V.; Kamenecka, T. M.; Koenig, M. Synthesis and SAR of novel isoxazoles as potent c-jun N-terminal kinase (JNK) inhibitors. *Bioorg. Med. Chem. Lett.* **2014**, *24*, 161-164.

165. Laufer, S. A.; Wagner, G. K.; Kotschenreuther, D. A.; Albrecht, W. Novel substituted pyridinyl imidazoles as potent anticytokine agents with low activity against hepatic cytochrome P450 enzymes. *J. Med. Chem.* **2003**, *46*, 3230-3244.

166. Marckwald, W. Ein Beitrag zur Kenntniss der Imidazole und der Constitution des Glyoxalins. *Ber. Dtsch. Chem. Ges.* **1892**, *25*, 2354-2373.
167. Scapin, G.; Patel, S. B.; Lisnock, J.; Becker, J. W.; LoGrasso, P. V. The structure of JNK3 in complex with small molecule inhibitors: Structural basis for potency and selectivity. *Chem. Biol.* **2003**, *10*, 705-712.
168. Wityak, J.; McGee, K. F.; Conlon, M. P.; Song, R. H.; Duffy, B. C.; Clayton, B.; Lynch, M.; Wang, G.; Freeman, E.; Haber, J.; Kitchen, D. B.; Manning, D. D.; Ismail, J.; Khmel'nitsky, Y.; Michels, P.; Webster, J.; Irigoyen, M.; Luche, M.; Hultman, M.; Bai, M.; Kuok, I. D.; Newell, R.; Lamers, M.; Leonard, P.; Yates, D.; Matthews, K.; Ongeri, L.; Clifton, S.; Mead, T.; Deupree, S.; Wheelan, P.; Lyons, K.; Wilson, C.; Kiselyov, A.; Toledo-Sherman, L.; Beconi, M.; Munoz-Sanjuan, I.; Bard, J.; Dominguez, C. Lead Optimization toward Proof-of-Concept Tools for Huntington's Disease within a 4-(1H-Pyrazol-4-yl)pyrimidine Class of Pan-JNK Inhibitors. *J. Med. Chem.* **2015**, *58*, 2967-2987.
169. Zhang, T.; Inesta-Vaquera, F.; Niepel, M.; Zhang, J. M.; Ficarro, S. B.; Machleidt, T.; Xie, T.; Marto, J. A.; Kim, N.; Sim, T.; Laughlin, J. D.; Park, H.; LoGrasso, P. V.; Patricelli, M.; Nomanbhoy, T. K.; Sorger, P. K.; Alessi, D. R.; Gray, N. S. Discovery of Potent and Selective Covalent Inhibitors of JNK. *Chem. Biol.* **2012**, *19*, 140-154.
170. Voss, M. E.; Beer, C. M.; Mitchell, S. A.; Blomgren, P. A.; Zhichkin, P. E. A simple and convenient one-pot method for the preparation of heteroaryl-2-imidazoles from nitriles. *Tetrahedron* **2008**, *64*, 645-651.
171. Ziegler, K.; Hauser, D. R. J.; Unger, A.; Albrecht, W.; Laufer, S. A. 2-Acylaminopyridin-4-ylimidazoles as p38 MAP Kinase Inhibitors: Design, Synthesis, and Biological and Metabolic Evaluations. *ChemMedChem* **2009**, *4*, 1939-1948.
172. Wagner, G. K.; Kotschenreuther, D.; Zimmermann, W.; Laufer, S. A. Identification of regioisomers in a series of N-substituted pyridin-4-yl imidazole derivatives by regiospecific synthesis, GC/MS, and H-1 NMR. *J. Org. Chem.* **2003**, *68*, 4527-4530.
173. Laufer, S.; Wagner, G.; Kotschenreuther, D. Ones, thiones, and N-oxides: An exercise in imidazole chemistry. *Angew. Chem., Int. Ed.* **2002**, *41*, 2290-2293.
174. Xi, N.; Xu, S. M.; Cheng, Y.; Tasker, A. S.; Hungate, R. W.; Reider, P. J. Regio-controlled synthesis of N-substituted imidazoles. *Tetrahedron Lett.* **2005**, *46*, 7315-7319.
175. Heider, F.; Haun, U.; Döring, E.; Kudolo, M.; Sessler, C.; Albrecht, W.; Laufer, S.; Koch, P. From 2-Alkylsulfanylimidazoles to 2-Alkylimidazoles: An Approach towards Metabolically More Stable p38 alpha MAP Kinase Inhibitors. *Molecules* **2017**, *22*, 1729.
176. Lin, J. H.; Lu, A. Y. Inhibition and induction of cytochrome P450 and the clinical implications. *Clin Pharmacokinet* **1998**, *35*, 361-90.





# Appendix

## Publication I

Ansideri, F.; Lange, A.; El-Gokha, A.; Boeckler, F. M.; Koch, P. Fluorescence polarization-based assays for detecting compounds binding to inactive c-Jun N-terminal kinase 3 and p38 alpha mitogen-activated protein kinase. *Anal. Biochem.* **2016**, *503*, 28-40.

**Reprinted with permission from Ansideri *et al.* 2016, 503, 28-40**

**Copyright 2016 Elsevier Inc. All rights reserved**

**Link to the published version:**

<https://www.sciencedirect.com/science/article/pii/S0003269716000968>



Contents lists available at ScienceDirect

Analytical Biochemistry

journal homepage: [www.elsevier.com/locate/yabio](http://www.elsevier.com/locate/yabio)

## Fluorescence polarization-based assays for detecting compounds binding to inactive c-Jun N-terminal kinase 3 and p38 $\alpha$ mitogen-activated protein kinase



Francesco Ansideri <sup>a</sup>, Andreas Lange <sup>b</sup>, Ahmed El-Gokha <sup>a,c</sup>, Frank M. Boeckler <sup>b</sup>, Pierre Koch <sup>a,\*</sup>

<sup>a</sup> Institute of Pharmaceutical Sciences, Department of Medicinal and Pharmaceutical Chemistry, Eberhard Karls Universität Tübingen, 72076 Tübingen, Germany

<sup>b</sup> Institute of Pharmaceutical Sciences, Molecular Design and Pharmaceutical Biophysics, Eberhard Karls Universität Tübingen, 72076 Tübingen, Germany

<sup>c</sup> Department of Chemistry, Faculty of Science, Menoufia University, Menoufia, Egypt

### ARTICLE INFO

**Article history:**  
Received 4 December 2015  
Received in revised form  
25 February 2016  
Accepted 26 February 2016  
Available online 5 March 2016

**Keywords:**  
Fluorescence polarization  
Binding assays  
c-Jun N-terminal kinase 3  
p38 $\alpha$  MAP kinase

### ABSTRACT

Two fluorescein-labeled pyridinylimidazoles were synthesized and evaluated as probes for the binding affinity determination of potential kinase inhibitors to the c-Jun N-terminal kinase 3 (JNK3) and p38 $\alpha$  mitogen-activated protein kinase (MAPK). Fluorescence polarization (FP)-based competition binding assays were developed for both enzymes using 1-(3',6'-dihydroxy-3-oxo-3H-spiro[isobenzofuran-1,9'-xanthen]-5-yl)-3-(4-((4-(4-fluorophenyl)-2-(methylthio)-1H-imidazol-5-yl)pyridin-2-yl)amino)phenyl)thiourea (**5**) as an FP probe (JNK3:  $K_d = 3.0$  nM; p38 $\alpha$  MAPK:  $K_d = 5.7$  nM). The validation of the assays with known inhibitors of JNK3 and p38 $\alpha$  MAPK revealed that both FP assays correlate very well with inhibition data received by the activity assays. This, in addition to the viability of both FP-based binding assays for the high-throughput screening procedure, makes the assays suitable as inexpensive prescreening protocols for JNK3 and p38 $\alpha$  MAPK inhibitors.

© 2016 Elsevier Inc. All rights reserved.

Within the mitogen-activated protein kinase (MAPK) family, the two serine/threonine kinases, c-Jun N-terminal kinase 3 (JNK3) and p38 $\alpha$  MAPK have emerged during recent decades as particularly attractive therapeutic targets due to their implication in several pathologic conditions. JNK3, which is predominantly expressed in the brain, is associated with neurodegenerative diseases such as Alzheimer's disease (AD), Parkinson's disease (PD), and Huntington's disease [1,2]. On the other hand, p38 $\alpha$  MAPK is responsible for

different inflammatory responses and thus has become a well-established target for some chronic inflammatory diseases such as rheumatoid arthritis [3], inflammatory bowel disease [4], and psoriasis [5]. Recently, several clinical trials investigating the benefit of p38 $\alpha$  MAPK inhibitors for the treatment of chronic obstructive pulmonary disease were terminated [6,7]. In addition, some studies have also highlighted p38 $\alpha$  MAPK as a key protein in the pathogenesis of neurodegenerative diseases, including AD, PD, and multiple sclerosis [8–10]. As a consequence, great efforts have been focused in finding inhibitors for both JNK3 and p38 $\alpha$  MAPK [11–13], which led to the achievement of molecules endowed with a good potency, although often lacking a satisfactory selectivity.

JNK3 and p38 $\alpha$  MAPK are both activated in response to environmental stress stimuli as well as pro-inflammatory cytokines and take part in different signaling pathways [14–17]. The activation is carried out by upstream MAPK kinases MKK4/MKK7 and MKK3/MKK6 for JNK3 and p38 $\alpha$  MAPK, respectively, via a concomitant phosphorylation of a threonine residue and a tyrosine residue situated at the activation loop [15,18]. Among others, the most evident conformational modification following is the shift of a tripeptide

**Abbreviations used:** MAPK, mitogen-activated protein kinase; JNK, c-Jun N-terminal kinase; AD, Alzheimer's disease; PD, Parkinson's disease; ATP, adenosine triphosphate; HTS, high throughput screening; FP, fluorescence polarization; FITC, fluorescein isothiocyanate; ELISA, enzyme-linked immunosorbent assay; MOE, Molecular Operating Environment; TLC, thin layer chromatography; UV, ultraviolet; HPLC, high-performance liquid chromatography; NMR, nuclear magnetic resonance; ppm, parts per million; ESI-MS, electrospray ionization mass spectrometry; RT, room temperature; DMF, dimethylformamide; BME,  $\beta$ -mercaptoethanol; BSA, bovine serum albumin; rpm, revolutions per minute; NCB, National Center for Biotechnology Information; %CV, percentage coefficient of variation; ITC, isothermal titration calorimetry.

\* Corresponding author.  
E-mail address: [pierre.koch@uni-tuebingen.de](mailto:pierre.koch@uni-tuebingen.de) (P. Koch).

<http://dx.doi.org/10.1016/j.ab.2016.02.058>  
0003-2697/© 2016 Elsevier Inc. All rights reserved.

Glu-Phe-Gly situated at the beginning of the activation loop, known as the DFG motif, from an “out” conformation on the inactive enzyme to an “in” conformation [19]. Such modification has been well characterized and widely described for p38 $\alpha$  MAPK [20,21], and recently the possible adoption of the DFG–out conformation has been reported for JNK3 as well [22]. The majority of the p38 $\alpha$  MAPK inhibitors and nearly all of the reported JNK3 inhibitors discovered so far are classified as type I inhibitors, binding at the adenosine triphosphate (ATP) binding site of the enzyme in its active conformation and thus being ATP competitive [23]. However, most of type I inhibitors are also able to bind to the inactive form of the enzyme, probably due to the fact that the position of the DFG motif does not affect the binding mode of these compounds [21,24]. On the other side, type II inhibitors bind the ATP cleft of the inactive enzyme, exploiting a hydrophobic pocket known as the deep pocket, which is present only in the DFG–out conformation [25]. Because the inactive form of the kinase is not able to bind ATP, this modality of binding avoids the competition with high intracellular ATP concentrations. Furthermore, because the amino acid composition of the deep pocket is low conserved within the catalytic site of related kinases, type II binding allows achieving an improved selectivity profile. Despite the high desirability of MAPK type II inhibitors, only a few of these inhibitors have been characterized for p38 $\alpha$  MAPK [26], whereas to date no type II inhibitors have been reported for JNK3.

The activity of type I inhibitors on JNK3 and p38 $\alpha$  MAPK is generally evaluated through biological assays quantifying the amount of MAPK substrate phosphorylated from the active enzymes in the presence and absence of the inhibitor [27,28]. These activity assays provide an exhaustive indication about the inhibitory activity of compounds but are generally expensive, time-consuming, and not amenable for high-throughput screening (HTS) due to multiple separation and washing steps. The evaluation of type II inhibitors is instead far more challenging, although some screening assays for inactive p38 $\alpha$  MAPK have been reported during recent years [29,30]. An additional strategy in the identification of new kinase inhibitors is the detection of the binding affinity of novel compounds for the enzymes, which is a substantial prerequisite for any inhibitory activity. With this scope, here we report the development and optimization of fluorescence polarization (FP)-based competition binding assays, which employ a novel fluorescein-labeled probe binding to both the active and inactive conformations of JNK3 and p38 $\alpha$  MAPK. FP is a technique increasingly used within recent years in the field of drug discovery due to its advantages such as versatility, speed, easy handling, and cost efficiency [31,32]. It is even useful for detecting weak binding events limited only by compound solubility [33]. The basic principle of this methodology is that after excitation by plane polarized light, the fluorophore's emission is polarized as well due to photoselection. However, the capability of the fluorophore to retain such polarization depends on its molecular size. Small molecules, such as the fluorophore alone, are prone to fast tumbling due to Brownian motions. Therefore, the light emitted easily loses the polarization achieved and produces a low FP signal. On the other hand, the FP signal dramatically increases when the fluorophore binds to a protein due to a slower tumbling of the high molecular weight complex. As a result, the displacement of a fluorescent probe from the enzyme by a tested compound can be followed by measuring the FP signal directly after the addition (mix and measure) without separation and washing steps. This feature, together with significantly improved safety, makes the FP-based binding assay superior in comparison with traditional binding assays based on radioligands [34,35].

The assay presented here, using slightly different conditions, was recently employed by our group on the wild-type form as well

as on gatekeeper mutations of JNK3 [36] and represents the first example of an FP-based binding assay on JNK3. On the other side, Munoz and coworkers in 2010 reported an FP competition assay for the inactive form of p38 $\alpha$  MAPK [37]. The probe employed in this assay (compound 2; Fig. 1) is based on the prototypical p38 $\alpha$  MAPK inhibitor SB203580, which was modified on its side chain and labeled with the 4'-isomer of fluorescein isothiocyanate (FITC). However, the FP assay reported by Munoz and coworkers does not show correlation with the p38 $\alpha$  MAPK activity assay ( $R^2 = -0.4005$ ) [37].

Here, we describe the development of two novel and wider applicable probes (compounds 5 and 6; Fig. 2) due to their derivation from dual JNK3/p38 $\alpha$  MAPK inhibitors (compounds 3 and 4; Fig. 2). Two analogous binding assays employing the inactive form of both kinases, JNK3 and p38 $\alpha$  MAPK, using the most promising probe 5 were optimized. The use of the inactive form of both kinases enhances the application spectrum of these assays because it enables the evaluation of binding affinity for type I inhibitors as well as type II inhibitors. The results obtained from the binding assays were correlated with the results obtained from enzyme-linked immunosorbent assay (ELISA) activity assays, and the viability of the optimized protocols in an HTS format was investigated.

## Materials and methods

### Computational docking analysis

#### Molecule and binding pocket preparation for docking

To prepare molecules for docking, we used the Molecular Operating Environment (MOE) suite's “molecule wash” function to deprotonate strong acids and protonate strong bases (MOE 2013.08; Chemical Computing Group, Montreal, QC, Canada). Energy minimization of all molecules was then performed by using the MMFF94x force field at a gradient of 0.0001 root mean square deviation (rmsd). Existing chirality was preserved and partial charges were calculated according to the parameters of the force field.

All crystal structures (3FF3 and 1OUK) [38,39] were downloaded from the Protein Data Bank (PDB) [40]. Subsequently, protonation of the protein–ligand complex was performed with the MOE “protonate 3D” function at standard settings ( $T = 300$  K, pH 7.0, ionic strength  $I = 0.1$  M).

#### Docking experiments

All docking experiments were performed using the docking program GOLD (version 5.2.2; Cambridge Crystallographic Data Centre, Cambridge, UK) in combination with the scoring functions ChemPLP [41] and GoldScore [42] for 3FF3 and the combination of GoldScore and ChemScore [43] for 1OUK. The search efficiency for the genetic algorithm was increased from standard 100% to 200% at automatic mode. Binding site residues were defined by specifying crystal structure ligand coordinates; and the active site radius setting remained at a default value of 6 Å with the “detect cavity” option enabled. For each target, we employed a test docking of the ligand from the crystal structure into its binding pocket. If pose retrieval was unsatisfying, we optimized docking parameters and continued with the best settings in respect of pose retrieval.

#### Probe synthesis

##### General

All reagents and solvents were of commercial quality and used without further purification. Thin layer chromatography (TLC) reaction controls were performed for all reactions using fluorescent

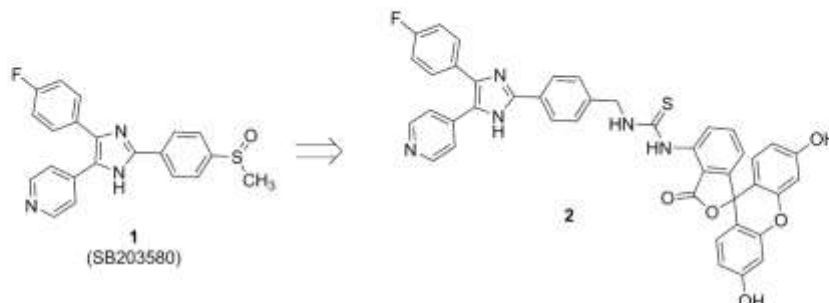


Fig. 1. Reported probe for p38 $\alpha$  MAPK FP assay based on the p38 $\alpha$  MAPK prototype inhibitor SB203580.

silica gel 60 F<sub>254</sub> plates (Merck) and visualized under natural light and ultraviolet (UV) illumination at 254 and 365 nm. The purity of all synthesized probes and tested compounds is greater than 95% as determined via reverse phase high-performance liquid chromatography (HPLC) on a Hewlett Packard HP 1090 series II LC device equipped with a UV diode array detector (DAD; detection at 230 and 254 nm). The chromatographic separation was performed on a Phenomenex Luna C8 column (150 × 4.6 mm, 5  $\mu$ m) at 35 °C oven temperature. The injection volume was 5  $\mu$ l and the flow was 1.5 ml/min using the following gradient: 0.01 M KH<sub>2</sub>PO<sub>4</sub> (pH 2.3) (solvent A), methanol (solvent B), 40% B to 85% B in 8 min; 85% B for 5 min; 85% to 40% B in 1 min; 40% B for 2 min; stop time 16 min. Column chromatography was performed on Davisil LC60A 20–45  $\mu$ m silica from Grace Davison and Geduran Si60 63–200  $\mu$ m silica from Merck for the precolumn using an Interchim Puriflash 430 automated flash chromatography system. Nuclear magnetic resonance (NMR) spectra were measured on a Bruker Avance NMR spectrometer at 250 MHz in the Organic Chemistry Institute, Eberhard Karls Universität Tübingen, or on a Bruker Avance 400 NMR spectrometer in the Institute of Pharmaceutical Sciences, Eberhard Karls Universität Tübingen. Chemical shifts are reported in parts per million (ppm) relative to tetramethylsilane. All spectra were calibrated against the (residual proton) peak of the deuterated solvent used. Mass spectra were performed on an Advion Expression S electrospray ionization mass spectrometry (ESI–MS) instrument with TLC interface in the Institute of Pharmaceutical Sciences, Eberhard Karls Universität Tübingen.

#### Experimental procedures

*N*-(4-(4-(4-Fluorophenyl)-2-(methylthio)-1H-imidazol-5-yl)pyridin-2-yl)benzene-1,4-diamine (**3**). In a pressure tube, compound **8** (500 mg, 1.65 mmol) and *p*-phenylenediamine (267 mg, 2.47 mmol) were suspended in *n*-butanol (30 ml), and then 1.25 M HCl in ethanol (1.32 ml, 1.65 mmol) was added. After sealing the tube, the mixture was stirred at 180 °C for 16 h. The solvent was evaporated at reduced pressure, and the residue was purified by flash column chromatography (dichloromethane/ethanol, 19:1 to 93:7), giving 568 mg of product (88%). <sup>1</sup>H NMR (400 MHz, DMSO-*d*<sub>6</sub>)  $\delta$  (ppm) 2.61 (s, 3H), 4.74 (br s, 2H), 6.49 (d, *J* = 7.1 Hz, 2H), 6.53–6.96 (m, 2H), 7.11 (d, *J* = 7.1 Hz, 2H), 7.16–7.37 (m, 2H), 7.50 (br s, 2H), 7.80–8.11 (m, 1H), 8.24–8.54 (m, 1H), 12.65 (br s, 1H); HPLC: *t* = 3.36 min, 98%; ESI–MS: [M+H]<sup>+</sup> calculated 392.13, found 392.2.

1-(3',6'-Dihydroxy-3-oxo-3H-spiro[isobenzofuran-1,9'-xanthen]-5-yl)-3-(4-((4-(4-(4-fluorophenyl)-2-(methylthio)-1H-imidazol-5-yl)pyridin-2-yl)amino)phenyl)thiourea (**5**). A suspension of **3** (200 mg, 0.51 mmol) and FITC isomer **5'** (298 mg, 0.76 mmol) in acetone (60 ml) was stirred at room temperature (RT) for 24 h covered from light. The solvent was evaporated at reduced pressure and the residue was purified by flash column chromatography (dichloromethane/ethanol, 19:1 to 4:1), giving 207 mg of the desired compound (52%). <sup>1</sup>H NMR (250 MHz, DMSO-*d*<sub>6</sub>)  $\delta$  (ppm) 2.62 (s, 3H), 6.55–6.85 (m, 7H), 7.05–7.35 (m, 6H), 7.45–7.65 (m, 4H), 7.83 (d, *J* = 8.2 Hz, 1H), 7.95–8.15 (m, 1H), 8.20 (br s, 1H), 9.10 (br s, 1H).

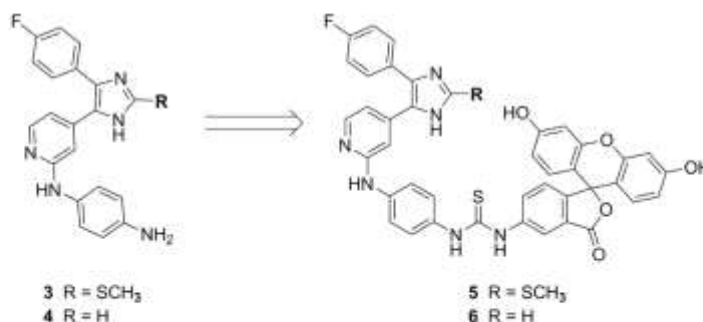


Fig. 2. Novel probes for JNK3 and p38 $\alpha$  MAPK FP assay based on potent dual JNK3/p38 $\alpha$  MAPK inhibitors **3** and **4**.



9.95–10.25 (m, 4H), 12.70 (br s, 1H); HPLC:  $t_r$  = 6.19 min, 95%; ESI–MS:  $[M-H]^-$  calculated 779.85, found 779.5.

**2-Fluoro-4-(4-(4-fluorophenyl)-1H-imidazol-5-yl)pyridine (11).** Compound **10** (2.00 g, 8.09 mmol) was dissolved in dimethylformamide (DMF; 5 mL), and then formaldehyde (243 mg, 8.09 mmol), ammonium acetate (6.23 g, 80.9 mmol), and glacial acetic acid (47 mg, 0.81 mmol) were added and the mixture was stirred at 70 °C for 1 h. The reaction mixture was poured into water and the precipitate formed was filtered, washed with water, and dried. The solid was then purified by column chromatography (dichloromethane/ethanol, 97:3 to 4:1), yielding 200 mg (10%) of **11**.

Spectroscopic data were in agreement with those in the literature [44].

**N1-(4-(4-(4-Fluorophenyl)-1H-imidazol-5-yl)pyridin-2-yl)benzene-1,4-diamine (4).** In a pressure tube, compound **11** (150 mg, 0.58 mmol) and *p*-phenylenediamine (315 mg, 2.91 mmol) were suspended in *n*-butanol (3 mL), and then 1.25 M HCl in ethanol (0.46 mL, 0.58 mmol) was added. After sealing the tube, the mixture was stirred at 180 °C for 16 h. The solvent was evaporated in vacuo and the residue was purified twice by column chromatography (dichloromethane/ethanol, 19:1 to 4:1), giving 124 mg of product (60%). <sup>1</sup>H NMR (250 MHz, DMSO-*d*<sub>6</sub>)  $\delta$  (ppm) 4.75 (br s, 2H), 6.46 (d,  $J$  = 8.6 Hz, 2H), 6.60 (dd,  $J_1$  = 5.3 Hz,  $J_2$  = 1.2 Hz, 1H), 6.77 (br s, 1H), 7.06 (d,  $J$  = 8.6 Hz, 2H), 7.20–7.30 (m, 2H), 7.45–7.55 (m, 2H), 7.80 (s, 1H), 7.95 (br s, 1H), 8.35 (br s, 1H), 12.60 (br s, 1H); HPLC:  $t_r$  = 2.25 min, 100%; ESI–MS:  $[M+H]^+$  calculated 346.38, found 346.3;  $[M-H]^-$  calculated 344.38, found 344.3.

**1-(3',6'-Dihydroxy-3-oxo-3H-spiro[isobenzofuran-1,9'-xanthen]-5-yl)-3-(4-(4-(4-fluorophenyl)-1H-imidazol-5-yl)pyridin-2-yl)amino)phenylthiourea (6).** A solution of compound **4** (70 mg, 0.20 mmol) and FITC isomer 5' (118 mg, 0.30 mmol) in acetone (20 mL) was stirred at RT for 24 h. The reaction mixture was concentrated to dryness and the residue was purified by column chromatography (dichloromethane/ethanol, 9:1 to 1:1) to yield 60 mg (40%) of product **6**. <sup>1</sup>H NMR (250 MHz, DMSO-*d*<sub>6</sub>)  $\delta$  (ppm) 6.50–6.67 (m, 6H), 6.73 (d,  $J$  = 5.5 Hz, 1H), 7.05–7.35 (m, 7H), 7.45–7.60 (m, 4H), 7.80–7.87 (m, 2H), 8.05 (br s, 1H), 8.26 (br s, 1H), 9.05 (br s, 1H), 10.00–10.60 (m, 4H), 12.52 (br s, 1H); HPLC:  $t_r$  = 3.77 min, 96%; ESI–MS:  $[M-H]^-$  calculated 733.76, found 733.4.

#### Expression and purification of inactive JNK3 and inactive p38 $\alpha$ MAPK

Inactive JNK3 and p38 $\alpha$  MAPK were expressed and purified following the procedure previously reported by Lange and co-workers [36].

#### Activity assay

Probes **5** and **6**, as well as compounds **1**, **3**, and **12** to **22**, were tested for their inhibitory activity for JNK3 and/or p38 $\alpha$  MAPK in previously reported ELISA activity assays [27,28].

#### FP assay

##### General

All FP measurements were performed in black, nonbinding 96-well plates (Greiner Bio-One) and conducted through a CLARIOstar microplate reader (BMG Labtech) using excitation and emission filters of 480 and 530 nm, respectively. For JNK3 measurements,

buffer A (25 mM Hepes [pH 7.0], 100 mM NaCl, 2 mM MgCl<sub>2</sub>, 10 mM  $\beta$ -mercaptoethanol [BME], and 0.05 mg/ml bovine serum albumin [BSA]) was used, whereas buffer B (25 mM Tris [pH 7.1], 100 mM NaCl, 10 mM MgCl<sub>2</sub>, 5 mM dithiothreitol [DTT], 5% glycerol, and 0.05 mg/ml BSA) was employed in the assay performed on p38 $\alpha$  MAPK. The concentration of DMSO used in every assay was 5% (v/v), and the final volume in every well was 200  $\mu$ L. Incubation was carried out for the respective time at RT on an Eppendorf MixMate at 400 revolutions per minute (rpm), including 2 min inside the plate reader in order to equilibrate at the measurement temperature (25 °C for JNK3 and 28 °C for p38 $\alpha$  MAPK), which deviated only marginally from the incubation temperature. Before every measurement, the focal height of the excitation beam was tuned in order to achieve the optimal fluorescence intensity and the gain value for both detectors was adjusted. All experiments were performed three times in quadruplicate. Absolute polarization values were normalized to the average values of first well and last well replicates and are reported as percentages. Data were fitted to a four-parameter logistic curve with variable slope using the software GraphPad Prism 4 (GraphPad Software, San Diego, CA, USA).  $K_i$  values for the competition assays were calculated from the measured IC<sub>50</sub> values using a modified Cheng–Prusoff equation from the Wang's group [45,46].

#### Probe characterization and time stability

A final concentration of 10 nM of probes **5** and **6** was titrated with 3-fold increasing concentrations of JNK3 and p38 $\alpha$  MAPK, ranging from 0 to 600 nM. Concentrations used for both kinases were 0, 0.01, 0.03, 0.09, 0.27, 0.82, 2.47, 7.40, 22.22, 66.66, 200, and 600 nM. Prior to the reading, plates were incubated for total times of 15, 30, and 60 min.

#### Optimization of assay conditions

A final concentration of 5 nM of probe **5** was titrated with 3-fold increasing concentrations of JNK3 and p38 $\alpha$  MAPK, ranging from 0 to 300 nM. Concentrations used for both kinases were 0, 0.005, 0.015, 0.045, 0.13, 0.41, 1.23, 3.70, 11.11, 33.33, 100, and 300 nM. The FP was measured after a total time of incubation of 30 min.

#### Autofluorescence assay

Prior to the measurement, compounds **1**, **3**, and **12** to **23** were tested for their fluorescence intensity at the excitation and emission wavelengths of 480 and 530 nm, respectively, using a concentration of 1  $\mu$ M of the test compound in buffer A. Buffer A containing 5% DMSO (v/v) served as a negative control, whereas two different concentrations of probe **5** (5 nM and 1  $\mu$ M) in the same buffer were used as positive controls.

#### Competition binding assay

Final concentrations of 10 nM of the respective protein kinase and 5 nM of probe **5** were measured after the addition of increasing concentrations of compounds **1**, **3**, **12** to **16**, **18**, and **20** to **23** (11 different concentrations including a well without inhibitor). For each measurement, a well containing a 5-nM concentration of probe **5** in buffer was included as a negative control. The range of compound concentrations was selected in order to achieve a full sigmoidal curve. The FP signal was measured after an incubation time of 30 min. Linear regression on plotted logarithmic results of the FP assay and the ELISA activity assay was calculated using GraphPad Prism 4.

#### HTS assay validation

The suitability for HTS of the competition binding assays on JNK3 and p38 $\alpha$  MAPK was evaluated following the National Center for Biotechnology Information (NCBI) guidelines manual [47]. The

interleaved signal format described was employed. For the assays, a 10-nM concentration of the enzyme in the respective assay buffer and a 5-nM concentration of probe **5** were employed in every well. DMSO (5%, v/v) was constantly used in all of the assay plates. As a negative control for both enzymes, probe **5** alone at the aforementioned concentration was chosen. In the JNK3 experiments, compound **3** at a concentration of 1  $\mu$ M was employed as a positive control, whereas the same compound at 20 nM concentration was used as middle control. Regarding the p38 $\alpha$  MAPK, the same compound (**3**) was employed at concentrations of 2  $\mu$ M and 50 nM for the positive and middle controls, respectively. The experiment was performed three times on 3 different days; controls were plated in a black, nonbinding 96-well plate following the scheme reported in the literature [47], and the FP signal was read after 30 min of incubation at RT. The measurement was carried out at 25 °C, and the focus height and the gain values were adjusted before every measurement. Percentage coefficients of variation (% CVs) for the negative, positive, and middle controls were calculated for each plate. Each single-well signal of middle control was normalized to the mean of negative and positive controls of the same plate in order to achieve a percentage of activity. After that, the means and standard deviations for the middle control were calculated on the normalized values. Finally, the Z-factor of every plate was calculated. The single-well signals of each day were plotted separately in graphs “by row, then column” and “by column, then row” using the software Graph Pad Prism 4 in order to detect drift or edge effects.

#### Isothermal titration calorimetry

A reverse isothermal titration calorimetry (ITC) was performed due to the lack of solubility of compounds to be tested. Solutions (10 mM) of probes **5** and **6** in DMSO were diluted 1:100 with pure DMSO and eventually further diluted 1:20 with buffer C (50 mM Hepes [pH 7.0], 100 mM NaCl, 2 mM MgCl<sub>2</sub>, and 2 mM tris(2-carboxyethyl)phosphine [TCEP]) for JNK3 and with buffer D (25 mM Tris [pH 7.1], 100 mM NaCl, 10 mM MgCl<sub>2</sub>, and 1 mM BME) for p38 $\alpha$  MAPK in order to achieve a 4- $\mu$ M concentration of compound with a 5% (v/v) final DMSO concentration. The aforementioned solutions were loaded into the sample cell of a MicroCal ITC200 (formerly GE Healthcare, now Malvern). A freshly concentrated solution of JNK3 or p38 $\alpha$  MAPK in buffer C or D, respectively, containing a 5% (v/v) DMSO concentration, was loaded in the titration syringe. Measurements were performed at 25 °C. Protein solution was titrated into the sample cell in 20 injection steps of 2  $\mu$ l each at a rate of 0.5  $\mu$ l/s with an interval of 120 s between the steps. Stirring was applied at 1000 rpm. Before the first step, 0.5  $\mu$ l of protein solution was injected into the sample cell in order to correct for protein diffusion from the syringe during experimental setup and equilibration. The data point of this pre-step was neglected during data analysis. Data analysis was performed using MicroCal Origin software (version 7.0552; OriginLab, Northampton, MA, USA).

## Results

#### Design, synthesis, and characterization of probes **5** and **6**

As a starting point for the design of the two probes, the two pyridinylimidazoles **3** and **4** were selected as precursor molecules (Fig. 2). Both compounds were identified in a current ongoing research program as potent dual inhibitors of JNK3 and p38 $\alpha$  MAPK (Table 1). The *p*-phenylenediamino group present in both compounds was chosen for the linking of the fluorescein tag. Computational docking studies of **3** with both kinases (see Fig. S1 in online

**Table 1**  
Biological activity of precursors **3** and **4** and probes **5** and **6** tested in ELISA activity assays.

Compound	IC <sub>50</sub> $\pm$ SEM (nM)	
	JNK3	p38 $\alpha$ MAPK
<b>3</b>	24 $\pm$ 1	17 $\pm$ 0
<b>4</b>	4.7 $\pm$ 0.4	7.5 $\pm$ 0.3
<b>5</b>	48 $\pm$ 2	26 $\pm$ 0
<b>6</b>	74 $\pm$ 1	29 $\pm$ 2

Note: n = 3.

supplementary material) as well as comparison of the binding mode with similar pyridinylimidazole- and pyrimidinylimidazole-based kinase inhibitors [38,48,49] revealed that this portion of the molecule occupies the hydrophobic region II of the enzyme. This is an area of the ATP binding pocket that is solvent exposed and thus is supposed to be able to tolerate the bulkiness of the fluorescein moiety. In contrast to the previously reported probe **2** by Munoz and coworkers (Fig. 1) [37], we chose the more easily available 5'-isomer of FITC as a starting material to insert the fluorophore. The design hypothesis of our probes was supported by computational docking studies of compound **5**, with both enzymes showing the bulky fluorescein group ranging outside the enzyme and therefore presumably not hampering the binding (see Fig. S2 in supplementary material).

The first probe, compound **5**, was synthesized as depicted in Scheme 1 starting from known 2-chloro-4-(4-(4-fluorophenyl)-2-(methylthio)-1*H*-imidazol-5-yl)pyridine (**8**). Pyridinylimidazole **8**, which is synthetically accessible from the commercially available 2-chloro-4-methylpyridine (**7**) in four synthetic steps [50], was subsequently reacted in a nucleophilic aromatic substitution reaction with *p*-phenylenediamine to obtain compound **3**. The precursor **3** was labeled with the fluorophore through the formation of a thiourea group between the primary amino group and the 5'-isomer of FITC at RT.

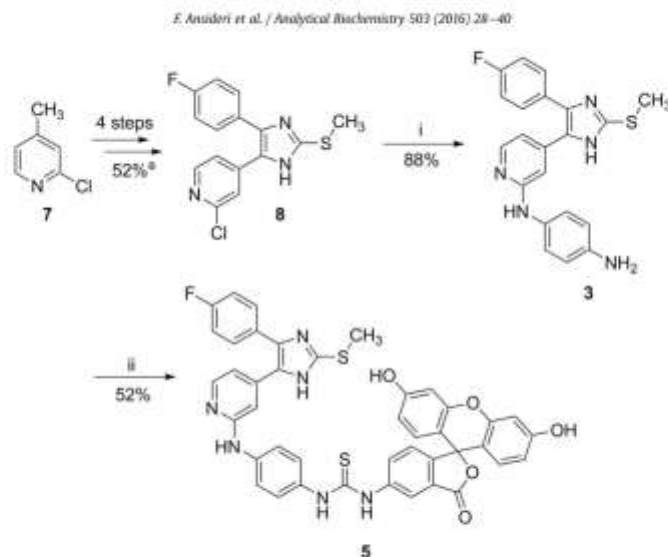
The second probe, compound **6** (PTD105016 in our previously published work [36]), was prepared starting from already reported ethane-1,2-dione **10**, which was synthesized according to our reported protocol in two steps from 2-fluoro-4-methylpyridine (**9**) (Scheme 2) [51]. Cyclization under Radziszewski conditions [52] of dione **10** using ammonium acetate and formaldehyde provided pyridinylimidazole **11**. Finally, the substitution with *p*-phenylenediamine and the introduction of the fluorophore yielding probe **6** were performed using the same conditions as described for probe **5**.

Probes **5** and **6** were also tested for their ability to inhibit JNK3 and p38 $\alpha$  MAPK, showing only a negligible decrease in potency in comparison with the unlabeled precursors **3** and **4** (Table 1). This demonstrates the low impact of the fluorescent moiety on the binding affinity, confirming our design hypothesis as well as the results of the docking studies.

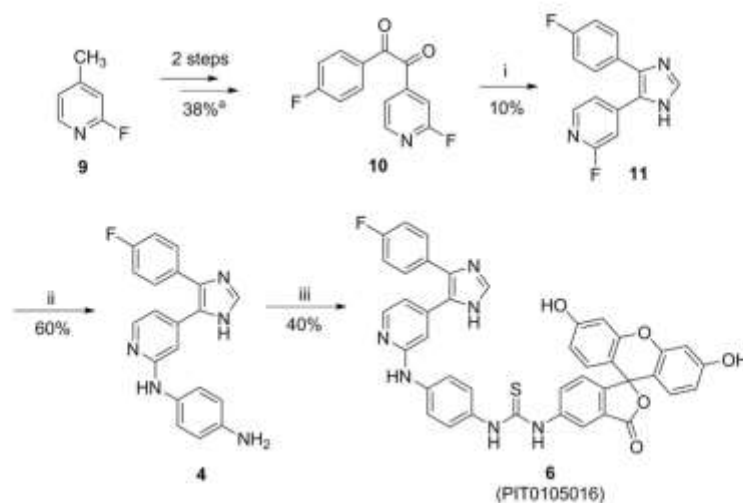
The insertion of a further spacer between the fluorescein moiety and the *p*-phenylenediamino group therefore was considered unnecessary and potentially detrimental because a higher flexibility of the fluorescein-labeled probe could cause a decrease in the width of the signal window [53].

#### K<sub>d</sub> determination of probes

With the aim to estimate the binding of the two probes to the inactive form of the protein kinases, a fixed concentration of 10 nM of probes **5** and **6** was titrated with increasing concentrations of JNK3 and p38 $\alpha$  MAPK (0–600 nM). The FP signal was read after incubation at RT for 15, 30, and 60 min, thereby also allowing



**Scheme 1.** Synthesis of probe **5** starting from 2-chloro-4-methylpyridine (**7**). Reagents and conditions: (i) *p*-phenylenediamine, HCl in ethanol (1.25 M), *n*-butanol, 180 °C, 16 h; (ii) FITC isomer (**5'**), acetone, RT, 24 h. <sup>a</sup>Yield derived from Laufer and Liedtke [50].

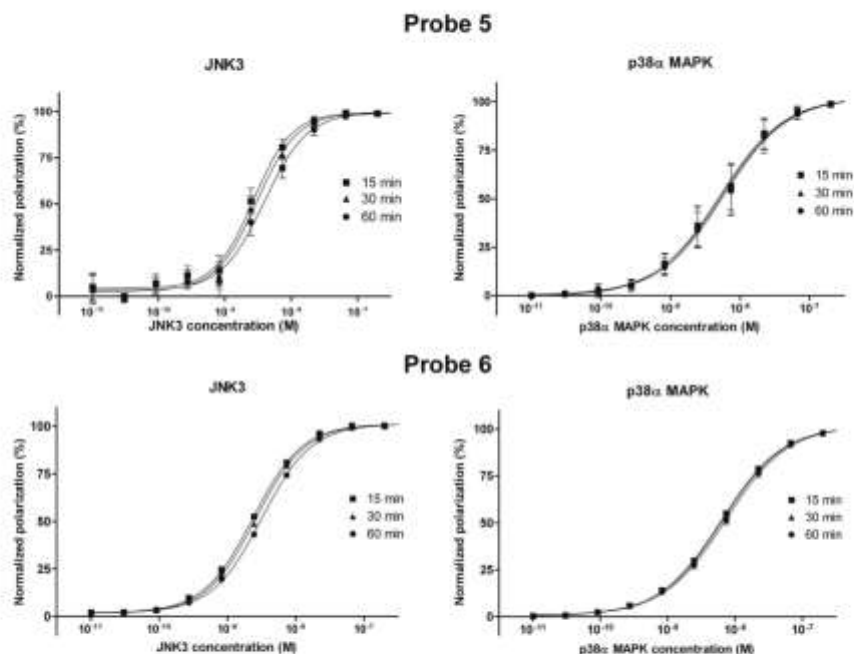


**Scheme 2.** Synthesis of probe **6** starting from 2-fluoro-4-methylpyridine (**9**). Reagents and conditions: (i) formaldehyde,  $\text{NH}_4\text{OAc}$ , acetic acid, DMF, 70 °C, 1 h; (ii) *p*-phenylenediamine, HCl in EtOH (1.25 M), *n*-butanol, 180 °C, 16 h; (iii) FITC isomer (**5'**), acetone, RT, 24 h. <sup>a</sup>Yield derived from Koch and coworkers [51].

evaluation of the time dependence of the experiments in terms of equilibrium onset and signal stability. Nonlinear fit of the data obtained in the titration experiments of the two probes (Fig. 3) resulted in very close  $K_d$  values in the low single-digit nanomolar range for both kinases (Table 2). Due to a very similar binding profile of the two compounds, the selection of probe **5** for the further optimization of the assays relied mainly on a higher overall

yield of the synthetic route (23% in the case of probe **5** vs. 1% in the case of probe **6**; cf. Scheme 1 vs. Scheme 2). Regarding the time dependence of the assays, both probes showed in both enzymes only a small variation in  $K_d$  value ( $\leq 1.3$  nM) between 15 and 60 min. This suggests a rapid onset of the binding equilibrium of the probes that is already reached after 15 min. Nevertheless, because an incubation time of 30 min was considered more suitable in binding





**Fig. 3.** Titration of probes **5** and **6** with inactive JNK3 and inactive p38 $\alpha$  MAPK. Probe concentration was 10 nM in 5% (v/v) DMSO. Data points represent mean values  $\pm$  standard deviations.

competition assays of inhibitors with unknown binding kinetics, the  $K_d$  values of the two probes after 30 min of incubation were selected as the  $K_d$  values to be considered in the competition assays.

The  $K_d$  values of probes **5** and **6** were further determined using ITC as an additional technique. The  $K_d$  values (Table 3; see also Fig. S3 in supplementary material) obtained by ITC experiments for both probes are slightly higher compared with those obtained by direct titration in the corresponding FP assays, probably due to different intrinsic characteristics of the two techniques and of the experimental protocols. Nevertheless, the high affinity of the probes for the two enzymes was again confirmed.

#### Optimization of assay conditions

After determination of  $K_d$  values for probe **5** (Table 2), a concentration of 5 nM was selected as a final concentration to be used

in the competition assays for both enzymes. This is in accordance with FP assay development guidelines [54], suggesting a probe concentration as low as possible, preferably not significantly higher than twice the probe  $K_d$  value. Using this probe concentration, a second titration with increasing concentrations of the two enzymes was performed in order to select the optimal protein concentration (see Fig. S4 in supplementary material). In line with practical considerations [54], such concentration should yield an increase in the polarization signal included between 50 and 80% of the overall signal window, thereby giving a still significant width of signal and at the same time being far from stoichiometric conditions, in order to provide the assay with a better sensitivity. Therefore, a concentration of 10 nM of both enzymes, yielding signal windows of approximately 140 and 165 mP for JNK3 and p38 $\alpha$  MAPK, respectively, was selected as the standard concentration employed in the competition assays.

**Table 2**  
Binding affinities of probes **5** and **6** for JNK3 and p38 $\alpha$  MAPK at different times of incubation tested in the FP assays.

Probe	$K_d \pm$ SEM [nM]					
	JNK3			p38 $\alpha$ MAPK		
	15 min	30 min	60 min	15 min	30 min	60 min
<b>5</b>	2.7 $\pm$ 0.2	3.0 $\pm$ 0.2	4.0 $\pm$ 0.3	5.4 $\pm$ 1.0	5.7 $\pm$ 1.1	6.2 $\pm$ 1.2
<b>6</b>	2.3 $\pm$ 0.1	2.6 $\pm$ 0.1	3.2 $\pm$ 0.1	6.2 $\pm$ 0.1	6.5 $\pm$ 0.2	7.2 $\pm$ 0.3

Note.  $n = 3$ . Concentration of probe used was 10 nM. Total volume of DMSO was 5% (v/v). SEM, standard error of the mean.

**Table 3**  
Binding affinities of probes **5** and **6** for JNK3 and p38 $\alpha$  MAPK determined by ITC.

Probe	$K_d \pm$ SEM [nM]	
	JNK3	p38 $\alpha$ MAPK
<b>5</b>	25 $\pm$ 5	35 $\pm$ 5
<b>6</b>	20 $\pm$ 1	33 $\pm$ 3

Note.  $n = 3$ . Results were obtained through reverse ITC. Protein concentration in the titration syringe was 55  $\mu$ M and compound concentration in the sample cell was 4  $\mu$ M. SEM, standard error of the mean.



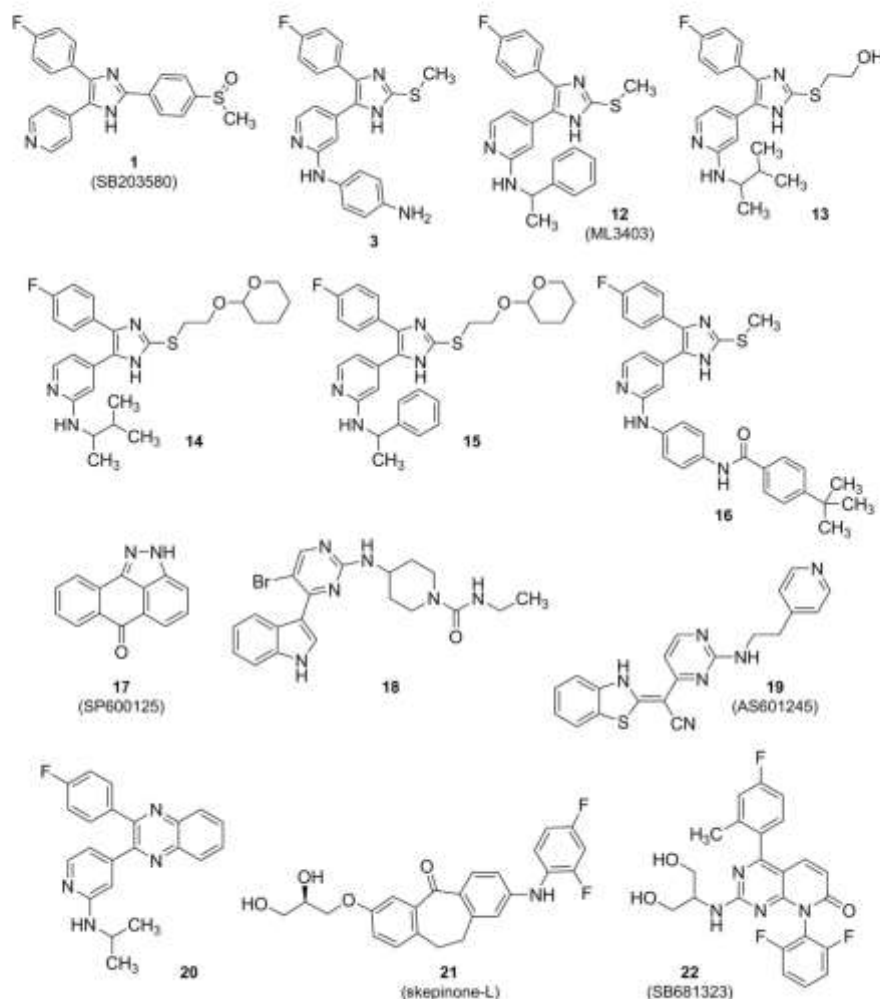


Fig. 4. Structures of tested compounds.

#### Assay validation and correlation

With the purpose of validating the optimized assays, as well as assessing their viability in predicting the potency of type I inhibitors in reference activity assays, a series of 13 compounds (Fig. 4) was selected to be evaluated for JNK3 and/or p38 $\alpha$  MAPK for their capability to displace the fluorescein-labeled probe **5**. This series consists of different pyridinylimidazoles from our compound library [55,56], including the nonlabeled precursor of probe **5** (compound **3**) as well as the two p38 $\alpha$  MAPK reference compounds SB203580 (**1**) and ML3403 (**12**). To demonstrate the full capacity of the probe, examples of non-pyridinylimidazole-type kinase

inhibitors were also selected to be investigated. The early JNK3 inhibitor SP600125 (**17**) [57], aminopyrimidine **18** [36], and clinical candidate AS601245 (**19**) [58] were chosen for the assay on JNK3, whereas high-quality kinase probe skepinone-L (**21**) [59] and clinical candidate SB681323 (**22**) [60] were tested on p38 $\alpha$  MAPK. Finally, pyridinylquinoxaline **20** [51] was tested on both enzymes.

All selected compounds were primarily tested for auto-fluorescence at the absorption and emission wavelengths used for

**Table 4**  
Comparison of activity of tested compounds on ELISA activity assays and FP assays.

Compound	JNK3		p38 $\alpha$ MAPK	
	Activity assay (IC <sub>50</sub> $\pm$ SEM) (nM)	FP binding assay (K <sub>i</sub> $\pm$ SEM) (nM)	Activity assay (IC <sub>50</sub> $\pm$ SEM) (nM)	FP binding assay (K <sub>i</sub> $\pm$ SEM) (nM)
<b>1</b>	727 $\pm$ 28 <sup>b</sup>	167 $\pm$ 10	50 $\pm$ 0.4 <sup>e</sup>	56 $\pm$ 1
<b>3</b>	24 $\pm$ 1	3 $\pm$ 0.2	17 $\pm$ 0.4	14 $\pm$ 2
<b>12</b>	176 $\pm$ 2	40 $\pm$ 6	40 $\pm$ 5 <sup>f</sup>	38 $\pm$ 1
<b>13</b>	181 $\pm$ 4	11 $\pm$ 1	11 $\pm$ 0.9 <sup>g</sup>	4 $\pm$ 1
<b>14</b>	370 $\pm$ 13	49 $\pm$ 2	53 $\pm$ 4	39 $\pm$ 9
<b>15</b>	742 $\pm$ 12	142 $\pm$ 18	170 $\pm$ 10	141 $\pm$ 10
<b>16</b>	67 $\pm$ 2	5 $\pm$ 1	97 $\pm$ 8	61 $\pm$ 7
<b>18</b>	147 $\pm$ 5	29 $\pm$ 2	n.l.	n.l.
<b>20</b>	3,950 $\pm$ 200 <sup>c</sup>	1,041 $\pm$ 32	81 $\pm$ 5 <sup>f</sup>	350 $\pm$ 10
<b>21</b>	n.l.	n.l.	5 $\pm$ 2 <sup>h</sup>	4.2 $\pm$ 0.4
<b>22</b>	n.l.	n.l.	13 $\pm$ 0.1	7 $\pm$ 0.1

Note:  $n = 3$ . SEM, standard error of the mean. n.l., not tested.

<sup>a</sup> Data previously reported by Goettert and coworkers [27].

<sup>b</sup> Data previously reported by Goettert and coworkers [28].

<sup>c</sup> Data previously reported by Laufer and coworkers [61].

<sup>d</sup> Data previously reported by Koch and coworkers [36].

<sup>e</sup> Data previously reported by Koch and coworkers [31].

<sup>f</sup> Data previously reported by Fischer and coworkers [62].

the fluorescein-labeled probe in order to ensure that the measured FP signal could be exclusively attributable to the probe. One of the drawbacks of FP assay indeed is its unsuitability for the evaluation of compounds showing autofluorescence at the same wavelengths employed for the fluorophore [53]. For this reason, SP600125 (**17**) and AS601245 (**19**), which displayed a fluorescence comparable to the positive control (5-nM probe), needed to be excluded from the assay (data not shown). To achieve for every measurement a complete displacement of the labeled probe, compounds were tested at different ranges of concentrations depending on their ability to bind the two protein kinases. The IC<sub>50</sub> values resulting from the competition binding assays were then converted into K<sub>i</sub> values through a modified Cheng–Prusoff equation [45,46] (Table 4).

As displayed in Fig. 5, the assays are valid for both enzymes because the unlabeled precursor of probe **5** (compound **3**) and other tested inhibitors are able to displace the probe in a dose-dependent manner. Subsequent to the assay validation, the correlation between the presented FP-based binding competition assays and the ELISA activity assays was investigated. A correlation between these two assays could make the binding assays useful tools for preliminary evaluation of new inhibitors of JNK3 and p38 $\alpha$  MAPK in a fast and relatively inexpensive manner with the aim to promote only better binders to a further characterization of the inhibition profile. Correlation was assessed through linear regression of the plotted logarithmic data for both assay methods (Fig. 6). With regard to JNK3, the enzyme activity assay and the FP-based competition binding assay proved to correlate remarkably ( $R^2 = 0.9555$ ). In the case of p38 $\alpha$  MAPK, a good correlation was observed ( $R^2 = 0.8447$ ), representing an advantage of our optimized p38 $\alpha$  MAPK FP assay in comparison with the existing one. These results display the suitability of both presented assays in the prediction of the inhibitory activity of novel compounds.

As it is possible to observe from Table 4, the K<sub>i</sub> values of the tested compounds are between the low single-digit nanomolar range and the low single-digit micromolar range. To estimate the limitation of binding affinity detection, a non-optimized inhibitor, namely 1-(4-fluorophenyl)-5-(pyridin-4-yl)imidazole (**23**), was tested as an example of a weak binder in both optimized FP assays. Compound **23** displayed K<sub>i</sub> values of 2,168  $\pm$  29 nM and 24,030  $\pm$  1,589 nM for JNK3 and p38 $\alpha$  MAPK, respectively (Fig. 7). Binders of JNK3 and p38 $\alpha$  MAPK with K<sub>i</sub> values up to the low

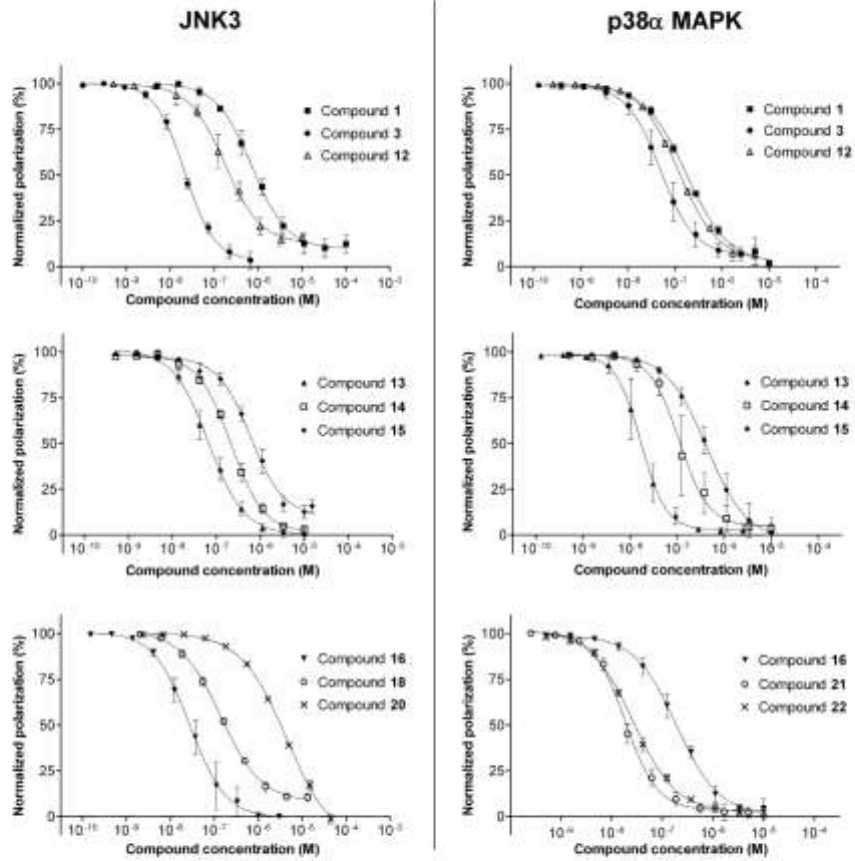
double-digit nanomolar range are detectable using the optimized FP assay protocols presented.

#### HTS assay validation

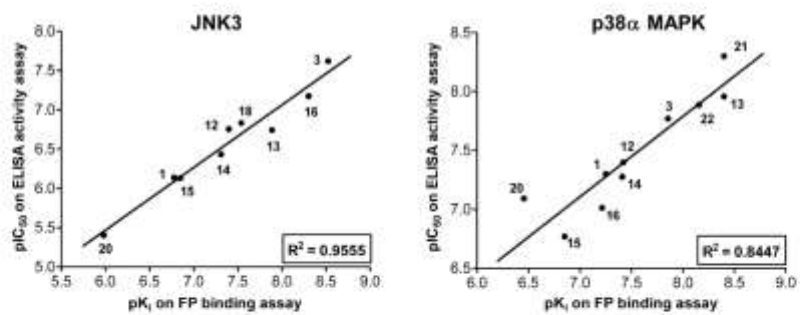
The outcome of the experiments performed in the previous section prompted us to exploit the correlation between the binding and the activity assays on both enzymes for the rapid estimation of the (potential) inhibitory activity for large compound sets. One of the advantages of FP assay is indeed the possibility to measure the signal directly after the addition of the components without washing or separation steps (mix and measure), which makes such assays suitable for the HTS format. To assess the viability of the FP assays developed for HTS, we followed the procedure reported in NCBI guidelines [47]. As negative control, probe **5** alone was selected. As a positive control, the unlabeled probe (compound **3**), at a concentration known to displace the probe completely, was added to the same concentration of probe **5**. Finally, compound **3** was used as a middle control at a concentration close to its IC<sub>50</sub> value. Results obtained (Tables 5 and 6) were in agreement with the acceptance criteria described in the guidelines (%CVs  $\leq$  20% for all controls, normalized standard deviations for the middle control  $\leq$  20, low inter-plate variability of the normalized middle signal, and Z-factor  $\geq$  0.4) and the plots of the single-well values showed the absence of significant drift and edge effects (see Figs. S5–S8 in supplementary material), highlighting the suitability of these assays for the HTS procedure.

#### Discussion

The research for novel inhibitors of the two protein kinases, JNK3 and p38 $\alpha$  MAPK, is still ongoing and aimed to the discovery of molecules displaying a high efficacy together with a satisfactory selectivity profile. A key approach might be represented by the identification of molecules, which bind preferentially the inactive conformation of these enzymes (type II inhibitors), taking advantage of binding pockets that are less conserved within the family of closely related kinases. With this scope, we developed two FP-based competition binding assays employing the inactive form of the two kinases able to measure the binding affinity of both type I and type II inhibitors. Classical activity assays using the active kinase exclude type II inhibitors predominantly binding to the



**Fig.5.** Results of competition binding assays for the selected compounds. Probe 5 concentration was 5 nM, and the concentration of enzyme was 10 nM. Data points represent mean values  $\pm$  standard deviations.



**Fig.6.** Linear regression of plotted results for the ELISA activity assay and the FP competition binding assay.

38

E. Anđević et al. / Analytical Biochemistry 503 (2016) 28–40

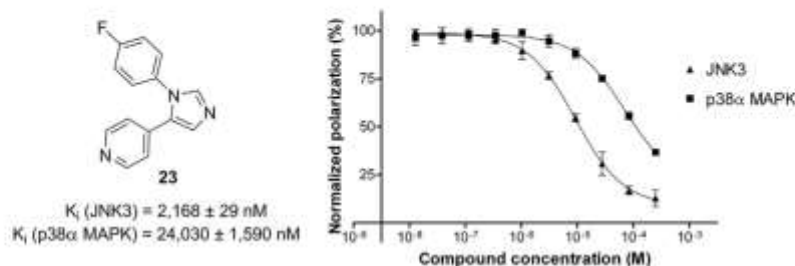
Fig. 7. Structure and binding affinity of 1-(4-fluorophenyl)-5-(pyridin-4-yl)imidazole (**23**).

Table 5

HTS assay validation results for JNK3.

#	Negative control		Positive control		Middle control		Normalized activity (%) (mean $\pm$ SD)	Z-Factor
	FP value (mP) (mean $\pm$ SD)	%CV	FP value (mP) (mean $\pm$ SD)	%CV	FP value (mP) (mean $\pm$ SD)	%CV		
1	300.3 $\pm$ 2.2	0.7	161.7 $\pm$ 2.8	1.7	220.8 $\pm$ 4.0	1.8	42.6 $\pm$ 2.9	0.89
2	300.5 $\pm$ 3.8	1.2	151.3 $\pm$ 3.3	2.2	210.7 $\pm$ 5.3	2.5	39.8 $\pm$ 3.5	0.86
3	298.0 $\pm$ 3.8	1.2	143.1 $\pm$ 3.2	2.2	195.1 $\pm$ 5.0	2.5	33.5 $\pm$ 3.2	0.86

Note: #, experiment number; SD, standard deviation.

Table 6

HTS assay validation results for p38 $\alpha$  MAPK.

#	Negative control		Positive control		Middle control		Normalized activity (%) (mean $\pm$ SD)	Z-Factor
	FP value (mP) (mean $\pm$ SD)	%CV	FP value (mP) (mean $\pm$ SD)	%CV	FP value (mP) (mean $\pm$ SD)	%CV		
1	296.1 $\pm$ 2.7	0.9	122.4 $\pm$ 4.3	3.5	256.0 $\pm$ 3.4	1.3	77.4 $\pm$ 2.0	0.88
2	304.9 $\pm$ 4.1	1.3	134.9 $\pm$ 3.5	2.6	226.9 $\pm$ 2.9	1.3	54.1 $\pm$ 1.7	0.86
3	291.9 $\pm$ 6.9	2.3	124.9 $\pm$ 4.6	3.6	214.6 $\pm$ 4.7	2.2	53.7 $\pm$ 2.8	0.79

Note: #, experiment number; SD, standard deviation.

inactive enzyme. Extending a previously reported assay for p38 $\alpha$  MAPK, the assay presented here broadens the range of applicability including JNK3 due to the use of a dual JNK3/p38 $\alpha$  MAPK inhibitor as a precursor of the probe employed. In addition, the comparison of the FP assays presented with well-known ELISA activity assays allowed observing a correlation between the two assays performed on both protein kinases. These results point out the potential of the assays presented as rapid and relatively inexpensive (e.g. low concentrations of kinase needed, no costly kinase substrates and antibodies required) alternatives to activity assays, which can be used to predict the inhibitory activity of new compounds at an early stage. Finally, the suitability of these assays to the HTS format allows the screening of wide libraries of compounds and therefore represents an improvement in the research of new JNK3 and p38 $\alpha$  MAPK inhibitors.

## Conclusion

The synthesis of two novel fluorescein-based pyridinylimidazoles and their evaluation for their ability to act as probes for the determination of binding affinity of kinase inhibitors to JNK3 and p38 $\alpha$  MAPK has been presented. Fast and inexpensive FP assays for both enzymes using probe **5** (JNK3:  $K_d$  = 3.0 nM; p38 $\alpha$  MAPK:  $K_d$  = 5.7 nM) were developed and validated with known inhibitors of JNK3 and p38 $\alpha$  MAPK. The comparison of the results obtained from the FP assays with the results of ELISA-based activity assays revealed a good to excellent correlation, which makes the p38 $\alpha$  MAPK FP assay superior to the reported one. Moreover, both FP assays are easily adaptable to the HTS procedure and therefore

are suitable as inexpensive prescreening protocols for JNK3 and p38 $\alpha$  MAPK inhibitors.

## Acknowledgments

The authors thank Katharina Bauer and Daniela Müller, who carried out the testing of the compounds in the ELISA activity assays. We are also grateful to Stefan Laufer (Chair of Pharmaceutical and Medicinal Chemistry, Institute of Pharmaceutical Sciences, Eberhard Karls Universität Tübingen) for providing samples of SP600125, compound **18**, AS601245, skepinone-L, and SB681323. We thank Tamer Kocakaya and Philip Krause for synthesizing compounds **16** and **23**, respectively. Miriam Gisevius, Regina Jedig, and Mark Kudolo (all students at the Institute of Pharmaceutical Sciences, Eberhard Karls Universität Tübingen) are gratefully acknowledged for their assistance in the FP assay. Special thanks go to Silke Bauer for helpful discussions.

## Appendix A. Supplementary data

Supplementary data related to this article can be found at <http://dx.doi.org/10.1016/j.ab.2016.02.018>.

## References

- [1] V. Perrin, N. Dufour, C. Raoul, R. Hassig, E. Brusaferri, P. Aebischer, R. Luthi-Carter, N. Deglon, Implication of the JNK pathway in a rat model of Huntington's disease, *Exp. Neurol.* 215 (2009) 191–200.
- [2] L. Resnick, M. Fennell, Targeting JNK3 for the treatment of neurodegenerative disorders, *Drug Discov. Today* 9 (2004) 932–936.



- [3] S. Kumar, S.M. Wake, J.G. Emery, Intracellular signaling pathways as a target for the treatment of rheumatoid arthritis, *Curr. Opin. Pharmacol.* 1 (2001) 307–313.
- [4] Y.J. Frang, Y.Y. Li, The role of p38 mitogen-activated protein kinase in the pathogenesis of inflammatory bowel disease, *J. Dig. Dis.* 12 (2011) 327–332.
- [5] A. Mavropoulos, E.A. Rigopoulou, C. Liaskos, D.P. Bogdanos, I.I. Sakkas, The role of p38 MAPK in the arthropathogenesis of psoriasis and psoriatic arthritis, *Clin. Dev. Immunol.* 2013 (2013), <http://dx.doi.org/10.1155/2013/568751>.
- [6] J.C. Betts, R.J. Mayer, R. Tai-Singer, L. Warnock, C. Claxton, S. Bates, B.E. Hoffman, C. Larmine, D. Singh, Gene expression changes caused by the p38 MAPK inhibitor ilmapimod in COPD patients: analysis of blood and sputum samples from a randomized, placebo-controlled clinical trial, *Pharmacol. Res. Perspect.* 3 (1) (2015) e00094.
- [7] W. MacNee, R.J. Allan, I. Jones, M.C. De Salvo, L.F. Tan, Efficacy and safety of the oral p38 inhibitor PF-27804 in chronic obstructive pulmonary disease: a randomized clinical trial, *Thorax* 68 (2013) 738–745.
- [8] S.A. Correa, K.L. Eales, The role of p38 MAPK and its substrates in neuronal plasticity and neurodegenerative disease, *J. Signal Transduct.* 2012 (2012), <http://dx.doi.org/10.1155/2012/6140079>.
- [9] D.N. Kremenetsov, T.M. Thomson, C. Teuchter, M. Ilinciu, The emerging role of p38 mitogen-activated protein kinase in multiple sclerosis and its models, *Mol. Cell. Biol.* 33 (2013) 3728–3734.
- [10] I. Munuz, A.J. Anstey, Targeting p38 MAPK pathway for the treatment of Alzheimer's disease, *Neuropharmacology* 58 (2010) 561–568.
- [11] P. Koch, M. Gehring, S.A. Laufer, Inhibitors of c-Jun N-terminal kinases: an update, *J. Med. Chem.* 58 (2015) 72–95.
- [12] M. Gehring, F. Muth, P. Koch, S.A. Laufer, c-Jun N-terminal kinase inhibitors: a patent review (2010–2014), *Expert Opin. Ther. Pat.* 23 (2013) 849–872.
- [13] S. Bühler, S.A. Laufer, p38 MAPK inhibitors: a patent review (2012–2011), *Expert Opin. Ther. Pat.* 24 (2014) 535–554.
- [14] A.M. Manning, R.J. Davis, Targeting JNK for therapeutic benefit: from junk to gold? *Nat. Rev. Drug Discov.* 2 (2003) 554–565.
- [15] A. Cuenca, S. Rousseau, p38 MAPK-kinases pathway regulation, function, and role in human diseases, *Biochim. Biophys. Acta* 1773 (2007) 1356–1375.
- [16] B. Kaminska, MAPK signalling pathways as molecular targets for anti-inflammatory therapy—From molecular mechanisms to therapeutic benefits, *Biochim. Biophys. Acta* 1754 (2005) 253–262.
- [17] S. Kumar, J. Bawden, J.C. Lee, p38 MAPK kinases: key signaling molecules as therapeutic targets for inflammatory diseases, *Nat. Rev. Drug Discov.* 2 (2003) 717–726.
- [18] R.J. Davis, Signal transduction by the JNK group of MAP kinases, *Cell* 103 (2000) 239–252.
- [19] Y. Liu, N.S. Gray, Rational design of inhibitors that bind to inactive kinase conformations, *Nat. Chem. Biol.* 2 (2006) 358–364.
- [20] J.E. Sudyan, G.A. Holmgren, D. Campbell, D. Tamura, S. Gerhardt, J. Brzezniak, A.L. Breeze, A. Bermingham, B.A. Pauplik, R.A. Norman, K.J. Embrey, J. Read, W.J. Vancycoc, W.H.J. Ward, Prevention of MEK3-dependent activation by binding to p38 $\alpha$  MAP kinase, *Biochemistry* 44 (2005) 16475–16480.
- [21] F. Filimova, F. De Rienzo, M.C. Menziani, Insights into MAPK p38 $\alpha$  flip mechanism by accelerated molecular dynamics, *Bioorg. Med. Chem.* 18 (2010) 6805–6812.
- [22] Z. Zhao, H. Wu, L. Wang, Y. Liu, S. Knapp, Q. Liu, N.S. Gray, Exploitation of type II binding mode: a privileged approach for kinase inhibitor focused drug discovery? *ACS Chem. Biol.* 9 (2014) 1230–1241.
- [23] A. Backes, R. Zech, B. Felber, B. Klebl, G. Müller, Small-molecule inhibitors binding to protein kinases. I. Exceptions from the traditional pharmacophore approach of type I inhibition, *Expert Opin. Drug Discov.* 3 (2008) 1409–1425.
- [24] M. Vogtherr, K. Saena, S. Hecker, S. Grimme, M. Brta, U. Schreiber, B. Pescatore, M. Robin, L. Delarbre, T. Langer, K.U. Wendt, H. Schwalbe, NMR characterization of kinase p38 dynamics in free and ligand-bound forms, *Angew. Chem. Int. Ed.* 45 (2006) 903–907.
- [25] A. Backes, R. Zech, B. Felber, B. Klebl, G. Müller, Small-molecule inhibitors binding to protein kinase. II. The novel pharmacophore approach of type II and type III inhibition, *Expert Opin. Drug Discov.* 3 (2008) 1427–1449.
- [26] C. Pargellis, L. Tong, L. Churchill, P.F. Cifello, T. Gilmore, A.G. Graham, P.M. Gros, J.H. Bradley, N. Moss, S. Pav, J. Beggs, Inhibition of p38 MAP kinase by utilizing a novel allosteric binding site, *Nat. Struct. Biol.* 9 (2002) 268–272.
- [27] M. Goettfert, S. Luik, B. Graeser, S.A. Laufer, A direct ELISA assay for quantitative determination of the inhibitory potency of small molecule inhibitors for JNK3, *J. Pharm. Biomed. Anal.* 55 (2011) 236–240.
- [28] M. Goettfert, B. Graeser, S.A. Laufer, Optimization of a nonradioactive immunoassay for p38 $\alpha$  mitogen-activated protein kinase activity, *Anal. Biochem.* 406 (2010) 231–234.
- [29] J.R. Simard, M. Getlik, C. Gutter, V. Pawar, S. Wulfert, M. Rabiller, D. Koch, Development of a fluorescent-tagged kinase assay system for the detection and characterization of allosteric kinase inhibitors, *J. Am. Chem. Soc.* 131 (2009) 13286–13296.
- [30] H. Terle, F. Ferris, H. Liu, C. Rubin, G. Remise, M. Morris, J. Shao, A.C. Cheng, D. Gokunju, J. Mirt, R. Culi, S.H. Xi, S.L. Chagston, S. Low, S. Kaminski, Y.H. Ding, Q. Cao, T.L. Johnson, G.D. Deshmukh, J.P. D'Onofrio, J.C. Wu, J.M. English, The design, synthesis, and potential utility of fluorescence probes that target DHG-out conformation of p38 $\alpha$  for high throughput screening binding assay, *Chem. Biol. Drug Des.* 74 (2009) 547–559.
- [31] T.J. Burke, K.R. Lomello, J.A. Beebe, K.M. Ervin, Development and applications of fluorescence polarization assays in drug discovery, *Comb. Chem. High Throughput Screen* 6 (2003) 183–194.
- [32] D.M. Jamison, J.C. Greeny, Fluorescence polarization: past, present, and future, *Comb. Chem. High Throughput Screen* 6 (2003) 167–173.
- [33] S.M. Vogel, M.B. Bauer, A.C. Joerger, E. Wilcken, T. Brandt, D.B. Veprikov, T.J. Rutherford, A.E. Fersht, F.M. Boeckler, Lithocholic acid is an endogenous inhibitor of MDM4 and MDM2, *Proc. Natl. Acad. Sci. U. S. A.* 109 (2012) 16006–16010.
- [34] J.R. Lakowicz, Principles of Fluorescence Spectroscopy, Springer, New York, 2006, pp. 353–380.
- [35] A.M. Rossi, C.W. Taylor, Analysis of protein–ligand interactions by fluorescence polarization, *Nat. Protoc.* 6 (2011) 365–387.
- [36] A. Lange, M. Günther, F. Michael Bittner, M.O. Zimmermann, J. Hedrich, S. Heising, S. Zahn, C. Schall, A. Sievers-Engler, F. Ansdelen, P. Koch, M. Laemmerhofer, T. Stehle, S.A. Laufer, F.M. Boeckler, Targeting the gate-keeper MET46 of C-Jun N-terminal kinase 3 induces a bivalent halogen chalcogen bond, *J. Am. Chem. Soc.* 137 (2015) 14640–14652.
- [37] L. Munuz, R. Selig, Y.T. Yeung, C. Peiffer, D. Hauner, S. Laufer, Fluorescence polarization binding assay to develop inhibitors of inactive p38 $\alpha$  mitogen-activated protein kinase, *Anal. Biochem.* 401 (2010) 125–133.
- [38] C.E. Fitzgerald, S.B. Patel, J.W. Becker, P.M. Camoron, D. Zaller, V.B. Plikous, S.J. O'Keefe, G. Scapin, Structural basis for p38 $\alpha$  MAP kinase quinazolinone and pyridol-pyrimidine inhibitor specificity, *Nat. Struct. Biol.* 10 (2003) 764–768.
- [39] T. Kamenecka, J. Habel, D. Dockett, W. Chen, Y.Y. Ling, B. Frackowiak, R. Jiang, Y. Shin, X. Song, P. LoGrasso, Structure–activity relationships and X-ray structures describing the selectivity of aminopyrazole inhibitors for c-Jun N-terminal kinase 3 (JNK3) over p38, *J. Biol. Chem.* 284 (2009) 12851–12861.
- [40] H.M. Berman, J. Westbrook, Z. Feng, G. Gilliland, T.N. Bhat, H. Weissig, I.N. Shindyalov, P.E. Bourne, The Protein Data Bank, *Nucleic Acids Res.* 28 (2000) 235–242.
- [41] D. Korb, T. Stutzle, T.E. Esser, Empirical scoring functions for advanced protein–ligand docking with PLANTS, *J. Chem. Inf. Model.* 49 (2009) 94–96.
- [42] G. Jones, P. Willett, R.C. Glen, A.R. Leach, R. Taylor, Development and validation of a genetic algorithm for flexible docking, *J. Mol. Biol.* 267 (1997) 727–748.
- [43] M.D. Edridge, C.W. Murray, T.R. Auton, G.V. Paulini, R.P. Mee, Empirical scoring functions: I. The development of a fast empirical scoring function to estimate the binding affinity of ligands to receptor complexes, *J. Comput. Aided Mol. Des.* 11 (1997) 425–445.
- [44] E. Reyes, E. Blum, E.E. Di Padova, T. Buhl, R. Felber, H. Gram, P. Hiestand, U. Manning, G. Kochlin, Novel p38 inhibitors with potent oral efficacy in several models of rheumatoid arthritis, *Bioorg. Med. Chem. Lett.* 14 (2004) 3595–3598.
- [45] Z. Nikolovska-Coleska, B. Wang, X. Fang, H. Pan, Y. Tomita, P. Li, P.P. Bidler, K. Krajewski, M.C. Saito, J.A. Stuckey, S. Wang, Development and optimization of a binding assay for the XIAP BIR3 domain using fluorescence polarization, *Anal. Biochem.* 332 (2004) 261–273.
- [46] R. Wang, Z. Nikolovska-Coleska, X. Fang, S. Wang, From IC<sub>50</sub> to K<sub>i</sub>: a general mathematical solution for fluorescence-based competitive binding assays, *Unpublished results*.
- [47] P.W. Berman, B. Beck, E.F. Chen, W. Demu, V. Devarajan, B.J. Eastwood, M.W. Fermi, S.J. Farrar, C. Moras, J.A. Moore, J.R. Weissner, G.S. Srinivasan, HTS assay validation, in: G.S. Srinivasan, N.P. Coussens, H. Nelson, M. Arkin, D. Auld, C. Austin, B. Bejcek, M. Glickman, J. Ingole, P.W. Iversen, Z. Li, J. McGee, O. McMurry, L. Minor, A. Napper, J.M. Peitler, T. Pitt, O.J. Tsiak Jr., J. Weidner (Eds.), *Assay Guidance Manual*, Eli Lilly and National Center for Advancing Translational Sciences, Bethesda, MD, 2004.
- [48] G. Scapin, S.B. Patel, J. Lisnock, J.W. Becker, P.V. LoGrasso, The structure of JNK3 in complex with small molecule inhibitors: structural basis for potency and selectivity, *Chem. Biol.* 10 (2003) 705–712.
- [49] Z.I. Wang, B.J. Canagarajah, J.C. Boehm, S. Kamata, M.H. Cobbs, P.R. Young, S. Abdel-Meguid, J.L. Adams, I.J. Goldsmith, Structural basis of inhibitor selectivity in MAP kinases, *Struct. Fold. Des.* 6 (1998) 1117–1128.
- [50] S.A. Laufer, A.J. Liedtke, A concise and optimized four-step approach toward 2-(aryl-alkylsulfanyl)-4(5)-aryl-5(4)-heteroaryl-substituted imidazoles using alkyl- or arylalkyl thiocyanates, *Tetrahedron Lett.* 47 (2006) 7199–7201.
- [51] P. Koch, H. Johns, V. Schättel, M. Goettfert, S. Laufer, Pyridinylquinazolines and pyridinylpyridopyrazines as lead compounds for novel p38 $\alpha$  mitogen-activated protein kinase inhibitors, *J. Med. Chem.* 53 (2010) 1128–1137.
- [52] B. Radziszewski, Über Glyoxal und seine Homologe, *Ber. Deut. Chem. Ges.* 15 (1882) 2706–2708.
- [53] W.A. Lea, A. Simeonov, Fluorescence polarization assays in small molecule screening, *Expert Opin. Drug Discov.* 6 (2011) 17–32.
- [54] N.J. Moerke, Fluorescence polarization (FP) assays for monitoring peptide–protein or nucleic acid–protein binding, *Curr. Protoc. Chem. Biol.* 1 (2009) 1–15.
- [55] A. El-Gokha, S.A. Laufer, P. Koch, An optimized and versatile synthesis to pyridinylimidazole-type p38 $\alpha$  mitogen-activated protein kinase inhibitors, *Org. Biomol. Chem.* 13 (2015) 10089–10094.
- [56] P. Koch, C. Häuerlein, H. Jank, S. Laufer, Targeting the ribose and phosphate binding site of p38 mitogen-activated protein (MAP) kinase: synthesis and biological testing of 2-alkylsulfanyl-, 4(5)-aryl-, 5(4)-heteroaryl-substituted imidazoles, *J. Med. Chem.* 51 (2008) 5630–5640.
- [57] B.L. Bennett, D.T. Suzuki, B.W. Murray, E.C. O'Leary, S.T. Sakata, W. Xu, J.C. Leisten, A. Matsuda, S. Pierce, Y. Saito, S.S. Bhargava, A.M. Manning, D.W. Anderson, SP600125, an anthracycline inhibitor of Jun N-terminal kinase, *Proc. Natl. Acad. Sci. U. S. A.* 98 (2001) 13681–13686.

- [58] P. Gaillán, I. Jean-Luude-Ester, V. Arribas, S. Arkinstall, V. Cambet, M. Camps, C. Chabert, D. Charth, R. Girón, D. Gortner, S. Halazy, A. Nichols, C. Szyndrakiewicz, P.A. Vitor, J.F. Gortner, Design and synthesis of the first generation of novel potent, selective, and in vivo active (benzothiazol-2-yl) acetonitrile inhibitors of the c-Jun N-terminal kinase. *J. Med. Chem.* 48 (2005) 4596–4607.
- [59] S.C. Koehler, J. Rasmir, S. Fischer, A. Kuchel, V. Schüttel, W. Allrecht, C. Grütter, O. Wenz, D. Rauh, T. Stehle, S.A. Laufer, Stepinone-1 is a selective p38 mitogen-activated protein kinase inhibitor. *Nat. Chem. Biol.* 8 (2012) 141–143.
- [60] L.J. Adams, J.C. Boehm, C. Jeffrey, R. Hall, Q. Jin, J. Kasperek, D.J. Silva, J.J. Taggart, Novel compounds, patent WO/2002/059083 A2, 2001.
- [61] S.A. Laufer, D.B. Hauser, D.M. Dimeyer, K. Simhal, A.J. Lindke, Design, synthesis, and biological evaluation of novel di- and tetrasubstituted imidazoles as highly potent and specific ATP-mimetic inhibitors of p38 MAP kinase: focus on optimized interactions with the enzyme's surface-exposed flint region. *J. Med. Chem.* 51 (2008) 4322–4349.
- [62] S. Fischer, H.K. Weitsch, S.C. Mayer-Wiangowski, M. Zimmermann, S.M. Bauer, K. Storch, R. Niess, S.C. Koehler, C. Grütter, F.M. Jeschke, D. Rauh, S.A. Laufer, Dihydroisobenzos as p38 mitogen-activated protein kinase inhibitors with low ATP competitiveness and outstanding whole blood activity. *J. Med. Chem.* 56 (2013) 241–253.

**Supplementary Material****Fluorescence polarization-based assays for detecting compounds binding to inactive JNK3 and p38 $\alpha$  MAP kinase**

Francesco Ansideri <sup>a</sup>, Andreas Lange <sup>b</sup>, Ahmed El-Gokha <sup>a,c</sup>, Frank M. Boeckler <sup>b</sup>, Pierre Koch<sup>a\*</sup>

**Address:**

<sup>a</sup>Institute of Pharmaceutical Sciences, Department of Medicinal and Pharmaceutical Chemistry, Eberhard Karls Universität Tübingen, Auf der Morgenstelle 8, 72076 Tübingen, Germany

<sup>b</sup>Institute of Pharmaceutical Sciences, Molecular Design and Pharmaceutical Biophysics, Eberhard Karls Universität Tübingen, Auf der Morgenstelle 8, 72076 Tübingen, Germany

<sup>c</sup>Menofia University, Chemistry Department, Faculty of Science, Menofia, Egypt

\*Corresponding author

Email: Pierre Koch\* - pierre.koch@uni-tuebingen.de

**Contents:**

Synthesis of compounds <b>16</b> and <b>23</b> .....	S2
Fig. S1. Docking poses of ligand <b>3</b> with JNK3 and p38 $\alpha$ MAPK .....	S3
Fig. S2. Docking poses of probe <b>5</b> with JNK3 and p38 $\alpha$ MAPK .....	S4
Fig. S3. Binding affinities of probes <b>5</b> and <b>6</b> for JNK3 and p38 $\alpha$ MAPK determined by ITC .....	S5
Fig. S4. Assay conditions optimization for probe <b>5</b> .....	S6
Fig. S5. HTS assay validation plot by column, then by row (JNK3) .....	S7
Fig. S6. HTS assay validation plot by row, then by column (JNK3) .....	S8
Fig. S7. HTS assay validation plot by column, then by row (p38 $\alpha$ MAPK) .....	S9
Fig. S8. HTS assay validation plot by row, then by column (p38 $\alpha$ MAPK) .....	S10
References .....	S11

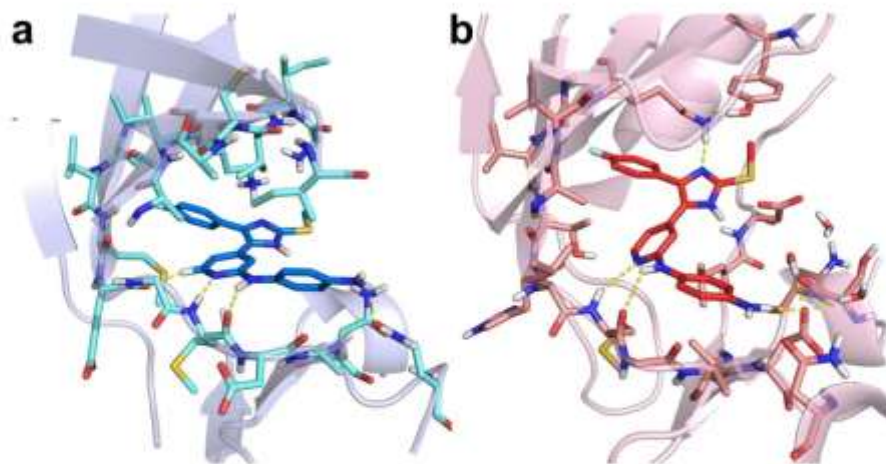
**Synthesis of compound 16**

Under dry conditions, compound **3** (100 mg, 0.26 mmol) was dissolved in pyridine (5 mL) followed by addition of 4-(*tert*-butyl)benzoyl chloride (60  $\mu$ L, 0.31 mmol) at r.t. The reaction mixture was stirred at r.t. for 48 h. The reaction was quenched with water (5 mL) and the aqueous layer was extracted 3 times with ethyl acetate (5 mL). The organic layers were dried over anhydrous  $\text{Na}_2\text{SO}_4$  and the solvent was then evaporated under reduced pressure. The crude product was purified by flash column chromatography (dichloromethane – ethanol 19:1) giving 69 mg (50%) of the desired product.  $^1\text{H-NMR}$  (250 MHz,  $\text{DMSO-}d_6$ ):  $\delta$  (ppm) 1.32 (s, 9 H), 2.62 (s, 3 H), 6.68 (dd,  $J_1 = 5.2$  Hz,  $J_2 = 1.1$  Hz, 1 H), 7.02 (br. s., 1 H), 7.27 (br. s., 2 H), 7.43-7.68 (m, 8 H), 7.88 (d,  $J = 8.54$  Hz, 2 H), 8.03 (br. s., 1 H), 8.97 (s, 1 H), 10.04 (s, 1 H), 12.68 (br. s, 1 H); HPLC:  $t = 10.12$  min, 99%; ESI-MS:  $[\text{M} + \text{H}]^+$  calculated 552.22, found 552.3.

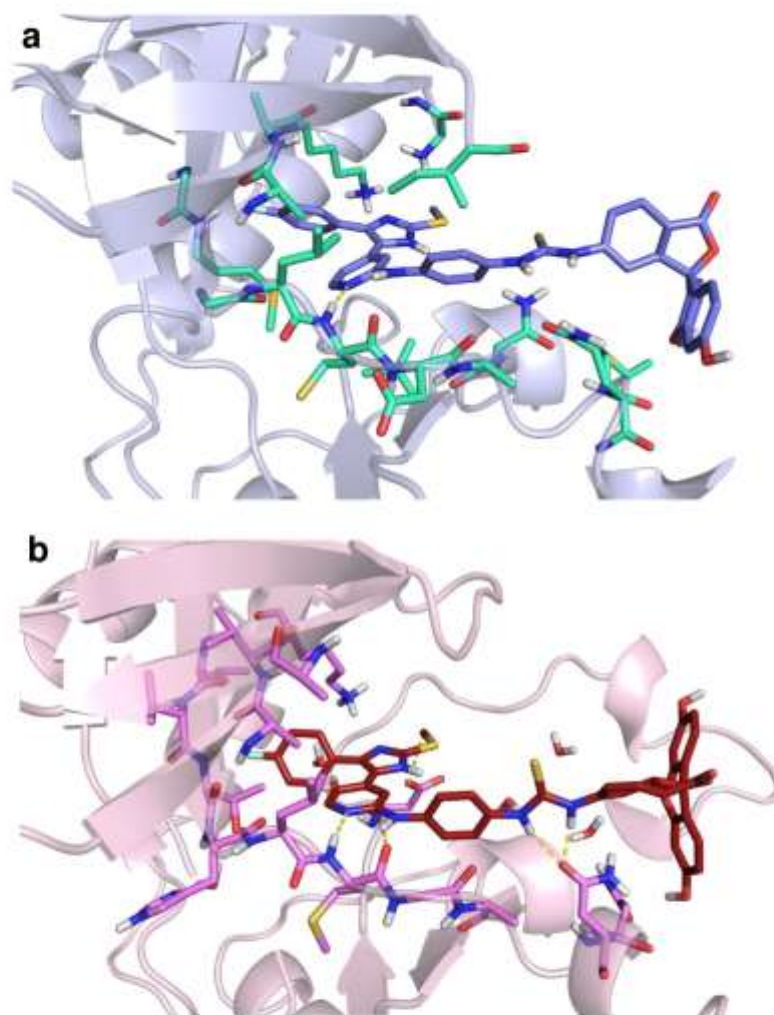
**Synthesis of 1-(4-fluorophenyl)-5-(pyridin-4-yl)imidazole (23)**

A solution of 4-fluoroaniline (118.7  $\mu$ L, 1.25 mmol), 4-pyridinecarboxaldehyde (117.4  $\mu$ L, 1.25 mmol) and acetic acid (125  $\mu$ L) in ethanol (10 mL) was heated to reflux temperature for 2 h. After cooling to r.t., the solvent was removed under reduced pressure and the remaining residue was dissolved in a mixture of methanol (8.75 mL) and dimethoxyethane (3.75 mL). To this solution,  $\text{K}_2\text{CO}_3$  (345 mg, 2.5 mmol) and *p*-toluenesulfonylmethyl isocyanide (366 mg, 1.87 mmol) was added and the reaction mixture was heated to reflux temperature for 3 h. After cooling to r.t., the solvent was removed under reduced pressure and the remaining residue was dissolved in dichloromethane and washed with water. The organic layer was dried over anhydrous  $\text{Na}_2\text{SO}_4$  and the solvent was then evaporated under reduced pressure. The crude product was purified by flash column chromatography (dichloromethane – methanol 1:0 to 9:1) yielding 92 mg (31%) of the desired product.  $^1\text{H-NMR}$  (250 MHz,  $\text{DMSO-}d_6$ ):  $\delta$  (ppm) 7.08 (d,  $J = 4$  Hz, 2H), 7.36-7.44 (m, 4H), 7.57 (s, 1H), 8.05 (s, 1H), 8.46 (d,  $J = 4$  Hz, 2H); HPLC:  $t = 3.54$  min, 100%; ESI-MS:  $[\text{M} + \text{H}]^+$  calculated 240.09, found 240.0.





**Figure S1:** Docking poses of ligand **3** in the active centre of JNK3 (a) and p38 $\alpha$  MAPK (b) using the software GOLD [1]. For the protein models, we used the crystal structures of Protein Data Bank entries 3FI3 and 1OUK for JNK3 and p38 $\alpha$  MAPK, respectively [2]. Possible hydrogen bonds are shown as dashed lines.



**Fig. S2.** Docking poses of probe 5 in the active centre of JNK3 (a) and p38 $\alpha$  MAPK (b) using the software GOLD [1]. For the protein models, we used the crystal structures of Protein Data Bank entries 3F13 and 1OUK for JNK3 and p38 $\alpha$  MAPK, respectively [2]. Possible hydrogen bonds are shown as dashed lines.

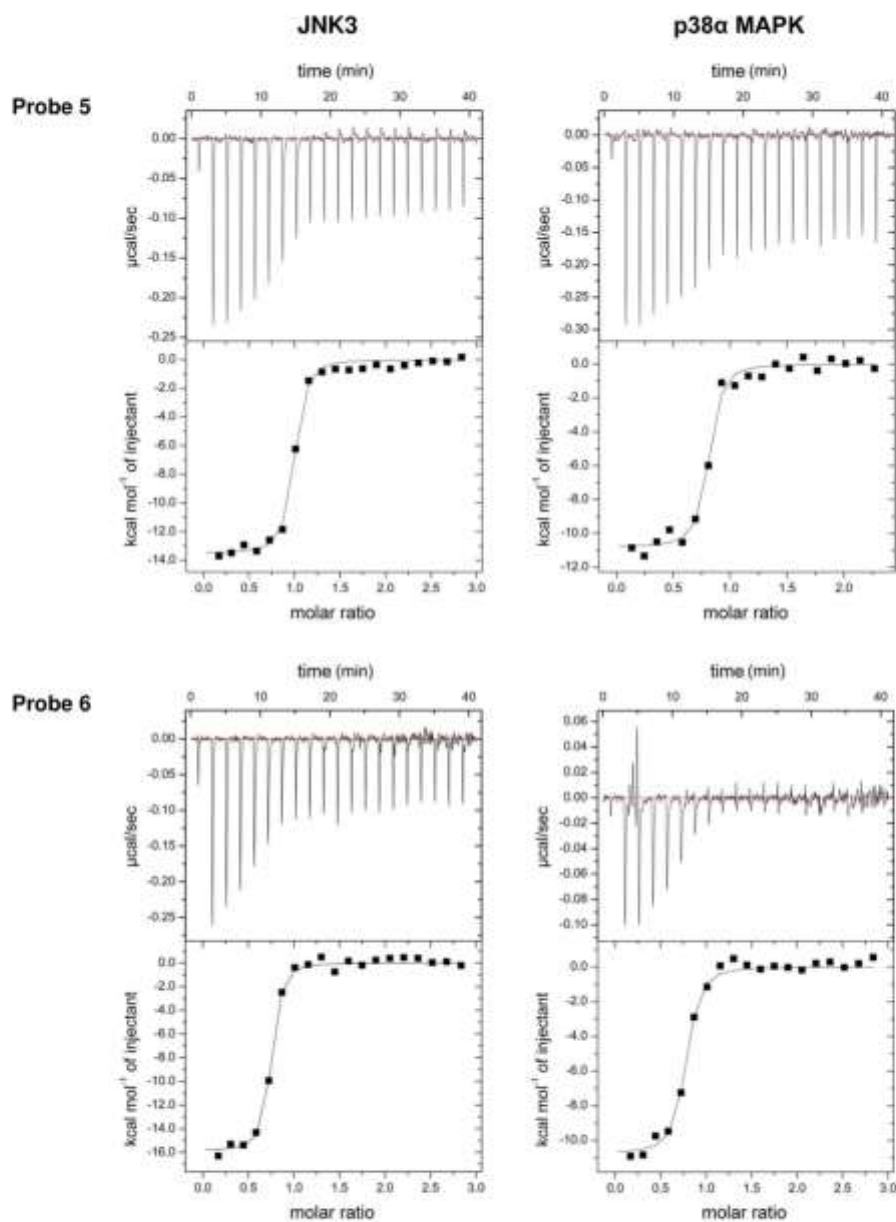
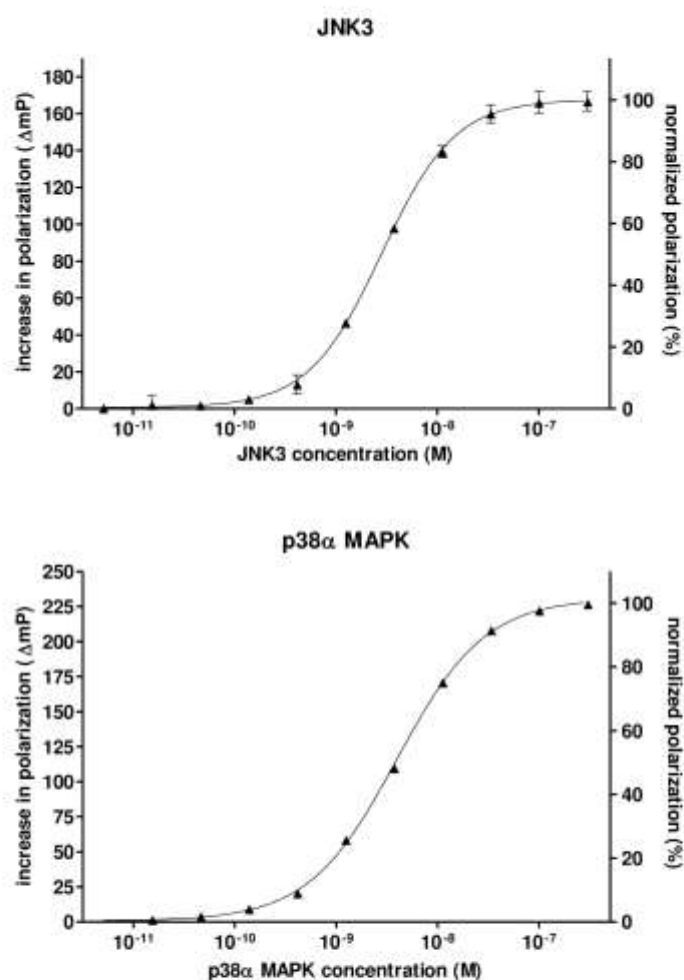
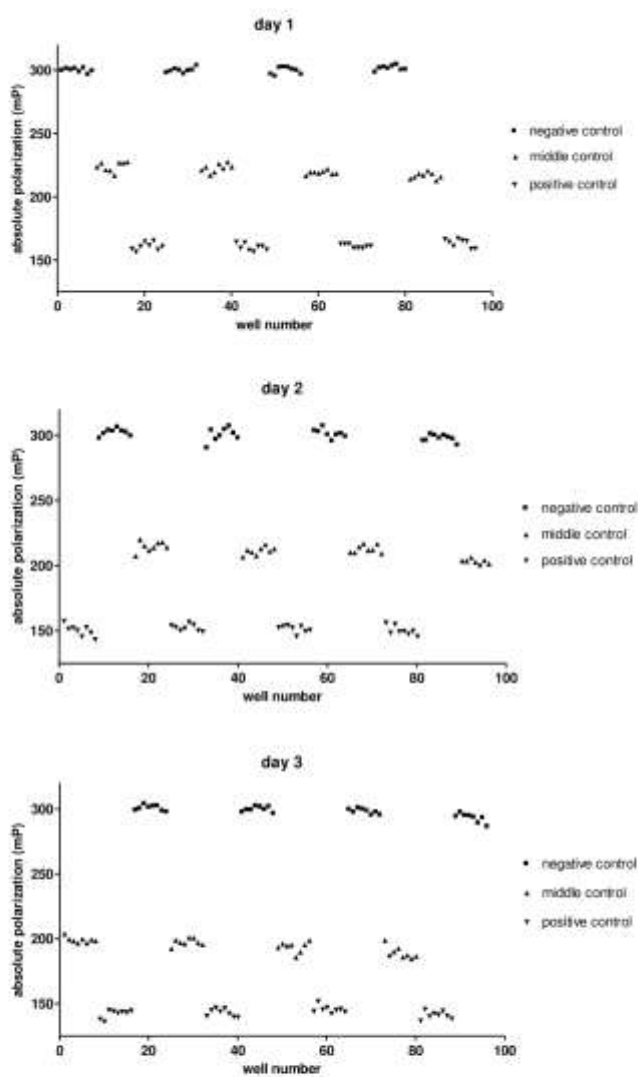


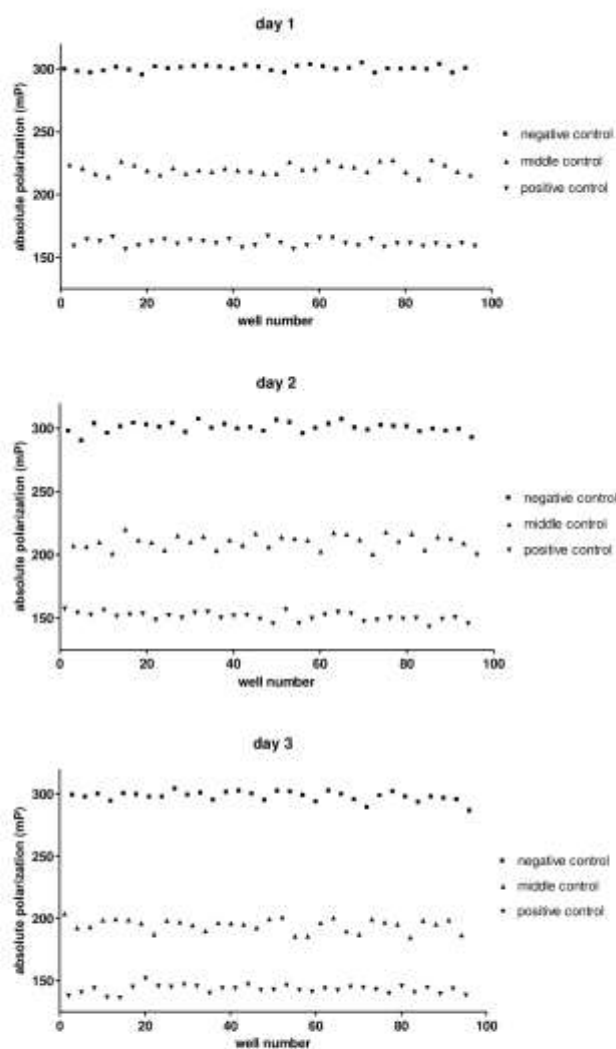
Fig. S3. Binding affinities of probes 5 and 6 for JNK3 and p38 $\alpha$  MAPK determined by ITC.



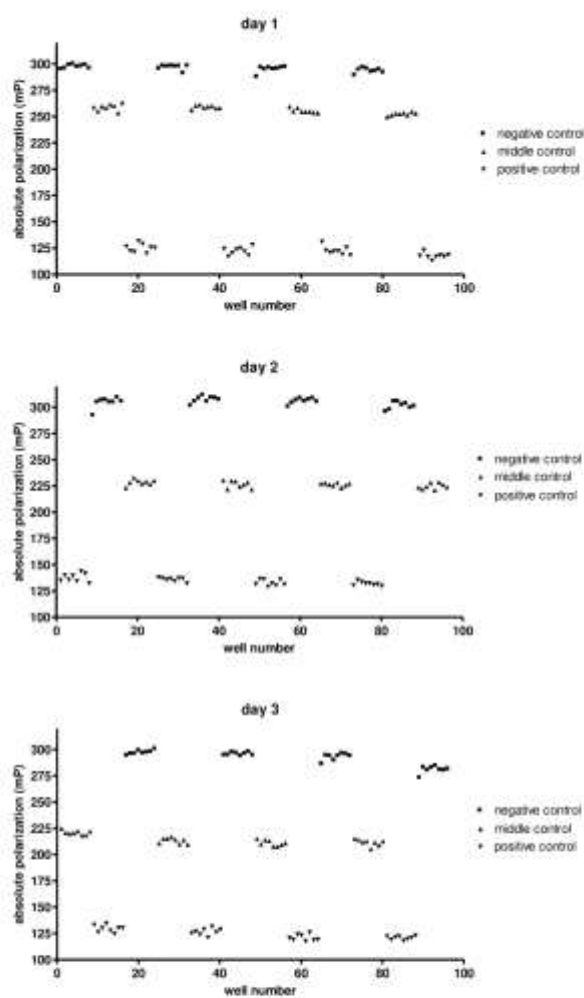
**Fig. S4.** Assay conditions optimization for probe 5. Data points represent mean values  $\pm$  SD. The concentration of probe 5 used was 5 nM and the incubation time was 30 minutes. The left Y-axis represents the increase in polarization calculated through baseline correction of the absolute polarization values whereas the right Y-axis displays the normalized polarization.



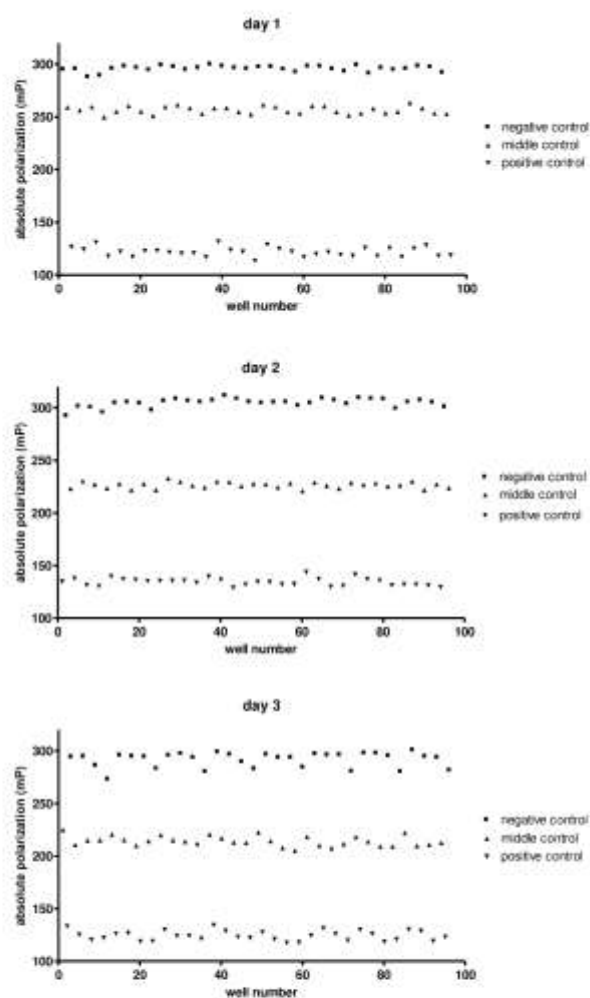
**Fig. S5.** HTS assay validation plot by column, then by row (JNK3). Experiment was performed on 3 different days using the interleaved plate format described in literature [3]. As a negative control a 5 nM concentration of probe **5** in 5% DMSO in buffer A was used. For positive and middle controls, we used the unlabelled probe (compound **3**) at a concentration of 1  $\mu$ M and 20 nM, respectively, in addition to the 5 nM probe **5**.



**Fig. S6.** HTS assay validation plot by row, then by column (JNK3). Experiment was performed on 3 different days using the interleaved plate format described in literature [3]. As a negative control a 5 nM concentration of probe **5** in 5% DMSO in buffer A was used. For positive and middle controls, we used the unlabeled probe (compound **3**) at a concentration of 1  $\mu$ M and 20 nM, respectively, in addition to the 5 nM probe **5**.



**Fig. S7.** HTS assay validation plot by column, then by row (p38 $\alpha$  MAPK). Experiment was performed on 3 different days using the interleaved plate format described in literature [3]. As a negative control a 5 nM concentration of probe **5** in 5% DMSO in buffer A was used. For positive and middle controls, we used the unlabelled probe (compound **3**) at a concentration of 1  $\mu$ M and 20 nM, respectively, in addition to the 5 nM probe **5**.



**Fig. S8.** HTS assay validation plot by row, then by column (p38 $\alpha$  MAPK). Experiment was performed on 3 different days using the interleaved plate format described in literature [3]. As a negative control a 5 nM concentration of probe **5** in 5% DMSO in buffer A was used. For positive and middle controls, we used the unlabelled probe (compound **3**) at a concentration of 1  $\mu$ M and 20 nM, respectively, in addition to the 5 nM probe **5**.



**References**

- [1] GOLD v5.2.2, The Cambridge Crystallographic Data Centre, Cambridge, UK, 2013
- [2] H.M. Berman, J. Westbrook, Z. Feng, G. Gilliland, T.N. Bhat, H. Weissig, I.N. Shindyalov, P.E. Bourne, The Protein Data Bank, *Nucleic Acids Res.*, 28 (2000) 235-242.
- [3] P.W. Iversen, B. Beck, Y.F. Chen, W. Dere, V. Devanarayan, B.J. Eastwood, M.W. Farnen, S.J. Iturria, C. Montrose, R.A. Moore, J.R. Weidner, G.S. Sittampalam, HTS Assay Validation, in: G.S. Sittampalam, N.P. Coussens, H. Nelson, M. Arkin, D. Auld, C. Austin, B. Bejcek, M. Glicksman, J. Inglese, P.W. Iversen, Z. Li, J. McGee, O. McManus, L. Minor, A. Napper, J.M. Peltier, T. Riss, O.J. Trask, Jr., J. Weidner (Eds.) *Assay Guidance Manual*, Bethesda (MD), 2004.



## Publication II

Ansideri, F.; Dammann, M.; Boeckler, F. M.; Koch, P. Fluorescence polarization-based competition binding assay for c-Jun N-terminal kinases 1 and 2. *Anal. Biochem.* 2017, 532, 26-28.

**Reprinted with permission from Ansideri *et al.* 2016, 503, 28-40**

**Copyright 2016 Elsevier Inc. All rights reserved**

**Link to the published version:**

<https://www.sciencedirect.com/science/article/pii/S0003269717302270>



Contents lists available at ScienceDirect

Analytical Biochemistry

journal homepage: [www.elsevier.com/locate/yabio](http://www.elsevier.com/locate/yabio)

## Fluorescence polarization-based competition binding assay for c-Jun N-terminal kinases 1 and 2



Francesco Ansideri <sup>a</sup>, Marcel Dammann <sup>b</sup>, Frank M. Boeckler <sup>b</sup>, Pierre Koch <sup>a,\*</sup>

<sup>a</sup> Institute of Pharmaceutical Sciences, Department of Medicinal and Pharmaceutical Chemistry, Eberhard Karls Universität Tübingen, Auf der Morgenstelle 8, 72076 Tübingen, Germany

<sup>b</sup> Institute of Pharmaceutical Sciences, Molecular Design and Pharmaceutical Biophysics, Eberhard Karls Universität Tübingen, Auf der Morgenstelle 8, 72076 Tübingen, Germany

### ARTICLE INFO

Article history:  
Received 21 April 2017  
Accepted 22 May 2017  
Available online 25 May 2017

Keywords:  
Fluorescence polarization  
Binding assay  
c-Jun N-terminal kinases  
JNK1  
JNK2

### ABSTRACT

In order to evaluate the isoform selectivity of novel inhibitors within the c-Jun N-terminal kinase (JNK) family, a fluorescence polarization-based competition binding assay, previously developed for JNK3, was extended to the other isoforms JNK1 and JNK2. The assay is based on the displacement of a versatile fluorescent pyridinylimidazole-based probe and was validated by testing the precursor of the probe as well as standard JNK inhibitors.

© 2017 Elsevier Inc. All rights reserved.

The c-Jun N-terminal kinases (JNKs) represent a subfamily of the mitogen-activated protein kinases (MAPKs) and are encoded by three different genes (*jnk1*, *jnk2* and *jnk3*) for a total of 10 isoforms arising from alternative splicing [1]. Despite their high sequence homology, the JNK isoforms present differences in tissue distribution. In contrast to the ubiquitous expression of JNK1 and JNK2, JNK3 is being restricted to the brain, heart and testis. In addition, these isoforms show dissimilarities in terms of substrate specificity, regulation from upstream kinases, and signal transduction pathways [1–3]. Several studies have highlighted the involvement of the JNKs in diverse pathological conditions, such as neurodegenerative diseases, stroke, diabetes and tumorigenesis [4–6], although the specific pathophysiological role of the single isoforms has not always been fully elucidated. For this reason, the development of novel JNK isoform-selective inhibitors as pharmacological tools would be highly desirable in order to dissect the contribution of the single isoforms in each pathological state. Furthermore, this would represent a starting point in the perspective of a JNK isoform-specific therapeutic approach. Nevertheless, given the considerable structural similarity between JNK1, JNK2 and JNK3, this goal has not been achieved yet [7,8].

In order to ease the biological evaluation of potential inhibitors of JNK3, we recently reported in this journal the development and optimization of a fluorescence polarization (FP)-based binding assay for this kinase [9]. This assay is based on the competitive displacement of probe **PIT0105006** (**1**), which was obtained by fluorescein-labelling of the potent pyridinylimidazole-based JNK3 inhibitor **PIT0104002** (Fig. 1) [9]. The necessity of evaluating *intra*-JNK selectivity prompted us to broaden this existing assay to JNK1 and JNK2, in order to improve the efficiency in the development of isoform specific inhibitors. As in the case of our reported JNK3 FP-assay, the JNK1 and JNK2 were employed in their inactive forms (for JNK1 and JNK2 expression and purification, see supplementary material). This allows the detection of compounds binding preferentially the kinases in such state (type-II inhibitors) as well as the detection of most type-I inhibitors [10,11].

The first step consisted in assessing the suitability of probe **1** for JNK1 and JNK2. This was evaluated by direct titration of a fixed concentration of probe **1** (5 nM) using threefold increasing concentrations of protein, ranging from 25 pM to 1.5 μM. A well containing no protein was also included as a negative control. The assays were performed in black, non-binding 96-well plates (Greiner Bio-One) reaching a final volume of 100 μL and were repeated three times in quadruplicate. A constant 5% DMSO concentration (v/v) was used in every well together with the assay buffer (20 mM TRIS pH 7.5, 250 mM NaCl, 5 mM β-mercaptoethanol

\* Corresponding author.  
E-mail address: [pierre.koch@uni-tuebingen.de](mailto:pierre.koch@uni-tuebingen.de) (P. Koch).

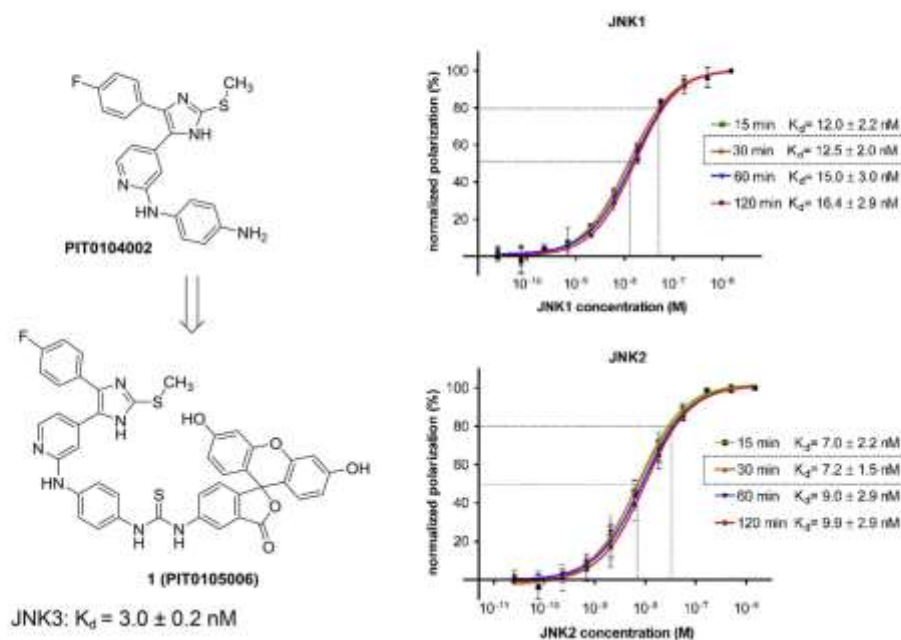


Fig. 1. Structure and binding affinity of probe 1 for JNK1 and JNK2. The levels of 50% and 80% polarization increase are marked as dashed lines.

and 0.05 mg/mL bovine serum albumin). In order to evaluate the time dependency of the binding event, the plate was incubated at room temperature for 15, 30, 60, and 120 min in an Eppendorf MixMate at 400 rpm before every reading. The measurement was then conducted through a CLARIOstar microplate reader (BMC Labtech GmbH) using excitation and emission filters of 480 nm and of 530 nm, respectively. Last 2 min of every incubation time were carried out inside the reader, previously equilibrated at 25 °C. Prior to every measurement, the excitation beam was focused at the optimal height and the gain values for both detectors were adjusted. The absolute polarization values were normalized using the software GraphPad Prism 4 (GraphPad Prism 4, GraphPad Software Inc., San Diego, CA, USA) and results were reported as percentages. Four-parameter logistic curves with variable slope were fitted to the data points using the same software. Probe 1 revealed to be suitable for both JNK1 and JNK2, displaying  $K_d$  values in the low nanomolar range (Fig. 1), though showing a slightly lower affinity in comparison with JNK3 ( $K_d = 3.0 \pm 0.2$  nM; 30 min) [9]. The versatility of probe 1 is the result of its poor *intra*-MAPK selectivity, as demonstrated by its capability to efficiently bind also the closely related p38 $\alpha$  MAPK ( $K_d = 5.7$  nM; 30 min). The measured  $K_d$  values appeared to remain overall stable over time, only showing a negligible time-dependent increase after incubation times longer than 1 h. The  $K_d$  values measured after 30 min incubation, (JNK1:  $K_d = 12.5 \pm 2.0$  nM; JNK2:  $K_d = 7.2 \pm 1.5$  nM) were selected as the parameters of probe 1 to be used in the competition assay. This choice, in agreement with our previously developed assay procedure, unifies the assay conditions for the three different JNK isoforms and therefore allows a better comparison of the results obtained. The titration experiment permitted

also the determination of the optimal protein concentration to use in the competition assay. As reported in literature [12], this concentration should produce an increase in the polarization signal laying between 50 and 80% in order to work in non-stoichiometric conditions and achieve at the same time a satisfactory signal window. The enzyme concentrations selected were therefore 50 nM for JNK1 and 30 nM for JNK2, both yielding an increase in polarization of approximately 80%.

The assays were validated by testing the non-labelled precursor of probe 1, compound PIT0104002, together with four chemically diverse JNK standard inhibitors (IQ-15 [13], JNK inhibitor VIII [14], SR-3576 [15] and SR-3306 [16]; for the structures of these inhibitors, see Fig. S1, supplementary material) purchased from Merck Millipore (Germany). The selected compounds were initially screened for autofluorescence using the same protocol previously described by us [9] and did not show significant intrinsic fluorescence at the excitation/emission wavelengths of 480/530 nm. Probe 1 (5 nM) and the corresponding kinase (50 nM and 30 nM for JNK1 and JNK2, respectively) were then incubated for 30 min with threefold increasing concentrations of inhibitor. A positive control containing no inhibitor and a negative control containing only probe 1 in assay buffer were also included in the measurement. The measurement parameters were maintained equal to the aforementioned ones. The absolute polarization values were normalized to the readout of positive and negative control and data points were fitted to logistic curves as previously described (for assay graphs, see Fig. S2, supplementary material). Finally,  $K_i$  values were derived from the measured  $IC_{50}$  values using a modified Cheng-Prusoff equation [17,18].

As displayed in Table 1, the assays can be considered valid for



**Table 1**  
Measured  $K_i$  values in the FP assay in comparison with data from literature.

	JNK1		JNK2	
	$K_i$ FP assay (mean $\pm$ SD) <sup>a</sup> (nM)	Literature data (nM)	$K_i$ FP assay (mean $\pm$ SD) <sup>a</sup> (nM)	Literature data (nM)
<b>PIT0104002</b>	18 $\pm$ 4	n.r. <sup>b</sup>	12 $\pm$ 1	n.r.
<b>IQ-15</b>	311 $\pm$ 43	390 ( $K_d$ ) <sup>c</sup>	390 $\pm$ 38	360 ( $K_d$ ) <sup>c</sup>
<b>JNK inh. VIII</b>	48 $\pm$ 12	2 ( $K_i$ ) <sup>d</sup>	35 $\pm$ 5	4 ( $K_i$ ) <sup>d</sup>
<b>SR3576</b>	40 $\pm$ 0	170 ( $K_{50}$ ) <sup>e</sup>	8 $\pm$ 2	n.r.
<b>SR3306</b>	79 $\pm$ 12	67 $\pm$ 19 ( $K_{50} \pm$ SD) <sup>f</sup>	215 $\pm$ 57	283 $\pm$ 3 ( $K_{50} \pm$ SD) <sup>f</sup>

<sup>a</sup> n = 3.

<sup>b</sup> Data not reported in literature.

<sup>c</sup> Data reported by Schepetkin et al. [13]; SD not reported.

<sup>d</sup> Data reported by Szczepankiewicz et al. [14]; SD not reported.

<sup>e</sup> Data reported by Kamenecka et al. [15]; SD not reported.

<sup>f</sup> Data reported by Chambers et al. [16].

both enzymes since all tested inhibitors are able to displace the probe in a dose-dependent manner. The  $K_i$  of compound **PIT0104002** and the  $K_d$  of probe **1**, measured on the same enzyme, showed analogous values (Table 1 and Fig. 1). This was observed also in the case of JNK3 (**PIT0104002**:  $K_i = 3.0 \pm 0.2$  nM; probe **1**:  $K_d = 3.0 \pm 0.2$  nM) and demonstrates that the introduction of the bulky fluorophore is well tolerated by all members of the JNK family.

In most cases, the measured  $K_i$  values correspond to the reported activities of the tested standard JNK inhibitors. However, a direct comparison of the obtained data with the reported ones from literature is not possible due to the diverse assay layouts, the differences in the inhibition parameters and the use of the kinases in different activation states. Instead, it can be stated that when test results were reported for both JNK1 and JNK2, the comparison with the data from the FP assay revealed an analogous trend on the inhibitory activity, despite their differences in absolute values.

To sum up, our previously reported convenient FP-based competition binding assay protocol for JNK3 was successfully extended for all members of the JNK family by using the same probe in analogous conditions. The easy handling and cost efficiency features of the FP technique in combination with the possibility to directly compare the results obtained from the three isoforms, provided a useful tool for both determining the binding affinity to these enzymes and for the assessment of selectivity within the JNK subfamily. This is particularly useful when trying to exploit subtle structural differences in the binding pockets for the induction of subtype selectivity [19].

#### Acknowledgement

Catharina Sessler is gratefully acknowledged for her assistance in the FP assay.

#### Appendix A. Supplementary data

Supplementary data related to this article can be found at <http://dx.doi.org/10.1016/j.ab.2017.05.022>.

#### References

- [1] S. Gupta, T. Barrett, A.J. Whitmarsh, J. Cavanagh, H.K. Shoss, B. Derjard, R.J. Davis, Selective interaction of JNK protein kinase isoforms with transcription factors, *Embo J.* 15 (1996) 2760–2770.
- [2] M.A. Bogoyevitch, K.R.W. Ng, T.Y. Zhao, Y.Y.C. Yeap, D.C.H. Ng, c-Jun N-terminal kinase (JNK) signaling: recent advances and challenges, *Biochim. Biophys. Acta Proteins Proteom.* 1804 (2010) 463–475.
- [3] R.J. Davis, Signal transduction by the JNK group of MAP kinases, *Cell* 103 (2000) 239–252.

- [4] M.A. Bogoyevitch, The isoform-specific functions of the c-Jun N-terminal kinases (JNKs): differences revealed by gene targeting, *Bioessays* 28 (2006) 923–934.
- [5] S. Brecht, R. Kirchhof, A. Chromik, M. Willesen, T. Nicolaus, G. Raivich, J. Weisig, V. Warting, M. Goetz, M. Glaussen, D. Pearse, C.Y. Kwon, E. Vaudan, A. Behrens, T. Wagner, R.A. Flavell, R.J. Davis, T. Herdegen, Specific pathophysiological functions of JNK isoforms in the brain, *Eur. J. Neurosci.* 21 (2005) 363–377.
- [6] P.P. Graczyk, JNK inhibitors as anti-inflammatory and neuroprotective agents, *Future Med. Chem.* 5 (2013) 539–551.
- [7] P. Koch, M. Gehring, S.A. Lauder, Inhibitors of c-Jun N-terminal kinases: an update, *J. Med. Chem.* 58 (2015) 72–95.
- [8] M. Gehring, F. Muth, P. Koch, S.A. Lauder, c-Jun N-terminal kinase inhibitors: a patent review (2010–2014), *Expert Opin. Ther. Pat.* 25 (2015) 849–872.
- [9] F. Anisderi, A. Lange, A. El-Gokha, F.M. Bockler, P. Koch, Fluorescence polarization-based assays for detecting compounds binding to inactive c-Jun N-terminal kinase 3 and p38 alpha mitogen-activated protein kinase, *Anal. Biochem.* 503 (2016) 28–40.
- [10] A. Bucher, B. Zech, B. Felber, B. Klebl, G. Müller, Small-molecule inhibitors binding to protein kinase, Part II: the novel pharmacophore approach of type II and type III inhibition, *Expert Opin. Drug Discov.* 3 (2008) 1427–1449.
- [11] A. Bucher, B. Zech, B. Felber, B. Klebl, G. Müller, Small-molecule inhibitors binding to protein kinases, Part I: exemplars from the traditional pharmacophore approach of type I inhibition, *Expert Opin. Drug Discov.* 3 (2008) 1409–1425.
- [12] N.J. Moorik, Fluorescence polarization (FP) assays for monitoring peptide-protein or nucleic acid-protein binding, *Curr. Protoc. Chem. Biol.* 1 (2009) 1–15.
- [13] I.A. Schepetkin, L.N. Karpova, A.I. Khlebnikov, T.S. Hanika, I. Kochenkova, D.W. Pascul, M.A. Jullia, M.T. Quinn, Identification and characterization of a novel class of c-Jun N-terminal kinase inhibitors, *Mol. Pharmacol.* 81 (2012) 832–845.
- [14] B.G. Szczepankiewicz, C. Komgol, L.T.J. Nelson, G. Liu, B. Liu, H.Y. Zhao, M.D. Serly, Z.L. Xin, M. Lin, R.J. Gam, D.J. Hausch, S.Y. Wang, J.E. Clampton, E.F. Johnson, T.H. Lubben, M.A. Stashko, E.T. Obojczak, C.H. Sun, S.A. Dorwin, K. Haskins, C. Albad-Zapatero, E.H. Fry, C.W. Hutchins, H.L. Sham, C.M. Roodman, J.M. Trevisyan, Aminopyridine-based c-Jun N-terminal kinase inhibitors with cellular activity and minimal cross-kinase activity, *J. Med. Chem.* 49 (2006) 3563–3580.
- [15] T. Kamenecka, J. Haber, D. Duckert, W. Chen, Y.Y. Ling, B. Frackowiak, R. Jung, Y. Shin, X. Song, P. LoGrasso, Structure-activity relationships and X-ray structures describing the selectivity of aminopyridine inhibitors for c-Jun N-terminal kinase 3 (JNK3) over p38, *J. Biol. Chem.* 284 (2009) 12851–12861.
- [16] J.W. Chambers, A. Pachori, S. Howard, M. Ganso, D. Hansen, T. Kamenecka, X.Y. Song, D. Duckert, W.M. Chen, Y.Y. Ling, L. Cherry, M.D. Cameron, L. Lin, C.H. Ruiz, P. LoGrasso, Small molecule c-Jun N-terminal kinase inhibitors protect dopaminergic neurons in a model of Parkinson's disease, *ACS Chem. Neurosci.* 2 (2011) 198–206.
- [17] Z. Mikolovska-Coleska, R. Wang, X. Fang, H. Pan, Y. Tamita, P. Li, P.P. Butler, K. Krajewski, N.G. Saito, J.A. Stuckey, S. Wang, Development and optimization of a binding assay for the XIAP BIR3 domain using fluorescence polarization, *Anal. Biochem.* 332 (2004) 261–273.
- [18] R. Wang, Z. Mikolovska-Coleska, X. Fang, S. Wang, From K50 to K1: A General Mathematical Solution for Fluorescence-Based Competitive Binding Assays, unpublished results.
- [19] A. Lange, M. Günther, F. Michael Büttsel, M.O. Zimmermann, J. Heidrich, S. Hennig, S. Zahn, C. Schall, A. Sievers-Englet, E. Anisderi, P. Koch, M. Laemmerhofer, T. Stehbe, S.A. Lauder, F.M. Bockler, Targeting the gate-keeper ME1146 of c-Jun N-terminal kinase 3 induces a bivalent halogen/thalogen bond, *J. Am. Chem. Soc.* 137 (2015) 14640–14652.

## Supplementary Material

### Fluorescence polarization-based competition binding assay for c-Jun N terminal kinases 1 and 2.

Francesco Ansideri<sup>a</sup>, Marcel Dammann<sup>b</sup>, Frank M. Boeckler<sup>b</sup>, Pierre Koch<sup>a\*</sup>

*<sup>a</sup>Institute of Pharmaceutical Sciences, Department of Medicinal and Pharmaceutical Chemistry, Eberhard Karls Universität Tübingen, Auf der Morgenstelle 8, 72076 Tübingen, Germany*

*<sup>b</sup>Institute of Pharmaceutical Sciences, Molecular Design and Pharmaceutical Biophysics, Eberhard Karls Universität Tübingen, Auf der Morgenstelle 8, 72076 Tübingen, Germany*

### TABLE OF CONTENTS

<b>JNK1 and JNK2 expression and purification</b> .....	S2
<b>Figure S1. Structures of tested standard JNK inhibitors</b> .....	S5
<b>Figure S2. Competition assay graphs</b> .....	S6

**JNK1 and JNK2 expression and purification**

The JNK1 gene was amplified and cloned into the expression vector pET-24a-HLT using the Gibson Assembly<sup>®</sup> Master Mix (New England Biolabs GmbH). The cloning was performed according to the manual with exception of the heat shock lasting 45 s instead of 30 s. Clones were cultured overnight in lysogeny broth media at 37 °C. The plasmid was finally extracted using the QIAprep Spin Miniprep Kit<sup>®</sup> (Qiagen) in agreement with the manual and checked by Eurofins Genomics.

The JNK2 gene was synthesized and cloned into the same expression vector pET-24a-HLT by GeneArt<sup>™</sup> (Thermo Fisher Scientific) and the plasmid was rechecked by Eurofins Genomics.

The plasmids were transformed in *Escherichia coli* BL21 competent cells using the following protocol: 2 µL of a 100 µg/mL plasmid solution were added to the competent cells and incubated on ice for 30 min. The cells were then heat-shocked at 42 °C for 2 min, followed by 5 min incubation on ice. 900 µL of 2xYT media were added and the cell suspension was incubated for 1 h at 37 °C. 200 µL were plated on plates of 2xYT agar, containing 50 µg/µL kanamycin and 30 µg/µL chloramphenicol whereas the remaining cell suspension was centrifuged at 3000 rpm for 2 min. The supernatant was discarded with exception of 200 µL which was used to resuspend the pellet and the resulting suspension was plated on another 2xYT plate. Both plates were incubated overnight at 37 °C. 10 mL of 2xYT media, containing both antibiotics, were used to wash the plates and were then added to 90 mL of the same media. The culture was grown at 37 °C and 200 rpm until reaching an  $OD_{600} = 1$ , at which point 10 mL of this pre-culture were inoculated into each of 6-8 2L flasks containing 1 L of 2xYT and antibiotics. The culture was grown at 37 °C and 220 rpm to an  $OD_{600} = 0.4 - 0.6$ . The temperature was then lowered to 18 °C and 800 µL of 1 M isopropyl-1-thio-β-D-S2



galactopyranoside (Roth) were added for induction. The protein was expressed overnight and afterwards the cells were harvested by centrifugation at 4000 rpm for 30 min.

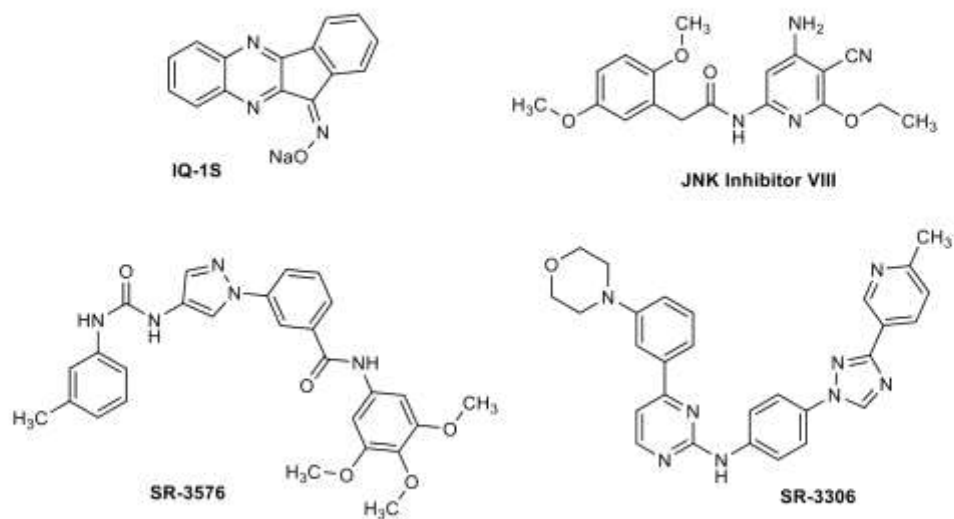
The pellet was resuspended in JNK lysis buffer (20 mM Tris pH 7.4, 500 mM NaCl, 15 mM imidazole, 5 mM  $\beta$ -mercaptoethanol (BME)). The suspension was added with DNase, RNase, and EDTA-free protease inhibitor cocktail tablets (Roche) and then lysis by ultrasound pulses was performed. The sonication procedure consisted in 5 consecutive 4 min programs, each alternating 15 s pulses and 30 s pause, using a Bandelin Sonoplus HD 3200 with KE76 sonicator tip. The resulting suspension was centrifuged at 18500 rpm for 1 h at 4 °C and the supernatant was filtered through a polyethersulfon membrane with 0.22  $\mu$ m pores. The first purification step was performed by a Ni<sup>2+</sup>-NTA column (GE Healthcare), previously equilibrated with lysis buffer. After loading, the lysate was eluted by JNK Elution Buffer (20 mM Tris pH 7.5, 500 mM NaCl, 300 mM imidazole, 5 mM BME) used in a linear gradient. Protein containing fractions were pooled and TEV protease was added at a final concentration of 1 mg/mL and diluted 1:2. The solution dialysed overnight with regenerated cellulose (12 kDa molecular weight cut-off) at 4 °C. The solution was loaded on a Ni<sup>2+</sup>-NTA column and eluted using JNK Elution Buffer in a two-step gradient (40 and 80%). The washing phase and the flow through were pooled and the resulting solution was concentrated using a Vivaspin® 15 (Sartorius) with a MW cut-off of 10 kDa. Last purification step was performed using a HiLoad 27/60 Superdex 75 prep grade gel filtration column, which was equilibrated with JNK gel filtration buffer (20 mM Tris pH 7.5, 250 mM NaCl, 5% (v/v) glycerol, 5 mM BME). The protein containing fractions were pooled and concentrated as described above.

The following sequence of JNK1 was expressed:

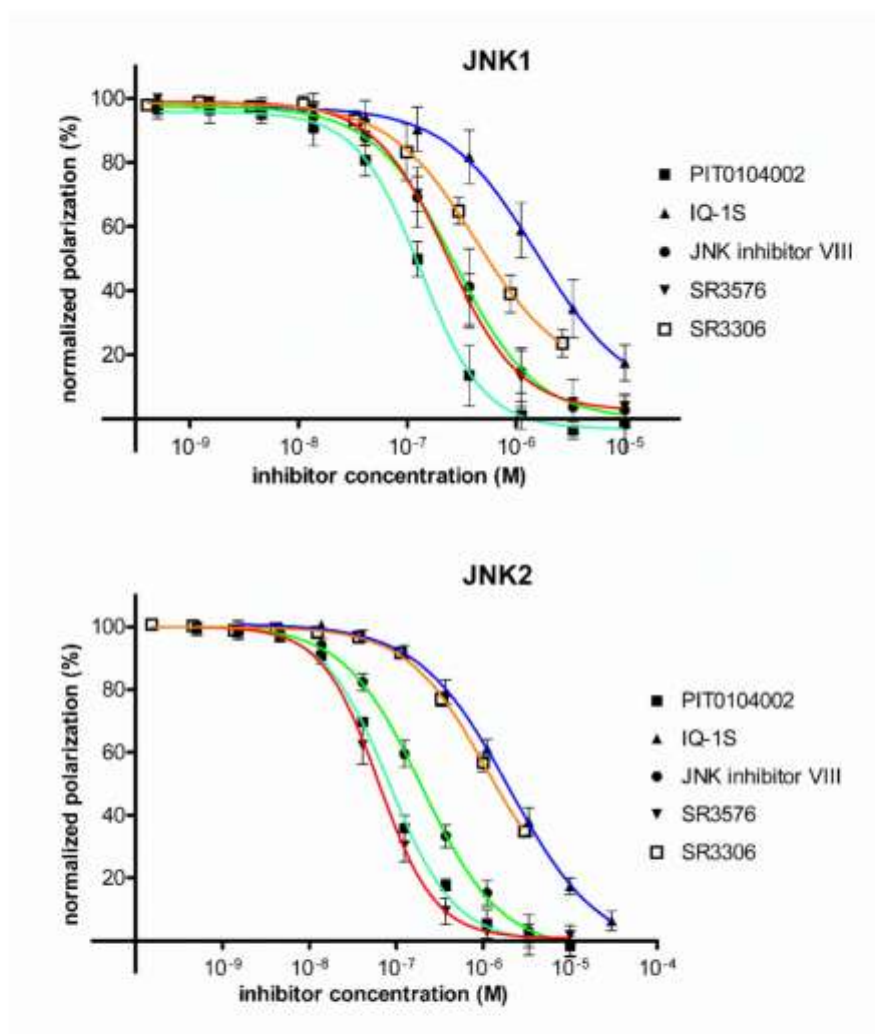
MHHHHHSGAFEFKLPDIGEGIEIVKWFVKGDEVNEDDVLCEVQNDKAVVEIPSPVKGKVL  
EILVPEGTVATVGQTLITLDAPGYENMTTGS DTGENLYFQGGSMSRSKRDN NFYSVEIGDSTFTVL  
KRYQNLKPIGSGAQGIVCAAYDAILERNVAIKLSRPFQNT HAKRAYREL VLMKCVNHKNIIGLLN  
VFTPQKSLEEFQDVYIVMELMDANLCQVIQME LDHERMSYLLYQMLCGIKHLHSAGIIHRDLKPSNI  
VVKSDCTLKILDFGLARTAGTSFM MTPYVVTRY YRAPEVILGMGYKENVDIWSVGCIMGEMIKGGV  
LFPGTDHIDQWNKVIEQLGTPCEPFMKK LQPTVRTYVENR PKYAGYSFEKLPDVLFPADSEHNK  
LKASQARDLLSKMLVIDASKRISVDEALQHPYINWYDPSEAEAPPPKIPDKQLDEREHTIEEWKEL  
IYKEVMDLE\*

The following sequence of JNK2 was expressed:

MHHHHHSGAFEFKLPDIGEGIEIVKWFVKGDEVNEDDVLCEVQNDKAVVEIPSPVKGKVL  
EILVPEGTVATVGQTLITLDAPGYENMTTGS DTGENLYFQGGSMDSQFYSVQVADSTFTVLKRYQ  
QLKPIGSGAQGIVCAAFDVLGINVAVKKLSRPFQNT HAKRAYREL VLLKCVNHKNIISLLNVFTP  
QKTLEEFQDVYIVMELMDANLCQVIHME LDHERMSYLLYQMLCGIKHLHSAGIIHRDLKPSNIVVK  
SDCTLKILDFGLARTASTNFM MTPYVVTRY YRAPEVILGMGYKENVDIWSVGCIMGELVKGSVIFQ  
GTDHIDQWNKVIEQLGTPSAEFMAALQPTVRNYVENR PAYPGIAFEELFPDWIFPSESERDKIKTS  
QARDLLSKMLVIDPDKRISVDEALRHPYITVWYDPAEAEAPPPQIYDAQLEEREHAIEEWKELIYKE  
VMD\*



**Figure S1.** Structures of tested standard JNK inhibitors.



**Figure S2.** Competition curves obtained from the FP assay on JNK1 (50 nM) and JNK2 (30 nM). Probe 1 was used at a concentration of 5 nM. Data point represent mean  $\pm$  SD of three independent experiments.

## Publication III

Koch, P.; Ansideri, F. 2-Alkylsufanyl-4(5)-aryl-5(4)-heteroarylimidazoles: An Overview on Synthetic Strategies and Biological Activity. *Arch. Pharm.* **2017**, *350*, e1700258.


Reprinted with permission from Koch and Ansideri, *Arch. Pharm.* **2017**, *350*, e1700258. Copyright 2017 Deutsche Pharmazeutische Gesellschaft

Link to the published version:

<https://onlinelibrary.wiley.com/doi/10.1002/ardp.201700258>

## Review Article

### 2-Alkylsulfanyl-4(5)-aryl-5(4)-heteroarylimidazoles: An Overview on Synthetic Strategies and Biological Activity

Pierre Koch  and Francesco Ansideri

Department of Pharmaceutical and Medicinal Chemistry, Institute of Pharmaceutical Sciences, Eberhard Karls Universität Tübingen, Tübingen, Germany

2-Alkylsulfanyl-4(5)-aryl-5(4)-heteroarylimidazoles represent an important class of ATP-competitive protein kinase inhibitors, offering the possibility of multiple interactions with different regions of the target enzyme. The necessity of exploring the effects of diverse chemical decorations around the imidazole core prompted the design of several synthetic routes aimed at achieving both efficiency and flexibility. Additionally, the optimization of established protocols and the extensive use of transition metal-catalyzed cross-coupling reactions have been broadening the spectrum of preparative methodologies within the last decade. This review summarizes the progress in the development of synthetic strategies leading to 2-alkylsulfanyl-4(5)-aryl-5(4)-heteroarylimidazoles and 1-alkyl-2-alkylsulfanyl-4(5)-aryl-5(4)-heteroarylimidazoles and offers a glance at the biological activities of this class of compounds.

**Keywords:** 1,2,4,5-Tetra-substituted imidazoles / 2,4,5-Tri-substituted imidazoles / Kinase inhibitors / Regioselective synthesis

Received: August 16, 2017; Revised: October 12, 2017; Accepted: October 13, 2017

DOI 10.1002/ardp.201700258

#### Introduction

The imidazole ring represents one of the most widely spread heterocyclic cores, being expressed in many natural products as well as in synthetic molecules. Due to favorable features like water solubility and the potential to act both as donor and acceptor of hydrogen bonds, such a scaffold has found many applications in the field of medicinal chemistry and is incorporated in a multitude of compounds exhibiting biological activities. The multiplicity of synthetic strategies for their preparation, allowing a high versatility in the functionalization of the different positions around the five-membered ring, represents an additional advantage of the imidazole-based derivatives' design. A recent extensive overview of imidazole-based medicinal chemistry was published by Zhang et al. in 2014 [1]. The synthesis of vicinal diaryl imidazoles as well as their biological activity was reviewed by Bellina et al. in 2007 [2]. The pharmacophore design of tri- and tetra-substituted imidazoles as inhibitors of p38 $\alpha$  mitogen-

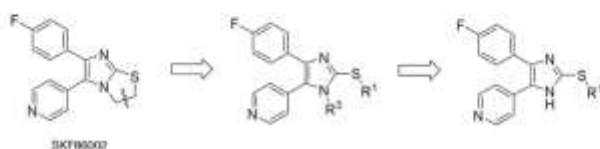
activated protein (MAP) kinase was listed by Scior et al. in 2011 [3].

The current review summarizes different synthetic methods for the preparation of 2-alkylsulfanyl-4(5)-aryl-5(4)-heteroarylimidazoles published until June 2017. Additionally, the biological activity of selected 2-alkylsulfanylimidazoles will be discussed. In fact, most of the herein presented compounds are inhibiting different protein kinases, e.g., p38 $\alpha$  MAP kinase, c-Jun N-terminal kinase (JNK) 3, protein kinase CK1 $\delta$ , and CK1 $\epsilon$ , as well as epidermal growth factor receptor kinase (EGFR).

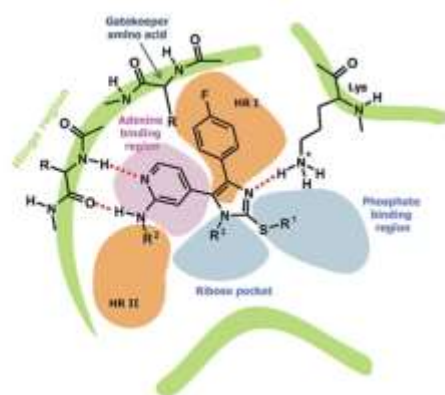
2-Alkylsulfanyl-4(5)-aryl-5(4)-heteroarylimidazoles can be considered as open analogs of the early lead p38 $\alpha$  MAP kinase inhibitor SKF86002 [4] developed by Smith Kline & French Laboratories (Scheme 1). Their kinase inhibitory activity is attributed to the imidazole ring distributing the substituents on positions 1, 2, 4, and 5 in optimal orientations in order to get multiple interaction possibilities within the ATP-binding site of the enzyme (Fig. 1). In detail, the imidazole-N3 atom is accepting either a direct or a water-mediated hydrogen bond from a highly conserved Lys side chain amino function [5] and a second hydrogen bond interaction involves the pyridine heteroatom and the backbone of the hinge region. The 4-fluorophenyl moiety occupies the hydrophobic region I, an additional pocket not targeted by ATP, while the residues at the imidazole-N1 and the imidazole-C2-5 positions are interacting with the sugar pocket and/or with the phosphate

**Correspondence:** Prof. Pierre Koch, Department of Pharmaceutical and Medicinal Chemistry, Institute of Pharmaceutical Sciences, Eberhard Karls Universität Tübingen, Auf der Morgenstelle 8, 72076 Tübingen, Germany.  
E-mail: pierre.koch@uni-tuebingen.de  
Fax: +49 7071 29 5037





**Scheme 1.** Derivation of 1,2,4,5-tetra-substituted and 2,4,5-tri-substituted imidazoles from SKF86002.



**Figure 1.** Binding mode of SKF86002-derived 2-alkylsulfanyl-4(5)-aryl-5(4)-heteroaryl-imidazoles within the ATP-binding sites of protein kinases (modified from Ref. [7]). HR I, hydrophobic region I; HR II, hydrophobic region II.

binding site. Optimized kinase inhibitors have an amino or amide function at the pyridine-C2 position, permitting the formation of an additional hydrogen bond interaction to the hinge region as well as introducing a suitable moiety  $R^2$  pointing toward the less conserved solvent-exposed hydrophobic region II. Different combinations in the substitution pattern of the imidazole ring and of the substituent at the pyridine-C2 position allowed the achievement of potency and selectivity within the kinase.

Among numerous 2-alkylsulfanyl-imidazoles, which have been synthesized within the last few decades, only two co-crystal structures of these derivatives complexed with protein kinases have been reported so far [6].

### Synthesis of 2,4,5-tri-substituted imidazoles

The first synthetic methods of vicinal 4,5-diaryl-substituted 2-mercaptoimidazoles were filed in a European patent application from researchers of Ciba-Geigy AG in 1979 [8]. The

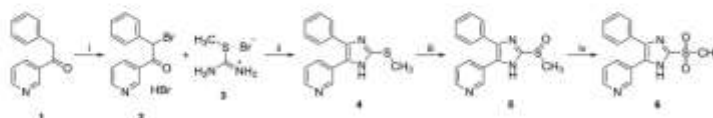
researchers claimed these 2-alkyl-imidazoles, as well as their corresponding sulfoxides and sulfones, to exhibit anti-inflammatory and/or anti-nociceptive and/or anti-thrombotic activity.

For their preparation, a short two-step synthetic sequence, which is illustrated for 2-methylsulfanyl-4(5)-phenyl-5(4)-(3-pyridyl)imidazole (**4**) in Scheme 2, starting from benzyl-(pyridin-3-yl)ketone (**1**) was used. This sequence involved bromination of ketone **1** in  $\alpha$ -position followed by ring closing reaction of **2** with 5-methylisothiuronium bromide (**3**) in presence of *N,N*-diisopropylethylamine (DIPEA) to yield 2-methylsulfanyl-imidazole **4**. Oxidation of the sulfur atom of **4** was also reported. Treatment of **4** with 84% *m*-chloroperbenzoic acid (*m*-CPBA) resulted in 2-methylsulfinyl-imidazole **5**, which was further oxidized to methylsulfonyl derivative **6** using 30% hydrogen peroxide.

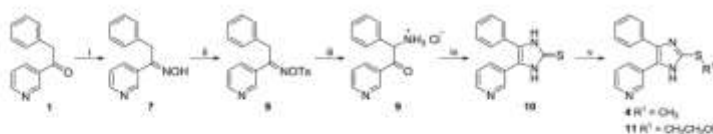
In order to diversify the substitution at the imidazole-C2-S position, another synthetic sequence was reported from the same researchers also using ketone **1** as starting material (Scheme 3). The building block **10**, 4(5)-aryl-5(4)-heteroaryl-imidazole-2-thione, was synthesized in an adaption of the Marckwald imidazole synthesis. This structural class represents a common intermediate in many of the described synthetic routes listed in this review. The  $\alpha$ -aminoketone **9** was obtained from a Neber rearrangement reaction of the *O*-tosyl oxime **8** with potassium *tert*-butoxide in absolute ethanol, and immediately converted into the imidazole-2-thione **10** by cyclization with sodium thiocyanate. The introduction of substituents (methyl and 2-hydroxyethyl) on the imidazole-C2-S position occurred by treatment of **10** with the corresponding alkyl halides in presence of a base.

During the optimization and identification of novel SKF86002-like p38 $\alpha$  MAP kinase inhibitors, Sisko and co-workers reported in 2000 an unexpected reactivity of imidazo[2,1-*b*]thiazolines with organolithium and Grignard reagents leading to 2-alkylsulfanyl-imidazoles [9]. For example, treatment of SKF86002 with *n*-butyllithium under low temperature proceeded smoothly to formation of 2-butylsulfanyl-imidazole **12** (Scheme 4). The release of the ring strain is supposed to represent the key driver for this reaction and the formation of **12** might arise from addition of the butyl group at the sulfur atom followed by elimination of ethylene.

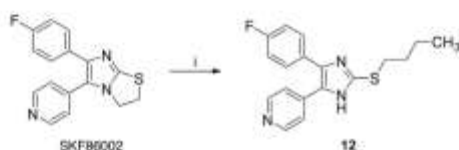
The aforementioned synthetic routes to 2,4,5-tri-substituted imidazoles allow modifications of the residue on the sulfur atom, but none of these take into account the option of introducing substituents at the six-membered heterocycle at the imidazole-C4(5) position.



**Scheme 2.** Synthesis of 2-methylsulfanyl-4(5)-phenyl-5(4)-(3-pyridyl)imidazole (**4**) and its oxidation products **5** and **6**. Reagents and conditions: (i)  $\text{Br}_2$ , acetic acid; (ii) DIPEA, acetonitrile; (iii) 84% *m*-CPBA, chloroform; (iv) 30% hydrogen peroxide, acetic acid, 70°C.



**Scheme 3.** Synthesis of 2-alkylsulfanyl-4(5)-phenyl-5(4)-(pyridin-3-yl)imidazoles **4** and **11**. Reagents and conditions: (i)  $\text{H}_2\text{N}\cdot\text{OH}\cdot\text{HCl}$ , pyridine, 100°C; (ii) *p*-toluenesulfonyl chloride, pyridine, -10°C; (iii) *t*-BuOK, ethanol, 0°C; (iv) NaSCN, aq. HCl, ethanol, reflux temperature; (v)  $\text{H}_2\text{C}\cdot\text{I}$ , methanol/2 M aq. NaOH 5:1 (v/v), room temperature (rt) in case of preparation of **4** or EtONa, 2-chloroethanol, ethanol, reflux temperature in case of preparation of **11**.



**Scheme 4.** Unexpected reaction of imidazo[2,1-*b*]thiazolines to 2-alkylsulfanylimidazoles. Reagents and conditions: (i) *n*-butyllithium, tetrahydrofuran, -78°C.

In 2003, Laufer and co-workers reported a six-step synthetic protocol to 2-methylsulfanyl- and 2-benzylsulfanyl-substituted imidazoles **19** starting from 2-halogeno-4-methylpyridines **13a–c** (Scheme 5), which was further optimized in 2006 [10, 11]. Analogously to the route depicted in Scheme 3, the formation of the imidazole ring takes place by cyclization of an  $\alpha$ -aminoketone with thiocyanate salt, although the preparation of the  $\alpha$ -aminoketones **16** was carried out in a different way. Ethanones **14**, synthesized starting from the corresponding 2-halogeno-4-methylpyridines, were first converted into the corresponding  $\alpha$ -oximino derivatives **15** and then regioselectively reduced to  $\alpha$ -aminoketones **16**. This reduction step was performed using hydrogen at atmospheric pressure, palladium on charcoal as catalyst, and 2-propanolic hydrogen chloride solution as solvent. The choice of the solvent during this step was described to be essential for its success. Most important, under these acidic conditions, the primary amino function of **16** resulting from the reduction is being protonated, thus preventing the possible intermolecular condensation reaction of two  $\alpha$ -aminoketone molecules to a 2,3,5,6-tetra-substituted pyrazine derivative. However, when using hydrogen chloride solution of linear alcohols as

a solvent, e.g., methanol or ethanol, these were able to react in an acid-catalyzed nucleophilic aromatic substitution reaction displacing the fluorine substituent at the pyridine ring. In detail, the use of methanolic hydrogen chloride solution in this reaction resulted in methoxy derivative **16c**. By employing a more sterically demanding alcohol such as isopropyl alcohol this collateral reaction could be avoided and compounds **16a** and **16b** could be obtained smoothly. Worth to mention, the reduction of oxime derivative **15c** was accompanied by a hydrogenolytic cleavage of the bromo atom yielding unsubstituted pyridine compound **16d**. The latter observation was used in another study to synthesize 4(5)-(4-fluorophenyl)-5(4)-(pyridin-4-yl)-1,3-dihydroimidazol-2-one from bromo-substituted oxime **15c** via  $\alpha$ -aminoketone **16d** [12].

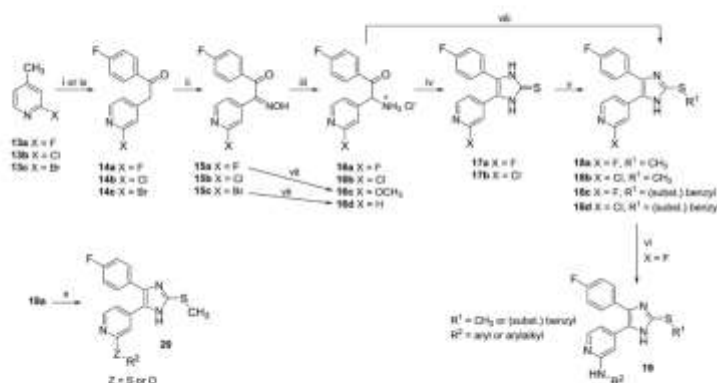
The imidazole-2-thiones **17** were synthesized by cyclization reaction of  $\alpha$ -aminoketones **16a** and **16b** with potassium thiocyanate. Subsequently, the exocyclic sulfur atom was alkylated (methyl or (substituted) benzyl) via a nucleophilic substitution reaction. Finally, the pyridine-C2-amino function was introduced through a nucleophilic aromatic substitution reaction of imidazoles **18a** and **18c** and different primary amines.

As already mentioned, this synthetic strategy was further optimized by Laufer and Liedtke [11]. Ethanones **14** were synthesized according to a protocol of Thompson et al., which consisted in reacting the 2-halogeno-4-methylpyridines with ethyl 4-fluorobenzoate instead of the Weinreb amide and in using sodium bis(trimethylsilyl)amide (NaHMDS) instead of lithium diisopropylamide (LDA) as a base. These modifications allowed the performance of this reaction at moderate temperatures and reduced the reaction time. Moreover, the reaction of  $\alpha$ -aminoketones **16a** and **16b** with alkyl or benzyl thiocyanates directly yielded the corresponding 2-alkylsulfanyl- or 2-benzylsulfanyl-substituted imidazoles **18**, thus



Arch. Pharm. Chem. Life Sci. 2017, 350, e1700258  
P. Koch and F. Ansideri

ARCH PHARM  
Archiv der Pharmazie



**Scheme 5.** Synthetic routes toward 2-alkyl-5-(2-aminopyridin-4-yl)-4-(4-fluorophenyl)imidazoles **19** and 2-methylsulfanylimidazoles **20**. Reagents and conditions: (i) LDA, 4-fluoro-*N*-methoxy-*N*-methylbenzamide, tetrahydrofuran,  $-85^{\circ}\text{C}$  then  $0^{\circ}\text{C}$ ; (ii)  $\text{NaNO}_2$ , acetic acid;  $10^{\circ}\text{C}$ ; (iii)  $\text{H}_2$ , Pd/C 10%, 1 atm, 2-propanolic HCl, rt; (iv) KSCN, *N,N*-dimethylformamide (DMF), reflux temperature; (v)  $\text{R}^1\text{-hal}$  (hal = I, Br, Cl;  $\text{R}^1 = \text{CH}_3$  or benzyl), ethanol-tetrahydrofuran (8:2), reflux temperature; (vi) excess  $\text{R}^2\text{-NH}_2$ , neat,  $160\text{--}180^{\circ}\text{C}$ ; (vii)  $\text{H}_2$ , Pd/C 10%, 1 atm, methanolic HCl, rt; (viii) methyl-/benzylthiocyanate, DMF,  $160^{\circ}\text{C}$ ; (ix) NaHMDS, ethyl 4-fluorobenzoate, tetrahydrofuran,  $0^{\circ}\text{C}$  then rt; (x)  $\text{R}^2\text{-SH}$  or  $\text{R}^2\text{-OH}$ , NaH, DMF,  $155\text{--}160^{\circ}\text{C}$ .

shortening the synthetic sequence by one step. The presented route is characterized by a good flexibility in the functionalization of the imidazole-C2-S position and in the substitution of the pyridine-C2 position, taking place in the last two synthetic steps. On the other side, the aryl and the heteroaryl moieties at the imidazole-C4 and -C5 positions need to be defined in the first step of the route.

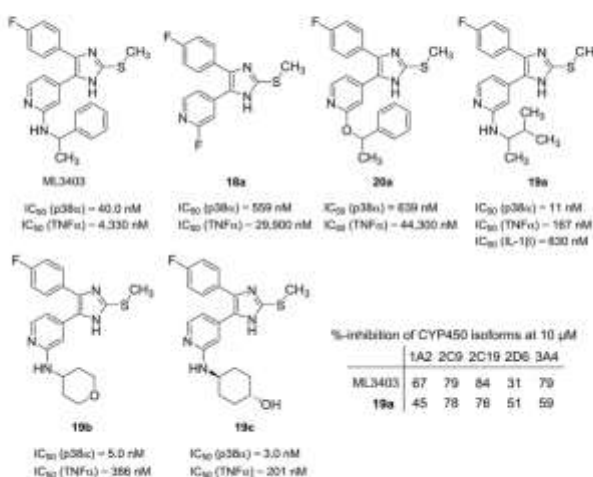
In 2008, Laufer and co-workers took on the optimized synthetic strategy extending the number of examples of imidazoles **19** [7]. Within this series, 2-methylsulfanylimidazoles having a meta-trifluorophenyl ring as aromatic substituent or a quinoline ring as heteroaromatic substituent on the imidazole-C4 and -C5 positions, were also synthesized. In addition, the substitution pattern at the pyridine-C2 amino group was extensively modified by introduction of alkyl, cycloalkyl, aromatic as well as heteroaromatic moieties, and the amino linker was replaced by an ether and a thioether function.

Examples of tri-substituted 2-alkylsulfanylimidazoles as potent p38 $\alpha$  MAP kinase inhibitors, which were synthesized following the synthetic routes depicted in Scheme 5, are displayed in Fig. 2. The most prominent example is represented by ML3403, which inhibits the target kinase in the double-digit nanomolar range and the release of TNF- $\alpha$  from human whole blood (HWB) in the low-micromolar range. ML3403 served both as lead compound for further optimization studies and as reference compound in *in vitro* and *in vivo* studies [7, 13–17]. The pharmacokinetic profile of ML3403 was extensively investigated by Kammerer et al. [18, 19]. *In vitro* (animal and human liver microsomes) as well as *in vivo* (Wistar rats) studies revealed the oxidation of

the 2-methylsulfanyl moiety at the imidazole-C2 position into a 2-methylsulfinyl being the predominant biotransformation reaction [17, 18]. Cytochrome P450 (CYP450)-3A4 was identified to be the key isoform for this sulfoxidation reaction. In a mouse arthritis model, ML3403 reduced the production of the proinflammatory cytokine IL-6 in the paw tissue, whereas it increased the levels of the anti-inflammatory cytokine IL-10 [14].

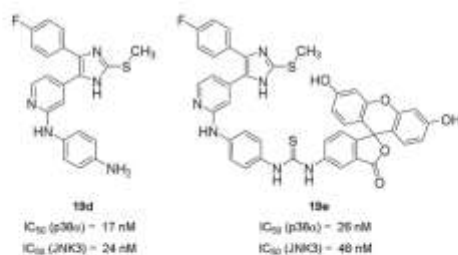
By comparing ML3403 with its precursor **18a** (Fig. 2), it could be observed that substitution of the fluorine atom at the pyridine-C2 position with a phenylalkylamino group proved to be beneficial for the inhibitory activity on the p38 $\alpha$  MAP kinase. As already mentioned, this is mainly due to the formation of an additional hydrogen bond with the backbone carbonyl group of Met109 and, as an additional factor, to the potential interaction with the enzyme's hydrophobic region II. As proof of this, the replacement of the nitrogen with a linker atom unable to donate a hydrogen bond (such as oxygen in compound **20a**) resulted in a dramatic drop in activity. Laufer and co-workers also showed compounds having branched alkyl (**19a**) or (polar) cycloalkyl groups (**19b**, **19c**) at the pyridine-C2 amino function to exhibit a markedly increased p38 $\alpha$  MAP kinase inhibition profile with IC<sub>50</sub> values down to the low single-digit nanomolar range (Fig. 2). Nevertheless, at a test concentration of  $10\ \mu\text{M}$ , ML3403 as well as **19a** display more than 50% inhibition of four CYP450 isoenzymes [7].

Recently, our group reported tri-substituted imidazole **19d** as a balanced dual p38 $\alpha$  MAP kinase/JNK3 inhibitor together with its fluorescent labelling by reaction with fluorescein isothiocyanate isomer S' giving **19e** (Fig. 3) [20]. The latter

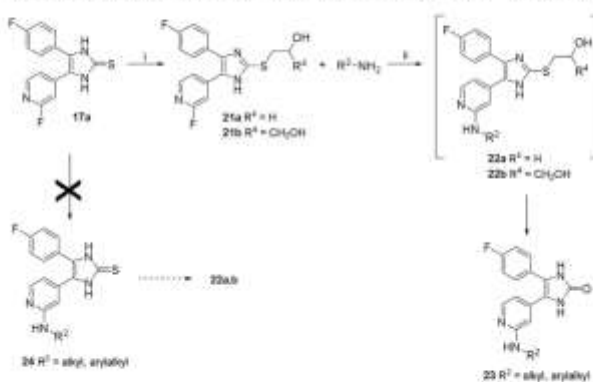


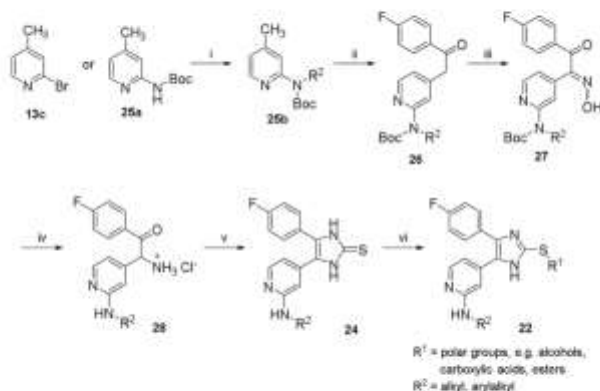
serves as a reporter molecule in fluorescence polarization-based competition binding assays to determine the affinity of potential inhibitors for p38 $\alpha$  MAP kinase as well as for all JNK isoforms [20–22].

The route depicted in Scheme 5 is limited by the nature of the moiety at the imidazole-C2 position. Attempts to synthesize a series of pyridinylimidazoles **22** having hydroxy-containing groups like hydroxyethyl or 2,3-dihydroxypropyl at the imidazole-C2-5 position starting from imidazole-2-thione **17a** (Scheme 6) failed [12]. The intended synthetic strategy included the introduction of the polar alkylsulfanyl moiety at the imidazole-C2 position by nucleophilic substitution of imidazole-2-thione **17a** and the appropriate alkyl halide followed by displacement of the fluorine



**Figure 3.** Dual p38 $\alpha$  MAP kinase/JNK3 inhibitor **19d** and reporter molecule **19e** [20].





**Scheme 7.** Preparation of 4(5)-(4-fluorophenyl)-5(4)-(2-(alkylamino)pyridin-4-yl)-1,3-dihydroimidazole-2-thiones **24** as well as their functionalization at the imidazole-C2-S position. Reagents and conditions: (i) NaH,  $R^2$ -Br, DMF, 0°C (in case of starting from **25a**) or a)  $R^2$ -NH<sub>2</sub>, Pd<sub>2</sub>(dba)<sub>3</sub>, t-BuONa, BINAP, toluene, b) Boc<sub>2</sub>O, dichloromethane (in case of starting from **13c**); (ii) NaHMDS, ethyl 4-fluorobenzoate, tetrahydrofuran, 0°C, then rt; (iii) NaNO<sub>2</sub>, acetic acid, 10°C to rt; (iv) Pd/C 10%, methanolic HCl, H<sub>2</sub>, atmospheric pressure, rt; (v) KSCN, DMF, reflux temperature; (vi)  $R^1$ -X (X = Cl, Br, I), t-BuOK or EtONa, methanol, 50°C to reflux temperature.

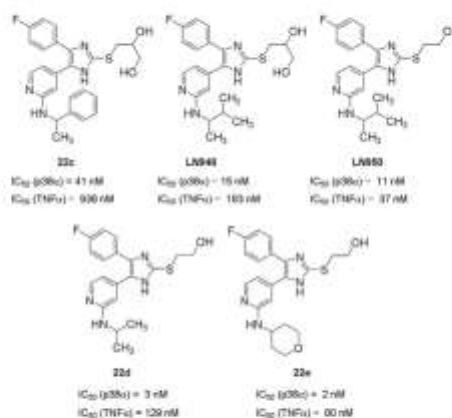
atom in **21a** and **21b** by heating with an excess of primary amine. However, the latter step was accompanied by an unexpected transformation of 2-alkylsulfanylimidazoles **22a** and **22b** into the imidazol-2-one derivatives **23** [12]. The progress of this reaction to the 2-alkylsulfanylimidazole and imidazole-2-one derivatives **22** and **23** is temperature-dependent. Reaction monitoring also indicated that imidazoles **21** first reacted with the primary amine in a nucleophilic aromatic substitution reaction to 2-alkylsulfanylimidazoles **22** followed by the conversion of **22** into imidazol-2-ones **23** as the predominant reaction.

Due to the fact that the introduction of the amino function at the pyridine-C2 position via a nucleophilic substitution reaction is not feasible without simultaneous conversion of 2-alkylsulfanylimidazoles **22** into imidazole-2-ones **23**, the reaction sequence was modified. The first attempt consisted in performing the nucleophilic aromatic substitution reaction on the imidazole-2-thione intermediate **17a** in order to functionalize the sulfur atom of thiones **24** in the last synthetic step. However, this approach was not successful due to a problematic isolation of the imidazole-2-thiones **24**, along with a scarce reproducibility of this reaction [23].

An alternative strategy succeeding in the preparation of compounds **22** was suggested by some of us in 2008 (Scheme 7) [24]. In the first step of this synthetic route, the substituent at the pyridine-C2 position was introduced either via a nucleophilic substitution reaction of Boc-protected 2-amino-4-picoline (**25a**) with alkyl halides or via Buchwald-Hartwig cross-coupling reaction of 2-bromo-4-picoline (**13c**) with primary amines followed by Boc-protection. Starting from 2-amino-4-methylpyridines **25b** the ethanone formation-nitrosation-reduction-cyclization sequence was applied to generate imidazole-2-thiones **24**. Alkylation of the exocyclic sulfur atom in building block **24** with different polar alkyl halide residues furnished target compounds **22**.

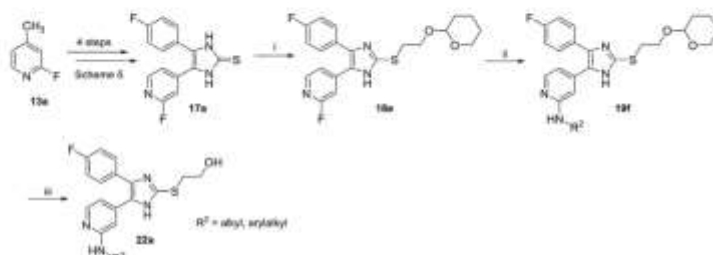
In contrast to the route depicted in Scheme 5, methanolic hydrogen chloride was applicable as a solvent in the reduction reaction of oximes **27** to the corresponding amine hydrochlorides **28**, determining at the same time the cleavage of the Boc protecting group.

Most potent p38 $\alpha$  MAP kinase inhibitors emerging from this series are presented in Fig. 4. As a general trend, bigger, polar moieties at the imidazole-C2 position, which may interact with the ribose and the phosphate binding site, are well tolerated by the target kinase. Whereas the compounds of this series have a similar inhibition profile of p38 $\alpha$  MAP kinase like their 5-methyl counterparts (Fig. 2), they are all showing an increased potency

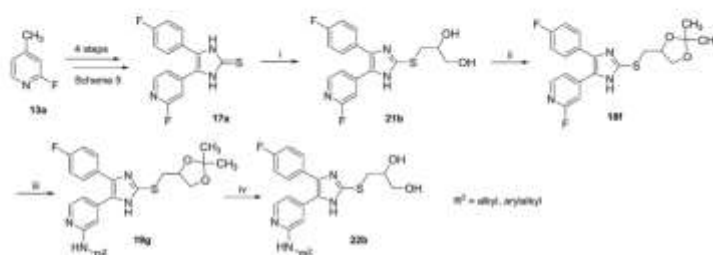


**Figure 4.** Optimized p38 $\alpha$  MAP kinase inhibitors synthesized through the route depicted in Scheme 7 [24].





**Scheme 8.** Optimized synthesis of **22a** using tetrahydropyranyl as the hydroxyl protecting group. Reagents and conditions: (i) *t*-BuONa, methanol, 2-(2-bromoethoxy)-tetrahydro-2*H*-pyran, 50°C; (ii) excess  $R^2$ -NH<sub>2</sub>, 160°C, sealed tube; (iii) 1.25 M HCl/ethanol, rt.



**Scheme 9.** Optimized synthesis of **22b** using acetal as the 1,2-dihydroxyl protecting group. Reagents and conditions: (i) *t*-BuONa, methanol, 3-bromopropane-1,2-diol, 70°C; (ii) acetone, *p*-toluenesulfonic acid, reflux temperature; (iii)  $R^2$ -NH<sub>2</sub>, 160°C, sealed tube; (iv) 2 M aq. HCl, rt.

in the *ex vivo* HWB assay. For example, imidazoles **22c** and LN950 are 3- and 5-times more active inhibitors of the LPS-stimulated TNF- $\alpha$  release compared to their parent compounds ML3403 and **19a** (Fig. 2), respectively.

The introduction of the amino moiety at the pyridine-C2 position in the first step of the synthesis (Scheme 7) limits the use of this synthetic strategy for both optimization and scale-up. For example, the overall yield in case of the synthesis of LN950 is 4%.

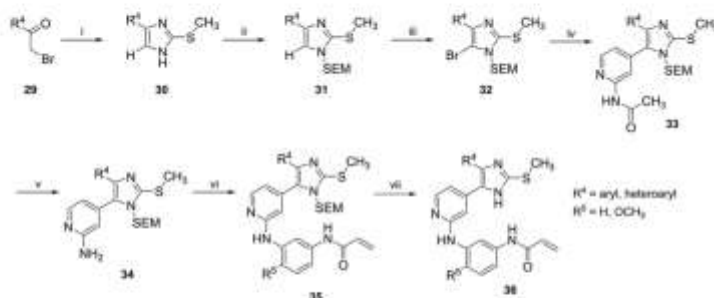
Therefore, our group reported an optimized, more versatile, and diverse protocol to prepare 2-hydroxyethylsulfanyl and 2,3-dihydroxypropyl imidazoles (Schemes 8 and 9) [25]. Differently from the aforementioned strategy, the introduction of the imidazole-C2-5 moiety as well as the pyridine-C2-amino function are performed in the last steps of the sequence, thus easing the access to a broad variety of derivatives.

In order to avoid the aforementioned conversion of 2-alkylsulfanylimidazoles **22a** and **22b** into the corresponding imidazol-2-one derivatives **23** (Scheme 6), the hydroxyl groups of **21a** and **21b** were protected as acetals. Then the amino function at the pyridine-C2 position of the *O*-protected

imidazoles **19f** and **19g** was introduced via nucleophilic aromatic substitution. Finally, the acid-labile protecting groups were cleaved off to liberate the 2-alkylimidazoles **22a** and **22b**, respectively.

This optimized strategy resulted in a remarkable increase in the overall yield of derivatives **22a** and **22b**, e.g., the overall yield for the synthesis of LN950 (Scheme 8) is 29.4%, thus eight times higher than the route illustrated in Scheme 7. Furthermore, the higher flexibility in introducing (phenyl)alkylamino substituents at the pyridine-C2 position enabled a broader exploration of this area. As an example, the use of enantiomerically pure alkylamino substituents allowed to assess that, in case of LN950, the eutomer is represented by the (5*S*)-enantiomer.

In 2016, Günther et al. reported a route to 2,4,5-trisubstituted imidazoles as covalent inhibitors of EGFR, in which the heteroaromatic ring at the imidazole-C4(5) position was introduced via palladium-catalyzed cross-coupling reaction (compounds **36**,  $R^4$  = 4-fluorophenyl, Scheme 10) [26]. With the aim to extend SAR insights in EGFR inhibition, Günther et al. took recently over the same route and broadened the range of the aryl substituents at the imidazole-C4(5) position by

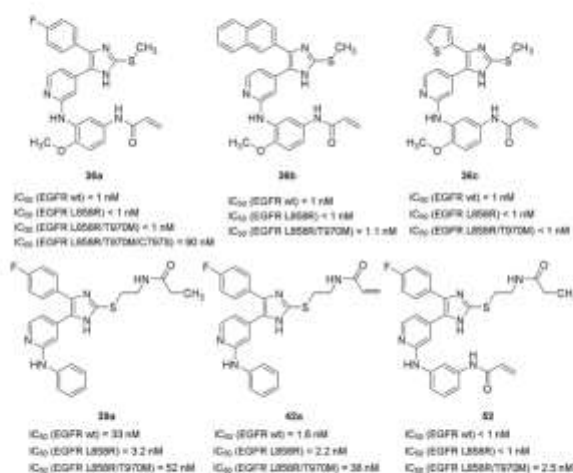


**Scheme 10.** Synthesis of covalent EGFR inhibitors **36**. Reagents and conditions: (i) 5-methylsulfonium sulfate, tetrahydrofuran/ $\text{H}_2\text{O}$ , reflux temperature; (ii) a) NaH, SEM-Cl, tetrahydrofuran,  $-15^\circ\text{C}$ ; b) SEM-Cl (cat.), acetonitrile,  $80^\circ\text{C}$ ; (iii) NBS, acetonitrile,  $85^\circ\text{C}$ ; (iv) (2-acetamidopyridin-4-yl)boronic acid ester,  $\text{Pd}(\text{OAc})_2/\text{XPhos}$  or  $\text{Pd}_2(\text{dba})_3/(\text{t-Bu})_3\text{P-HBF}_4$ ,  $\text{K}_3\text{PO}_4$ , dioxane/ $\text{H}_2\text{O}$ , reflux temperature; (v) 5M NaOH/methanol,  $60^\circ\text{C}$ ; (vi) subst. bromoanilines, Brettphos Pd G1,  $\text{Cs}_2\text{CO}_3$ , dioxane/*t*-BuOH,  $130^\circ\text{C}$ , (vii) trifluoroacetic acid, dichloromethane, rt.

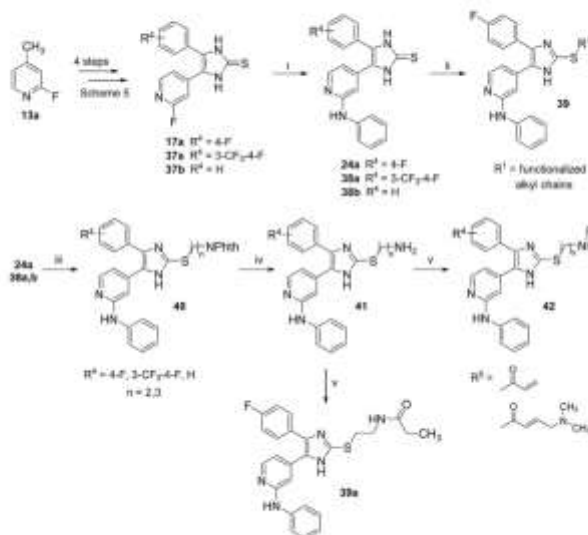
introducing an unsubstituted phenyl ring, as well as 2-naphthyl and 2-thienyl moieties [27]. 2-Methylsulfanylimidazole **30** was built up in analogy to the route depicted in Scheme 2 by reaction of an  $\alpha$ -bromoketone and an 5-methylsulfonium salt. Prior to the Suzuki cross-coupling reaction, the NH of the imidazole was protected by the SEM group and the imidazole-C5 position was brominated using *N*-bromosuccinimide (NBS) in acetonitrile. Suzuki cross-coupling of **32** and (2-acetamidopyridin-4-yl) boronic acid ester yielded 1,2,4,5-tetra-substituted imidazole **33**. Removal of the acetyl group under basic conditions liberated primary amine **34**, which was functionalized via

palladium-catalyzed Buchwald-Hartwig arylation with predecorated bromoanilines carrying the electrophilic warhead. Finally, removal of the SEM group under mild acidic conditions liberated 2-methylsulfanylimidazoles **36**.

Computational studies showed that these pyridinylimidazole-based inhibitors bind to the ATP cleft of the target enzyme in an analogous manner as for the p38 $\alpha$  MAP kinase. The 2-aminopyridine moiety forms a bidentate hydrogen bond to the Met793 of the hinge region while the 4-fluorophenyl moiety is located in the hydrophobic region I. Additionally, the substituent on the pyridine-C2 position



**Figure 5.** 2-Alkylsulfanyl-5(4)-pyridin-4-ylimidazoles as wt and mutants EGFR inhibitors [26, 27].



**Scheme 11.** Synthesis of 2,4,5-tri-substituted imidazoles **39**, **42**, and **39a** featuring a diverse substitution pattern at the imidazole-C2-S position. Reagents and conditions: (i) aniline, *N*-methylpyrrolidinone, conc. aq. HCl, reflux temperature; (ii) alkyl halide,  $K_2CO_3$ , tetrahydrofuran, reflux temperature; (iii) *N*-(2-bromoethyl)phthalimide or *N*-(3-iodopropyl)phthalimide,  $K_2CO_3$ , tetrahydrofuran, reflux temperature; (iv) hydrazine hydrate, ethanol, 70°C; (v) carboxylic acid, TBTU, DIPEA, tetrahydrofuran, rt.

carries an electrophilic warhead able to covalently target the non-catalytic Cys797, thus increasing potency and residence time of the inhibitor. The most promising covalent inhibitor **36a** (Figure 5) revealed to efficiently inhibit not only the wild type (wt) and both the single (L858R) and double (L858R/T790M) mutants of the EGFR, but also the one carrying a triple L858R/T790M/C797S mutation. Although the latter mutant is missing the Cys797 residue and can therefore not be targeted by the acrylamide moiety, the strong reversible binding of these derivatives is reported to be the determinant for the still satisfying inhibitory activity against this enzyme variant. In addition, inhibitor **36a** proved to be effective in proliferation assays on tumor-relevant cancer cell lines carrying different EGFR mutations and showed additionally a high selectivity over the wt cell line. When tested at a concentration of 200 nM in a panel of 410 kinases, compound **36a** inhibited 27 kinases including EGFR wt, 10 disease-relevant EGFR mutants and all three JNK isoforms [26]. Replacement of the 4-fluorophenyl ring with other aryl and heteroaryl moieties seemed not to produce a remarkable effect on the inhibition of wt and mutant forms of EGFR, as compounds **36b** and **36c**, bearing, respectively, a 2-naphthyl and a 2-thienyl moiety still displayed  $IC_{50}$  values in the picomolar range [27].

In addition, in order to diversify the substitution on the sulfur atom at the imidazole-C2 position, the same authors suggested a strategy analogous to the one outlined in Scheme 5, starting from 2-fluoro-4-picoline (**13a**, Scheme 11). The major difference from the previously reported synthetic pathway was the possibility to introduce the moiety at the pyridine-C2 position directly on the imidazole-2-thione derivatives **17a** and **37**, thus shifting the functionalization

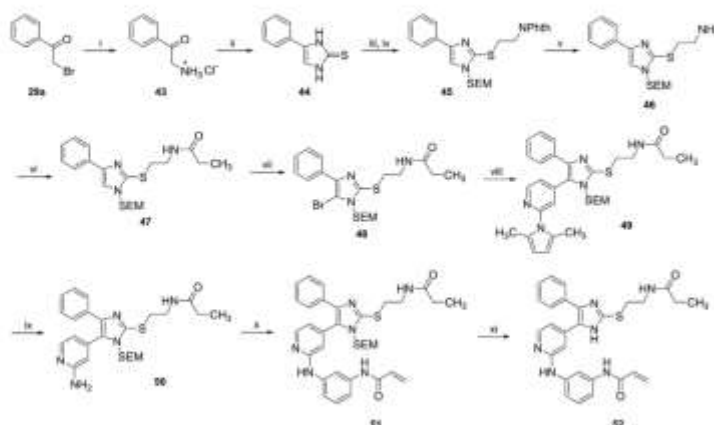
of the sulfur atom to the last step of the route. Nevertheless, only an aniline was introduced in this position and, as reported from the authors, the same reaction could not be reproduced using differently substituted aromatic amines. After functionalization of the pyridine ring, different aliphatic moieties were installed on the sulfur atom by nucleophilic substitution of compounds **24a** and **38** with the appropriate alkyl halide. Among these, alkyl amines protected as phthalimides could be introduced (compounds **40**). After deprotection by hydrazinolysis, primary amines **41** were coupled with different carboxylic acids resulting either in amides **42** having different electrophilic warheads or in saturated counterpart **39a**.

As previously mentioned, the preparation of analogs of compounds **39**, bearing substituted anilines at the pyridine-C2 position, required a different strategy. This route, in analogy to the one reported in Scheme 10, is based on the construction and functionalization of the imidazole core followed by introduction of the pyridine moiety at a late stage (Scheme 12) [27]. The  $\alpha$ -aminoketone **43**, obtained by Delépine reaction from the  $\alpha$ -bromoketone **29a**, was cyclized with potassium thiocyanate and the imidazole-2-thione intermediate **44** was then substituted on the sulfur atom by reaction with *N*-(2-bromoethyl)phthalimide. After SEM protection of the imidazole-N atom, the aliphatic amino group was liberated by hydrazinolysis. Subsequently, compound **46** was coupled with propionic acid and, analogously to the previously reported route, the imidazole-C5 position was brominated using NBS. The 2-aminopyridin-4-yl moiety could be introduced by a one-pot (two-step) tandem borylation/Suzuki cross-coupling reaction affording compound **49**.



Arch. Pharm. Chem. Life Sci. 2017, 350, e1700258  
P. Koch and F. Ansideri

ARCH PHARM  
Archiv der Pharmazie



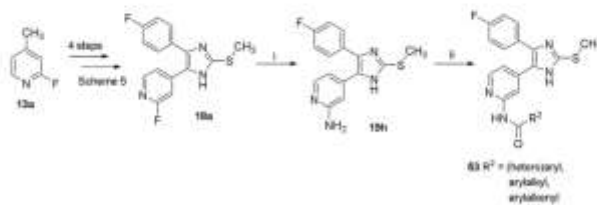
**Scheme 12.** Synthesis of compound **52**. Reagents and conditions: (i) urotropine, chloroform, 50°C, then conc. aq. HCl, ethanol, rt; (ii) KSCN, acetic acid, reflux temperature; (iii) *N*-(2-bromoethyl)phthalimide, K<sub>2</sub>CO<sub>3</sub>, tetrahydrofuran, reflux temperature; (iv) NaH, SEM-Cl, DMF, rt; (v) hydrazine hydrate, ethanol, 50°C; (vi) propionic acid, TBTU, DIPEA, tetrahydrofuran, rt; (vii) NBS, DMF, rt; (viii) 4-bromo-2-(2,5-dimethyl-1*H*-pyrrol-1-yl)pyridine, bis(pinacolato)diboron, KOAc, Pd(OAc)<sub>2</sub>, XPhos, 0.5 M aq. K<sub>3</sub>PO<sub>4</sub>, dioxane, 130°C; (ix) H<sub>2</sub>N-OH·HCl, DIPEA, ethanol/H<sub>2</sub>O, 45°C, sealed reaction vessel; (x) *N*-(3-bromophenyl)acrylamide, Cs<sub>2</sub>CO<sub>3</sub>, Brettphos Pd G1, dioxane/*t*-BuOH; (xi) trifluoroacetic acid, dichloromethane, rt.

Differently from the pathway depicted in Scheme 10, a 2,5-dimethylpyrrole protecting group was employed for the 2-amino moiety, allowing a controlled deprotection step without the simultaneous cleavage of the amide functionality. Derivative **50** was reacted in a palladium-catalyzed arylation reaction with an aryl bromide group carrying the electrophilic Michael acceptor. Finally, the SEM protecting group was cleaved off to obtain the desired compound **52**.

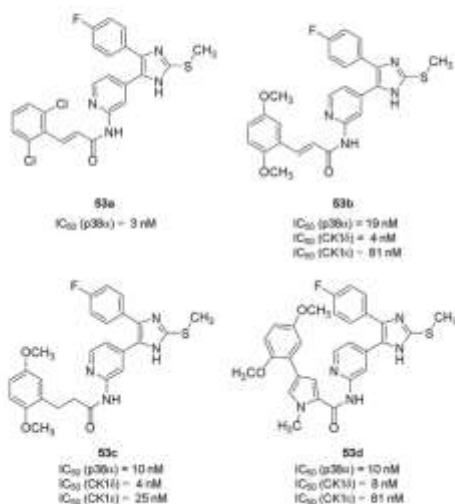
Targeting the phosphate binding cleft by introducing diversely functionalized alkyl chains at the imidazole-C2-5 position produced good results in case of amine or amide moieties with an ethylene spacer. Compounds **39a** and **42a** (Fig. 5) proved to inhibit the different forms of EGFR more efficiently than their 5-methylated precursor, presumably due to the formation of an additional hydrogen bond interaction with the Asp855. Nevertheless, placing the electrophilic

warhead on the flexible chain at the imidazole-C2-5 position (compound **42a**) did not result in the same high potency of compounds **36a–c**, although an irreversible mechanism of action was confirmed by mass experiments. Also compound **52**, bearing both the covalent tag at the pyridine-C2 position and the amide moiety at the imidazole-C2-5 atom did not overcome the potency of the covalent inhibitors **36a–c** on the EGFR L858R/T790M mutant [27].

In 2010, Laufer and co-workers reported a synthetic strategy toward 2,4,5-tri-substituted imidazoles having an acyl group at the pyridine-C2-amino position that starts from building block **18a** (Scheme 13) [28]. After substitution of the fluorine atom by ammonium hydroxide, target compounds **53** were obtained by coupling of **19h** with the corresponding carboxylic acids after *N,N*-carbonyldiimidazole (CDI) activation. The most potent p38 $\alpha$  MAP kinase inhibitor out of this



**Scheme 13.** Synthetic pathway to 2,4,5-tri-substituted imidazoles having an acyl group at the pyridine-C2-amino position. Reagents and conditions: (i) NH<sub>4</sub>OH, 180°C; (ii) R<sup>1</sup>-COOH, CDI, *N*-methylpyrrolidinone, rt then 120°C.



**Figure 6.** Tri-substituted imidazoles featuring an acyl group at the pyridine-C2 amino position, synthesized through the route outlined in Scheme 13 [6, 28, 29].

series is imidazole **53a** displaying IC<sub>50</sub> values in the low single-digit nanomolar range (Fig. 6). Despite the presence of an α,β-unsaturated carbonyl group, a potential covalent inhibition mechanism was not commented.

Peifer et al. showed that an analogous compound of **53a** (2-methylsulfanylimidazole **53b**), which was originally designed as a p38α MAP kinase inhibitor, is also inhibiting two isoforms of protein kinase CK1, formerly known as casein kinase 1 [29]. Although inhibitor **53b** also possesses a Michael acceptor system, in this case a possible irreversible mode of action was excluded by the authors. Recently, Peifer and co-workers reported an optimization study of **53b** resulting in balanced dual CK1β/CK1γ inhibitor **53c** [6]. A selectivity screening of **53c** against a panel of 321 kinases revealed that six other protein kinases, including CK1α, p38α MAP kinase and related kinases JNK2 and JNK3, were inhibited higher than 50% at a test concentration of 100 nM. Compounds **53b** and **53c** are the first 2-alkylsulfanylimidazole-based kinase inhibitors for which a co-crystal structure with the target kinase was solved. Inhibitors **53b** and **53c** were co-crystallized with p38α MAP kinase (PDB code: 5ML5) and CK1β (PDB code: 5MQV), respectively. In case of **53b**-p38α MAP kinase complex, the crystallographic data confirmed the general binding mode discussed in the introduction with the addition of a potential interaction of Phe169 with the imidazole core and with the Lys53 through π-π and π-cation-stacking, respectively.

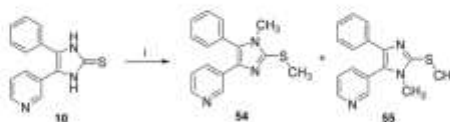
### Synthesis of 1,2,4,5-tetra-substituted imidazoles

The alkylation of 2,4,5-tri-substituted 1*H*-imidazoles represents one possible strategy to obtain 1,2,4,5-tetra-substituted imidazoles which can, however, result in two different regioisomers. The substituents on position (2), 4, and 5 may influence this reaction by directing the substitution on one of the two imidazole nitrogen atoms, therefore favoring the formation of one regioisomer over the other.

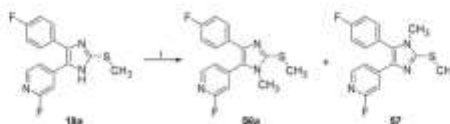
In the patent application described in Scheme 2 [8], the researchers reported the alkylation reaction of imidazole-2-thione **10** with methyl iodide to tri-substituted imidazole **4** to also result in methylation of the imidazole-N atom. As displayed in Scheme 14, this led to two different regioisomers **54** and **55**, which could be separated by chromatography on silica gel. However, the authors did not comment on the analytical techniques to define the position of the methylation and neither a yield nor the ratio of the two isomers was reported for this reaction.

In 2003, Wagner et al. studied the methylation of the imidazole ring of different tri-substituted 1*H*-imidazoles, e.g., **18a**, and reported analytical methods to distinguish both *N*-substituted regioisomers (Scheme 15) [30]. Alkylation under basic conditions occurred with a remarkable selectivity yielding isomer **57** as major product (57/56a = 93:7; use of Na<sub>2</sub>CO<sub>3</sub> or Cs<sub>2</sub>CO<sub>3</sub> as base) or sole product (use of NaH as base) of this reaction.

The authors also demonstrated that the alkylation of the correct imidazole nitrogen is critical for the inhibitors'

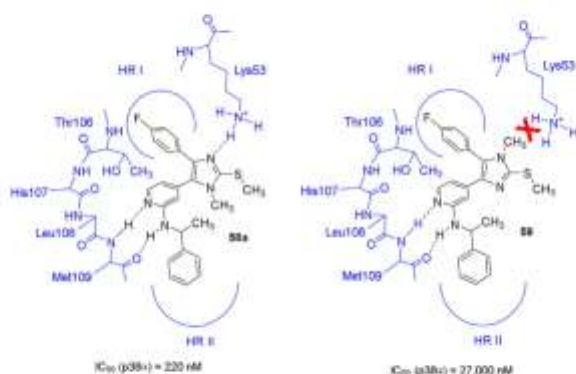


**Scheme 14.** Synthesis of 1-methyl-2-methylsulfanyl-4(5)-phenyl-5(4)-(pyridin-3-yl)imidazoles **54** and **55**. Reagents and conditions: (i) H<sub>3</sub>C-I, methanol/2 M aq. NaOH 2.5:1 (v/v), rt.



**Scheme 15.** Alkylation of *N*-unsubstituted imidazole **18a**. Reagents and conditions: (i) H<sub>3</sub>C-I, different base/solvent mixtures.





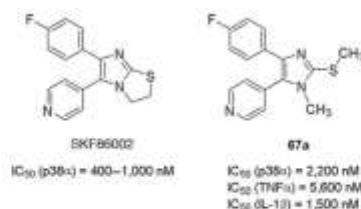
**Figure 7.** Influence on regioisomerism for p38 $\alpha$  MAP kinase inhibition [10] (modified from Ref. [31]; HR, hydrophobic region).

potency. Tetra-substituted imidazole **58a** bearing the methyl group at the imidazole nitrogen adjacent to the pyridine ring shows a more than 100-fold higher inhibition of p38 $\alpha$  MAP kinase in comparison to compound **59** having the same substituent at the N atom adjacent to the 4-fluorophenyl ring, due to the impossibility of the latter to accept a hydrogen bond from Lys53 (Fig. 7).

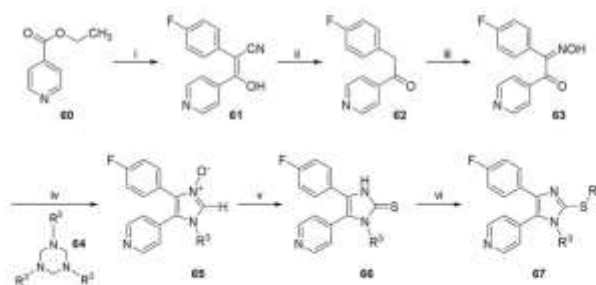
A six-step reaction sequence for synthesizing 1-alkyl-2-alkylsulfanyl-4-(4-fluorophenyl)-5-(pyridin-4-yl)imidazoles **67** starting from ethyl 4-fluorophenylacetate (**60**) (Scheme 16) was reported by Laufer and co-workers in a patent application in 2002 [32]. Key steps of this pathway are the assembling of the imidazole ring by reaction of  $\alpha$ -oximinoketone **63** with different *N*-substituted 1,3,5-trialkylhexahydro-1,3,5-triazines **64** resulting regioselectively in 1-alkylimidazole-3-oxides **65**, followed by treatment with 2,2,4,4-tetramethyl-3-thiocyclobutan-1-one or 2,2,4,4-tetramethylcyclobutane-1,3-dithiane to yield imidazole-2-thiones **66**. In the last step, the moiety at the imidazole-C2-5 position was introduced, as in previous examples, by nucleophilic substitution reaction with appropriate alkyl halides. However, this route is not

suitable for the introduction of aryl or heteroaryl moieties at the imidazole-N1 position.

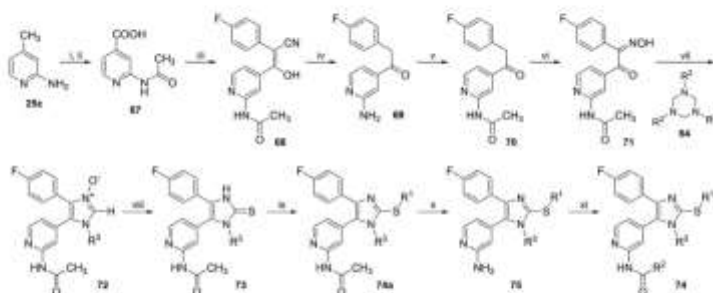
Compound **67a**, the open analog of prototype p38 $\alpha$  MAP kinase inhibitor SKF86002, shows a two- to fourfold decrease in kinase inhibition compared to its parent compound (Fig. 8) [33].



**Figure 8.** Biological activity of 1,2,4,5-tetra-substituted imidazole **67a** [33] in comparison with its cyclic analogue SKF86002 [34, 35].



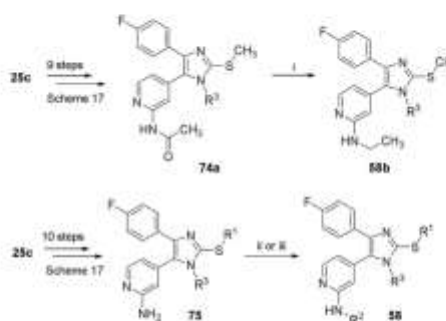
**Scheme 16.** Synthetic pathway toward 1-alkyl-2-methylsulfanyl-4-(4-fluorophenyl)-5-(pyridin-4-yl)imidazoles **67**. Reagents and conditions: (i) 4-fluorophenylacetone, sodium, ethanol, reflux temperature; (ii) 48% aq. HBr, reflux temperature; (iii) NaNO<sub>2</sub>, H<sub>2</sub>O, acetic acid, rt; (iv) ethanol, reflux temperature; (v) 2,2,4,4-tetramethyl-3-thiocyclobutan-1-one, chloroform, 0°C then rt or 2,2,4,4-tetramethylcyclobutane-1,3-dithione, dichloromethane, 0°C then rt; (vi) R<sup>1</sup>-X (X = I, Br), Na<sub>2</sub>CO<sub>3</sub>, ethanol, reflux temperature.



**Scheme 17.** Synthetic pathway toward 1,2,4,5-tetra-substituted imidazoles **74** bearing an acyl moiety at the pyridine-C2 position. Reagents and conditions: (i) acetic anhydride, 4-dimethylaminopyridine (DMAP), reflux temperature; (ii)  $\text{KMnO}_4$ ,  $\text{H}_2\text{O}_2$ ; (iii) a) CDI, DMF, rt; b)  $t\text{-BuOK}$ , 4-fluorophenylacetonitrile, DMF,  $120^\circ\text{C}$ ; (iv) 48% aq. HBr, reflux temperature; (v) acetic anhydride, DMAP, reflux temperature; (vi) isopropyl nitrite, MeONa, methanol, rt; (vii) ethanol, reflux temperature; (viii) 2,2,4,4-tetramethylcyclobutane-1,3-dithione, dichloromethane, rt; (ix)  $\text{R}^1\text{-X}$ ,  $\text{Na}_2\text{CO}_3$ , ethanol, rt; (x) 10% aq. HCl, reflux temperature; (xi)  $\text{R}^2\text{-COCl}$ , triethylamine, tetrahydrofuran,  $0^\circ\text{C}$  or  $\text{R}^2\text{-COOH}$ , CDI, *N*-methylpyrrolidinone, rt then  $120^\circ\text{C}$ .

In order to improve the inhibitory potency of tetra-substituted imidazoles **67**, two modifications of this synthetic strategy were reported by the same group, enabling the introduction of acyl or amino moieties at the pyridine-C2 position (Schemes 17–19) [10, 36]. Both multi-step reaction sequences encompass ethanone **69** as a common synthetic intermediate. Prior to the formation of the corresponding  $\alpha$ -oximinoketone, the amino function of **69** has to be protected due to the possible interference in the cyclization step with triazinanes **64**. The two alternative strategies applied consisted either in protecting the amino function of **69** as *N*-acetyl (Scheme 17), or in transferring it into a fluorine group using Olah's reagent (Scheme 19). In the penultimate step of both sequences, the *N*-protecting group was removed under acidic conditions (Scheme 17) or the F-atom was displaced via a nucleophilic substitution reaction with ammonia in a reactor, both resulting in a primary amine (Scheme 19). Finally, the moieties at the pyridine-C2 amino function were installed. For the introduction of acyl moieties at the pyridine-C2 amino function, a coupling with activated carboxylic acids (acid chlorides or CDI method) was carried out in both synthetic routes. In case of the strategy depicted in Scheme 17, the authors also reported the possibility to introduce alkyl moieties at this position by reducing the amide function of **74a** to secondary amines **58b** or by nucleophilic substitution of primary amines **75** with appropriate alkyl halides (Scheme 18). Alternatively, the exocyclic amino group of **75** can also be functionalized by palladium-catalyzed Buchwald-Hartwig coupling reaction with predecorated aryl halides (Scheme 18) [37]. Furthermore, by following the same route displayed in Scheme 19, Laufer et al. reported the introduction of (aryl)alkylamino groups at the pyridine-C2 position by directly reacting intermediate **56** in a nucleophilic aromatic substitution reaction with primary amines [38].

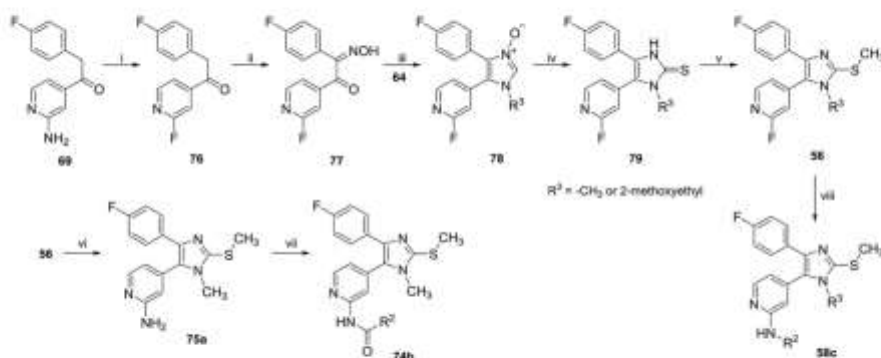
A broad range of tetra-substituted imidazoles **74** were reported by Laufer and co-workers varying the substituents at the imidazole-N1, at the imidazole-C2-5 as well as at the pyridine-C2-amino position (Fig. 9) [10, 28, 36–41]. The active metabolite (CBS-3595) of 2-methylsulfanylimidazole **74c** is the first out of this series being tested in pre-clinical studies [42]. CBS-3595 is a dual p38 $\alpha$  MAP kinase/phosphodiesterase (PDE)-4 inhibitor exhibiting good TNF- $\alpha$  inhibition in the HWB assay. One of the advantages of substituting the imidazole-N1 position is represented by



**Scheme 18.** Synthetic pathway toward 1,2,4,5-tetra-substituted imidazoles **58** bearing an amino function at the pyridine-C2 position. Reagents and conditions: (i)  $\text{LiAlH}_4$ , tetrahydrofuran, reflux temperature; (ii)  $\text{R}^2\text{-Br}$ , NaH, DMF, reflux temperature; (iii) aryl bromide, Brettphos Pd G1,  $\text{C}_5\text{CO}_3$ , dioxane/*t*-BuOH 4:1 (v/v),  $110^\circ\text{C}$ .

Arch. Pharm. Chem. Life Sci. 2017, 350, e1700258  
P. Koch and F. Ansideri

ARCH PHARM  
Archiv der Pharmazie



**Scheme 19.** Synthetic pathway toward 1,2,4,5-tetra-substituted imidazoles **58c** and **74b**. Reagents and conditions: (i)  $\text{NaNO}_2$ , 70% HF-pyridine,  $-15$  to  $-10^\circ\text{C}$  then rt; (ii)  $\text{NaNO}_2$ , glacial acetic acid, rt; (iii) ethanol, reflux temperature; (iv) 2,2,4,4-tetramethylcyclobutane-1,3-dithione, dichloromethane, rt; (v)  $\text{H}_2\text{C}=\text{I}$ ,  $\text{K}_2\text{CO}_3$ , methanol, rt; (vi)  $\text{NH}_3$ , reactor; (vii)  $\text{R}^2\text{-COOH}$ , CDI, *N*-methylpyrrolidinone,  $120^\circ\text{C}$ ; (viii) excess  $\text{R}^2\text{-NH}_2$ , neat,  $170^\circ\text{C}$ .

the possibility of reducing the CYP450 inhibition, particularly when introducing bulky moieties. This is exemplified by compound **74d**, presenting a clean CYP450 inhibition profile (at a test concentration of  $10\ \mu\text{M}$ , no or only slight inhibition (<15%) of CYP450 isoenzymes 1A2, 2C9, 2C19, 2D6, and 79% inhibition of CYP450 isoenzyme 3A4) [10]. The introduction of a methoxy-substituted phenyl ring with two methyl spacers from the acyl function combined with a 2-methoxyethyl moiety at the imidazole-N1 position resulted in the potent  $\text{p}38\alpha$  MAP kinase inhibitor **74e** with  $\text{IC}_{50}$  value down to the low double-digit nanomolar range [40].

In 2015, Muth et al. reported a series of tetra-substituted imidazoles displaying balanced  $\text{p}38\alpha$  MAP kinase/JNK3 inhibition [37]. Imidazole **74f** bearing an (*E*)-acrylic acid substituent at the imidazole-C2-5 position represents the most potent derivative of this series. Docking studies performed on an analogous derivative assumed that this particular moiety is able to establish hydrogen bond interactions with a conserved Lys (Lys53 in  $\text{p}38\alpha$  MAP kinase and Lys93 in JNK3) as well as with Arg107 (JNK3) in the phosphate binding site.

Recently, the potent covalent JNK3 inhibitor **58d** showing an excellent selectivity profile was reported [41]. The acrylamide moiety targets the non-catalytic Cys154 located in the hydrophobic region II, which is only conserved among all three JNK isoforms but not in the rest of the kinase [43]. Both, the irreversible mode of action and the specific amino acid targeted from the electrophilic warhead were confirmed by mass shift experiments.

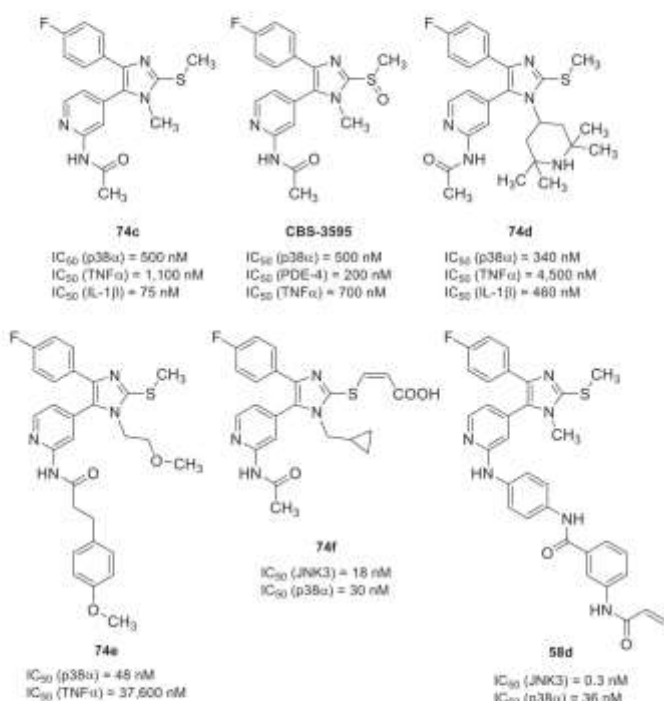
In 2008, Laufer et al. reported a shorter route to 1,2,4,5-tetra-substituted imidazoles **58c** (Scheme 20) [38]. The regioselective alkylation of the desired imidazole-N is achieved through  $\alpha$ -halogenation of ethanones **14a** and **80**

followed by nucleophilic substitution reaction of **81** with primary amines to yield  $\alpha$ -aminoketones **83** and **84** as their hydrochloride salts. 2-Methylsulfanylimidazoles **56** were then obtained either by direct cyclization of **83** with methyl thiocyanate or via imidazole-2-thiones **79** followed by methylation of the sulfur atom. In the last step, the F-atom was substituted with different amines.

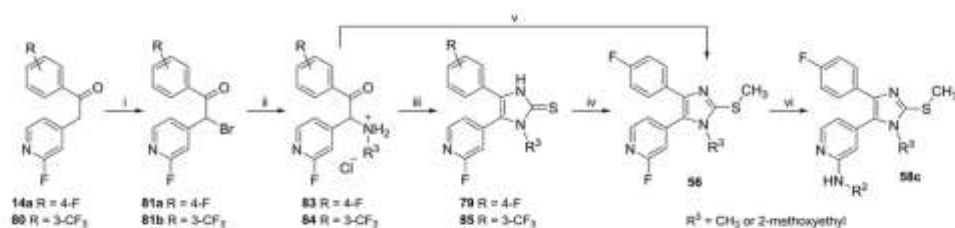
A series of derivatives was generated by transferring to the pyridine-C2 position of tetra-substituted imidazoles **58c** (**58e-g**, Fig. 10) the same moieties, which had been resulting in tri-substituted imidazoles with a high inhibitory activity on  $\text{p}38\alpha$  MAP kinase [7]. In case of the tetrahydropyranyl-substituted imidazole **58f**, a one order of magnitude reduced  $\text{p}38\alpha$  MAP kinase inhibition was measured compared to **19b**. However, in case of hydroxycyclohexyl-substituted imidazole **58g** no loss in kinase activity was observed compared to its tri-substituted counterpart **19c**. Nevertheless, in comparison to their tri-substituted analogs, tetra-substituted imidazoles **58f** and **58g** showed a markedly reduced inhibition of LPS-stimulated TNF- $\alpha$  release in HWB assay.

In the same publication [38], the authors reported an alternative strategy towards 1,2,4,5-tetra-substituted imidazole **56a** wherein the heteroaromatic ring was introduced by palladium-catalyzed cross-coupling reaction (Scheme 21). The 2-methylsulfanylimidazole ring was built up in analogy to Scheme 20 starting from an  $\alpha$ -bromoketone via nucleophilic substitution reaction with primary amines, thione formation, and alkylation of the exocyclic sulfur atom. 1,2,4-tri-substituted imidazole **88** was brominated in position 5 using NBS and finally the pyridine ring was installed via Suzuki cross-coupling reaction to obtain tetra-substituted imidazole **56a**. This route, together with the ones depicted in Schemes 10 and 12, represent the sole strategies permitting





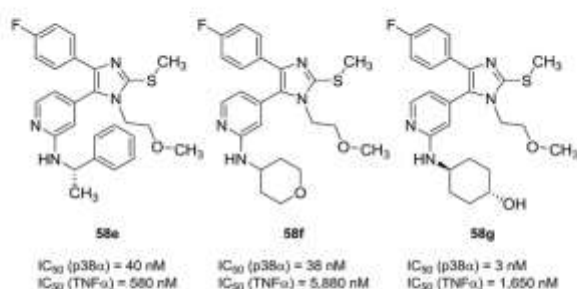
**Figure 9.** Diverse 1,2,4,5-tetra-substituted imidazoles synthesized by following the routes described in Schemes 17–19 [10, 37, 40–42].



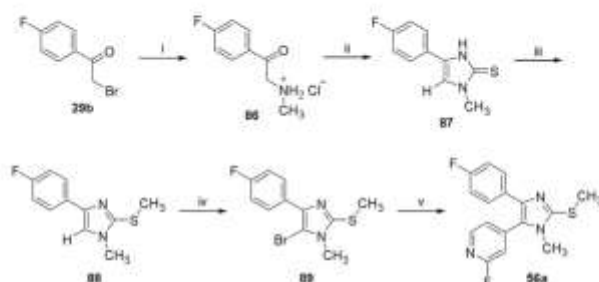
**Scheme 20.** Alternative synthetic pathway toward 1,2,4,5-tetra-substituted imidazoles **58c**. Reagents and conditions: (i) Br<sub>2</sub>, glacial acetic acid, rt; (ii) R<sup>2</sup>-NH<sub>2</sub>, dichloromethane, -5 to 0°C, then 1.25 M HCl/ethanol; (iii) KSCN, DMF, reflux temperature; (iv) H<sub>2</sub>C-I, K<sub>2</sub>CO<sub>3</sub>, methanol, rt (starting from **79**); (v) methylthiocyanate, DMF, reflux temperature (starting from **83**); (vi) excess R<sup>2</sup>-NH<sub>2</sub>, 140–155°C (in case of aliphatic amines) or aniline, NaH, diglyme, 70°C.

Arch. Pharm. Chem. Life Sci. 2017, 350, e1700258  
P. Koch and F. Ansideri

ARCH PHARM  
Archiv der Pharmazie



**Figure 10.** Selected examples of tetra-substituted imidazoles **58** synthesized via the route depicted in Scheme 20 [7].



**Scheme 21.** Alternative synthetic pathway toward 1,2,4,5-tetra-substituted imidazole **56a**. Reagents and conditions: (i) ethanolic  $H_2C-NH_2$ , dichloromethane,  $-5$  to  $0^\circ C$ , then 1.25 M HCl/ethanol; (ii) KSCN, DMF, reflux temperature; (iii)  $H_2C-I$ ,  $K_2CO_3$ , methanol, rt; (iv) NBS, tetrachloromethane,  $0^\circ C$  to rt; (v) (2-fluoropyridin-4-yl)-boronic acid,  $Pd(PPh_3)_4$ ,  $Na_2CO_3$ , toluene,  $120^\circ C$ .

the introduction of the heteroaromatic moiety in the last steps of the synthetic pathway, thus offering a higher flexibility in the investigation of the substitution at the imidazole-C5 position.

## Conclusions

2-Alkylsulfanyl-4(5)-aryl-5(4)-heteroarylimidazole has emerged as a privileged scaffold in the field of kinase inhibition due to its capability of mimicking the basic interactions of ATP while exploiting additional areas of the protein not addressed by the endogenous cofactor. The high flexibility in the substitution of the central imidazole ring permitted to switch the selectivity towards several target enzymes (p38 $\alpha$  MAP kinase, EGFR, CK1 $\delta/\epsilon$ , and JNK3), yielding highly potent inhibitors in each case. The pyridinylimidazole structure also proved to be advantageous for the labeling with fluorophores in the development of assay probes as well as for the introduction of reactive electrophilic moieties, thus obtaining covalent inhibition of the desired kinase. Diverse synthetic strategies, developed during the last few decades, have achieved a wide versatility in the substitution pattern of this important class of molecules. In particular, functionalization of key positions in a late stage of the synthetic pathway allowed the preparation of a broad range

of derivatives, resulting in a fast assessment of SAR. Nevertheless, a strategy leading to the introduction of the aromatic ring at the imidazole-C4 position in the last steps is still missing and extensive investigation in this area might be beneficial.

The authors have declared no conflicts of interest.

## References

- [1] L. Zhang, X. M. Peng, G. L. V. Damu, R. X. Geng, C. H. Zhou, *Med. Res. Rev.* **2014**, *34*, 340–437.
- [2] F. Bellina, S. Cauteruccio, R. Rossi, *Tetrahedron* **2007**, *63*, 4571–4624.
- [3] T. Scior, D. M. Domeyer, K. Cuanalo-Contreras, S. A. Laufer, *Curr. Med. Chem.* **2011**, *18*, 1526–1539.
- [4] D. E. Griswold, P. J. Marshall, E. F. Webb, R. Godfrey, J. Newton, Jr., M. J. DiMartino, H. M. Sarau, J. G. Gleason, G. Poste, N. Hanna, *Biochem. Pharmacol.* **1987**, *36*, 3463–3470.
- [5] B. Abu Thaher, P. Koch, V. Schattel, S. Laufer, *J. Med. Chem.* **2009**, *52*, 2613–2617.
- [6] J. Halekotte, L. Witt, C. Ianes, M. Krüger, M. Bührmann, D. Rauh, C. Pichlo, E. Brunstein, A. Luxenburger, U. Baumann, U. Knippschild, J. Bischof, C. Peifer, *Molecules* **2017**, *22*, 522.

- [7] S. A. Laufer, D. R. J. Hauser, D. M. Domeyer, K. Kinkel, A. J. Liedtke, *J. Med. Chem.* **2008**, *51*, 4122–4149.
- [8] P. G. Ferrini, R. Goeschke, Mercaptoimidazole derivatives, 1979, Switz. 79-100962[4648], 43. EP. 30-3-1979.
- [9] J. Sisko, A. J. Kassick, S. B. Shetzline, *Org. Lett.* **2000**, *2*, 2877–2880.
- [10] S. A. Laufer, G. K. Wagner, D. A. Kotschenreuther, W. Albrecht, *J. Med. Chem.* **2003**, *46*, 3230–3244.
- [11] S. A. Laufer, A. J. Liedtke, *Tetrahedron Lett.* **2006**, *47*, 7199–7203.
- [12] P. Koch, S. Laufer, *J. Med. Chem.* **2010**, *53*, 4798–4802.
- [13] L. Graziosi, A. Mencarelli, C. Santorelli, B. Renga, S. Cipriani, E. Cavazzoni, G. Palladino, S. Laufer, M. Burnet, A. Donini, S. Fiorucci, *Eur. J. Pharmacol.* **2012**, *674*, 143–152.
- [14] D. A. Koch, R. B. M. Silva, A. H. de Souza, C. E. Leite, N. F. Nicoletti, M. M. Campos, S. Laufer, F. B. Morrone, *Rheumatology* **2014**, *53*, 425–432.
- [15] L. Munoz, E. E. Ramsay, M. Manetsch, Q. Ge, C. Peifer, S. Laufer, A. J. Ammit, *Eur. J. Pharmacol.* **2010**, *635*, 212–218.
- [16] N. V. Ryazantseva, V. V. Novitsky, N. Y. Chasovskih, E. V. Kaygorodova, E. G. Starikova, Y. V. Starikov, T. T. Radzivil, *B. Exp. Biol. Med.* **2008**, *145*, 569–572.
- [17] F. Heider, U. Haun, E. Döring, M. Kudolo, C. Sessler, W. Albrecht, S. Laufer, P. Koch, *Molecules* **2017**, *22*, 1729.
- [18] B. Kammerer, H. Scheible, W. Albrecht, C. H. Gleiter, S. Laufer, *Drug Metab. Dispos.* **2007**, *35*, 875–883.
- [19] B. Kammerer, H. Scheible, G. Zurek, M. Godejohann, K. P. Zeller, C. H. Gleiter, W. Albrecht, S. Laufer, *Xenobiotica* **2007**, *37*, 280–297.
- [20] F. Ansideri, A. Lange, A. El-Gokha, F. M. Boeckler, P. Koch, *Anal. Biochem.* **2016**, *503*, 28–40.
- [21] A. Lange, M. Günther, F. M. Büttner, M. O. Zimmermann, J. Heidrich, S. Hennig, S. Zahn, C. Schall, A. Sievers-Engler, F. Ansideri, P. Koch, M. Laemmerhofer, T. Stehlie, S. A. Laufer, F. M. Boeckler, *J. Am. Chem. Soc.* **2015**, *137*, 14640–14652.
- [22] F. Ansideri, M. Dammann, F. M. Boeckler, P. Koch, *Anal. Biochem.* **2017**, *532*, 26–28.
- [23] S. Laufer, P. Koch, *Org. Biomol. Chem.* **2008**, *6*, 437–439.
- [24] P. Koch, C. Bäuerlein, H. Jank, S. Laufer, *J. Med. Chem.* **2008**, *51*, 5630–5640.
- [25] A. El-Gokha, S. A. Laufer, P. Koch, *Org. Biomol. Chem.* **2015**, *13*, 10699–10704.
- [26] M. Günther, M. Juchum, G. Kelter, H. Fiebig, S. Laufer, *Angew. Chem. Int. Ed.* **2016**, *55*, 10890–10894.
- [27] M. Günther, J. Lategahn, M. Juchum, E. Döring, M. Keul, J. Engel, H. L. Tumbrink, D. Rauh, S. Laufer, *J. Med. Chem.* **2017**, *60*, 5613–5637.
- [28] S. Laufer, D. Hauser, T. Stegmiller, C. Bracht, K. Ruff, V. Schattel, W. Albrecht, P. Koch, *Bioorg. Med. Chem. Lett.* **2010**, *20*, 6671–6675.
- [29] C. Peifer, M. Abadleh, J. Bischof, D. Hauser, V. Schattel, H. Hirner, U. Knippschild, S. Laufer, *J. Med. Chem.* **2009**, *52*, 7618–7630.
- [30] G. K. Wagner, D. Kotschenreuther, W. Zimmermann, S. A. Laufer, *J. Org. Chem.* **2003**, *68*, 4527–4530.
- [31] P. Koch, H. Jahns, V. Schattel, M. Goettert, S. Laufer, *J. Med. Chem.* **2010**, *53*, 1128–1137.
- [32] S. Laufer, D. Kotschenreuther, P. Merckle, K. Tollmann, H.-G. Striegel, 2-Thio-substituted imidazole derivatives and the use thereof in the pharmaceutical industry, 2002, WO 02/066458 A2.
- [33] S. Laufer, G. Wagner, D. Kotschenreuther, *Angew. Chem. Int. Ed.* **2002**, *41*, 2290–2293.
- [34] S. Laufer, C. Greim, T. Bertsche, *Osteoarthr. Cartil.* **2002**, *10*, 961–967.
- [35] A. Trejo, H. Arzeno, M. Browner, S. Chanda, S. Cheng, D. D. Comer, S. A. Dalrymple, P. Dunten, J. Lafargue, B. Lovejoy, J. Freire-Moar, J. Lim, J. McIntosh, J. Miller, E. Papp, D. Reuter, R. Roberts, F. Sanpablo, J. Saunders, K. Song, A. Villasenor, S. D. Warren, M. Welch, P. Weller, P. E. Whiteley, L. Zeng, D. M. Goldstein, *J. Med. Chem.* **2003**, *46*, 4702–4713.
- [36] R. Selig, V. Schattel, M. Goettert, D. Schollmeyer, W. Albrecht, S. Laufer, *MedChemComm* **2011**, *2*, 261–269.
- [37] F. Muth, M. Günther, S. M. Bauer, E. Döring, S. Fischer, J. Maier, P. Drückes, J. Köppler, J. Trappe, U. Rothbauer, P. Koch, S. A. Laufer, *J. Med. Chem.* **2015**, *58*, 2567–2567.
- [38] S. A. Laufer, D. R. J. Hauser, A. J. Liedtke, *Synthesis-Stuttgart* **2008**, 253–266.
- [39] S. A. Laufer, W. Zimmermann, K. J. Ruff, *J. Med. Chem.* **2004**, *47*, 6311–6325.
- [40] K. Ziegler, D. R. J. Hauser, A. Unger, W. Albrecht, S. A. Laufer, *ChemMedChem* **2009**, *4*, 1939–1948.
- [41] F. Muth, A. El-Gokha, F. Ansideri, M. Eitel, E. Döring, A. Sievers-Engler, A. Lange, F. M. Boeckler, M. Lämmerhofer, P. Koch, S. A. Laufer, *J. Med. Chem.* **2017**, *60*, 594–607.
- [42] W. Albrecht, A. Unger, S. M. Bauer, S. A. Laufer, *J. Med. Chem.* **2017**, *60*, 5290–5305.
- [43] A. Chaikvad, P. Koch, S. A. Laufer, S. Knapp, *Angew. Chem. Int. Ed.*, in press, <https://doi.org/10.1002/anie.201707875>.

## Publication IV

Muth, F.; El-Gokha, A.; Ansideri, F.; Eitel, M.; Döring, E.; Sievers-Engler, A.; Lange, A.; Boeckler, F. M.; Lämmerhofer, M.; Koch, P.; Laufer, S. A. Tri- and Tetrasubstituted Pyridinylimidazoles as Covalent Inhibitors of c-Jun N-Terminal Kinase 3. *J. Med. Chem.* 2017, 60, 594-607.

Reprinted with permission from Muth *et al.* *J. Med. Chem.* 2017, 60, 594-607.

Copyright 2016 American Chemical Society

Link to the published version:

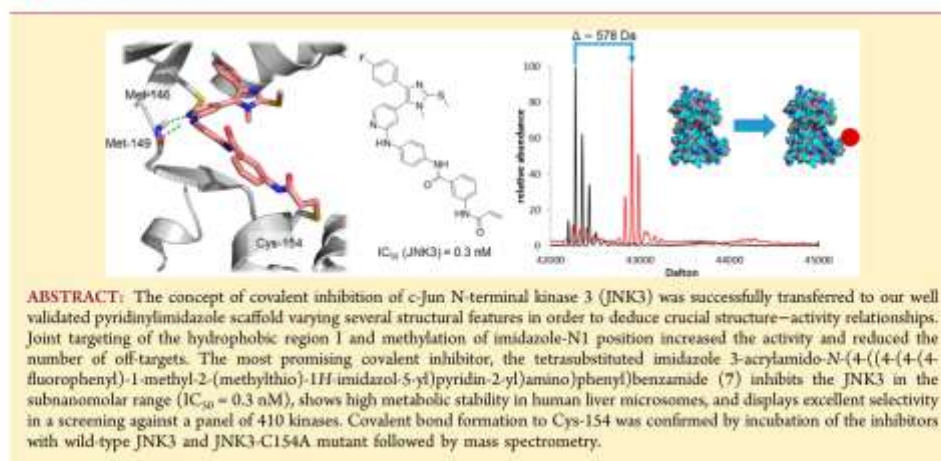
<https://pubs.acs.org/doi/10.1021/acs.jmedchem.6b01180>



## Tri- and Tetrasubstituted Pyridinylimidazoles as Covalent Inhibitors of c-Jun N-Terminal Kinase 3

Felix Muth,<sup>†,§</sup> Ahmed El-Gokha,<sup>†,†,§</sup> Francesco Ansideri,<sup>†</sup> Michael Eitel,<sup>†</sup> Eva Döring,<sup>†</sup> Adrian Sievers-Engler,<sup>†</sup> Andreas Lange,<sup>†</sup> Frank M. Boeckler,<sup>†</sup> Michael Lämmerhofer,<sup>†</sup> Pierre Koch,<sup>\*,†</sup> and Stefan A. Laufer<sup>†,1</sup><sup>†</sup>Department of Pharmaceutical Chemistry, Institute of Pharmaceutical Sciences, Eberhard Karls Universität Tübingen, Auf der Morgenstelle 8, 72076 Tübingen, Germany<sup>§</sup>Chemistry Department, Faculty of Science, Menofia University, Menofia, Egypt

Supporting Information



## INTRODUCTION

The c-Jun N-terminal kinase 3 (JNK3) belongs to the mitogen-activated protein (MAP) kinase family, which comprises 10 members: p38 MAP kinases (p38 $\alpha$ , - $\beta$ , - $\gamma$ , - $\delta$ ), JNKs (JNK1, -2, -3), and three extracellular-regulated kinases.<sup>1</sup> The three genes *jnk1*, *jnk2*, *jnk3* encode for a total of 10 alternatively spliced JNK isoforms with a molecular weight between 46 and 55 kDa.<sup>2,3</sup> Although structurally highly conserved, JNKs differ in tissue distribution fundamentally. JNK1 and JNK2 are ubiquitously expressed, whereas JNK3 expression is primarily restricted to the heart, testis, and brain.<sup>4</sup>

On the basis of results from several knock out experiments<sup>5–7</sup> and due to its specific tissue distribution, JNK3 has been identified as a promising target for potential treatment of neurodegenerative disorders such as Huntington's disease, Parkinson's disease, and Alzheimer's disease.<sup>8</sup>

Within the past years, covalent inhibition of enzymes has experienced a resurgence.<sup>9</sup> Carefully designed irreversible inhibitors have been proven to be even more selective than their reversibly binding counterparts.<sup>10,11</sup> With approval of the

covalent inhibitor of the epidermal growth factor receptor afatinib in 2013,<sup>12</sup> the design of irreversible inhibitors raised the attention of the protein kinase research community.

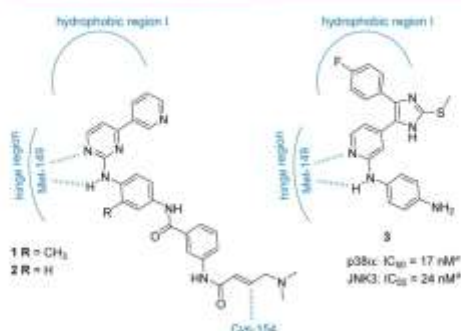
The recently highlighted high quality kinase probe JNK-IN-8<sup>1,3</sup> (1, Figure 1) was discovered by Zhang et al.<sup>11</sup> and provided the first highly selective covalent pan-JNK inhibitor. The reported aminopyrimidine-based pan-JNK inhibitors possess an electrophilic moiety and target a cysteine (Cys-154, JNK3 numbering) conserved among all JNKs (in the hinge 7 position) that is not present in other protein kinases.<sup>10</sup>

In the search for new covalent inhibitors, researchers mostly follow two different paths: either a nonspecific weak reversible binder is used as a lead structure or a noncovalent, relatively potent inhibitor already optimized for the target kinase is chosen to be refined.<sup>14</sup> In continuing efforts to enhance both selectivity and activity of pyridinylimidazole-based JNK3 inhibitors, we applied the latter approach of covalent targeting

Received: August 11, 2016

Published: December 15, 2016



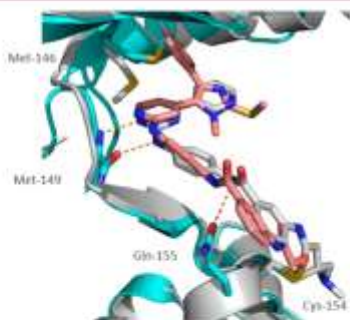


**Figure 1.** Pan-JNK inhibitors **1** and **2** and dual JNK3/p38 $\alpha$  inhibitor **3**. Data previously reported by Ansideri and co-workers.<sup>15</sup>

to our previously reported potent dual JNK3/p38 $\alpha$  inhibitor **3** (Figure 1).<sup>15</sup> This scaffold was designed to align all moieties for optimal interaction with the active site of the enzymes. Computational docking studies with inhibitor **3** as well as comparison of known crystal structures of similar pyrimidiny-imidazole inhibitors<sup>10</sup> (PDB codes 1PMN and 4Z9L) bound to JNK3 suggest that the 4-fluorophenyl ring of **3** is located in the hydrophobic region I of JNK3 and two hydrogen bond interactions are formed with Met-149 positioned in the hinge region. Therefore, it provides a suitable starting point to examine structure–activity relationships (SARs).

Due to the fact that the hinge binding motifs present in **1** and in our 2-aminopyridine scaffold are forming two hydrogen bonds to Met-149 (Figures 1 and 2), derivatives of **3** bearing an appropriate side chain at the pyridine-C2 position containing an electrophilic warhead should be able to target the unique cysteine (Cys-154).

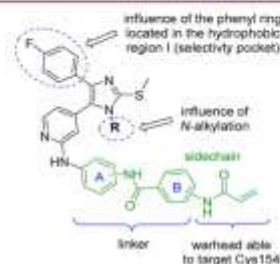
This design hypothesis was supported by the comparing of the binding mode of JNK-IN-7 (**2**, Figure 1) in the crystal structure with JNK3 (PDB code 3V6S) and one of our



**Figure 2.** Superimposition of **2** (gray) in crystal structure with JNK3 (PDB code: 3V6S, cyan) and **7** (salmon) covalently docked into JNK3 (PDB code 1PMN, gray) using Schrödinger Glide.<sup>17</sup> Polar contacts of **2** and JNK3 are depicted as orange dashes. The image was generated with PyMOL.<sup>18</sup> Amino acid sequence was partially hidden for clarity.

designed inhibitors, compound **7**, computationally docked into the active site (Figure 2).

Herein, we report the synthesis of tri- and tetrasubstituted pyridinylimidazoles (compounds **4–23**) as well as their evaluation as covalent JNK3 inhibitors (Figure 3). The effects



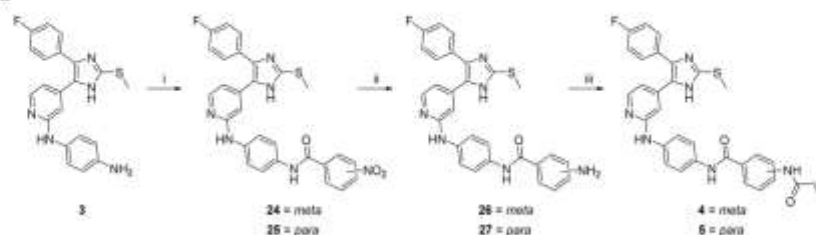
**Figure 3.** Structural modifications of imidazole scaffold and depiction of the terminology used throughout this article.

of the 4-fluorophenyl ring at the imidazole-C4 position as well as those of an imidazole N-alkylation were evaluated. Moreover, the influence of the substitution pattern of both phenyl rings A and B on the biological activity was investigated extensively. An acrylamide-type electrophilic warhead was chosen for the design of the herein presented compounds, since the  $\alpha,\beta$ -unsaturated carbonyl group represents a soft electrophile, which reacts preferentially with the soft thiol present in cysteine side chains.<sup>19</sup> Furthermore, the presence of this Michael acceptor in several launched covalent kinase inhibitors (afatinib, ibrutinib, osimertinib)<sup>20</sup> as well as in drug candidates (neratinib, dacomitinib)<sup>20,21</sup> allows the assessment of a general safety profile for compounds bearing this moiety. However, in contrast to the *N,N*-dimethylaminomethyl acrylamide present in afatinib or neratinib as well as in compounds **1** and **2**, the unsubstituted acrylamide was preferred as electrophilic warhead for our series of inhibitors. In fact, although the tertiary amine has proven to improve properties as solubility and cellular half-life,<sup>22</sup> it also significantly increases the reactivity of the acrylamide by catalyzing the Michael addition<sup>23</sup> and therefore could be potentially responsible for off-target side effects.

## RESULTS AND DISCUSSION

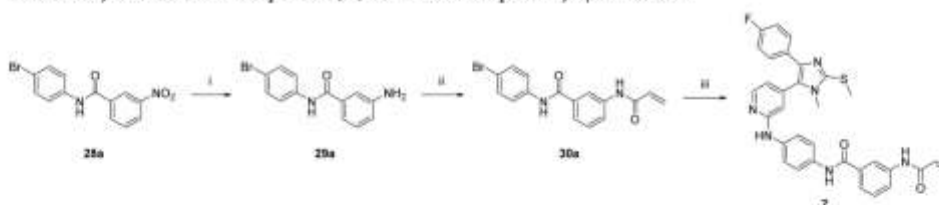
**Chemistry.** The synthesis of trisubstituted imidazole derivatives **4** and **5** bearing a 4-fluorophenyl moiety at the imidazole-C4 position was accomplished in three steps starting from reported inhibitor **3**<sup>15</sup> (Scheme 1). First, the primary amine was reacted with the respective nitrobenzoic acid using benzotriazol-1-yl-oxytripyrrolidinophosphonium hexafluorophosphate (PyBOP) as a coupling reagent to yield amides **24** and **25**. Second, the nitro compounds **24** and **25** were reduced to the corresponding amines **26** and **27** using tin(II) chloride. Finally, the Michael acceptor system was introduced by reaction of the anilines **26** and **27** with acryloyl chloride in the presence of *N,N*-diisopropylethylamine (DIPEA) as a base. As a negative control for evaluation of covalent binding to the enzyme, compound **6** (the saturated analog of **4**) was synthesized by reaction of **3** with 3-propionamidobenzoic acid and PyBOP as coupling reagent (Scheme S1, Supporting Information).

**Scheme 1. Synthesis of Trisubstituted Pyridinylimidazoles 4 and 5 Bearing a 4-Fluorophenyl Ring at the Imidazole-C4 Position<sup>14</sup>**



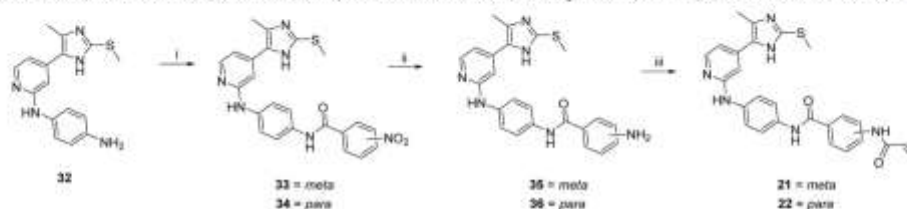
<sup>14</sup>Reagents and conditions: (i) *m*- or *p*-nitrobenzoic acid, PyBOP, DIPEA in dichloromethane, 5 h, rt; (ii)  $\text{SnCl}_2 \cdot 2\text{H}_2\text{O}$ , EtOH, reflux, 6 h; (iii) acryloyl chloride, DIPEA, DMF, 0 °C to rt.

**Scheme 2. Synthesis of Final Compounds 7, 8, and 10–20 Exemplified by Synthesis of 7<sup>14</sup>**



<sup>14</sup>Reagents and conditions: (i)  $\text{SnCl}_2 \cdot 2\text{H}_2\text{O}$ , EtOH, 75 °C, 2.5 h; (ii) acryloyl chloride, DIPEA, 1,4-dioxane, rt, 2 h; (iii) 31,  $\text{Cs}_2\text{CO}_3$ , BrettPhos precatalyst, 1,4-dioxane(abs)/*tert*-butanol 4:1, 125 °C, 5 h.

**Scheme 3. Synthesis of Trisubstituted Pyridinylimidazoles 21 and 22 Bearing a Methyl Moiety at the Imidazole-C4 Position<sup>14</sup>**



<sup>14</sup>Reagents and conditions: (i) *m*-nitrobenzoic acid,  $\text{SOCl}_2$ , pyridine, rt or *p*-nitrobenzoyl chloride, pyridine, rt; (ii)  $\text{SnCl}_2 \cdot 2\text{H}_2\text{O}$ , EtOH, reflux, 6 h; (iii) acryloyl chloride, DIPEA, DMF, -20 °C to rt, 3 h.

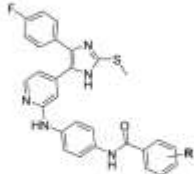
The tetrasubstituted imidazoles 7, 8, and 10–20 were prepared using a convergent synthetic strategy starting from the corresponding nitrobenzoic acid and bromoaniline (Scheme 2). Compounds 28a–h were synthesized in good yields by adding *O*-(benzotriazol-1-yl)-*N,N,N',N'*-tetramethyluronium tetrafluoroborate (TBTU) and the corresponding bromoaniline to a suspension of nitrobenzoic acid in dichloromethane at mild conditions using DIPEA as base. In order to reduce the nitro group to a primary amine, compounds 28a–h were treated with tin(II) chloride in ethanol at 75 °C. The acrylamide warhead and its saturated counterpart were introduced using the corresponding acid chlorides. Compounds 29a–h were suspended in dry 1,4-dioxane and treated with the activated carboxylic acid at mild conditions using DIPEA as base. In the last step of this synthetic route, a Buchwald–Hartwig cross-coupling reaction was applied. Optimized conditions for the


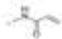

introduction of substituted aryl moieties at the pyridine-C2 amino position have been previously described.<sup>24</sup> The scaffold 4-(4-(4-fluorophenyl)-1-methyl-2-(methylthio)-1*H*-imidazol-5-yl)pyridin-2-amine (31)<sup>25</sup> and the side chains 30a–m were coupled using BrettPhos Pd G1 precatalyst as the catalyst/ligand system and cesium carbonate as base.<sup>19</sup> Compound 9 was synthesized by performing the Buchwald–Hartwig aryl amination reaction with 28a and 31 followed by a reduction step (Scheme S2, Supporting Information).

This synthetic strategy allows the introduction of the side chain using optimized Buchwald–Hartwig cross-coupling reaction conditions in the last step, thus providing a high degree of flexibility in terms of varying the scaffold or the side chain.

As further modifications, compounds 21 and 22 bearing a small methyl moiety at the imidazole-C4 position were

Table 1. Biological Activity of Trisubstituted Imidazoles 4–6



Cmp	R	JNK3 <sup>a</sup>		p38 $\alpha$ <sup>b</sup>		Q <sup>c</sup>
		IC <sub>50</sub> [nM] <sup>d</sup>	SEM	IC <sub>50</sub> [nM] <sup>d</sup>	SEM	
4	<i>meta</i> 	0.6	0.04	0.8	0.11	~1
5	<i>para</i> 	3	0.07	3	0.69	1
6	<i>meta</i> 	2	0.07	4	0.27	2

<sup>a</sup>Incubation time, 50 min. <sup>b</sup>Incubation time, 60 min. <sup>c</sup>IC<sub>50</sub> values are the mean of three experiments. <sup>d</sup>Ratio: IC<sub>50</sub>(p38 $\alpha$ )/IC<sub>50</sub>(JNK3).

synthesized in three steps (Scheme 3) starting from *N*'-(4-(4-methyl-2-(methylthio)-1*H*-imidazol-5-yl)pyridin-2-yl)benzene-1,4-diamine (**32**; for synthesis of imidazole **32**, see Scheme S3, Supporting Information). The buildup of the linker bearing the electrophilic warhead at the aniline function was conducted similarly to the strategy described for the trisubstituted imidazoles bearing a 4-fluorophenyl ring at the imidazole core. The conditions used to synthesize compound **23**, the saturated analog of **21**, starting with precursor **32** are identical to those used for the synthesis of **6** (Scheme S4, Supporting Information).

**Biological Evaluation.** All synthesized inhibitors were evaluated in enzyme-linked immunosorbent assays (ELISA)<sup>26,27</sup> to determine the IC<sub>50</sub> values for JNK3 and p38 $\alpha$ . Compounds **7** and **21** were examined for their metabolic stability and further screened in a panel against 410 kinases to determine their selectivity within the kinome. Results are presented in Tables 1–4 as well as in Tables S1 and S4 (Supporting Information).

Both examples of the trisubstituted pyridinylimidazoles series bearing a 4-fluorophenyl ring at the imidazole-C4 position (compounds **4** and **5**) are very potent dual JNK3/p38 $\alpha$  inhibitors displaying IC<sub>50</sub> values down to the picomolar range (Table 1). While no preference for either tested kinase was detectable, compounds **4** and **5** deduced from compound **3** (Figure 1) revealed that the bulky side chain not only was well tolerated by both enzymes but also caused an increase in inhibitory activity that is distinct in compound **4** having the Michael acceptor in *meta* position. However, within the series of 4-fluorophenyl-substituted imidazoles, the influence of the Michael acceptor system in terms of JNK3 inhibition is rather low, since the saturated analog of **4**, compound **6**, shows no significant decrease in terms of JNK3 affinity.

We could not observe any beneficial effect of introducing electrophilic warheads in terms of selectivity regarding the trisubstituted imidazoles bearing a 4-fluorophenyl moiety. Therefore, as a parallel concept, we chose to alkylate the

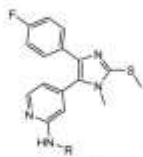
imidazole-N1 position with the utmost simple substituent as prior investigations of our group correlate the *N*-alkylation with a reduced p38 $\alpha$  inhibition.<sup>28</sup>


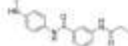
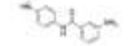

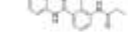


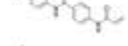
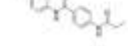
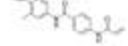
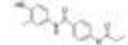
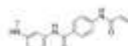
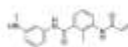
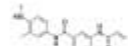
It is crucial for the linker between the scaffold and the warhead to comprise the optimal length and angle in order to orient the warhead ideally for the nucleophilic attack of the thiol to occur and simultaneously retain the original binding mode of the scaffold. Therefore, we synthesized a broad variety of linkers, altering the *meta* and *para* substitution patterns consequently. Furthermore, we introduced methyl groups at different positions of the A and B rings to slightly increase the torsion angle.

In order to elucidate the contribution of each moiety on ring B of **7** and **8**, we synthesized compound **9** (IC<sub>50</sub>: JNK3, 30 nM; p38 $\alpha$ , 149 nM). The *para/meta* substitution pattern (whereupon *para* refers to ring A and *meta* to ring B) with the unsubstituted aniline, presenting a 5-fold prevalence for JNK3 over p38 $\alpha$ , was rather encouraging since the covalent tag was yet to be introduced. The *para/meta* substituted compound **7** (IC<sub>50</sub>: JNK3, 0.3 nM; p38 $\alpha$ , 36 nM), bearing an acrylamide warhead, features a picomolar inhibitory effect for JNK3 and 120-fold preference compared to the IC<sub>50</sub> value of p38 $\alpha$ , emerging as the most potent inhibitor synthesized in this series. Surprisingly, we observed a lower IC<sub>50</sub> value for p38 $\alpha$  alongside the JNK3 inhibition compared to compound **9**. The initial assumption that the carbonyl oxygen of the acrylamide forms an additional hydrogen bond to p38 $\alpha$  and thereby increases its inhibitory effect was invalidated by compound **8**. It shows a 4-fold decreased inhibition for p38 $\alpha$  compared to its unsaturated counterpart, compound **7**. More interestingly, JNK3 inhibition of compound **8** is significantly decreased compared to compound **7**. This can be considered as a strong indication for the formation of a covalent bond of **7** to the JNK3.

Compound **10** (IC<sub>50</sub>: JNK3, 2 nM; p38 $\alpha$ , 2 nM), which features the *para/meta* substitution pattern and a methyl group in *ortho* position at the B ring, inhibits both kinases in the low single digit nanomolar range. The methyl group at that position

Table 2. Biological Activities of Tetrasubstituted Imidazoles 7–20



Cmp	R	JNK3 <sup>a</sup>		p38 $\alpha$ <sup>b</sup>		Q <sup>c</sup>
		IC <sub>50</sub> [nM]	SEM	IC <sub>50</sub> [nM]	SEM	
7		0.3	0.03	36	4.38	120
8		23	0.5	126	21.18	5
9		30	0.54	149	2.71	5
10		2	0.07	2	0.08	1
11		17	0.92	38	3.25	2
12		3	0.16	217	10.39	72
13		175	17.56	241	6.28	1
14		10	1.01	47	1.23	5
15		27	1.08	17	0.83	1
16		8	1.62	35	1.64	4
17		25	0.68	22	0.92	1
18		4	0.24	26	1.43	7
19		3	0.07	100	8.60	33
20		2	0.65	3	0.34	1

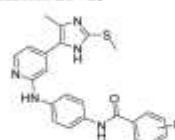
<sup>a</sup>Incubation time, 50 min. <sup>b</sup>Incubation time, 60 min. <sup>c</sup>IC<sub>50</sub> values are the mean of three experiments. <sup>d</sup>Ratio: IC<sub>50</sub>(p38 $\alpha$ )/IC<sub>50</sub>(JNK3).

seems to increase the potency on p38 $\alpha$  drastically. The saturated analog **11** (IC<sub>50</sub>: JNK3, 17 nM; p38 $\alpha$ , 38 nM) lacking the electrophilic warhead supports this assumption since JNK3

and p38 $\alpha$  inhibition are alike. The inversion of the *para*/*meta* substitution pattern led to compound **18** (IC<sub>50</sub>: JNK3, 4 nM; p38 $\alpha$ , 26 nM) exhibiting a low preference for JNK3. The



Table 3. Biological Activity of Trisubstituted Imidazoles 21–23



Cmp	R	JNK3 <sup>a</sup>		p38 $\alpha$ <sup>b</sup>		Q <sup>c</sup>
		IC <sub>50</sub> [nM] <sup>d</sup>	SEM	IC <sub>50</sub> [nM] <sup>d</sup>	SEM	
21	meta	2	0.02	1,952	62	976
22	para	200	12	5,920	107	30
23	meta	253	8.7	>10,000	—	>39

<sup>a</sup>Incubation time, 50 min. <sup>b</sup>Incubation time, 60 min. <sup>c</sup>IC<sub>50</sub> values are the mean of three experiments. <sup>d</sup>Ratio: IC<sub>50</sub>(p38 $\alpha$ )/IC<sub>50</sub>(JNK3).

introduction of an ortho methyl group at the A ring, which was described by Zhang et al.<sup>14</sup> to be the key determinant for selectivity, bred compound **20** (IC<sub>50</sub>: JNK3, 2 nM; p38 $\alpha$ , 3 nM). Since we could not observe a selectivity increase with respect to JNK3 and p38 $\alpha$  inhibition, we introduced the ortho methyl group to the para/para substituted compound **16** (IC<sub>50</sub>: JNK3, 8 nM; p38 $\alpha$ , 35 nM) and its propionamide analog **17**. However, this did not yield the desired effect.

Judged by the small difference in inhibition between compounds **14** (IC<sub>50</sub>: JNK3, 10 nM; p38 $\alpha$ , 47 nM) and **15** (IC<sub>50</sub>: JNK3, 27 nM; p38 $\alpha$ , 17 nM) it appears that compound **14** does not establish a covalent bond with JNK3. Remarkably, compound **15** bearing the propionamide moiety is better tolerated by p38 $\alpha$  compared to **14**, which stands in contrast to the prior observation. The meta/meta substituted **12** (IC<sub>50</sub>: JNK3, 3 nM; p38 $\alpha$ , 217 nM) features a 72-fold preference for JNK3 compared to the IC<sub>50</sub> value of p38 $\alpha$ . Additionally, the almost 70 times lower JNK3 inhibition of **13** (IC<sub>50</sub>: JNK3, 175 nM; p38 $\alpha$ , 241 nM) and the almost constant p38 $\alpha$  inhibition suggest the successful formation of a covalent bond between compound **12** and Cys-154. The unfavorable ortho methylation at the B ring seen with compounds **19** and **20** (increasing p38 $\alpha$  inhibition) is in agreement with a similar observation in compounds **16** and **17**.

Since our efforts of optimizing the linker did not result in a JNK3 inhibitor exceeding 120-fold preference over p38 $\alpha$ , we chose to replace the 4-fluorophenyl ring of compounds **4–6** by a small methyl group leading to compounds **21–23**.

The rationale behind this modification is the fact that numerous examples of known JNK selective inhibitors are not targeting the hydrophobic region I (for recent reviews on JNK inhibitors, see Koch et al.<sup>28</sup> and Gehring et al.<sup>29</sup>). The most selective JNK3 inhibitor in this series (Table 3), compound **21**, shows an IC<sub>50</sub> value in the low nanomolar range and is 976-fold selective against p38 $\alpha$  (IC<sub>50</sub>: JNK3, 2 nM; p38 $\alpha$ , 1,952 nM). Comparison of **21** and **22** demonstrates that the position of the electrophilic warhead on ring B is crucial for improving both JNK3 activity and selectivity. Compound **22** (IC<sub>50</sub>: JNK3, 200 nM), having the acrylamide in para-position, is 100-fold less active than its isomer **21**, which has the same substituent in

meta-position. Compound **23** lacks the Michael acceptor system and shows a tremendous drop (>125-fold) in JNK3 inhibition compared to **21**. SARs of the trisubstituted pyridinylimidazoles series, which carry a small methyl moiety at the imidazole-C4 position, indicate the formation of covalent bond between JNK3 and the inhibitor **21**. Compound **22**, presenting a para/para substitution pattern, apparently does not establish a covalent bond to the cysteine in JNK3, since its inhibitory effect was similar to the saturated compound **23**, unable to form a covalent bond.

Inhibitors **7** and **21**, displaying the best inhibition profile within the series, were further investigated. In order to confirm the formation of a covalent bond to Cys-154, the enzyme–inhibitor complex was analyzed by liquid chromatography–mass spectrometry (LC–MS). Both compounds were incubated with JNK3, and subsequently subjected to LC–MS analysis. Unbound and reversibly bound ligand were removed both by chromatography and by application of a high declustering potential in the course of ionization (for further details, see Supporting Information). These two passages are aimed at disrupting reversible electrostatic interactions, allowing only the detection of covalently bound ligand. The expected mass shift of ~578 Da and ~484 Da in the case of incubation with inhibitor **7** and **21**, respectively, could be measured on the intact protein level using LC- $\mu$ ESI-QTOF mass spectrometry (for further details, see Table S2 and Figures S1–S3a,b,d, Supporting Information). Moreover, performing the same experiment with compounds **8** and **23**, the saturated analogs of **7** and **21**, no mass shift could be observed, since the noncovalent inhibitors do not sustain the binding to JNK3 during the LC–MS experiment (Figures S3c and S3e, Supporting Information). Interestingly, MS analysis carried out on compound **14** (Figure S4a, Supporting Information), which bears the electrophilic warhead in para position and had been assumed not capable of binding covalently, displayed the mass shift of ~578 Da relative to the irreversible bond with the target. However, the shifted peak had a significantly decreased intensity compared to the mass shift of the aforementioned compounds **7** and **21**, revealing that the para/para substitution pattern of the linker can still permit the formation of the

covalent bond, although with a nonfavorable efficiency. As expected, incubation of compound **15**, the noncovalent counterpart of **14**, did not give rise to any enzyme mass increase (Figure S4b, Supporting Information). Finally, the analogous MS experiment was performed by incubating compounds **7**, **14**, and **21** with a JNK3 mutant, where the reactive Cys-154 was replaced by alanine (Figure S5, Supporting Information). Results for the three compounds tested showed absence of mass shift, proving our hypothesis both on the formation of the covalent bond and on the specific amino acid (Cys-154) targeted.

Covalent inhibitors **7** and **21** were further tested in a panel of 410 kinases, including 70 disease-relevant protein kinase mutants and 13 lipid kinases (Table S1, Supporting Information) to evaluate their selectivity within the kinome. At a testing concentration of 1  $\mu\text{M}$ , which represents 500 times its  $\text{IC}_{50}$  value, imidazole **21** inhibited only 15 kinases (including all JNK isoforms) out of the tested kinase panel, resulting in a low  $S$  ( $S_0$ ) score of 0.037. This parameter is defined as the portion of kinases that are inhibited to more than 50%, in relation to all tested kinases.<sup>31</sup> Notably, the tetrasubstituted imidazole **7** reveals a remarkable selectivity profile. Besides the JNKs, **7** inhibits only three other protein kinases (Table 4) at a

**Table 4.** Off-Target Activity of Compounds **21** and **7** in a Panel of 410 Kinases

<b>21</b> at 1 $\mu\text{M}$				<b>7</b> at 0.5 $\mu\text{M}$
CK-1- $\delta$	CLK4	MKK7	TAOK2	TIE2-wt
CK-1- $\gamma 2$	MAP3K10	PKC-mu	TSF1	MAPKAP2
CK-1- $\gamma 3$	MAP3K11	SGK1	ZAK	CK-1- $\delta$
10–29 % <sup>a</sup>				30–50 % <sup>a</sup>

<sup>a</sup>Residual activity.

screening concentration of 0.5  $\mu\text{M}$  (representing more than 1500-fold its  $\text{IC}_{50}$  value) and possesses an excellent  $S$  ( $S_0$ ) score of 0.015. The slightly changed selectivity is mainly attributed to the methylation of the imidazole-N1 position and specific interactions within the hydrophobic region I, the so-called selectivity pocket, which is not targeted by compound **21**. As expected, no selectivity was seen within the JNK family, since the targeted cysteine is conserved among all isoforms.

All final compounds were checked for being potential pan-assay interference compounds (PAINS) using the ZINC Patterns tool,<sup>32</sup> which led to no hits. Since acrylamides might interfere with intracellular proteins in a nondiscriminatory manner,<sup>33</sup> the most promising covalent inhibitor **7** (10  $\mu\text{M}$ ) was incubated with the nonspecific thiol glutathione (present in almost all cells, 5 mM) under similar conditions used in the kinase activity assay (maximum concentration 10  $\mu\text{M}$ , 54 min, 37 °C). Subsequent high performance liquid chromatography (HPLC) analysis revealed only low depletion of **7** (Table S3, Supporting Information). This observation together with the rather clean profile of acrylamide compounds **7** and **21** in the selectivity screening shows no evidence of unpredictable interactions with other cysteine side chains.

Inhibitors **7** and **21** were further tested for their metabolic stability in male human liver microsomes (HLMs). Both covalent inhibitors undergo a partial biotransformation. Nevertheless, both tested compounds are exhibiting 13% and 31% degradation over a time span of 180 and 190 min, respectively,

and can therefore be considered to be metabolically stable (Table S4 and Figures S6 and S7, Supporting Information). In agreement with prior findings,<sup>34</sup> the metabolic degradation leads most likely to the oxidation of the imidazole-C2 sulfur.

## CONCLUSION

We successfully transferred the concept of covalently inhibiting the JNKs to our pyridinylimidazole scaffold, which was elaborated for JNK interaction. Compounds **7** and **21** with their para/meta substitution pattern comprise the optimal linker length and angle for the electrophilic warhead to form a covalent bond to the Cys-154. Incubation of JNK3 with compounds **7** and **21** followed by mass experiments substantiated the assumption of a covalent bond formation. Both covalent inhibitors are metabolically relatively stable when exposed to HLM. Targeting the hydrophobic region I with a 4-fluorophenyl ring combined with a methylation of the imidazole-N1 position reduced the number of off targets, resulting in compound **7** with a remarkable selectivity profile.

## EXPERIMENTAL SECTION

**Chemistry.** General. The purity of all tested compounds is  $\geq 95\%$  and was determined via reverse phase HPLC.

**General Procedure for the Reduction of Nitro Group of Compounds **24**, **25**, **33**, and **34** Using Tin(II) Chloride (General Procedure A).** In 100 mL round-bottom flask, the nitro compound was dissolved in ethanol. Tin(II) chloride was added, and the reaction mixture was refluxed for 6 h. After cooling to rt, a saturated solution of sodium bicarbonate (20 mL) was added. The aqueous layer was extracted with ethyl acetate (3  $\times$  10 mL), and the combined organic layer was dried over anhydrous  $\text{Na}_2\text{SO}_4$ . The solvent was evaporated under reduced pressure, and the crude product was purified by flash chromatography ( $\text{SiO}_2$ , dichloromethane/ethanol, 95:05 to 90:10).

**General Procedure for the Preparation of Final Compounds **4**, **5**, **21**, and **22** (General Procedure B).** The respective primary amine **26**, **27**, **35**, or **36** was dissolved in DMF (2 mL) and placed in a round-bottom flask under argon atmosphere. DIPEA was added in one portion followed by dropwise addition of acryloyl chloride diluted in dry dichloromethane (1 mL) at 0 °C (in the cases of preparation of **4** and **5**) or in dry DMF (0.2 mL) at  $-20$  °C (in the cases of preparation of **21** and **22**). The reaction mixture was further stirred for 2 h at rt, then poured over ice and stirred for 30 min. If the crude product precipitated, the precipitate was filtered off and purified by column chromatography. In the case of preparation of **21**, the crude product did not precipitate. Therefore, the aqueous phase was extracted with ethyl acetate (3  $\times$  10 mL). The combined organic layers were dried over  $\text{Na}_2\text{SO}_4$ , the solvent was evaporated under reduced pressure, and the residue was purified with flash chromatography.

**General Procedure for Synthesis of Amides **28a–h** (General Procedure C).** To a stirred suspension of corresponding nitrobenzoic acid (1.1 equiv) in dichloromethane (9 mL/mmol aniline), THTU (1.1 equiv), the corresponding bromoaniline (1 equiv), and DIPEA (2 equiv) were added at 0 °C. The yellowish suspension cleared up as it was allowed to warm to room temperature and was subsequently stirred for 3 h until complete consumption of the respective bromoaniline was detected by TLC. The reaction mixture was poured on a pad of silica and eluted with a mixture of ethyl acetate and petrol ether 50/50.

**General Procedure for Synthesis of **29a–h** by Reduction of Nitrobenzene Analogs **28a–h** (General Procedure D).** To a suspension of tin(II) chloride (5 equiv) in ethanol (100 mL/mmol nitrobenzene) was added the corresponding nitrobenzene (1 equiv), and the reaction mixture was heated to 75 °C for 2.5 h until complete conversion was detected by TLC. The solvent was evaporated under reduced pressure. The white residue was treated with saturated  $\text{NaHCO}_3$  solution and brine. The aqueous layer was extracted with ethyl acetate (3  $\times$  60 mL). The combined organic phases were dried over  $\text{Na}_2\text{SO}_4$  and evaporated under reduced pressure to yield the



desired title compound as a white solid, which was used without further purification.

**General Procedure for Synthesis of Compounds 30a–m via Amide Coupling (General Procedure E).** To a suspension of corresponding aniline **29** (1 equiv) in 1,4-dioxane (12 mL/mmol aniline), DIPEA (2.5 equiv) was added followed by the corresponding acid chloride (1.1 equiv) at 0 °C. The mixture was allowed to warm up to room temperature and was stirred for 2 h until complete conversion was detected by TLC. After removal of all volatiles under reduced pressure, methanol was added and the mixture was evaporated again. This process was repeated three times, and the solid obtained was used without further purification.

**General Procedure for Synthesis of Final Compounds 7, 8, 10–20 via Buchwald–Hartwig Cross-Coupling Reaction (General Procedure F).** BrettPhos precatalyst (2.5 mol %) was added to a dry mixture of *tert*-butanol and 1,4-dioxane (1:4; 54 mL/mmol **31**) in an argon flushed glass tube. Compound **31** (1 equiv) was added to the reaction mixture followed by cesium carbonate (2.5 equiv) and the respective aryl bromide **30** (1.1 equiv). The reaction mixture was heated to 125 °C and stirred for 2 h after sealing the glass tube tightly. Another 2.5 mol % BrettPhos precatalyst was added, and the reaction mixture was heated to 125 °C and stirred for an additional 3 h until HPLC confirmed complete conversion. The reaction mixture was allowed to cool to room temperature, filtered, and washed with ethyl acetate (20 mL). All volatiles were removed under reduced pressure, and the residue was purified by silica flash chromatography.

**3-Acrylamido-N-(4-((4-(4-fluorophenyl)-2-(methylthio)-1H-imidazol-5-yl)pyridin-2-yl)amino)phenyl)benzamide (4).** Compound **4** was synthesized according to general procedure B, using compound **26** (80 mg, 0.16 mmol), DIPEA (30  $\mu$ L, 0.17 mmol), and acryloyl chloride (16  $\mu$ L, 0.19 mmol). Purification by flash chromatography (SiO<sub>2</sub>, dichloromethane/ethanol, 92:08) afforded 35 mg (40%) of a light yellow solid product. <sup>1</sup>H NMR (250 MHz, DMSO-*d*<sub>6</sub>)  $\delta$  12.67 (br s, 1H), 10.35 (s, 1H), 10.14 (s, 1H), 8.97 (br s, 1H), 8.21–7.96 (m, 2H), 7.96–7.87 (m, 1H), 7.73–7.40 (m, 3H), 7.38–7.13 (m, 2H), 7.12–6.77 (m, 1H), 6.68 (d, *J* = 4.6 Hz, 1H), 6.48 (dd, *J* = 9.9, 17.0 Hz, 1H), 6.30 (dd, *J* = 2.3, 17.0 Hz, 1H), 5.88–5.72 (m, 1H), 2.62 (s, 3H). <sup>13</sup>C NMR (101 MHz, DMSO-*d*<sub>6</sub>)  $\delta$  164.9, 163.3, 161.9 (d, *J* = 247.0 Hz), 156.3, 147.2, 142.8, 141.9, 139.1, 137.9, 135.9, 134.7, 132.0, 131.7, 130.7 (d, *J* = 8.9 Hz), 129.5 (d, *J* = 3.5 Hz), 128.7, 127.1, 122.3, 122.0, 121.0, 118.8, 118.2, 115.7 (d, *J* = 23.0 Hz), 112.4, 111.8, 107.0, 15.0; HPLC *t*<sub>R</sub> = 6.25 min. ESI-MS: calculated, 565.1817 [M + H]<sup>+</sup>; found, 565.1812.

**4-Acrylamido-N-(4-((4-(4-fluorophenyl)-2-(methylthio)-1H-imidazol-5-yl)pyridin-2-yl)amino)phenyl)benzamide (5).** Compound **5** was synthesized according to general procedure B, using compound **27** (78 mg, 0.15 mmol), DIPEA (30  $\mu$ L, 0.17 mmol), and acryloyl chloride (15  $\mu$ L, 0.18 mmol). Purification by flash chromatography (SiO<sub>2</sub>, dichloromethane/ethanol, 92:08) afforded 22 mg (27%) of a light yellow solid product. <sup>1</sup>H NMR (400 MHz, DMSO-*d*<sub>6</sub>)  $\delta$  12.68 (br s, 1H), 10.44 (s, 1H), 10.03 (s, 1H), 8.99 (br s, 1H), 8.12 (br s, 1H), 8.02–7.89 (m, 2H), 7.85–7.74 (m, 2H), 7.62 (d, *J* = 8.3 Hz, 2H), 7.57 (d, *J* = 8.6 Hz, 2H), 7.51 (br s, 2H), 7.31 (br s, 1H), 7.23 (br s, 1H), 7.12–6.74 (m, 1H), 6.74–6.60 (m, 1H), 6.49 (dd, *J* = 10.1, 17.0 Hz, 1H), 6.31 (d, *J* = 17.2 Hz, 1H), 5.81 (d, *J* = 10.1 Hz, 1H), 2.63 (s, 3H). <sup>13</sup>C NMR (101 MHz, DMSO-*d*<sub>6</sub>)  $\delta$  164.3, 163.4, 161.3 (d, *J* = 246.2 Hz), 156.3, 147.7, 147.1, 142.9, 142.7, 141.7, 137.6, 131.6, 130.6 (d, *J* = 5.5 Hz), 129.7, 128.4, 127.4, 126.8, 121.0, 118.5, 118.4, 118.3, 115.7 (d, *J* = 26.7 Hz), 111.8, 107.1, 99.9, 15.0; HPLC *t*<sub>R</sub> = 6.11 min. ESI-MS: calculated, 565.1817 [M + H]<sup>+</sup>; found, 565.1804.

**N-(4-((4-(4-fluorophenyl)-2-(methylthio)-1H-imidazol-5-yl)pyridin-2-yl)amino)phenyl)-3-propionamidobenzamide (6).** Under argon atmosphere, compound **3** (100 mg, 0.23 mmol) was suspended in dry dichloromethane (10 mL) and DIPEA (54  $\mu$ L, 0.31 mmol) was added. Finally, a suspension of 3-propionamidobenzamide (54 mg, 0.28 mmol) and PyBOP (161 mg, 0.31 mmol) in dry dichloromethane (10 mL) was added and the reaction mixture was stirred at rt for 18 h. The reaction mixture was concentrated at reduced pressure and the crude was purified twice by flash column

chromatography (SiO<sub>2</sub>, dichloromethane/ethanol, 97:03 to 80:20) yielding product **6** (30 mg, 21%). <sup>1</sup>H NMR (300 MHz, DMSO-*d*<sub>6</sub>)  $\delta$  12.67 (br s, 1H), 10.11 (br s, 1H), 10.06 (s, 1H), 9.08–8.87 (m, 1H), 8.17–7.94 (m, 2H), 7.84 (d, *J* = 8.0 Hz, 1H), 7.67–7.15 (m, 10H), 7.10–6.76 (m, 1H), 6.73–6.64 (m, 1H), 2.63 (s, 3H), 2.36 (q, *J* = 7.5 Hz, 2H), 1.11 (t, *J* = 7.5 Hz, 3H). <sup>13</sup>C NMR (101 MHz, DMSO-*d*<sub>6</sub>)  $\delta$  172.2, 165.1, 163.1, 161.4 (d, *J* = 244.9 Hz), 156.3, 148.0, 147.2, 142.9, 142.0, 139.4, 138.9, 137.9, 137.4, 135.9, 134.7, 133.8, 132.5, 132.1, 130.7 (d, *J* = 8.0 Hz), 129.5 (d, *J* = 6.0 Hz), 128.6, 126.8, 126.2, 121.7, 121.0, 118.6, 118.5, 118.2, 115.8 (d, *J* = 22.0 Hz), 115.3 (d, *J* = 22.0 Hz), 112.4, 111.8, 111.4, 107.3, 107.0, 29.5, 15.1, 9.6. The peaks of the carbon are double due to the amide tautomerism. HPLC *t*<sub>R</sub> = 5.47 min. ESI-MS: calculated, 567.1973 [M + H]<sup>+</sup>; found, 567.1957.

**3-Acrylamido-N-(4-((4-(4-fluorophenyl)-1-methyl-2-(methylthio)-1H-imidazol-5-yl)pyridin-2-yl)amino)phenyl)benzamide (7).** According to general procedure F, **7** was synthesized from **31** and **30a**. Eluent ethyl acetate/*n*-hexane 45:55 to 75:25. Another flash chromatography was performed to purify the product; eluent dichloromethane/methanol 100:0 to 92:8 afforded 31% yield. <sup>1</sup>H NMR (200 MHz, DMSO-*d*<sub>6</sub>)  $\delta$  10.34 (s, 1H), 10.15 (s, 1H), 9.12 (s, 1H), 8.26 (d, *J* = 5.4 Hz, 1H), 8.15 (s, 1H), 7.92 (d, *J* = 7.8 Hz, 1H), 7.70–7.59 (m, 5H), 7.53–7.40 (m, 3H), 7.14 (t, *J* = 8.9 Hz, 2H), 6.78–6.69 (m, 2H), 6.55–6.17 (m, 2H), 5.84–5.72 (m, 1H), 3.43 (s, 3H), 2.65 (s, 3H). <sup>13</sup>C NMR (101 MHz, DMSO-*d*<sub>6</sub>)  $\delta$  165, 163.3, 161.0 (d, *J* = 243.7 Hz), 156.5, 148.3, 143.5, 139.1, 138.9, 137.3, 136.8, 135.9, 132.5, 131.7, 130.6 (d, *J* = 2.9 Hz), 128.7, 128.3 (d, *J* = 8.0 Hz), 128.3, 127.1, 122.3, 122.0, 121.0, 118.8, 118.4, 115.1 (d, *J* = 21.5 Hz), 114.8, 111.1, 31.5, 15.3. ESI-MS: calculated, 578.1900 [M + H]<sup>+</sup>; found, 578.1876. HPLC *t*<sub>R</sub> = 5.87 min.

**N-(4-((4-(4-fluorophenyl)-1-methyl-2-(methylthio)-1H-imidazol-5-yl)pyridin-2-yl)amino)phenyl)-3-propionamidobenzamide (8).** According to general procedure F, **8** was synthesized from **31** and **30j**. Eluent ethyl acetate/*n*-hexane 45:55 to 75:25. Another flash chromatography was performed to purify the product; eluent dichloromethane/methanol 100:0 to 92:8 afforded 62% yield. <sup>1</sup>H NMR (200 MHz, CDCl<sub>3</sub>)  $\delta$  8.33–8.15 (m, 2H), 7.98 (d, *J* = 10.6 Hz, 2H), 7.72 (d, *J* = 8.6 Hz, 1H), 7.55–7.28 (m, 6H), 7.23–7.12 (m, 2H), 7.04 (s, 1H), 6.93 (t, *J* = 8.6 Hz, 2H), 6.67–6.58 (m, 2H), 3.44 (s, 3H), 2.65 (s, 3H), 2.33 (q, *J* = 7.7 Hz, 2H), 1.17 (t, *J* = 7.5 Hz, 3H). <sup>13</sup>C NMR (101 MHz, DMSO-*d*<sub>6</sub>)  $\delta$  172.2, 165.1, 161.0 (d, *J* = 243.4 Hz), 156.4, 148.2, 143.6, 139.5, 138.9, 137.2, 136.8, 135.9, 132.6, 130.5 (d, *J* = 2.9 Hz), 128.6, 128.3 (d, *J* = 7.9 Hz), 128.3, 121.8, 121.7, 121.0, 118.5, 115.2 (d, *J* = 21.4 Hz), 114.8, 111.1, 31.6, 29.5, 15.3, 9.6. ESI-MS: calculated, 580.2057 [M + H]<sup>+</sup>; found, 580.2054. HPLC *t*<sub>R</sub> = 7.55 min.

**3-Amino-N-(4-((4-(4-fluorophenyl)-1-methyl-2-(methylthio)-1H-imidazol-5-yl)pyridin-2-yl)amino)phenyl)benzamide (9).** Compound **9** was synthesized from **S1**, zinc dust (6 equiv), and ammonium formate (6 equiv) in ethanol (62 mL/mmol **S1**). The mixture was heated under reflux for 4 h until complete reduction of the nitro group was detected by TLC. The mixture was filtered through a pad of Celite, which was washed with ethanol. All volatiles were removed under reduced pressure, and the residue was purified using flash chromatography. Eluent ethyl acetate/*n*-hexane 45:55 to 75:25 afforded 75% yield. <sup>1</sup>H NMR (200 MHz, CDCl<sub>3</sub>)  $\delta$  8.24 (d, *J* = 5.7 Hz, 1H), 7.83 (s, 1H), 7.57–7.37 (m, 5H), 7.24–7.10 (m, 6H), 7.05–6.74 (m, 4H), 6.69–6.59 (m, 2H), 3.46 (s, 3H), 2.68 (s, 4H). <sup>13</sup>C NMR (50 MHz, CDCl<sub>3</sub>)  $\delta$  165.8, 161.8 (d, *J* = 245.9 Hz), 156.7, 149.1, 146.9, 144.5, 140.1, 138.6, 136.2, 136, 133.4, 130.1 (d, *J* = 3.2 Hz), 129.5, 128.9 (d, *J* = 7.9 Hz), 128.1, 121.4, 121.3, 118.1, 116.2, 115.6, 115.1 (d, *J* = 21.4 Hz), 113.7, 109, 31.8, 16. ESI-MS: calculated, 524.1795 [M + H]<sup>+</sup>; found, 524.1761. HPLC *t*<sub>R</sub> = 4.13 min.

**3-Acrylamido-N-(4-((4-(4-fluorophenyl)-1-methyl-2-(methylthio)-1H-imidazol-5-yl)pyridin-2-yl)amino)phenyl)-2-methylbenzamide (10).** According to general procedure F, **10** was synthesized from **31** and **30l**. Eluent: ethyl acetate/*n*-hexane 45:55 to 75:25. Another flash chromatography was performed to purify the product; eluent dichloromethane/methanol 100:0 to 92:8 afforded 12% yield. <sup>1</sup>H NMR (400 MHz, DMSO-*d*<sub>6</sub>)  $\delta$  10.25 (s, 1H), 9.65 (s, 1H), 9.13 (s, 1H), 8.25 (d, *J* = 5.1 Hz, 1H), 7.67–7.52 (m, 5H), 7.51–

7.41 (m, 2H), 7.33–7.24 (m, 2H), 7.15 (t,  $J = 8.9$  Hz, 2H), 6.77–6.71 (m, 2H), 6.61–6.51 (m, 1H), 6.31–6.22 (m, 1H), 5.81–5.74 (m, 1H), 3.43 (s, 3H), 2.65 (s, 3H), 2.24 (s, 3H).  $^{13}\text{C}$  NMR (101 MHz, DMSO- $d_6$ )  $\delta$  167.2, 163.4, 161.0 (d,  $J = 243.3$  Hz), 156.5, 148.3, 143.5, 138.9, 138.9, 137.2, 136.8, 136.6, 132.7, 131.6, 130.6 (d,  $J = 3.1$  Hz), 129.4, 128.26 (d,  $J = 8.0$  Hz), 128.3, 126.7, 126.4, 125.5, 124.1, 120.2, 118.5, 115.2 (d,  $J = 21.5$  Hz), 114.8, 111.1, 31.5, 15.3, 14.6. ESI-HRMS: calculated, 592.2057 [M + H] $^+$ ; found, 592.2049. HPLC  $t_R = 6.60$  min.

**N-[(4-[(4-(4-fluorophenyl)-1-methyl-2-(methylthio)-1H-imidazol-5-yl)pyridin-2-yl]amino)phenyl]-2-methyl-3-propionamidobenzamide (11).** According to general procedure F, 11 was synthesized from 31 and 30b. Eluent ethyl acetate/*n*-hexane 45:55 to 75:25 afforded 63% yield.  $^1\text{H}$  NMR (200 MHz, DMSO- $d_6$ )  $\delta$  10.23 (s, 1H), 9.36 (s, 1H), 9.12 (s, 1H), 8.25 (d,  $J = 5.5$  Hz, 1H), 7.71–7.52 (m, 4H), 7.52–7.39 (m, 3H), 7.30–7.06 (m, 4H), 6.80–6.66 (m, 2H), 3.43 (s, 3H), 2.65 (s, 3H), 2.37 (q,  $J = 7.3$  Hz, 2H), 2.22 (s, 3H), 1.11 (t,  $J = 7.5$  Hz, 3H).  $^{13}\text{C}$  NMR (50 MHz, DMSO- $d_6$ )  $\delta$  172.1, 167.3, 161.0 (d,  $J = 243.7$  Hz), 156.5, 148.3, 143.5, 138.9 (d,  $J = 2.9$  Hz), 137.1, 137.0, 136.76, 132.8, 130.6, 130.5, 129.5, 128.3, 128.2 (d,  $J = 8.0$  Hz), 126.6, 125.4, 123.8, 120.2, 118.5, 115.1 (d,  $J = 21.5$  Hz), 114.8, 111.0, 31.5, 28.8, 15.3, 14.5, 9.8. ESI-HRMS: calculated, 594.2231 [M + H] $^+$ ; found, 594.2231. HPLC  $t_R = 7.27$  min.

**3-Acrylamido-N-[(4-[(4-(4-fluorophenyl)-1-methyl-2-(methylthio)-1H-imidazol-5-yl)pyridin-2-yl]amino)phenyl]benzamide (12).** According to general procedure F, 12 was synthesized from 31 and 30c. Eluent ethyl acetate/*n*-hexane 45:55 to 75:25. Another flash chromatography was performed to purify the product; eluent dichloromethane/methanol 100:0 to 92:8 afforded 30% yield.  $^1\text{H}$  NMR (400 MHz, DMSO- $d_6$ )  $\delta$  10.37 (s, 1H), 10.24 (s, 1H), 9.26 (s, 1H), 8.26 (d,  $J = 5.2$  Hz, 1H), 8.15 (s, 1H), 8.10 (s, 1H), 7.92 (d,  $J = 8.0$  Hz, 1H), 7.65 (d,  $J = 7.4$  Hz, 1H), 7.54–7.41 (m, 4H), 7.29–7.10 (m, 4H), 6.81 (s, 1H), 6.77 (d,  $J = 5.2$  Hz, 1H), 6.52–6.41 (m, 2H), 6.30 (d,  $J = 16.9$  Hz, 1H), 5.79 (d,  $J = 10.6$  Hz, 1H), 3.44 (s, 3H), 2.65 (s, 3H).  $^{13}\text{C}$  NMR (101 MHz, DMSO- $d_6$ )  $\delta$  165.5, 163.3, 161.1 (d,  $J = 243.6$  Hz), 156.3, 148.3, 143.7, 141.4, 139.4, 139.1, 136.8, 135.9, 131.7, 130.4 (d,  $J = 2.6$  Hz), 128.75, 128.62, 128.33 (d,  $J = 8.0$  Hz), 128.2, 127.2, 122.5, 122.2, 118.9, 115.2 (d,  $J = 21.5$  Hz), 115.2, 114.0, 113.5, 111.6, 110.8, 31.6, 15.3. ESI-HRMS: calculated, 578.1900 [M + H] $^+$ ; found, 578.1885. HPLC  $t_R = 6.38$  min.

**N-[(4-[(4-(4-fluorophenyl)-1-methyl-2-(methylthio)-1H-imidazol-5-yl)pyridin-2-yl]amino)phenyl]-3-propionamidobenzamide (13).** According to general procedure F, 13 was synthesized from 31 and 30d. Eluent ethyl acetate/*n*-hexane 45:55 to 75:25 afforded 62% yield.  $^1\text{H}$  NMR (400 MHz, DMSO- $d_6$ )  $\delta$  10.21 (s, 1H), 10.07 (s, 1H), 9.21 (s, 1H), 8.27 (d,  $J = 5.2$  Hz, 1H), 8.09 (d,  $J = 9.2$  Hz, 2H), 7.85–7.80 (m, 1H), 7.63–7.58 (m, 1H), 7.56–7.50 (m, 1H), 7.49–7.40 (m, 3H), 7.27–7.18 (m, 2H), 7.14 (t,  $J = 8.9$  Hz, 2H), 6.81 (s, 1H), 6.78–6.73 (m, 1H), 3.44 (s, 3H), 2.65 (s, 3H), 2.35 (q,  $J = 7.5$  Hz, 2H), 1.10 (t,  $J = 7.5$  Hz, 3H).  $^{13}\text{C}$  NMR (101 MHz, DMSO- $d_6$ )  $\delta$  172.1, 165.5, 161 (d,  $J = 243.5$  Hz), 156.4, 148.2, 143.5, 141.5, 139.4, 139.3, 138.9, 136.8, 135.8, 130.5 (d,  $J = 3.0$  Hz), 128.5, 128.2 (d,  $J = 7.8$  Hz), 121.8, 118.6, 115.1, 115.1 (d,  $J = 21.4$  Hz), 113.9, 113.4, 111.5, 110.6, 31.5, 29.5, 15.3, 9.5. ESI-HRMS: calculated, 580.2057 [M + H] $^+$ ; found, 580.2056. HPLC  $t_R = 7.19$  min.

**4-Acrylamido-N-[(4-[(4-(4-fluorophenyl)-1-methyl-2-(methylthio)-1H-imidazol-5-yl)pyridin-2-yl]amino)phenyl]benzamide (14).** According to general procedure F, 14 was synthesized from 31 and 30e. Eluent ethyl acetate/*n*-hexane 45:55 to 75:25. Another flash chromatography was performed to purify the product; eluent dichloromethane/methanol 100:0 to 92:8 afforded 32% yield.  $^1\text{H}$  NMR (400 MHz, CDCl $_3$ /methanol- $d_4$ )  $\delta$  8.13 (d,  $J = 5.2$  Hz, 1H), 7.86 (d,  $J = 8.6$  Hz, 2H), 7.72 (d,  $J = 8.6$  Hz, 2H), 7.54 (d,  $J = 8.6$  Hz, 2H), 7.40–7.34 (m, 2H), 7.20 (d,  $J = 8.7$  Hz, 2H), 6.97 (t,  $J = 8.7$  Hz, 2H), 6.66 (s, 1H), 6.60 (d,  $J = 5.3$  Hz, 1H), 6.43–6.36 (m, 2H), 5.75 (dd,  $J = 7.5, 4.2$  Hz, 1H), 3.53 (s, 3H), 2.60 (s, 3H).  $^{13}\text{C}$  NMR (101 MHz, CDCl $_3$ /methanol- $d_4$ )  $\delta$  166.9, 165.4, 162.6 (d,  $J = 246.4$  Hz), 157.4, 148.9, 145.1, 142.0, 140.3, 139.2, 136.9, 134.1, 131.3, 130.6, 130.1 (d,  $J = 3.2$  Hz), 129.8 (d,  $J = 8.0$  Hz), 129, 128.7, 128.1, 122.4, 121.5, 120, 115.6, 115.6 (d,  $J = 21.6$  Hz), 110.3, 32.4, 16.7. ESI-HRMS: calculated, 578.1900 [M + H] $^+$ ; found, 578.1894. HPLC  $t_R = 5.70$  min.

**N-[(4-[(4-(4-fluorophenyl)-1-methyl-2-(methylthio)-1H-imidazol-5-yl)pyridin-2-yl]amino)phenyl]-4-propionamidobenzamide (15).** According to general procedure F, 15 was synthesized from 31 and 30f. Eluent ethyl acetate/*n*-hexane 45:55 to 75:25. Another flash chromatography was performed to purify the product; eluent dichloromethane/methanol 100:0 to 92:8 afforded 48% yield.  $^1\text{H}$  NMR (400 MHz, DMSO- $d_6$ )  $\delta$  10.15 (s, 1H), 10.01 (s, 1H), 9.13 (s, 1H), 8.26 (d,  $J = 5.2$  Hz, 1H), 7.92 (d,  $J = 8.7$  Hz, 2H), 7.73 (d,  $J = 8.7$  Hz, 2H), 7.67–7.57 (m, 4H), 7.51–7.43 (m, 2H), 7.15 (t,  $J = 8.9$  Hz, 2H), 6.77–6.71 (m, 2H), 3.43 (s, 3H), 2.65 (s, 3H), 2.37 (q,  $J = 7.5$  Hz, 2H), 1.10 (t,  $J = 7.5$  Hz, 3H).  $^{13}\text{C}$  NMR (101 MHz, DMSO- $d_6$ )  $\delta$  172.3, 164.4, 161.0 (d,  $J = 243.5$  Hz), 156.5, 148.3, 143.5, 142.1, 138.9, 137.1, 136.8, 132.7, 130.6 (d,  $J = 3.1$  Hz), 129.1, 128.4, 128.3, 128.2 (d,  $J = 7.9$  Hz), 121.0, 118.4, 118.1, 115.1 (d,  $J = 21.5$  Hz), 114.8, 111.1, 31.5, 29.5, 15.2, 9.4. ESI-HRMS: calculated, 580.2057 [M + H] $^+$ ; found, 580.2054. HPLC  $t_R = 7.04$  min.

**N-[(4-[(4-(4-fluorophenyl)-1-methyl-2-(methylthio)-1H-imidazol-5-yl)pyridin-2-yl]amino)phenyl]-3-propionamidobenzamide (16).** According to general procedure F, 16 was synthesized from 31 and 30g. Eluent ethyl acetate/*n*-hexane 45:55 to 75:25. Another flash chromatography was performed to purify the product; eluent dichloromethane/methanol 100:0 to 92:8 afforded 37% yield.  $^1\text{H}$  NMR (200 MHz, CDCl $_3$ /methanol- $d_4$ )  $\delta$  8.46 (s, 1H), 8.30–8.17 (m, 2H), 7.83–7.69 (m, 2H), 7.66–7.49 (m, 3H), 7.45–7.27 (m, 3H), 7.14–7.06 (m, 1H), 6.92 (t,  $J = 8.8$  Hz, 2H), 6.62 (d,  $J = 5.1$  Hz, 1H), 6.51–6.19 (m, 4H), 5.79–5.67 (m, 1H), 3.45 (s, 3H), 2.63 (s, 3H), 2.16 (s, 3H).  $^{13}\text{C}$  NMR (50 MHz, CDCl $_3$ /methanol- $d_4$ )  $\delta$  166.4, 164.8, 162 (d,  $J = 246.3$  Hz), 157.9, 148.4, 144.5, 141.5, 140.1, 138.7, 135.8, 133.8, 133.5, 130.8, 130, 129.5 (d,  $J = 3.2$  Hz), 129.2 (d,  $J = 8.1$  Hz), 128.4, 128.2, 127.8, 125.0, 123.2, 119.4, 119.2, 115.0 (d,  $J = 21.5$  Hz), 114.7, 108.4, 32, 17.7, 16.2. ESI-HRMS: calculated, 592.2057 [M + H] $^+$ ; found, 592.2068. HPLC  $t_R = 6.90$  min.

**N-[(4-[(4-(4-fluorophenyl)-1-methyl-2-(methylthio)-1H-imidazol-5-yl)pyridin-2-yl]amino)-3-methylphenyl]-4-propionamidobenzamide (17).** According to general procedure F, 17 was synthesized from 31 and 30h. Eluent ethyl acetate/*n*-hexane 45:55 to 75:25 afforded 72% yield.  $^1\text{H}$  NMR (200 MHz, DMSO- $d_6$ )  $\delta$  10.23 (s, 1H), 9.36 (s, 1H), 9.11 (s, 1H), 8.25 (d,  $J = 5.2$  Hz, 1H), 7.68–7.53 (m, 4H), 7.52–7.39 (m, 3H), 7.33–7.03 (m, 4H), 6.79–6.65 (m, 2H), 3.43 (s, 3H), 2.65 (s, 3H), 2.37 (q,  $J = 7.5$  Hz, 2H), 2.21 (s, 3H), 1.11 (t,  $J = 7.5$  Hz, 3H).  $^{13}\text{C}$  NMR (50 MHz, CDCl $_3$ /methanol- $d_4$ )  $\delta$  174.5, 169, 162.1 (d,  $J = 246.4$  Hz), 156.9, 148.6, 144.7, 140, 138.8, 138.6, 136.2, 135.9, 133.9, 130.9, 129.7 (d,  $J = 3.2$  Hz), 129.3 (d,  $J = 8.0$  Hz), 128.4 (d,  $J = 0.7$  Hz), 127.6, 126.2, 125.1, 121.4, 121.0, 115.2, 115.2 (d,  $J = 21.5$  Hz), 109.4, 32.1, 29.6, 16.3, 14.6, 9.8. ESI-HRMS: calculated, 594.2213 [M + H] $^+$ ; found, 594.2213. HPLC  $t_R = 6.68$  min.

**4-Acrylamido-N-[(3-[(4-(4-fluorophenyl)-1-methyl-2-(methylthio)-1H-imidazol-5-yl)pyridin-2-yl]amino)phenyl]benzamide (18).** According to general procedure F, 18 was synthesized from 31 and 30i. Eluent ethyl acetate/*n*-hexane 45:55 to 75:25. Another flash chromatography was performed to purify the product; eluent dichloromethane/methanol 100:0 to 92:8 afforded 26% yield.  $^1\text{H}$  NMR (200 MHz, CDCl $_3$ /methanol- $d_4$ )  $\delta$  7.93 (d,  $J = 5.3$  Hz, 1H), 7.70–7.43 (m, 5H), 7.21–7.10 (m, 2H), 7.07–6.89 (m, 2H), 6.89–6.79 (m, 1H), 6.72 (t,  $J = 8.8$  Hz, 2H), 6.54 (s, 1H), 6.39 (d,  $J = 5.2$  Hz, 1H), 6.17 (d,  $J = 5.6$  Hz, 2H), 5.58–5.47 (m, 1H), 3.33 (s, 3H), 2.38 (s, 3H).  $^{13}\text{C}$  NMR (50 MHz, CDCl $_3$ /methanol- $d_4$ )  $\delta$  166.4, 164.8, 161.9 (d,  $J = 246.3$  Hz), 156.5, 148.1, 144.4, 141.5, 140.5, 139.6, 138.9, 138.5, 130.7, 129.8, 129.4 (d,  $J = 3.2$  Hz), 129.1 (d,  $J = 8.0$  Hz), 129.0, 128.3, 128.1, 127.5, 119.2, 115.7, 115.3, 115, 114.9 (d,  $J = 21.6$  Hz), 112.5, 310.4, 31.8, 16.1. ESI-HRMS: calculated, 578.1900 [M + H] $^+$ ; found, 578.1900. HPLC  $t_R = 5.95$  min.

**3-Acrylamido-N-[(3-[(4-(4-fluorophenyl)-1-methyl-2-(methylthio)-1H-imidazol-5-yl)pyridin-2-yl]amino)phenyl]-2-methylbenzamide (19).** According to general procedure F, 19 was synthesized from 31 and 30j. Eluent ethyl acetate/*n*-hexane 45:55 to 75:25. Another flash chromatography was performed to purify the product; eluent dichloromethane/methanol 100:0 to 92:8 afforded 30% yield.  $^1\text{H}$  NMR (400 MHz, DMSO- $d_6$ )  $\delta$  10.35 (s, 1H), 9.65 (s, 1H), 9.21 (s, 1H), 8.25 (d,  $J = 5.2$  Hz, 1H), 8.07 (s, 1H), 7.62–7.50



(m, 2H), 7.50–7.42 (m, 2H), 7.33–7.25 (m, 2H), 7.24–7.18 (m, 2H), 7.18–7.09 (m, 2H), 6.80 (s, 1H), 6.75 (d,  $J = 5.2$  Hz, 1H), 6.62–6.50 (m, 1H), 6.26 (d,  $J = 17.1$  Hz, 1H), 5.77 (d,  $J = 10.3$  Hz, 1H), 3.43 (s, 3H), 2.69–2.60 (m, 3H), 2.23 (s, 3H).  $^{13}\text{C}$  NMR (101 MHz, DMSO- $d_6$ )  $\delta$  167.7, 163.5, 161.0 (d,  $J = 243.6$  Hz), 156.5, 148.2, 143.6, 141.6, 139.4, 138.9, 136.8, 136.6, 130.6 (d,  $J = 3.0$  Hz), 130.5, 129.4, 128.7, 128.3 (d,  $J = 7.8$  Hz), 128.2, 126.7, 126.5, 125.6, 124.1, 115.2, 115.1 (d,  $J = 21.4$  Hz), 113.7, 112.6, 111.5, 109.8, 31.6, 15.3, 14.6. The missing signal is most probably overlaid by another signal. ESI-HRMS: calculated, 592.2057 [M + H] $^+$ ; found, 592.2045. HPLC  $t_R = 6.32$  min.

**3-Acrylamido-N-(4-((4-(4-fluorophenyl)-1-methyl-2-(methylthio)-1H-imidazol-5-yl)pyridin-2-yl)amino)-3-methylphenyl)benzamide (20).** According to general procedure F, **20** was synthesized from **31** and **30m**. Eluent acetate/*n*-hexane 45:55 to 75:25. Another flash chromatography was performed to purify the product; eluent dichloromethane/methanol 100:0 to 92:8 afforded 43% yield.  $^1\text{H}$  NMR (400 MHz, DMSO- $d_6$ )  $\delta$  10.36 (s, 1H), 10.16 (s, 1H), 8.31 (s, 1H), 8.18–8.12 (m, 2H), 7.92 (d,  $J = 8.0$  Hz, 1H), 7.67–7.58 (m, 2H), 7.52–7.37 (m, 5H), 7.18–7.10 (m, 2H), 6.69 (dd,  $J = 5.2, 1.2$  Hz, 1H), 6.55–6.42 (m, 2H), 6.30 (dd,  $J = 17.0, 1.9$  Hz, 1H), 5.82–5.74 (m, 1H), 3.42 (s, 3H), 2.63 (s, 3H), 2.17 (s, 3H).  $^{13}\text{C}$  NMR (101 MHz, DMSO- $d_6$ )  $\delta$  165.1, 163.3, 161.0 (d,  $J = 243.6$  Hz), 157.8, 148.5, 143.4, 139.1, 139.1, 136.8, 135.9, 135.1, 134.3, 131.9, 131.7, 130.6 (d,  $J = 3.0$  Hz), 128.7, 128.4, 128.3 (d,  $J = 8.0$  Hz), 127.1, 124.2, 122.5, 122.3, 122.1, 118.8, 118.4, 115.1 (d,  $J = 21.4$  Hz), 114.3, 109.4, 31.5, 18.2, 15.4, 15.3. ESI-HRMS: calculated, 592.2057 [M + H] $^+$ ; found, 592.2064. HPLC  $t_R = 6.60$  min.

**3-Acrylamido-N-(4-((4-(4-methyl-2-(methylthio)-1H-imidazol-5-yl)pyridin-2-yl)amino)phenyl)benzamide (21).** Compound **21** was prepared according to general procedure B starting from **35** (87.5 mg, 0.20 mmol), DIPEA (46  $\mu\text{L}$ , 0.26 mmol), and acryloyl chloride (22  $\mu\text{L}$ , 0.24 mmol). Purification: flash column chromatography (SiO $_2$ , dichloromethane/ethanol, 92:08). Yield: 40 mg (41%) as a light yellow solid product.  $^1\text{H}$  NMR (250 MHz, DMSO- $d_6$ )  $\delta$  12.28 (s, 1H), 10.35 (s, 1H), 10.13 (s, 1H), 8.99 (s, 1H), 8.14 (s, 1H), 8.08 (d,  $J = 5.4$  Hz, 1H), 7.92 (d,  $J = 8.3$  Hz, 1H), 7.71–7.59 (m, 5H), 7.52–7.38 (m, 1H), 7.15 (s, 1H), 6.98 (d,  $J = 5.6$  Hz, 1H), 6.56–6.38 (m, 1H), 6.36–6.20 (m, 1H), 5.86–5.70 (m, 1H), 2.55 (s, 3H), 2.42 (s, 3H).  $^{13}\text{C}$  NMR (101 MHz, DMSO- $d_6$ )  $\delta$  164.9, 163.3, 156.3, 147.2, 143.1, 139.1, 138.2, 137.0, 135.9, 134.0, 131.8, 131.7, 128.7, 127.1, 122.2, 122.0, 121.1, 118.8, 118.3, 117.9, 111.0, 105.9, 15.5, 11.4. HPLC  $t_R = 5.29$  min. ESI-HRMS: calculated, 485.1754 [M + H] $^+$ ; found, 485.1738.

**4-Acrylamido-N-(4-((4-(4-methyl-2-(methylthio)-1H-imidazol-5-yl)pyridin-2-yl)amino)phenyl)benzamide (22).** Compound **22** was synthesized according to general procedure B, using compound **36** (100 mg, 0.23 mmol), DIPEA (53  $\mu\text{L}$ , 0.3 mmol), and acryloyl chloride (23  $\mu\text{L}$ , 0.28 mmol). Purification by flash chromatography (SiO $_2$ , dichloromethane/ethanol, 98:08) afforded 20 mg (22%) of a light yellow solid product.  $^1\text{H}$  NMR (250 MHz, DMSO- $d_6$ )  $\delta$  12.29 (br s, 1H), 10.42 (s, 1H), 10.01 (s, 1H), 8.98 (s, 1H), 8.09 (d,  $J = 5.4$  Hz, 1H), 7.99–7.92 (m,  $J = 8.8$  Hz, 2H), 7.84–7.76 (m,  $J = 9.0$  Hz, 2H), 7.70–7.59 (m, 4H), 7.15 (s, 1H), 6.98 (d,  $J = 5.1$  Hz, 1H), 6.48 (dd,  $J = 9.9, 17.0$  Hz, 1H), 6.30 (dd,  $J = 2.2, 17.1$  Hz, 1H), 5.76–5.85 (m, 1H), 2.55 (s, 3H), 2.42 (s, 3H). HPLC  $t_R = 2.66$  min. ESI-HRMS: calculated, 485.1754 [M + H] $^+$ ; found, 485.1752.

**N-(4-((4-(4-Methyl-2-(methylthio)-1H-imidazol-5-yl)pyridin-2-yl)amino)phenyl)-3-propionamidobenzamide (23).** Under argon atmosphere, compound **32** (80 mg, 0.26 mmol) was suspended in a mixture of dry dichloromethane (10 mL) and DIPEA (0.054 mL, 0.31 mmol) was added. Finally, a solution of 3-propionamidobenzamide acid (54 mg, 0.28 mmol) and PyBOP (162 mg, 0.31 mmol) in (5:1) mixture of dichloromethane/DMF (6 mL) was added. The reaction was stirred at rt for 6 h. The reaction mixture was poured in water, and the aqueous layer was extracted 3 times with ethyl acetate. The organic layers were washed with saturated NaCl solution, dried over anhydrous Na $_2$ SO $_4$ , and concentrated at reduced pressure. The residue was finally purified twice by flash column chromatography (SiO $_2$ , dichloromethane/ethanol, 92:08 to 85:15) yielding 27 mg of product (21%).  $^1\text{H}$  NMR (300 MHz, DMSO- $d_6$ )  $\delta$  10.15 (s, 1H),

10.06 (s, 1H), 9.17 (br s, 1H), 8.10 (br s, 1H), 8.07 (d,  $J = 5.6$  Hz, 1H), 7.83 (d,  $J = 7.9$  Hz, 1H), 7.73–7.58 (m, 5H), 7.49–7.40 (m, 1H), 7.15 (s, 1H), 7.01 (d,  $J = 5.4$  Hz, 1H), 2.57 (s, 3H), 2.43 (s, 3H), 2.36 (q,  $J = 7.5$  Hz, 2H), 1.11 (t,  $J = 7.4$  Hz, 3H).  $^{13}\text{C}$  NMR (101 MHz, DMSO- $d_6$ )  $\delta$  172.2, 165.1, 155.8, 146.0, 143.2, 142.9, 139.8, 139.4, 137.3, 135.8, 132.6, 128.6, 121.7, 121.1, 118.8, 118.5, 113.8, 113.4, 111.0, 105.9, 29.5, 15.4, 9.6, 8.6. HPLC  $t_R = 4.12$  min. ESI-HRMS: calculated, 487.1911 [M + H] $^+$ ; found, 487.1896.

**N-(4-((4-(4-Fluorophenyl)-2-(methylthio)-1H-imidazol-5-yl)pyridin-2-yl)amino)phenyl)-3-nitrobenzamide (24).** In 100 mL round-bottom flask, *m*-nitrobenzoic acid (341.5 mg, 2.00 mmol), PyBOP (1.28 g, 2.40 mmol), and DIPEA (463  $\mu\text{L}$ , 2.60 mmol) were mixed together in 30 mL of dichloromethane. The mixture was stirred for 1 h at rt. Then, amine **3** (800 mg, 2.00 mmol) was added to the reaction mixture in one portion and the reaction stirred for 5 h at rt. The solvent was evaporated under vacuum, then ethyl acetate (50 mL) was added and washed with water (3  $\times$  15 mL). The combined water layers were extracted with ethyl acetate one time. The combined organic layers were dried over anhydrous Na $_2$ SO $_4$ . The solvent was evaporated and the crude product was purified by flash chromatography (SiO $_2$ , dichloromethane/ethanol, 95:05 to 90:10) to afford 462 mg (42%) of an orange solid product.  $^1\text{H}$  NMR (400 MHz, DMSO- $d_6$ )  $\delta$  12.69 (br s, 1H), 10.48 (br s, 1H), 9.05 (br s, 1H), 8.80 (br s, 1H), 8.50–8.30 (m, 2H), 8.01 (br s, 1H), 7.89–7.75 (m, 1H), 7.64 (br s, 4H), 7.52 (br s, 2H), 7.30 (br s, 2H), 7.13–6.75 (m, 1H), 6.70 (br s, 1H), 2.63 (s, 3H).  $^{13}\text{C}$  NMR (101 MHz, DMSO- $d_6$ )  $\delta$  162.7, 162.2 (d,  $J = 249.5$  Hz), 156.2, 147.7, 147.1, 142.9, 142.1, 139.6, 138.2, 136.5, 134.0, 131.6 (d,  $J = 4.6$  Hz), 130.6 (d,  $J = 7.3$  Hz), 130.1, 129.6, 128.2, 125.9, 122.3, 121.3, 118.5, 115.8 (d,  $J = 24.8$  Hz), 112.0, 107.3, 15.0. HPLC  $t_R = 6.87$  min. FAB-MS: ( $m/z$ ) calculated, 541.15 [M + H] $^+$ ; found: 541.2.

**N-(4-((4-(4-Fluorophenyl)-2-(methylthio)-1H-imidazol-5-yl)pyridin-2-yl)amino)phenyl)-4-nitrobenzamide (25).** Compound **25** was synthesized similarly to **24** using *p*-nitrobenzoic acid (310 mg, 1.85 mmol), PyBOP (1.1 g, 2.02 mmol) and DIPEA (353  $\mu\text{L}$ , 2.03 mmol) and amine **3** (660 mg, 1.85 mmol) affording 637 mg (70%) of an orange solid product.  $^1\text{H}$  NMR (400 MHz, DMSO- $d_6$ )  $\delta$  12.69 (br s, 1H), 10.46 (br s, 1H), 9.06 (br s, 1H), 8.46–8.29 (m, 2H), 8.26–8.13 (m, 2H), 8.03 (br s, 1H), 7.75–7.57 (m, 4H), 7.52 (br s, 2H), 7.28 (br s, 2H), 7.07 (br s, 1H), 6.76–6.62 (m, 1H), 2.63 (d,  $J = 2.3$  Hz, 3H).  $^{13}\text{C}$  NMR (101 MHz, DMSO- $d_6$ )  $\delta$  163.2, 161.7 (d,  $J = 248.9$  Hz), 156.2, 149.0, 142.2, 140.8, 138.2, 131.7 (d,  $J = 1.8$  Hz), 129.1 (d,  $J = 2.4$  Hz), 129.0, 123.6, 123.4, 122.5, 121.4, 121.2, 120.8, 119.0, 118.3, 115.7 (d,  $J = 22.2$  Hz), 112.1, 107.3, 15.0. HPLC  $t_R = 6.80$  min. FAB-MS: ( $m/z$ ) calculated, 541.15 [M + H] $^+$ ; found: 541.2.

**3-Amino-N-(4-((4-(4-fluorophenyl)-2-(methylthio)-1H-imidazol-5-yl)pyridin-2-yl)amino)phenyl)benzamide (26).** Compound **26** was synthesized according to general procedure A, using compound **24** (160 mg, 0.30 mmol), EtOH (20 mL), and tin(II) chloride (167 mg, 0.74 mmol). Yield: 88 mg (58%) of a light yellow solid product.  $^1\text{H}$  NMR (400 MHz, DMSO- $d_6$ )  $\delta$  12.67 (br s, 1H), 10.03–9.83 (m, 1H), 9.08–8.84 (m, 1H), 8.23–7.90 (m, 1H), 7.61 (d,  $J = 6.1$  Hz, 2H), 7.58–7.44 (m, 4H), 7.37–7.17 (m, 2H), 7.17–6.99 (m, 4H), 6.84–6.72 (m, 1H), 6.72–6.63 (m, 1H), 5.29 (br s, 2H), 2.63 (br s, 3H).  $^{13}\text{C}$  NMR (101 MHz, DMSO- $d_6$ )  $\delta$  165.8, 161.9 (d,  $J = 247.4$  Hz), 161.3 (d,  $J = 241.8$  Hz), 156.4, 148.6, 148.0, 147.2, 142.8, 142.0, 138.9, 137.9, 137.6, 137.2, 136.1, 134.7, 132.8, 132.4, 131.0, 130.7 (d,  $J = 8.1$  Hz), 129.4 (d,  $J = 10.3$  Hz), 128.6, 126.8, 126.8, 126.2, 120.9, 118.7, 118.3, 116.6, 115.9 (d,  $J = 22.3$  Hz), 115.1 (d,  $J = 21.2$  Hz), 114.7, 113.0, 112.3, 111.8, 107.2, 107.0, 15.1, 15.0. The peaks of the carbon are double due to the amide tautomerism. HPLC  $t_R = 5.32$  min. FAB-MS: ( $m/z$ ) calculated, 511.2 [M + H] $^+$ ; found: 511.3.

**4-Amino-N-(4-((4-(4-fluorophenyl)-2-(methylthio)-1H-imidazol-5-yl)pyridin-2-yl)amino)phenyl)benzamide (27).** Compound **27** was synthesized according to general procedure A, using compound **25** (352 mg, 0.65 mmol), EtOH (70 mL), tin(II) chloride (368 mg, 1.6 mmol). Yield: 183 mg (55%) of a light yellow solid product.  $^1\text{H}$  NMR (400 MHz, DMSO- $d_6$ )  $\delta$  12.67 (br s, 1H), 9.65 (br s, 1H), 9.02–8.85 (m, 1H), 8.20–7.88 (m, 1H), 7.72 (d,  $J = 7.3$  Hz,

2H), 7.56–7.55 (m, 1H), 7.64–7.41 (m, 6H), 7.39–7.11 (m, 2H), 7.11–6.73 (m, 1H), 6.67 (br s, 1H), 6.60 (d,  $J = 7.3$  Hz, 2H), 5.72 (br s, 2H), 2.62 (s, 3H).  $^{13}\text{C}$  NMR (101 MHz, DMSO- $d_6$ )  $\delta$  164.8, 161.9 (d,  $J = 241.0$  Hz), 156.4, 151.8, 148.0, 147.1, 142.8, 141.9, 137.2, 132.8, 130.6 (d,  $J = 7.0$  Hz), 129.1, 126.8 (d,  $J = 3.8$  Hz), 121.4, 120.8, 118.7, 118.3, 115.8 (d,  $J = 21.3$  Hz), 112.5, 111.7, 106.9, 15.0. HPLC  $t_R = 4.86$  min. FAB-MS: ( $m/z$ ) calculated, 511.2 [ $M + H$ ] $^+$ ; found: 511.3.

**N-(4-Bromophenyl)-3-nitrobenzamide (28a).** According to general procedure C, **28a** was synthesized from 4-bromoaniline and 3-nitrobenzoic acid. All volatiles were evaporated under reduced pressure to afford 56% yield as an off-white solid.  $^1\text{H}$  NMR (200 MHz, DMSO- $d_6$ )  $\delta$  10.68 (s, 1H), 8.78 (s, 1H), 8.51–8.33 (m, 2H), 7.91–7.70 (m, 3H), 7.56 (d,  $J = 8.8$  Hz, 2H). Exact mass: 320.0. ESI-MS ( $m/z$ ): 319.4, 321.4 [ $M - H$ ] $^-$  (peaks were measured at half-intensity due to isotopic pattern of bromine).

**N-(4-Bromophenyl)-2-methyl-3-nitrobenzamide (28b).** According to general procedure C, **28b** was synthesized from 4-bromoaniline and 2-methyl-3-nitrobenzoic acid. All volatiles were evaporated under reduced pressure to afford 89% yield as an off-white solid.  $^1\text{H}$  NMR (200 MHz, DMSO- $d_6$ )  $\delta$  10.71 (s, 1H), 8.01 (d,  $J = 7.5$  Hz, 1H), 7.89–7.45 (m, 6H), 2.41 (s, 3H). Exact mass: 334.0. ESI-MS ( $m/z$ ): 332.8, 334.8 [ $M - H$ ] $^-$  (peaks were measured at half-intensity due to isotopic pattern of bromine).

**N-(3-Bromophenyl)-3-nitrobenzamide (28c).** According to general procedure C, **28c** was synthesized from 3-bromoaniline and 3-nitrobenzoic acid. All volatiles were evaporated under reduced pressure to afford 79% yield as an off-white solid.  $^1\text{H}$  NMR (200 MHz, DMSO- $d_6$ )  $\delta$  10.70 (s, 1H), 8.79 (t,  $J = 1.9$  Hz, 1H), 8.50–8.33 (m, 2H), 8.14–8.05 (m, 1H), 7.91–7.70 (m, 2H), 7.42–7.28 (m, 2H). Exact mass: 320.0. ESI-MS ( $m/z$ ): 318.8, 320.8 [ $M - H$ ] $^-$  (peaks were measured at half-intensity due to isotopic pattern of bromine).

**N-(3-Bromophenyl)-2-methyl-3-nitrobenzamide (28d).** According to general procedure C, **28d** was synthesized from 3-bromoaniline and 2-methyl-3-nitrobenzoic acid. All volatiles were evaporated under reduced pressure to afford 67% yield as an off-white solid.  $^1\text{H}$  NMR (200 MHz, DMSO- $d_6$ )  $\delta$  10.73 (s, 1H), 8.11–7.97 (m, 2H), 7.85–7.75 (m, 1H), 7.70–7.50 (m, 2H), 7.40–7.26 (m, 2H), 2.44 (s, 3H). Exact mass: 334.0. ESI-MS ( $m/z$ ): 333.4, 335.4 [ $M - H$ ] $^-$  (peaks were measured at half-intensity due to isotopic pattern of bromine).

**N-(4-Bromophenyl)-4-nitrobenzamide (28e).** According to general procedure C, **28e** was synthesized from 4-bromoaniline and 4-nitrobenzoic acid. All volatiles were evaporated under reduced pressure to afford 89% yield as a yellow solid.  $^1\text{H}$  NMR (200 MHz, DMSO- $d_6$ )  $\delta$  10.66 (s, 1H), 8.37 (d,  $J = 8.9$  Hz, 2H), 8.17 (d,  $J = 8.8$  Hz, 2H), 7.77 (d,  $J = 8.9$  Hz, 2H), 7.56 (d,  $J = 8.9$  Hz, 2H). Exact mass: 320.0. ESI-MS ( $m/z$ ): 319.4, 321.4 [ $M - H$ ] $^-$  (peaks were measured at half-intensity due to isotopic pattern of bromine).

**N-(4-Bromo-3-methylphenyl)-4-nitrobenzamide (28f).** According to general procedure C, **28f** was synthesized from 4-bromo-3-methylaniline and 4-nitrobenzoic acid. All volatiles were evaporated under reduced pressure to afford 89% yield as an off-white solid.  $^1\text{H}$  NMR (200 MHz, DMSO- $d_6$ )  $\delta$  10.59 (s, 1H), 8.36 (d,  $J = 8.8$  Hz, 2H), 8.17 (d,  $J = 8.8$  Hz, 2H), 7.78 (s, 1H), 7.56 (s, 2H), 2.35 (s, 3H). Exact mass: 334.0. ESI-MS ( $m/z$ ): 333.4, 335.4 [ $M - H$ ] $^-$  (peaks were measured at half-intensity due to isotopic pattern of bromine).

**N-(3-Bromophenyl)-4-nitrobenzamide (28g).** According to general procedure C, **28g** was synthesized from 3-bromoaniline and 4-nitrobenzoic acid. All volatiles were evaporated under reduced pressure to afford 70% yield as an off-white solid.  $^1\text{H}$  NMR (200 MHz, DMSO- $d_6$ )  $\delta$  10.68 (s, 1H), 8.37 (d,  $J = 8.8$  Hz, 2H), 8.24–8.05 (m, 3H), 7.82–7.67 (m, 1H), 7.41–7.26 (m, 2H). Exact mass: 320.0. ESI-MS ( $m/z$ ): 319.4, 321.4 [ $M - H$ ] $^-$  (peaks were measured at half-intensity due to isotopic pattern of bromine).

**N-(4-Bromo-3-methylphenyl)-3-nitrobenzamide (28h).** According to general procedure C, **28h** was synthesized from 4-bromo-3-methylaniline and 3-nitrobenzoic acid. All volatiles were evaporated under reduced pressure to afford 72% yield as an off-white solid.  $^1\text{H}$  NMR (200 MHz, DMSO- $d_6$ )  $\delta$  10.60 (s, 1H), 8.82–8.74 (m, 1H),

8.47–8.33 (m, 2H), 7.89–7.73 (m, 2H), 7.64–7.49 (m, 2H), 2.35 (s, 3H). Exact mass: 334.0. ESI-MS ( $m/z$ ): 333.3, 335.3 [ $M - H$ ] $^-$  (peaks were measured at half-intensity due to isotopic pattern of bromine).

**3-Amino-N-(4-bromophenyl)benzamide (29a).** According to general procedure D, **29a** was synthesized from **28a**. Yield: 96%.  $^1\text{H}$  NMR (200 MHz, DMSO- $d_6$ )  $\delta$  10.18 (s, 1H), 7.75 (d,  $J = 8.9$  Hz, 2H), 7.51 (d,  $J = 8.8$  Hz, 2H), 7.23–6.97 (m, 3H), 6.75 (d,  $J = 7.1$  Hz, 1H), 5.33 (s, 2H). Exact mass: 290.0. ESI-MS ( $m/z$ ): 289.3, 291.3 [ $M - H$ ] $^-$  (peaks were measured at half-intensity due to isotopic pattern of bromine).

**3-Amino-N-(4-bromophenyl)-2-methylbenzamide (29b).** According to general procedure D, **29b** was synthesized from **28b**. Yield: 93%.  $^1\text{H}$  NMR (200 MHz, DMSO- $d_6$ )  $\delta$  10.33 (s, 1H), 7.72 (d,  $J = 8.7$  Hz, 1H), 7.50 (d,  $J = 8.6$  Hz, 1H), 6.98 (t,  $J = 7.7$  Hz, 1H), 6.73 (d,  $J = 7.9$  Hz, 1H), 6.61 (d,  $J = 7.3$  Hz, 1H), 5.07 (s, 1H), 2.05 (s, 2H). Exact mass: 304.0. ESI-MS ( $m/z$ ): 303.3, 305.3 [ $M - H$ ] $^-$  (peaks were measured at half-intensity due to isotopic pattern of bromine).

**3-Amino-N-(3-bromophenyl)benzamide (29c).** According to general procedure D, **29c** was synthesized from **28c**. Yield: 91%.  $^1\text{H}$  NMR (200 MHz, DMSO- $d_6$ )  $\delta$  10.21 (s, 1H), 8.10 (s, 1H), 7.82–7.65 (m, 1H), 7.37–7.00 (m, 5H), 6.76 (d,  $J = 8.0$  Hz, 1H), 5.32 (s, 2H). Exact mass: 290.0. ESI-MS ( $m/z$ ): 289.3, 291.3 [ $M - H$ ] $^-$  (peaks were measured at half-intensity due to isotopic pattern of bromine).

**3-Amino-N-(3-bromophenyl)-2-methylbenzamide (29d).** According to general procedure D, **29d** was synthesized from **28d**. Yield: 57%.  $^1\text{H}$  NMR (200 MHz, DMSO- $d_6$ )  $\delta$  10.38 (s, 1H), 8.11 (s, 1H), 7.68 (d,  $J = 6.4$  Hz, 1H), 7.35–7.18 (m, 2H), 6.99 (t,  $J = 7.7$  Hz, 1H), 6.75 (d,  $J = 7.7$  Hz, 1H), 6.63 (d,  $J = 7.3$  Hz, 1H), 5.12 (s, 2H), 2.08 (s, 3H). Exact mass: 304.0. ESI-MS ( $m/z$ ): 303.4, 304.3 [ $M - H$ ] $^-$  (peaks were measured at half-intensity due to isotopic pattern of bromine).

**4-Amino-N-(4-bromophenyl)benzamide (29e).** According to general procedure D, **29e** was synthesized from **28e**. Yield: 34%.  $^1\text{H}$  NMR (200 MHz, DMSO- $d_6$ )  $\delta$  9.88 (s, 1H), 7.79–7.65 (m, 4H), 7.48 (d,  $J = 8.9$  Hz, 2H), 6.60 (d,  $J = 8.6$  Hz, 2H), 5.79 (s, 2H). Exact mass: 290.0. ESI-MS ( $m/z$ ): 289.4, 291.5 [ $M - H$ ] $^-$  (peaks were measured at half-intensity due to isotopic pattern of bromine).

**4-Amino-N-(4-bromo-3-methylphenyl)benzamide (29f).** According to general procedure D, **29f** was synthesized from **28f**. Yield: 80%.  $^1\text{H}$  NMR (200 MHz, DMSO- $d_6$ )  $\delta$  9.81 (s, 1H), 7.85–7.65 (m, 3H), 7.63–7.39 (m, 2H), 6.61 (d,  $J = 8.6$  Hz, 2H), 5.78 (s, 2H), 2.32 (s, 3H). Exact mass: 304.0. ESI-MS ( $m/z$ ): 303.3, 305.4 [ $M - H$ ] $^-$  (peaks were measured at half-intensity due to isotopic pattern of bromine).

**4-Amino-N-(3-bromophenyl)benzamide (29g).** According to general procedure D, **29g** was synthesized from **28g**. Yield: 50%.  $^1\text{H}$  NMR (200 MHz, DMSO- $d_6$ )  $\delta$  9.89 (s, 1H), 8.10 (s, 1H), 7.78–7.64 (m, 3H), 7.35–7.14 (m, 2H), 6.61 (d,  $J = 8.6$  Hz, 2H), 5.81 (s, 2H). Exact mass: 290.0. ESI-MS ( $m/z$ ): 289.3, 291.3 [ $M - H$ ] $^-$  (peaks were measured at half-intensity due to isotopic pattern of bromine).

**3-Amino-N-(4-bromo-3-methylphenyl)benzamide (29h).** According to general procedure D, **29h** was synthesized from **28h**. Yield: 78%.  $^1\text{H}$  NMR (200 MHz, CDCl $_3$ )  $\delta$  8.00 (s, 1H), 7.54 (d,  $J = 2.0$  Hz, 1H), 7.44 (d,  $J = 8.6$  Hz, 1H), 7.35–7.07 (m, 4H), 6.84–6.73 (m, 1H), 3.78 (s, 2H), 2.35 (s, 3H). Exact mass: 304.0. ESI-MS ( $m/z$ ): 303.3, 305.3 [ $M - H$ ] $^-$  (peaks were measured at half-intensity due to isotopic pattern of bromine).

**3-Acrylamido-N-(4-bromophenyl)benzamide (30a).** According to general procedure E, **30a** was synthesized from **29a** and acryloyl chloride. Yield: 51%.  $^1\text{H}$  NMR (200 MHz, CDCl $_3$ )  $\delta$  8.06–7.96 (m, 1H), 7.90 (d,  $J = 7.4$  Hz, 1H), 7.71–7.51 (m, 4H), 7.51–7.40 (m, 2H), 6.67–6.44 (m, 2H), 6.39–5.98 (m, 2H), 5.80 (dd,  $J = 10.3, 1.6$  Hz, 1H). Exact mass: 344.0. ESI-MS ( $m/z$ ): 343.5, 345.5 [ $M - H$ ] $^-$  (peaks were measured at half-intensity due to isotopic pattern of bromine).

**N-(4-Bromophenyl)-2-methyl-3-propionamidobenzamide (30b).** According to general procedure E, **30b** was synthesized from **29b** and propionyl chloride. Yield: 77%.  $^1\text{H}$  NMR (200 MHz, DMSO- $d_6$ )  $\delta$  10.51 (s, 1H), 9.39 (s, 1H), 7.74 (d,  $J = 8.5$  Hz, 2H), 7.63–7.38 (m, 3H), 7.26 (d,  $J = 4.4$  Hz, 2H), 2.37 (q,  $J = 7.1$  Hz, 2H), 2.21 (s,



3H), 1.11 (t,  $J = 7.5$  Hz, 3H). Exact mass: 360.0. ESI-MS ( $m/z$ ): 358.8, 360.8 [M - H]<sup>-</sup> (peaks were measured at half-intensity due to isotopic pattern of bromine).

**3-Acrylamido-*N*-(3-bromophenyl)benzamide (30c).** According to general procedure E, 30c was synthesized from 29c and acryloyl chloride. Yield: 48%. <sup>1</sup>H NMR (200 MHz, DMSO-*d*<sub>6</sub>)  $\delta$  10.40 (d,  $J = 10.5$  Hz, 2H), 8.20–8.08 (m, 2H), 7.99–7.90 (m, 1H), 7.81–7.61 (m, 2H), 7.50 (t,  $J = 7.8$  Hz, 1H), 7.39–7.25 (m, 2H), 6.56–6.22 (m, 2H), 5.79 (dd,  $J = 9.6, 2.5$  Hz, 1H). Exact mass: 344.0. ESI-MS ( $m/z$ ): 343.4, 345.4 [M - H]<sup>-</sup> (peaks were measured at half-intensity due to isotopic pattern of bromine).

**3-Acrylamido-*N*-(3-bromophenyl)-2-methylbenzamide (30d).** According to general procedure E, 30d was synthesized from 29d and acryloyl chloride. Yield: 77%. <sup>1</sup>H NMR (200 MHz, DMSO-*d*<sub>6</sub>)  $\delta$  10.57 (s, 1H), 9.67 (s, 1H), 8.11 (s, 1H), 7.79–7.47 (m, 2H), 7.40–7.21 (m, 4H), 6.68–6.44 (m, 1H), 6.27 (d,  $J = 16.9$  Hz, 1H), 5.78 (d,  $J = 9.8$  Hz, 1H), 2.23 (s, 3H). Exact mass: 358.0. ESI-MS ( $m/z$ ): 357.5, 359.5 [M - H]<sup>-</sup> (peaks were measured at half-intensity due to isotopic pattern of bromine).

**4-Acrylamido-*N*-(4-bromophenyl)benzamide (30e).** According to general procedure E, 30e was synthesized from 29e and acryloyl chloride. Yield: 60%. <sup>1</sup>H NMR (200 MHz, DMSO-*d*<sub>6</sub>)  $\delta$  10.44 (s, 1H), 10.26 (s, 1H), 7.96 (d,  $J = 8.7$  Hz, 2H), 7.87–7.68 (m, 4H), 7.53 (d,  $J = 8.9$  Hz, 2H), 6.59–6.18 (m, 2H), 5.81 (dd,  $J = 9.7, 2.3$  Hz, 1H). Exact mass: 344.0. ESI-MS ( $m/z$ ): 343.4, 345.4 [M - H]<sup>-</sup> (peaks were measured at half-intensity due to isotopic pattern of bromine).

**4-Acrylamido-*N*-(4-bromo-3-methylphenyl)benzamide (30f).** According to general procedure E, 30f was synthesized from 29f and acryloyl chloride. Yield: 68%. <sup>1</sup>H NMR (200 MHz, DMSO-*d*<sub>6</sub>)  $\delta$  10.44 (s, 1H), 10.19 (s, 1H), 7.95 (d,  $J = 8.8$  Hz, 2H), 7.81 (d,  $J = 8.7$  Hz, 3H), 7.64–7.46 (m, 2H), 6.57–6.21 (m, 2H), 5.81 (dd,  $J = 9.7, 2.3$  Hz, 1H), 2.34 (s, 3H). Exact mass: 358.0. ESI-MS ( $m/z$ ): 356.8, 358.8 [M - H]<sup>-</sup> (peaks were measured at half-intensity due to isotopic pattern of bromine).

**4-Acrylamido-*N*-(3-bromophenyl)benzamide (30g).** According to general procedure E, 30g was synthesized from 29g and acryloyl chloride. Titration with cold methanol afforded 74% yield. <sup>1</sup>H NMR (200 MHz, DMSO-*d*<sub>6</sub>)  $\delta$  10.45 (s, 1H), 10.28 (s, 1H), 8.11 (s, 1H), 8.01–7.89 (m, 2H), 7.88–7.69 (m, 3H), 7.38–7.21 (m, 2H), 6.58–6.22 (m, 2H), 5.81 (dd,  $J = 9.6, 1.9$  Hz, 1H). Exact mass: 344.0. ESI-MS ( $m/z$ ): 342.8, 344.8 [M - H]<sup>-</sup> (peaks were measured at half-intensity due to isotopic pattern of bromine).

***N*-(3-Bromophenyl)-3-propionamidobenzamide (30h).** According to general procedure E, 30h was synthesized from 29c and propionyl chloride. Yield: 68%. <sup>1</sup>H NMR (400 MHz, DMSO-*d*<sub>6</sub>)  $\delta$  10.40 (s, 1H), 10.08 (s, 1H), 8.10 (s, 2H), 7.84 (d,  $J = 8.0$  Hz, 1H), 7.77–7.71 (m, 1H), 7.60 (d,  $J = 7.8$  Hz, 1H), 7.45 (t,  $J = 7.9$  Hz, 1H), 7.37–7.26 (m, 2H), 2.35 (q,  $J = 7.5$  Hz, 2H), 1.10 (t,  $J = 7.5$  Hz, 3H). Exact mass: 346.0. ESI-MS ( $m/z$ ): 344.8, 346.8 [M - H]<sup>-</sup> (peaks were measured at half-intensity due to isotopic pattern of bromine).

***N*-(4-Bromo-3-methylphenyl)-4-propionamidobenzamide (30i).** According to general procedure E, 30i was synthesized from 29f and propionyl chloride. Yield: 64%. <sup>1</sup>H NMR (200 MHz, DMSO-*d*<sub>6</sub>)  $\delta$  10.15 (s, 2H), 7.98–7.84 (m, 2H), 7.83–7.67 (m, 3H), 7.65–7.47 (m, 2H), 2.44–2.26 (m, 5H) (CH<sub>3</sub> and methyl group overlay), 1.09 (t,  $J = 7.5$  Hz, 3H). Exact mass: 360.0. ESI-MS ( $m/z$ ): 358.8, 360.8 [M - H]<sup>-</sup> (peaks were measured at half-intensity due to isotopic pattern of bromine).

***N*-(4-Bromophenyl)-3-propionamidobenzamide (30j).** According to general procedure E, 30j was synthesized from 29a and propionyl chloride. Yield: 63%. <sup>1</sup>H NMR (200 MHz, DMSO-*d*<sub>6</sub>)  $\delta$  10.37 (s, 1H), 10.07 (s, 1H), 8.10 (s, 1H), 7.94–7.69 (m, 3H), 7.66–7.38 (m, 4H), 2.35 (q,  $J = 7.5$  Hz, 2H), 1.10 (t,  $J = 7.5$  Hz, 3H). Exact mass: 346.0. ESI-MS ( $m/z$ ): 344.8, 346.8 [M - H]<sup>-</sup> (peaks were measured at half-intensity due to isotopic pattern of bromine).

***N*-(4-Bromophenyl)-4-propionamidobenzamide (30k).** According to general procedure E, 30k was synthesized from 29e and propionyl chloride. Yield: 90%. <sup>1</sup>H NMR (200 MHz, DMSO-*d*<sub>6</sub>)  $\delta$  10.19 (d,  $J = 13.5$  Hz, 2H), 7.92 (d,  $J = 8.6$  Hz, 2H), 7.82–7.68 (m, 4H), 7.52 (d,  $J = 8.5$  Hz, 2H), 2.37 (q,  $J = 7.6$  Hz, 2H), 1.09 (t,  $J = 7.5$

Hz, 3H). Exact mass: 346.0. ESI-MS ( $m/z$ ): 344.8, 346.8 [M - H]<sup>-</sup> (peaks were measured at half-intensity due to isotopic pattern of bromine).

**3-Acrylamido-*N*-(4-bromophenyl)-2-methylbenzamide (30l).** According to general procedure E, 30l was synthesized from 29b and acryloyl chloride. Yield: 55%. <sup>1</sup>H NMR (200 MHz, DMSO-*d*<sub>6</sub>)  $\delta$  10.55 (s, 1H), 7.73 (d,  $J = 8.5$  Hz, 2H), 7.52 (d,  $J = 8.5$  Hz, 3H), 7.28 (d,  $J = 4.5$  Hz, 2H), 6.76–6.53 (m, 1H), 6.25 (d,  $J = 16.0$  Hz, 1H), 5.75 (d,  $J = 11.2$  Hz, 1H), 2.22 (s, 3H). Exact mass: 358.0. ESI-MS ( $m/z$ ): 358.9, 360.9 [M + H]<sup>+</sup> (peaks were measured at half-intensity due to isotopic pattern of bromine).

**3-Acrylamido-*N*-(4-bromo-3-methylphenyl)benzamide (30m).** According to general procedure E, 30m was synthesized from 29h and acryloyl chloride. Yield: 61%. <sup>1</sup>H NMR (200 MHz, DMSO-*d*<sub>6</sub>)  $\delta$  10.33 (d,  $J = 7.0$  Hz, 1H), 8.15 (s, 1H), 7.91 (d,  $J = 7.5$  Hz, 1H), 7.77 (s, 1H), 7.68–7.39 (m, 4H), 6.55–6.18 (m, 2H), 5.77 (dd,  $J = 9.8, 1.7$  Hz, 1H), 2.32 (s, 3H). Exact mass: 358.0. ESI-MS ( $m/z$ ): 357.5, 359.5 [M - H]<sup>-</sup> (peaks were measured at half-intensity due to isotopic pattern of bromine).

***N*-(4-((4-(4-Methyl-2-(methylthio)-1*H*-imidazol-5-yl)pyridin-2-ylamino)phenyl)-3-nitrobenzamide (33).** In a round-bottom flask under dry conditions, *m*-nitrobenzoic acid (222.2 mg, 1.33 mmol) was dissolved in 3 mL of thionyl chloride. The reaction mixture was refluxed for 2 h. The solvent was removed under high vacuum and compound 32 (230 mg, 0.74 mmol) dissolved in 5 mL pyridine was added to the reaction mixture and the reaction was stirred at rt for 60 h. The reaction mixture was poured in water (10 mL) finding the formation of a precipitate. The precipitate was filtered off and purified by flash chromatography (SiO<sub>2</sub>, dichloromethane/ethanol, 95:05 to 80:20) to afford 135 mg (40%) of a red solid. <sup>1</sup>H NMR (400 MHz, DMSO-*d*<sub>6</sub>)  $\delta$  12.29 (br s, 1H), 10.48 (s, 1H), 9.05 (s, 1H), 8.80 (br s, 1H), 8.49–8.34 (m, 2H), 8.10 (d,  $J = 5.1$  Hz, 1H), 7.91–7.78 (m, 1H), 7.72 (d,  $J = 8.6$  Hz, 2H), 7.66 (d,  $J = 8.9$  Hz, 2H), 7.18 (s, 1H), 6.99 (d,  $J = 5.3$  Hz, 1H), 2.56 (s, 3H), 2.46–2.32 (m, 3H). <sup>13</sup>C NMR (101 MHz, DMSO-*d*<sub>6</sub>)  $\delta$  162.7, 156.3, 147.7, 147.2, 143.1, 139.1, 138.6, 136.5, 134.0, 131.2, 130.1, 127.2, 125.9, 122.3, 121.3, 118.3, 117.9, 111.1, 106.1, 15.5, 11.4. HPLC  $t_R = 7.35$  min. ESI-MS: ( $m/z$ ) calculated, 461.14 [M + H]<sup>+</sup>; found: 461.1.

***N*-(4-((4-(4-Methyl-2-(methylthio)-1*H*-imidazol-5-yl)pyridin-2-ylamino)phenyl)-4-nitrobenzamide (34).** In a round-bottom flask under dry conditions, compound 34 (100 mg, 0.32 mmol) and *p*-nitrobenzoyl chloride (71.5 mg, 0.39 mmol) were stirred in pyridine (3 mL) at rt for 48 h. The reaction mixture was poured in water (10 mL) finding the formation of a precipitate. The precipitate was filtered off and purified by flash chromatography two times (SiO<sub>2</sub>, dichloromethane/ethanol, 95:05 to 80:20) to afford 70 mg (47%) of a red solid. <sup>1</sup>H NMR (250 MHz, DMSO-*d*<sub>6</sub>)  $\delta$  12.31 (br s, 1H), 10.44 (s, 1H), 9.04 (s, 1H), 8.47–8.31 (m, 2H), 8.27–8.14 (m, 2H), 8.10 (d,  $J = 5.4$  Hz, 1H), 7.77–7.68 (m, 2H), 7.68–7.55 (m, 2H), 7.15 (br s, 1H), 6.98 (d,  $J = 3.9$  Hz, 1H), 2.56 (s, 3H), 2.42 (s, 3H). <sup>13</sup>C NMR (101 MHz, DMSO-*d*<sub>6</sub>)  $\delta$  163.2, 156.3, 149.0, 147.2, 140.8, 138.6, 134.0, 131.3, 129.0, 127.5, 127.1, 123.4, 121.2, 117.9, 116.7, 111.1, 106.0, 15.4, 11.4. HPLC  $t_R = 5.73$  min. ESI-MS: ( $m/z$ ) calculated, 461.14 [M + H]<sup>+</sup>; found, 461.1.

**3-Amino-*N*-(4-((4-(4-methyl-2-(methylthio)-1*H*-imidazol-5-yl)pyridin-2-ylamino)phenyl)benzamide (35).** Compound 35 was synthesized according to general procedure A, using compound 33 (135 mg, 0.29 mmol), EtOH (20 mL), tin(II) chloride (661.5 mg, 2.9 mmol). Yield: 110 mg (87%) of a light yellow solid product. <sup>1</sup>H NMR (250 MHz, DMSO-*d*<sub>6</sub>)  $\delta$  12.36 (br s, 1H), 9.93 (s, 1H), 9.00 (s, 1H), 8.08 (d,  $J = 5.6$  Hz, 1H), 7.73–7.55 (m, 4H), 7.20–7.02 (m, 4H), 6.97 (d,  $J = 4.9$  Hz, 1H), 6.79–6.63 (m, 1H), 5.29 (s, 2H), 2.55 (s, 3H), 2.42 (s, 3H). <sup>13</sup>C NMR (101 MHz, DMSO-*d*<sub>6</sub>)  $\delta$  165.7, 156.4, 148.6, 147.1, 143.0, 139.0, 137.9, 136.1, 134.0, 132.1, 128.6, 127.1, 120.9, 117.9, 116.5, 114.6, 112.9, 111.0, 105.9, 15.5, 11.4. HPLC  $t_R = 3.99$  min. ESI-MS: ( $m/z$ ) calculated, 431.17 [M + H]<sup>+</sup>; found, 431.2.

**4-Amino-*N*-(4-((4-(4-methyl-2-(methylthio)-1*H*-imidazol-5-yl)pyridin-2-ylamino)phenyl)benzamide (36).** Compound 36 was synthesized according to general procedure A, using compound 34 (135 mg, 0.29 mmol), EtOH (20 mL), tin(II) chloride (661.5 mg,

2.9 mmol). Yield: 120 mg (95%) of a light yellow solid product.  $^1\text{H}$  NMR (250 MHz,  $\text{DMSO-}d_6$ )  $\delta$  12.27 (br s, 1H), 9.62 (s, 1H), 8.92 (s, 1H), 8.07 (d,  $J = 5.4$  Hz, 1H), 7.71 (d,  $J = 8.3$  Hz, 2H), 7.61 (s, 4H), 7.14 (s, 1H), 6.96 (d,  $J = 5.6$  Hz, 1H), 6.59 (d,  $J = 8.3$  Hz, 2H), 5.70 (s, 2H), 2.55 (s, 3H), 2.42 (s, 3H);  $^{13}\text{C}$  NMR (101 MHz,  $\text{DMSO-}d_6$ )  $\delta$  164.8, 156.4, 151.8, 147.2, 143.0, 139.0, 137.5, 134.1, 132.6, 129.1, 127.0, 121.4, 120.8, 118.0, 112.5, 110.9, 105.8, 15.5, 11.4. HPLC  $t_R = 1.69$  min. ESI-MS: ( $m/z$ ) calculated, 431.17 [ $M + H$ ] $^+$ ; found, 431.4.

**Biochemistry.** JNK3<sup>99–100</sup> was expressed and purified as described previously.<sup>14</sup> JNK3-C154A was prepared using the NEB Q5 site-directed mutagenesis kit. Expression and purification of the C154A mutant were performed exactly as for wild-type JNK3.

## ■ ASSOCIATED CONTENT

### Supporting Information

The Supporting Information is available free of charge on the ACS Publications website at DOI: 10.1021/acs.jmedchem.6b01180.

Details for the synthesis and characterization of compound **32**; structures of intermediates **28–30**; kinase profile; description of the ELISA activity assay; in vitro reactivity study of inhibitor **7** with glutathione; metabolism in human male liver microsomes; mass measurements (PDF).

SMILES strings and some data (CSV)

3D coordinates of the JNK3 in complex with **7** (PDB)

## ■ AUTHOR INFORMATION

### Corresponding Authors

\*P.K.: phone, +49 7071 2974579; e-mail, pierre.koch@uni-tuebingen.de.

\*S.A.L.: phone, +49 7071 2972459; e-mail, stefan.lauffer@uni-tuebingen.de.

### ORCID

Stefan A. Lauffer: 0000-0001-6952-1486

### Author Contributions

<sup>§</sup>F.M. and A. E.-G. contributed equally.

### Notes

The authors declare no competing financial interest.

## ■ ACKNOWLEDGMENTS

Daniela Müller and Katharina Bauer are acknowledged for skilful technical assistance in compound testing. Julianer Rainer and Pascal Pross are acknowledged for assisting with the preparation of some of the linkers. Furthermore, we thank Niklas Walter and Marcel Günther for proofreading of the manuscript. M.L. acknowledges the support by the "Struktur- und Innovationsfonds Baden-Württemberg" and by the German Research Foundation DFG for funding scientific equipment as part of the DFG's Major Research Instrumentation Program as per Art.91b GG (INST 37/821-1 FUGG).

## ■ ABBREVIATIONS USED

MAP, mitogen activated protein; JNK, c-Jun N-terminal kinase; PyBOP, benzotriazol-1-yloxytrispyrrolidinophosphonium hexafluorophosphate; TBTU, *O*-(benzotriazol-1-yl)-*N,N,N'*-tetramethyluronium tetrafluoroborate; ELISA, enzyme-linked immunosorbent assay;  $\text{IC}_{50}$ , half maximal inhibitory concentration; HLM, male human liver microsomes; PAINS, pan assay interference compounds; LC-MS, liquid chromatography-mass spectrometry

## ■ REFERENCES

- (1) Cargnello, M.; Roux, P. P. Activation and function of the MAPKs and their substrates, the MAPK-activated protein kinases. *Microbiol. Mol. Biol. Rev.* **2011**, *75*, 50–83.
- (2) Davis, R. J. Signal transduction by the JNK group of MAP kinases. *Cell* **2000**, *103*, 239–252.
- (3) Gupta, S.; Barrett, T.; Whitmarsh, A. J.; Cavanagh, J.; Sluss, H. K.; Dérijard, B.; Davis, R. J. Selective interaction of JNK protein kinase isoforms with transcription factors. *EMBO J.* **1996**, *15*, 2760–2770.
- (4) Bogoyevitch, M. A.; Kobe, B. Uses for JNK: the many and varied substrates of the c-Jun N-terminal kinases. *Microbiol. Mol. Biol. Rev.* **2006**, *70*, 1061–1095.
- (5) Yoon, S. O.; Park, D. J.; Ryu, J. C.; Ozer, H. G.; Tep, C.; Shin, Y. J.; Lim, T. H.; Pastorino, L.; Kunwar, A. J.; Walton, J. C.; Nagahara, A. H.; Lu, K. P.; Nelson, R. J.; Tuszyński, M. H.; Huang, K. JNK3 perpetuates metabolic stress induced by A $\beta$  peptides. *Neuron* **2012**, *75*, 824–837.
- (6) Ungerstedt, U. 6-Hydroxy-dopamine induced degeneration of central monoamine neurons. *Eur. J. Pharmacol.* **1968**, *5*, 107–110.
- (7) Ungerstedt, U.; Arbuthnot, G. W. Quantitative recording of rotational behavior in rats after 6-hydroxy-dopamine lesions of the nigrostriatal dopamine system. *Brain Res.* **1970**, *24*, 485–493.
- (8) Antoniou, X.; Falconi, M.; Di Marino, D.; Bonsello, T. JNK3 as a therapeutic target for neurodegenerative diseases. *J. Alzheimer's Dis.* **2011**, *24*, 633–642.
- (9) Singh, J.; Petter, R. C.; Baillie, T. A.; Whitty, A. The resurgence of covalent drugs. *Nat. Rev. Drug Discovery* **2011**, *10*, 307–317.
- (10) Liu, Q.; Sabnis, Y.; Zhao, Z.; Zhang, T.; Buhlage, S.; Sara, J.; Jones, L.; Gray, N. S.; Nathanael, S. Developing irreversible inhibitors of the protein kinase cys215. *Chem. Biol.* **2013**, *20*, 146–159.
- (11) Sanderson, K. Irreversible kinase inhibitors gain traction. *Nat. Rev. Drug Discovery* **2013**, *12*, 649–651.
- (12) Genova, C.; Rjavec, E.; Barletta, G.; Burratino, G.; Biello, F.; Dal Bello, M. G.; Coco, S.; Truini, A.; Alami, A.; Boccardo, F.; Grossi, F. Afatinib for the treatment of advanced non-small-cell lung cancer. *Expert Opin. Pharmacother.* **2014**, *15*, 889–903.
- (13) Knapp, S.; Arruda, P.; Blagg, J.; Burley, S.; Drewry, D. H.; Edwards, A.; Fabbo, D.; Gillespie, P.; Gray, N. S.; Kuster, B.; Lackey, K. E.; Mazafera, P.; Tomkinson, N. C. O.; Willson, T. M.; Workman, P.; Zuercher, W. J. A public-private partnership to unlock the untargeted kinase. *Nat. Chem. Biol.* **2013**, *9*, 3–6.
- (14) Zhang, T.; Inesta-Vaquera, F.; Niepel, M.; Zhang, J.; Ficarro, S. B.; Machleidt, T.; Xie, T.; Marto, J. A.; Kim, N. J.; Sun, T.; Langhin, J. D.; Park, H.; LoGrasso, P. V.; Paticelli, M.; Nomanbhoy, T. K.; Sorger, P. K.; Alessi, D. R.; Gray, N. S. Discovery of potent and selective covalent inhibitors of JNK. *Chem. Biol.* **2012**, *19*, 140–154.
- (15) Ansidei, F.; Lange, A.; El-Gokha, A.; Boeckler, F. M.; Koch, P. Fluorescence polarization-based assays for detecting compounds binding to inactive c-Jun N-terminal kinase 3 and p38 $\alpha$  mitogen-activated protein kinase. *Anal. Biochem.* **2016**, *503*, 28–40.
- (16) Scapin, G.; Patel, S. B.; Lisnock, J.; Becker, J. W.; LoGrasso, P. V. The structure of JNK3 in complex with small molecule inhibitors: Structural basis for potency and selectivity. *Chem. Biol.* **2003**, *10*, 705–712.
- (17) *Small-Molecule Drug Discovery Suite 2015-4: Guide*, version 6.9; Schrödinger, LLC: New York, 2015.
- (18) *The PyMOL Molecular Graphics System*, version 0.99; Schrödinger, LLC: New York, 2006.
- (19) Kalgutar, A. S.; Dalvie, D. K. Drug discovery for a new generation of covalent drugs. *Expert Opin. Drug Discovery* **2012**, *7*, 561–581.
- (20) Baillie, T. A. Targeted covalent inhibitors for drug design. *Angew. Chem., Int. Ed.* **2016**, *55*, 13408–13421.
- (21) Gonzalez, A. J.; Hook, K. E.; Althaus, I. W.; Ellis, P. A.; Trachet, E.; Delaney, A. M.; Harvey, P. J.; Ellis, T. A.; Amato, D. M.; Nelson, J. M.; Fry, D. W.; Zhu, T.; Loi, C. M.; Fakhoury, S. A.; Schlosser, K. M.; Sexton, K. E.; Winters, R. T.; Reed, J. E.; Bridges, A. J.; Lettiere, D. J.; Baker, D. A.; Yang, J. X.; Lee, H. T.; Teale, H.; Vincent, P. W. Antitumor activity and pharmacokinetic properties of PF-00299804, a

second-generation irreversible pan-erbB receptor tyrosine kinase inhibitor. *Med. Cancer Ther.* **2008**, *7*, 1880–1889.

(22) Lanning, B. R.; Whitby, L. R.; Dix, M. M.; Douhan, J.; Gilbert, A. M.; Hett, E. C.; Johnson, T.; Joslyn, C.; Kath, J. C.; Niessen, S.; Roberts, L. R.; Schulte, M. E.; Wang, C.; Hulce, J. J.; Wei, B. X.; Whiteley, L. O.; Hayward, M. M.; Cravatt, B. F. A road map to evaluate the proteome-wide selectivity of covalent kinase inhibitors. *Nat. Chem. Biol.* **2014**, *10*, 760–767.

(23) Tsou, H. R.; Mamuya, N.; Johnson, B. D.; Reich, M. F.; Gruber, B. C.; Yu, F.; Nilakantas, R.; Shen, R.; Discasani, C.; DeBlanc, R.; Davis, R.; Koehn, F. E.; Greenberger, L. M.; Wang, Y. F.; Wissner, A. 6-Substituted-4-(3-bromophenylamino)quinazolines as putative irreversible inhibitors of the epidermal growth factor receptor (EGFR) and human epidermal growth factor receptor (HER-2) tyrosine kinases with enhanced antitumor activity. *J. Med. Chem.* **2001**, *44*, 2719–2734.

(24) Muth, F.; Günther, M.; Bauer, S. M.; Döring, E.; Fischer, S.; Maier, J.; Drückes, P.; Köppler, J.; Trappe, J.; Rothbauer, U.; Koch, P.; Laufer, S. A. Tetra-substituted pyridinylimidazoles as dual inhibitors of p38 $\alpha$  mitogen-activated protein kinase and c-Jun N-terminal kinase 3 for potential treatment of neurodegenerative diseases. *J. Med. Chem.* **2015**, *58*, 443–456.

(25) Laufer, S.; Hauser, D.; Stegmüller, T.; Bracht, C.; Ruff, K.; Schattel, V.; Albrecht, W.; Koch, P. Tri- and tetrasubstituted imidazoles as p38 $\alpha$  mitogen-activated protein kinase inhibitors. *Bioorg. Med. Chem. Lett.* **2010**, *20*, 6671–6675.

(26) Goettert, M.; Graessr, R.; Laufer, S. A. Optimization of a nonradioactive immunosorbent assay for p38 $\alpha$  mitogen-activated protein kinase activity. *Anal. Biochem.* **2010**, *406*, 233–234.

(27) Goettert, M.; Luik, S.; Graessr, R.; Laufer, S. A. A direct ELISA assay for quantitative determination of the inhibitory potency of small molecules inhibitors for JNK3. *J. Pharm. Biomed. Anal.* **2011**, *55*, 236–240.

(28) Selig, R.; Schattel, V.; Goettert, M.; Schollmeyer, D.; Albrecht, W.; Laufer, S. Conformational effects on potency of thioimidazoles and dihydrothiazolines. *MedChemComm* **2011**, *2*, 261–269.

(29) Koch, P.; Gehringer, M.; Laufer, S. A. Inhibitors of c-Jun N-terminal kinases: an update. *J. Med. Chem.* **2015**, *58*, 72–95.

(30) Gehringer, M.; Muth, F.; Koch, P.; Laufer, S. A. c-Jun N-terminal kinase inhibitors: a patent review (2010 – 2014). *Expert Opin. Ther. Pat.* **2015**, *25*, 849–872.

(31) Karaman, M. W.; Heergard, S.; Treiber, D. K.; Gallant, P.; Attenridge, C. E.; Campbell, B. T.; Chan, K. W.; Cicci, P.; Davis, M. L.; Edson, P. T.; Farsoni, R.; Floyd, M.; Hunt, J. P.; Lockhart, D. J.; Milanov, Z. V.; Morrison, M. J.; Pallares, G.; Patel, H. K.; Pritchard, S.; Wodicka, L. M.; Zarrinkar, P. P. A quantitative analysis of kinase inhibitor selectivity. *Nat. Biotechnol.* **2008**, *26*, 127–132.

(32) Sterling, T.; Irwin, J. J. ZINC 15 – Ligand discovery for everyone. *J. Chem. Inf. Model.* **2015**, *55*, 2324–2337.

(33) Baell, J. B.; Ferrins, L.; Falk, H.; Nikolakopoulos, G. PAINS: Relevance to tool compound discovery and fragment-based screening. *Aust. J. Chem.* **2013**, *66*, 1483–1494.

(34) Lange, A.; Günther, M.; Büttner, F. M.; Zimmermann, M. O.; Heidrich, J.; Hennig, S.; Zahn, S.; Schall, C.; Sievers-Engler, A.; Ansider, F.; Koch, P.; Laemmerhofer, M.; Stehle, T.; Laufer, S. A.; Boeckler, F. M. Targeting the gatekeeper MET146 of c-Jun N-terminal kinase 3 induces a bivalent halogen/chalcogen bond. *J. Am. Chem. Soc.* **2015**, *137*, 14640–14652.



## Supporting Information

**Tri- and Tetra-substituted Pyridinylimidazoles as Covalent Inhibitors of c-Jun N-Terminal Kinase 3**

Felix Muth,<sup>a,†</sup> Ahmed El-Gokha,<sup>a,b,†</sup> Francesco Ansideri,<sup>a</sup> Michael Eitel,<sup>a</sup> Eva Döring,<sup>a</sup> Adrian Sievers-Engler,<sup>a</sup> Andreas Lange,<sup>a</sup> Frank M. Boeckler,<sup>a</sup> Michael Laemmerhofer,<sup>a</sup> Pierre Koch<sup>b,\*</sup> and Stefan A. Laufer<sup>a,\*</sup>

<sup>a</sup>Department of Pharmaceutical Chemistry, Institute of Pharmaceutical Sciences, Eberhard Karls Universität Tübingen, Auf der Morgenstelle 8, 72076 Tübingen, Germany.

<sup>b</sup>Menofia University, Chemistry Department, Faculty of Science, Menofia, Egypt.

**Table of Contents**

<b>General information</b>	S2
<b>Schemes S1-S4</b>	S3
<b>Experimental procedures</b>	S5
<b>Structure of intermediates 28-30</b>	S8
<b>Screening data</b>	S13
<b>Description of the ELISA</b>	S21
<b>LC-<math>\mu</math>ESI-QTOF mass spectrometry</b>	S22
<b>In vitro reactivity of inhibitor 7</b>	S29
<b>Metabolism in Human Male Liver Microsomes</b>	S30
<b>References</b>	S32

### General information

All reagents and (anhydrous) solvents are commercially available and were used without further purification. 4-(4-(4-Fluorophenyl)-1-methyl-2-(methylthio)-1*H*-imidazol-5-yl)pyridin-2-amine (**31**) was synthesized according to literature.<sup>1</sup> *N*<sup>1</sup>-(4-(4-(4-Fluorophenyl)-2-(methylthio)-1*H*-imidazol-5-yl)pyridin-2-yl)benzene-1,4-diamine (**3**) was synthesized according to literature.<sup>2</sup>

### NMR:

<sup>1</sup>H- and <sup>13</sup>C-NMR spectra were obtained with Bruker 200 Avance, Bruker ARX 250, Bruker Avance III HD 300 NanoBay or with Bruker 400 Avance. The spectra were obtained in the indicated solvent and calibrated against the residual proton peak of the deuterated solvent. Chemical shifts ( $\delta$ ) are reported in parts per million (ppm).

### Mass Spectrometry:

Mass spectra were recorded on Advion Expression S ESI-MS coupled with a TLC interface. High-resolution mass spectra (FT-ICR-MS) were obtained from the Institute of Pharmaceutical Sciences, Department of Pharmaceutical Analytics and Bioanalytics, Eberhard Karls Universität Tübingen. GC/MS analyses were carried out on a Hewlett Packard HP 6890 series GC-system equipped with a HP-5MS capillary column (0.25  $\mu$ m film thickness, 30 m x 250  $\mu$ m) and a HP 5973 mass selective detector (EI ionization). Helium was used as carrier gas in the following temperature program: start at 100 °C and hold for 1 min, then increase to 270 °C in 27.3 min, then increase to 300 °C in 9 min and hold for 2 min.

### TLC:

Analyses were performed on fluorescent silica gel 60 F<sub>254</sub> plates (Merck) and visualized under UV illumination at 254 nm and 366 nm.

### Column chromatography:

Column chromatography was performed on Davisil LC60A 20-45 micron silica from Grace Davison and Geduran Si60 63-200 micron silica from Merck for the pre-column using an Interchim PuriFlash 430 automated flash chromatography system.

### HPLC:

The purity of all tested compounds was determined via reverse phase high performance liquid chromatography. The purity of all tested compounds is  $\geq$  95 %.

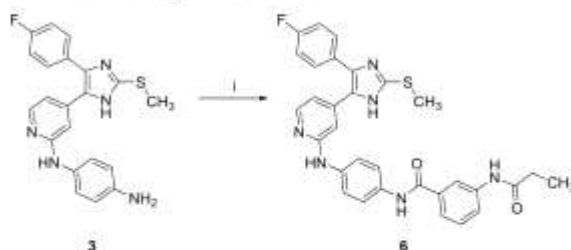
In case of compounds **4,5** and **7-22**: Hewlett Packard HP 1090 Series II LC equipped with a UV diode array detector (DAD, detection at 230 nm and 254 nm); Phenomenex Luna 5u C8 column (150 mm x 4.6 mm, 5  $\mu$ m); 35 °C oven temperature; injection volume: 5  $\mu$ L; gradient (flow: 1.5 mL/min): 0.01 M KH<sub>2</sub>PO<sub>4</sub>, pH 2.3 (solvent A), methanol (solvent B): 40 % B to 85 % B in 8 min, 85 % B for 5 min, 85% to 40 % B in 1 min, 40 % B for 2 min, stop time 16 min.

In case of compounds **6** and **23**: Agilent 1100; XBridge™ C18 (150 mm x 4.6 mm, 5  $\mu$ m); 30 °C oven temperature; injection volume: 10  $\mu$ L; gradient (flow: 1.5 mL/min): 0.01 M KH<sub>2</sub>PO<sub>4</sub>, pH 2.3 (solvent A), methanol (solvent B): 45 % B to 85 % B in 9 min, 85 % B for 6 min, stop time 15 min.

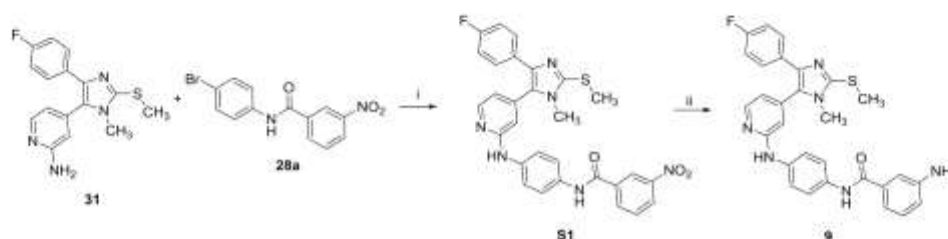
### Docking:

The docking studies were carried out using Schrodinger Glide Docking Tool.<sup>3</sup> The presented docking results were the best ranked ones. For visualization and generation of pharmacophore models, PyMOL Molecular Graphics System, Version 0.99 Schrödinger, LLC<sup>4</sup> was used.

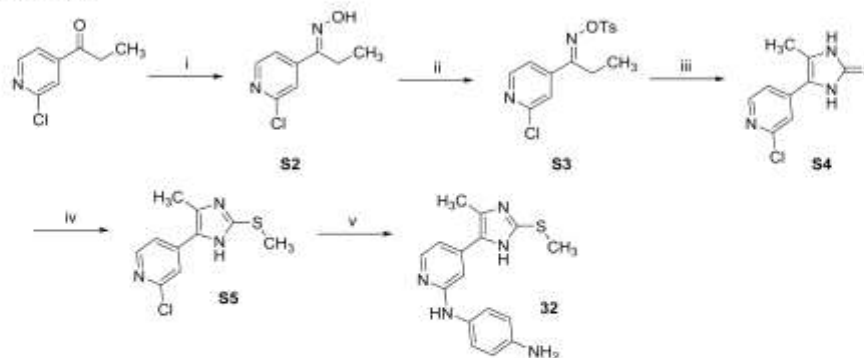
## Schemes S1-S4

Scheme S1. Synthesis of *tri*-substituted pyridinylimidazole 6.<sup>a</sup>

<sup>a</sup>Reagents and conditions: (i) 3-propionamidobenzoic acid, PyBOP, DIPEA, DMF, DCM, rt, 18 h.

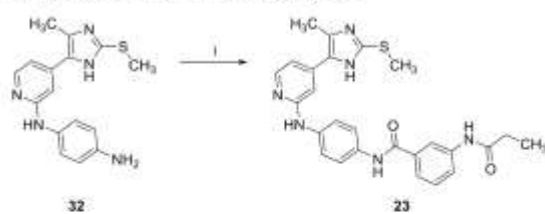
Scheme S2. Synthesis of *tetra*-substituted pyridinylimidazole 9.<sup>a</sup>

<sup>a</sup>Reagents and conditions: (i) Cs<sub>2</sub>CO<sub>3</sub>, BrettPhos precatalyst, 1,4-dioxane(abs)/tert-butanol 4:1, 125 °C, 5 h; (ii) Zn, ammonium formate, EtOH, reflux temperature, 4 h.

Scheme S3. Synthesis of *N*1-(4-(4-Methyl-2-(methylthio)-1*H*-imidazol-5-yl)pyridin-2-yl)benzene-1,4-diamine (32).<sup>a</sup>

<sup>a</sup>Reagents and conditions: (i) NH<sub>2</sub>OH·HCl, NaOH, CH<sub>3</sub>OH, 0 °C, 2 h; (ii) *p*-toluenesulfonylchloride, pyridine, 24 h; (iii) a) K, EtOH, 0 °C to rt, Et<sub>2</sub>O, 16h; b) HCl, 50 °C, 4 h; c) KSCN, MeOH, reflux temperature, 4 h; (iv) NaOtBu, MeI, MeOH, 0 °C to 55 °C; (v) *p*-phenylenediamine, *n*-butanol, 1.25 M HCl in ethanol, 160 °C, 18 h.

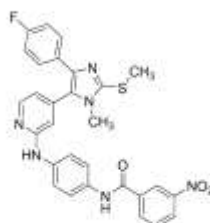


**Scheme S4. Synthesis of *tri*-substituted pyridinylimidazole 23.<sup>a</sup>**

<sup>a</sup>Reagents and conditions: (i) 3-propionamidobenzoic acid, PyBOP, DIPEA, DMF, DCM, rt, 18 h.

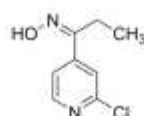
## Experimental procedures

### *N*-4-((4-(4-(4-Fluorophenyl)-1-methyl-2-(methylthio)-1*H*-imidazol-5-yl)pyridin-2-yl)amino)phenyl)-3-nitrobenzamide (**S1**)



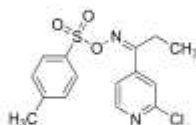
According to general procedure **F**, **S1** was synthesized from **31** and **28a**. Eluent: ethyl acetate/*n*-hexane 30/70 → ethyl acetate/*n*-hexane 60/40. The product containing fractions were unified and all volatiles were evaporated under reduced pressure. Yield: 28 %. <sup>1</sup>H NMR (200 MHz, DMSO-*d*<sub>6</sub>) δ 10.49 (s, 1H), 9.18 (s, 1H), 8.82–8.75 (m, 1H), 8.47–8.36 (m, 2H), 8.27 (d, *J* = 5.6 Hz, 1H), 7.83 (t, *J* = 8.0 Hz, 1H), 7.66 (s, 4H), 7.53–7.41 (m, 2H), 7.21–7.08 (m, 2H), 6.79–6.71 (m, 2H), 3.43 (s, 3H), 2.65 (s, 3H). **Exact Mass**: 554.2; **ESI-MS** (*m/z*): 353.2 [M-H]<sup>-</sup>

### 1-(2-Chloropyridin-4-yl)propan-1-one oxime (**S2**).

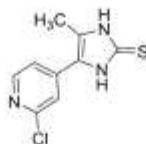


A solution of sodium hydroxide (20%; 10 mL) and hydroxylamine hydrochloride (1.79 g, 25.69 mmol) in water (10 mL) was added to a solution of 2-chloro-4-propionylpyridine (3.96 g, 23.25 mmol) in methanol (20 mL) at 0 °C. After the reaction was stirred for 2 h at 0 °C, the product was extracted by ethyl acetate and the solvent was evaporated under reduced pressure to obtain the product as a white-yellowish solid (90 %; 3.56 g). <sup>1</sup>H NMR (400 MHz, DMSO-*d*<sub>6</sub>) δ 11.88 (s, 1H), 8.42 (d, *J* = 5.1 Hz, 1H), 7.65 (dd, *J* = 4.4, 5.9 Hz, 2H), 2.72 (q, *J* = 7.3 Hz, 2H), 1.02 (t, *J* = 7.5 Hz, 3H); <sup>13</sup>C NMR (101 MHz, DMSO-*d*<sub>6</sub>) δ 155.5, 151.0, 150.2, 146.6, 120.2, 119.5, 17.6, 10.4. **GC-MS** (*m/z*) calculated: 184.04 [M]<sup>+</sup>; found: 184.0.

### 1-(2-Chloropyridin-4-yl)propan-1-one *O*-tosyl oxime (**S3**)

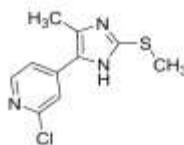


*p*-Toluenesulfonylchloride (10.58 g, 55.50 mmol) was added to a solution of 2-chloro-4-propionylpyridine oxime (**S2**) (6.81 g, 37.00 mmol) in dry pyridine (40 mL) under argon atmosphere. After the reaction was stirred for 24 h at rt, the solution was diluted with ice water (300 mL) and stirred for further 3 h. The water layer was extracted with ethyl acetate, washed with water and purified by flash chromatography (SiO<sub>2</sub>, *n*-hexane/ethyl acetate, 100:00 to 90:10) to get a viscous yellow oil (yield: 83 %; 10.47 g). <sup>1</sup>H NMR (400 MHz, DMSO-*d*<sub>6</sub>) δ 8.50 (d, *J* = 5.1 Hz, 1H), 7.91 (d, *J* = 7.8 Hz, 2H), 7.64 (s, 1H), 7.56 (d, *J* = 5.1 Hz, 1H), 7.49 (d, *J* = 7.8 Hz, 2H), 2.81 (d, *J* = 7.5 Hz, 2H), 2.41 (s, 3H), 0.99 (s, 3H); <sup>13</sup>C NMR (101 MHz, DMSO-*d*<sub>6</sub>) δ 166.6, 151.2, 150.8, 145.8, 143.0, 131.4, 130.1, 128.5, 121.7, 120.5, 21.1, 20.6, 10.4. **FABMS**: (*m/z*) calculated: 339.06 [M+H]<sup>+</sup>; found: 339.1.

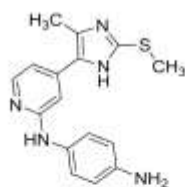
**4-(2-Chloropyridin-4-yl)-5-methyl-1,3-dihydro-2H-imidazole-2-thione (S4)**

The preparation of **S4** was performed in three steps:

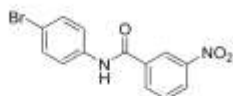
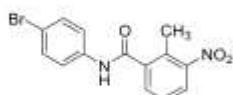
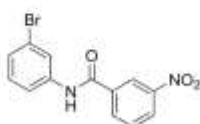
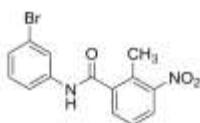
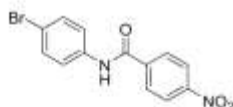
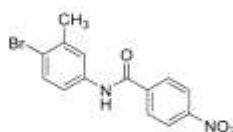
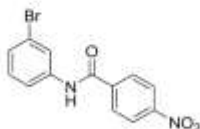
- 1) Solid potassium (1.21 g, 30.92 mmol) was added in pieces to absolute ethanol (50 mL). After the potassium was totally dissolved the reaction mixture was cooled to 0 °C and 1-(2-chloropyridin-4-yl)propan-1-one O-tosyl oxime (**S3**) (10.47 g, 30.92 mmol) in absolute ethanol (350 mL) was added dropwise to the solution. After completion of the addition the reaction was warmed to rt and stirred for 1 h. The solution was diluted with diethyl ether (100 mL) and stirred for 16 h. The precipitate was removed by filtration and washed with diethyl ether and the filtrate was concentrated at reduced pressure to obtain a yellow viscous liquid (7.80 g).
- 2) Concentrated hydrochloric acid (60 mL) was added to the crude product (7.80 g) obtained in step 1 and stirred for 4 h at 50 °C. Then, the solvent was evaporated under reduced pressure and a yellow solid (8.15 g) was obtained.
- 3) Potassium thiocyanate (15.02 g; 154.60 mmol) was added to the crude product (8.15 g) obtained in step 2 in methanol (160 mL) and stirred for 4 h at 90 °C. The formed yellow precipitate was filtered, washed with water and dried under vacuum to get the product as a yellow solid (4.56 g; 65 % over 3 steps). <sup>1</sup>H NMR (400 MHz, DMSO-*d*<sub>6</sub>) δ 12.50 (br. s, 1H), 12.43 (br. s, 1H), 8.43 - 8.27 (m, 1H), 7.59 (s, 1H), 7.51 - 7.40 (m, 1H), 2.27 (s, 3H); <sup>13</sup>C NMR (101 MHz, DMSO-*d*<sub>6</sub>) δ 161.5, 151.1, 150.1, 139.1, 126.9, 120.1, 118.8, 118.3, 10.8. HPLC tR = 2.67 min, purity: 100% (λ = 254 nm). FABMS: (m/z) calculated: 226.02 [M+H]<sup>+</sup>; found: 226.1.

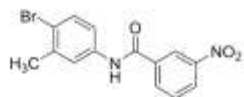
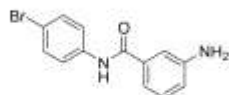
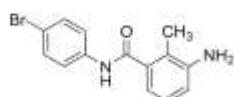
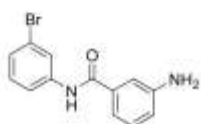
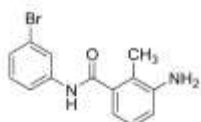
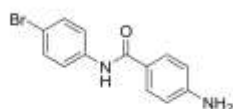
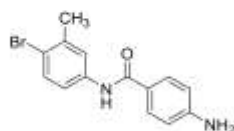
**2-Chloro-4-(4-methyl-2-(methylthio)-1H-imidazol-5-yl)pyridine (S5)**

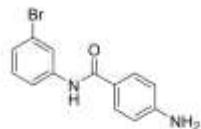
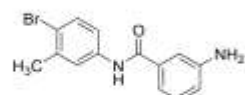
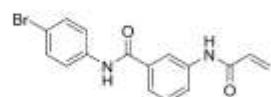
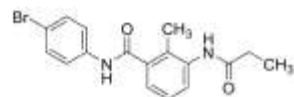
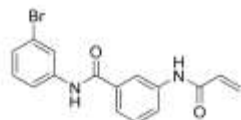
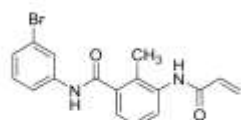
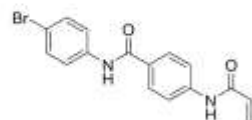
Sodium *tert*-butoxide (427 mg, 4.44 mmol) was added to a solution of **40** (500 mg, 2.22 mmol) in absolute methanol (20 mL). The reaction mixture was cooled to 0 °C and methyl iodide (147.5 μL, 2.22 mmol) was added slowly under argon atmosphere. The reaction mixture was stirred for 30 min at 0 °C and 3 h at 55 °C. After cooling to rt, the solvent was removed under vacuum, the residue was dissolved in water, extracted with ethyl acetate and dried over Na<sub>2</sub>SO<sub>4</sub>. The solvent was evaporated under reduced pressure and the residue was purified by flash chromatography (SiO<sub>2</sub>, dichloromethane/ethanol, 100:0 to 90:10) to obtain the product as a yellowish solid (76 %; 404 mg). <sup>1</sup>H NMR (400 MHz, DMSO-*d*<sub>6</sub>) δ 12.46 (br. s, 1H), 8.32 (d, *J* = 4.8 Hz, 1H), 7.62 (br. s, 1H), 7.59 (d, *J* = 4.8 Hz, 1H), 2.57 (s, 3H), 2.44 (s, 3H); <sup>13</sup>C NMR (101 MHz, DMSO-*d*<sub>6</sub>) δ 150.8, 149.8, 145.6, 140.2, 132.2, 129.3, 118.9, 118.6, 15.2, 11.4. HPLC: tR = 4.6 min. ESIMS: (m/z) calculated: 240.04 [M+H]<sup>+</sup>; found: 240.0.

***N***1-(4-(4-Methyl-2-(methylthio)-1*H*-imidazol-5-yl)pyridin-2-yl)benzene-1,4-diamine (**32**)

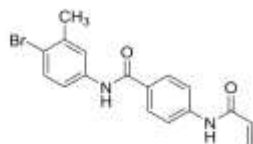
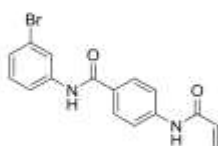
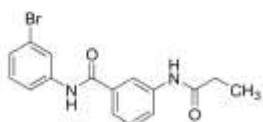
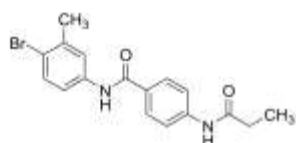
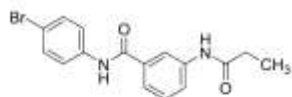
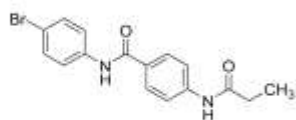
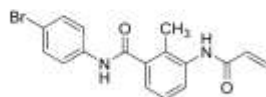
In a pressure glass tube, compound **41** (100 mg, 0.42 mmol) and *p*-phenylenediamine (67.7 mg, 0.63 mmol) were suspended in *n*-butanol (5 mL). 1.25 M HCl in ethanol (345  $\mu$ L, 0.42 mmol) was added and the reaction was heated overnight at 160 °C. After cooling to rt, the solvent was removed and the residue was purified twice by flash chromatography (SiO<sub>2</sub>, dichloromethane/ethanol, 90:10) to afford 80 mg (62%) as a brown solid. <sup>1</sup>H NMR (250 MHz, DMSO-*d*<sub>6</sub>)  $\delta$  12.23 (br. s, 1H), 8.36 (s, 1H), 7.97 (d, *J* = 5.4 Hz, 1H), 7.33 - 7.13 (m, 2H), 6.97 (s, 1H), 6.91 - 6.64 (m, 1H), 6.59 - 6.43 (m, 2H), 5.01 - 4.26 (m, 2H), 2.53 (s, 3H), 2.37 (s, 3H); <sup>13</sup>C NMR (101 MHz, DMSO-*d*<sub>6</sub>)  $\delta$  157.4, 147.3, 143.1, 142.8, 138.8, 134.3, 131.1, 126.8, 121.2, 114.2, 110.0, 104.4, 15.5, 11.3. HPLC *t*<sub>R</sub> = 1.89 min. ESIMS: (*m/z*) calculated: 312.42 [M+H]<sup>+</sup>; found: 312.2.

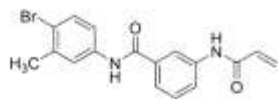
**Structure of intermediates 28-30*****N*-(4-Bromophenyl)-3-nitrobenzamide (28a)*****N*-(4-Bromophenyl)-2-methyl-3-nitrobenzamide (28b)*****N*-(3-Bromophenyl)-3-nitrobenzamide (28c)*****N*-(3-Bromophenyl)-2-methyl-3-nitrobenzamide (28d)*****N*-(4-Bromophenyl)-4-nitrobenzamide (28e)*****N*-(4-Bromo-3-methylphenyl)-4-nitrobenzamide (28f)*****N*-(3-Bromophenyl)-4-nitrobenzamide (28g)**

***N*-(4-Bromo-3-methylphenyl)-3-nitrobenzamide (28h)****3-Amino-*N*-(4-bromophenyl)benzamide (29a)****3-Amino-*N*-(4-bromophenyl)-2-methylbenzamide (29b)****3-Amino-*N*-(3-bromophenyl)benzamide (29c)****3-Amino-*N*-(3-bromophenyl)-2-methylbenzamide (29d)****4-Amino-*N*-(4-bromophenyl)benzamide (29e)****4-Amino-*N*-(4-bromo-3-methylphenyl)benzamide (29f)**

**4-Amino-N-(3-bromophenyl)benzamide (29g)****3-Amino-N-(4-bromo-3-methylphenyl)benzamide (29h)****3-Acrylamido-N-(4-bromophenyl)benzamide (30a)****N-(4-Bromophenyl)-2-methyl-3-propionamidobenzamide (30b)****3-Acrylamido-N-(3-bromophenyl)benzamide (30c)****3-Acrylamido-N-(3-bromophenyl)-2-methylbenzamide (30d)****4-Acrylamido-N-(4-bromophenyl)benzamide (30e)**



**4-Acrylamido-N-(4-bromo-3-methylphenyl)benzamide (30f)****4-Acrylamido-N-(3-bromophenyl)benzamide (30g)****N-(3-Bromophenyl)-3-propionamidobenzamide (30h)****N-(4-Bromo-3-methylphenyl)-4-propionamidobenzamide (30i)****N-(4-Bromophenyl)-3-propionamidobenzamide (30j)****N-(4-Bromophenyl)-4-propionamidobenzamide (30k)****3-Acrylamido-N-(4-bromophenyl)-2-methylbenzamide (30l)**

**3-Acrylamido-N-(4-bromo-3-methylphenyl)benzamide (30m)**

### Selectivity Screen

Compounds **7** and **21** were tested at ProQinase GmbH (Freiburg, Germany) against 410 kinases at concentrations of 1  $\mu$ M, 5  $\mu$ M and 0.1  $\mu$ M, 0.5  $\mu$ M respectively. Activities are specified as residual activities (% of control) and values under 50 % are highlighted in orange.

**Table S1**

#	Kinase Name	Kinase Family*	<b>7</b> c = 0.1 $\mu$ M	<b>7</b> c = 0.5 $\mu$ M	<b>21</b> c = 1 $\mu$ M	<b>21</b> c = 5 $\mu$ M
1	ABL1 E255K	TK	106	114	94	88
2	ABL1 F317I	TK	102	102	102	82
3	ABL1 G250E	TK	96	75	88	89
4	ABL1 H396P	TK	99	91	93	71
5	ABL1 M351T	TK	101	80	87	61
6	ABL1 Q252H	TK	101	93	96	65
7	ABL1 T315I	TK	94	93	91	82
8	ABL1 wt	TK	108	109	96	71
9	ABL1 Y253F	TK	105	108	85	64
10	ABL2	TK	134	113	74	84
11	ACK1	TK	130	128	100	95
12	ACV-R1	TKL	107	93	85	54
13	ACV-R1B	TKL	92	91	94	94
14	ACV-R2A	TKL	97	92	81	80
15	ACV-R2B	TKL	88	82	88	68
16	ACV-RL1	TKL	93	86	74	52
17	AKT1 aa106-480	AGC	104	87	84	69
18	AKT2 aa107-481	AGC	108	105	92	78
19	AKT3 aa106-479	AGC	108	122	95	90
20	ALK C1156Y (GST-HIS-tag)	TK	122	117	86	69
21	ALK F1174L (GST-HIS-tag)	TK	113	106	84	74
22	ALK F1174S (GST-HIS-tag)	TK	132	119	92	72
23	ALK L1196M (GST-HIS-tag)	TK	114	102	72	55
24	ALK R1275Q (GST-HIS-tag)	TK	119	123	85	73
25	ALK wt (GST-HIS-tag)	TK	111	105	98	72
26	AMPK-alpha1 aa1-550	CAMK	70	62	100	93
27	ARK5	CAMK	85	91	97	88
28	ASK1	STE	108	104	92	95
29	Aurora-A	OTHER	97	98	74	34
30	Aurora-B	OTHER	102	103	73	40
31	Aurora-C	OTHER	84	81	86	57
32	AXL	TK	105	102	99	76
33	BLK	TK	101	97	77	81
34	BMPR1A	TKL	96	84	83	88
35	BMX	TK	108	111	106	85
36	B-RAF V600E	TKL	91	103	110	113
37	B-RAF wt	TKL	107	107	96	82
38	BRK	TK	109	125	101	105
39	BRSK1	CAMK	101	109	107	95
40	BRSK2	CAMK	98	95	103	85
41	BTK	TK	107	107	101	87
42	BUB1B	OTHER	129	112	95	80
43	CAMK1D	CAMK	99	97	90	75
44	CAMK2A	CAMK	88	81	90	90
45	CAMK2B	CAMK	103	89	97	79
46	CAMK2D	CAMK	101	106	95	92
47	CAMK2G	CAML	68	58	81	54

48	CAMK4	CAMK	130	115	110	91
49	CAMKK1	OTHER	64	66	98	108
50	CAMKK2	OTHER	123	122	83	86
51	CCDC6-RET	TK	106	98	84	84
52	CDC42BPA	AGC	93	89	102	91
53	CDC42BPB	AGC	90	85	89	82
54	CDC7/DBF4	OTHER	105	109	94	89
55	CDK1/CycA2	CMGC	96	116	89	79
56	CDK1/CycB1	CMGC	98	100	94	77
57	CDK1/CycE1	CMGC	98	88	90	74
58	CDK12 R722C/CycK	CMGC	90	99	93	66
59	CDK12/CycK wt	CMGC	71	65	82	57
60	CDK16/CycY	CMGC	103	108	88	87
61	CDK19/CycC	CMGC	93	105	72	65
62	CDK2/CycA2	CMGC	109	98	78	56
63	CDK2/CycE1	CMGC	105	106	88	62
64	CDK3/CycC	CMGC	105	108	91	74
65	CDK3/CycE1	CMGC	103	97	98	79
66	CDK4/CycD1	CMGC	107	115	94	76
67	CDK4/CycD3	CMGC	124	117	92	83
68	CDK5/p25NCK	CMGC	100	95	77	54
69	CDK5/p35NCK	CMGC	96	98	74	36
70	CDK6/CycD1	CMGC	106	119	91	87
71	CDK6/CycD3	CMGC	106	109	93	86
72	CDK7/CycH/MAT1	CMGC	112	114	89	86
73	CDK8/CycC	CMGC	109	100	67	29
74	CDK9/CycK	CMGC	99	107	85	39
75	CDK9/CycT1	CMGC	98	93	63	38
76	CHK1	CAMK	110	100	94	100
77	CHK2	CAMK	91	93	70	36
78	CK1-alpha1	CK1	100	85	70	38
79	CK1-delta	CK1	59	20	13	3
80	CK1-epsilon	CK1	87	54	57	21
81	CK1-gamma1	CK1	97	96	65	31
82	CK1-gamma2	CK1	81	75	22	5
83	CK1-gamma3	CK1	92	77	38	12
84	CK2-alpha1	OTHER	91	91	92	75
85	CK2-alpha2	OTHER	92	94	80	52
86	CLK1	CMGC	91	98	67	37
87	CLK2	CMGC	94	92	81	51
88	CLK3	CMGC	83	68	98	89
89	CLK4	CMGC	83	86	46	20
90	COT	STE	92	99	95	103
91	CSF1-R	TK	102	89	106	69
92	CSK	TK	102	96	87	81
93	DAPK1	CAMK	103	98	100	94
94	DAPK2	CAMK	76	83	92	78
95	DAPK3	CAMK	88	84	88	88
96	DCAMKL2	CAMK	97	101	95	94
97	DDR2 N456S	TK	76	81	88	67
98	DDR2 T654M	TK	79	82	89	70
99	DDR2 wt	TK	92	91	90	76
100	DMPK	AGC	107	97	97	92
101	DNA-PK	ATYPICAL	86	98	92	103
102	DYRK1A	CMGC	122	103	92	70
103	DYRK1B	CMGC	106	102	85	53
104	DYRK2	CMGC	96	105	72	30
105	DYRK3	CMGC	101	101	82	39

106	DYRK4	CMGC	90	89	90	84
107	EEF2K	ATYPICAL	100	98	91	92
108	EGF-R d746-750	TK	126	109	115	88
109	EGF-R d747-749/A750P	TK	133	132	101	101
110	EGF-R d747-752/P753S	TK	111	104	85	86
111	EGF-R d752-759	TK	107	101	88	96
112	EGF-R G719C	TK	68	100	96	75
113	EGF-R G719S	TK	107	104	88	97
114	EGF-R L858R	TK	111	119	95	83
115	EGF-R L861Q	TK	114	98	104	91
116	EGF-R T790M	TK	106	108	91	84
117	EGF-R T790M/L858R	TK	114	110	96	96
118	EGF-R wt	TK	138	125	108	101
119	EIF2AK2	OTHER	123	129	84	55
120	EIF2AK3	OTHER	100	94	92	97
121	EML-ALK	TKL	108	107	91	89
122	EML-ALK F117L	TKL	105	106	93	80
123	EPHA1	TK	105	98	90	63
124	EPHA2	TK	142	128	92	81
125	EPHA3	TK	103	92	98	89
126	EPHA4	TK	99	99	93	78
127	EPHA5	TK	118	113	94	87
128	EPHA6	TK	114	105	99	100
129	EPHA7	TK	106	96	93	89
130	EPHA8	TK	104	101	96	99
131	EPHB1	TK	122	116	83	82
132	EPHB2	TK	108	97	93	78
133	EPHB3	TK	129	115	106	108
134	EPHB4	TK	143	131	110	111
135	ERBB2	TK	111	104	92	94
136	ERBB4	TK	121	108	93	90
137	ERK1	CMGC	108	107	101	99
138	ERK2	CMGC	95	95	96	100
139	ERK5	CMGC	93	94	83	73
140	ERK7	CMGC	93	84	66	31
141	FAK aa2-1052	TK	136	133	106	92
142	FER	TK	114	114	104	93
143	FES	TK	117	110	88	91
144	FGF-R1 V561M	TK	115	123	99	65
145	FGF-R1 wt	TK	116	103	105	87
146	FGF-R2	TK	136	128	105	87
147	FGF-R3 G697C	TK	141	130	103	83
148	FGF-R3 K650E	TK	128	116	104	79
149	FGF-R3 K650M	TK	116	121	97	72
150	FGF-R3 wt	TK	118	112	98	78
151	FGF-R4	TK	125	128	88	91
152	FGR	TK	100	113	87	79
153	FLT3 D835Y	TK	90	90	65	32
154	FLT3 ITD	TK	107	107	78	49
155	FLT3 wt	TK	96	105	94	62
156	FRK	TK	104	112	99	75
157	FYN wt	TK	140	132	101	100
158	GRK2	AGC	94	105	101	88
159	GRK3	AGC	123	110	94	95
160	GRK4	AGC	92	88	101	97
161	GRK5	AGC	87	84	97	94
162	GRK6	AGC	61	76	88	90
163	GRK7	AGC	87	84	100	99

164	GSG2	OTHER	137	146	84	56
165	GSK3-alpha	CMGC	103	88	90	61
166	GSK3-beta	CMGC	112	111	91	85
167	HCK	TK	117	115	105	88
168	HIPK1	CMGC	91	84	103	143
169	HIPK2	CMGC	111	106	100	87
170	HIPK3	CMGC	91	94	93	90
171	HIPK4	CMGC	112	104	76	37
172	HRI	OTHER	100	87	85	66
173	IGF1-R	TK	101	95	92	86
174	IKK-alpha	OTHER	109	111	78	57
175	IKK-beta	OTHER	104	93	77	63
176	IKK-epsilon	OTHER	99	94	88	70
177	INS-R	TK	103	97	91	83
178	INSR-R	TK	137	131	81	72
179	IRAK1	TKL	103	100	50	11
180	IRAK4 (untagged)	TKL	117	123	85	56
181	ITK	TK	120	118	95	81
182	JAK1 aa583-1154 wt	TK	86	101	98	96
183	JAK2	TK	96	97	80	72
184	JAK3	TK	96	104	79	54
185	JNK1	CMGC	84	16	5	1
186	JNK2	CMGC	27	5	8	1
187	JNK3	CMGC	20	4	3	0
188	KIT A829P	TK	118	120	68	75
189	KIT D816H	TK	124	121	91	66
190	KIT D816V	TK	129	120	87	55
191	KIT T670I	TK	100	104	107	98
192	KIT V559D	TK	144	138	102	94
193	KIT V559D/T670I	TK	103	109	96	77
194	KIT V559D/V654A	TK	148	145	94	85
195	KIT V560G	TK	137	135	95	67
196	KIT V654A	TK	144	113	103	80
197	KIT wt	TK	138	119	98	101
198	LCK	TK	120	107	85	89
199	LIMK1	TKL	104	102	72	46
200	LIMK2	TKL	102	102	90	80
201	LRRK2 G2019S	TKL	102	100	72	52
202	LRRK2 I2020T	TKL	108	96	71	49
203	LRRK2 R1441C	TKL	103	96	80	51
204	LRRK2 wt	TKL	84	92	77	47
205	LTK	TK	131	123	108	99
206	LYN	TK	118	110	99	94
207	MAP3K1	STE	86	91	100	96
208	MAP3K10	STE	95	87	27	4
209	MAP3K11	STE	112	140	28	13
210	MAP3K7/MAP3K7IP1	STE	96	86	101	77
211	MAP3K9	STE	89	89	80	45
212	MAP4K2	STE	100	89	89	50
213	MAP4K4	STE	100	104	79	55
214	MAP4K5	STE	74	72	71	49
215	MAPKAPK2	CAMK	43	38	71	42
216	MAPKAPK3	CAMK	101	100	100	65
217	MAPKAPK5	CAMK	87	84	96	97
218	MARK1	CAMK	107	101	100	88
219	MARK2	CAMK	109	108	93	84
220	MARK3	CAMK	105	100	82	92
221	MARK4	CAMK	92	87	92	99

222	MATK	TK	146	119	92	111
223	MEK1 wt	STE	98	90	96	113
224	MEK2	STE	99	98	76	36
225	MEK5	STE	92	92	87	60
226	MEKK2	STE	88	88	99	88
227	MEKK3	STE	92	89	102	103
228	MELK	CAMK	102	95	95	70
229	MERTK	TK	125	118	76	41
230	MET D1228H	TK	113	117	76	65
231	MET D1228N	TK	104	96	89	74
232	MET F1200I	TK	111	111	81	59
233	MET M1250T	TK	117	115	88	65
234	MET wt	TK	106	103	93	78
235	MET Y1230A	TK	108	111	97	85
236	MET Y1230C	TK	108	114	90	76
237	MET Y1230D	TK	112	114	88	73
238	MET Y1230H	TK	97	97	92	72
239	MET Y1235D	TK	113	106	105	86
240	MINK1	STE	116	107	75	44
241	MKK4	STE	113	134	71	90
242	MKK6 S207D/T211D	STE	103	85	103	126
243	MKK7	STE	100	84	45	39
244	MKNK1	CAMK	120	118	90	55
245	MKNK2	CAMK	96	93	80	31
246	MLK4	TKL	105	131	81	59
247	MST1	STE	119	112	96	80
248	MST2	STE	106	104	83	69
249	MST3	STE	85	82	85	89
250	MST4	STE	111	124	94	97
251	mTOR	ATYPICAL	117	107	88	91
252	MUSK	TK	118	120	74	31
253	MYLK	CAMK	107	96	84	60
254	MYLK2	CAMK	111	98	83	59
255	MYLK3	CAMK	104	108	89	68
256	NEK1	OTHER	85	87	80	64
257	NEK11	OTHER	103	96	103	87
258	NEK2	OTHER	102	124	92	78
259	NEK3	OTHER	111	123	73	50
260	NEK4	OTHER	111	101	79	51
261	NEK6	OTHER	109	108	91	92
262	NEK7	OTHER	76	81	91	95
263	NEK9	OTHER	107	104	97	73
264	NIK	STE	107	96	91	87
265	NLK	CMGC	107	98	86	37
266	NPM1ALK	TK	108	105	94	96
267	NPM1ALK F1174L	TK	127	105	104	106
268	p38-alpha	CMGC	98	50	90	67
269	p38-beta	CMGC	104	93	93	75
270	p38-delta	CMGC	87	77	91	80
271	p38-gamma	CMGC	114	103	94	87
272	PAK1	STE	97	100	90	84
273	PAK2	STE	105	90	99	86
274	PAK3	STE	98	88	98	83
275	PAK4	STE	98	98	92	76
276	PAK6	STE	101	98	92	76
277	PAK7	STE	98	91	90	67
278	PASK	CAMK	107	99	81	55
279	PBK	OTHER	112	107	141	89



280	PDGFR-alpha D842V	TK	107	101	68	41
281	PDGFR-alpha T674I	TK	100	118	96	84
282	PDGFR-alpha V561D	TK	104	91	91	68
283	PDGFR-alpha wt	TK	96	104	97	72
284	PDGFR-beta	TK	109	101	74	46
285	PDK1	AGC	117	91	74	39
286	PHKG1	CAMK	110	127	80	44
287	PHKG2	CAMK	104	94	94	96
288	PIM1	CAMK	103	107	87	67
289	PIM2	CAMK	74	64	101	69
290	PIM3	CAMK	97	92	93	82
291	PKA	AGC	102	103	84	66
292	PKC-alpha	AGC	116	114	102	80
293	PKC-beta1	AGC	121	116	111	106
294	PKC-beta2	AGC	101	100	103	81
295	PKC-delta	AGC	110	117	84	94
296	PKC-epsilon	AGC	113	95	97	108
297	PKC-eta	AGC	107	106	91	78
298	PKC-gamma	AGC	105	113	88	100
299	PKC-iota	AGC	123	102	80	52
300	PKC-mu	AGC	100	93	68	31
301	PKC-nu	AGC	87	76	44	15
302	PKC-theta	AGC	114	115	97	96
303	PKC-zeta	AGC	102	85	87	86
304	PKC-zeta wt aa 184-592 (PKM-zeta)	AGC	109	108	90	68
305	PKMYT1	OTHER	95	101	74	56
306	PKN3	AGC	111	122	79	54
307	PLK1	OTHER	106	106	98	96
308	PLK3	OTHER	111	106	103	75
309	PRK1	AGC	104	104	100	91
310	PRK2	AGC	110	114	90	76
311	PRKD2	CAMK	92	92	69	43
312	PRKG1	AGC	100	91	92	87
313	PRKG2	AGC	105	97	84	81
314	PRKX	AGC	108	67	86	61
315	PYK2	TK	107	119	91	96
316	RAF1 Y340D/Y341D (untagged)	TKL	97	97	96	92
317	RET E762Q	TK	121	114	95	78
318	RET G691S	TK	112	119	90	77
319	RET M918T	TK	154	124	97	82
320	RET R749T	TK	121	113	96	76
321	RET R813Q	TK	126	117	98	75
322	RET S891A	TK	114	112	95	74
323	RET V804L	TK	107	105	88	80
324	RET V804M	TK	141	131	98	90
325	RET wt	TK	128	161	87	72
326	RET Y791F	TK	145	123	96	71
327	RIPK2	TKL	99	97	77	43
328	RIPK5	TKL	93	95	90	67
329	ROCK1	AGC	93	100	104	80
330	ROCK2	AGC	100	111	95	75
331	RON	TK	156	145	92	104
332	ROS	TK	117	109	87	74
333	RPS6KA1	AGC	85	86	82	64
334	RPS6KA2	AGC	107	90	88	69
335	RPS6KA3	AGC	86	77	81	58
336	RPS6KA4	AGC	84	104	97	94
337	RPS6KA5	AGC	103	100	94	87

338	RPS6KA6	AGC	103	115	88	68
339	S6K	AGC	124	119	105	87
340	S6K-beta	AGC	116	102	87	79
341	SAK	OTHER	103	79	77	57
342	SGK1	AGC	92	109	49	15
343	SGK2	AGC	85	84	93	71
344	SGK3	AGC	122	102	82	76
345	SIK1	CAMK	107	107	107	102
346	SIK2	CAMK	98	95	108	90
347	SIK3	CAMK	109	107	65	47
348	SLK	STE	114	133	102	76
349	SNARK	CAMK	98	99	99	87
350	SNK	OTHER	100	103	86	81
351	SRC (GST-HIS-tag)	TK	123	123	98	86
352	SRM5	TK	107	104	95	92
353	SRPK1	CMGC	92	106	99	86
354	SRPK2	CMGC	104	87	82	75
355	STK17A	CAMK	84	78	78	35
356	STK23	CAMK	115	107	97	101
357	STK25	STE	86	81	88	95
358	STK33	CAMK	99	98	76	71
359	STK39	STE	105	77	100	73
360	SYK aa1-635	TK	114	110	94	86
361	TAOK2	STE	107	92	38	16
362	TAOK3	STE	95	102	95	72
363	TBK1	OTHER	88	95	84	69
364	TEC	TK	98	96	99	81
365	TGFB-R1	TKL	96	94	106	92
366	TGFB-R2	TKL	111	128	53	4
367	TIE2 R849W	TK	87	96	92	107
368	TIE2 wt	TK	136	18	85	81
369	TIE2 Y1108F	TK	128	128	95	96
370	TIE2 Y897S	TK	118	110	85	85
371	TLK1	AGC	105	112	97	90
372	TLK2	AGC	92	91	92	83
373	TNK1	TK	103	111	91	61
374	TRK-A	TK	115	111	81	58
375	TRK-B	TK	96	105	89	81
376	TRK-C	TK	116	110	99	79
377	TSF1	OTHER	96	93	23	6
378	TSK2	CAMK	91	87	90	97
379	TSSK1	CAMK	86	77	76	72
380	TTBK1	CK1	96	102	102	106
381	TTBK2	CK1	96	84	94	93
382	TTK	OTHER	107	111	72	34
383	TXK	TK	98	98	87	77
384	TYK2	TK	97	94	77	46
385	TYRO3	TK	114	104	100	86
386	VEGF-R1	TK	106	93	84	66
387	VEGF-R2	TK	121	110	78	50
388	VEGF-R3	TK	112	93	73	68
389	VRK1	CK1	72	70	95	97
390	VRK2	CK1	101	73	97	83
391	WEE1	OTHER	113	120	73	79
392	WNK1	OTHER	127	106	95	81
393	WNK2	OTHER	74	85	98	78
394	WNK3	OTHER	120	99	79	67
395	YES	TK	113	100	89	75

396	ZAK	TKL	98	95	48	15
397	ZAP70	TK	127	114	88	93
398	PI4K2A	Lipid Kinase	113	113	117	133
399	PI4K2B	Lipid Kinase	113	112	128	120
400	PI4KB	Lipid Kinase	91	92	101	79
401	PIK3C2A	Lipid Kinase	138	152	189	183
402	PIK3C2B	Lipid Kinase	109	139	132	133
403	PIK3C2G	Lipid Kinase	145	155	129	108
404	PIK3C3	Lipid Kinase	98	99	108	103
405	PIK3CA/PIK3R1	Lipid Kinase	108	108	118	106
406	PIK3CB/PIK3R1	Lipid Kinase	132	131	138	166
407	PIK3CD/PIK3R1	Lipid Kinase	110	108	119	113
408	PIK3CG	Lipid Kinase	109	115	176	156
409	PIPSK1A	Lipid Kinase	94	100	102	44
410	PIPSK1C	Lipid Kinase	114	111	107	102
Selectivity Score (<50 % residual activity):			<b>0.007</b>	<b>0.015</b>	<b>0.037</b>	<b>0.146</b>

\*Classification of protein kinase families:<sup>2</sup>

**AGC:** containing PKA, PKG and PKC families

**CAMK:** Calcium/Calmoduline-dependent protein kinases

**CK1:** Casein kinase 1-like

**CMGC:** containing CDK, MAPK, GSK3 and CLK families

**TK:** Tyrosine Kinase

**TKL:** Tyrosine Kinase-like

**STE:** Homologs of Yeast Sterile 7, Sterile 11, Sterile 20 Kinases

**Direct enzyme-linked immunosorbent assay (ELISA) for routine screening of p38 $\alpha$  MAPK and JNK3 inhibitors**

Being a natural substrate of both p38 $\alpha$  MAP kinase and JNK3, activation transcription factor 2 (ATF-2) purchased from ProQinase, Freiburg, Germany (# 0594-0000-2) as full-length protein is adsorbed to the 96 well assay plates (Nunc Maxisorp<sup>®</sup>) yielding a concentration of 10  $\mu$ g/mL.

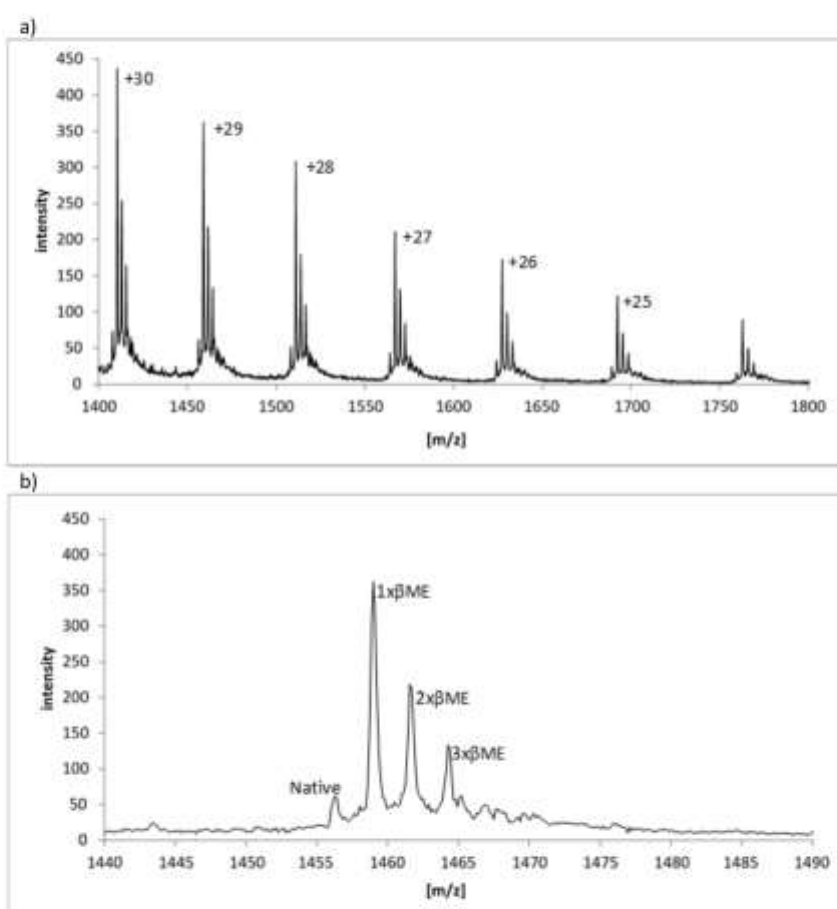
Dilution rows of candidate inhibitor are prepared in a kinase buffer containing active p38 $\alpha$  MAP kinase or activate JNK3 enzyme. The active p38 $\alpha$  MAP kinase was obtained from Prof. Dr. J. Schultz (University of Tübingen, Germany), whereas the active JNK3 enzyme was purchased from ProQinase, Freiburg, Germany (#0900-0000-1). The ATP concentrations used in the respective kinase buffers are adjusted to twice the  $K_m$  value, depending on the kinase.

The activity of p38 $\alpha$  MAP kinase or JNK3 kinase after one hour of incubation at 37°C with the candidate inhibitors is measured by the phosphorylation degree of ATF-2, which is directly detected by a monoclonal peroxidase-conjugated antibody purchased from Sigma Aldrich (#A6228). The phosphorylation degree achieved with the respective kinase in absence of inhibitor is taken as positive control (STIM). Pure kinase buffer without kinase serves for detection of non-specific binding (NSB). After staining with 3,3',5,5'-tetramethylbenzidine reagent (BD Biosciences Europe) and termination of colour development using 1M sulphuric acid, the optical density is read out in an ELISA reader at 450 nm. As phosphorylation is inversely correlated with the inhibitor potency, the calculation of inhibition is carried out according to the formula.<sup>6,7</sup>

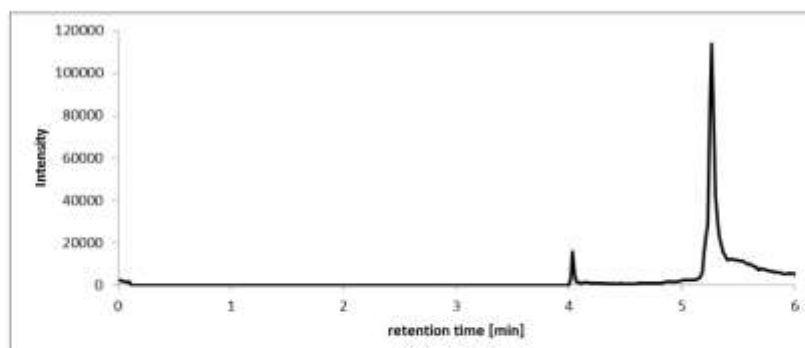
$$\text{Inhibition[\%]} = 100 - \left( \frac{OD_{450} \text{Sample} - OD_{450} \text{NSB}}{OD_{450} \text{STIM} - OD_{450} \text{NSB}} \right) \times 100$$

### Investigation of the covalent bond formation using LC- $\mu$ ESI-QTOF mass spectrometry

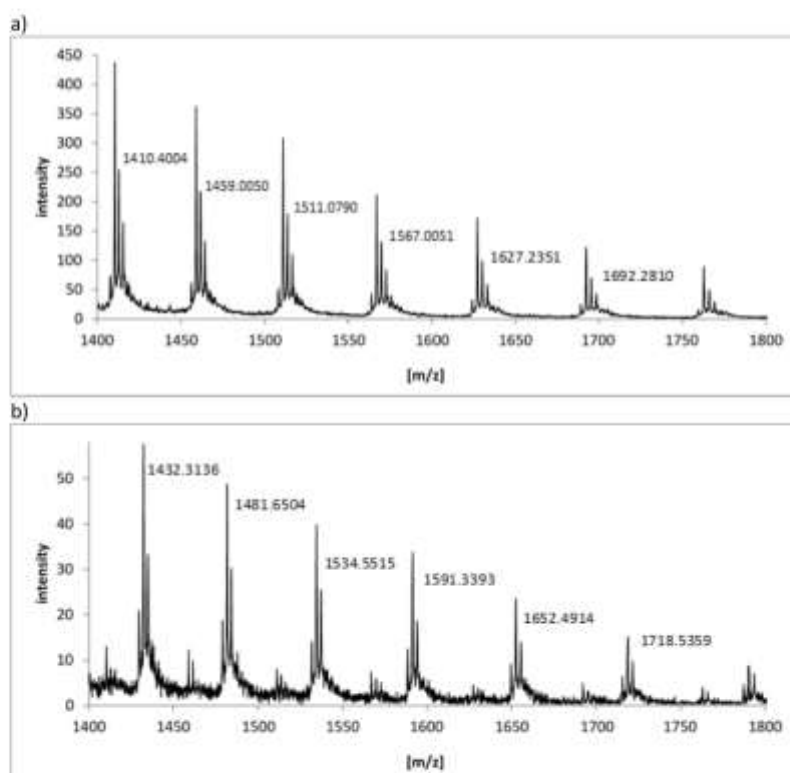
Covalent bonding has been verified by LC- $\mu$ ESI-QTOF mass spectrometry of intact JNK3. Potential noncovalent interactions have been eliminated by chromatography prior to ESI-ionisation and the employment of a high declustering potential (DP) of 230V. This is substantiated by the charge series of intact JNK3 consisting only of  $[M+nH]^{n+}$  ions, i.e. only  $H^+$ -adduct series has been found. Further evidence is provided by **15**, an analogue of **7** with inactive, non-Michael-reactive warhead. Presumably noncovalent bonding to the ATP-binding site is disrupted during chromatography and/or the ESI-process due to application of high declustering potential. Results show (s. Figures S3a, S3c and S3e), that inactive species produce the same spectrum like the control (unmodified JNK3), confirming that only active ligands result in a mass shift corresponding to the mass of the inhibitor (Figures S3b and S3d) by covalent modification of JNK3.

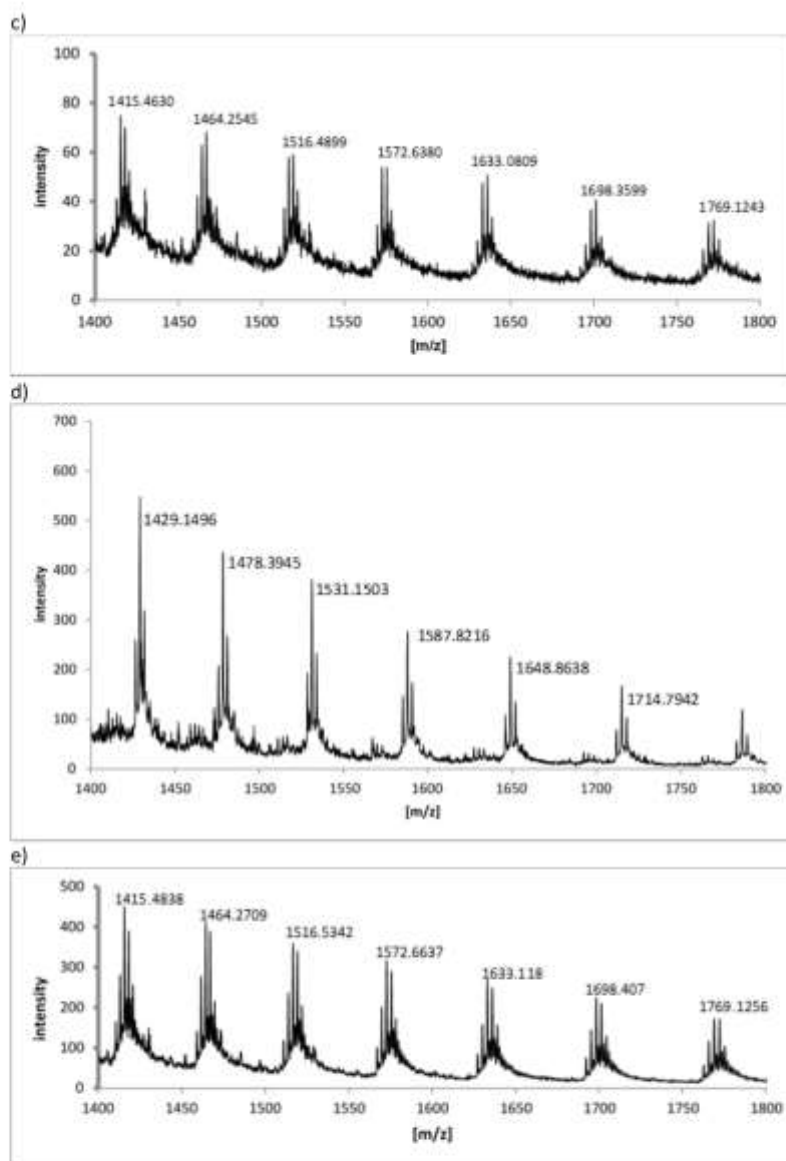


**Figures S1. Charge series of JNK3.** a) Charge series consists exclusively of  $H^+$ -adducts. Charge states from +30 to +25 have been used for intact protein mass deconvolution. Charge series deconvolutes to  $M = 42281.9073$  (1x $\beta$ ME-JNK3). Calculated  $M$  for 1x $\beta$ ME-JNK3 is 42281.8941, mass accuracy 0.3ppm; b) Triplet structure of charge series is caused by 1-3 times  $\beta$ -mercaptoethanoylation.

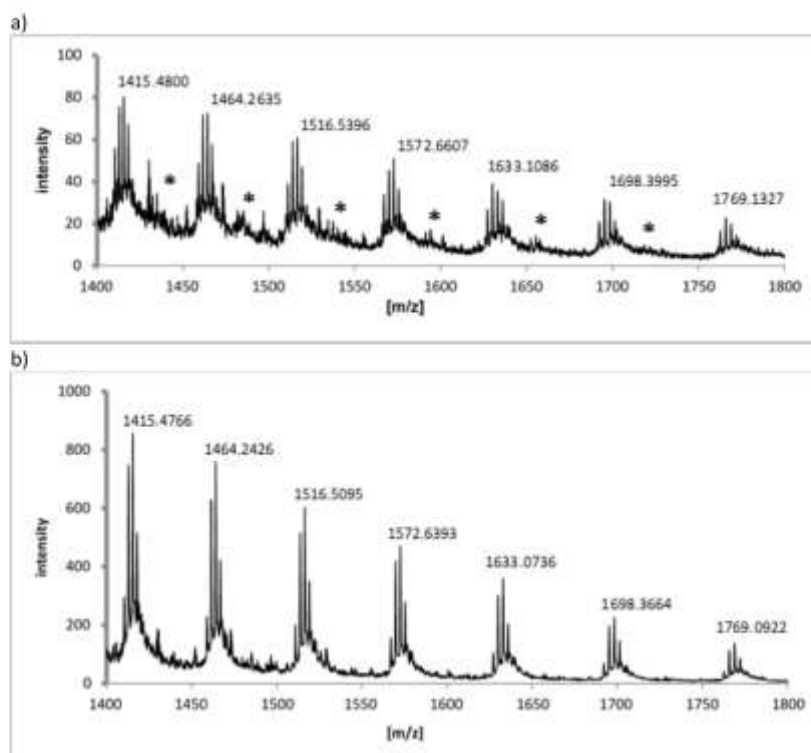


**Figure S2. Chromatogram of JNK3.** First 4 minutes have been switched to waste via valve, effectively preventing the reaction buffer from entering the ESI-source. JNK3 eluting at  $t = 5.2$  min.



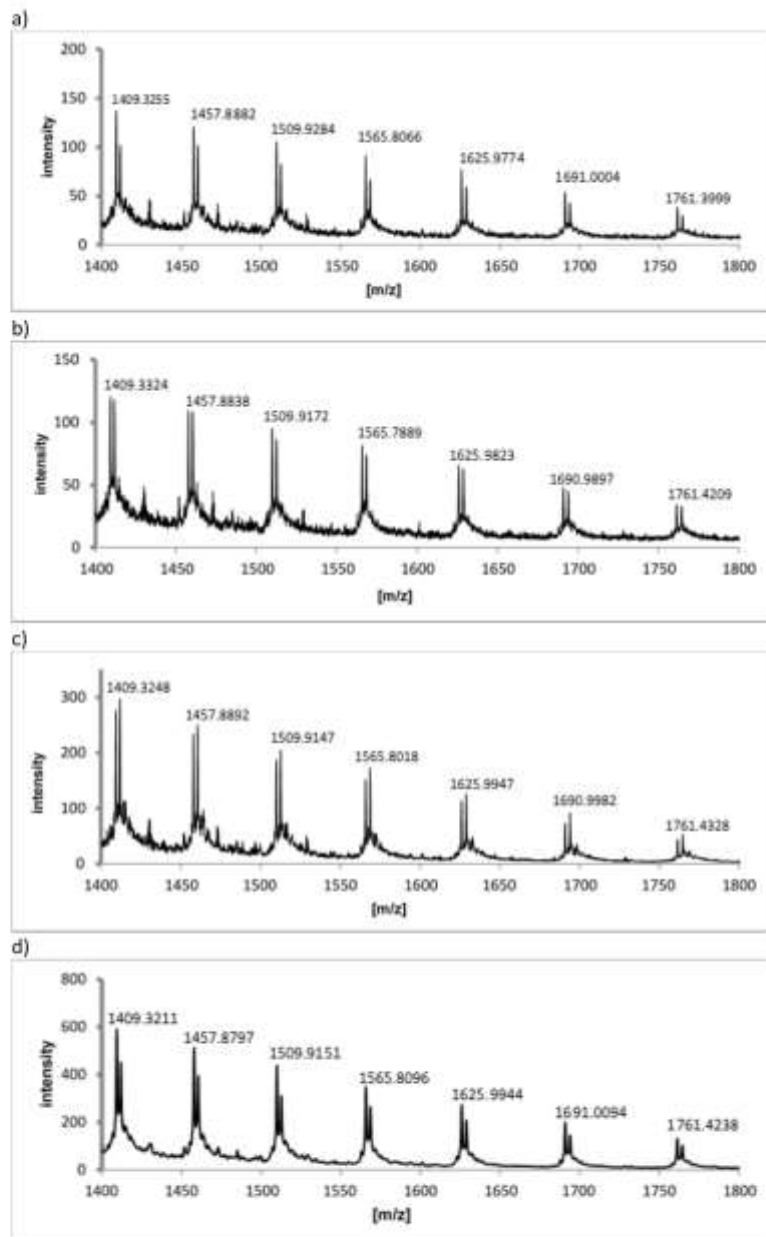


**Figures S3. Charge series after 1 h of incubation of JNK3 wt with 5 molar excess of inhibitor.** a) Control, only JNK3; b) **7**, reactive warhead (para/meta substituent), mass shift according to mass of ligand. Small residual of unmodified JNK3 present; c) **8**, no reactive warhead (saturated counterpart of **7**), spectrum identical to control, no covalent bonding to JNK3; d) **21**, reactive warhead, mass shift according to mass of ligand; e) **23**, no reactive warhead (saturated counterpart of **21**), spectrum identical to control, no covalent bonding to JNK3.



**Figures S4. Charge series after 1 h of incubation of JNK3 wt with 5 molar excess of inhibitor.** a) Binding assay with **14**. For **14**, that exhibits some activity in  $IC_{50}$ -Assay, binding to some extent was observed, as minor charge series denoted by (\*). For identification, most intense charge series of [JNK3-3x $\beta$ ME-1x410] was chosen, with m/z-series of 1434.8416; 1484.2622; 1537.2659; 1594.1314; 1655.3635; 1721.6486; 1793.2949; for deconvolution. Binding ratio was calculated comparing area in 50mDa corridor around target mass after baseline subtraction to 29% bound and 71 unbound. Unmodified [JNK3+3x $\beta$ ME] charge series: 1415.4822; 1464.2572; 1516.5161; 1572.6461; 1633.0937; 1698.3772; 1769.1009; b) **15**, no reactive warhead (saturated counterpart of **14**), spectrum identical to control, no covalent bonding to JNK3.





**Figure S5. Charge series after 1h of incubation of with Cys154 → Ala154-mutant of JNK3 with 5 molar excess of inhibitor.** a) control; b) 7; c) 21; d) 14; No covalent modification by inhibitors could be observed, precluding reactivity with other than target Cys154. Protein was visible as  $\beta$ -ME-adduct-series ranging from 0 to 4 mercaptoethanoylations. For mass accuracy, the intense 1x  $\beta$ -mercaptoethanol-adduct was chosen (left one of each peak doublets) for evaluation. Theoretical charge series of unmodified [Cys→Ala-JNK3-1x $\beta$ -ME]: 1409.3247; 1457.8874; 1509.9188; 1565.8044; 1625.9889; 1690.9882; 1761.4041.

**Table S2. Calculations of ligand masses from charge series deconvolution.**

Cmp #	Protein Mass			Ligand Mass shift	
	Calculated	Measured	error ppm	Expected	Found
7	42784.5576	42784.2239	-7.8	578.3280	578.6617
8	42205.8959	42205.51046	9.1	0	0
15	42205.8959	42205.9047	0.2	0	0
21	42690.4710	42690.1030	-8.6	484.2071	484.2071
23	42205.8959	42206.342	10.5	0	0

All calculations show the covalent binding of the inhibitors could be proved by sub Dalton mass accuracy. Inhibitor models without reactive warhead do not show any binding to JNK3.

Note: Ligand masses are denoted as average masses, as protein mass spectrometry in the mass range of the target is performed on average rather than monoisotopic peaks. For easy comparison the deconvoluted masses of the protein-ligand adducts have been corrected for mercaptoethanoylation.

## Materials and Methods

### LC-QTOF- $\mu$ ESI-MS of intact JNK3-Ligand adducts

Analysis was performed on a Sciex (Concord, Ontario, Canada) 5600+ TripleTOF mass spectrometer equipped with an Agilent (Waldbronn, Germany) 1290 Series UHPLC and a PAL-xts (CTC, Zwingen, Switzerland) autosampler for injection. Chromatographic separation was conducted using a ProsWIFT (Thermo Scientific, Waltham, USA) 100 x 0.5 mm monolithic polystyrene-divinylbenzene copolymer capillary column. Mobile phases consisted of A: H<sub>2</sub>O, 0.1 % formic acid and B: acetonitrile, 0.1 % formic acid. Gradient profile was 0 - 1.5 min 20 % B, 1.5 - 4.5 min: 20 - 80 % B, 4.5 - 6 min 95 % B. Flow rate: 50  $\mu$ l/min. First 4 minutes were switched to waste to prevent buffer components from entering the ESI-source. Column temperature was kept at 22 °C. Injection volume was 5  $\mu$ l, corresponding to 5 pmol JNK3 absolute per injection. Acetonitrile and formic acid were of Ultra-MS-grade, purchased from Carl Roth (Karlsruhe, Germany). Ultra-MS-grade water was produced using an Elga (Veolia Water Technologies, Germany) Purelab Ultra system.

For  $\mu$ flow-electrospray ionization ( $\mu$ ESI) the Sciex Duospray Ionsource was outfitted with a 50  $\mu$ m I.D. PEEKsil-stainless steel tip hybrid micro-electrode. Mass spectrometry was done using SCIEX "Intact Protein Mode"-Script with a detector voltage (CEM) lowered by 100V. MS parameters were as follows: gas1 (nebulizer) 50 psi, gas2 (drying gas) 40 psi, curtain gas 30 psi, source temperature 400 °C, ion source floating voltage (ISFV) 5200V. Collision energy (CE) was set to protein mode typical 30V facilitating clearance of Q2 (collision cell). Declustering potential (DP) was set to 230V for removal of non-covalent species. Q1 transmission: 100 % at 1250 m/z. time bins: 100. Positive-TOF-mode mass scan: 500-4000 m/z.

### Sequence of recombinant JNK3 (average mass was 42205.8959 Da)

GGSMSSKSKVDNQFYSEVVDSTFTVLKRYQNLKPIGSGAQGIVCAAYDAVLDNRNVAIKKLSRPFQNTQTHAKRAYRELVLMLK  
CVNHKNIISLLNVFTPQKTLLEEFQDVYLVMEMLMDANLCQVIQMELDHERMSYLLYQMLCGIKHLHSAGIIHRDLKPSNIVVKS  
DCTLKILDFGLARTAGTSFMMTPYVVTRYRAPEVILGMGYKENVDIWSVGCIMGEMVRHKILFPGRDYIDQWNVKIEQLG  
TPCPPEFMKKLQPTVRNYVENRPKYAGLTFPKLFPDSLFPADSEHNKLGKASQARDLLSKMLVIDPAKRISVDDALQHPYINVVY  
DPAEVEAPPPQIYDKQLDEREHTIEEWKELIYKEVMNSE

### Sequence of mutant JNK3 (average mass 42173.8359 Da)

GGSMSSKSKVDNQFYSEVVDSTFTVLKRYQNLKPIGSGAQGIVCAAYDAVLDNRNVAIKKLSRPFQNTQTHAKRAYRELVLMLK  
CVNHKNIISLLNVFTPQKTLLEEFQDVYLVMEMLMDANL(A)QVIQMELDHERMSYLLYQMLCGIKHLHSAGIIHRDLKPSNIVV  
KSDCTLKILDFGLARTAGTSFMMTPYVVTRYRAPEVILGMGYKENVDIWSVGCIMGEMVRHKILFPGRDYIDQWNVKIEQLG  
LGTCPPEFMKKLQPTVRNYVENRPKYAGLTFPKLFPDSLFPADSEHNKLGKASQARDLLSKMLVIDPAKRISVDDALQHPYINVVY  
WYDPAEVEAPPPQIYDKQLDEREHTIEEWKELIYKEVMNSE

**Binding assay**

Binding assay was performed in 60 mM ammonium acetate. Reaction volume was 200  $\mu$ l, containing 200 pmol of JNK3 and 1 nmol of inhibitor and 0.5 % (v/v) DMSO. Binding reaction was performed at 37 °C for 1h. Samples were analyzed immediately afterwards, stored at 4 °C in the autosampler during analysis.

### In vitro reactivity study of inhibitor 7 with glutathione

The *in vitro* reactivity of covalent inhibitor **7** was determined similar to a protocol published by Schmidt *et al.*<sup>8</sup> This protocol was adapted by using the conditions of our in house kinase assay (buffer, reaction time and temperature). *N*-Phenylacrylamide (PAA) served as a positive control since it is known that PAA forms adducts with glutathione under physiological conditions.<sup>9</sup>

Buffer: 50 mM Tris [pH 7.5], 10 mM MgCl<sub>2</sub>, 10mM β-glycerolphosphate, 100 μg/ml BSA, 1 mM dithiothreitol, 0.1 mM Na<sub>3</sub>VO<sub>4</sub>

**Table S3.** Incubation of compound **7** (10 μM) and PAA (10 μM) with 5 mM glutathione

time [min]	cpd <b>7</b> [%]	PAA [%]
0	99.9	100
9	99.2	91.6
18	98.5	86.1
27	97.6	81.0
36	96.8	76.7
45	96.1	70.5
54	93.7	66.5

### In Vitro Metabolism Studies

Pooled human male liver microsomes (HLM) were purchased from Sigma-Aldrich (Steinheim, Germany). These microsomes were characterized in protein and cytochrome P-450 content. All incubations were made in the presence of an NADPH-regenerating system, consisting of 5 mM Glucose-6-phosphate, 5 U/mL Glucose-6-phosphate dehydrogenase and 1 mM NADP<sup>+</sup>. The substrate (100  $\mu$ M), the NADPH regenerating system and 3.8 mM MgCl<sub>2</sub> x 6 H<sub>2</sub>O in 0.1 M Tris-buffer (pH = 7.4 at 37 °C) were preincubated for 5 min in a shaking heating block at 37 °C and 550 rpm.<sup>10</sup> The incubation mix was split into 75  $\mu$ L aliquots and the reaction was started by addition of the HLM. Thereby the microsomal protein content was standardized to 1 mg/mL. To follow the course of metabolism, the reaction tubes were quenched at selected time points (0, 10, 20, 30, 45, 60, 130/135 and 180/190 min; analyte **7/21**) by adding 225  $\mu$ L icecooled internal standard at a concentration of 100  $\mu$ M for **7** and 20  $\mu$ M for **21** in acetonitrile (ACN). The samples were vortexed for 30 s and centrifuged (19800 relative centrifugal force/4°C/20 min). The supernatant was directly used for LC-MS analysis. All incubations were conducted in triplicates and incubations with heat-inactivated HLM were used to proof that analyte reduction results from metabolic degradation only. In all incubations a limit of 1 % organic solvent was not exceeded.<sup>11</sup>

### Screening of Metabolites by LC-MS Analysis

Metabolite formation was analyzed with an Alliance 2695 Separations Module (Waters GmbH, Eschborn). Samples were maintained at 4 °C, the column temperature was set to 40 °C and injection volume was 10  $\mu$ L. The chromatographic separation of analyte **7** was performed on a Waters Symmetry<sup>®</sup>C18 (150 x 4.6 mm; 5  $\mu$ m); **21** on a Phenomenex Synergi Max RP column (150 x 4.6 mm; 5  $\mu$ m) with a precolumn of the same material, respectively. An isocratic elution of 11.0 min for **7** and 8.0 min for **21** with 63 % solvent A (90 % H<sub>2</sub>O, 10 % ACN, 0.1 % formic acid) and 37 % solvent B (ACN, 0.1 % formic acid) at a flow rate of 400  $\mu$ L/min was used. The detection was performed on a Micromass Quattro micro triple quadrupole mass spectrometer (Waters GmbH, Eschborn) using the electrospray ionization in the positive-mode. Correspondent to the analyte the spray voltage was set to 3.5 - 4.25 kV. The heated capillary operated at 250 °C and the desolvation gas flow worked at 500 L/h.

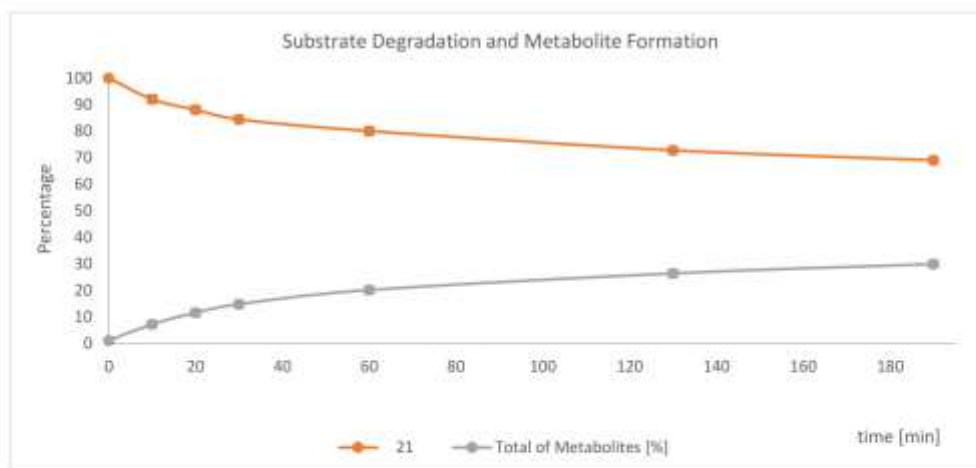
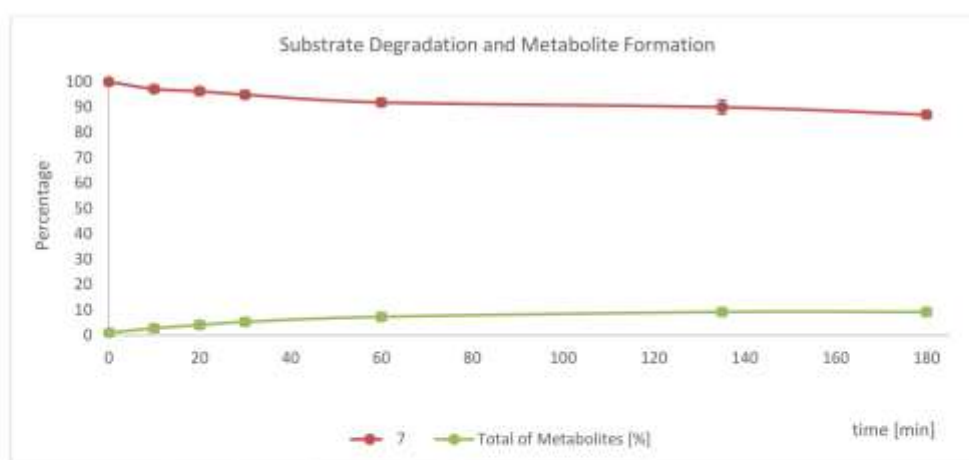


Figure S6. Degradation scheme of compound **21** while incubating in HLM for 190 min.



**Figure S7.** Degradation scheme of compound **7** while incubating in HLM for 180 min.

**Table S4.** Metabolic stability

Cmp	IC <sub>50</sub> [nM]		
	JNK3	p38α	OxMet <sup>a</sup>
21	2	1,952	69 <sup>b</sup>
7	<1	36	87 <sup>c</sup>

<sup>a</sup>Percent remaining after incubation with HLM; <sup>b</sup>incubation time: 190 min; <sup>c</sup>incubation time: 180 min.

**References**

1. Laufer, S.; Hauser, D.; Stegmüller, T.; Bracht, C.; Ruff, K.; Schattel, V.; Albrecht, W.; Koch, P. Tri- and tetrasubstituted imidazoles as p38 alpha mitogen-activated protein kinase inhibitors. *Bioorg. Med. Chem. Lett.* **2010**, *20*, 6671-6675.
2. Ansideri, F.; Lange, A.; El-Gokha, A.; Boeckler, F. M.; Koch, P. Fluorescence polarization-based assays for detecting compounds binding to inactive c-Jun N-terminal kinase 3 and p38 $\alpha$  mitogen-activated protein kinase. *Anal. Biochem.* **2016**, *503*, 28-40.
3. Schrödinger, LLC. Small-Molecule Drug Discovery Suite 2015-4: Glide, version 6.9. In New York, 2015.
4. Schrödinger, LLC. The PyMOL molecular graphics system, version 0.99. In New York, 2006.
5. Manning, G.; Whyte, D. B.; Martinez, R.; Hunter, T.; Sudarsanam, S. The Protein Kinase Complement of the Human Genome. *Science* **2002**, *298*, 1912-1934.
6. Goettert, M.; Graeser, R.; Laufer, S. A. Optimization of a nonradioactive immunosorbent assay for p38 alpha mitogen-activated protein kinase activity. *Anal. Biochem.* **2010**, *406*, 233-234.
7. Goettert, M.; Luik, S.; Graeser, R.; Laufer, S. A. A direct ELISA assay for quantitative determination of the inhibitory potency of small molecules inhibitors for JNK3. *J. Pharm. Biomed. Anal.* **2011**, *55*, 236-240.
8. Schmidt, T. J.; Ak, M.; Mrowietz, U. Reactivity of dimethyl fumarate and methylhydrogen fumarate towards glutathione and N-acetyl-L-cysteine - Preparation of S-substituted thiosuccinic acid esters. *Bioorg. Med. Chem.* **2007**, *15*, 333-342.
9. Cee, V. J.; Volak, L. P.; Chen, Y. P.; Bartberger, M. D.; Tegley, C.; Arvedson, T.; McCarter, J.; Tasker, A. S.; Fotsch, C. Systematic study of the glutathione (GSH) reactivity of N-arylacrylamides: 1. Effects of aryl substitution. *J. Med. Chem.* **2015**, *58*, 9171-9178.
10. Baur, B.; Storch, K.; Martz, K. E.; Goettert, M. I.; Richters, A.; Rauh, D.; Laufer, S. A. Metabolically stable dibenzo[b,e]oxepin-11(6H)-ones as highly selective p38 MAP kinase inhibitors: optimizing anti-cytokine activity in human whole blood. *J. Med. Chem.* **2013**, *56*, 8561-8578.
11. Chauret, N.; Gauthier, A.; Nicoll-Griffith, D. A. Effect of common organic solvents on in vitro cytochrome P450-mediated metabolic activities in human liver microsomes. *Drug Metab. Dispos.* **1998**, *26*, 1-4.





## Publication V

Ansideri, F.; Andreev, S.; Kuhn, A.; Albrecht, W.; Laufer, S. A.; Koch, P. A Diverse and Versatile Regiospecific Synthesis of Tetrasubstituted Alkylsulfanylimidazoles as p38 $\alpha$  Mitogen-Activated Protein Kinase Inhibitors. *Molecules* **2018**, *23*, 221.

**Open access publication**


**Link to the published version:**

<http://www.mdpi.com/1420-3049/23/1/221>



Article

## A Diverse and Versatile Regiospecific Synthesis of Tetrasubstituted Alkylsulfanylimidazoles as p38 $\alpha$ Mitogen-Activated Protein Kinase Inhibitors

Francesco Ansideri<sup>1</sup>, Stanislav Andreev<sup>1</sup>, Annette Kuhn<sup>1</sup>, Wolfgang Albrecht<sup>2</sup>,  
Stefan A. Laufer<sup>1</sup> and Pierre Koch<sup>1,\*</sup> 

<sup>1</sup> Institute of Pharmaceutical Sciences, Department of Medicinal and Pharmaceutical Chemistry, Eberhard Karls Universität Tübingen, Auf der Morgenstelle 8, 72076 Tübingen, Germany; francesco.ansideri@uni-tuebingen.de (F.A.); stanislav.andreev@uni-tuebingen.de (S.A.); annette.kuhn@uni-tuebingen.de (A.K.); stefan.laufer@uni-tuebingen.de (S.A.L.)

<sup>2</sup> Teva-Ratiopharm, Graf-Arco-Str. 3, 89079 Ulm, Germany; wolfgang.albrecht@ratiopharm.de

\* Correspondence: pierre.koch@uni-tuebingen.de; Tel.: +49-7071-29-74579

Received: 12 December 2017; Accepted: 17 January 2018; Published: 20 January 2018

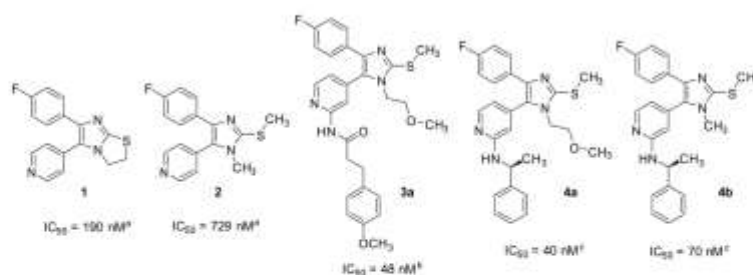
**Abstract:** An alternative strategy for the synthesis of 1-aryl- and 1-alkyl-2-methylsulfanyl-4-(4-fluorophenyl)-5-(pyridin-4-yl)imidazoles as potential p38 $\alpha$  mitogen-activated protein kinase inhibitors is reported. The regioselective *N*-substitution of the imidazole ring was achieved by treatment of  $\alpha$ -aminoketones with different aryl or alkyl isothiocyanates. In contrast to previously published synthesis routes starting from 2-amino-4-methylpyridine, the presented route is characterized by a higher flexibility and a lower number of steps. This strategy was also applied to access 1-alkyl-2-methylsulfanyl-5-(4-fluorophenyl)-4-(pyridin-4-yl)imidazoles in six steps starting from 2-chloro-4-methylpyridine.

**Keywords:** regiospecific synthesis; tetrasubstituted imidazoles; p38 $\alpha$  MAP kinase

### 1. Introduction

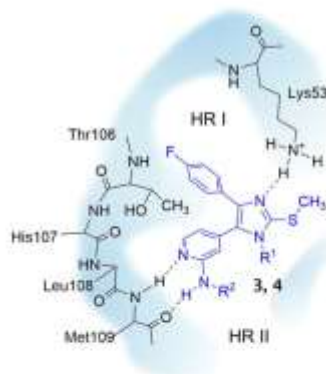
The p38 $\alpha$  mitogen-activated protein (MAP) kinase is a serine/threonine kinase, which plays a role in signal transduction pathways, modulating the cellular response to external stress stimuli like infection, heat or osmotic shock, UV light, and inflammatory cytokines [1]. Through phosphorylation of multiple downstream targets, this kinase triggers a wide range of cellular processes mostly resulting in the stimulation of the inflammatory reaction (e.g., release of pro-inflammatory cytokines like tumor necrosis factor- $\alpha$ , interleukin-1 $\beta$ , and interleukin-6 and induction of COX-2 transcription) [1,2]. The function of the p38 $\alpha$  MAP kinase has therefore been regarded as crucial in those cytokine-driven chronic inflammatory conditions like rheumatoid arthritis, Crohn's disease, psoriasis, and chronic asthma [3,4]. Additionally, several studies suggested that the p38 $\alpha$  MAP kinase may also play a role as a major character in the pathogenesis of neurodegenerative diseases such as Alzheimer's disease, Parkinson's disease and multiple sclerosis [5–8]. Due to this well-documented physiopathological role, inhibition of the p38 $\alpha$  MAP kinase has been widely pursued in many medicinal chemistry programs [9,10].

Pyridinylimidazoles represent a privileged scaffold in the field of kinase inhibition, especially concerning the targeting of the p38 $\alpha$  MAP kinase, as very recently reviewed by some of us [11]. In particular, tetrasubstituted pyridinylimidazoles like compounds **2**, **3a**, **4a** and **4b** [12–15] represent adenosine triphosphate (ATP)-competitive inhibitors of p38 $\alpha$  MAP kinase, which might be considered as open analogues of the imidazolthiazolidine-based early lead compound SKF86002 (**1**) from SmithKline & French [16] (Figure 1).



**Figure 1.** Early lead compound SKF86002 (1) and 1,2,4,5-tetrasubstituted imidazoles 2, 3a, 4a and 4b as p38 $\alpha$  MAP kinase inhibitors. <sup>a</sup> unpublished data from our research group; compounds tested in assay conditions described by Goettert et al. [17]; <sup>b</sup> data taken from [14]; <sup>c</sup> data taken from [15].

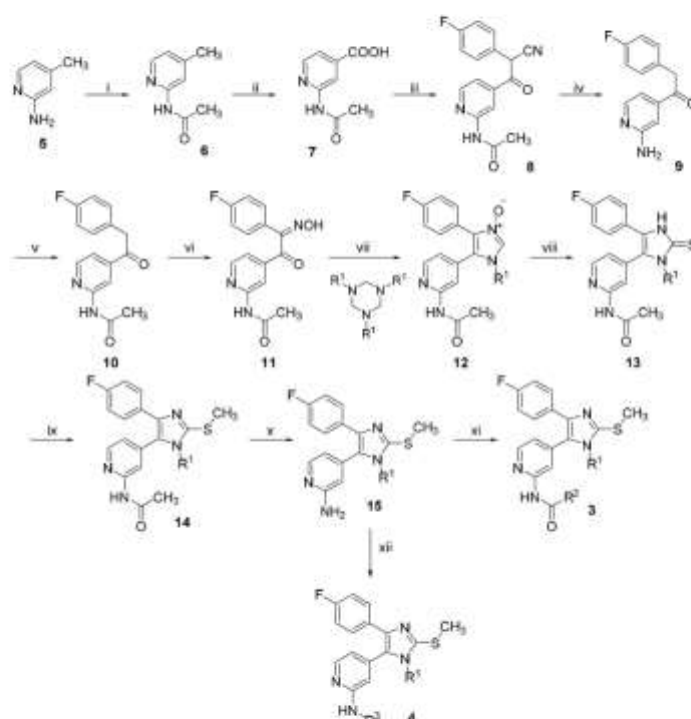
Figure 2 shows the well-described binding mode of tetrasubstituted pyridinylimidazoles like compounds 2, 3a, 4a and 4b within the ATP cleft of the p38 $\alpha$  MAP kinase. Worth to mention are the occupation of two hydrophobic pockets named hydrophobic region (HR) I and HR II as well as the formation of a hydrogen bond with the conserved Lys53 side chain. Tetrasubstituted pyridinylimidazoles were initially reported to display a lower inhibitory activity in comparison to the analogous trisubstituted derivatives lacking the substituent on the imidazole-N1 atom [18]. Nevertheless, it was observed that by inserting opportune substituents at this position, a high potency could still be maintained, probably thanks to additional interactions. Furthermore, some tetrasubstituted pyridinylimidazoles showed a markedly reduced inhibition of the CYP450 enzymes, considered one of the major drawbacks of their trisubstituted counterparts [13].



**Figure 2.** Binding mode of tetrasubstituted imidazoles bearing an acylamino or alkylamino group at the pyridine-C2 position. Figure modified from ref. [19].

Due to the binding mode of this class of inhibitors, a compulsory structural requisite is that the substituted imidazole-N atom is the one adjacent to the pyridine ring. Substitution on the imidazole-N atom proximal to the 4-fluorophenyl ring would instead prevent the formation of the hydrogen bond with Lys53 and has been reported to cause a tremendous drop in inhibitory activity [20]. For this reason, in order to preserve their binding affinity to the p38 $\alpha$  MAP kinase, these inhibitors need to be accessed through a regiospecific synthetic route.

The first synthetic route toward tetrasubstituted 2-alkylsulfanylimidazoles was reported in 2002 and 2003 (Scheme 1) [21,22] and was subsequently employed in several studies on kinase inhibitors [13–15,23–25]. This route, comprising eleven steps, starts from 2-amino-4-methylpyridine (5) which was first protected as an acetamide and successively oxidized to a carboxylic acid. Ethanone 9 was then obtained by coupling with 4-fluorophenylacetonitrile followed by hydrolysis-decarboxylation reaction of the resulting cyanoketone 8, causing the simultaneous cleavage of the *N*-acetyl protecting group. After repeating the protection step, ethanone 10 was converted into the  $\alpha$ -oximinoketone 11, and then cyclized with an opportunistically substituted 1,3,5-trialkyltriazinane to regioselectively afford imidazole-*N*-oxides 12. Intermediates 12 were then transformed into the corresponding imidazole-2-thiones 13 and then methylated on the exocyclic sulphur. Finally, the amino group of compounds 14 was deprotected and then coupled with different carboxylic acids to produce final compounds 3. From intermediates 15 it is also possible to obtain alkylamino derivatives 4 by nucleophilic substitution reaction with alkyl halides [13].



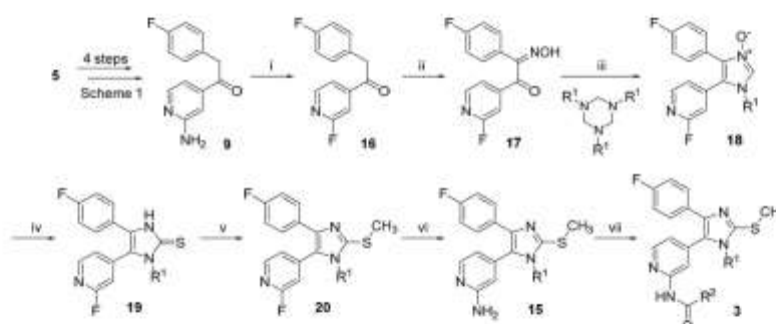
**Scheme 1.** Synthetic pathway toward 1,2,4,5-tetrasubstituted imidazoles 3 and 4. Reagents and conditions: (i)  $\text{Ac}_2\text{O}$ , DMAP, reflux temperature; (ii)  $\text{KMnO}_4$ ,  $\text{H}_2\text{O}$ , 50–90 °C; (iii) CDI, DME, *t*-BuOK, 120 °C; (iv)  $\text{HBr}$ , reflux temperature; (v)  $\text{Ac}_2\text{O}$ , DMAP, reflux temperature; (vi) isoamyl nitrite, MeONa, MeOH, rt; (vii) EtOH, reflux temperature; (viii) 2,2,4,4-tetramethylcyclobutane-1,3-dithione, DCM, rt; (ix) iodomethane,  $\text{Na}_2\text{CO}_3$ , EtOH, rt; (x) 10%  $\text{HCl}_{(\text{aq})}$ , reflux temperature; (xi)  $\text{R}^2\text{-COCl}$ ,  $\text{NEt}_3$ , THE, 0 °C or  $\text{R}^2\text{-COOH}$ , CDI, *N*-methylpyrrolidinone, rt, then 120 °C; (xii)  $\text{R}^3\text{-Br}$ , NaH, DME, rt.

This reported route noticeably entails a large number of steps and the preparation of intermediate 10 is particularly inconvenient due to the repeated introduction and cleavage of the *N*-acetyl



protecting group. An additional drawback of the reported route is the flexibility of application. As reported from the authors, this route is indeed not suitable for the introduction of aryl or heteroaryl moieties at the imidazole-N1 position [22]. Moreover, the functionalization of the pyridine-C2 position by nucleophilic substitution reaction of 2-aminopyridine derivatives **15** and alkyl halides represents a limitation when introducing alkyl groups featuring a stereocenter adjacent to the amino moiety. The use of chiral alkyl halides can indeed result in inversion of configuration or racemization, thus hampering the stereoselective synthesis of some derivatives (e.g., compound **4a**, wherein the hypothetical use of the corresponding benzyl halide would favor an  $S_N1$  mechanism with the consequent loss of chirality). For this reason, preparation of derivatives **4a** and **4b** could only be achieved by converting the 2-amino group into a fluorine atom and introducing the chiral amine by nucleophilic aromatic substitution, as reported in 2008 [12].

In 2011, Selig et al. published an alternative synthetic route to tetrasubstituted imidazoles **3** (Scheme 2) [18]. This route is overall similar to the previously reported one and only differs in the replacement of the amino group of intermediate **9** with a fluorine, allowing the realization of the following steps without the necessity of the protecting group. The amino group was then reintroduced at the penultimate step, before its functionalization with different acyl derivatives yielding compounds **3**. Nevertheless, because of the replacement of the amino group only after the preparation of ethanone **9**, this route does not bypass the issues relative to the installation and cleavage of the *N*-acetyl protecting group and encompasses the same number of steps as the one presented in Scheme 1.



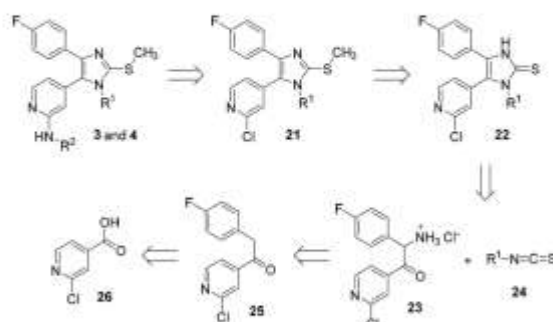
**Scheme 2.** Synthetic pathway toward 1,2,4,5-tetrasubstituted imidazoles **3**. Reagents and conditions: (i)  $\text{NaNO}_2$ , 70% HF-pyridine;  $-15$  to  $-10$  °C, then rt; (ii)  $\text{NaNO}_2$ , glacial AcOH, rt; (iii) EtOH, reflux temperature; (iv) 2,2,4,4-tetramethylcyclobutane-1,3-dithione, DCM, rt; (v) iodomethane,  $\text{K}_2\text{CO}_3$ , MeOH, rt; (vi)  $\text{NH}_3$ , reactor; (vii)  $\text{R}^2\text{-COOH}$ , CDI, *N*-methylpyrrolidinone, rt, then 120 °C.

## 2. Results and Discussion

### 2.1. Chemistry

Our retrosynthetically-planned synthetic strategy towards 1,2,4,5-tetrasubstituted imidazoles **3** and **4** is depicted in Scheme 3. In contrast to the aforementioned routes, we sought to introduce the whole alkyl- or acylamino group at the pyridine-C2 position starting from 2-chloropyridine derivatives **21** since the higher stability of the 2-halopyridine moiety avoids the need for protection/deprotection steps. However, in contrast to the route reported by Selig et al., chlorine was preferred over fluorine, as it can be displaced through both nucleophilic aromatic substitution reaction and Buchwald-Hartwig arylation/amidation. Moreover, this choice would allow the introduction of chiral amines having the stereocenter adjacent to the amino group without leading to racemization or inversion of configuration, as the reaction mechanism does not involve the chiral center. Key passage of the synthesis is then the cyclization reaction of  $\alpha$ -aminoketone **23** and alkyl/aryl-substituted

isothiocyanates **24**, allowing the regioselective introduction of the imidazole-N-substituent, followed by methylation of resulting intermediates **22**. Finally, a suitable precursor for the preparation of  $\alpha$ -aminoketone **23** could be represented by ethanone derivative **25**, which in turn can arise from the commercially available 2-chloroisonicotinic acid (**26**).



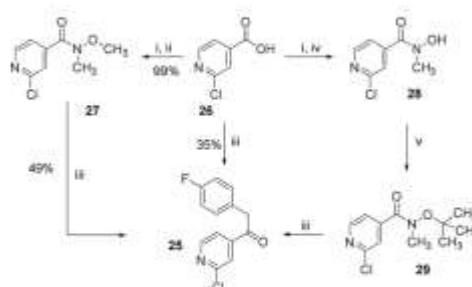
**Scheme 3.** Retrosynthetic strategy for the preparation of 1,2,4,5-tetrasubstituted imidazoles **3** and **4**.

The initial step of our alternative route consisted in the preparation of the 1-(2-chloropyridin-4-yl)-2-(4-fluorophenyl)ethan-1-one (**25**). This compound represents the 2-chloropyridine-substituted analogue of derivative **9**, a common intermediate of both published synthetic pathways toward tetrasubstituted pyridinylimidazoles (Schemes 1 and 2). As already mentioned, the preparation of ethanone **9** constituted one of the major bottlenecks of both previously reported routes and as a consequence, the new synthetic strategy would benefit from a more efficient method to achieve its analogue **25**. Several attempts were carried out in order to yield compound **25**, which are displayed in Scheme 4.

Despite their similarity, it was not possible to prepare compound **25** in an analogous fashion as ethanone **9**, namely by condensation of the 2-chloroisonicotinic acid with 4-fluorophenylacetonitrile followed by hydrolysis of the resulting cyanoketone. A convenient method for the synthesis of ketones is generally represented by the addition of Grignard reagents to Weinreb amides. Unfortunately, Grignard reaction of 4-fluorobenzyl magnesium chloride with 2-chloro-*N*-methoxy-*N*-methylisonicotinamide (**27**) afforded ethanone **25** in a non-satisfactory yield of 49%. A reason for the reduced yield is probably a well-described E<sub>2</sub> elimination reaction starting with the extraction of a proton from the *N*-methoxy group and resulting in the formation of the corresponding *N*-methylamide and formaldehyde [26]. In order to avoid this undesired side reaction a previously described approach was followed [27], consisting in the use of a modified Weinreb amide wherein the methoxy group was replaced by a *tert*-butoxy moiety. Such group has no H atoms adjacent to the oxygen atom and is therefore not prone to deprotonation by the Grignard reagent. *N*-(*tert*-butoxy)-2-chloro-*N*-methylisonicotinamide (**29**) could be prepared in good yield via a two-step procedure starting from the corresponding carboxylic acid **26**. In detail, coupling of **26** with *N*-methylhydroxylamine afforded the corresponding hydroxamic acid **28**, which was then converted into the Weinreb amide **29** by acid-catalyzed esterification with *tert*-butyl acetate. The use of amide **29** in the Grignard reaction with 4-fluorobenzyl magnesium chloride permitted a significantly increased yield of up to 81%, with an overall yield of 62% over 3 steps for the preparation of intermediate **25**. It is worth mentioning that the ethanone derivative **25** could also be prepared by direct Grignard reaction of 2-chloroisonicotinic acid (**26**) with 4-fluorobenzyl magnesium chloride, adapting a procedure previously reported by Reeves et al. [28]. The latter method allows the preparation of key intermediate **25** in a single step and consists in reacting the carboxylic acid with two equivalents of organomagnesium reactant in order to achieve nucleophilic addition on the carboxylate derivative. This

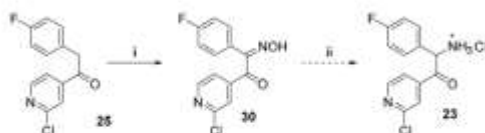


approach afforded derivative **25** in a low yield (35%) and the formation of 1,2-bis(4-fluorophenyl)ethane as a by-product was observed.



**Scheme 4.** Diverse strategies for the synthesis of ethanone derivative **25**. Reagents and conditions: (i)  $\text{SOCl}_2$ , reflux temperature; (ii) *N,O*-dimethylhydroxylamine hydrochloride,  $\text{NEt}_3$ , DCM, rt; (iii) 4-fluorobenzyl magnesium chloride, dry THF,  $-10^\circ\text{C}$ , then rt; (iv) *N*-methylhydroxylamine hydrochloride,  $\text{NEt}_3$ , dry DCM, rt; (v) *t*-BuOAc, 70%  $\text{HClO}_4(\text{aq})$ , 1,4-dioxane,  $60^\circ\text{C}$ , sealed vial.

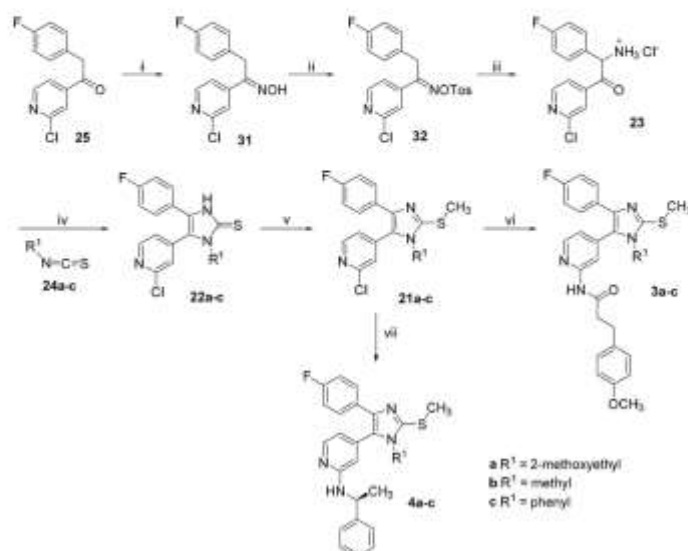
After obtaining a convenient method for the preparation of ethanone intermediate **25**, a strategy for its conversion into  $\alpha$ -aminoketone **23** was pursued. As shown in Scheme 5, reduction of the  $\alpha$ -ketoxime **30** did not succeed in producing the desired  $\alpha$ -aminoketone **23** starting from ethanone **25**. Such transformation was instead successfully achieved through a three-step procedure involving a base-mediated Neber rearrangement of an *O*-tosyl-oxime derivative (Scheme 6). In detail, ethanone **25** was first reacted in a nucleophilic addition with hydroxylamine and the resulting oxime **31** was tosylated. Following the tosylation protocol of Lantos and coworkers for a related ketoxime [29], a significantly slower conversion was observed, accompanied by the formation of by-products, which deteriorated under increased thermal conditions. Carrying out the reaction at room temperature afforded a sufficiently clean tosylation, yet requiring a high excess of *p*-toluenesulfonylchloride to compensate for the resultant low conversion rate. Intermediate **32** was then reacted in a Neber rearrangement with potassium ethoxide, affording an aziridine derivative, which was immediately hydrolyzed in acidic conditions, yielding  $\alpha$ -aminoketone **23** as a hydrochloride salt.



**Scheme 5.** Attempted short strategy for the preparation of  $\alpha$ -aminoketone **23**. Reagents and conditions: (i)  $\text{NaNO}_2$ , glacial AcOH, rt; (ii) Pd/C 10%,  $\text{H}_2$ , isopropanolic HCl, rt.

Construction of the imidazole ring was performed by reaction of the  $\alpha$ -aminoketone **23** and alkyl or aryl isothiocyanates **24** in a single two-step procedure. First, the nucleophilic addition of the amino group to the isothiocyanate took place using triethylamine as both base and solvent. The cyclization was then promoted by evaporating the triethylamine and by heating the reaction mixture in glacial acetic acid, succeeding in the regioselective preparation of *N*-alkyl and -aryl substituted imidazole-2-thiones **22** in moderate yields. Tetrasubstituted imidazole derivatives **21** were then easily accessible through nucleophilic substitution of compounds **22** with iodomethane in the presence of a base. The last step of our alternative route consisted in the introduction of the alkyl- or acylamino functions at the pyridine-C2 position. In case of aliphatic amines this was obtained by

nucleophilic aromatic substitution of synthones **21** with large excess of amine in solvent-free conditions. Amide moieties could instead be introduced starting from the same derivative via palladium-catalyzed Buchwald-Hartwig reaction.

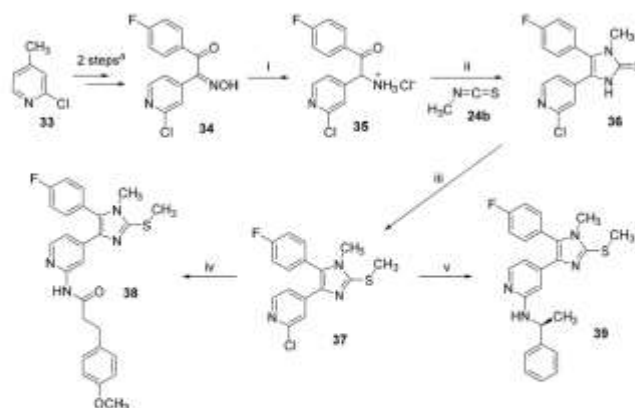


**Scheme 6.** Optimized synthesis of tetrasubstituted imidazoles **3** and **4**. Reagents and conditions: (i) hydroxylamine hydrochloride, NaOH<sub>(aq)</sub>, MeOH, rt; (ii) tosyl chloride, pyridine, rt; (iii) (a) EtOK, EtOH<sub>(abs)</sub>, 0 °C, then rt; (b) conc. HCl<sub>(aq)</sub>, 50 °C; (iv) (a) NEt<sub>3</sub>, 50 °C; (b) glacial AcOH, 80 °C; (v) iodomethane, *t*-BuONa, MeOH, 50 °C; (vi) 3-(4-methoxyphenyl)propanamide, Pd<sub>2</sub>(dba)<sub>3</sub>, XantPhos, Cs<sub>2</sub>CO<sub>3</sub>, DMF, 100 °C; (vii) (*S*)-phenylethan-1-amine, 180 °C, sealed tube.

As already mentioned, derivatization of the imidazole-N atom adjacent to the 4-fluorophenyl ring is detrimental for inhibitory activity on the p38 $\alpha$  MAPK, as the introduced alkyl or aryl substituent prevents the formation of a hydrogen bond interaction with the Lys53 of the enzyme. Nevertheless, in order to broaden the applicability of our alternative synthetic pathway, we tested its suitability for the regioselective synthesis of 1,2,4,5-tetrasubstituted pyridinylimidazoles bearing the substituent on the imidazole-N atom distal from the pyridine ring (Scheme 7). In this series, derivatives **38** and **39**, bearing a methyl group on the imidazole-N atom, were prepared as an example to prove the applicability of the presented synthetic route. In order to invert the substitution pattern on the imidazole ring, the cyclization step clearly needs to be performed starting from  $\alpha$ -aminoketone **36**, a regioisomer of compound **23**. This derivative could be obtained via a previously described procedure consisting in the condensation of 2-chloro-4-picoline (**33**) with ethyl 4-fluorobenzoate followed by  $\alpha$ -nitrosylation of the ethanone intermediate **34** and reduction of the resulting  $\alpha$ -ketoxime **34**. Differently from the attempt depicted in Scheme 4, the  $\alpha$ -ketoxime **34**, presenting the opposite arrangement of the two aryl substituents, could be smoothly reduced affording aminoketone **35** in very good yields. Starting from the  $\alpha$ -aminoketone **35**, the cyclization-methylation steps were carried out in an analogous fashion as the ones described in Scheme 6. Finally, using the same conditions as for compounds **3** and **4**, compounds **38** and **39** could be obtained by Buchwald-Hartwig amidation and by nucleophilic aromatic substitution, respectively.

Molecules 2018, 23, 221

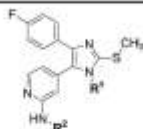
8 of 19

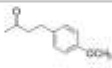
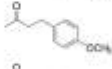

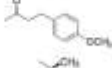
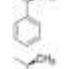
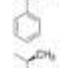




**Scheme 7.** Synthesis of tetrasubstituted imidazoles **38** and **39**. <sup>a</sup> Procedure reported by Laufer et al. [30]. Reagents and conditions: (i) Pd/C 10%, H<sub>2</sub>, isopropanolic HCl, rt; (ii) (a) NEt<sub>3</sub>, 60 °C; (b) glacial AcOH, 80 °C; (iii) iodomethane, *t*-BuONa, MeOH, 50 °C; (iv) 3-(4-methoxyphenyl)propanamide, Pd<sub>2</sub>(dba)<sub>3</sub>, XantPhos, Cs<sub>2</sub>CO<sub>3</sub>, DMF, 100 °C; (v) (*S*)-1-phenylethan-1-amine, 180 °C, sealed tube.

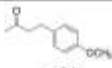

## 2.2. Biological Evaluation and SAR Insights

Compounds **3b–c**, **4c**, **38** and **39** were tested in an enzyme-linked immunosorbent assay (ELISA) in order to evaluate their capability to inhibit the p38 $\alpha$  MAP kinase and the results were compared to the ones of compounds **3a** and **4a–b**, which were previously tested in the same assay [17] (Table 1). Although the scant number of evaluated compounds does not allow an exhaustive analysis of structure-activity relationships, tetrasubstituted pyridinylimidazoles were confirmed as potent inhibitors of the p38 $\alpha$  MAP kinase, reaching IC<sub>50</sub> values down to the low double-digit nanomolar range (compound **3b**). As expected, substitution of the N atom adjacent to the 4-fluorophenyl ring (compounds **38** and **39**) was detrimental for the inhibitory activity, due to the suppression of the hydrogen bond with the Lys53. When comparing the two compound series **3a–c** and **4a–c** it appears evident that substitution of the imidazole-N atom with a phenyl ring (compounds **3c** and **4c**) has a negative effect on the inhibitory activity, even reaching an IC<sub>50</sub> value in the micromolar range in case of compound **4c**. This can be either due to unfavorable interactions with the phosphate/sugar pocket or to a sterical hindrance with the 2-alkylamino- or 2-acylamino-pyridine moiety, which does not allow a correct positioning of the molecule in the binding pocket of the enzyme. Finally, whereas the acylamino substituent appears to be overall preferable to the alkylamino group at the pyridine-C2 position, no clear indication could be obtained regarding the superiority of either the methyl or the methoxyethyl substituent at the imidazole-N atom.

**Table 1.** Biological activity of tetrasubstituted pyridinylimidazoles 3a-c, 4a-c, 38, and 39.


Cpd.	R <sup>1</sup>	R <sup>2</sup>	IC <sub>50</sub> (μM) Mean ± SEM <sup>a</sup>
3a	-(CH <sub>2</sub> ) <sub>2</sub> OCH <sub>3</sub>		0.048 ± 0.010 <sup>b</sup>
3b	-CH <sub>3</sub>		0.020 ± 0.004
3c			0.413 ± 0.072
4a	-(CH <sub>2</sub> ) <sub>2</sub> OCH <sub>3</sub>		0.040 ± 0.010 <sup>c</sup>
4b	-CH <sub>3</sub>		0.070 ± 0.030 <sup>c</sup>
4c			1.51 ± 0.15

Cpd.	R <sup>1</sup>	R <sup>2</sup>	IC <sub>50</sub> (μM) Mean ± SEM <sup>a</sup>
38	-CH <sub>3</sub>		2.70 ± 0.02
39	-CH <sub>3</sub>		3.19 ± 0.78

<sup>a</sup> n = 3; <sup>b</sup> data taken from ref. [14]; <sup>c</sup> data taken from ref. [15], n = 4.

To sum up, the herein reported route represents a valid alternative for the synthesis of tetrasubstituted pyridinylimidazoles, a class of molecules counting several examples in the field of kinase inhibition due to the capability of reaching high inhibitory potency together with reduced interaction with the CYP450 enzymes. This route comprises a lower number of synthetic steps in comparison with previously reported strategies along with an increased versatility. Both aliphatic and aromatic moieties can be introduced at the imidazole-N1 atom without modifying the synthetic path. Furthermore, the range of possible substituents is extremely broad thanks to both the commercial availability of diversely substituted isothiocyanates and to reported procedures describing facile preparation methods for these intermediates [31–33]. The presence of a Cl atom at the pyridine-C2 position eliminates the necessity of protection/deprotection steps and permits the functionalization with both amines and amides in the last step of the route. Furthermore, chiral amines featuring

the stereocenter in the  $\alpha$ -position can be introduced without the risk of inversion of configuration or racemization.

The introduction of an aromatic ring on the imidazole-N atom, constituting one of the advantages of the presented route with respect to published ones, did not emerge as a beneficial substitution to increase the inhibitory activity on the p38 $\alpha$  MAP kinase; likewise, functionalization of the imidazole-N atom distal to the pyridine ring results in a significantly reduced potency on the same target. Nevertheless, since pyridinylimidazoles represent a privileged scaffold in the realm of kinase inhibition, these synthetic improvements can still result helpful in the targeting of different kinases having dissimilar structural features compared to the p38 $\alpha$  MAP kinase.

### 3. Materials and Methods

#### 3.1. General Information

All reagents and solvents were of commercial quality and utilized without further purification. Thin layer chromatography (TLC) reaction controls were performed for all reactions using fluorescent silica gel 60 F<sub>254</sub> plates (Merck, Darmstadt, Germany) and visualized under natural light and UV illumination at 254 and 366 nm. The purity of all tested compounds are >95% as determined via reverse phase high performance liquid chromatography (HPLC) on a 1100 Series HPLC system (Agilent, Santa Clara, CA, USA) equipped with a UV diode array detector (detection at 218 nm, 254 nm and 280 nm). The chromatographic separation was performed on a XBridge™ C18 column (150 mm  $\times$  4.6 mm, 5  $\mu$ m) at 24 °C oven temperature. The injection volume was 10  $\mu$ L and the flow was 1.5 mL/min using the following gradient: 0.01 M KH<sub>2</sub>PO<sub>4</sub>, pH 2.3 (solvent A), MeOH (solvent B), 45% B to 85% B in 10 min; 85% B for 6 min; stop time 16 min. Column chromatography was performed on Davisil LC60A 20–45  $\mu$ m silica from Grace Davison (Columbia, MD, USA) and Geduran Si60 63–200  $\mu$ m silica from Merck for the pre-column using an PuriFlash 430 automated flash chromatography system (Interchim, Montluçon, France). Nuclear magnetic resonance (NMR) spectra were measured at 300/75 MHz on an Avance III HD NMR spectrometer (Bruker, Billerica, MA, USA) at the Organic Chemistry Institute, Eberhard Karls Universität Tübingen. Chemical shifts are reported in parts per million (ppm) relative to tetramethylsilane. All spectra were calibrated against the (residual proton) peak of the deuterated solvent used. Mass spectra were performed on an Expression S electrospray ionization mass spectrometer (ESI-MS, Advion, Ithaca, NY, USA) with TLC interface in the Institute of Pharmaceutical Sciences, Eberhard Karls Universität Tübingen. High-resolution mass spectra (HRMS) were measured on a Bruker maXis 4G ESI time of flight mass spectrometer (ESI-TOF-MS) in the positive mode in the Organic Chemistry Institute, Eberhard Karls Universität Tübingen.

#### 3.2. Experimental Procedures

##### 3.2.1. General Procedure for the Preparation of Imidazole-2-Thione Derivatives **22a–c** and **36** (General Procedure A)

In a pressure vial the corresponding alkyl or aryl isothiocyanate **24** (3–5 equiv.) was dissolved in NEt<sub>3</sub> (2 mL) and then the appropriate  $\alpha$ -aminoketone derivative **35** or **23** (1 equiv.) was added. The closed vial was heated at 50 °C and stirred until the starting compound resulted completely consumed as detected by HPLC analysis (1.5–4 h). The NEt<sub>3</sub> was then evaporated at reduced pressure and the residue was taken up in glacial AcOH and stirred at 80 °C for 2 to 16 h. After concentrating the mixture at reduced pressure, a NaHCO<sub>3</sub> saturated solution was added until reaching pH  $\approx$  8 and the aqueous layer was then extracted with EtOAc. The combined organic layers were then washed with NaCl saturated solution, dried over anhydrous Na<sub>2</sub>SO<sub>4</sub>, and concentrated at reduced pressure. The residue was finally purified by flash column chromatography.



### 3.2.2. General Procedure for the Preparation of 2-Methylsulfanylimidazole Derivatives **21a–c** and **37** (General Procedure B)

In a pressure vial the appropriate imidazole-2-thione derivative (**22a–c** or **36**, 1 equiv.) was suspended in MeOH (4–10 mL) and after that *t*-BuONa (1.2 equiv.) was added. After cooling the mixture at 0 °C, iodomethane (5 equiv.) was added and the tightly closed vial was heated to 50 °C and stirred for 45 min to 2 h. After removing the solvent at reduced pressure H<sub>2</sub>O was added and the aqueous phase was extracted with DCM. The combined organic layers were then washed with NaCl saturated solution, dried over anhydrous Na<sub>2</sub>SO<sub>4</sub>, and concentrated at reduced pressure. The residue was finally purified by flash column chromatography or directly used for the following step.

### 3.2.3. General Procedure for the Preparation of Amides **3a–c** and **38** (General Procedure C)

Under argon atmosphere the corresponding imidazole derivative **21a–c** or **37** (1 equiv.), 3-(4-methoxyphenyl)propanamide (1.5 equiv.), Pd<sub>2</sub>(dba)<sub>3</sub> (0.05 equiv.), XantPhos (0.1 equiv.), and Cs<sub>2</sub>CO<sub>3</sub> (3 equiv.) were suspended in dry DMF and after that the reaction mixture was heated at 100 °C and stirred overnight (18 h). The reaction mixture was poured in H<sub>2</sub>O and the aqueous phase was extracted with EtOAc. The combined organic layers were then washed with NaCl saturated solution, dried over anhydrous Na<sub>2</sub>SO<sub>4</sub>, and concentrated at reduced pressure. The residue was finally purified by flash column chromatography.

### 3.2.4. General Procedure for the Preparation of Amines **4a–c** and **39** (General Procedure D)

In a pressure vial, the corresponding imidazole derivative **21a–c** or **37** (1 equiv.) was suspended in (S)-1-phenylethan-1-amine (1.5 mL) and the closed vial was stirred at 180 °C for 18–40 h. The reaction mixture was poured in H<sub>2</sub>O and the aqueous phase was extracted with EtOAc. The combined organic layers were then washed with NaCl saturated solution, dried over anhydrous Na<sub>2</sub>SO<sub>4</sub>, and concentrated at reduced pressure. The residue was finally purified by flash column chromatography.

### 3.2.5. Detailed Procedures for the Preparation of Synthesized Compounds

**2-Chloro-N-methoxy-N-methylisonicotinamide (27)**. 2-Chloroisonicotinic acid (**26**, 21.0 g, 133.3 mmol) was suspended in SOCl<sub>2</sub> (60 mL) and the mixture was stirred at reflux temperature for 5 h. After removing the excess of solvent, the residue was taken up in dry DCM and added dropwise to an ice-cooled previously prepared suspension of *N,O*-dimethylhydroxylamine hydrochloride (15.6 g, 160 mmol) and NEt<sub>3</sub> (45.0 mL, 320 mmol) in dry DCM (50 mL). After completion of the addition the mixture was let heating at rt and stirred overnight. After evaporating the solvent at reduced pressure H<sub>2</sub>O was added and the aqueous phase was extracted with DCM. The combined organic layers were then washed with NaCl saturated solution, dried over anhydrous Na<sub>2</sub>SO<sub>4</sub>, and concentrated at reduced pressure giving 26.0 g of product as a light brown solid, which was directly used for the following step without further purification (97% yield); <sup>1</sup>H-NMR (300 MHz, CDCl<sub>3</sub>) δ 3.35 (s, 3H), 3.53 (s, 3H), 7.43 (dd, *J* = 5.0, 1.2 Hz, 1H), 7.54 (s, 1H), 8.45 (d, *J* = 5.1 Hz, 1H); <sup>13</sup>C-NMR (75 MHz, CDCl<sub>3</sub>) δ 32.9, 61.5, 120.7, 122.8, 144.5, 149.8, 151.6, 166.0; ESI-MS: (*m/z*) 201.1 [M + H]<sup>+</sup>; HPLC: *t*<sub>r</sub> = 2.051 min.

**2-Chloro-N-hydroxy-N-methylisonicotinamide (28)**. 2-Chloroisonicotinic acid (**26**, 5.0 g, 31.7 mmol) was suspended in SOCl<sub>2</sub> (25 mL) and the mixture was stirred at reflux temperature for 6 h. After removing the excess of solvent, the residue was taken up in dry DCM and added dropwise to an ice-cooled previously prepared suspension of *N*-methylhydroxylamine hydrochloride (3.2 g, 38.0 mmol) and NEt<sub>3</sub> (9.7 mL, 76.1 mmol) in dry DCM (15 mL). After completion of the addition the mixture was let heating at rt and stirred overnight. After evaporating the solvent at reduced pressure H<sub>2</sub>O was added and the aqueous phase was extracted with EtOAc. The combined organic layers were then washed with NaCl saturated solution, dried over anhydrous Na<sub>2</sub>SO<sub>4</sub>, and concentrated at reduced pressure giving 5.6 g of product as a white-pink solid, which was directly used for the following step without further purification (95% yield); <sup>1</sup>H-NMR (300 MHz, DMSO-*d*<sub>6</sub>) δ 3.27 (s, 3H), 7.53 (dd, *J* = 5.0,

1.2 Hz, 1H), 7.61 (dd,  $J = 1.2, 0.5$  Hz, 1H), 8.49 (dd,  $J = 5.0, 0.5$  Hz, 1H), 10.40 (br. s, 1H);  $^{13}\text{C-NMR}$  (75 MHz,  $\text{DMSO-}d_6$ )  $\delta$  36.9, 122.1, 123.1, 146.5, 150.50, 150.56, 165.7; ESI-MS: ( $m/z$ ) 187.2 [ $\text{M} + \text{H}$ ] $^+$ , 185.1 [ $\text{M} - \text{H}$ ] $^-$ ; HPLC:  $t_r = 1.568$  min.

*N*-(*tert*-butoxy)-2-chloro-*N*-methylisonicotinamide (29). In a pressure vial 2-chloro-*N*-hydroxy-*N*-methylisonicotinamide (27, 500 mg, 2.68 mmol) was suspended in dry 1,4-dioxane (5 mL) and *t*-BuOAc (20 mL). After adding 70%  $\text{HClO}_4(\text{aq})$  (27 mg, 0.27 mmol) the vial was tightly closed and the mixture was stirred at 60 °C for 48 h. After cooling down, the mixture was poured in a  $\text{K}_2\text{CO}_3$  saturated solution and the aqueous phase was extracted with EtOAc. The combined organic layers were then dried over anhydrous  $\text{Na}_2\text{SO}_4$  and the solvent was evaporated at reduced pressure giving 402 mg of the desired compound, which was used for the following step without further purification;  $^1\text{H-NMR}$  (300 MHz,  $\text{CDCl}_3$ )  $\delta$  1.10 (s, 9H), 3.43 (s, 3H), 7.48 (dd,  $J = 5.1, 1.2$  Hz, 1H), 7.60 (br. s, 1H), 8.43 (dd,  $J = 5.0, 0.5$  Hz, 1H); ESI-MS: ( $m/z$ ) 243.1 [ $\text{M} + \text{H}$ ] $^+$ ; HPLC:  $t_r = 4.733$  min.

1-(2-Chloropyridin-4-yl)-2-(4-fluorophenyl)ethan-1-one (25). The title compound could be obtained alternatively through the following three procedures:

(1) Under argon atmosphere Mg turnings (1.2 g, 50.0 mmol) were suspended in dry THF (120 mL) and after that 4-fluorobenzyl chloride (6.0 g, 41.5 mmol) was added in one portion. After the reaction was initiated, the mixture warmed up and was stirred until it cooled down to rt. The residual Mg was let decanting and the supernatant was added dropwise to a solution of 2-chloro-*N*-methoxy-*N*-methylisonicotinamide (27, 3.2 g, 16.0 mmol) in dry THF (35 mL) under argon atmosphere. The mixture was then stirred for 2 h at a temperature of 30–35 °C. The reaction was quenched with  $\text{NH}_4\text{Cl}$  saturated solution (100 mL) and stirred overnight at rt. The two formed phases were separated and the aqueous phase was then further extracted by EtOAc. The combined organic layers were then washed with NaCl saturated solution, dried over anhydrous  $\text{Na}_2\text{SO}_4$ , and concentrated at reduced pressure. Finally, the residue was purified by flash column chromatography ( $\text{SiO}_2$ , petroleum ether 40/60: EtOAc 4:1) giving 1.96 g of pure product as a yellow oil, which solidifies after cooling (49% yield).

(2) Under argon atmosphere Mg turnings (1.22 g, 50.1 mmol) were suspended in dry THF (15 mL) and then 4-fluorobenzyl chloride (1.07 g, 7.4 mmol) was added in one portion. When the mixture started to become warm it was immediately cooled with an ice bath and then stirred for 2 h. After letting the residual Mg decanting, the supernatant was added dropwise to a solution of *N*-(*tert*-butoxy)-2-chloro-*N*-methylisonicotinamide (29, 900 mg, 3.7 mmol) in dry THF (10 mL), previously cooled at  $-10$  °C. After completion of the addition the mixture was let slowly heating at rt and stirred for 3 h.  $\text{NH}_4\text{Cl}$  saturated solution (80 mL) was added and the two formed phases were separated. The aqueous phase was then further extracted 3 times with EtOAc. The combined organic layers were then washed with NaCl saturated solution, dried over anhydrous  $\text{Na}_2\text{SO}_4$ , and concentrated at reduced pressure. Finally, the residue was purified by flash column chromatography ( $\text{SiO}_2$ , *n*-hexane: EtOAc gradient elution from 4:1 to 3:2) giving 747 mg of pure product as a yellow oil, which solidifies after cooling (81% yield).

(3) Under argon atmosphere Mg turnings (6.94 g, 285.6 mmol) were suspended in dry THF (35 mL). After that 4-fluorobenzyl chloride (13.6 g, 92.5 mmol) was added in portions: after adding 1 mL and starting the reaction, the mixture was cooled at 0 °C with an ice bath and the addition continued by 0.5 mL/min at the same temperature. After the addition was completed the mixture was let stirring until warming up to rt. After letting the Mg decanting the supernatant was added slowly dropwise to a suspension of 2-chloroisonicotinic acid (26, 6.0 g, 38.1 mmol) in dry THF (24 mL), previously cooled at  $-30$  °C. During the addition the temperature was maintained between  $-25$  and  $-30$  °C. After complete addition the mixture was let heating to rt and stirred overnight. The mixture was poured on  $\text{NH}_4\text{Cl}$  saturated solution (100 mL). The aqueous phase was extracted twice with EtOAc and the combined organic layers were dried over anhydrous  $\text{Na}_2\text{SO}_4$ , and concentrated at reduced pressure. Finally, the residue was purified by flash column chromatography ( $\text{SiO}_2$ , petroleum



ether 40/60:EtOAc gradient elution from 3:1 to 1:1) giving 3.37 g of pure compound as a yellow oil, which solidifies after cooling (35% yield);  $^1\text{H-NMR}$  (300 MHz,  $\text{CDCl}_3$ )  $\delta$  4.24 (s, 2H), 6.99–7.10 (m, 2H), 7.15–7.23 (m, 2H), 7.67 (dd,  $J = 5.1, 1.5$  Hz, 1H), 7.79 (dd,  $J = 1.4, 0.7$  Hz, 1H), 8.56 (dd,  $J = 5.1, 0.5$  Hz, 1H);  $^{13}\text{C-NMR}$  (75 MHz,  $\text{CDCl}_3$ )  $\delta$  44.9, 115.9 (d,  $J = 21.6$  Hz), 120.2, 122.7, 128.4 (d,  $J = 3.3$  Hz), 131.1 (d,  $J = 8.3$  Hz), 145.2, 151.0, 153.0, 162.2 (d,  $J = 246.6$  Hz); ESI-MS: ( $m/z$ ) 249.9  $[\text{M} + \text{H}]^+$ ; HPLC:  $t_r = 5.555$  min.

**1-(2-Chloropyridin-4-yl)-2-(4-fluorophenyl)-2-(hydroxyimino)ethan-1-one (30).** Ethanone derivative **25** (1.96 g, 7.85 mmol) was dissolved in glacial AcOH (15 mL) and after that  $\text{NaNO}_2$  (1.67 g, 24.2 mmol), previously dissolved in  $\text{H}_2\text{O}$  (7 mL), was added dropwise and the reaction mixture was stirred overnight at rt. Afterwards 50 mL  $\text{H}_2\text{O}$  were added and the voluminous precipitate formed was filtered off and washed with  $\text{H}_2\text{O}$ . The residue was then suspended in  $\text{H}_2\text{O}$  and the suspension was extracted with EtOAc. The combined organic layers were dried over anhydrous  $\text{Na}_2\text{SO}_4$  and the solvent was then removed at reduced pressure, affording 1.8 g of the desired product, which was used for the following step without further purification (82% yield);  $^1\text{H-NMR}$  (300 MHz,  $\text{DMSO-}d_6$ )  $\delta$  7.23–7.37 (m, 2H), 7.51–7.62 (m, 2H), 7.73 (dd,  $J = 5.0, 1.4$  Hz, 1H), 7.89 (dd,  $J = 1.2, 0.7$  Hz, 1H), 8.58 (dd,  $J = 5.0, 0.7$  Hz, 1H), 13.14 (s, 1H);  $^{13}\text{C-NMR}$  (75 MHz,  $\text{DMSO-}d_6$ )  $\delta$  115.3 (d,  $J = 21.6$  Hz), 122.8, 124.3, 125.6 (d,  $J = 3.9$  Hz), 132.5 (d,  $J = 8.3$  Hz), 149.2, 150.5, 150.6, 154.3, 162.8 (d,  $J = 246.6$  Hz), 190.4; ESI-MS: ( $m/z$ ) 276.9  $[\text{M} - \text{H}]^-$ ; HPLC:  $t_r = 7.405$  min.

**1-(2-Chloropyridin-4-yl)-2-(4-fluorophenyl)ethan-1-one oxime (31).** Hydroxylamine hydrochloride (1.52 g, 21.93 mmol) was dissolved in  $\text{H}_2\text{O}$  (3.5 mL) and then 20%  $\text{NaOH}_{(\text{aq})}$  (0.7 mL) and a solution of ethanone derivative **25** (3.65 g, 14.62 mmol) in MeOH (17.5 mL) were added. The reaction mixture was stirred at rt for 48 h while a precipitate formed. Saturated  $\text{NH}_4\text{Cl}$  solution (50 mL) was added and the precipitate was filtered off, rinsed with  $\text{H}_2\text{O}$  and dried *in vacuo* over  $\text{P}_2\text{O}_5$  affording 3.71 g of the desired product as an off-white solid, which was used for the following step without further purification (96% yield). Extraction with EtOAc represents an alternative work-up procedure giving similar yields;  $^1\text{H-NMR}$  (300 MHz,  $\text{DMSO-}d_6$ )  $\delta$  4.16 (s, 2H), 7.12–7.02 (m, 2H), 7.28–7.20 (m, 2H), 7.64 (dd,  $J = 5.2, 1.5$  Hz, 1H), 7.71–7.68 (m, 1H), 8.37 (d,  $J = 5.2$  Hz, 1H), 12.27 (s, 1H);  $^{13}\text{C-NMR}$  (75 MHz,  $\text{DMSO-}d_6$ )  $\delta$  29.0, 115.4 (d,  $J = 21.3$  Hz), 119.7, 120.5, 130.2 (d,  $J = 8.0$  Hz), 132.5 (d,  $J = 3.1$  Hz), 146.5, 150.2, 151.0, 152.7, 160.9 (d,  $J = 242.4$  Hz); ESI-MS: 265.0  $[\text{M} + \text{H}]^+$ , 263.0  $[\text{M} - \text{H}]^-$ ; HPLC:  $t_r = 6.934$  min.

**1-(2-Chloropyridin-4-yl)-2-(4-fluorophenyl)ethan-1-one O-tosyl oxime (32).** A solution of ketoxime **31** (1.20 g, 4.53 mmol) and *p*-toluenesulfonyl chloride (3.46 g, 18.14 mmol) in dry pyridine (6 mL) was stirred at rt under  $\text{N}_2$  atmosphere for 50 h. The mixture was poured into a NaCl saturated solution (30 mL) and extracted three times with EtOAc. The combined organic layers were then washed 3 times with a NaCl saturated solution, dried over anhydrous  $\text{Na}_2\text{SO}_4$  and concentrated at reduced pressure. Finally, the residue was purified by flash column chromatography ( $\text{SiO}_2$ , petroleum ether 40/60:EtOAc 2:3) giving 1.68 g of the desired product as a yellow oil (88% yield);  $^1\text{H-NMR}$  (300 MHz,  $\text{CDCl}_3$ )  $\delta$  2.48 (s, 3H), 4.12 (s, 2H), 6.89–7.06 (m, 4H), 7.33 (dd,  $J = 5.2, 1.5$  Hz, 1H), 7.39 (d,  $J = 8.2$  Hz, 2H), 7.42–7.46 (m, 1H), 7.89 (d,  $J = 8.3$  Hz, 2H), 8.39 (d,  $J = 5.2$  Hz, 1H);  $^{13}\text{C-NMR}$  (75 MHz,  $\text{CDCl}_3$ )  $\delta$  21.8, 32.6, 116.1 (d,  $J = 21.6$  Hz), 120.0, 122.1, 128.8 (d,  $J = 3.3$  Hz), 129.0, 129.9 (d,  $J = 7.7$  Hz), 129.9, 131.9, 143.4, 145.9, 150.3, 152.4, 162.5 (d,  $J = 246.6$  Hz), 161.5; ESI-MS: ( $m/z$ ) 473.2  $[\text{M} + \text{Na} + \text{MeOH}]^+$ ; HPLC:  $t_r = 9.342$  min.

**2-Amino-1-(2-chloropyridin-4-yl)-2-(4-fluorophenyl)ethan-1-one hydrochloride (23).** In a three-necks round bottom flask under argon atmosphere K chunks (175 mg, 4.4 mmol) were added portionwise to  $\text{EtOH}_{(\text{abs})}$  (20 mL). After complete dissolution the mixture was cooled at 0 °C and 1-(2-chloropyridin-4-yl)-2-(4-fluorophenyl)ethan-1-one O-tosyl oxime (**31**, 1.70 g, 4.0 mmol), previously dissolved in  $\text{EtOH}_{(\text{abs})}$  (50 mL) was added slowly dropwise. The mixture was then stirred at 0 °C for 3 h and after that dry  $\text{Et}_2\text{O}$  (250 mL) was added and the mixture was stirred for 30 min at rt. The white precipitate formed was removed by filtration and the filtrate was concentrated at reduced pressure.

The residue was taken up in conc.  $\text{HCl}_{(\text{aq})}$  and the mixture was stirred at 60 °C for 2 h. The residual solvent was removed at reduced pressure and the residue was treated with a mixture of THF:Et<sub>2</sub>O 1:2. The white precipitate obtained was filtered off and dried affording 725 mg of the desired product, which was used for the following step without further purification (60% yield); ESI-MS: ( $m/z$ ) 264.9  $[\text{M} + \text{H}]^+$ , 263.0  $[\text{M} - \text{H}]^-$ ; HPLC:  $t_r$  = 2.329 min.

**5-(2-Chloropyridin-4-yl)-4-(4-fluorophenyl)-1-(2-methoxyethyl)-1,3-dihydro-2H-imidazole-2-thione (22a).** The title compound was prepared following general procedure A starting from compound **23** (500 mg, 1.65 mmol) and 2-methoxyethyl isothiocyanate (**24a**, 965 mg, 8.25 mmol); The residue was then treated with Et<sub>2</sub>O obtaining a precipitate, which was filtered off and dried. The filtrate was then concentrated at reduced pressure and the residue was purified by flash column chromatography (SiO<sub>2</sub>, *n*-hexane:EtOAc gradient elution from 7:3 to 1:1). 293 mg of the desired product were obtained in total (49% yield); <sup>1</sup>H-NMR (300 MHz, DMSO-*d*<sub>6</sub>) δ 3.06 (s, 3H), 3.52–3.60 (m, 2H), 3.99–4.14 (m, 2H), 7.08–7.32 (m, 4H), 7.42 (d, *J* = 4.6 Hz, 1H), 7.64 (s, 1H), 8.49 (d, *J* = 4.9 Hz, 1H), 13.07 (br. s, 1H); ESI-MS: ( $m/z$ ) 364.2  $[\text{M} + \text{H}]^+$ , 362.2  $[\text{M} - \text{H}]^-$ ; HPLC:  $t_r$  = 5.321 min.

**5-(2-Chloropyridin-4-yl)-4-(4-fluorophenyl)-1-methyl-1,3-dihydro-2H-imidazole-2-thione (22b).** The title compound was prepared following general procedure A starting from compound **23** (400 mg, 1.32 mmol) and methyl isothiocyanate (**24b**, 643 mg, 6.62 mmol); After the addition of NaHCO<sub>3</sub> saturated solution, a precipitate was formed, which was filtered off and purified twice by flash column chromatography (SiO<sub>2</sub>, DCM:EtOH gradient elution from 100:0 to 97:03) and (SiO<sub>2</sub>, DCM:EtOH 99:01). The obtained solid was treated with a mixture of Et<sub>2</sub>O:*n*-hexane 1:2 and the yellow precipitate obtained was then filtered off and dried, affording 255 mg of the desired compound (60% yield); <sup>1</sup>H-NMR (300 MHz, DMSO-*d*<sub>6</sub>) δ 3.43 (s, 3H), 7.16–7.25 (m, 2H), 7.26–7.35 (m, 2H), 7.42 (dd, *J* = 5.1, 1.3 Hz, 1H), 7.6 (s, 1H), 8.49 (d, *J* = 5.0 Hz, 1H), 13.01 (br. s, 1H); <sup>13</sup>C-NMR (75 MHz, DMSO-*d*<sub>6</sub>) δ 32.1, 115.9 (d, *J* = 22.1 Hz), 123.1, 123.9 (d, *J* = 2.8 Hz), 124.3, 125.1, 125.6, 129.7 (d, *J* = 8.3 Hz), 139.9, 150.7, 151.0, 161.9 (d, *J* = 246.6 Hz), 162.7; ESI-MS: ( $m/z$ ) 318.3  $[\text{M} - \text{H}]^-$ ; HPLC:  $t_r$  = 4.389 min.

**5-(2-Chloropyridin-4-yl)-4-(4-fluorophenyl)-1-phenyl-1,3-dihydro-2H-imidazole-2-thione (22c).** The title compound was prepared following general procedure A starting from compound **23** (400 mg, 1.32 mmol) and phenyl isothiocyanate (**24c**, 535 mg, 3.96 mmol); The residue was purified by flash column chromatography (SiO<sub>2</sub>, DCM:EtOH gradient elution from 100:0 to 98:02). The solid obtained was treated with a mixture of Et<sub>2</sub>O:*n*-hexane 1:2 and the white precipitate formed was then filtered off and dried, affording 260 mg of the desired compound (51% yield); <sup>1</sup>H-NMR (300 MHz, CDCl<sub>3</sub>) δ 6.69 (d, *J* = 4.7 Hz, 1H), 6.81 (s, 1H), 6.89–7.03 (m, 2H), 7.11–7.21 (m, 2H), 7.21–7.30 (m, 2H), 7.32–7.46 (m, 3H), 8.11 (d, *J* = 5.2 Hz, 1H), 12.63 (br. s, 1H); ESI-MS: ( $m/z$ ) 380.5  $[\text{M} - \text{H}]^-$ ; HPLC:  $t_r$  = 5.867 min.

**2-Chloro-4-(4-(4-fluorophenyl)-1-(2-methoxyethyl)-2-(methylthio)-1H-imidazol-5-yl)pyridine (21a).** The title compound was prepared following general procedure B starting from compound **22a** (263 mg, 0.72 mmol), *t*-BuONa (83 mg, 0.86 mmol), and iodomethane (511 mg, 3.6 mmol) obtaining 270 mg of the desired product, which was used for the following step without further purification (99% yield); <sup>1</sup>H-NMR (300 MHz, CDCl<sub>3</sub>) δ 2.73 (s, 3H), 3.25 (s, 3H), 3.55 (t, *J* = 5.5 Hz, 2H), 4.00 (t, *J* = 5.5 Hz, 2H), 6.87–6.98 (m, 2H), 7.21 (dd, *J* = 5.1, 1.4 Hz, 1H), 7.33–7.41 (m, 2H), 7.42 (dd, *J* = 1.3, 0.6 Hz, 1H), 8.40 (dd, *J* = 5.1, 0.6 Hz, 1H); <sup>13</sup>C-NMR (75 MHz, CDCl<sub>3</sub>) δ 16.0, 44.4, 58.9, 70.5, 115.3 (d, *J* = 21.6 Hz), 124.1, 125.7, 126.3, 128.9 (d, *J* = 8.3 Hz), 129.5 (d, *J* = 3.3 Hz), 139.5, 141.9, 145.4, 150.1, 152.1, 162.0 (d, *J* = 246.6 Hz); ESI-MS: ( $m/z$ ) 378.3  $[\text{M} + \text{H}]^+$ ; HPLC:  $t_r$  = 7.524 min.

**2-Chloro-4-(4-(4-fluorophenyl)-1-methyl-2-(methylthio)-1H-imidazol-5-yl)pyridine (21b).** The title compound was prepared following general procedure B starting from compound **22b** (225 mg, 0.70 mmol), *t*-BuONa (81 mg, 0.84 mmol), and iodomethane (497 mg, 3.5 mmol). The crude product was purified by flash column chromatography (SiO<sub>2</sub>, DCM:EtOH gradient elution from 100:0 to 99:01) giving 189 mg of the desired compound (80% yield); <sup>1</sup>H-NMR (300 MHz, CDCl<sub>3</sub>) δ 2.73 (s, 3H), 3.49 (s, 3H), 6.90–7.02 (m, 2H), 7.13 (dd, *J* = 5.1, 1.4 Hz, 1H), 7.34–7.45 (m, 2H), 8.42 (d, *J* = 5.1 Hz, 1H); <sup>13</sup>C-NMR (75 MHz, CDCl<sub>3</sub>)

$\delta$  15.8, 32.0, 115.4 (d,  $J = 21.6$  Hz), 123.4, 124.8, 126.1, 129.1 (d,  $J = 7.7$  Hz), 129.5 (d,  $J = 3.3$  Hz), 139.8, 141.6, 146.1, 150.4, 152.4, 162.2 (d,  $J = 246.6$  Hz); ESI-MS: ( $m/z$ ) 334.3 [M + H]<sup>+</sup>; HPLC:  $t_r = 6.695$  min.

**2-Chloro-4-(4-(4-fluorophenyl)-2-(methylthio)-1-phenyl-1H-imidazol-5-yl)pyridine (21c).** The title compound was prepared following general procedure B starting from compound **22c** (219 mg, 0.57 mmol), *t*-BuONa (55 mg, 0.57 mmol), and iodomethane (404 mg, 2.85 mmol). After adding H<sub>2</sub>O a precipitate was formed, which was filtered off and dried, giving 185 mg of the desired product that was used for the following step without further purification (82% yield); <sup>1</sup>H-NMR (300 MHz, CDCl<sub>3</sub>)  $\delta$  2.68 (s, 3H), 6.82 (d,  $J = 4.7$  Hz, 1H), 6.93 (s, 1H), 6.96–7.09 (m, 2H), 7.11–7.25 (m, 2H), 7.37–7.58 (m, 5H), 8.15 (d,  $J = 4.9$  Hz, 1H); <sup>13</sup>C-NMR (75 MHz, CDCl<sub>3</sub>)  $\delta$  15.1, 115.5 (d,  $J = 21.6$  Hz), 122.6, 124.2, 126.2, 127.6, 129.5 (d,  $J = 3.3$  Hz), 129.6, 129.7, 135.1, 140.8 (d,  $J = 7.7$  Hz), 147.6, 149.6, 151.7, 162.4 (d,  $J = 247.1$  Hz); ESI-MS: ( $m/z$ ) 396.6 [M + H]<sup>+</sup>; HPLC:  $t_r = 9.718$  min.

***N*-(4-(4-(4-Fluorophenyl)-1-(2-methoxyethyl)-2-(methylthio)-1H-imidazol-5-yl)pyridin-2-yl)-3-(4-methoxyphenyl)propanamide (3a) [14].** The title compound was prepared according to general procedure C starting from imidazole **21a** (100 mg, 0.26 mmol), 3-(4-methoxyphenyl)propanamide (72 mg, 0.40 mmol), Pd<sub>2</sub>(dba)<sub>3</sub> (12 mg, 0.013 mmol), XantPhos (15 mg, 0.026 mmol), and Cs<sub>2</sub>CO<sub>3</sub> (254 mg, 0.78 mmol). The residue was purified twice by flash column chromatography (SiO<sub>2</sub>, DCM:EtOH gradient elution from 100:0 to 95:05) and (SiO<sub>2</sub>, DCM:EtOH gradient elution from 100:0 to 97:03) giving 50 mg of the desired product (37% yield); <sup>1</sup>H-NMR (300 MHz, CDCl<sub>3</sub>)  $\delta$  2.64–2.77 (m, 5H), 3.00 (t,  $J = 7.6$  Hz, 2H), 3.24 (s, 3H), 3.51 (t,  $J = 6.0$  Hz, 2H), 3.79 (s, 3H), 4.10 (t,  $J = 6.0$  Hz, 2H), 6.79–6.88 (m, 2H), 6.88–6.99 (m, 3H), 7.11–7.20 (m, 2H), 7.36–7.47 (m, 2H), 8.16 (br. s, 1H), 8.24 (d,  $J = 5.1$  Hz, 1H), 8.29 (s, 1H); ESI-MS: ( $m/z$ ) 521.5 [M + H]<sup>+</sup>, 543.4 [M + Na]<sup>+</sup>, 519.5 [M – H]<sup>–</sup>; HPLC:  $t_r = 8.476$  min.

***N*-(4-(4-(4-Fluorophenyl)-1-methyl-2-(methylthio)-1H-imidazol-5-yl)pyridin-2-yl)-3-(4-methoxyphenyl)propanamide (3b).** The title compound was prepared according to general procedure C starting from imidazole **21b** (70 mg, 0.21 mmol), 3-(4-methoxyphenyl)propanamide (75 mg, 0.41 mmol), Pd<sub>2</sub>(dba)<sub>3</sub> (10 mg, 0.01 mmol), XantPhos (12 mg, 0.021 mmol), and Cs<sub>2</sub>CO<sub>3</sub> (205 mg, 0.63 mmol). The residue was purified twice by flash column chromatography (SiO<sub>2</sub>, DCM:EtOH gradient elution from 99:01 to 95:05) and (SiO<sub>2</sub>, *n*-hexane:EtOAc gradient elution from 4:1 to 1:1) giving 44 mg of the desired product (45% yield); <sup>1</sup>H-NMR (300 MHz, CDCl<sub>3</sub>)  $\delta$  2.62–2.81 (m, 5H), 3.00 (t,  $J = 7.5$  Hz, 2H), 3.54 (s, 3H), 3.79 (s, 3H), 6.84 (d,  $J = 8.6$  Hz, 2H), 6.88–7.00 (m, 3H), 7.14 (d,  $J = 8.6$  Hz, 2H), 7.36–7.50 (m, 2H), 8.21 (d,  $J = 5.1$  Hz, 1H), 8.27 (s, 1H), 8.36 (br. s, 1H); <sup>13</sup>C-NMR (75 MHz, CDCl<sub>3</sub>)  $\delta$  16.1, 30.3, 32.1, 39.6, 55.3, 114.0, 114.6, 115.3 (d,  $J = 21.6$  Hz), 121.1, 127.6, 129.1 (d,  $J = 7.7$  Hz), 129.3, 130.0 (d,  $J = 3.3$  Hz), 132.3, 139.3, 141.1, 145.3, 148.1, 151.9, 158.2, 162.1 (d,  $J = 246.6$  Hz), 171.0; ESI-TOF-HRMS: ( $m/z$ ) [M + H]<sup>+</sup> calcd. for C<sub>26</sub>H<sub>25</sub>FN<sub>4</sub>O<sub>2</sub>S 477.1755, found 477.1762; HPLC:  $t_r = 8.855$  min.

***N*-(4-(4-(4-Fluorophenyl)-2-(methylthio)-1-phenyl-1H-imidazol-5-yl)pyridin-2-yl)-3-(4-methoxyphenyl)propanamide (3c).** The title compound was prepared according to general procedure C starting from imidazole **21c** (70 mg, 0.18 mmol), 3-(4-methoxyphenyl)propanamide (64 mg, 0.36 mmol), Pd<sub>2</sub>(dba)<sub>3</sub> (8 mg, 0.009 mmol), XantPhos (10 mg, 0.018 mmol), and Cs<sub>2</sub>CO<sub>3</sub> (173 mg, 0.53 mmol). The residue was purified twice by flash column chromatography (SiO<sub>2</sub>, DCM:EtOH gradient elution from 99:01 to 95:05) and (SiO<sub>2</sub>, *n*-hexane:EtOAc gradient elution from 4:1 to 1:1) giving 24 mg of the desired product (25% yield); <sup>1</sup>H-NMR (300 MHz, DMSO-*d*<sub>6</sub>)  $\delta$  2.54–2.68 (m, 5H), 2.70–2.84 (m, 2H), 3.71 (s, 3H), 6.77–6.90 (m, 3H), 7.05–7.22 (m, 4H), 7.25–7.36 (m, 2H), 7.39–7.60 (m, 5H), 7.93 (s, 1H), 8.16 (dd,  $J = 5.1$ , 0.7 Hz, 1H), 10.44 (s, 1H); <sup>13</sup>C-NMR (75 MHz, CDCl<sub>3</sub>)  $\delta$  15.3, 30.3, 39.7, 55.2, 113.9, 114.5, 115.3 (d,  $J = 21.6$  Hz), 120.5, 127.9, 129.1, 129.2, 129.4, 129.5 (d,  $J = 7.7$  Hz), 129.8 (d,  $J = 2.8$  Hz), 132.3, 135.4, 140.0, 140.8, 146.8, 147.2, 151.4, 158.1, 162.2 (d,  $J = 246.6$  Hz), 170.4; ESI-TOF-HRMS: ( $m/z$ ) [M + H]<sup>+</sup> calcd. for C<sub>31</sub>H<sub>27</sub>FN<sub>4</sub>O<sub>2</sub>S 539.1911, found 539.1915; HPLC:  $t_r = 10.160$  min.

**(*S*)-4-(4-(4-Fluorophenyl)-1-(2-methoxyethyl)-2-(methylthio)-1H-imidazol-5-yl)-*N*-(1-phenylethyl)pyridin-2-amine (4a) [15].** The title compound was prepared according to general procedure D starting from



compound **21a** (100 mg, 0.26 mmol). The reaction was stopped after 24 h. The residue was then purified twice by flash column chromatography (SiO<sub>2</sub>, DCM:EtOH gradient elution from 100:0 to 95:05) and (SiO<sub>2</sub>, DCM:EtOH gradient elution from 99:01 to 97:03) giving 50 mg of the desired product (41% yield); <sup>1</sup>H-NMR (300 MHz, DMSO-*d*<sub>6</sub>) δ 1.42 (d, *J* = 6.8 Hz, 3H), 2.63 (s, 3H), 3.06 (s, 3H), 3.22–3.32 (m, 2H, partially overlapping with H<sub>2</sub>O signal), 3.78–3.95 (m, 2H), 4.90–5.09 (m, 1H), 6.35–6.52 (m, 2H), 7.01–7.13 (m, 2H), 7.13–7.24 (m, 2H), 7.24–7.46 (m, 6H), 8.03 (d, *J* = 5.1 Hz, 1H); ESI-MS: (*m/z*) 463.5 [M + H]<sup>+</sup>, 461.5 [M – H]<sup>–</sup>; HPLC: *t*<sub>r</sub> = 6.398 min.

(*S*)-4-(4-(4-Fluorophenyl)-1-methyl-2-(methylthio)-1H-imidazol-5-yl)-N-(1-phenylethyl)pyridin-2-amine (**4b**) [15]. The title compound was prepared according to general procedure D starting from compound **21b** (35 mg, 0.105 mmol). The reaction was stopped after 32 h although not completed. The residue was then purified by preparative TLC (SiO<sub>2</sub>, DCM:EtOH 95:05) and by flash column chromatography (SiO<sub>2</sub>, *n*-hexane:EtOAc gradient elution from 7:3 to 1:1) giving 17 mg of the desired product (39% yield); <sup>1</sup>H-NMR (300 MHz, CDCl<sub>3</sub>) δ 1.54 (d, *J* = 6.7 Hz, 3H), 2.64 (s, 3H), 3.08 (s, 3H), 4.47–4.69 (m, 1H), 5.51 (br. s, 1H), 6.05 (s, 1H), 6.42 (d, *J* = 4.7 Hz, 1H), 6.76–6.95 (m, 2H), 7.14–7.53 (m, 7H, overlapping with the solvent peak), 8.05 (d, *J* = 5.1 Hz, 1H); ESI-MS: (*m/z*) 419.3 [M + H]<sup>+</sup>, 417.2 [M – H]<sup>–</sup>; HPLC: *t*<sub>r</sub> = 7.063 min.

(*S*)-4-(4-(4-Fluorophenyl)-2-(methylthio)-1-phenyl-1H-imidazol-5-yl)-N-(1-phenylethyl)pyridin-2-amine (**4c**). The title compound was prepared according to general procedure D starting from compound **21b** (42 mg, 0.106 mmol). The reaction was stopped after 26 h. The residue was purified by flash column chromatography (SiO<sub>2</sub>, *n*-hexane:EtOAc gradient elution from 9:1 to 1:1) giving 42 mg of the desired product (82% yield); <sup>1</sup>H-NMR (300 MHz, CDCl<sub>3</sub>) δ 1.41 (d, *J* = 6.8 Hz, 3H), 2.63 (s, 3H), 4.16–4.34 (m, 1H), 5.18–5.36 (m, 1H), 5.90 (s, 1H), 6.21 (dd, *J* = 5.3, 1.2 Hz, 1H), 6.86–6.98 (m, 2H), 7.00–7.10 (m, 2H), 7.11–7.31 (m, 5H, overlapping with the solvent peak), 7.31–7.41 (m, 3H), 7.41–7.51 (m, 2H), 7.83 (d, *J* = 5.2 Hz, 1H); <sup>13</sup>C-NMR (75 MHz, CDCl<sub>3</sub>) δ 15.3, 24.4, 52.2, 107.4, 114.1, 115.2 (d, *J* = 21.6 Hz), 125.6, 127.1, 127.6, 128.4, 128.7, 128.9, 129.2 (d, *J* = 7.7 Hz), 129.3, 129.9 (d, *J* = 3.3 Hz), 135.5, 139.2, 139.8, 144.0, 146.0, 147.4, 157.8, 162.0 (d, *J* = 246.0 Hz); ESI-TOF-HRMS: (*m/z*) [M + H]<sup>+</sup> calcd. for C<sub>29</sub>H<sub>25</sub>FN<sub>4</sub>S 481.1857, found 481.1865; HPLC: *t*<sub>r</sub> = 9.148 min.

2-Amino-2-(2-chloropyridin-4-yl)-1-(4-fluorophenyl)ethan-1-one hydrochloride (**35**) [13,30]. Oxime **34** [13,30] (500 mg, 1.8 mmol) and 10% Pd on charcoal (100 mg, 0.095 mmol) were placed in a Schlenk reaction tube, which was then evacuated and filled with a H<sub>2</sub> atmosphere. Isopropanolic HCl (10 mL) was then added and the mixture was vigorously stirred at rt under a constant supply of H<sub>2</sub> for 1 h. The solvent was evaporated at reduced pressure and then MeOH was added. The Pd catalyst was removed by filtration and the filtrate was concentrated at reduced pressure. Finally, the residue was treated with EtOAc and the white solid obtained was filtered off and dried, affording 520 mg of the desired product, which were used for the following step without further purification (92% yield); ESI-MS: (*m/z*) 264.9 [M + H]<sup>+</sup>, 262.9 [M – H]<sup>–</sup>; HPLC: *t*<sub>r</sub> = 2.486 min.

4-(2-Chloropyridin-4-yl)-5-(4-fluorophenyl)-1-methyl-1,3-dihydro-2H-imidazole-2-thione (**36**). The title compound was prepared following general procedure A starting from compound **35** (550 mg, 1.82 mmol) and methyl isothiocyanate (**24b**, 665 mg, 9.1 mmol); the residue was then purified by flash column chromatography (SiO<sub>2</sub>, DCM:EtOH gradient elution from 100:0 to 95:05) obtaining 267 mg of the desired product (46% yield); <sup>1</sup>H-NMR (300 MHz, DMSO-*d*<sub>6</sub>) δ 3.27 (s, 3H), 7.03 (dd, *J* = 5.3, 1.6 Hz, 1H), 7.32 (d, *J* = 1.1 Hz, 1H), 7.37–7.48 (m, 2H), 7.51–7.63 (m, 2H), 8.22 (d, *J* = 5.3 Hz, 1H), 13.09 (br. s, 1H); ESI-MS: (*m/z*) 318.0 [M – H]<sup>–</sup>; HPLC: *t*<sub>r</sub> = 5.864 min.

2-Chloro-4-(5-(4-fluorophenyl)-1-methyl-2-(methylthio)-1H-imidazol-4-yl)pyridine (**37**). The title compound was prepared following general procedure B starting from compound **36** (267 mg, 0.83 mmol), *t*-BuONa (96.1 mg, 1.0 mmol), and iodomethane (639 mg, 4.15 mmol) obtaining 255 mg of the desired product, which was used for the following step without further purification (92% yield); <sup>1</sup>H-NMR (300 MHz, CDCl<sub>3</sub>) δ 2.65 (s, 3H), 3.28 (s, 3H), 7.03 (d, *J* = 5.0 Hz, 1H), 7.08–7.31 (m, 4H), 7.44 (s, 1H), 8.02 (d,

$J = 5.2$  Hz, 1H);  $^{13}\text{C}$ -NMR (75 MHz,  $\text{CDCl}_3$ )  $\delta$  15.6, 31.3, 116.7 (d,  $J = 21.6$  Hz), 118.7, 120.4, 125.6 (d,  $J = 3.3$  Hz), 132.3 (d,  $J = 8.3$  Hz), 132.5, 134.3, 144.7, 144.9, 149.2, 151.7, 163.3 (d,  $J = 251.0$  Hz); ESI-MS: ( $m/z$ ) 334.0  $[\text{M} + \text{H}]^+$ ; HPLC:  $t_r = 8.065$  min.

*N*-(4-(5-(4-Fluorophenyl)-1-methyl-2-(methylthio)-1H-imidazol-4-yl)pyridin-2-yl)-3-(4-methoxyphenyl)propanamide (38). The title compound was prepared according to general procedure C starting from imidazole 37 (90 mg, 0.27 mmol), 3-(4-methoxyphenyl)propanamide (73 mg, 0.41 mmol),  $\text{Pd}_2(\text{dba})_3$  (12 mg, 0.013 mmol), XantPhos (16 mg, 0.027 mmol), and  $\text{Cs}_2\text{CO}_3$  (264 mg, 0.81 mmol). The residue was purified by flash column chromatography ( $\text{SiO}_2$ , DCM:EtOH gradient elution from 100:0 to 95:05) affording 82 mg of the desired product (64% yield);  $^1\text{H}$ -NMR (300 MHz,  $\text{CDCl}_3$ )  $\delta$  2.59 (t,  $J = 7.7$  Hz, 2H), 2.76 (s, 3H), 2.94 (t,  $J = 7.6$  Hz, 2H), 3.37 (s, 3H), 3.78 (s, 3H), 6.82 (d,  $J = 8.6$  Hz, 2H), 7.05–7.15 (m, 3H), 7.18–7.27 (m, 2H), 7.29–7.38 (m, 2H), 8.00 (d,  $J = 5.4$  Hz, 1H), 8.21–8.42 (m, 2H);  $^{13}\text{C}$ -NMR (75 MHz,  $\text{CDCl}_3$ )  $\delta$  15.7, 30.3, 31.3, 39.6, 55.2, 110.8, 113.9, 116.5 (d,  $J = 21.6$  Hz), 116.8, 125.9 (d,  $J = 3.3$  Hz), 129.3, 132.2, 132.4 (d,  $J = 8.3$  Hz), 132.6, 135.7, 144.4, 144.5, 146.9, 151.5, 158.0, 163.3 (d,  $J = 246.6$  Hz), 170.4; ESI-TOF-HRMS: ( $m/z$ )  $[\text{M} + \text{H}]^+$  calcd. for  $\text{C}_{26}\text{H}_{25}\text{FN}_4\text{O}_2\text{S}$  477.1755, found 477.1763; HPLC:  $t_r = 7.745$  min.

(*S*)-4-(5-(4-Fluorophenyl)-1-methyl-2-(methylthio)-1H-imidazol-4-yl)-*N*-(1-phenylethyl)pyridin-2-amine (39). The title compound was prepared according to general procedure D starting from compound 21a (55 mg, 0.16 mmol). The reaction was stopped after 40 h although not fully completed. The residue was then purified by flash column chromatography ( $\text{SiO}_2$ , *n*-hexane:EtOAc gradient elution from 4:1 to 1:1) obtaining 39 mg of the desired product (58% yield);  $^1\text{H}$ -NMR (300 MHz,  $\text{CDCl}_3$ )  $\delta$  1.39 (d,  $J = 6.8$  Hz, 3H), 2.60 (s, 3H), 3.22 (s, 3H), 4.37–4.50 (m, 1H), 4.91 (d,  $J = 6.4$  Hz, 1H), 6.30 (s, 1H), 6.57 (dd,  $J = 5.5, 1.4$  Hz, 1H), 6.98–7.31 (m, 9H overlapping with the solvent peak), 7.80 (d,  $J = 5.4$  Hz, 1H);  $^{13}\text{C}$ -NMR (75 MHz,  $\text{CDCl}_3$ )  $\delta$  15.8, 24.2, 31.2, 51.7, 103.4, 110.9, 116.3 (d,  $J = 21.6$  Hz), 125.8, 126.3 (d,  $J = 3.9$  Hz), 126.8, 128.4, 131.3, 132.4 (d,  $J = 8.3$  Hz), 136.1, 143.1, 143.8, 144.6, 147.6, 158.0, 163.0 (d,  $J = 249.9$  Hz); ESI-TOF-HRMS: ( $m/z$ )  $[\text{M} + \text{H}]^+$  calcd. for  $\text{C}_{24}\text{H}_{23}\text{FN}_4\text{S}$  419.1700, found 419.1706; HPLC:  $t_r = 6.899$  min.

**Acknowledgments:** The authors acknowledge Lars Kuckuck for contribution in the synthesis of compounds 3a and 4a. In addition, Jens Strobach, Katharina Bauer, and Mark Kudolo are gratefully acknowledged for the biological assay of synthesized compounds. This study was supported by the Federal Ministry of Education and Research (BMBF) within the BioPharma—Neuroallianz consortium.

**Author Contributions:** F.A., S.A., A.K., W.A., S.A.L. and P.K. conceived and designed the experiments; F.A., S.A. and A.K. performed syntheses; F.A., W.A., S.A.L. and P.K. analyzed the data; F.A., S.A. and P.K. wrote the paper.

**Conflicts of Interest:** The authors declare no conflict of interest.

## References

1. Cuenda, A.; Rousseau, S. p38 MAP-kinases pathway regulation, function and role in human diseases. *Biochim. Biophys. Acta* **2007**, *1773*, 1358–1375. [[CrossRef](#)] [[PubMed](#)]
2. Zarubin, T.; Han, J.H. Activation and signaling of the p38 MAP kinase pathway. *Cell Res.* **2005**, *15*, 11–18. [[CrossRef](#)] [[PubMed](#)]
3. Kaminska, B. MAPK signalling pathways as molecular targets for anti-inflammatory therapy—From molecular mechanisms to therapeutic benefits. *Biochim. Biophys. Acta* **2005**, *1754*, 253–262. [[CrossRef](#)] [[PubMed](#)]
4. Kumar, S.; Boehm, J.; Lee, J.C. p38 MAP kinases: Key signalling molecules as therapeutic targets for inflammatory diseases. *Nat. Rev. Drug Discov.* **2003**, *2*, 717–726. [[CrossRef](#)] [[PubMed](#)]
5. Correa, S.A.; Eales, K.L. The Role of p38 MAPK and Its Substrates in Neuronal Plasticity and Neurodegenerative Disease. *J. Signal Transduct.* **2012**, *2012*, 649079. [[CrossRef](#)] [[PubMed](#)]
6. Kremontsov, D.N.; Thornton, T.M.; Teuscher, C.; Rincon, M. The emerging role of p38 mitogen-activated protein kinase in multiple sclerosis and its models. *Mol. Cell. Biol.* **2013**, *33*, 3728–3734. [[CrossRef](#)] [[PubMed](#)]
7. Munoz, L.; Ammit, A.J. Targeting p38 MAPK pathway for the treatment of Alzheimer's disease. *Neuropharmacology* **2010**, *58*, 561–568. [[CrossRef](#)] [[PubMed](#)]



8. Lee, J.K.; Kim, N.J. Recent Advances in the Inhibition of p38 MAPK as a Potential Strategy for the Treatment of Alzheimer's Disease. *Molecules* **2017**, *22*, 1287. [[CrossRef](#)] [[PubMed](#)]
9. Bühler, S.; Laufer, S.A. p38 MAPK inhibitors: A patent review (2012–2013). *Expert Opin. Ther. Pat.* **2014**, *24*, 535–554. [[CrossRef](#)] [[PubMed](#)]
10. Fischer, S.; Koeberle, S.C.; Laufer, S.A. p38 alpha mitogen-activated protein kinase inhibitors, a patent review (2005–2011). *Expert Opin. Ther. Pat.* **2011**, *21*, 1843–1866. [[CrossRef](#)] [[PubMed](#)]
11. Koch, P.; Ansideri, F. 2-Alkylsulfanyl-4(5)-aryl-5(4)-heteroarylimidazoles: An Overview on Synthetic Strategies and Biological Activity. *Arch. Pharm.* **2017**, *350*, e1700258. [[CrossRef](#)] [[PubMed](#)]
12. Laufer, S.A.; Hauser, D.R.J.; Liedtke, A.J. Regiospecific and highly flexible synthesis of 1,4,5-trisubstituted 2-sulfanylimidazoles from structurally diverse ethanone precursors. *Synthesis* **2008**, 253–266. [[CrossRef](#)]
13. Laufer, S.A.; Wagner, G.K.; Kotschenreuther, D.A.; Albrecht, W. Novel substituted pyridinyl imidazoles as potent anticytokine agents with low activity against hepatic cytochrome P450 enzymes. *J. Med. Chem.* **2003**, *46*, 3230–3244. [[CrossRef](#)] [[PubMed](#)]
14. Ziegler, K.; Hauser, D.R.J.; Unger, A.; Albrecht, W.; Laufer, S.A. 2-Acylaminopyridin-4-ylimidazoles as p38 MAP Kinase Inhibitors: Design, Synthesis, and Biological and Metabolic Evaluations. *ChemMedChem* **2009**, *4*, 1939–1948. [[CrossRef](#)] [[PubMed](#)]
15. Laufer, S.A.; Hauser, D.R.; Domeyer, D.M.; Kinkel, K.; Liedtke, A.J. Design, synthesis, and biological evaluation of novel tri- and tetrasubstituted imidazoles as highly potent and specific ATP-mimetic inhibitors of p38 MAP kinase: Focus on optimized interactions with the enzyme's surface-exposed front region. *J. Med. Chem.* **2008**, *51*, 4122–4149. [[CrossRef](#)] [[PubMed](#)]
16. Griswold, D.E.; Marshall, P.J.; Webb, E.F.; Godfrey, R.; Newton, J.; Dimartino, M.J.; Sarau, H.M.; Gleason, J.G.; Poste, G.; Hanna, N. SK-F-86002—A Structurally Novel Antiinflammatory Agent That Inhibits Lipoxygenase-Mediated and Cyclooxygenase-Mediated Metabolism of Arachidonic Acid. *Biochem. Pharmacol.* **1987**, *36*, 3463–3470. [[CrossRef](#)]
17. Goettert, M.; Graeser, R.; Laufer, S.A. Optimization of a nonradioactive immunosorbent assay for p38alpha mitogen-activated protein kinase activity. *Anal. Biochem.* **2010**, *406*, 233–234. [[CrossRef](#)] [[PubMed](#)]
18. Selig, R.; Schattel, V.; Goettert, M.; Schollmeyer, D.; Albrecht, W.; Laufer, S. Conformational effects on potency of thioimidazoles and dihydrothiazolines. *MedChemComm* **2011**, *2*, 261–269. [[CrossRef](#)]
19. Koch, P.; Jahns, H.; Schattel, V.; Goettert, M.; Laufer, S. Pyridinylquinoxalines and pyridinylpyridopyrazines as lead compounds for novel p38 alpha mitogen-activated protein kinase inhibitors. *J. Med. Chem.* **2010**, *53*, 1128–1137. [[CrossRef](#)] [[PubMed](#)]
20. Wagner, G.K.; Kotschenreuther, D.; Zimmermann, W.; Laufer, S.A. Identification of regioisomers in a series of N-substituted pyridin-4-yl imidazole derivatives by regiospecific synthesis, GC/MS, and H-1 NMR. *J. Org. Chem.* **2003**, *68*, 4527–4530. [[CrossRef](#)] [[PubMed](#)]
21. Laufer, S.; Kotschenreuther, D.; Merckle, P.; Tollmann, K.; Striegel, H.G. 2-thio-Substituted Imidazole Derivatives and the Use Thereof in the Pharmaceutical Industry. U.S. Patents 10/467,064, 7 August 2007.
22. Laufer, S.; Wagner, G.; Kotschenreuther, D. Ones, thiones, and N-oxides: An exercise in imidazole chemistry. *Angew. Chem. Int. Ed.* **2002**, *41*, 2290–2293. [[CrossRef](#)]
23. Laufer, S.; Hauser, D.; Stegmüller, T.; Bracht, C.; Ruff, K.; Schattel, V.; Albrecht, W.; Koch, P. Tri- and tetrasubstituted imidazoles as p38 alpha mitogen-activated protein kinase inhibitors. *Bioorg. Med. Chem. Lett.* **2010**, *20*, 6671–6675. [[CrossRef](#)] [[PubMed](#)]
24. Muth, F.; El-Gokha, A.; Ansideri, F.; Eitel, M.; Döring, E.; Sievers-Engler, A.; Lange, A.; Boeckler, F.M.; Lämmerhofer, M.; Koch, P.; et al. Tri- and Tetrasubstituted Pyridinylimidazoles as Covalent Inhibitors of c-Jun N-Terminal Kinase. *J. Med. Chem.* **2017**, *60*, 594–607. [[CrossRef](#)] [[PubMed](#)]
25. Muth, F.; Günther, M.; Bauer, S.M.; Döring, E.; Fischer, S.; Maier, J.; Drückes, P.; Köppler, J.; Trappe, J.; Rothbauer, U.; et al. Tetra-Substituted Pyridinylimidazoles As Dual Inhibitors of p38 alpha Mitogen-Activated Protein Kinase and c-Jun N-Terminal Kinase 3 for Potential Treatment of Neurodegenerative Diseases. *J. Med. Chem.* **2015**, *58*, 443–456. [[CrossRef](#)] [[PubMed](#)]
26. Graham, S.L.; Scholz, T.H. A New Mode of Reactivity of N-Methoxy-N-Methylamides with Strongly Basic Reagents. *Tetrahedron Lett.* **1990**, *31*, 6269–6272. [[CrossRef](#)]
27. Labeeuw, O.; Phansavath, P.; Genet, J.P. Synthesis of modified Weinreb amides: N-tert-butoxy-N-methylamides as effective acylating agents. *Tetrahedron Lett.* **2004**, *45*, 7107–7110. [[CrossRef](#)]

28. Reeves, J.T.; Tan, Z.L.; Reeves, D.C.; Song, J.H.J.; Han, Z.X.S.; Xu, Y.B.; Tang, W.J.; Yang, B.S.; Razavi, H.; Harcken, C.; et al. Development of an Enantioselective Hydrogenation Route to (S)-1-(2-(Methylsulfonyl)pyridin-4-yl)propan-1-amine. *Org. Process Res. Dev.* **2014**, *18*, 904–911. [[CrossRef](#)]
29. Lantos, I.; Gombatz, K.; McGuire, M.; Pridgen, L.; Remich, J.; Shilcrat, S. Synthetic and Mechanistic Studies on the Preparation of Pyridyl-Substituted Imidazothiazoles. *J. Org. Chem.* **1988**, *53*, 4223–4227. [[CrossRef](#)]
30. Laufer, S.A.; Liedtke, A.J. A concise and optimized four-step approach toward 2-(aryl)-alkylsulfanyl-, 4(5)-aryl-, 5(4)-heteroaryl-substituted imidazoles using alkyl- or arylalkyl thiocyanates. *Tetrahedron Lett.* **2006**, *47*, 7199–7203. [[CrossRef](#)]
31. Li, Z.Y.; Ma, H.Z.; Han, C.; Xi, H.T.; Meng, Q.; Chen, X.; Sun, X.Q. Synthesis of Isothiocyanates by Reaction of Amines with Phenyl Chlorothionoformate via One-Pot or Two-Step Process. *Synthesis* **2013**, *45*, 1667–1674. [[CrossRef](#)]
32. Sun, N.; Li, B.; Shao, J.P.; Mo, W.M.; Hu, B.X.; Shen, Z.L.; Hu, X.Q. A general and facile one-pot process of isothiocyanates from amines under aqueous conditions. *Beilstein J. Org. Chem.* **2012**, *8*, 61–70. [[CrossRef](#)] [[PubMed](#)]
33. Wong, R.; Dolman, S.J. Isothiocyanates from tosyl chloride mediated decomposition of in situ generated dithiocarbamic acid salts. *J. Org. Chem.* **2007**, *72*, 3969–3971. [[CrossRef](#)] [[PubMed](#)]

**Sample Availability:** Samples of the compounds **38** and **39** are available from the authors.



© 2018 by the authors. Licensee MDPI, Basel, Switzerland. This article is an open access article distributed under the terms and conditions of the Creative Commons Attribution (CC BY) license (<http://creativecommons.org/licenses/by/4.0/>).



## Publication VI

Ansideri, F.; Schollmeyer, D.; Koch, P. 1-(3',6'-Dihydroxy-3-oxo-3H-spiro[isobenzofuran-1,9'-xanthen]-5-yl)-3-[4-({4-[1-(4-fluorophenyl)-1H-imidazol-5-yl]pyridin-2-yl}amino)phenyl]thiourea methanol monosolvate. *IUCrData* **2016**, *1*, x160840.

**Open access publication**

**Link to the published version:**

<http://iucrdata.iucr.org/x/issues/2016/05/00/hb4047/index.html>



data reports



ISSN 2474-3146

# 1-(3',6'-Dihydroxy-3-oxo-3*H*-spiro[isobenzofuran-1,9'-xanthen]-5-yl)-3-[4-([4-[1-(4-fluorophenyl)-1*H*-imidazol-5-yl]pyridin-2-yl]amino)phenyl]thiourea methanol monosolvate

Francesco Ansideri,<sup>a</sup> Dieter Schollmeyer<sup>b</sup> and Pierre Koch<sup>a\*</sup>

Received 14 May 2016  
Accepted 25 May 2016

Edited by W. T. A. Harrison, University of Aberdeen, Scotland

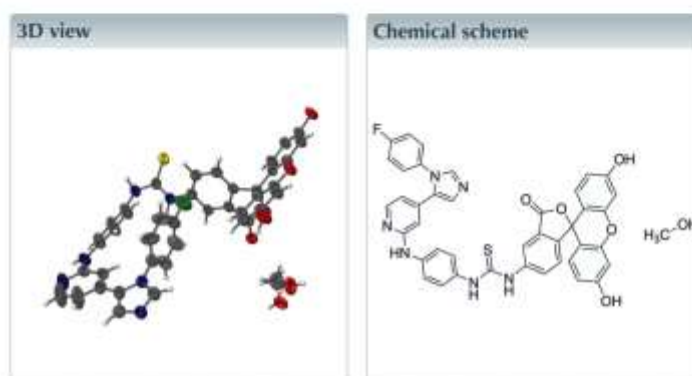
**Keywords:** crystal structure; fluorescein; thiourea; pyridenylimidazole.

CCDC reference: 1481316

Structural data: full structural data are available from [icrdata.iucr.org](http://icrdata.iucr.org)

<sup>a</sup>Institute of Pharmaceutical Sciences, Department of Pharmaceutical and Medicinal Chemistry, Eberhard Karls Universität Tübingen, Auf der Morgenstelle 8, 72076 Tübingen, Germany, and <sup>b</sup>Department of Organic Chemistry, Johannes Gutenberg-University Mainz, Duesbergweg 10-14, 55099 Mainz, Germany. \*Correspondence e-mail: [pierre.koch@uni-tuebingen.de](mailto:pierre.koch@uni-tuebingen.de)

The title compound, which crystallized as a methanol monosolvate,  $C_{23}H_{22}FN_6O_5S \cdot CH_3OH$ , was synthesized as a probe for a fluorescence polarization-based competition binding assay. The isobenzofuran fused-ring system is close to planar and orientated almost perpendicular to the central ring of the xanthene system. The dihedral angle between the benzene rings of the xanthene system is  $10.0(2)^\circ$ , indicating a butterfly-like orientation. A short intramolecular  $C-F \cdots \pi$  contact [ $F \cdots \pi = 3.100(4) \text{ \AA}$  and  $C-F \cdots \pi = 139.9(3)^\circ$ ] to the six-membered ring of the isobenzofuran system may influence the molecular conformation. The methanol solvent molecule is disordered over two orientations in a 0.6:0.4 ratio. In the crystal, the components are linked by numerous hydrogen bonds, generating a three-dimensional network.



## Structure description

The title compound was synthesized by reaction of *N*1-[4-[1-(4-fluorophenyl)-1*H*-imidazol-5-yl]pyridin-2-yl]benzene-1,4-diamine and 5(6)-fluorescein-isothiocyanate as a probe for a fluorescence polarization-based competition binding assay. The design and application of similar probes was recently published by our group (Ansideri *et al.*, 2016). As a commercially available isomeric mixture of the 5'- and 6'-isomers of fluorescein-isothiocyanate had been used as a starting material, single-crystal analysis was performed to confirm the isolated isomer. X-ray data confirmed that solely the 5'-isomer was isolated. The title molecule is shown in Fig. 1.

OPEN ACCESS

IUCrData (2016), 1, x160840

<http://dx.doi.org/10.1107/52414314616008401> 1 of 3

## data reports

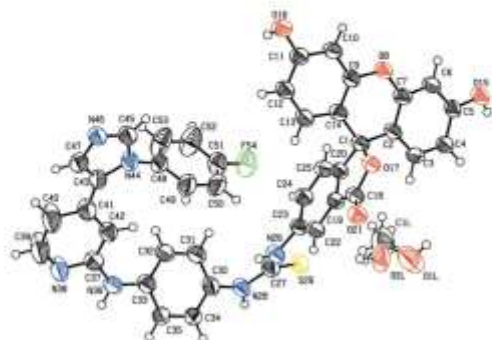


Figure 1  
The molecular structure of the title compound, with displacement ellipsoids drawn at the 50% probability level.

The isobenzofuran fused-ring system is almost planar (r.m.s. deviation = 0.038 Å) and almost perpendicular to the central ring of the xanthene system [dihedral angle = 86.44 (17)°]. The dihedral angle between the benzene rings of the xanthene system is 10.0 (2)°. The thiourea unit of the molecule makes dihedral angles of 53.64 (17)° and 56.3 (2)° with the isobenzofuran ring system and the pyridine-C2 position, respectively. The imidazole ring makes a dihedral angle of 14.8 (3)° with the 4-fluorophenyl ring. The pyridine ring is almost perpendicular to the imidazole core, subtending a dihedral angle of 84.9 (3)°. A short intramolecular C—F... $\pi$  contact [F... $\pi$  = 3.100 (4) Å and C—F... $\pi$  = 139.9 (3)°] to the six-membered ring of the isobenzofuran system may influence the molecular conformation.

The crystal packing features numerous hydrogen bonds (Table 1), generating a three-dimensional network, and incorporates one disordered molecule of methanol.

## Synthesis and crystallization

A solution of N1-[4-[1-(4-fluorophenyl)-1H-imidazol-5-yl]-pyridin-2-yl]benzene-1,4-diamine (200 mg, 0.58 mmol) and 5(6)-fluorescein-isothiocyanate (248 mg, 0.77 mmol) in acetone (30 ml) was stirred at 298 K for 48 h with light excluded. The mixture was evaporated to dryness and the residue was purified by flash chromatography (dichloromethane-ethanol 95:05-90:10) obtaining 160 mg of the desired product (yield 37%). Crystals of the title compound suitable for X-ray diffraction were obtained by slow evaporation of a solution of the solid in methanol at 298 K.

<sup>1</sup>H NMR (250 MHz, DMSO-*d*<sub>6</sub>):  $\delta$  6.45 (dd,  $J_1$  = 5.3 Hz,  $J_2$  = 1.4 Hz, 1H), 6.53–6.63 (m, 5H), 6.67 (d,  $J$  = 2.0 Hz, 2H), 7.18 (d,  $J$  = 8.4 Hz, 1H), 7.27 (d,  $J$  = 8.9 Hz, 2H), 7.35–7.45 (m, 5H), 7.47 (d,  $J$  = 9.0 Hz, 2H), 7.82 (dd,  $J_1$  = 8.4 Hz,  $J_2$  = 2.0 Hz), 8.00 (d,  $J$  = 1.0 Hz, 1H), 8.05 (d,  $J$  = 5.4 Hz, 1H), 8.17 (d,  $J$  = 1.9 Hz, 1H), 9.06 (br s, 1H), 9.94 (br s, 1H), 10.00 (s, 1H), 10.17 (s, 2H); <sup>13</sup>C NMR (100 MHz, DMSO-*d*<sub>6</sub>)  $\delta$  83.6, 102.9, 108.3, 111.4,

Table 1  
Hydrogen-bond geometry (Å, °).

D—H...A	D—H	H...A	D...A	D—H...A
O15—H15...N46 <sup>i</sup>	0.84	1.84	2.667 (5)	168
O16—H16...O21 <sup>ii</sup>	0.84	2.04	2.808 (5)	153
C22—H22...O15 <sup>ii</sup>	0.95	2.59	3.315 (5)	133
C24—H24...S29 <sup>ii</sup>	0.95	2.99	3.804 (5)	145
N26—H26...O15 <sup>ii</sup>	1.09	2.17	3.061 (5)	138
N28—H28...N38 <sup>ii</sup>	1.17	1.94	3.009 (6)	162
C34—H34...O1L <sup>iii</sup>	0.95	2.46	3.334 (9)	154
N36—H36...S29 <sup>iii</sup>	0.88	2.64	3.437 (4)	152
C40—H40...O2L <sup>iiii</sup>	0.95	2.32	3.103 (12)	139
C45—H45...O17 <sup>i</sup>	0.95	2.49	3.379 (6)	155
C53—H53...S29 <sup>ii</sup>	0.95	2.87	3.743 (6)	153
C1L—H2M...O2i	0.98	2.56	3.267 (7)	129
O1L—H1L...S29 <sup>ii</sup>	0.84	2.46	3.202 (8)	147

Symmetry codes: (i)  $x, y-1, z$ ; (ii)  $-x+\frac{1}{2}, -y+\frac{1}{2}, -z+1$ ; (iii)  $x-\frac{1}{2}, y+\frac{1}{2}, z$ ; (iv)  $-x+1, y, -z+\frac{1}{2}$ ; (v)  $-x+\frac{1}{2}, y-\frac{1}{2}, -z+\frac{1}{2}$ ; (vi)  $-x+\frac{1}{2}, -y+\frac{1}{2}, -z+1$ ; (vii)  $-x+\frac{1}{2}, y+\frac{1}{2}, -z+\frac{1}{2}$ ; (viii)  $-x+1, -y+1, -z+1$ ; (ix)  $x+\frac{1}{2}, y+\frac{1}{2}, z$ ; (x)  $-x+1, -y, -z+1$ .

Table 2  
Experimental details.

Crystal data	
Chemical formula	C <sub>22</sub> H <sub>22</sub> FN <sub>6</sub> O <sub>5</sub> S·CH <sub>3</sub> O
<i>M</i> <sub>r</sub>	766.79
Crystal system, space group	Monoclinic, <i>C2/c</i>
Temperature (K)	193
<i>a</i> , <i>b</i> , <i>c</i> (Å)	15.1825 (8), 17.7557 (7), 26.2236 (13)
$\beta$ (°)	92.283 (4)
<i>V</i> (Å <sup>3</sup> )	7063.6 (6)
<i>Z</i>	8
Radiation type	Mo <i>K</i> $\alpha$
$\mu$ (mm <sup>-1</sup> )	0.16
Crystal size (mm)	0.09 × 0.08 × 0.07
Data collection	
Diffractometer	Stoe IPDS 2T
No. of measured, independent and observed [ $I > 2\sigma(I)$ ] reflections	23065, 8960, 3244
<i>R</i> <sub>int</sub>	0.085
( $\sin \theta$ ) <sub>max</sub> (Å <sup>-1</sup> )	0.674
Refinement	
$R$ [ $F^2 > 2\sigma(F^2)$ ], <i>wR</i> [ $F^2$ ], <i>S</i>	0.070, 0.240, 0.92
No. of reflections	8960
No. of parameters	516
No. of restraints	2
H-atom treatment	H-atom parameters constrained
$\Delta\rho_{max}$ , $\Delta\rho_{min}$ (e Å <sup>-3</sup> )	0.35, -0.38

Computer programs: *X-AREA* and *X-RED* (Stoe & Cie, 2011), *SIR2004* (Burla et al., 2005) and *SHELXL2014* (Sheldrick, 2015).

113.3, 113.4, 117.3 (*d*,  $J$  = 22.9 Hz), 118.4, 119.1, 124.6, 125.7, 127.2, 128.7 (*d*,  $J$  = 8.8 Hz), 129.8, 130.8, 131.3, 132.7, 133.3 (*d*,  $J$  = 2.4 Hz), 138.4, 139.6, 141.8, 142.3, 148.5, 148.7, 152.8, 156.9, 160.5, 162.6 (*d*,  $J$  = 245.6 Hz), 169.6, 180.8. HPLC: *t* = 11.54 min, purity: 98% ( $\lambda$  = 254 nm).

## Refinement

Crystal data, data collection and structure refinement details are summarized in Table 2. The methanol solvent molecule is disordered over two orientations in a 0.6:0.4 ratio.

---

**data reports****References**

- Ansideri, F., Lange, A., El-Gokha, A., Boeckler, F. M. & Koch, P. (2016). *Anal. Biochem.* **503**, 28–40.
- Burla, M. C., Caliandro, R., Camalli, M., Carrozzini, B., Cascarano, G. L., De Caro, L., Giacovazzo, C., Polidori, G. & Spagna, R. (2005). *J. Appl. Cryst.* **38**, 381–388.
- Sheldrick, G. M. (2015). *Acta Cryst.* **C71**, 3–8.
- Stoe & Cie (2011). *X-RED* and *X-AREA*. Stoe & Cie, Darmstadt, Darmstadt, Germany.

## full crystallographic data

*IUCrData* (2016), 1, x160840 [doi:10.1107/S2414314616008403]

**1-(3',6'-Dihydroxy-3-oxo-3*H*-spiro[isobenzofuran-1,9'-xanthen]-5-yl)-3-[4-((4-[1-(4-fluorophenyl)-1*H*-imidazol-5-yl]pyridin-2-yl)amino)phenyl]-thiourea methanol monosolvate**

Francesco Ansideri, Dieter Schollmeyer and Pierre Koch

1-(3',6'-Dihydroxy-3-oxo-3*H*-spiro[isobenzofuran-1,9'-xanthen]-5-yl)-3-[4-((4-[1-(4-fluorophenyl)-1*H*-imidazol-5-yl]pyridin-2-yl)amino)phenyl]thiourea; methanol

*Crystal data*

$C_{21}H_{17}FN_4O_5S \cdot CH_2O$   
 $M_r = 766.79$   
 Monoclinic,  $C2/c$   
 $a = 15.1825$  (8) Å  
 $b = 17.7557$  (7) Å  
 $c = 26.2236$  (13) Å  
 $\beta = 92.283$  (4)°  
 $V = 7063.6$  (6) Å<sup>3</sup>  
 $Z = 8$

$F(000) = 3184$   
 $D_x = 1.442$  Mg m<sup>-3</sup>  
 Mo  $K\alpha$  radiation,  $\lambda = 0.71073$  Å  
 Cell parameters from 7245 reflections  
 $\theta = 2.3\text{--}27.9^\circ$   
 $\mu = 0.16$  mm<sup>-1</sup>  
 $T = 193$  K  
 Block, colourless  
 $0.09 \times 0.08 \times 0.07$  mm

*Data collection*

Stoe IPDS 2T  
 diffractometer  
 Radiation source: sealed X-ray tube, 12 x 0.4  
 mm long-fine focus  
 Detector resolution: 6.67 pixels mm<sup>-1</sup>  
 rotation method scans  
 23065 measured reflections

8960 independent reflections  
 3244 reflections with  $I > 2\sigma(I)$   
 $R_{int} = 0.085$   
 $\theta_{max} = 28.6^\circ$ ,  $\theta_{min} = 2.3^\circ$   
 $h = -20\text{--}+20$   
 $k = -21\text{--}+23$   
 $l = -35\text{--}+35$

*Refinement*

Refinement on  $F^2$   
 Least-squares matrix: full  
 $R[F^2 > 2\sigma(F^2)] = 0.070$   
 $wR(F^2) = 0.240$   
 $S = 0.92$   
 8960 reflections  
 516 parameters  
 2 restraints  
 Hydrogen site location: mixed

H-atom parameters constrained  
 $w = 1/[\sigma^2(F_o^2) + (0.110P)^2]$   
 where  $P = (F_o^2 + 2F_c^2)/3$   
 $(\Delta/\sigma)_{max} < 0.001$   
 $\Delta\rho_{max} = 0.35$  e Å<sup>-3</sup>  
 $\Delta\rho_{min} = -0.38$  e Å<sup>-3</sup>  
 Extinction correction: *SHELXL2014* (Sheldrick,  
 2015),  $F_c = kF_c[1 + 0.001x\text{Fc}^2/\text{sin}(2\theta)]^{-1/4}$   
 Extinction coefficient: 0.00101 (19)

## data reports

*Special details*

**Geometry.** All esds (except the esd in the dihedral angle between two l.s. planes) are estimated using the full covariance matrix. The cell esds are taken into account individually in the estimation of esds in distances, angles and torsion angles; correlations between esds in cell parameters are only used when they are defined by crystal symmetry. An approximate (isotropic) treatment of cell esds is used for estimating esds involving l.s. planes.

*Fractional atomic coordinates and isotropic or equivalent isotropic displacement parameters ( $\text{\AA}^2$ )*

	x	y	z	$U_{\text{eq}}^*(U_{\text{eq}})$	Occ. (<1)
C1	0.7146 (3)	0.0416 (2)	0.45826 (18)	0.0456 (10)	
C2	0.7446 (3)	-0.0387 (2)	0.45478 (17)	0.0438 (9)	
C3	0.6854 (3)	-0.0980 (2)	0.45158 (19)	0.0491 (11)	
H3	0.6242	-0.0874	0.4526	0.059*	
C4	0.7120 (3)	-0.1717 (2)	0.44691 (18)	0.0485 (10)	
H4	0.6698	-0.2113	0.4457	0.058*	
C5	0.8021 (3)	-0.1878 (2)	0.44396 (18)	0.0466 (10)	
C6	0.8623 (3)	-0.1298 (2)	0.44888 (19)	0.0503 (11)	
H6	0.9237	-0.1402	0.4484	0.060*	
C7	0.8333 (3)	-0.0563 (2)	0.45448 (18)	0.0469 (10)	
O8	0.89947 (18)	-0.00298 (16)	0.45973 (14)	0.0535 (8)	
C9	0.8766 (3)	0.0723 (2)	0.45771 (19)	0.0467 (10)	
C10	0.9461 (3)	0.1221 (3)	0.45871 (19)	0.0519 (11)	
H10	1.0050	0.1041	0.4617	0.062*	
C11	0.9296 (3)	0.1988 (3)	0.4553 (2)	0.0525 (11)	
C12	0.8432 (3)	0.2243 (3)	0.4504 (2)	0.0578 (12)	
H12	0.8314	0.2767	0.4469	0.069*	
C13	0.7748 (3)	0.1734 (2)	0.45061 (19)	0.0523 (11)	
H13	0.7158	0.1915	0.4481	0.063*	
C14	0.7897 (3)	0.0962 (2)	0.45448 (18)	0.0454 (10)	
O15	0.83304 (19)	-0.25782 (16)	0.43631 (13)	0.0548 (8)	
H15	0.7917	-0.2856	0.4254	0.082*	
O16	0.99968 (19)	0.24600 (18)	0.45616 (15)	0.0636 (9)	
H16	0.9845	0.2883	0.4672	0.095*	
O17	0.67552 (18)	0.05307 (17)	0.51047 (12)	0.0470 (7)	
C18	0.5937 (3)	0.0830 (2)	0.50544 (18)	0.0453 (10)	
C19	0.5674 (3)	0.0866 (2)	0.45147 (18)	0.0453 (10)	
C20	0.6358 (3)	0.0599 (2)	0.42341 (18)	0.0441 (10)	
O21	0.5539 (2)	0.10267 (18)	0.54287 (13)	0.0541 (8)	
C22	0.4891 (3)	0.1127 (2)	0.42833 (18)	0.0462 (10)	
H22	0.4421	0.1305	0.4479	0.055*	
C23	0.4827 (3)	0.1116 (2)	0.37583 (18)	0.0470 (10)	
C24	0.5513 (3)	0.0831 (2)	0.34715 (19)	0.0488 (11)	
H24	0.5447	0.0814	0.3110	0.059*	
C25	0.6285 (3)	0.0575 (3)	0.37110 (19)	0.0487 (11)	
H25	0.6753	0.0387	0.3518	0.058*	
N26	0.4075 (2)	0.1462 (2)	0.35115 (15)	0.0497 (9)	
H26	0.3989	0.2001	0.3703	0.060*	
C27	0.3620 (3)	0.1219 (3)	0.30850 (18)	0.0491 (11)	

## data reports

N28	0.3064 (2)	0.1732 (2)	0.28696 (16)	0.0525 (9)	
H28	0.2590	0.1411	0.2583	0.063*	
S29	0.36943 (8)	0.03475 (7)	0.28470 (5)	0.0582 (4)	
C30	0.3108 (3)	0.2532 (2)	0.29427 (19)	0.0511 (11)	
C31	0.3902 (3)	0.2919 (3)	0.2939 (2)	0.0591 (12)	
H31	0.4438	0.2645	0.2924	0.071*	
C32	0.3928 (3)	0.3699 (3)	0.2956 (2)	0.0576 (12)	
H32	0.4477	0.3955	0.2953	0.069*	
C33	0.3145 (3)	0.4108 (3)	0.29767 (19)	0.0513 (11)	
C34	0.2351 (3)	0.3715 (3)	0.29846 (19)	0.0527 (11)	
H34	0.1812	0.3986	0.2995	0.063*	
C35	0.2338 (3)	0.2942 (3)	0.29771 (19)	0.0526 (11)	
H35	0.1792	0.2684	0.2996	0.063*	
N36	0.3091 (2)	0.4896 (2)	0.29414 (17)	0.0570 (10)	
H36	0.2562	0.5064	0.2850	0.068*	
C37	0.3706 (3)	0.5452 (3)	0.30223 (19)	0.0532 (11)	
N38	0.3436 (3)	0.6124 (3)	0.2834 (2)	0.0799 (15)	
C39	0.3977 (5)	0.6696 (4)	0.2922 (4)	0.126 (4)	
H39	0.3783	0.7182	0.2815	0.151*	
C40	0.4795 (5)	0.6642 (4)	0.3158 (3)	0.115 (3)	
H40	0.5173	0.7068	0.3177	0.138*	
C41	0.5070 (3)	0.5962 (3)	0.3369 (2)	0.0607 (13)	
C42	0.4508 (3)	0.5361 (3)	0.32982 (19)	0.0528 (11)	
H42	0.4663	0.4882	0.3437	0.063*	
C43	0.5906 (3)	0.5970 (3)	0.36659 (19)	0.0534 (11)	
N44	0.6417 (2)	0.5368 (2)	0.38405 (15)	0.0509 (9)	
C45	0.7124 (3)	0.5661 (3)	0.4102 (2)	0.0561 (12)	
H45	0.7584	0.5368	0.4257	0.067*	
N46	0.7097 (2)	0.6401 (2)	0.41169 (16)	0.0534 (9)	
C47	0.6355 (3)	0.6593 (3)	0.38449 (19)	0.0548 (11)	
H47	0.6168	0.7097	0.3785	0.066*	
C48	0.6348 (3)	0.4580 (3)	0.37468 (19)	0.0523 (11)	
C49	0.5898 (4)	0.4127 (3)	0.4064 (2)	0.0721 (16)	
H49	0.5584	0.4341	0.4335	0.087*	
C50	0.5895 (4)	0.3352 (3)	0.3992 (3)	0.0799 (18)	
H50	0.5583	0.3030	0.4211	0.096*	
C51	0.6341 (4)	0.3071 (3)	0.3607 (2)	0.0675 (15)	
C52	0.6814 (5)	0.3505 (3)	0.3291 (3)	0.091 (2)	
H52	0.7139	0.3286	0.3027	0.109*	
C53	0.6807 (5)	0.4272 (3)	0.3365 (2)	0.084 (2)	
H53	0.7127	0.4590	0.3147	0.101*	
F54	0.6336 (3)	0.23112 (17)	0.35271 (16)	0.0939 (11)	
C1L	0.5122 (6)	0.1316 (5)	0.6625 (3)	0.123 (3)	
H1M	0.4629	0.1554	0.6435	0.185*	0.6
H2M	0.5428	0.0971	0.6401	0.185*	0.6
H3M	0.5534	0.1705	0.6752	0.185*	0.6
H4M	0.5767	0.1337	0.6620	0.185*	0.4
H5M	0.4867	0.1573	0.6323	0.185*	0.4



## data reports

H6M	0.4930	0.0789	0.6625	0.185*	0.4
O1L	0.4803 (5)	0.0914 (5)	0.7038 (3)	0.111 (3)	0.6
H1L	0.5221	0.0681	0.7188	0.166*	0.6
O2L	0.4841 (7)	0.1673 (5)	0.7067 (3)	0.081 (3)	0.4
H2L	0.4341	0.1864	0.7008	0.122*	0.4

Atomic displacement parameters ( $\text{\AA}^2$ )

	$U^{11}$	$U^{22}$	$U^{33}$	$U^{12}$	$U^{13}$	$U^{23}$
C1	0.0352 (19)	0.044 (2)	0.057 (3)	0.0036 (17)	-0.0048 (18)	-0.006 (2)
C2	0.0364 (19)	0.042 (2)	0.052 (3)	0.0047 (17)	-0.0059 (17)	-0.002 (2)
C3	0.0342 (19)	0.043 (2)	0.070 (3)	0.0017 (17)	0.0030 (19)	-0.002 (2)
C4	0.039 (2)	0.038 (2)	0.068 (3)	-0.0018 (17)	-0.0038 (19)	-0.003 (2)
C5	0.044 (2)	0.034 (2)	0.061 (3)	0.0040 (17)	-0.003 (2)	-0.0025 (19)
C6	0.035 (2)	0.043 (2)	0.072 (3)	0.0047 (17)	-0.003 (2)	-0.003 (2)
C7	0.036 (2)	0.045 (2)	0.059 (3)	-0.0005 (17)	-0.0040 (19)	-0.006 (2)
O8	0.0363 (14)	0.0361 (15)	0.087 (2)	0.0002 (12)	-0.0070 (15)	-0.0041 (15)
C9	0.043 (2)	0.035 (2)	0.062 (3)	-0.0002 (17)	-0.005 (2)	-0.005 (2)
C10	0.035 (2)	0.047 (2)	0.073 (3)	0.0026 (18)	-0.004 (2)	-0.009 (2)
C11	0.043 (2)	0.045 (2)	0.069 (3)	-0.0048 (19)	-0.002 (2)	-0.006 (2)
C12	0.045 (2)	0.042 (2)	0.085 (4)	0.0045 (19)	-0.005 (2)	-0.004 (2)
C13	0.041 (2)	0.040 (2)	0.075 (3)	0.0040 (18)	-0.008 (2)	-0.005 (2)
C14	0.038 (2)	0.041 (2)	0.056 (3)	0.0026 (17)	-0.0028 (18)	-0.010 (2)
O15	0.0430 (15)	0.0361 (15)	0.085 (2)	0.0058 (13)	-0.0048 (15)	-0.0086 (16)
O16	0.0409 (15)	0.0425 (17)	0.107 (3)	-0.0043 (13)	0.0025 (17)	-0.0120 (18)
O17	0.0389 (14)	0.0475 (17)	0.0541 (19)	0.0063 (12)	-0.0050 (13)	-0.0031 (14)
C18	0.037 (2)	0.043 (2)	0.055 (3)	0.0050 (17)	-0.0051 (19)	-0.006 (2)
C19	0.037 (2)	0.041 (2)	0.058 (3)	0.0024 (17)	0.0013 (19)	-0.001 (2)
C20	0.038 (2)	0.040 (2)	0.054 (3)	0.0023 (17)	0.0015 (18)	-0.0023 (19)
O21	0.0514 (17)	0.0521 (19)	0.059 (2)	0.0047 (15)	0.0018 (15)	-0.0044 (16)
C22	0.037 (2)	0.046 (2)	0.055 (3)	0.0064 (17)	-0.0010 (18)	-0.002 (2)
C23	0.0340 (19)	0.045 (2)	0.061 (3)	0.0011 (17)	-0.0048 (18)	-0.002 (2)
C24	0.044 (2)	0.046 (2)	0.056 (3)	-0.0010 (18)	-0.003 (2)	-0.005 (2)
C25	0.038 (2)	0.051 (3)	0.057 (3)	0.0035 (18)	0.0034 (19)	-0.006 (2)
N26	0.0429 (18)	0.046 (2)	0.060 (2)	0.0064 (16)	-0.0094 (17)	-0.0054 (18)
C27	0.042 (2)	0.048 (2)	0.056 (3)	-0.0002 (18)	-0.0078 (19)	0.002 (2)
N28	0.046 (2)	0.041 (2)	0.069 (3)	0.0028 (16)	-0.0160 (17)	-0.0009 (18)
S29	0.0543 (6)	0.0454 (6)	0.0736 (9)	0.0011 (5)	-0.0144 (6)	-0.0027 (6)
C30	0.050 (2)	0.039 (2)	0.063 (3)	0.0015 (19)	-0.010 (2)	0.001 (2)
C31	0.044 (2)	0.051 (3)	0.082 (4)	0.004 (2)	-0.007 (2)	0.000 (3)
C32	0.044 (2)	0.044 (2)	0.084 (4)	0.0012 (19)	-0.005 (2)	-0.003 (2)
C33	0.049 (2)	0.041 (2)	0.063 (3)	0.0012 (19)	-0.006 (2)	-0.005 (2)
C34	0.044 (2)	0.044 (2)	0.070 (3)	-0.0028 (18)	-0.006 (2)	0.004 (2)
C35	0.045 (2)	0.048 (3)	0.064 (3)	-0.0009 (19)	-0.005 (2)	0.009 (2)
N36	0.043 (2)	0.044 (2)	0.083 (3)	0.0023 (16)	-0.0078 (19)	-0.006 (2)
C37	0.050 (2)	0.046 (3)	0.063 (3)	-0.002 (2)	-0.009 (2)	-0.010 (2)
N38	0.079 (3)	0.051 (3)	0.107 (4)	-0.006 (2)	-0.039 (3)	0.014 (3)
C39	0.119 (6)	0.058 (4)	0.192 (9)	-0.034 (4)	-0.103 (6)	0.041 (5)

## data reports

C40	0.108 (5)	0.062 (4)	0.170 (8)	-0.029 (4)	-0.081 (5)	0.039 (4)
C41	0.063 (3)	0.050 (3)	0.068 (3)	-0.006 (2)	-0.022 (2)	0.001 (2)
C42	0.056 (3)	0.040 (2)	0.062 (3)	0.001 (2)	-0.007 (2)	-0.004 (2)
C43	0.055 (3)	0.047 (2)	0.057 (3)	-0.004 (2)	-0.007 (2)	0.009 (2)
N44	0.054 (2)	0.0402 (19)	0.058 (2)	-0.0027 (17)	-0.0079 (17)	0.0009 (18)
C45	0.048 (2)	0.047 (3)	0.073 (3)	-0.004 (2)	-0.012 (2)	-0.001 (2)
N46	0.049 (2)	0.045 (2)	0.065 (3)	-0.0013 (17)	-0.0119 (18)	-0.0027 (19)
C47	0.056 (3)	0.047 (3)	0.061 (3)	-0.006 (2)	-0.007 (2)	-0.002 (2)
C48	0.051 (2)	0.043 (2)	0.062 (3)	-0.007 (2)	-0.003 (2)	0.004 (2)
C49	0.077 (3)	0.049 (3)	0.092 (4)	0.005 (3)	0.027 (3)	0.010 (3)
C50	0.080 (4)	0.046 (3)	0.116 (5)	-0.005 (3)	0.029 (4)	0.011 (3)
C51	0.074 (3)	0.036 (2)	0.092 (4)	-0.005 (2)	-0.004 (3)	-0.007 (3)
C52	0.138 (6)	0.053 (3)	0.085 (5)	-0.015 (4)	0.036 (4)	-0.016 (3)
C53	0.133 (6)	0.053 (3)	0.069 (4)	-0.027 (3)	0.033 (4)	-0.011 (3)
F54	0.110 (3)	0.0416 (17)	0.130 (3)	-0.0085 (17)	0.003 (2)	-0.0046 (18)
C1L	0.151 (8)	0.113 (6)	0.108 (7)	0.029 (6)	0.026 (6)	0.039 (5)
O1L	0.099 (6)	0.122 (7)	0.111 (7)	0.036 (5)	-0.006 (5)	0.026 (6)
O2L	0.108 (8)	0.052 (6)	0.086 (7)	0.018 (5)	0.027 (6)	0.007 (5)

*Geometric parameters (Å, °)*

C1—C2	1.501 (6)	C31—H31	0.9500
C1—C14	1.503 (6)	C32—C33	1.395 (6)
C1—C20	1.511 (6)	C32—H32	0.9500
C1—O17	1.527 (5)	C33—C34	1.394 (6)
C2—C7	1.383 (5)	C33—N36	1.404 (6)
C2—C3	1.385 (6)	C34—C35	1.374 (6)
C3—C4	1.376 (6)	C34—H34	0.9500
C3—H3	0.9500	C35—H35	0.9500
C4—C5	1.403 (6)	N36—C37	1.371 (6)
C4—H4	0.9500	N36—H36	0.8800
C5—O15	1.347 (5)	C37—N38	1.348 (6)
C5—C6	1.380 (6)	C37—C42	1.400 (6)
C6—C7	1.386 (6)	N38—C39	1.322 (7)
C6—H6	0.9500	C39—C40	1.368 (9)
C7—O8	1.383 (5)	C39—H39	0.9500
O8—C9	1.382 (5)	C40—C41	1.385 (8)
C9—C10	1.377 (6)	C40—H40	0.9500
C9—C14	1.385 (6)	C41—C42	1.375 (6)
C10—C11	1.387 (6)	C41—C43	1.462 (7)
C10—H10	0.9500	C42—H42	0.9500
C11—O16	1.354 (5)	C43—C47	1.373 (6)
C11—C12	1.389 (6)	C43—N44	1.388 (6)
C12—C13	1.378 (6)	N44—C45	1.354 (6)
C12—H12	0.9500	N44—C48	1.423 (6)
C13—C14	1.393 (6)	C45—N46	1.314 (6)
C13—H13	0.9500	C45—H45	0.9500
O15—H15	0.8400	N46—C47	1.353 (6)

## data reports

O16—H16	0.8400	C47—H47	0.9500
O17—C18	1.354 (5)	C48—C53	1.358 (7)
C18—O21	1.223 (5)	C48—C49	1.360 (7)
C18—C19	1.456 (7)	C49—C50	1.389 (7)
C19—C20	1.381 (6)	C49—H49	0.9500
C19—C22	1.392 (6)	C50—C51	1.333 (8)
C20—C25	1.372 (7)	C50—H50	0.9500
C22—C23	1.376 (6)	C51—C52	1.358 (8)
C22—H22	0.9500	C51—F54	1.365 (6)
C23—C24	1.402 (6)	C52—C53	1.376 (8)
C23—N26	1.429 (5)	C52—H52	0.9500
C24—C25	1.384 (6)	C53—H53	0.9500
C24—H24	0.9500	C1L—O1L	1.3998 (10)
C25—H25	0.9500	C1L—O2L	1.4009 (10)
N26—C27	1.362 (6)	C1L—H1M	0.9800
N26—H26	1.0913	C1L—H2M	0.9800
C27—N28	1.350 (6)	C1L—H3M	0.9800
C27—S29	1.675 (5)	C1L—H4M	0.9800
N28—C30	1.434 (6)	C1L—H5M	0.9800
N28—H28	1.1665	C1L—H6M	0.9800
C30—C35	1.383 (6)	O1L—H1L	0.8400
C30—C31	1.389 (6)	O2L—H2L	0.8400
C31—C32	1.386 (7)		
C2—C1—C14	112.1 (3)	C32—C31—C30	121.3 (4)
C2—C1—C20	113.8 (4)	C32—C31—H31	119.4
C14—C1—C20	113.9 (4)	C30—C31—H31	119.4
C2—C1—O17	108.1 (4)	C31—C32—C33	119.8 (4)
C14—C1—O17	107.2 (3)	C31—C32—H32	120.1
C20—C1—O17	100.8 (3)	C33—C32—H32	120.1
C7—C2—C3	117.3 (4)	C34—C33—C32	118.6 (4)
C7—C2—C1	120.9 (4)	C34—C33—N36	116.8 (4)
C3—C2—C1	121.8 (3)	C32—C33—N36	124.3 (4)
C4—C3—C2	122.4 (4)	C35—C34—C33	120.7 (4)
C4—C3—H3	118.8	C35—C34—H34	119.6
C2—C3—H3	118.8	C33—C34—H34	119.6
C3—C4—C5	119.2 (4)	C34—C35—C30	121.1 (4)
C3—C4—H4	120.4	C34—C35—H35	119.5
C5—C4—H4	120.4	C30—C35—H35	119.5
O15—C5—C6	118.0 (4)	C37—N36—C33	132.1 (4)
O15—C5—C4	122.8 (4)	C37—N36—H36	114.0
C6—C5—C4	119.2 (4)	C33—N36—H36	114.0
C5—C6—C7	120.0 (4)	N38—C37—N36	112.7 (4)
C5—C6—H6	120.0	N38—C37—C42	122.5 (4)
C7—C6—H6	120.0	N36—C37—C42	124.7 (4)
O8—C7—C2	123.3 (4)	C39—N38—C37	116.0 (5)
O8—C7—C6	115.0 (3)	N38—C39—C40	124.8 (6)
C2—C7—C6	121.8 (4)	N38—C39—H39	117.6

## data reports

C9—O8—C7	118.5 (3)	C40—C39—H39	117.6
C10—C9—O8	115.4 (4)	C39—C40—C41	119.7 (6)
C10—C9—C14	122.2 (4)	C39—C40—H40	120.1
O8—C9—C14	122.5 (4)	C41—C40—H40	120.1
C9—C10—C11	119.5 (4)	C42—C41—C40	116.5 (5)
C9—C10—H10	120.2	C42—C41—C43	126.9 (4)
C11—C10—H10	120.2	C40—C41—C43	116.5 (4)
O16—C11—C12	122.6 (4)	C41—C42—C37	120.1 (4)
O16—C11—C10	117.8 (4)	C41—C42—H42	119.9
C12—C11—C10	119.6 (4)	C37—C42—H42	119.9
C13—C12—C11	119.7 (4)	C47—C43—N44	104.1 (4)
C13—C12—H12	120.2	C47—C43—C41	126.7 (4)
C11—C12—H12	120.2	N44—C43—C41	129.1 (4)
C12—C13—C14	121.7 (4)	C45—N44—C43	107.0 (4)
C12—C13—H13	119.1	C45—N44—C48	121.2 (4)
C14—C13—H13	119.1	C43—N44—C48	131.5 (4)
C9—C14—C13	117.3 (4)	N46—C45—N44	112.0 (4)
C9—C14—C1	121.4 (4)	N46—C45—H45	124.0
C13—C14—C1	121.2 (4)	N44—C45—H45	124.0
C5—O15—H15	109.5	C45—N46—C47	105.2 (4)
C11—O16—H16	109.5	N46—C47—C43	111.6 (4)
C18—O17—C1	110.7 (3)	N46—C47—H47	124.2
O21—C18—O17	120.9 (4)	C43—C47—H47	124.2
O21—C18—C19	130.0 (4)	C53—C48—C49	119.9 (5)
O17—C18—C19	109.1 (4)	C53—C48—N44	119.1 (4)
C20—C19—C22	122.0 (4)	C49—C48—N44	120.8 (5)
C20—C19—C18	108.7 (4)	C48—C49—C50	120.2 (5)
C22—C19—C18	129.4 (4)	C48—C49—H49	119.9
C25—C20—C19	120.7 (4)	C50—C49—H49	119.9
C25—C20—C1	129.0 (4)	C51—C50—C49	118.3 (5)
C19—C20—C1	110.2 (4)	C51—C50—H50	120.9
C23—C22—C19	117.1 (4)	C49—C50—H50	120.9
C23—C22—H22	121.4	C50—C51—C52	123.1 (5)
C19—C22—H22	121.4	C50—C51—F54	119.1 (5)
C22—C23—C24	121.2 (4)	C52—C51—F54	117.8 (5)
C22—C23—N26	118.0 (4)	C51—C52—C53	118.0 (6)
C24—C23—N26	120.6 (4)	C51—C52—H52	121.0
C25—C24—C23	120.5 (5)	C53—C52—H52	121.0
C25—C24—H24	119.7	C48—C53—C52	120.6 (5)
C23—C24—H24	119.7	C48—C53—H53	119.7
C20—C25—C24	118.5 (4)	C52—C53—H53	119.7
C20—C25—H25	120.7	O1L—C1L—H1M	109.5
C24—C25—H25	120.7	O1L—C1L—H2M	109.5
C27—N26—C23	127.3 (4)	H1M—C1L—H2M	109.5
C27—N26—H26	126.1	O1L—C1L—H3M	109.5
C23—N26—H26	106.1	H1M—C1L—H3M	109.5
N28—C27—N26	114.8 (4)	H2M—C1L—H3M	109.5
N28—C27—S29	121.2 (4)	O2L—C1L—H4M	109.5

## data reports

N26—C27—S29	124.0 (3)	O2L—C1L—H5M	109.5
C27—N28—C30	125.9 (4)	H4M—C1L—H5M	109.5
C27—N28—H28	107.4	O2L—C1L—H6M	109.5
C30—N28—H28	126.4	H4M—C1L—H6M	109.5
C35—C30—C31	118.4 (4)	H5M—C1L—H6M	109.5
C35—C30—N28	119.6 (4)	C1L—O1L—H1L	109.5
C31—C30—N28	121.8 (4)	C1L—O2L—H2L	109.5
C14—C1—C2—C7	7.2 (6)	C22—C23—C24—C25	-2.0 (7)
C20—C1—C2—C7	138.2 (4)	N26—C23—C24—C25	172.5 (4)
O17—C1—C2—C7	-110.7 (4)	C19—C20—C25—C24	0.7 (7)
C14—C1—C2—C3	-172.6 (4)	C1—C20—C25—C24	-174.6 (4)
C20—C1—C2—C3	-41.6 (6)	C23—C24—C25—C20	0.7 (7)
O17—C1—C2—C3	69.5 (5)	C22—C23—N26—C27	-142.2 (5)
C7—C2—C3—C4	-1.7 (7)	C24—C23—N26—C27	43.1 (7)
C1—C2—C3—C4	178.1 (5)	C23—N26—C27—N28	-166.0 (4)
C2—C3—C4—C5	-1.6 (8)	C23—N26—C27—S29	16.3 (7)
C3—C4—C5—O15	-175.9 (5)	N26—C27—N28—C30	20.6 (7)
C3—C4—C5—C6	3.8 (7)	S29—C27—N28—C30	-161.7 (4)
O15—C5—C6—C7	177.1 (4)	C27—N28—C30—C35	-141.9 (5)
C4—C5—C6—C7	-2.7 (7)	C27—N28—C30—C31	43.5 (7)
C3—C2—C7—O8	-177.0 (4)	C35—C30—C31—C32	-1.6 (8)
C1—C2—C7—O8	3.2 (7)	N28—C30—C31—C32	173.1 (5)
C3—C2—C7—C6	2.9 (7)	C30—C31—C32—C33	-0.1 (9)
C1—C2—C7—C6	-176.9 (5)	C31—C32—C33—C34	0.6 (8)
C5—C6—C7—O8	179.2 (4)	C31—C32—C33—N36	-173.1 (5)
C5—C6—C7—C2	-0.7 (8)	C32—C33—C34—C35	0.6 (8)
C2—C7—O8—C9	-9.8 (7)	N36—C33—C34—C35	174.7 (5)
C6—C7—O8—C9	170.3 (4)	C33—C34—C35—C30	-2.4 (8)
C7—O8—C9—C10	-174.6 (4)	C31—C30—C35—C34	2.8 (8)
C7—O8—C9—C14	4.9 (7)	N28—C30—C35—C34	-172.0 (5)
O8—C9—C10—C11	178.0 (5)	C34—C33—N36—C37	165.4 (5)
C14—C9—C10—C11	-1.5 (8)	C32—C33—N36—C37	-20.9 (9)
C9—C10—C11—O16	-179.7 (4)	C33—N36—C37—N38	165.5 (5)
C9—C10—C11—C12	-0.6 (8)	C33—N36—C37—C42	-18.5 (9)
O16—C11—C12—C13	-178.9 (5)	N36—C37—N38—C39	176.4 (7)
C10—C11—C12—C13	2.0 (8)	C42—C37—N38—C39	0.3 (9)
C11—C12—C13—C14	-1.5 (8)	C37—N38—C39—C40	4.4 (14)
C10—C9—C14—C13	2.0 (7)	N38—C39—C40—C41	-6.7 (16)
O8—C9—C14—C13	-177.5 (4)	C39—C40—C41—C42	4.0 (12)
C10—C9—C14—C1	-174.3 (5)	C39—C40—C41—C43	-173.0 (8)
O8—C9—C14—C1	6.2 (7)	C40—C41—C42—C37	0.3 (9)
C12—C13—C14—C9	-0.5 (8)	C43—C41—C42—C37	176.9 (5)
C12—C13—C14—C1	175.8 (5)	N38—C37—C42—C41	-2.5 (8)
C2—C1—C14—C9	-11.7 (6)	N36—C37—C42—C41	-178.2 (5)
C20—C1—C14—C9	-142.7 (4)	C42—C41—C43—C47	-162.3 (5)
O17—C1—C14—C9	106.7 (5)	C40—C41—C43—C47	14.3 (9)
C2—C1—C14—C13	172.1 (4)	C42—C41—C43—N44	16.3 (9)

## data reports

C20—C1—C14—C13	41.2 (6)	C40—C41—C43—N44	-167.1 (6)
O17—C1—C14—C13	-69.4 (5)	C47—C43—N44—C45	-0.4 (5)
C2—C1—O17—C18	-127.2 (4)	C41—C43—N44—C45	-179.2 (5)
C14—C1—O17—C18	111.8 (4)	C47—C43—N44—C48	-173.9 (5)
C20—C1—O17—C18	-7.6 (4)	C41—C43—N44—C48	7.3 (9)
C1—O17—C18—O21	-173.6 (4)	C43—N44—C45—N46	1.1 (6)
C1—O17—C18—C19	6.0 (5)	C48—N44—C45—N46	175.4 (4)
O21—C18—C19—C20	178.0 (5)	N44—C45—N46—C47	-1.3 (6)
O17—C18—C19—C20	-1.5 (5)	C45—N46—C47—C43	1.1 (6)
O21—C18—C19—C22	-0.8 (8)	N44—C43—C47—N46	-0.4 (6)
O17—C18—C19—C22	179.6 (4)	C41—C43—C47—N46	178.5 (5)
C22—C19—C20—C25	-0.7 (7)	C45—N44—C48—C53	-79.0 (7)
C18—C19—C20—C25	-179.6 (4)	C43—N44—C48—C53	93.6 (7)
C22—C19—C20—C1	175.4 (4)	C45—N44—C48—C49	94.7 (6)
C18—C19—C20—C1	-3.6 (5)	C43—N44—C48—C49	-92.6 (7)
C2—C1—C20—C25	-62.3 (6)	C53—C48—C49—C50	-1.1 (9)
C14—C1—C20—C25	67.8 (6)	N44—C48—C49—C50	-174.8 (5)
O17—C1—C20—C25	-177.8 (4)	C48—C49—C50—C51	0.0 (10)
C2—C1—C20—C19	122.1 (4)	C49—C50—C51—C52	1.6 (11)
C14—C1—C20—C19	-107.8 (4)	C49—C50—C51—F54	-179.2 (6)
O17—C1—C20—C19	6.6 (4)	C50—C51—C52—C53	-2.0 (11)
C20—C19—C22—C23	-0.6 (6)	F54—C51—C52—C53	178.8 (6)
C18—C19—C22—C23	178.1 (4)	C49—C48—C53—C52	0.7 (10)
C19—C22—C23—C24	1.9 (6)	N44—C48—C53—C52	174.5 (6)
C19—C22—C23—N26	-172.8 (4)	C51—C52—C53—C48	0.7 (11)

## Hydrogen-bond geometry (Å, °)

<i>D</i> —H... <i>A</i>	<i>D</i> —H	H... <i>A</i>	<i>D</i> ... <i>A</i>	<i>D</i> —H... <i>A</i>
O15—H15...N46 <sup>i</sup>	0.84	1.84	2.667 (5)	168
O16—H16...O21 <sup>ii</sup>	0.84	2.04	2.808 (5)	153
C22—H22...O15 <sup>iii</sup>	0.95	2.59	3.315 (5)	133
C24—H24...S29 <sup>iv</sup>	0.95	2.99	3.804 (5)	145
N26—H26...O15 <sup>v</sup>	1.09	2.17	3.061 (5)	138
N28—H28...N38 <sup>vi</sup>	1.17	1.94	3.069 (6)	162
C34—H34...O1L <sup>vii</sup>	0.95	2.46	3.334 (9)	154
N36—H36...S29 <sup>viii</sup>	0.88	2.64	3.437 (4)	152
C40—H40...O2L <sup>ix</sup>	0.95	2.32	3.103 (12)	139
C45—H45...O17 <sup>x</sup>	0.95	2.49	3.379 (6)	155
C53—H53...S29 <sup>xi</sup>	0.95	2.87	3.743 (6)	153
C1L—H2M...O21	0.98	2.56	3.267 (7)	129
O1L—H1L...S29 <sup>xii</sup>	0.84	2.46	3.202 (8)	147

Symmetry codes: (i)  $x, y-1, z$ ; (ii)  $-x+3/2, -y+1/2, -z+1$ ; (iii)  $x-1/2, y+1/2, z$ ; (iv)  $-x+1, y, -z+1/2$ ; (v)  $-x+1/2, y-1/2, -z+1/2$ ; (vi)  $-x+1/2, -y+1/2, -z+1$ ; (vii)  $-x+1/2, y+1/2, -z+1/2$ ; (viii)  $-x+1, -y+1, -z+1$ ; (ix)  $x+1/2, y+1/2, z$ ; (x)  $-x+1, -y, -z+1$ .







## Publication VII

Ansideri, F.; Macedo, T. J.; Eitel, M.; El-Gokha, A.; Zinad, D. S.; Scarpellini, C.; Kudolo, M.; Schollmeyer, D.; Boeckler, F. M.; Blaum, B. S.; Laufer, S. A.; Koch, P. Structural Optimization of a Pyridinylimidazole Scaffold: Shifting the Selectivity from p38 $\alpha$  Mitogen-Activated Protein Kinase to c-Jun N-terminal Kinase 3; *ACS Omega* **2018**, 3, 7809-7831.

**Open access publication**

**Link to the published version:**

<https://pubs.acs.org/doi/10.1021/acsomega.8b00668>

**further permissions related to the material excerpted should be directed to the  
American Chemical Society**

This is an open access article published under an ACS AuthorChoice license, which permits copying and redistribution of the article or any adaptations for non-commercial purposes.



Cite This: ACS Omega 2018, 3, 7809–7831

Article

## Structural Optimization of a Pyridinylimidazole Scaffold: Shifting the Selectivity from p38 $\alpha$ Mitogen-Activated Protein Kinase to c-Jun N-Terminal Kinase 3

Francesco Ansideri,<sup>†</sup> Joana T. Macedo,<sup>‡</sup> Michael Eitel,<sup>†</sup> Ahmed El-Gokha,<sup>†,§</sup> Dhafer S. Zinad,<sup>†,||</sup> Camilla Scarpellini,<sup>†</sup> Mark Kudolo,<sup>†</sup> Dieter Schollmeyer,<sup>‡</sup> Frank M. Boeckler,<sup>†</sup> Bärbel S. Blaum,<sup>‡</sup> Stefan A. Laufer,<sup>†</sup> and Pierre Koch<sup>\*,†,||</sup>

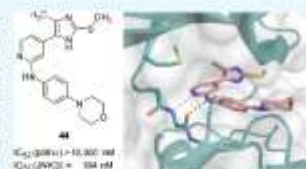
<sup>†</sup>Department of Pharmaceutical and Medicinal Chemistry, Institute of Pharmaceutical Sciences, Eberhard Karls Universität Tübingen, Auf der Morgenstelle 8, 72076 Tübingen, Germany

<sup>‡</sup>Interfaculty Institute of Biochemistry, Eberhard Karls Universität Tübingen, Hoppe-Seyler-Straße 4, 72076 Tübingen, Germany

<sup>§</sup>Department of Organic Chemistry, Johannes Gutenberg University Mainz, Duesbergweg 10-14, D-55099 Mainz, Germany

### Supporting Information

**ABSTRACT:** Starting from known p38 $\alpha$  mitogen-activated protein kinase (MAPK) inhibitors, a series of inhibitors of the c-Jun N-terminal kinase (JNK) 3 was obtained. Altering the substitution pattern of the pyridinylimidazole scaffold proved to be effective in shifting the inhibitory activity from the original target p38 $\alpha$  MAPK to the closely related JNK3. In particular, a significant improvement for JNK3 selectivity could be achieved by addressing the hydrophobic region I with a small methyl group. Furthermore, additional structural modifications permitted to explore structure–activity relationships. The most potent inhibitor 4-(4-methyl-2-(methylthio)-1H-imidazol-5-yl)-N-(4-morpholinophenyl)pyridin-2-amine showed an IC<sub>50</sub> value for the JNK3 in the low triple digit nanomolar range and its binding mode was confirmed by X-ray crystallography.



### INTRODUCTION

The mitogen-activated protein kinases (MAPKs) represent a family of enzymes involved in several signal transduction pathways, whose activation is part of a phosphorylation cascade triggered by diverse extracellular stimuli. Among the members of this family, the c-Jun N-terminal kinases (JNKs) mostly respond to a variety of stress stimuli such as radiation, osmotic or heat shock, oxidative insult, and proinflammatory cytokines, modulating responses such as cell survival and apoptosis.<sup>1</sup> The JNK subfamily is encoded by the three genes *jak1*, *jak2*, and *jak3*, which in turn give rise to 10 different isoforms through alternative splicing.<sup>2</sup> Despite their structural homology and the partially functional redundancy, these isoforms follow a different tissue distribution pattern, JNK3 being restricted to the central nervous system, heart, and testis oppositely to the ubiquitous expression of JNK1 and 2.<sup>3,4</sup> In addition to this, a different substrate specificity of the JNK1, 2, and 3 suggests the existence of isoform-specific roles of these enzymes, which were partially disclosed through gene knock-out studies.<sup>5</sup> There is well-documented evidence for the critical role of the JNK subfamily members in several neurodegenerative diseases such as Parkinson's and Alzheimer's disease, as well as in neuronal death derived by stroke and ischemia/reperfusion injury.<sup>3–6</sup> Furthermore, some members of the JNKs are also involved in metabolic and inflammatory diseases, and several studies suggest that these kinases might

contribute to the development and diffusion of some forms of cancer,<sup>7–9</sup> thus emerging as particularly attractive drug targets. Despite the intense endeavor in the research of JNK inhibitors, only a scarce number of candidates have reached clinical trial phases and to date, none of them have been approved.<sup>10–12</sup> Until early 2010s, a major challenge in the development of JNK inhibitors has been the achievement of selectivity over the closely related p38 $\alpha$  MAPK,<sup>11</sup> a member of the same family which, analogously to the JNKs, participates in regulating the cellular response to stress stimuli. This protein kinase was also shown to assume a key function in different inflammatory and neurodegenerative diseases<sup>13–15</sup> and the simultaneous inhibition of JNK and p38 $\alpha$  MAPK is assumed to obtain a synergistic effect in the treatment of some pathological conditions.<sup>16</sup> Nevertheless, obtaining a JNK-selective inhibitor would be beneficial to fully elucidate the effective role of this protein kinase in the aforementioned pathological conditions and thereby assess its therapeutic potential. Furthermore, most of the reported clinical trials on selective p38 $\alpha$  MAPK inhibitors have been discontinued because of the insurgence of adverse effects mostly related to liver toxicity,<sup>17</sup> leading to

Received: April 6, 2018

Accepted: June 26, 2018

Published: July 12, 2018

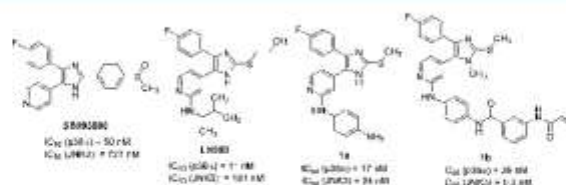
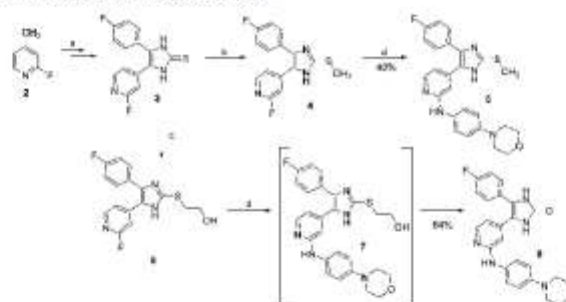


Figure 1. Tri- and tetrasubstituted pyridinylimidazoles. Data are taken from Ansideri et al.<sup>19</sup> and Muth et al.<sup>21</sup>

#### Scheme 1. Synthesis of Imidazole 5 and Imidazol-2-one 8<sup>44</sup>



<sup>a</sup>Reagents and conditions: (a) four-step route reported by Laufer and co-workers;<sup>23</sup> (b) MeI,  $K_2CO_3$ , MeOH, rt, 18 h; (c) 2-bromoethyl acetate, *t*-BuONa, MeOH, 55 °C, 3 h; and (d) 4-morpholinoaniline, 1.25 M HCl in EtOH, *o*-BuOH, 180 °C, 16 h.

the assumption the activity on the p38 $\alpha$  MAPK to be undesired for an improved safety profile of JNK inhibitors.

Regarding the selectivity within the JNK subfamily, the achievement of JNK isoform-selective inhibitors would be desirable to dissect the contribution of the different isoforms in various pathological conditions. However, the JNK1, 2, and 3 share more than 80% sequence identity, making the development of isoform-specific inhibitors extremely challenging.

In the last decades, pyridinylimidazoles have encountered a remarkable success in the field of p38 $\alpha$  MAPK inhibition. This class of inhibitors counts a large number of examples starting from the precursor SB203580 to the optimized compound LN950 (Figure 1), until reaching derivatives with low single digit nanomolar  $IC_{50}$  values (a review on this class of compounds has recently been published).<sup>19</sup> As can be seen from Figure 1, the reported p38 $\alpha$  MAPK inhibitors are also able to inhibit the JNK3 with  $IC_{50}$  values in the submicromolar range, thus offering a suitable starting point for optimization when aiming to target this enzyme. In 2016, we published compound 1a as a balanced dual JNK3/p38 $\alpha$  MAPK inhibitor, which served as a precursor for the synthesis of a fluorescent probe used in fluorescence polarization-based binding assays.<sup>19,20</sup> As it is evident from the biological activity of 1a in comparison to the activity of previous inhibitors, modifying the substitution pattern around the pyridinylimidazole scaffold can contribute to a shift in selectivity toward the JNK3.

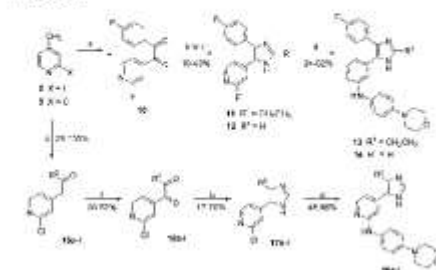
Some of us have recently reported the optimization of compound 1a following a covalent inhibition approach (compound 1b), which was based on the introduction of an electrophilic moiety able to target a noncatalytic cysteine of the JNK3 that is not conserved in the closely related p38 $\alpha$  MAPK.<sup>21</sup> The aim of the herein presented work consists

instead in the achievement of a potent and selective JNK inhibitor by structural modification of the pyridinylimidazole scaffold following the canonical concept of reversible inhibition.

## RESULTS AND DISCUSSION

**Chemistry.** Despite the overall similarity of their structures, the herein reported compounds were synthesized following considerably diverse routes, especially with regard to the construction of the five-membered heterocyclic central core. The synthesis of compounds 5 and 8 was achieved as displayed in Scheme 1. The route leading to the common intermediate 3, starting from 2-fluoro-4-methylpyridine (2), is based on the Marcwald imidazole synthesis<sup>22</sup> and was previously reported by Laufer et al.<sup>23</sup> The substitution on the imidazole-C2-S position was obtained by reacting imidazole-2-thione 3 with the appropriate alkyl halide. Finally, the introduction of the 4-morpholinoaniline moiety was carried out through nucleophilic aromatic substitution in acidic conditions, this representing the final step for most of the herein presented compounds. Applying these conditions to the hydroxyethyl derivative 6 unexpectedly yielded imidazol-2-one 8, instead of imidazole 7, as a result of a previously described rearrangement.<sup>24</sup>

The preparation of 2,4,5-trisubstituted imidazole 13 and of 4,5-disubstituted imidazoles 14 and 18a–1 is outlined in Scheme 2. The route providing  $\alpha$ -diketone 10 starting from 2-fluoro-4-methylpyridine (2) was recently described by Ansideri et al.,<sup>19</sup> whereas the synthesis of intermediates 16a–1 was achieved following a similar approach. Ethanones 15a–1 were obtained by condensation of the appropriate ethyl ester with 2-chloro-4-methylpyridine (9) and were subsequently oxidized

**Scheme 2. Synthesis of 4,5-Disubstituted Imidazoles 13, 14, and 18a–l<sup>18</sup>**

<sup>18</sup>Reagents and conditions: (a) route reported by Asideri et al.<sup>18</sup> (b)  $\text{HCHO}_{(aq)}$ ,  $\text{NH}_4\text{OAc}$ ,  $\text{AcOH}$ ,  $180\text{ }^\circ\text{C}$  microwave irradiation, 2–5 min; (c) propionaldehyde, 7 M  $\text{NH}_3$  in  $\text{MeOH}$ ,  $80\text{ }^\circ\text{C}$ , 4 h; (d) 4-morpholinoaniline, 1.25 M  $\text{HCl}$  in  $\text{EtOH}$ , *n*- $\text{BuOH}$ ,  $180\text{ }^\circ\text{C}$ , 16 h; (e) ethyl arylcarboxylate or ethyl alkylcarboxylate,  $\text{NaHMDS}$ , dry  $\text{THF}$ ,  $0\text{ }^\circ\text{C}$ , 1–5 h; and (f)  $\text{SeO}_2$ ,  $\text{AcOH}$ ,  $70\text{ }^\circ\text{C}$ , 2–3 h; ( $\text{R}^1$  = see Table 2).

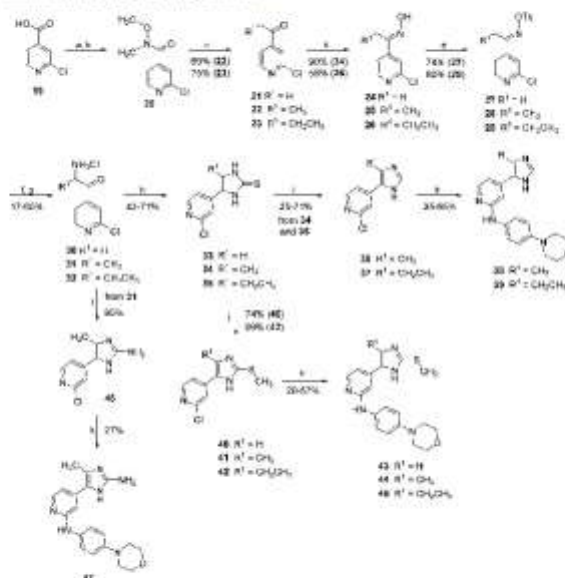
by  $\text{SeO}_2$  to the corresponding diketones (16a–l). Microwave-assisted cyclization with formaldehyde and  $\text{NH}_4\text{OAc}$  in Radziszewski conditions<sup>25</sup> then afforded the disubstituted imidazoles 12 and 17a–l, whereas propionaldehyde and

methanolic  $\text{NH}_3$  were employed to obtain the 2-ethylimidazole 11. Finally, introduction of the 4-morpholinoaniline moiety at the pyridine-C2 position, giving the final compounds 13, 14, and 18a–l, was accomplished by the aforementioned nucleophilic aromatic substitution.

The synthesis of 4,5-disubstituted pyridinylimidazoles 38 and 39, featuring a linear alkyl group at the imidazole-C4 position, required a different strategy than the examples having aromatic or branched aliphatic moieties (14 and 18a–l). This was mainly due to the fact that alkyl esters of linear alkanic acids did not undergo condensation with 2-chloro-4-methylpyridine (9) to give the desired ethanone intermediates.

An alternative approach to compounds 38 and 39 could also be employed for the synthesis of the 2,4(2,5)-disubstituted imidazole 43 as well as for the 2,4,5-trisubstituted imidazoles 44 and 45 (Scheme 3). This route started from the commercially available 1-(2-chloropyridin-4-yl)ethan-1-one (21) or from the acylpyridines 22 and 23, which were synthesized by Grignard reaction of the appropriate alkylmagnesium bromide with Weinreb amide 20.

Formation of the corresponding oximes 24–26 and following tosylation of the hydroxyl groups led to intermediates 27–29. Tosylated oximes 27–29 were then first converted into the  $\alpha$ -aminoketones 30–32 through Neber rearrangement<sup>26</sup> and subsequently cyclized by  $\text{KSCN}$ , yielding imidazole-2-thione derivatives 33–35. From these intermediates, it was possible to achieve the disubstituted imidazoles 36

**Scheme 3. Synthesis of Imidazoles 38, 39, 43–45, and 47<sup>19</sup>**

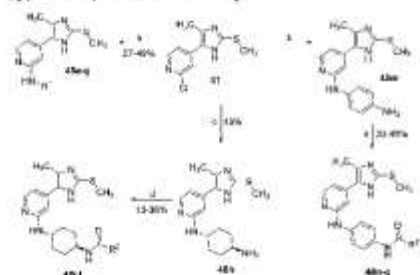
<sup>19</sup>Reagents and conditions: (a)  $\text{SOCl}_2$ , reflux temperature, 5 h; (b) *N,O*-dimethylhydroxylamine hydrochloride,  $\text{Et}_3\text{N}$ , dry  $\text{DCM}$ , 16 h; (c)  $\text{EtMgBr}$  or *n*- $\text{PrMgBr}$ , dry  $\text{THF}$ ,  $-10\text{ }^\circ\text{C}$ , 1–3 h; (d)  $\text{NH}_2\text{OH}\cdot\text{HCl}$ , 20%  $\text{NaOH}_{(aq)}$ ,  $\text{MeOH}$ ,  $\text{H}_2\text{O}$ ,  $0\text{ }^\circ\text{C}$ , 1–2 h; (e)  $\text{TsCl}$ , pyridine, rt, 24–72 h; (f)  $\text{EtOH}_{(sol)}$ ,  $\text{K}$ ,  $0\text{ }^\circ\text{C}$ , 2–16 h; (g)  $\text{KSCN}$ ,  $\text{MeOH}$ , reflux temperature, 4 h; (h)  $\text{H}_2\text{O}_2$ ,  $\text{AcOH}$ , rt, 15 min; (i)  $\text{MeI}$ , *t*- $\text{BuONa}$ ,  $\text{MeOH}$ ,  $50\text{ }^\circ\text{C}$ , 0.5–3 h; (j) 4-morpholinoaniline, 1.25 M  $\text{HCl}$  in  $\text{EtOH}$ , *n*- $\text{BuOH}$ ,  $180\text{ }^\circ\text{C}$ , 16 h; and (l) cyanamide,  $\text{EtOH}$ , reflux temperature, 2 h.



and 37 by oxidative desulfurization<sup>27</sup> as well as the 2-methylsulfanylimidazoles 40–42 via monomethylation. Alternatively, compound 46 displaying a 2-aminoimidazole core could be prepared by cyclization of the  $\alpha$ -aminoketone 31 with cyanamide. Intermediates 36, 37, 40–42, and 47 were then reacted with 4-morpholinoaniline, as previously mentioned, to afford the final compounds 38, 39, 43–45, and 47, respectively.

Several analogues of compound 44 featuring a different substituent at the pyridine-C2 position (compounds 48a–h and 48m, Scheme 4) could be prepared by nucleophilic

**Scheme 4. Synthesis of 4(5)-Methyl-2-methylsulfanyl-5-(4)pyridin-4-ylimidazoles 48a–q**



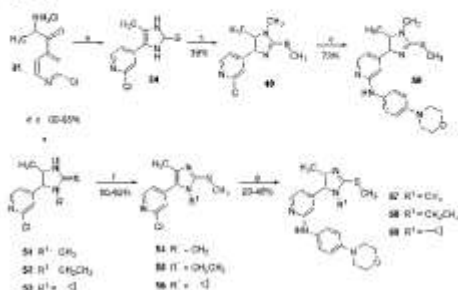
“Reagents and conditions: (a) cycloalkylamine (NEAT or *n*-BuOH), 180 °C, 24–72 h; (b) *p*-phenylenediamine, 1.25 M HCl in EtOH, *n*-BuOH, 180 °C, 16 h; (c) *trans*-diaminocyclohexane, *n*-BuOH, 180 °C, 72 h; and (d) acyl chloride or anhydride, dry pyridine, rt, 16 h; (R<sup>1</sup>, R<sup>2</sup> = see Table 6).

aromatic substitution of synthon 41 with *p*-phenylenediamine, 1-phenylethanamine, or with diverse branched or cycloalkyl amines. In addition, compound 48h and the previously reported 48m<sup>21</sup> were coupled with different acid chlorides or anhydrides to obtain the corresponding amides 48i–l and 48n–q (Scheme 4).

The introduction of a methyl substituent on the imidazole-N atom, providing 1,2,4,5-tetrasubstituted imidazoles 50 and 57, required a distinct approach depending on the desired N-methylated regioisomer. In fact, double nucleophilic substitution of imidazole-2-thione 34 using excess of methyl iodide almost exclusively afforded the regioisomer bearing the substituent on the N atom away from the pyridine ring (49, Scheme 5). The regioselectivity of the methylation reaction was confirmed by crystal structure analysis of intermediate 49 (see Figure S1 in the Supporting Information) and was attributed to the lower steric hindrance offered by the methyl group compared to the pyridine ring. The regioisomer 54, having the methyl group on the N atom adjacent to the pyridine ring, was instead achieved by cyclizing the  $\alpha$ -aminoketone 31 with methyl isothiocyanate, followed by methylation of the sulfur of the resulting N1-methylimidazole-2-thione 51.

This approach, adapting a procedure published by Xi et al.,<sup>27</sup> represents an unusual route to tetrasubstituted pyridinylimidazoles and was recently reported by some of us for the preparation of tetrasubstituted imidazoles bearing two aromatic moieties at the 4 and 5 positions.<sup>28</sup> The same method could also be employed, using the appropriate alkyl

**Scheme 5. Synthesis of Tetrasubstituted Imidazoles 50 and 57–59**

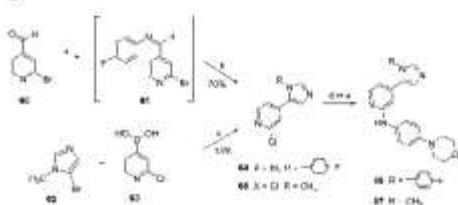


“Reagents and conditions: (a) KSCN, MeOH, reflux temperature, 4 h; (b) MeI, *t*-BuONa, MeOH, 80 °C, 3 h; (c) 4-morpholinoaniline, Pd<sub>2</sub>(dba)<sub>3</sub>, Xantphos, Cs<sub>2</sub>CO<sub>3</sub>, dry 1,4-dioxane, 100 °C, 18 h; (d) allyl isothiocyanate, Et<sub>3</sub>N, 60 °C, 16 h; (e) AcOH, 80 °C, 1 h; (f) MeI, *t*-BuONa, MeOH, 50 °C, 30 min; and (g) 4-morpholinoaniline, Pd<sub>2</sub>(dba)<sub>3</sub>, XPhos, Cs<sub>2</sub>CO<sub>3</sub>, dry 1,4-dioxane, 100 °C, 16 h.

isothiocyanate, to achieve the N-ethyl- and the N-cyclopropylimidazole derivatives 55 and 56, respectively. Unlike the majority of the reported compounds, the introduction of the 4-morpholinoaniline moiety, yielding compounds 50 and 57–59, was carried out by palladium-catalyzed Buchwald–Hartwig aryl amination.

The synthesis of the 1,5-disubstituted imidazole 66, bearing an aromatic substituent on the imidazole-N1 atom, was performed starting from 2-bromoisonicotinaldehyde (60) via a two-step procedure as depicted in Scheme 6. Such a route

**Scheme 6. Synthesis of 1,5-Disubstituted Imidazoles 66 and 67**



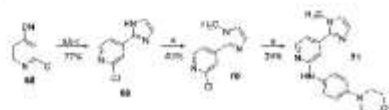
“Reagents and conditions: (a) 4-fluoroaniline, AcOH, EtOH, reflux temperature, 2 h; (b) TOSMIC, K<sub>2</sub>CO<sub>3</sub>, MeOH/dimethoxyethane 2:1, reflux temperature, 3 h; (c) Pd(PPh<sub>3</sub>)<sub>4</sub>, Cs<sub>2</sub>CO<sub>3</sub>, H<sub>2</sub>O, DMF, 60 °C, 24 h; and (d) 4-morpholinoaniline, *t*-BuONa, Pd<sub>2</sub>(dba)<sub>3</sub>, BINAP, toluene, 80 °C, 3 h; (e) 4-morpholinoaniline, 1.25 M HCl in EtOH, *n*-BuOH, 180 °C, 16 h.

entails the formation of the imine derivative 61 and its direct cyclization through the Van Leusen reaction<sup>29</sup> using toluene sulfonylmethylisocyanide (TOSMIC) and K<sub>2</sub>CO<sub>3</sub>. The analogous route was unfortunately not accessible for the synthesis of the N1-methyl substituted derivative 67 because of the instability of the corresponding imine intermediate. As an alternative, the preformed N1-methyl imidazole group was introduced through Suzuki cross-coupling reaction<sup>30</sup> between 5-bromo-1-methyl-1H-imidazole (62) and pyridinylboronic

acid **63** (Scheme 6). The last step of both routes consisted of the introduction of the 4-morpholinoaniline moiety. In the case of the 4-fluorophenyl derivative **64**, this was performed by Buchwald–Hartwig amination giving compound **66**, whereas the acid-catalyzed nucleophilic aromatic substitution was employed for the synthesis of compound **67**.

The 1,2-disubstituted imidazole derivative **71** was obtained starting from 2-chloroisonicotinonitrile (**68**), which was initially reacted in a one-pot procedure described by Voss et al.<sup>31</sup> (Scheme 7). This reaction involves the formation of an

**Scheme 7.** Synthesis of Imidazol-2-yl Pyridine Derivative **71**<sup>a</sup>

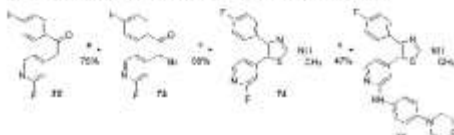


<sup>a</sup>Reagents and conditions: (a) 30% NaOMe in MeOH, MeOH, 40 °C, 1 h; (b) aminoacetaldehyde dimethylacetal, AcOH, MeOH, reflux temperature, 30 min; (c) 6 M HCl, reflux temperature, 18 h; (d) MeI, NaH, dry DMF, rt, 2 h; and (e) 4-morpholinoaniline, 1.25 M HCl in EtOH, *n*-BuOH, 180 °C, 16 h.

imidate, followed by substitution with acetal-protected aminoacetaldehyde and final ring closure by deprotection, affording 2-(pyridine-4-yl)imidazole **69** in good yield. At last, *N*-methylimidazole **70** was obtained by nucleophilic substitution with methyl iodide and subsequently reacted with 4-morpholinoaniline as previously discussed, yielding compound **71**.

For the synthesis of compounds **75** and **78**, presenting a methylaminothiazole central core, an approach related to Hantzsch thiazole synthesis<sup>32</sup> was employed (Schemes 8 and

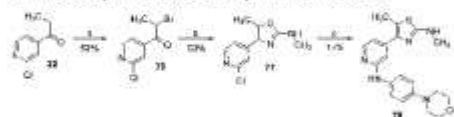
**Scheme 8.** Synthesis of 2-Methylaminothiazole **75**<sup>a</sup>



<sup>a</sup>Reagents and conditions: (a) Br<sub>2</sub>, 30% HBr in AcOH, 75 °C, 2 h; (b) *N*-methylthiourea, EtOH, reflux temperature, 1 h; and (c) 4-morpholinoaniline, 1.25 M HCl in EtOH, *n*-BuOH, 180 °C, 16 h.

9). Thiazole **75** was obtained starting from 1-(4-fluorophenyl)-2-(2-fluoropyridin-4-yl)ethan-1-one (**72**),<sup>23</sup> whereas com-

**Scheme 9.** Synthesis of 2-Methylaminothiazole **78**<sup>a</sup>



<sup>a</sup>Reagents and conditions: (a) Br<sub>2</sub>, 30% HBr in AcOH, 75 °C, 4 h; (b) *N*-methylthiourea, EtOH, reflux temperature, 1 h; and (c) 4-morpholinoaniline, 1.25 M HCl in EtOH, *n*-BuOH, 180 °C, 16 h.

ound **78** was synthesized starting from 1-pyridinyl-propan-1-one (**22**). Both ketones **72** and **22** were monohalogenated at the  $\alpha$ -position under acidic conditions and then cyclized via *N*-methylthiourea, affording intermediates **74** and **77**, respectively. Conclusively, substitution with 4-morpholinoaniline yielded the desired compounds **75** and **78**.

**Biological Evaluation.** All synthesized inhibitors were evaluated by enzyme-linked immunosorbent assays<sup>33,34</sup> to determine their ability to inhibit JNK3 and p38 $\alpha$  MAPK, and the results are presented in Tables 1–4 and 6.

**Table 1.** Core Modifications on 4-F-Phenyl-Substituted Derivatives<sup>a</sup>

Cpl	Core	IC <sub>50</sub> ± SD [n = 4] <sup>b</sup>	
		JNK3	p38 $\alpha$ MAPK
<b>5</b>		38 ± 2	17 ± 1
<b>8</b>		142 ± 28	54 ± 4
<b>12</b>		31 ± 0.7	9 ± 1
<b>14</b>		31 ± 2	21 ± 1
<b>66</b>		276 ± 10	325 ± 10
<b>75</b>		75 ± 5	2 ± 0
<b>SB203580</b>	—	—	56 ± 10 <sup>c</sup>
<b>SP600125</b>	—	171 ± 30 <sup>c</sup>	—

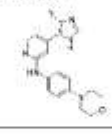
<sup>a</sup>Data of standard inhibitors SB203580 (p38 $\alpha$  MAPK) and SP600125 (JNK3) in our in-house activity assay are included. <sup>b</sup>IC<sub>50</sub> values are the mean of three experiments. <sup>c</sup>*n* = 16, <sup>d</sup>*n* = 20.

The free terminal aniline moiety of compound **1a** is considered to be potentially responsible for aggregation and therefore might result in assay interference, as also pointed out by analysis through the ZINC 15 pattern tool.<sup>35</sup> For this reason, the *p*-phenylendiamine moiety at the pyridine-C2 position of compound **1a** was modified in a 4-morpholinoaniline group, which has already been reported as a beneficial substituent in this position.<sup>30</sup> Resulting compound **5** (Table 1) displayed extremely close inhibition values to its analogue **1a** (IC<sub>50</sub>(JNK3) = 24 nM, IC<sub>50</sub>(p38 $\alpha$  MAPK) = 17 nM) and this moiety was, therefore, maintained constant during the investigation of other positions of the scaffold.

The first attempt, which was carried out to shift the preference of compound **5** toward the JNK3, consisted of modifying the central imidazole core together with acting on the substitution at the imidazole-C2 position (Table 1). Transformation of the methylsulfanyl group at the imidazole-C2 position into an ethyl group or removal of the same group,



**Table 2.** Effect of Different Aryl and Alkyl Substituents at the Imidazole C4(5) Position



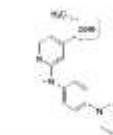
Cpd	R	IC <sub>50</sub> ± SD [μM] <sup>a</sup>	
		JNK3	p38α MAPK
14		31 ± 2	24 ± 1
18a		37 ± 3	34 ± 3
18b		60 ± 8	38 ± 2
18c		131 ± 31	64 ± 7
18d		143 ± 12	22 ± 3
18e		31 ± 3	16 ± 3
18f		758 ± 49	3,250 ± 181
18g		1,774 ± 179	736 ± 74
18h		2,189 ± 0.136	1,716 ± 81
18i		1,787 ± 133	2,265 ± 177
18j		1,089 ± 165	4,923 ± 193
18k		>10,000 (32%) <sup>b</sup>	>10,000 (41%) <sup>b</sup>
18l		2,833 ± 46	10,000 (50%) <sup>b</sup>
38		833 ± 139	>10,000 (41%) <sup>b</sup>
39		1,198 ± 193	>10,000 (37%) <sup>b</sup>

<sup>a</sup>IC<sub>50</sub> values are the mean of three experiments. <sup>b</sup>Percent inhibition at indicated concentration.

resulting in compounds 13 and 14, respectively, did not seem to affect the inhibitory activity on the two enzymes. Replacement of the imidazole core with an imidazol-2-one ring instead caused a decrease in the JNK3 inhibitory activity while leaving the inhibition of p38α MAPK unchanged (8: IC<sub>50</sub>(JNK3) = 142 nM; IC<sub>50</sub>(p38α MAPK) = 34 nM). The position of the two nitrogen atoms at the central imidazole core seems to be essential for the inhibition of both enzymes, as the different arrangements of substituents around the five-membered ring of 1,5-disubstituted imidazole 66 resulted in a drop in activity on both target kinases. On the other hand, exchange of 2-sulfanylimidazole with 2-methylaminothiazole (75) yielded an increase in inhibitory activity of 2.5- and 8-fold for JNK3 and p38α MAPK, respectively.

To assess the effect of the substituent located in the hydrophobic region (HR) I, the 4-fluorophenyl group was

**Table 3.** Modification of the Core on Methyl-Substituted Derivatives



Cpd	Core	IC <sub>50</sub> ± SD [nM] <sup>a</sup>	
		JNK3	p38α MAPK
38		833 ± 139	>10,000 (41%) <sup>b</sup>
44		363 ± 34	>10,000 (48%) <sup>b</sup>
47		1,395 ± 230	>10,000 (37%) <sup>b</sup>
50		1,279 ± 179	>10,000 (37%) <sup>b</sup>
57		2,514 ± 342	>10,000 (10%) <sup>b</sup>
58		2,091 ± 108	>10,000 (21%) <sup>b</sup>
59		6,509 ± 1,326	>10,000 (40%) <sup>b</sup>
67		714 ± 21	>10,000 (32%) <sup>b</sup>
71		>10,000 (42%) <sup>b</sup>	>10,000 (15%) <sup>b</sup>
78		2,500 ± 92	>10,000 (9%) <sup>b</sup>

<sup>a</sup>IC<sub>50</sub> values are the mean of three experiments. <sup>b</sup>Percent inhibition at indicated concentration.

**Table 4.** Effect of Small Alkyl Substituents in the HR I



Cpd	R	IC <sub>50</sub> ± SD [nM] <sup>a</sup>	
		JNK3	p38α MAPK
43	H	562 ± 21	>10,000 (43%) <sup>b</sup>
44	Me	363 ± 34	>10,000 (48%) <sup>b</sup>
45	Et	1,095 ± 64	>10,000 (38%) <sup>b</sup>

<sup>a</sup>IC<sub>50</sub> values are the mean of three experiments. <sup>b</sup>Percent inhibition at indicated concentration.

replaced by different aromatic, alkyl, and cycloalkyl moieties (Table 2). In terms of both ligand efficiency (L.E.) as well as

lipophilic LE (LLE), the 4,5-disubstituted derivative **14** is the most efficient one out of the series of Table 1 and serves, therefore, as the optimal starting point for these modifications. Moreover, this scaffold presents a substantially equal activity compared to its 5-methylated analogue **5**, along with a convenient synthetic strategy, facilitating the preparation of a broad range of derivatives.

Most of the 4,5-disubstituted pyridinylimidazoles having an aromatic moiety at the imidazole-C4 position (compounds **18a–f**) revealed to be potent inhibitors for both enzymes, displaying  $IC_{50}$  values down to the low double digit nanomolar range. In general, addressing the HR I with a phenyl or monosubstituted phenyl ring resulted in dual inhibitors displaying a slight preference toward p38 $\alpha$  MAPK over JNK3. This trend is most distinct in the case of compound **18d** having a 3-(trifluoromethyl)phenyl moiety, which presents a 6-fold higher activity for p38 $\alpha$  MAPK than for JNK3. The only aromatic substituent stepping out of this trend was the heteroaromatic *N*-methylpyrazole of compound **18f**, producing an overall decrease in activity on both kinases while conserving a moderate preference toward JNK3 (**18f**:  $IC_{50}(JNK3) = 758$  nM;  $IC_{50}(p38\alpha\text{ MAPK}) = 3259$  nM). These findings indicate that substitution on the phenyl ring is not beneficial when pursuing selectivity on JNK3 and instead seems to be counterproductive, increasing the activity on p38 $\alpha$  MAPK. The reason behind this lack of selectivity can be intuitively explained by considering the dimensions of the hydrophobic pocket known as HR I in the two target kinases. This cleft is wider in the p38 $\alpha$  MAPK than in JNK3 mostly because of a difference in the "gatekeeper" residue (Thr106 in p38 $\alpha$  MAPK vs Met146 in JNK3). However, as already mentioned in some cocrystallization studies,<sup>37</sup> aromatic moieties can induce a shift of the flexible side chain of Met146 (JNK3), thus essentially abolishing the size differences between the two pockets. As a proof of that, even the bulky 2-naphthyl group of compound **18e** seems to be accommodated in the "reshaped" hydrophobic pocket of JNK3, therefore resulting in a high inhibitory potency. Moreover, attempts of substituting the ortho and meta positions of the phenyl ring, seeking for additional interactions, did not succeed and produced negative outcomes instead (compounds **18b–d**).

The replacement of the aromatic ring at the imidazole-C4 position by cycloalkyl moieties resulted in a dramatic decrease in activity for both enzymes, with  $IC_{50}$  values in the low micromolar range. The only exception was the cyclohexyl derivative **18g** that was able to interact with p38 $\alpha$  MAPK with an  $IC_{50}$  value of 726 nM, 2-fold more potent than on JNK3. The inhibitory effect of compounds **18g–j** on p38 $\alpha$  MAPK, decreasing alongside the reduction of the ring size, is symptomatic of a gradually diminished capability of the cyclic group to occupy the spacious cavity of the enzyme. On the other side, JNK3 activity of derivatives **18g–i**, bearing a four- to six-membered ring at the imidazole-C4 position, remained substantially constant, although significantly decreased compared to the parent compound **14**. An analogous scenario occurred in the case of compounds featuring branched aliphatic groups at the same position. The isopropyl derivative **18l**, analogously to the closely related **18j**, showed a significant drop in activity on p38 $\alpha$  MAPK, while conserving an  $IC_{50}$  value on JNK3 in the low micromolar range. On the other hand, introduction of a *tert*-butyl moiety (**18k**) resulted in a complete loss of activity on both JNK3 and p38 $\alpha$  MAPK. Because of their flexibility and low electron density, cyclic and

branched aliphatic groups are presumably unable to promote the Met146 shift and therefore cannot fit in the narrow hydrophobic back pocket of JNK3. A reasonable consequence of this would therefore consist of the flip of the imidazole ring, directing the branched or cyclic alkyl moieties away from the hydrophobic back pocket of the JNK3, thus explaining the similarity of the inhibitory activity regardless of the substituent size.

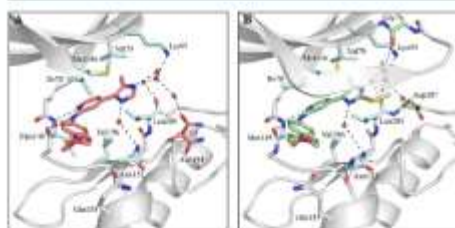
In agreement with the trend of the series, methyl- and ethyl-substituted imidazoles **38** and **39**, respectively, displayed no inhibition of the p38 $\alpha$  MAPK ( $IC_{50} > 10$   $\mu$ M), however, preserving activity on the JNK3. In particular, the methyl derivative **38** represented the sole compound of this series reaching a submicromolar activity on JNK3 without any remarkable effect on the p38 $\alpha$  MAPK. Moreover, this inhibitor also represents the most efficient selective inhibitor of this series in terms of LE and LLE and was therefore chosen as the starting point for further investigations.

Once the methyl substituent at the imidazole-C4 position was selected, our attention was refocused on the central core (Table 3). Because of the presence of the methyl substituent, all derivatives presented in this series lost their potency on the p38 $\alpha$  MAPK, with each one displaying an  $IC_{50}$  value higher or equal 10  $\mu$ M. Altering the arrangement of the substituents around the imidazole ring proved beneficial in the case of the 1,5-disubstituted imidazole **67**, slightly increasing its potency compared to the precursor **38**, whereas it was deleterious for the 1,2-disubstituted derivative **71**. Replacement of the imidazole core with a 2-aminomethyl thiazole (**78**) also revealed to be detrimental for the inhibitory activity. A different approach consisted of the introduction of an additional substituent on the imidazole-N atom, together with a reintroduction of the 5-methyl group at the C2 position, yielding the tetrasubstituted imidazole scaffold already reported in potent dual JNK3/p38 $\alpha$  MAPK as well as JNK3 selective inhibitors.<sup>10,21</sup> In the case of p38 $\alpha$  MAPK, the effect of an additional alkyl substituent on the imidazole ring has been reported to be strictly dependent on the position of the substituted N atom. Several examples have demonstrated alkylation of the imidazole-N atom away from the pyridine ring to cause a severe reduction of the activity because of the impossibility to establish a hydrogen bond with the Lys53 of the p38 $\alpha$  MAPK.<sup>38,39</sup> Because the same interaction has shown to also occur in the binding to JNK3 (Lys93), an analogous effect was expected on this enzyme as well and was confirmed by the remarkably reduced JNK3 inhibition by compound **50**, carrying a methyl group on the distal imidazole N atom. On the other hand, because several tetrasubstituted JNK3/p38 $\alpha$  MAPK inhibitors have been reported with an alkyl substituent on the imidazole N adjacent to the pyridine ring, we assumed this modification to be suitable with our 4-methyl substituted scaffold as well. However, derivatives **57** and **58**, featuring a methyl and an ethyl substituent on the N atom proximal to pyridine, respectively, unexpectedly presented an even lower potency on JNK3 than the supposedly "wrong" regioisomer **50**. The drop in activity appeared to increase with the size of the alkyl substituent, as *N*-cyclopropyl substituted **59** was almost 3-fold less active compared to its *N*-methyl analogue **57**. This outcome suggests that despite not hampering the formation of a H bond with the Lys93, alkyl substituents at the imidazole N atom proximal to pyridine reduce the tightness of the binding to the JNK3 active site.

To complete this series, starting from 4,5-disubstituted imidazole **38**, the original 5-methyl group or a free amino substituent was introduced at the imidazole-C2 position, affording compounds **44** and **47**, respectively. Although the 2-amino imidazole derivative showed a drop in activity compared to the parent compound **38**, reintroduction of the 5-methyl group at the imidazole-C2 position surprisingly produced a 2-fold increase in the inhibitory potency on JNK3 (**44**:  $IC_{50(JNK3)} = 363$  nM;  $IC_{50(p38\alpha\ MAPK)} > 10$   $\mu$ M). This outcome prompted us to reconsider our previous assumption regarding the role of the 2-methylsulfanyl moiety. Although the 5-methyl group exerts no influence on the inhibitory activity when the 4-fluorophenyl moiety is installed at the imidazole-C4 position, it has a significant impact in the case of 4-methyl imidazole derivatives.

In a closer evaluation concerning the influence of the alkyl chain in position 4 of the imidazole core combined with the 2-methylsulfanyl moiety in C2 position, the methyl group (**44**) emerged once more as the substituent presenting the optimal length to target the JNK3 HR I, when compared to the 4-unsubstituted and to the 4-ethyl derivatives **43** and **45**, respectively (Table 4). Comparison of imidazoles **5** (Table 1) and **44** (Table 4) reveals the replacement of the 4-fluorophenyl ring at the imidazole-C4(5) position by a smaller methyl group to result in a 1 order of magnitude loss in JNK3 inhibition and in a complete loss of p38 $\alpha$  MAPK inhibitory activity.

To elucidate the binding mode of the 4-methyl-substituted-5-(pyridine-4-yl)imidazole derivatives, as well as to gain insight into the role of the 2-methylsulfanyl group, crystal structures of JNK3 in complex with compounds **38** and **44** were determined (Figure 2).



**Figure 2.** Crystal structures of JNK3 in complex with inhibitors **38** (A) and **44** (B) featuring a pyridylimidazole scaffold. Only the JNK3 active site is shown. The protein backbone is displayed in gray. The compounds, the side chain of gatekeeper Met146, and a part of the Gly-rich loop are highlighted in stick display. Active site residues with common orientations and interactions are shown in light blue, whereas residues that differ between both complexes are highlighted in the same color as the respective inhibitor. Side chains for which multiple orientations are observed (Asn194 in complex with **38** and Asn152 in complex with **44**) are shown in both orientations. Water molecules are represented as red spheres and hydrogen bonds are shown as black dashed lines.

The structures revealed a similar binding mode of the inhibitors within the adenosine 5'-triphosphate (ATP) pocket of JNK3 (Figure 2). As expected, both scaffolds interacted with the hinge region of the kinase via two hydrogen bonds involving the main chain carbonyl and backbone amine groups of Met149 and mimicking the interactions of the enzyme with ATP<sup>40</sup> as well as with its nonhydrolyzable analogue  $\beta\gamma$ -

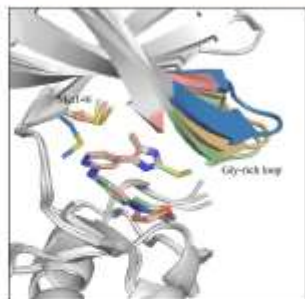
methyleneadenosine-5'-triphosphate (AMP-PCP; Figure S3, Supporting Information). In both structures, the imidazole-N atom distal from the pyridine ring is part of a network of water-mediated hydrogen bonds, involving the side chain of Lys93 and the main chain of Leu206. Further water-mediated hydrogen bonds in the JNK3-**38** crystal structure (Figure 2A) include the side chain of Asn194, whereas in the JNK3-**44** structure (Figure 2B), the backbone of Gly76 and the side chain of Asp207 are involved. The structure of JNK3 in complex with inhibitor **38** also showed that the imidazole-N atom proximal to the pyridine ring participates in a water-mediated hydrogen bond with the Asn152 side chain and the same interaction seems to be present in the JNK3-**44**, thus explaining the detrimental effect produced by the substitution of this position (compounds **57**–**59**). Multiple hydrophobic interactions comprising the gatekeeper Met146 and the side chains of Ile70, Val78, Val196, and Leu206 were also observed. These interactions have been previously described by Scapin et al.<sup>37</sup> and confer JNK3 selectivity as they cannot be formed in the larger binding pocket of p38 $\alpha$  MAPK. The methyl group present in both inhibitors was oriented toward the HR I, which resulted in an identical orientation of the side chain of the gatekeeper residue Met146. The 4-morpholinylaniline moiety, which occupied the solvent-exposed HR II, exhibited higher flexibility and no direct interactions with JNK3, that is, this moiety likely contributes barely or not at all to the binding.

A major structural difference between the two complex structures was observed for the Gly-rich loop. In the JNK3-**38** complex structure, no electron density for residues Gly71–Gly76 was visible because of high local flexibility, a phenomenon also encountered in other JNK3 crystal structures.<sup>41–43</sup> In the JNK3-**44** complex, however, the electron density for this loop was clearly defined, hinting to a structural stabilization of this region upon interaction with the 2-methylsulfanyl moiety in compound **44**.

A superposition of our inhibitor complex structures with crystal structures of JNK3 bound to AMP-PCP and the dual JNK3/p38 $\alpha$  MAPK inhibitor by Scapin et al.<sup>37</sup> (PDB code: IPMN) yielded insights into the structural basis for the observed selectivity of compounds **38** and **44** (Figure 3).

As can be seen from this structural comparison, no movement of the gatekeeper Met146 side chain is induced by compounds **38** and **44** when compared to the AMP-PCP complex, contrary to the dual kinase inhibitor studied by Scapin et al. In the latter crystal structure, an induced fit of side chain 146 occurred to accommodate the dichlorophenyl moiety of the dual kinase inhibitor. Conversely, it appears that the methyl substituent of compounds **38** and **44** was unable to occupy the wider HR I of the p38 $\alpha$  MAPK, while possessing the optimal length to target the respective region of JNK3. Therefore, this moiety determined the selectivity achieved over p38 $\alpha$  MAPK, demonstrated by the activities of compounds listed in Tables 2–4. In the case of AMP-PCP and compound **44**, another result of the interaction is a downward positioning of the flexible Gly-rich loop. A similar compression of the binding pocket caused by a repositioning of the Gly-rich loop was reported for a JNK3 complex crystal structure by Kamenecka et al.<sup>44</sup> and might be a result of hydrophobic interactions and water-mediated hydrogen bonds provided by inhibitor **44**, which stabilized this otherwise flexible section. Overall, as a result of inhibitor binding, the JNK3 ATP binding pocket in our crystal structures appears somewhat narrower in comparison to the p38 $\alpha$  MAPK binding





**Figure 3.** Comparison of the gatekeeper Met146 orientation and the Gly-rich loop positioning upon JNK3 inhibitor binding with other ligand-bound JNK3 structures. Overlay of the JNK3-44 complex structure (light green), the JNK3-38 complex structure (light red), the AMP-PCP-bound JNK3 structure (light orange), and the 1PMN structure reported by Scapin, et al.<sup>37</sup> (blue). The superposition was performed using the "align" function in PyMOL. The side chains of the gatekeeper Met146 and the Gly-rich loop are highlighted. Only compounds 38 and 44 are shown for the sake of clarity.

site (where the gatekeeper is Thr106), an effect that is less prominent for the dual kinase inhibitor (Figure 3) and probably responsible for the selectivity of compounds 38 and 44. With respect to the 2-fold increase in the inhibitory potency on JNK3 of compound 44 over its analogue 38, the influence of the *S*-methyl group on the positioning of the Gly-rich loop is the most likely structural reason for the significant gain in affinity.

An additional characterization of the two compounds 38 and 44 included the determination of the protein melting temperature ( $T_m$ ) in the presence and absence of inhibitors by nano differential scanning fluorimetry (nanoDSF). This methodology consists of assessing the influence of the binding event on the stability of the target protein and is carried out by monitoring temperature-dependent changes in the intrinsic protein fluorescence as a consequence of unfolding. The corresponding curves (Figure S2, Supporting Information) exhibited a significant increase in stability of JNK3 upon inhibitor binding, as can be seen from the associated  $T_m$  values (Table 5). The  $T_m$  value of JNK3 alone was determined to be 46.3 °C and increased to 53.8 and 54.8 °C in the presence of compounds 38 and 44, respectively, which correlates well with the results concerning the inhibitory activity and stability of the Gly-rich loop.

**Table 5.** Determined Melting Temperatures ( $T_m$ ) for JNK3 Alone and in Complex with Inhibitors 38 and 44

sample	$T_m$ (°C) <sup>a</sup>
JNK3	46.28 ± 0.50
JNK3-38	53.87 ± 0.04
JNK3-44	54.83 ± 0.04

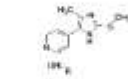
<sup>a</sup>Data represent mean value ± SD of a single experiment performed in triplicate. nanoDSF measurements (Figure S2, Supporting Information) were conducted using Prometheus NT.48 (NanoTemper Technologies, Munich).

A further approach in the pursuit of a tighter binding with the JNK3 consisted of modifying the amino moiety at the pyridine-C2 position (Table 6).

An initial attempt was carried out by introducing  $\alpha$ -methyl(phenyl)alkylamino moieties (compounds 48a–b) as well as cycloalkylamino groups (compounds 48c–e). The former moieties have been reported in potent p38 $\alpha$  MAPK inhibitors, for example, LN950 (Figure 1) and ML3403,<sup>45</sup> and were thus introduced to evaluate their effect on JNK3 inhibitory potency. In detail, these substituents were hypothesized to yield an increase in the JNK3 inhibitory activity while conserving selectivity over the p38 $\alpha$  MAPK because of the combination with the 4-methyl substituent on the imidazole ring. However, the 3-methyl-2-butylamino group (48a) resulted in a loss of activity compared to the 4-morpholinoaniline precursor 44, although maintaining some selectivity over the p38 $\alpha$  MAPK. Substitution with the  $\alpha$ -methylbenzylamine, giving rise to compound 48b, was instead counterproductive as it not only caused a tremendous drop in JNK3 inhibition but also a recovery of the activity on the p38 $\alpha$  MAPK (48b:  $IC_{50}(\text{JNK3}) = 7610 \text{ nM}$ ;  $IC_{50}(\text{p38}\alpha\text{-MAPK}) = 3460 \text{ nM}$ ). On the other hand, although not reaching the potency of the parent compound 44, the JNK3 inhibitory activity of compounds bearing cycloalkylamino moieties at the pyridine-C2 position (48c–e) increased alongside the size of the aliphatic ring, a trend suggesting the importance of hydrophobic interactions in this area of the molecule. Nevertheless, replacement of the cyclohexyl ring of 48e with the similar tetrahydropyranyl group (48f) yielded, unexpectedly, a remarkable loss of activity on JNK3.

A possible strategy to gain activity and selectivity on JNK3 would consist of targeting the side chain of Gln155 as this residue is replaced by a shorter Asn in the p38 $\alpha$  MAPK.<sup>46</sup> As suggested by the structure of the JNK3-44 complex (Figure 2), this amino acidic residue is located about 4 Å away from the 4-morpholinoaniline-N atom but cannot be reached because of the rigidity of this substituent. Moreover, the 4-morpholinoanilino moiety is only able to accept a hydrogen bond, whereas the Gln residue has the potential to act as both acceptor and donor of hydrogen bonds. For this reason, *trans*-4-aminocyclohexanol and *trans*-1,4-diaminocyclohexyl moieties were selected for compounds 48g and 48h, respectively, because of a higher flexibility and their additional capability to donate hydrogen bond interactions. In particular, the former moiety is also present in the structure of clinical candidate CC-930, wherein it is reported to interact with the aforementioned Gln155,<sup>47</sup> and included in potent p38 $\alpha$  MAPK inhibitors.<sup>45</sup> Unfortunately, despite preserving the selectivity over the p38 $\alpha$  MAPK, none of the two inhibitors 48g and 48h succeeded in overcoming the activity of the parent compound 44 on the JNK3, with the latter displaying a 3-fold drop in potency. This observation suggests an inability of the introduced moiety to form the desired interaction with the Gln155 side chain or this interaction being compensated by other factors. Additionally, it underlines the necessity of the aromatic moiety at the pyridine-C2 amino function for the binding to the JNK3. The significantly lower activity of compound 48b could also derive from the not tolerated protonation of its terminal amino functionality. With the aim to reach the Gln155 side chain by the introduction of an additional hydrogen bond acceptor, a series of amides of compound 48h and of its aromatic counterpart 48m was synthesized. This approach also permits to seek additional interactions with the enzyme HR II.

**Table 6. Influence of Substituents at the Pyridine-C2 Position**



Cpd	R	IC <sub>50</sub> ± SD [nM] <sup>a</sup>	
		JNK3	p38α MAPK
48a		2,590 ± 173	>10,000 (31%) <sup>b</sup>
48b		7,610 ± 145	3,460 ± 1,630
48c		3,040 ± 194	>10,000 (36%) <sup>b</sup>
48d		1,566 ± 124	>10,000 (47%) <sup>b</sup>
48e		671 ± 74	>10,000 (31%) <sup>b</sup>
48f		2,602 ± 406	>10,000 (27%) <sup>b</sup>
48g		457 ± 72	>10,000 (33%) <sup>b</sup>
48h		941 ± 75	>10,000 (46%) <sup>b</sup>
48i		819 ± 141	>10,000 (37%) <sup>b</sup>
48j		1,218 ± 723	>10,000 (12%) <sup>b</sup>
48k		2,231 ± 380	>10,000 (10%) <sup>b</sup>
48l		2,538 ± 261	>10,000 (13%) <sup>b</sup>
48m		353 ± 38	>10,000 (38%) <sup>b</sup>
48n		415 ± 40	>10,000 (32%) <sup>b</sup>
48o		432 ± 57	>10,000 (33%) <sup>b</sup>
48p		1,539 ± 349	>10,000 (27%) <sup>b</sup>
48q		2,573 ± 304	>10,000 (13%) <sup>b</sup>

<sup>a</sup>IC<sub>50</sub> values are the mean of three experiments. <sup>b</sup>Percent inhibition at indicated concentration. <sup>c</sup>According to the ZINC patterns tool, compound 48m represents a potential pan-assay interference compound. However, this compound was synthesized as the intermediate for the preparation of inhibitors 48n–q. To estimate the impact of the amide moiety present in compounds 48n–q on the

**Table 6. continued**

inhibition of the two kinases, the activities of 48m are listed in this table.

Unfortunately, in neither of the two series, the introduction of amide moieties permitted to gain an inhibitory activity comparable with the precursor 44. In the series featuring a cycloaliphatic amine (48i–l), only the small acetamide derivative 48i exhibited an almost similar activity to the precursor, whereas bulkier alkyl and aromatic residues displayed a 2- to 3-fold decrease in potency. In an analogous fashion, when considering the series derived from the aromatic intermediate 48m, compounds bearing a *tert*-butyl or a cyclohexyl amide (48p and 48q, respectively) showed a significant drop in inhibitory activity, with IC<sub>50</sub> values in the micromolar range. On the other hand, both inhibitors carrying an acetamido or benzamido moiety (48n and 48o, respectively) were still able to inhibit the JNK3 with a potency akin to the free amine derivative 48m. The comparison of the two amide series also supports the theory of a higher suitability of aromatic substituents at the pyridine-C2 amino position when targeting the JNK3.

Compound 44 resulted as the best inhibitor of the synthesized series and was, therefore, further investigated to achieve a comprehensive characterization. At a first instance, to evaluate the intra-JNK selectivity, compound 44 was tested on the three JNK isoforms (Table 7). As expected, compound 44 inhibited the three isoforms with a similar potency but showed a moderate preference for JNK1 and JNK3 over JNK2.

**Table 7. Inhibition Data of Compound 44 on the Three JNK Isoforms**

IC <sub>50</sub> [nM] <sup>a</sup>		
JNK1	JNK2	JNK3
119	468	184

<sup>a</sup>Compound 44 was tested by Reaction Biology corporation (Malvern, PA, USA) using a radiometric assay.

Moreover, inhibitor 44 was further screened against a panel of 45 diverse kinases to achieve a preliminary evaluation of its selectivity within the kinome. Out of the kinase panel, 10 kinases (including JNK1) were inhibited more than 50% at a testing concentration of 10 μM (Table S3, Supporting Information).

Additional studies were aimed at evaluating the inhibition of the human-ether-à-go-go related gene (hERG) potassium channels as well as liver cytochromes P450 (CYP450) to highlight potential liabilities of the synthesized scaffold. As displayed in Table 8, compound 44 showed a reduced interference with the hERG channels (IC<sub>50</sub> > 10 μM).

Regarding interaction with hepatic enzymes, compound 44 displayed low to moderate inhibition of four of the five tested

**Table 8. Inhibitory Activity of Compound 44 on hERG Channels and on the Most Relevant CYP Isoforms**

hERG inhibition [% inhibition at 10 μM]	CYP450 inhibition [% inhibition at 10 μM]				
	1A9	2C9	2C19	2D6	3A4
38.8	51.5	53.9	35.6	19.0	75.1



isoenzymes, this representing a significantly cleaner profile in comparison with previously reported inhibitors of this class.<sup>40</sup> However, the elevated blockage of the most abundant CYP450 isoform 3A4 still constitutes a serious limit, which needs to be solved by subsequent optimization strategies.

Finally, additional tests were performed to assess the metabolic stability of methyl-substituted pyridinylimidazole **44** upon incubation with human liver microsomes. One of the most serious limitations of previously reported 2-alkylsulfanylimidazoles is their severe metabolism consisting of oxidation of the thioether function to the corresponding sulfoxide.<sup>40</sup> Nevertheless, *in vitro* assays performed on compound **44** demonstrated a substantial metabolic stability, as approximately 80% of the unmodified compound was still present after 4 h incubation (Figure S6, Supporting Information). The major metabolite formed still appears to be represented by the sulfoxide derivative (8.49%), although modifications at the 4-morpholinoaniline substituent might also be present.

## CONCLUSIONS

Optimization of 4-(4-fluorophenyl)-5-(pyridin-4-yl)imidazole-based p38 $\alpha$  MAPK inhibitors by modification of the five-membered heterocyclic core, the aryl moiety at the imidazole-C4 position, and the pyridine-C2 amino function resulted in a novel series of JNK3 inhibitors exhibiting high selectivity over the closely related p38 $\alpha$  MAPK. Biological evaluation of the different pyridinyl-substituted five-membered rings provided valuable insights into the structure activity relationship of this scaffold with respect to JNK3 and p38 $\alpha$  MAPK inhibitory potencies. By addressing the HR 1 with a small methyl group, a significant selectivity toward JNK3 was achieved. This feature is not yet reported for this class of compounds, which have been generally described as p38 $\alpha$  MAPK inhibitors. The binding mode at the ATP binding site of the enzyme for this class of compounds was confirmed by X-ray structures of JNK3 crystals incubated with imidazoles **38** and **44**. The most potent inhibitor 4-(4-methyl-2-(methylthio)-1H-imidazol-5-yl)-N-(4-morpholinophenyl)pyridin-2-amine (**44**) inhibits the JNK3 in the low triple digit nanomolar range, is metabolically stable, and displays a slight selectivity over the JNK2 isoform. Further characterization of this inhibitor highlighted reduced interactions with the hERG channel as well with most of the tested CYP450 isoforms.

## EXPERIMENTAL SECTION

**Chemistry, General.** All chemicals were purchased from commercial sources unless otherwise specified and used without further purification. Thin-layer chromatography (TLC) reaction controls were performed for all reactions using fluorescent silica gel 60 F<sub>254</sub> plates (Merck) and visualized under natural light and UV illumination at 254 and 366 nm. The purities of all tested compounds were confirmed to be >95% as determined by reverse-phase high-performance liquid chromatography (HPLC) using one of the two following methods. In the case of method 1, the instrument used was a Hewlett Packard HP 1090 Series II LC equipped with a UV diode array detector (DAD) (detection at 230 and 254 nm). The chromatographic separation was performed on a Phenomenex Luna 5u C8 column (150 mm  $\times$  4.6 mm, 5  $\mu$ m) at 35  $^{\circ}$ C oven temperature. The injection volume was 5  $\mu$ L and the flow

was 1.5 mL/min using the following gradient: 0.01 M KH<sub>2</sub>PO<sub>4</sub> pH 2.3 (solvent A), MeOH (solvent B), 40% B to 85% B in 8 min; 85% B for 5 min; 85% to 40% B in 1 min; 40% B for 2 min; stop time 16 min. In the case of method 2, an Agilent 1100 Series HPLC system was used, equipped with a UV DAD (detection at 218, 254, and 280 nm). The chromatographic separation was performed on an XBridge C18 column (150 mm  $\times$  4.6 mm, 5  $\mu$ m) and the oven temperature was set to 30  $^{\circ}$ C. The injection volume was 10  $\mu$ L and the flow was 1.5 mL/min using the following gradient: 0.01 M KH<sub>2</sub>PO<sub>4</sub> pH 2.3 (solvent A), MeOH (solvent B), 45% B to 85% B in 9 min; 85% B for 6 min; stop time 16 min. Flash column chromatography was performed using an Interchim puriFlash 430 automated flash chromatography system with Davisil LC60A 20–45  $\mu$ m silica from Grace Davison and Geduran S160 63–200  $\mu$ m silica from Merck for the precolumn. Nuclear magnetic resonance (NMR) data were obtained on a Bruker ARX NMR spectrometer at 250 MHz, on a Bruker AVANCE III HD NMR spectrometer at 300 MHz, or on a Bruker AVANCE NMR spectrometer at 400 MHz at ambient temperature. Chemical shifts are reported in parts per million (ppm) relative to tetramethylsilane. All spectra were calibrated against the (residual proton) peak of the deuterated solvent used. Mass spectra were recorded on an Advion expression 5 electrospray ionization mass spectrometer (ESI-MS) with TLC interface.

**Experimental Procedures, General Procedure for the Nucleophilic Aromatic Substitution with 4-Morpholinoaniline (General Procedure A).** In a pressure vial, the 2-halide pyridine intermediate (1 equiv) and 4-morpholinoaniline (1.5 equiv) were suspended in *n*-butanol (3 mL) and 1.25 M HCl in EtOH (1 equiv) was added. After tightly closing the vial, the reaction mixture was heated in a heating block at 180  $^{\circ}$ C and stirred for 18 h. After removing the solvent at reduced pressure, the residue was purified by flash column chromatography.

**General Procedure for the Synthesis of Compounds 15a–I (General Procedure B).** In a three-neck round-bottom flask under anhydrous conditions, 2-chloro-4-methylpyridine (**9**) (1 equiv) and the appropriate ethyl ester (1 equiv) were dissolved in dry tetrahydrofuran (THF) (2 mL). After cooling the reaction mixture to 0  $^{\circ}$ C, 2 M sodium bis(trimethylsilyl)amide (NaHDMS) in dry THF (2.2 equiv) was added dropwise and the mixture was stirred at 0  $^{\circ}$ C for 1.5–5 h. After adding H<sub>2</sub>O, the aqueous phase was extracted three times with dichloromethane (DCM) or EtOAc and washed with NaCl saturated solution. The combined organic layers were dried over anhydrous Na<sub>2</sub>SO<sub>4</sub> and the solvent was evaporated at reduced pressure. The residue was finally purified by flash column chromatography.

**General Procedure for the Synthesis of Compounds 16a–I (General Procedure C).** Ethan-1-one intermediates 15a–I (1 equiv) and SeO<sub>2</sub> (1.1 equiv) were suspended in 5–10 mL of glacial AcOH and the reaction mixture was stirred at 65  $^{\circ}$ C for 2–3 h. After cooling to room temperature (rt), the formed solid residue of Se was removed by filtration and the filtrate was diluted with EtOAc and then washed with saturated NaHCO<sub>3</sub> solution four times. Finally, the organic phase was washed with saturated NaCl solution, dried over anhydrous Na<sub>2</sub>SO<sub>4</sub>, and concentrated at reduced pressure. The residue was purified by flash column chromatography.

**General Procedure for the Synthesis of Compounds 17a–I (General Procedure D).** In a pressure vial, ethane-1,2-dione

derivatives **16a–l** (1 equiv) and  $\text{NH}_4\text{OAc}$  (10 equiv) were suspended in 3 mL of glacial AcOH and after that a 37% aqueous solution of formaldehyde (1 equiv) was added. The reaction vessel was heated in a CEM microwave reactor at 180 °C, with an initial power of 200 W, for 2–5 min. The mixture was added dropwise to  $\text{NH}_4\text{OH}$  concentrated solution at 0 °C. The suspension obtained was extracted three times with EtOAc and the combined organic layers were dried over anhydrous  $\text{Na}_2\text{SO}_4$  and concentrated at reduced pressure. The residue was purified by flash column chromatography.

**General Procedure for the Synthesis of Compounds 48a–h (General Procedure E).** In a pressure vial, 2-chloro-4-(4-methyl-2-(methylthio)-1H-imidazol-5-yl)pyridine (**41**) was suspended in  $\approx 2$  mL of *n*-butanol. The closed vial was then heated at 180 °C and stirred for 48–120 h. The reaction mixture was poured in  $\text{H}_2\text{O}$  and the aqueous layer was extracted three times with EtOAc. The combined organic layers were dried over anhydrous  $\text{Na}_2\text{SO}_4$  and concentrated at reduced pressure. The residue was finally purified by flash column chromatography.

**General Procedure for the Synthesis of Compounds 48i–l and 48n–q (General Procedure F).** Under an argon atmosphere, *trans*-N1-(4-(4-methyl-2-(methylthio)-1H-imidazol-5-yl)pyridin-2-yl)cyclohexane-1,4-diamine (**48h**) or N1-(4-(4-methyl-2-(methylthio)-1H-imidazol-5-yl)pyridin-2-yl)-benzene-1,4-diamine (**48m**) was dissolved in 1.5 mL of dry pyridine and after that the appropriate acid chloride or anhydride was added and the reaction mixture was stirred at rt for 16 h. The reaction mixture was poured in  $\text{H}_2\text{O}$  and the aqueous layer was extracted three times with EtOAc. The combined organic layers were dried over anhydrous  $\text{Na}_2\text{SO}_4$  and concentrated at reduced pressure. The residue was finally purified by flash column chromatography.

**2-Fluoro-4-(4-(4-fluorophenyl)-2-(methylthio)-1H-imidazol-5-yl)pyridine (4).**<sup>21</sup> The title compound was synthesized as described in the literature<sup>21</sup> and analytical data were in agreement with the reported ones.

**4-(4-(4-Fluorophenyl)-2-(methylthio)-1H-imidazol-5-yl)-N-(4-morpholinophenyl)pyridin-2-amine (5).** The title compound was synthesized according to general procedure A starting from compound **4** (100 mg, 0.33 mmol) and 4-morpholinoaniline (88.1 mg, 0.49 mmol). Purification by flash column chromatography ( $\text{SiO}_2$ , DCM/EtOH 100:0 to 9:1) afforded 61 mg of the desired compound (40% yield);  $^1\text{H}$  NMR (400 MHz,  $\text{DMSO}-d_6$ ):  $\delta$  2.61 (s, 3H), 3.00 (br s, 4H), 3.73 (br s, 4H), 6.53–6.75 and 6.88–7.00 (m, 2H), 6.82 (d,  $J = 7.6$  Hz, 2H), 7.09–7.42 (m, 4H), 7.43–7.61 (m, 2H), 7.82–8.12 (m, 1H), 8.55–8.84 (m, 1H), 12.65 ppm (br s, 1H);  $^{13}\text{C}$  NMR (101 MHz,  $\text{DMSO}-d_6$ ):  $\delta$  15.0, 15.1, 49.4, 66.2, 106.1, 106.4, 111.4, 111.7, 115.2 (d,  $J = 21.2$  Hz), 115.7, 115.9, 119.9, 120.3, 126.2, 126.9, 129.5 (d,  $J = 8.1$  Hz), 130.7 (d,  $J = 8.0$  Hz), 133.7, 134.2, 134.8, 137.9, 138.7, 141.9, 142.7, 145.6, 145.9, 147.3, 148.1, 156.7, 161.9 ppm (d,  $J = 244.4$  Hz); MS–FAB  $m/z$  [M] calcd for  $\text{C}_{22}\text{H}_{24}\text{FN}_4\text{OS}$ , 461.2; found, 461.3; HPLC (method 1):  $t_R = 5.326$  min (100%).

**2-((4-(4-Fluorophenyl)-5-(2-fluoropyridin-4-yl)-1H-imidazol-2-yl)thio)ethan-1-ol (6).**<sup>49</sup> The title compound was synthesized as described in the literature<sup>49</sup> and analytical data were in agreement with the reported ones.

**4-(4-Fluorophenyl)-5-(2-((4-morpholinophenyl)amino)pyridin-4-yl)-1,3-dihydro-2H-imidazol-2-one (8).** The title

compound was prepared according to general procedure A starting from **6** (300 mg, 0.90 mmol) and 4-morpholinoaniline (240.6 mg, 1.35 mmol). Purification by flash column chromatography ( $\text{SiO}_2$ , DCM/EtOH 97:03 to 85:15) afforded 200 mg of the desired compound (64% yield);  $^1\text{H}$  NMR (400 MHz,  $\text{DMSO}-d_6$ ):  $\delta$  2.81–3.11 (m, 4H), 3.58–3.85 (m, 4H), 6.42–6.65 (m, 2H), 6.80 (d,  $J = 6.6$  Hz, 2H), 7.12–7.36 (m, 4H), 7.36–7.59 (m, 2H), 7.99 (dd,  $J = 4.7, 2.4$  Hz, 1H), 8.65 (br s, 1H), 10.64 (br s, 1H), 10.72 ppm (br s, 1H);  $^{13}\text{C}$  NMR (101 MHz,  $\text{DMSO}-d_6$ ):  $\delta$  49.3, 66.2, 105.2, 111.9, 115.6, 115.8, 115.9 (d,  $J = 19.0$  Hz), 119.7, 120.5, 126.2 (d,  $J = 2.9$  Hz), 129.9 (d,  $J = 8.0$  Hz), 133.6, 138.2, 145.9, 147.9, 153.9, 156.6, 161.7 ppm (d,  $J = 245.9$  Hz); MS–FAB  $m/z$ : [M + H]<sup>+</sup> calcd for  $\text{C}_{24}\text{H}_{22}\text{FN}_4\text{O}_2$ , 431.18; found, 431.30; HPLC (method 1):  $t_R = 4.552$  min (96.7%).

**1-(4-Fluorophenyl)-2-(2-fluoropyridin-4-yl)ethane-1,2-dione (10).** The title compound was synthesized according to the literature and the analytical data were in agreement with the reported ones.<sup>10</sup>

**4-(2-Ethyl-4-(4-fluorophenyl)-1H-imidazol-5-yl)-2-fluoropyridine (11).** To a solution of **10** (250 mg, 1.01 mmol) in MeOH (5 mL), 7 M ammonia in MeOH (2.89 mL, 20.23 mmol) and propionaldehyde (88.11 mg, 1.52 mmol) were added and the reaction mixture was heated to reflux temperature and stirred for 4 h. After cooling down, the solvent was evaporated at reduced pressure and the residue was purified by flash column chromatography ( $\text{SiO}_2$ , DCM/EtOH 97:03 to 94:06), obtaining 125 mg of the desired product (43% yield);  $^1\text{H}$  NMR (300 MHz,  $\text{DMSO}-d_6$ ):  $\delta$  1.28 (t,  $J = 7.6$  Hz, 3H), 2.64–2.77 (m, 2H), 7.09 (s, 1H), 7.17–7.40 (m, 3H), 7.47–7.56 (m, 2H), 8.06 (d,  $J = 5.4$  Hz, 1H), 12.41 ppm (br s, 1H); MS–ESI  $m/z$ : [M + H]<sup>+</sup> calcd for  $\text{C}_{24}\text{H}_{23}\text{F}_2\text{N}_3$ , 286.1; found, 286.0;  $m/z$ : [M – H]<sup>–</sup> calcd for  $\text{C}_{24}\text{H}_{21}\text{F}_2\text{N}_3$ , 284.1; found, 284.0; HPLC (method 2):  $t_R = 3.680$  min.

**4-(2-Ethyl-4-(4-fluorophenyl)-1H-imidazol-5-yl)-N-(4-morpholinophenyl)pyridin-2-amine (13).** The title compound was synthesized according to general procedure A starting from 4-(2-ethyl-4-(4-fluorophenyl)-1H-imidazol-5-yl)-2-fluoropyridine (**11**) (85 mg, 0.30 mmol) and 4-morpholinoaniline (80.2 mg, 0.45 mmol). The crude residue was purified twice by flash column chromatography ( $\text{SiO}_2$ , DCM/EtOH 96:04 to 94:06) and (RP-C18, *iso*-propanol/ $\text{H}_2\text{O}$  1:1), obtaining 32 mg of the desired compound (24% yield);  $^1\text{H}$  NMR (300 MHz,  $\text{DMSO}-d_6$ ):  $\delta$  1.27 (t,  $J = 7.6$  Hz, 3H), 2.69 (q,  $J = 7.6$  Hz, 2H), 2.96–3.06 (m, 4H), 3.70–3.79 (m, 4H), 6.63–6.92 (m, 3H), 6.97 (br s, 1H), 7.12–7.57 (m, 6H), 7.86–8.08 (m, 1H), 8.60–8.79 (m, 1H), 12.20 ppm (br s, 1H);  $^{13}\text{C}$  NMR (101 MHz,  $\text{DMSO}-d_6$ ):  $\delta$  12.7, 21.2, 49.4, 66.2, 106.2, 115.9, 119.9, 120.2, 127.6, 129.6, 130.6, 134.4, 143.5, 149.6, 156.7, 162.6 ppm; MS–ESI  $m/z$ : [M + H]<sup>+</sup> calcd for  $\text{C}_{30}\text{H}_{29}\text{FN}_4\text{O}$ , 444.2; found, 444.2;  $m/z$ : [M – H]<sup>–</sup> calcd for  $\text{C}_{30}\text{H}_{27}\text{FN}_4\text{O}$ , 442.2; found, 442.2; HPLC (method 2):  $t_R = 4.960$  min (98.6%).

**4-(4-(4-Fluorophenyl)-1H-imidazol-5-yl)-N-(4-morpholinophenyl)pyridin-2-amine (14).** The title compound was synthesized according to general procedure A starting from 2-fluoro-4-(4-(4-fluorophenyl)-1H-imidazol-5-yl)pyridine (**12**)<sup>19</sup> (70 mg, 0.27 mmol) and 4-morpholinoaniline (71.3 mg, 0.40 mmol). Purification by flash column chromatography ( $\text{SiO}_2$ , DCM/EtOH 95:05 to 90:10) afforded 70 mg of the desired compound (62% yield);  $^1\text{H}$  NMR (250 MHz,  $\text{DMSO}-d_6$ ):  $\delta$  2.93–3.07 (m, 4H), 3.66–3.79 (m, 4H),



6.63–7.00 (m, 4H), 7.12–7.41 (m, 4H), 7.42–7.60 (m, 2H), 7.81 (s, 1H), 7.89–8.13 (m, 1H), 8.57–8.80 (m, 1H), 12.53–12.78 ppm (m, 1H); MS-ESI  $m/z$ :  $[M + H]^+$  calcd for  $C_{24}H_{23}FN_3O$ , 415.18; found, 416.2;  $m/z$ :  $[M - H]^-$  calcd for  $C_{24}H_{22}FN_3O$ , 414.2; found, 414.2; HPLC (method 2):  $t_R$  = 3.692 min (97.9%).

***N*-(4-Morpholinophenyl)-4-(4-phenyl-1H-imidazol-5-yl)pyridin-2-amine (18a)**. The title compound was synthesized according to general procedure A starting from compound 17a (100 mg, 0.39 mmol) (for the synthesis of 17a see Supporting Information) and 4-morpholinoaniline (103.4 mg, 0.58 mmol). Purification by flash column chromatography ( $SiO_2$ , DCM/EtOH 97:03 to 90:10) afforded 138 mg of the desired compound (89% yield);  $^1H$  NMR (300 MHz,  $DMSO-d_6$ ):  $\delta$  2.92–3.08 (m, 4H), 3.66–3.80 (m, 4H), 6.68 (dd,  $J$  = 5.3, 0.9 Hz, 1H), 6.82 (d,  $J$  = 9.0 Hz, 2H), 6.93 (br s, 1H), 7.30–7.53 (m, 7H), 7.82 (s, 1H), 7.97 (d,  $J$  = 5.3 Hz, 1H), 8.70 (s, 1H), 12.66 ppm (br s, 1H);  $^{13}C$  NMR (101 MHz,  $DMSO-d_6$ ):  $\delta$  49.4, 66.1, 106.5, 111.8, 115.9, 120.1, 127.6, 128.1, 128.6, 132.0, 134.0, 136.0, 142.4, 145.7, 147.2, 156.6 ppm; MS-ESI  $m/z$ :  $[M + H]^+$  calcd for  $C_{24}H_{23}N_5O$ , 398.2; found, 398.2;  $m/z$ :  $[M - H]^-$  calcd for  $C_{24}H_{22}N_5O$ , 396.2; found, 396.3; HPLC (method 1):  $t_R$  = 3.513 min (99.1%).

**4-(4-(2-Chlorophenyl)-1H-imidazol-5-yl)-N-(4-morpholinophenyl)pyridin-2-amine (18b)**. The title compound was synthesized according to general procedure A starting from compound 17b (100 mg, 0.34 mmol) (for the synthesis of 17b see Supporting Information) and 4-morpholinoaniline (90.9 mg, 0.51 mmol). Purification by flash column chromatography ( $SiO_2$ , DCM/EtOH 97:03 to 90:10) afforded 127 mg of the desired compound (87% yield);  $^1H$  NMR (300 MHz,  $DMSO-d_6$ ):  $\delta$  2.85–3.17 (m, 4H), 3.59–3.89 (m, 4H), 6.51 (d,  $J$  = 4.8 Hz, 1H), 6.81 (d,  $J$  = 8.5 Hz, 2H), 6.92 (br s, 1H), 7.28 (d,  $J$  = 7.5 Hz, 2H), 7.37–7.67 (m, 4H), 7.79–8.01 (m, 2H), 8.60 (s, 1H), 12.63 ppm (br s, 1H);  $^{13}C$  NMR (101 MHz,  $DMSO-d_6$ ):  $\delta$  49.4, 66.2, 104.8, 110.4, 115.9, 120.1, 127.4, 129.8, 130.5, 130.6, 132.5, 133.3, 134.0, 136.0, 136.0, 142.8, 145.7, 146.1, 147.4, 156.7 ppm; MS-ESI  $m/z$ :  $[M + H]^+$  calcd for  $C_{24}H_{22}ClN_5O$ , 432.1; found, 432.1;  $m/z$ :  $[M - H]^-$  calcd for  $C_{24}H_{21}ClN_5O$ , 430.15; found, 429.8; HPLC (method 2):  $t_R$  = 3.671 min (99.4%).

**4-(4-(2-Bromophenyl)-1H-imidazol-5-yl)-N-(4-morpholinophenyl)pyridin-2-amine (18c)**. The title compound was synthesized according to general procedure A starting from compound 17c (100 mg, 0.30 mmol) (for the synthesis of 17c see Supporting Information) and 4-morpholinoaniline (80.2 mg, 0.45 mmol). Purification by flash column chromatography ( $SiO_2$ , DCM/EtOH 97:03 to 90:10) afforded 100 mg of the desired compound (71% yield);  $^1H$  NMR (300 MHz,  $DMSO-d_6$ ):  $\delta$  2.91–3.15 (m, 4H), 3.62–3.95 (m, 4H), 6.51 (d,  $J$  = 4.2 Hz, 1H), 6.82 (m,  $J$  = 8.0 Hz, 3H), 7.09–7.60 (m, 5H), 7.67–8.01 (m, 3H), 8.65–8.97 (m, 1H), 12.66 ppm (br s, 1H);  $^{13}C$  NMR (101 MHz,  $DMSO-d_6$ ):  $\delta$  49.3, 66.1, 104.7, 110.3, 115.9, 120.4, 124.0, 127.9, 130.6, 130.8, 132.5, 132.9, 133.6, 135.8, 145.9, 145.9, 146.9, 146.9, 156.4 ppm; MS-ESI  $m/z$ :  $[M + H]^+$  calcd for  $C_{24}H_{23}BrN_5O$ , 476.1; found, 476.0;  $m/z$ :  $[M - H]^-$  calcd for  $C_{24}H_{22}BrN_5O$ , 474.1; found, 473.9; HPLC (method 2):  $t_R$  = 3.669 min (99.3%).

***N*-(4-Morpholinophenyl)-4-(4-(3-trifluoromethyl)phenyl)-1H-imidazol-5-yl)pyridin-2-amine (18d)**. The title compound was synthesized according to general procedure A starting

from compound 17d (100 mg, 0.30 mmol) (for the synthesis of 17d see Supporting Information). Purification by flash column chromatography ( $SiO_2$ , DCM/EtOH 97:03 to 90:10) afforded 120 mg of the desired compound (86% yield);  $^1H$  NMR (300 MHz,  $DMSO-d_6$ ):  $\delta$  2.96–3.10 (m, 4H), 3.68–3.80 (m, 4H), 6.73 (d,  $J$  = 5.4 Hz, 1H), 6.80–6.92 (m, 3H), 7.34 (d,  $J$  = 8.8 Hz, 1H), 7.61–7.81 (m, 3H), 7.84 (br s, 1H), 7.96 (s, 1H), 7.99–8.09 (m, 1H), 8.94 (br s, 1H), 13.01 ppm (br s, 1H); MS-ESI  $m/z$ :  $[M + H]^+$  calcd for  $C_{22}H_{22}F_3N_5O$ , 466.2; found, 465.9;  $m/z$ :  $[M - H]^-$  calcd for  $C_{22}H_{21}F_3N_5O$ , 464.18; found, 463.8; HPLC (method 2):  $t_R$  = 5.413 min (100%).

***N*-(4-Morpholinophenyl)-4-(4-(naphthalen-2-yl)-1H-imidazol-5-yl)pyridin-2-amine (18e)**. The title compound was synthesized according to general procedure A starting from compound 17e (100 mg, 0.327 mmol) (for the synthesis of 17e see Supporting Information) and 4-morpholinoaniline (87.5 mg, 0.49 mmol). Purification by flash column chromatography ( $SiO_2$ , DCM/EtOH 100:0 to 90:10) afforded 88 mg of the desired compound (60% yield);  $^1H$  NMR (250 MHz,  $DMSO-d_6$ ):  $\delta$  2.79–2.96 (m, 4H), 3.61–3.80 (m, 4H), 6.53 (d,  $J$  = 9.0 Hz, 2H), 6.80 (d,  $J$  = 5.1 Hz, 1H), 6.87 (br s, 1H), 7.18 (d,  $J$  = 8.8 Hz, 2H), 7.47–7.65 (m, 3H), 7.88 (s, 1H), 7.90–8.12 (m, 5H), 8.60 (s, 1H), 12.72 ppm (br s, 1H);  $^{13}C$  NMR (101 MHz,  $DMSO-d_6$ ):  $\delta$  49.3, 66.1, 106.0, 111.8, 115.7, 120.1, 126.2, 126.5, 126.8, 127.6, 128.0, 128.1, 132.3, 133.1, 133.7, 136.4, 145.6, 147.7, 156.6 ppm; MS-ESI  $m/z$ :  $[M + H]^+$  calcd for  $C_{28}H_{23}N_5O$ , 448.2; found, 448.3;  $m/z$ :  $[M - H]^-$  calcd for  $C_{28}H_{22}N_5O$ , 446.2; found, 446.3; HPLC (method 2):  $t_R$  = 5.541 min (98.5%).

**4-(4-(1-Methyl-1H-pyrazol-4-yl)-1H-imidazol-5-yl)-N-(4-morpholinophenyl)pyridin-2-amine (18f)**. The title compound was synthesized according to general procedure A starting from compound 17f (105.0 mg, 0.40 mmol) (for the synthesis of 17f see Supporting Information) and 4-morpholinoaniline (107.0 mg, 0.60 mmol). Purification by flash column chromatography ( $SiO_2$ , DCM/EtOH 100:0 to 70:30) afforded 148 mg of the desired compound (92% yield);  $^1H$  NMR (250 MHz,  $DMSO-d_6$ ):  $\delta$  2.92–3.09 (m, 4H), 3.65–3.79 (m, 4H), 3.88 (s, 3H), 6.83–6.93 (m, 3H), 7.08 (s, 1H), 7.45 (d,  $J$  = 8.8 Hz, 2H), 7.60 (s, 1H), 7.79 (s, 1H), 7.93 (s, 1H), 8.00 (d,  $J$  = 5.4 Hz, 1H), 8.87 ppm (br s, 1H);  $^{13}C$  NMR (101 MHz,  $DMSO-d_6$ ):  $\delta$  38.6, 49.4, 66.2, 106.2, 111.3, 112.1, 115.9, 120.2, 123.4, 129.4, 131.1, 134.0, 135.6, 137.7, 142.9, 145.8, 146.7, 156.5 ppm; MS-ESI  $m/z$ :  $[M + H]^+$  calcd for  $C_{22}H_{23}N_5O$ , 402.2; found, 402.4;  $m/z$ :  $[M - H]^-$  calcd for  $C_{22}H_{22}N_5O$ , 400.2; found, 400.5; HPLC (method 2):  $t_R$  = 1.766 min (100%).

**4-(4-(Cyclohexyl)-1H-imidazol-5-yl)-N-(4-morpholinophenyl)pyridin-2-amine (18g)**. The title compound was synthesized according to general procedure A starting from compound 17g (100 mg, 0.38 mmol) (for the synthesis of 17g see Supporting Information) and 4-morpholinoaniline (107.6 mg, 0.57 mmol). Purification by flash column chromatography ( $SiO_2$ , DCM/EtOH 97:03 to 90:10) afforded 120 mg of the desired compound (78% yield);  $^1H$  NMR (300 MHz,  $DMSO-d_6$ ):  $\delta$  1.14–1.86 (m, 10H), 2.85–2.97 (m, 1H), 2.98–3.06 (m, 4H), 3.65–3.80 (m, 4H), 6.81–6.97 (m, 4H), 7.47 (d,  $J$  = 8.9 Hz, 2H), 7.64 (s, 1H), 8.04 (d,  $J$  = 5.3 Hz, 1H), 8.72 (br s, 1H), 12.25 ppm (br s, 1H);  $^{13}C$  NMR (101 MHz,  $DMSO-d_6$ ):  $\delta$  25.4, 26.0, 32.4, 34.9, 49.4, 66.2, 105.7, 111.5, 116.0, 120.5, 126.4, 127.7, 134.2,

134.5, 143.2, 145.8, 147.3, 156.9 ppm; MS-ESI  $m/z$ :  $[M + H]^+$  calcd for  $C_{24}H_{20}N_2O$ , 404.2; found, 404.4;  $m/z$ :  $[M - H]^-$  calcd for  $C_{24}H_{20}N_2O$ , 402.2; found, 402.2; HPLC (method 2):  $t_R = 4.730$  min (100%).

**4-(4-Cyclopentyl-1H-imidazol-5-yl)-N-(4-morpholinophenyl)pyridin-2-amine (17h).** The title compound was synthesized according to general procedure A starting from compound 17h (100 mg, 0.40 mmol) (for the synthesis of 17h see Supporting Information) and 4-morpholinoaniline (107.0 mg, 0.60 mmol). Purification by flash column chromatography ( $SiO_2$ , DCM/EtOH 97:03 to 9:1) afforded 107 mg of the desired compound (69% yield);  $^1H$  NMR (300 MHz,  $DMSO-d_6$ ):  $\delta$  1.57–1.86 (m, 6H), 1.86–2.05 (m, 2H), 2.96–3.06 (m, 4H), 3.30–3.50 (m, 1H), 3.69–3.77 (m, 4H), 6.85–6.93 (m, 3H), 6.96 (s, 1H), 7.49 (d,  $J = 8.8$  Hz, 2H), 7.70 (s, 1H), 8.05 (d,  $J = 5.4$  Hz, 1H), 8.78 ppm (s, 1H);  $^{13}C$  NMR (101 MHz,  $DMSO-d_6$ ):  $\delta$  25.1, 32.9, 36.3, 49.5, 66.2, 106.1, 111.6, 116.0, 120.3, 130.9, 131.5, 134.3, 134.8, 142.7, 145.7, 147.2, 156.8 ppm; MS-ESI  $m/z$ :  $[M + H]^+$  calcd for  $C_{23}H_{27}N_5O$ , 390.2; found, 390.0;  $m/z$ :  $[M - H]^-$  calcd for  $C_{23}H_{27}N_5O$ , 388.2; found, 387.9; HPLC (method 2):  $t_R = 4.071$  min (99.6%).

**4-(4-Cyclobutyl-1H-imidazol-5-yl)-N-(4-morpholinophenyl)pyridin-2-amine (17i).** The title compound was synthesized according to general procedure A starting from compound 17i (100 mg, 0.43 mmol) (for the synthesis of 17i see Supporting Information) and 4-morpholinoaniline (114.0 mg, 0.64 mmol). Purification by flash column chromatography ( $SiO_2$ , DCM/EtOH 97:03 to 90:10) afforded 77 mg of the desired compound (48% yield);  $^1H$  NMR (300 MHz,  $DMSO-d_6$ ):  $\delta$  1.77–2.04 (m, 2H), 2.08–2.37 (m, 4H), 2.90–3.11 (m, 4H), 3.70–3.76 (m, 4H), 3.78–3.93 (m, 1H), 6.67–7.00 (m, 4H), 7.50 (d,  $J = 8.9$  Hz, 2H), 7.59–7.73 (m, 1H), 8.03 (d,  $J = 5.0$  Hz, 1H), 8.62–8.79 (m, 1H), 12.18–12.40 ppm (m, 1H);  $^{13}C$  NMR (101 MHz,  $DMSO-d_6$ ):  $\delta$  7.7, 28.6, 31.1, 49.4, 66.2, 106.0, 111.3, 116.0, 120.7, 128.0, 129.8, 133.7, 134.9, 142.3, 146.1, 146.5, 156.5 ppm; MS-ESI  $m/z$ :  $[M + H]^+$  calcd for  $C_{22}H_{25}N_5O$ , 376.2; found, 376.1;  $m/z$ :  $[M - H]^-$  calcd for  $C_{22}H_{25}N_5O$ , 374.2; found, 373.9; HPLC (method 2):  $t_R = 3.480$  min (100%).

**4-(4-Cyclopropyl-1H-imidazol-5-yl)-N-(4-morpholinophenyl)pyridin-2-amine (17j).** The title compound was synthesized according to general procedure A starting from compound 17j (150 mg, 0.68 mmol) (for the synthesis of 17j see Supporting Information) and 4-morpholinoaniline (181.8 mg, 1.02 mmol). Purification by flash column chromatography ( $SiO_2$ , DCM/EtOH 100:0 to 80:20) afforded 153 mg of the desired compound (62% yield);  $^1H$  NMR (250 MHz,  $DMSO-d_6$ ):  $\delta$  0.70–0.81 (m, 2H), 0.91–1.02 (m, 2H), 2.06 (t,  $J = 8.3$ , 5.2 Hz, 1H), 2.92–3.10 (m, 4H), 3.60–3.84 (m, 4H), 6.88 (d,  $J = 9.0$  Hz, 2H), 7.08 (d,  $J = 5.1$  Hz, 1H), 7.22 (s, 1H), 7.51 (d,  $J = 8.8$  Hz, 2H), 7.55 (s, 1H), 8.05 (d,  $J = 5.6$  Hz, 1H), 8.74 (s, 1H), 12.12 ppm (br s, 1H);  $^{13}C$  NMR (101 MHz,  $DMSO-d_6$ ):  $\delta$  7.4, 7.5, 49.5, 66.2, 105.4, 110.9, 116.0, 120.0, 134.1, 134.5, 145.6, 147.2, 156.8 ppm; MS-ESI  $m/z$ :  $[M + H]^+$  calcd for  $C_{21}H_{23}N_5O$ , 362.2; found, 362.6;  $m/z$ :  $[M - H]^-$  calcd for  $C_{21}H_{23}N_5O$ , 360.2; found, 360.5; HPLC (method 2):  $t_R = 2.699$  min (100%).

**4-(4-(tert-Butyl)-1H-imidazol-5-yl)-N-(4-morpholinophenyl)pyridin-2-amine (17k).** The title compound was synthesized according to general procedure A starting from compound 17k (100 mg, 0.43 mmol) (for the

synthesis of 17k see Supporting Information) and 4-morpholinoaniline (115.0 mg, 0.64 mmol). Purification by flash column chromatography ( $SiO_2$ , DCM/EtOH 97:03 to 90:10) afforded 155 mg of the desired compound (96% yield);  $^1H$  NMR (300 MHz,  $DMSO-d_6$ ):  $\delta$  1.20–1.35 (m, 9H), 3.04 (br s, 4H), 3.74 (br s, 4H), 6.70–6.94 (m, 4H), 7.47–7.52 (m, 2H), 8.14–8.20 (m, 1H), 9.04 (br s, 1H), 9.10 ppm (br s, 1H);  $^{13}C$  NMR (101 MHz,  $DMSO-d_6$ ):  $\delta$  29.9, 31.6, 49.3, 66.1, 111.4, 114.9, 116.0, 120.6, 125.6, 133.4, 137.5, 138.7, 147.0, 156.1, 158.3, 158.7 ppm; ES-MS  $m/z$ :  $[M + H]^+$  calcd for  $C_{22}H_{27}N_5O$ , 378.2; found, 378.3; ES-MS  $m/z$ :  $[M - H]^-$  calcd for  $C_{22}H_{27}N_5O$ , 376.2; found, 376.1; HPLC (method 2):  $t_R = 2.860$  min (100%).

**4-(4-Isopropyl-1H-imidazol-5-yl)-N-(4-morpholinophenyl)pyridin-2-amine (17l).** The title compound was synthesized according to general procedure A starting from compound 17l (100 mg, 0.45 mmol) (for the synthesis of 17l see Supporting Information) and 4-morpholinoaniline (119.4 mg, 0.67 mmol). Purification by flash column chromatography ( $SiO_2$ , DCM/EtOH 97:03 to 90:10) afforded 124 mg of the desired compound (76% yield);  $^1H$  NMR (300 MHz, methanol- $d_4$ ):  $\delta$  1.31 (d,  $J = 7.0$  Hz, 6H), 3.07–3.16 (m, 4H), 3.25–3.45 (m, 1H), 3.80–3.91 (m, 4H), 6.86–6.94 (m, 2H), 6.96–7.03 (m, 2H), 7.30–7.39 (m, 2H), 7.65 (s, 1H), 8.03 ppm (d,  $J = 6.2$  Hz, 1H);  $^{13}C$  NMR (101 MHz,  $DMSO-d_6$ ):  $\delta$  22.4, 24.6, 49.5, 66.1, 106.2, 111.6, 115.9, 119.8, 131.9, 134.4, 134.5, 134.6, 143.8, 145.5, 147.2, 156.8 ppm; MS-ESI  $m/z$ :  $[M + H]^+$  calcd for  $C_{21}H_{25}N_5O$ , 364.2; found, 364.5;  $m/z$ :  $[M - H]^-$  calcd for  $C_{21}H_{25}N_5O$ , 362.2; found, 362.3; HPLC (method 2):  $t_R = 2.492$  min (98.6%).

**2-Chloro-4-(4-methyl-1H-imidazol-5-yl)pyridine (36).** Compound 34<sup>21</sup> (1.0 g, 4.43 mmol) was suspended in glacial AcOH (10 mL) and subsequently 30%  $H_2O_2$  (602.7 mg, 17.72 mmol) was added dropwise and the reaction mixture was stirred at rt for 15 min. After adding  $H_2O$ , the pH was adjusted to 8 using  $K_2CO_3$  saturated solution and the aqueous phase was extracted five times with EtOAc. The combined organic layers were dried over anhydrous  $Na_2SO_4$  and concentrated at reduced pressure, affording 230 mg of the product which was used in the following step without further purification (25% yield);  $^1H$  NMR (300 MHz,  $DMSO-d_6$ ):  $\delta$  2.47 (s, 3H), 7.62 (dd,  $J = 5.3$ , 1.3 Hz, 1H), 7.65 (br s, 1H), 7.69 (s, 1H), 8.33 ppm (d,  $J = 5.2$  Hz, 1H);  $^{13}C$  NMR (101 MHz,  $DMSO-d_6$ ):  $\delta$  11.7, 118.8, 119.1, 127.9, 130.5, 134.9, 145.9, 149.8, 150.8 ppm; MS-ESI  $m/z$ :  $[M + H]^+$  calcd for  $C_9H_9ClN_2$ , 194.0; found, 194.0;  $m/z$ :  $[M - H]^-$  calcd for  $C_9H_9ClN_2$ , 192.0; found, 191.8; HPLC (method 2):  $t_R = 1.375$  min.

**2-Chloro-4-(4-ethyl-1H-imidazol-5-yl)pyridine (37).** Compound 35 (400 mg, 1.67 mmol) (for the synthesis of compound 35 see Supporting Information) was suspended in glacial AcOH (10 mL) and subsequently 30%  $H_2O_2$  (227.2 mg, 6.68 mmol) was added dropwise and the reaction mixture was stirred at rt for 40 min. The reaction mixture was concentrated at reduced pressure and after that 20 mL of  $K_2CO_3$  saturated solution was added. The aqueous layer was extracted five times with EtOAc and the combined organic layers were dried over anhydrous  $Na_2SO_4$  and concentrated at reduced pressure, affording 230 mg of the product which was used in the following step without further purification (71% yield);  $^1H$  NMR (300 MHz,  $DMSO-d_6$ ):  $\delta$  1.22 (t,  $J = 7.4$  Hz, 3H), 2.85 (q,  $J = 7.4$  Hz, 2H), 7.58 (d,  $J = 5.0$  Hz, 1H), 7.62 (s, 1H), 7.70 (s, 1H), 8.33 ppm (d,  $J = 5.1$  Hz, 1H);  $^{13}C$  NMR (101 MHz,  $DMSO-d_6$ ):  $\delta$  13.4, 18.8, 119.1, 119.4, 129.7,



133.8, 135.2, 145.8, 149.9, 150.8 ppm; MS-ESI  $m/z$ :  $[M + H]^+$  calcd for  $C_{19}H_{16}ClN_3$ , 208.0; found, 208.1;  $m/z$ :  $[M - H]^-$  calcd for  $C_{19}H_{16}ClN_3$ , 206.0; found, 205.9; HPLC (method 2):  $t_R = 1.653$  min.

**4-(4-Methyl-1H-imidazol-5-yl)-N-(4-morpholinophenyl)pyridin-2-amine (38).** The title compound was synthesized according to general procedure A starting from compound 36 (100 mg, 0.47 mmol). The crude product was purified twice by flash column chromatography ( $SiO_2$ , DCM/EtOH 90:10 to 80:20), ( $SiO_2$ , EtOAc), obtaining 38 mg of the desired compound (25% yield);  $^1H$  NMR (300 MHz,  $DMSO-d_6$ ):  $\delta$  2.42 (s, 3H), 2.94–3.09 (m, 4H), 3.63–3.81 (m, 4H), 6.88 (d,  $J = 9.0$  Hz, 2H), 6.94 (d,  $J = 5.1$  Hz, 1H), 7.07 (s, 1H), 7.51 (d,  $J = 9.1$  Hz, 2H), 7.60 (s, 1H), 8.04 (d,  $J = 5.4$  Hz, 1H), 8.69 (s, 1H), 12.15 ppm (br s, 1H);  $^{13}C$  NMR (101 MHz,  $DMSO-d_6$ ):  $\delta$  11.4, 49.5, 66.2, 105.3, 110.8, 116.0, 119.7, 124.7, 133.0, 133.9, 134.6, 143.6, 145.5, 147.2, 156.8 ppm; MS-ESI  $m/z$ :  $[M + H]^+$  calcd for  $C_{17}H_{21}N_5O$ , 336.2; found, 336.2;  $m/z$ :  $[M - H]^-$  calcd for  $C_{17}H_{21}N_5O$ , 334.2; found, 334.1; HPLC (method 2):  $t_R = 1.871$  min (100%).

**4-(4-Ethyl-1H-imidazol-5-yl)-N-(4-morpholinophenyl)pyridin-2-amine (39).** The title compound was synthesized according to general procedure A starting from compound 37 (100 mg, 0.48 mmol). The crude product was purified twice by flash column chromatography ( $SiO_2$ , DCM/EtOH 90:10 to 80:20), ( $SiO_2$ , EtOAc), obtaining 110 mg of the desired compound (65% yield);  $^1H$  NMR (300 MHz,  $DMSO-d_6$ ):  $\delta$  1.22 (t,  $J = 7.5$  Hz, 3H), 2.70–2.90 (m, 2H), 2.92–3.11 (m, 4H), 3.62–3.85 (m, 4H), 6.80–6.98 (m, 3H), 7.07 (br s, 1H), 7.51 (d,  $J = 9.0$  Hz, 2H), 7.61 (s, 1H), 8.04 (d,  $J = 5.0$  Hz, 1H), 8.70 (br s, 1H), 12.03–12.48 ppm (m, 1H);  $^{13}C$  NMR (101 MHz,  $DMSO-d_6$ ):  $\delta$  13.9, 18.5, 49.5, 66.2, 105.6, 111.0, 116.0, 119.8, 130.6, 132.5, 134.2, 134.6, 143.7, 145.5, 147.3, 156.9 ppm; MS-ESI  $m/z$ :  $[M + H]^+$  calcd for  $C_{22}H_{25}N_5O$ , 350.4; found, 350.4;  $m/z$ :  $[M - H]^-$  calcd for  $C_{22}H_{25}N_5O$ , 348.2; found, 348.2; HPLC (method 2):  $t_R = 1.774$  min (99.4%).

**2-Chloro-4-(2-(methylthio)-1H-imidazol-5-yl)pyridine (40).** Under an argon atmosphere, compound 33 (500 mg, 2.36 mmol) (for the synthesis of compound 33 see Supporting Information) and  $t-BuONa$  (454 mg, 4.72 mmol) were dissolved in dry MeOH (20 mL) and after cooling the reaction mixture to 0 °C, methyl iodide (147.5  $\mu$ L, 2.36 mmol) was added and the reaction mixture was stirred at 0 °C for 30 min. The reaction mixture was then heated to 55 °C and stirred for 3 h. After cooling to rt, the solvent was evaporated at reduced pressure and  $H_2O$  was added. The aqueous phase was then extracted two times with EtOAc and the combined organic layers were dried over anhydrous  $Na_2SO_4$  and concentrated at reduced pressure. The residue was finally purified by flash column chromatography ( $SiO_2$ , DCM/EtOH 100:0 to 90:10) giving 396 mg of the desired compound (74% yield);  $^1H$  NMR (400 MHz,  $DMSO-d_6$ ):  $\delta$  2.59 (s, 3H), 7.64–7.72 (m, 1H), 7.73–7.79 (m, 1H), 8.03 (s, 1H), 8.31 (dd,  $J = 5.3, 1.8$  Hz, 1H), 12.70 ppm (br s, 1H); MS-ESI  $m/z$ :  $[M + H]^+$  calcd for  $C_9H_9ClN_3S$ , 226.0; found, 225.9;  $m/z$ :  $[M - H]^-$  calcd for  $C_9H_9ClN_3S$ , 224.0; found, 223.9; HPLC (method 1):  $t_R = 4.096$  min.

**2-Chloro-4-(4-methyl-2-(methylthio)-1H-imidazol-5-yl)pyridine (41).** The title compound was prepared as previously described<sup>31</sup> and analytical data were in agreement with the reported ones.

**2-Chloro-4-(4-ethyl-2-(methylthio)-1H-imidazol-5-yl)pyridine (42).** In a pressure vial, compound 35 (400 mg, 1.67 mmol) (for the synthesis of compound 35 see Supporting Information) and  $t-BuONa$  (160.5 mg, 1.67 mmol) were dissolved in dry MeOH (15 mL) and after cooling the reaction mixture to 0 °C, methyl iodide (203  $\mu$ L, 3.26 mmol) was added. The vial was tightly closed and the mixture was stirred at 50 °C for 1 h. The solvent was evaporated at reduced pressure and the residue was purified by flash column chromatography ( $SiO_2$ , DCM/EtOH 99:01 to 95:05), affording 378 mg of the product (89% yield);  $^1H$  NMR (300 MHz,  $CDCl_3$ ):  $\delta$  1.32 (t,  $J = 7.6$  Hz, 3H), 2.63 (s, 3H), 2.89 (q,  $J = 7.6$  Hz, 2H), 7.50 (dd,  $J = 5.3, 1.5$  Hz, 1H), 7.64 (br s, 1H), 8.35 ppm (dd,  $J = 5.3, 0.4$  Hz, 1H);  $^{13}C$  NMR (101 MHz,  $CDCl_3$ ):  $\delta$  13.5, 16.6, 19.4, 119.3, 120.7, 132.4, 135.1, 141.7, 145.0, 149.4, 151.9 ppm; MS-ESI  $m/z$ :  $[M + H]^+$  calcd for  $C_{11}H_{12}ClN_3S$ , 254.0; found, 254.0;  $m/z$ :  $[M - H]^-$  calcd for  $C_{11}H_{12}ClN_3S$ , 252.0; found, 252.0; HPLC (method 2):  $t_R = 3.575$  min.

**4-(2-(Methylthio)-1H-imidazol-5-yl)-N-(4-morpholinophenyl)pyridin-2-amine (43).** The title compound was synthesized according to general procedure A starting from 40 (100 mg, 0.44 mmol) and 4-morpholinoaniline (117.6 mg, 0.66 mmol). Purification by flash column chromatography ( $SiO_2$ , DCM/EtOH 100:0 to 90:10) afforded 92 mg of the desired compound (57% yield);  $^1H$  NMR (400 MHz,  $DMSO-d_6$ ):  $\delta$  2.54–2.62 (m, 3H), 2.92–3.09 (m, 4H), 3.63–3.78 (m, 4H), 6.87 (d,  $J = 7.8$  Hz, 2H), 6.96 (d,  $J = 4.5$  Hz, 1H), 7.17 (br s, 1H), 7.53 (d,  $J = 7.8$  Hz, 2H), 7.76 (br s, 1H), 8.00 (d,  $J = 4.5$  Hz, 1H), 8.75 (br s, 1H), 12.34–12.62 ppm (m, 1H);  $^{13}C$  NMR (101 MHz,  $DMSO-d_6$ ):  $\delta$  15.3, 49.5, 66.2, 104.1, 109.5, 116.0, 116.8, 119.7, 120.3, 134.6, 139.2, 142.0, 145.4, 147.3, 156.9 ppm; MS-FAB  $m/z$ :  $[M]$  calcd for  $C_{19}H_{21}N_5OS$ , 367.1; found, 367.2; HPLC (method 1):  $t_R = 2.501$  min (100%).

**4-(4-Methyl-2-(methylthio)-1H-imidazol-5-yl)-N-(4-morpholinophenyl)pyridin-2-amine (44).** The title compound was synthesized according to general procedure A starting from 41 (100 mg, 0.42 mmol) and 4-morpholinoaniline (112.3 mg, 0.63 mmol). Purification by flash column chromatography ( $SiO_2$ , DCM/EtOH 100:0 to 80:20) afforded 42 mg of the desired compound (26% yield);  $^1H$  NMR (400 MHz,  $DMSO-d_6$ ):  $\delta$  2.39 (br s, 3H), 2.52–2.60 (m, 3H), 2.93–3.09 (m, 4H), 3.61–3.83 (m, 4H), 6.78–6.94 (m, 3H), 7.06 (br s, 1H), 7.52 (d,  $J = 7.8$  Hz, 2H), 8.03 (d,  $J = 4.3$  Hz, 1H), 8.74 (br s, 1H), 12.27 ppm (br s, 1H);  $^{13}C$  NMR (101 MHz,  $DMSO-d_6$ ):  $\delta$  15.4, 25.4, 49.5, 66.2, 105.3, 110.5, 116.0, 119.6, 134.6, 145.4, 147.3, 156.7 ppm; MS-FAB  $m/z$ :  $[M + H]^+$  calcd for  $C_{20}H_{23}N_5OS$ , 382.2; found, 382.3; HPLC (method 1):  $t_R = 3.024$  min (96.4%).

**4-(4-Ethyl-2-(methylthio)-1H-imidazol-5-yl)-N-(4-morpholinophenyl)pyridin-2-amine (45).** The title compound was synthesized according to general procedure A starting from compound 42 (100 mg, 0.39 mmol) and 4-morpholinoaniline (103.4 mg, 0.58 mmol). Purification by flash column chromatography ( $SiO_2$ , DCM/EtOH 99:01 to 90:10) afforded 51 mg of the desired compound (33% yield);  $^1H$  NMR (300 MHz,  $DMSO-d_6$ ):  $\delta$  1.21 (t,  $J = 7.5$  Hz, 3H), 2.55 (s, 3H), 2.78 (q,  $J = 7.4$  Hz, 2H), 2.96–3.08 (m, 4H), 3.66–3.81 (m, 4H), 6.69–6.96 (m, 3H), 7.03 (br s, 1H), 7.52 (d,  $J = 8.8$  Hz, 2H), 8.03 (d,  $J = 5.3$  Hz, 1H), 8.67–8.81 (m, 1H), 12.07–12.37 ppm (m, 1H);  $^{13}C$  NMR (101 MHz,  $DMSO-d_6$ ):  $\delta$  13.9, 15.3, 18.7, 49.5, 66.2, 105.5, 110.8, 116.0,

119.8, 133.2, 134.5, 139.7, 143.0, 145.5, 147.3, 151.6, 156.8 ppm; MS-ESI  $m/z$ :  $[M + H]^+$  calcd for  $C_{21}H_{25}N_3OS$ , 396.2; found, 396.3;  $m/z$ :  $[M - H]^-$  calcd for  $C_{21}H_{23}N_3OS$ , 394.2; found, 394.1; HPLC (method 2):  $t_R = 3.499$  min (97.0%).

**4-(2-Chloropyridin-4-yl)-5-methyl-1H-imidazol-2-amine (46).** Cyanamide (652 mg, 15.52 mmol) was dissolved in EtOH (30 mL) and after heating at reflux temperature, compound 31 was added portionwise over 1 h and the mixture was stirred at the same temperature further for 3 h. After cooling down, the solvent was evaporated at reduced pressure and the residue was purified by flash column chromatography ( $SiO_2$ , DCM/EtOH/Et<sub>3</sub>N 95:05:0 to 80:18:2), obtaining 900 mg of the desired product (95% yield); <sup>1</sup>H NMR (300 MHz, DMSO-*d*<sub>6</sub>):  $\delta$  2.37 (s, 3H), 7.53 (d,  $J = 4.9$  Hz, 1H), 7.62 (br s, 3H), 8.42 (d,  $J = 5.1$  Hz, 1H), 12.86 ppm (br s, 1H); <sup>13</sup>C NMR (75 MHz, DMSO-*d*<sub>6</sub>):  $\delta$  10.7, 117.6, 118.9, 119.4, 124.4, 139.2, 147.0, 150.3, 151.1 ppm; MS-ESI  $m/z$ :  $[M + H]^+$  calcd for  $C_9H_8ClN_4$ , 209.0; found, 208.9;  $m/z$ :  $[M - H]^-$  calcd for  $C_9H_6ClN_4$ , 207.0; found, 206.9; HPLC (method 2):  $t_R = 1.524$  min.

**4-(2-Amino-5-methyl-1H-imidazol-4-yl)-N-(4-morpholinophenyl)pyridin-2-amine (47).** The title compound was synthesized according to general procedure A starting from compound 46 (100 mg, 0.48 mmol) and 4-morpholinooaniline (128.3 mg, 0.72 mmol). Purification by flash column chromatography ( $SiO_2$ , DCM/MeOH 99:01 to 90:10) and ( $SiO_2$ , DCM/MeOH 95:05 to 80:20) afforded 46 mg of the desired compound (27% yield); <sup>1</sup>H NMR (300 MHz, DMSO-*d*<sub>6</sub>):  $\delta$  2.30 (s, 3H), 2.95–3.07 (m, 4H), 3.67–3.79 (m, 4H), 6.76 (dd,  $J = 5.4, 1.4$  Hz, 1H), 6.83 (s, 1H), 6.89 (d,  $J = 9.0$  Hz, 2H), 7.25 (br s, 2H), 7.50 (d,  $J = 9.0$  Hz, 2H), 8.11 (d,  $J = 5.4$  Hz, 1H), 8.91 (s, 1H), 12.37 ppm (br s, 1H); <sup>13</sup>C NMR (101 MHz, DMSO-*d*<sub>6</sub>):  $\delta$  11.0, 49.9, 66.7, 105.9, 110.6, 116.4, 120.1, 120.6, 122.2, 134.4, 137.5, 146.4, 147.4, 148.4, 157.2 ppm; MS-ESI  $m/z$ :  $[M + H]^+$  calcd for  $C_{19}H_{22}N_6O$ , 351.2; found, 351.1;  $m/z$ :  $[M + Z]^-$  calcd for  $C_{17}H_{20}N_6OS$ , 349.2; found, 349.1; HPLC (method 2):  $t_R = 1.876$  min (96%).

**4-(4-Methyl-2-(methylthio)-1H-imidazol-5-yl)-N-(3-methylbutan-2-yl)pyridin-2-amine (48a).** The title compound was synthesized according to general procedure E starting from 41 (85 mg, 0.355 mmol) and 3-methylbutan-2-amine. The crude residue was purified by flash column chromatography ( $SiO_2$ , DCM/EtOH 100:0 to 80:20), affording 35 mg of pure product (34% yield); <sup>1</sup>H NMR (400 MHz, DMSO-*d*<sub>6</sub>):  $\delta$  0.79–0.94 (m, 6H), 1.03 (d,  $J = 6.6$  Hz, 3H), 1.70–1.86 (m, 1H), 2.36 (br s, 3H), 2.54 (br s, 3H), 3.72–3.89 (m, 1H), 6.35 (d,  $J = 7.1$  Hz, 1H), 6.53–6.92 (m, 2H), 7.86 (d,  $J = 5.3$  Hz, 1H), 12.23 ppm (br s, 1H); <sup>13</sup>C NMR (101 MHz, DMSO-*d*<sub>6</sub>):  $\delta$  15.4, 16.7, 17.9, 19.2, 32.1, 50.5, 104.1, 108.4, 127.0, 134.5, 139.0, 142.9, 146.5, 158.6 ppm; HPLC (method 1):  $t_R = 3.355$  min (95%).

**4-(4-Methyl-2-(methylthio)-1H-imidazol-5-yl)-N-(1-phenylethyl)pyridin-2-amine (48b).** The title compound was synthesized according to general procedure E starting from 41 (100 mg, 417 mmol) and 1-phenylethan-1-amine. The crude residue was purified by flash column chromatography ( $SiO_2$ , DCM/EtOH 100:0 to 80:20), affording 42 mg of pure product (31% yield); <sup>1</sup>H NMR (400 MHz, CDCl<sub>3</sub>):  $\delta$  1.38–1.55 (m, 3H), 1.96–2.13 (m, 3H), 2.36–2.54 (m, 3H), 4.50–4.69 (m, 1H), 5.50 (br s, 1H), 6.33 (br s, 1H), 6.77 (br s, 1H), 7.08–7.34 (m, 6H), 7.84–7.98 ppm (m, 1H); <sup>13</sup>C NMR (101 MHz, CDCl<sub>3</sub>):  $\delta$  12.2, 16.8, 24.4, 52.3, 103.5, 110.7, 125.8, 127.0,

128.7, 140.7, 142.5, 144.6, 147.1, 158.0 ppm; HPLC (method 1):  $t_R = 2.748$  min (100%).

**N-Cyclobutyl-4-(4-methyl-2-(methylthio)-1H-imidazol-5-yl)pyridin-2-amine (48c).** The title compound was synthesized according to general procedure E starting from 41 (150 mg, 0.62 mmol) and cyclobutylamine (48 h). The crude residue was purified by flash column chromatography ( $SiO_2$ , DCM/EtOH 97:03 to 90:10), affording 83 mg of pure product (49% yield); <sup>1</sup>H NMR (300 MHz, DMSO-*d*<sub>6</sub>):  $\delta$  1.55–1.73 (m, 2H), 1.77–1.95 (m, 2H), 2.19–2.41 (m, 5H), 2.53 (s, 3H), 4.16–4.40 (m, 1H), 6.41–6.77 (m, 3H), 7.84–7.97 (m, 1H), 12.08–12.34 ppm (m, 1H); <sup>13</sup>C NMR (101 MHz, DMSO-*d*<sub>6</sub>):  $\delta$  11.3, 14.7, 15.5, 30.7, 46.1, 103.3, 109.0, 126.6, 134.5, 138.7, 142.7, 147.5, 158.3 ppm; MS-ESI  $m/z$ :  $[M + H]^+$  calcd for  $C_{14}H_{18}N_4S$ , 275.1; found, 275.0;  $m/z$ :  $[M - H]^-$  calcd for  $C_{14}H_{16}N_4S$ , 273.1; found, 273.0; HPLC (method 2):  $t_R = 2.499$  min (99%).

**N-Cyclopentyl-4-(4-methyl-2-(methylthio)-1H-imidazol-5-yl)pyridin-2-amine (48d).** The title compound was synthesized according to general procedure E starting from 41 (100 mg, 0.42 mmol) and cyclopentylamine (120 h). The crude residue was purified by flash column chromatography ( $SiO_2$ , DCM/EtOH 95:05 to 90:10), affording 51 mg of pure product (42% yield); <sup>1</sup>H NMR (400 MHz, DMSO-*d*<sub>6</sub>):  $\delta$  1.36–1.74 (m, 6H), 1.84–1.98 (m, 2H), 2.37 (s, 3H), 2.54 (s, 3H), 3.99–4.15 (m, 1H), 6.60–7.02 (m, 3H), 7.88 (d,  $J = 5.6$  Hz, 1H), 12.32 ppm (br s, 1H); MS-ESI  $m/z$ :  $[M + H]^+$  calcd for  $C_{17}H_{22}N_4S$ , 289.1; found, 289.0;  $m/z$ :  $[M - H]^-$  calcd for  $C_{17}H_{20}N_4S$ , 287.1; found, 287.0; HPLC (method 2):  $t_R = 3.265$  min (98%).

**N-Cyclohexyl-4-(4-methyl-2-(methylthio)-1H-imidazol-5-yl)pyridin-2-amine (48e).** The title compound was synthesized according to general procedure E starting from 41 (100 mg, 0.42 mmol) and cyclohexylamine (72 h). The crude residue was purified twice by flash column chromatography ( $SiO_2$ , DCM/EtOH 97:03 to 90:10) and ( $SiO_2$ , DCM/EtOH 95:05 to 90:10), affording 35 mg of pure product (27% yield); <sup>1</sup>H NMR (400 MHz, DMSO-*d*<sub>6</sub>):  $\delta$  1.11–1.32 (m, 5H), 1.35 (br s, 1H), 1.52–1.63 (m, 1H), 1.64–1.76 (m, 2H), 1.80–1.96 (m, 2H), 2.35 (br s, 3H), 2.53 (s, 3H), 3.62–3.74 (m, 1H), 6.29 (d,  $J = 7.6$  Hz, 1H), 6.53–6.83 (m, 2H), 7.88 (d,  $J = 5.3$  Hz, 1H), 12.19 ppm (br s, 1H); MS-ESI  $m/z$ :  $[M + H]^+$  calcd for  $C_{18}H_{22}N_4S$ , 303.2; found, 303.1;  $m/z$ :  $[M - H]^-$  calcd for  $C_{18}H_{20}N_4S$ , 301.2; found, 301.2; HPLC (method 2):  $t_R = 4.347$  min (100%).

**4-(4-Methyl-2-(methylthio)-1H-imidazol-5-yl)-N-(tetrahydro-2H-pyran-4-yl)pyridin-2-amine (48f).** The title compound was synthesized according to general procedure E starting from 41 (80 mg, 0.33 mmol) and 4-aminotetrahydropyran (120 h). The crude residue was purified by flash column chromatography ( $SiO_2$ , DCM/EtOH 95:05 to 90:10), affording 30 mg of pure product (30% yield); <sup>1</sup>H NMR (400 MHz, DMSO-*d*<sub>6</sub>):  $\delta$  1.33–1.48 (m, 2H), 1.87 (d,  $J = 10.6$  Hz, 2H), 2.36 (br s, 3H), 2.53 (s, 3H), 3.40–3.45 (m, 2H), 3.76–3.99 (m, 3H), 6.29–6.86 (m, 3H), 7.90 (d,  $J = 4.5$  Hz, 1H), 12.20 ppm (br s, 1H); <sup>13</sup>C NMR (101 MHz, DMSO-*d*<sub>6</sub>):  $\delta$  11.3, 15.4, 32.9, 46.2, 66.0, 104.2, 108.9, 126.6, 134.4, 138.7, 142.6, 147.2, 158.4 ppm; MS-ESI  $m/z$ :  $[M + H]^+$  calcd for  $C_{15}H_{20}N_4OS$ , 305.1; found, 305.0;  $m/z$ :  $[M - H]^-$  calcd for  $C_{15}H_{18}N_4OS$ , 303.1; found, 303.1; HPLC (method 2):  $t_R = 1.570$  min (96%).

**trans-4-((4-(4-Methyl-2-(methylthio)-1H-imidazol-5-yl)pyridin-2-yl)amino)cyclohexan-1-ol (48g).** The title com-



compound was synthesized according to general procedure E starting from **41** (100 mg, 0.42 mmol) and *trans*-4-amino-cyclohexanol (484 mg, 4.20 mmol) and adding 2 mL of *n*-butanol (120 h). The crude residue was purified by flash column chromatography (SiO<sub>2</sub>, DCM/EtOH 92:08 to 80:20), affording 37 mg of pure product (27% yield); <sup>1</sup>H NMR (400 MHz, DMSO-*d*<sub>6</sub>): δ 1.10–1.35 (m, 4H), 1.76–2.00 (m, 4H), 2.22–2.42 (m, 3H); 2.52 (s, 3H), 3.41 (br s, 1H), 3.61 (br s, 1H), 4.47–4.70 (m, 1H), 6.14–6.85 (m, 3H), 7.78–8.02 (m, 1H), 12.06–12.36 ppm (m, 1H); <sup>13</sup>C NMR (101 MHz, DMSO-*d*<sub>6</sub>): δ 11.3, 15.5, 30.6, 34.1, 48.5, 68.5, 104.1, 108.7, 126.5, 134.5, 138.6, 142.5, 147.3, 158.7 ppm; MS-ESI *m/z*: [M + H]<sup>+</sup> calcd for C<sub>16</sub>H<sub>22</sub>N<sub>2</sub>O<sub>2</sub>, 319.1; found, 319.1; *m/z*: [M – H]<sup>–</sup> calcd for C<sub>16</sub>H<sub>22</sub>N<sub>2</sub>O<sub>2</sub>, 317.1; found, 317.2; HPLC (method 2): *t*<sub>R</sub> = 1.640 min (98%).

*trans*-*N*-(4-(4-Methyl-2-(methylthio)-1*H*-imidazol-5-yl)pyridin-2-yl)cyclohexane-1,4-diamine (**48h**). The title compound was synthesized according to general procedure E starting from **41** (300 mg, 1.25 mmol) and *trans*-1,4-diaminocyclohexane (2.8 g, 25 mmol) and adding 2 mL of *n*-butanol (72 h). The crude residue was purified by flash column chromatography (SiO<sub>2</sub>, DCM/EtOH 95:05 to 90:10), affording 172 mg of pure product (43% yield); <sup>1</sup>H NMR (300 MHz, methanol-*d*<sub>4</sub>): δ 1.23–1.42 (m, 4H), 1.85–2.13 (m, 4H), 2.41 (s, 3H), 2.55 (s, 3H), 2.58–2.75 (m, 1H), 3.56–3.67 (m, 1H), 6.67 (br s, 1H), 6.73 (dd, *J* = 5.6, 1.5 Hz, 1H), 7.89 ppm (dd, *J* = 5.6, 0.6 Hz, 1H); <sup>13</sup>C NMR (75 MHz, DMSO-*d*<sub>6</sub>): δ 12.6, 15.9, 32.0, 35.5, 49.3, 50.4, 104.4, 109.0, 129.2, 133.0, 139.6, 142.0, 148.0, 159.2 ppm; MS-ESI *m/z*: [M + H]<sup>+</sup> calcd for C<sub>16</sub>H<sub>23</sub>N<sub>3</sub>S, 318.2; found, 318.0; *m/z*: [M – H]<sup>–</sup> calcd for C<sub>16</sub>H<sub>23</sub>N<sub>3</sub>S, 316.2; found, 316.1; HPLC (method 2): *t*<sub>R</sub> = 1.234 min (100%).

*N*-(*trans*-4-(4-(4-Methyl-2-(methylthio)-1*H*-imidazol-5-yl)pyridin-2-yl)amino)cyclohexyl)acetamide (**48i**). The title compound was synthesized according to general procedure F starting from **48h** (180 mg, 0.57 mmol) and acetic anhydride (116 mg, 1.14 mmol). Purification by flash column chromatography (SiO<sub>2</sub>, DCM/EtOH 90:10 to 80:20) afforded 74 mg of the desired product (36% yield); <sup>1</sup>H NMR (300 MHz, DMSO-*d*<sub>6</sub>): δ 1.14–1.35 (m, 4H), 1.74–1.87 (m, 5H), 1.90–2.06 (m, 2H), 2.26–2.41 (m, 3H), 2.53 (s, 3H), 3.43–3.57 (m, 1H), 3.63 (br s, 1H), 6.21–6.80 (m, 3H), 7.75 (d, *J* = 7.8 Hz, 1H), 7.84–7.98 (m, 1H), 12.11–12.32 ppm (m, 1H); <sup>13</sup>C NMR (101 MHz, DMSO-*d*<sub>6</sub>): δ 11.3, 15.4, 22.7, 31.2, 31.4, 47.3, 48.4, 104.2, 108.7, 126.6, 134.4, 138.7, 142.5, 147.1, 158.5, 168.1 ppm; MS-ESI *m/z*: [M + H]<sup>+</sup> calcd for C<sub>21</sub>H<sub>25</sub>N<sub>3</sub>O<sub>2</sub>, 360.2; found, 360.1; *m/z*: [M – H]<sup>–</sup> calcd for C<sub>21</sub>H<sub>25</sub>N<sub>3</sub>O<sub>2</sub>, 358.2; found, 358.1; HPLC (method 2): *t*<sub>R</sub> = 1.647 min (99%).

*N*-(*trans*-4-(4-(4-Methyl-2-(methylthio)-1*H*-imidazol-5-yl)pyridin-2-yl)amino)cyclohexyl)benzamide (**48j**). The title compound was synthesized according to general procedure F starting from **48h** (120 mg, 0.38 mmol) and benzoyl chloride (80 mg, 0.57 mmol). Purification by flash column chromatography (SiO<sub>2</sub>, DCM/EtOH 90:10 to 80:20) afforded 22 mg of the desired product (13% yield); <sup>1</sup>H NMR (300 MHz, DMSO-*d*<sub>6</sub>): δ 1.20–1.57 (m, 4H), 1.78–2.11 (m, 4H), 2.28–2.43 (m, 3H), 2.54 (s, 3H), 3.60–3.90 (m, 2H), 6.26–6.88 (m, 3H), 7.36–7.58 (m, 3H), 7.75–8.01 (m, 3H), 8.27 (d, *J* = 7.9 Hz, 1H), 12.04–12.44 ppm (m, 1H); <sup>13</sup>C NMR (101 MHz, DMSO-*d*<sub>6</sub>): δ 11.3, 15.4, 31.1, 31.6, 48.1, 48.6, 104.2, 108.7, 126.6, 127.2, 128.1, 130.9, 134.4, 134.8, 138.7, 142.7, 147.0, 158.5, 165.5 ppm; MS-ESI *m/z*: [M + H]<sup>+</sup> calcd for

C<sub>23</sub>H<sub>27</sub>N<sub>3</sub>O<sub>2</sub>, 422.2; found, 422.0; *m/z*: [M – H]<sup>–</sup> calcd for C<sub>23</sub>H<sub>27</sub>N<sub>3</sub>O<sub>2</sub>, 420.2; found, 420.0; HPLC (method 2): *t*<sub>R</sub> = 4.076 min (97%).

*N*-(*trans*-4-(4-(4-Methyl-2-(methylthio)-1*H*-imidazol-5-yl)pyridin-2-yl)amino)cyclohexyl)cyclohexanecarboxamide (**48k**). The title compound was synthesized according to general procedure F starting from **48h** (120 mg, 0.38 mmol) and cyclohexane carbonyl chloride (83 mg, 0.57 mmol). Purification by flash column chromatography (SiO<sub>2</sub>, DCM/EtOH 95:05 to 80:20) afforded 29 mg of the desired product (18% yield); <sup>1</sup>H NMR (300 MHz, DMSO-*d*<sub>6</sub>): δ 1.05–1.43 (m, 9H), 1.54–1.87 (m, 7H), 1.90–2.10 (m, 3H), 2.23–2.42 (m, 3H), 2.53 (s, 3H), 3.45–3.72 (m, 2H), 6.15–6.84 (m, 3H), 7.56 (d, *J* = 7.6 Hz, 1H), 7.76–8.03 (m, 1H), 12.20 ppm (br s, 1H); MS-ESI *m/z*: [M + H]<sup>+</sup> calcd for C<sub>23</sub>H<sub>33</sub>N<sub>3</sub>O<sub>2</sub>, 428.2; found, 428.0; *m/z*: [M – H]<sup>–</sup> calcd for C<sub>23</sub>H<sub>33</sub>N<sub>3</sub>O<sub>2</sub>, 426.2; found, 426.1; HPLC (method 2): *t*<sub>R</sub> = 5.391 min (98%).

*N*-(*trans*-4-(4-(4-Methyl-2-(methylthio)-1*H*-imidazol-5-yl)pyridin-2-yl)amino)cyclohexyl)pivalamide (**48l**). The title compound was synthesized according to general procedure F starting from **48h** (120 mg, 0.38 mmol) and pivaloyl chloride (69 mg, 0.57 mmol). Purification by flash column chromatography (SiO<sub>2</sub>, DCM/EtOH 90:10 to 80:20) afforded 29 mg of the desired product (19% yield); <sup>1</sup>H NMR (400 MHz, DMSO-*d*<sub>6</sub>): δ 1.08 (s, 9H), 1.35–1.40 (m, 4H), 1.64–1.77 (m, 2H), 1.92–2.05 (m, 2H), 2.25–2.41 (m, 3H), 2.53 (s, 3H), 3.46–3.70 (m, 2H), 6.23–6.77 (m, 3H), 7.13 (d, *J* = 8.1 Hz, 1H), 7.89 (d, *J* = 4.5 Hz, 1H), 12.04–12.35 ppm (m, 1H); <sup>13</sup>C NMR (101 MHz, DMSO-*d*<sub>6</sub>): δ 11.3, 15.5, 27.4, 31.0, 31.6, 37.8, 47.5, 48.6, 104.1, 108.6, 126.6, 134.4, 138.7, 142.6, 147.1, 158.5, 176.5 ppm; MS-ESI *m/z*: [M + H]<sup>+</sup> calcd for C<sub>23</sub>H<sub>27</sub>N<sub>3</sub>O<sub>2</sub>, 402.2; found, 402.0; *m/z*: [M – H]<sup>–</sup> calcd for C<sub>23</sub>H<sub>27</sub>N<sub>3</sub>O<sub>2</sub>, 400.2; found, 400.0; HPLC: *t*<sub>R</sub> = 4.114 min (99%).

*N*-(4-(4-(4-Methyl-2-(methylthio)-1*H*-imidazol-5-yl)pyridin-2-yl)benzene-1,4-diamine (**48m**).<sup>21</sup> The title compound was prepared as previously described<sup>21</sup> and analytical data were in agreement with the reported ones.

*N*-(4-(4-(4-Methyl-2-(methylthio)-1*H*-imidazol-5-yl)pyridin-2-yl)amino)phenyl)acetamide (**48n**). The title compound was synthesized according to general procedure F starting from **48m** (100 mg, 0.32 mmol) and acetic anhydride (49 mg, 0.48 mmol). Purification by flash column chromatography (SiO<sub>2</sub>, DCM/EtOH 97:03 to 90:10) afforded 37 mg of the desired product (33% yield); <sup>1</sup>H NMR (400 MHz, DMSO-*d*<sub>6</sub>): δ 2.01 (s, 3H), 2.28–2.44 (m, 3H), 2.54 (s, 3H), 6.75–7.04 (m, 1H), 7.10 (s, 1H), 7.43 (d, *J* = 8.8 Hz, 2H), 7.58 (d, *J* = 8.8 Hz, 2H), 8.01–8.13 (m, 1H), 8.80–8.98 (m, 1H), 9.78 (s, 1H), 12.19–12.47 ppm (m, 1H); <sup>13</sup>C NMR (101 MHz, DMSO-*d*<sub>6</sub>): δ 11.5, 15.6, 23.8, 105.9, 111.1, 118.4, 119.9, 127.3, 132.3, 134.2, 137.6, 139.2, 143.1, 147.3, 156.5, 167.9 ppm; MS-ESI *m/z*: [M + H]<sup>+</sup> calcd for C<sub>19</sub>H<sub>19</sub>N<sub>3</sub>O<sub>2</sub>, 354.1; found, 354.1; *m/z*: [M – H]<sup>–</sup> calcd for C<sub>19</sub>H<sub>19</sub>N<sub>3</sub>O<sub>2</sub>, 352.1; found, 352.2; HPLC (method 2): *t*<sub>R</sub> = 2.035 min (98%).

*N*-(4-(4-(4-Methyl-2-(methylthio)-1*H*-imidazol-5-yl)pyridin-2-yl)amino)phenyl)benzamide (**48o**). The title compound was synthesized according to general procedure F starting from **48m** (100 mg, 0.32 mmol) and benzoyl chloride (67 mg, 0.48 mmol). Purification by flash column chromatography (SiO<sub>2</sub>, DCM/EtOH 98:02 to 90:10) afforded 27 mg of the desired product (33% yield); <sup>1</sup>H NMR (400 MHz, DMSO-*d*<sub>6</sub>): δ 2.41 (s, 3H), 2.56 (s, 3H), 6.97 (br s, 1H), 7.14 (br s,

1H), 7.46–7.73 (m, 7H), 7.90–8.00 (m, 2H), 8.10 (d,  $J = 5.3$  Hz, 1H), 9.01 (s, 1H), 10.12 (s, 1H), 12.29 ppm (br s, 1H);  $^{13}\text{C}$  NMR (101 MHz,  $\text{DMSO-}d_6$ ):  $\delta$  14.2, 15.9, 106.4, 111.5, 118.6, 121.6, 128.0, 128.8, 129.2, 131.4, 131.7, 132.5, 135.6, 138.6, 139.9, 143.7, 147.7, 156.9, 165.5 ppm; MS-ESI  $m/z$ :  $[\text{M} + \text{H}]^+$  calcd for  $\text{C}_{23}\text{H}_{21}\text{N}_3\text{O}_8$ , 416.1; found, 415.7;  $m/z$ :  $[\text{M} - \text{H}]^-$  calcd for  $\text{C}_{22}\text{H}_{21}\text{N}_3\text{O}_8$ , 414.1; found, 413.7; HPLC (method 2):  $t_R = 4.357$  min (97%).

***N*-(4-((4-(4-Methyl-2-(methylthio)-1H-imidazol-5-yl)pyridin-2-yl)amino)phenyl)cyclohexanecarboxamide (48p)**. The title compound was synthesized according to general procedure F starting from **48m** (100 mg, 0.32 mmol) and cyclohexane carbonyl chloride (70 mg, 0.48 mmol). Purification by flash column chromatography ( $\text{SiO}_2$ , DCM/EtOH 97:03 to 90:10) afforded 40 mg of the desired product (30% yield);  $^1\text{H}$  NMR (300 MHz,  $\text{DMSO-}d_6$ ):  $\delta$  1.11–1.50 (m, 5H), 1.56–1.85 (m, 5H), 2.22–2.36 (m, 1H), 2.40 (s, 3H), 2.55 (s, 3H), 6.94 (d,  $J = 5.0$  Hz, 1H), 7.09 (br s, 1H), 7.47 (d,  $J = 9.0$  Hz, 2H), 7.58 (d,  $J = 9.0$  Hz, 2H), 8.06 (d,  $J = 5.4$  Hz, 1H), 8.91 (s, 1H), 9.62 (s, 1H), 12.28 ppm (br s, 1H);  $^{13}\text{C}$  NMR (101 MHz,  $\text{DMSO-}d_6$ ):  $\delta$  11.5, 15.4, 25.2, 25.4, 29.2, 44.7, 105.7, 110.9, 118.3, 119.7, 127.1, 132.5, 134.2, 137.3, 139.4, 142.8, 147.2, 156.4, 173.6 ppm; MS-ESI  $m/z$ :  $[\text{M} + \text{H}]^+$  calcd for  $\text{C}_{21}\text{H}_{22}\text{N}_4\text{O}_8$ , 422.2; found, 422.0;  $m/z$ :  $[\text{M} - \text{H}]^-$  calcd for  $\text{C}_{20}\text{H}_{22}\text{N}_4\text{O}_8$ , 420.2; found, 420.1; HPLC (method 2):  $t_R = 4.646$  min (99%).

***N*-(4-((4-(4-Methyl-2-(methylthio)-1H-imidazol-5-yl)pyridin-2-yl)amino)phenyl)pivalamide (48q)**. The title compound was synthesized according to general procedure F starting from **48m** (120 mg, 0.39 mmol) and pivaloyl chloride (70 mg, 0.58 mmol). Purification by flash column chromatography ( $\text{SiO}_2$ , DCM/EtOH 97:03 to 90:10) afforded 74 mg of the desired product (48% yield);  $^1\text{H}$  NMR (400 MHz,  $\text{DMSO-}d_6$ ):  $\delta$  1.22 (s, 9H), 2.41 (s, 3H), 2.55 (s, 3H), 6.96 (d,  $J = 5.6$  Hz, 1H), 7.11 (s, 1H), 7.50 (d,  $J = 8.8$  Hz, 2H), 7.58 (d,  $J = 8.8$  Hz, 2H), 8.07 (d,  $J = 5.3$  Hz, 1H), 9.00 (s, 1H), 9.07 (s, 1H), 12.35 ppm (br s, 1H);  $^{13}\text{C}$  NMR (101 MHz,  $\text{DMSO-}d_6$ ):  $\delta$  11.9, 15.4, 27.3, 38.9, 105.7, 110.9, 118.2, 121.1, 128.8, 132.5, 137.3, 139.5, 142.6, 146.7, 156.2, 175.9 ppm; MS-ESI  $m/z$ :  $[\text{M} + \text{H}]^+$  calcd for  $\text{C}_{21}\text{H}_{23}\text{N}_4\text{O}_8$ , 396.2; found, 395.7;  $m/z$ :  $[\text{M} - \text{H}]^-$  calcd for  $\text{C}_{20}\text{H}_{23}\text{N}_4\text{O}_8$ , 394.2; found, 393.7; HPLC (method 2):  $t_R = 3.999$  min (100%).

**2-Chloro-4-(1,5-dimethyl-2-(methylthio)-1H-imidazol-4-yl)pyridine (49)**. Under an argon atmosphere, compound **34** (250 mg, 1.11 mmol) and *t*-BuONa (213 mg, 2.22 mmol) were dissolved in dry MeOH (10 mL), and after cooling the reaction mixture to 0 °C, methyl iodide (205  $\mu\text{L}$ , 3.32 mmol) was added and the reaction mixture was let to heat to rt. The reaction mixture was then heated to 80 °C and stirred for 3 h. After cooling to rt, the solvent was evaporated at reduced pressure and  $\text{H}_2\text{O}$  was added. The aqueous phase was then extracted two times with EtOAc and the combined organic layers were dried over anhydrous  $\text{Na}_2\text{SO}_4$  and concentrated at reduced pressure. The residue was finally purified by flash column chromatography ( $\text{SiO}_2$ , DCM/EtOH 100:0 to 90:10) giving 110 mg of the desired compound (39% yield);  $^1\text{H}$  NMR (400 MHz,  $\text{DMSO-}d_6$ ):  $\delta$  2.44 (s, 3H), 2.54–2.62 (m, 3H), 3.34 (s, 3H), 7.47–7.77 (m, 2H), 8.34 ppm (d,  $J = 4.5$  Hz, 1H);  $^{13}\text{C}$  NMR (101 MHz,  $\text{DMSO-}d_6$ ):  $\delta$  10.5, 15.4, 30.6, 119.1, 119.4, 130.5, 132.4, 142.3, 145.6, 149.8, 150.8 ppm; HPLC (method 1):  $t_R = 4.812$  min.

**4-(1,5-Dimethyl-2-(methylthio)-1H-imidazol-4-yl)-*N*-(4-morpholinophenyl)pyridin-2-amine (50)**. Under an argon

atmosphere, tris(dibenzylideneaceton)dipalladium(0) ( $\text{Pd}_2(\text{dba})_3$ ) (17.5 mg, 0.02 mmol) and 9,9-dimethyl-4,5-bis(diphenylphosphino)xanten (Xantphos) (22.1 mg, 0.04 mmol) were dissolved in dry 1,4-dioxane (5 mL) and stirred for 10 min. After that compound **49** (50 mg, 0.21 mmol),  $\text{C}_2\text{S}_2\text{CO}_3$  (138.1 mg, 0.42 mmol), and 4-morpholinylaniline (56.7 mg, 0.32 mmol) were added and the reaction mixture was heated to 100 °C and stirred for 15 h. After cooling to rt, the reaction mixture was diluted with DCM and the solid residue was removed by filtration. The filtrate was then concentrated at reduced pressure and the residue was purified by flash column chromatography (DCM/EtOH 100:0 to 90:10) giving 61 mg of the desired product (73% yield);  $^1\text{H}$  NMR (400 MHz,  $\text{DMSO-}d_6$ ):  $\delta$  2.36–2.44 (m, 3H), 2.54 (m, 3H), 2.93–3.05 (m, 4H), 3.45–3.55 (m, 3H), 3.67–3.76 (m, 4H), 6.79–6.96 (m, 3H), 7.07 (s, 1H), 7.54 (d,  $J = 7.3$  Hz, 2H), 8.00–8.09 (m, 1H), 8.76 ppm (br s, 1H);  $^{13}\text{C}$  NMR (101 MHz,  $\text{DMSO-}d_6$ ):  $\delta$  10.5, 15.8, 30.5, 49.5, 66.2, 106.0, 111.0, 115.9, 119.5, 128.4, 134.4, 134.6, 140.9, 142.9, 145.4, 147.2, 156.7 ppm; MS-FAB  $m/z$ :  $[\text{M}]^+$  calcd for  $\text{C}_{21}\text{H}_{22}\text{N}_4\text{O}_8$ , 395.2; found, 395.3; HPLC (method 1):  $t_R = 3.156$  min (98.7%).

**5-(2-Chloropyridin-4-yl)-1,4-dimethyl-1,3-dihydro-2H-imidazole-2-thione (51)**. In a pressure vial, compound **31** (200 mg, 0.77 mmol) (for the synthesis of compound **31** see Supporting Information) and methyl isothiocyanate (284 mg, 3.88 mmol) were suspended in triethylamine (2 mL), and after closing the vial tightly, the reaction mixture was stirred at 60 °C for 16 h. The excess of triethylamine was evaporated at reduced pressure and the residue was suspended in glacial AcOH and stirred at 80 °C for 1.5 h. The reaction mixture was concentrated at reduced pressure and after that  $\text{NaHCO}_3$  saturated solution (20 mL) was added and the aqueous phase was extracted four times with EtOAc. The combined organic layers were washed with  $\text{H}_2\text{O}$  and NaCl saturated solution, dried over anhydrous  $\text{Na}_2\text{SO}_4$  and concentrated at reduced pressure. Finally, the residue was purified by flash column chromatography ( $\text{SiO}_2$ , DCM/EtOH 100:0 to 95:05), affording 110 mg of the desired product (60% yield);  $^1\text{H}$  NMR (300 MHz,  $\text{DMSO-}d_6$ ):  $\delta$  2.11 (s, 3H), 3.45 (s, 3H), 7.47 (dd,  $J = 5.2, 1.4$  Hz, 1H), 7.55–7.63 (m, 1H), 8.47 (d,  $J = 5.1$  Hz, 1H), 12.51 ppm (br s, 1H);  $^{13}\text{C}$  NMR (75 MHz,  $\text{DMSO-}d_6$ ):  $\delta$  9.6, 32.4, 122.7, 122.9, 123.3, 124.4, 139.5, 150.2, 150.9, 161.8 ppm; MS-ESI  $m/z$ :  $[\text{M} - \text{H}]^-$  calcd for  $\text{C}_{10}\text{H}_{10}\text{ClN}_2\text{S}$ , 238.0; found, 238.0; HPLC (method 2):  $t_R = 2.353$  min.

**5-(2-Chloropyridin-4-yl)-1-ethyl-4-methyl-1,3-dihydro-2H-imidazole-2-thione (52)**. The title compound was prepared following the same procedure of compound **51** starting from **31** (200 mg, 0.77 mmol) (for the synthesis of compound **31** see Supporting Information) and ethyl isothiocyanate (335.5 mg, 3.85 mmol). Purification by flash column chromatography ( $\text{SiO}_2$ , DCM/EtOH 99:01 to 95:05) afforded 128 mg of the desired compound (65% yield);  $^1\text{H}$  NMR (300 MHz,  $\text{CDCl}_3$ ):  $\delta$  1.15 (t,  $J = 6.9$  Hz, 3H), 2.14 (s, 3H), 4.04 (q,  $J = 6.7$  Hz, 2H), 7.11 (d,  $J = 4.5$  Hz, 1H), 7.21 (s, 1H), 8.46 (d,  $J = 4.8$  Hz, 1H), 12.32 ppm (br s, 1H);  $^{13}\text{C}$  NMR (101 MHz,  $\text{CDCl}_3$ ):  $\delta$  9.6, 14.1, 40.3, 122.5, 123.2, 124.2, 124.8, 139.5, 150.4, 152.4, 160.1 ppm; MS-ESI  $m/z$ :  $[\text{M} - \text{H}]^-$  calcd for  $\text{C}_{11}\text{H}_{12}\text{ClN}_2\text{S}$ , 252.0; found, 252.0; HPLC (method 2):  $t_R = 3.168$  min.

**5-(2-Chloropyridin-4-yl)-1-cyclopropyl-4-methyl-1,3-dihydro-2H-imidazole-2-thione (53)**. The title compound was prepared following the same procedure of compound **51** starting from **31** (500 mg, 1.94 mmol) (for the synthesis of



compound **31** see Supporting Information) and cyclopropyl isothiocyanate (962.4 mg, 9.70 mmol). Purification by flash column chromatography (SiO<sub>2</sub>, DCM/EtOH 100:0 to 95:05) afforded 335 mg of the desired compound (60% yield); <sup>1</sup>H NMR (300 MHz, DMSO-*d*<sub>6</sub>): δ 0.43–0.53 (m, 2H), 0.79–0.96 (m, 2H), 2.09 (s, 3H), 3.17–3.29 (m, 1H), 7.49 (dd, *J* = 5.2, 1.4 Hz, 1H), 7.55–7.64 (m, 1H), 8.45 (d, *J* = 5.2 Hz, 1H), 12.42 ppm (br s, 1H); <sup>13</sup>C NMR (101 MHz, DMSO-*d*<sub>6</sub>): δ 6.5, 9.6, 27.0, 122.5, 122.9, 123.3, 124.4, 139.6, 149.6, 150.4, 163.9 ppm; MS-ESI *m/z*: [M – H]<sup>–</sup> calcd for C<sub>12</sub>H<sub>12</sub>ClN<sub>2</sub>S, 264.0; found, 264.0; HPLC (method 2): *t*<sub>R</sub> = 3.057 min.

**2-Chloro-4-(1,4-dimethyl-2-(methylthio)-1H-imidazol-5-yl)pyridine (54)**. In a pressure vial, compound **51** (285 mg, 1.19 mmol) and *t*-BuONa (114.3 mg, 1.19 mmol) were dissolved in dry MeOH (15 mL), and after cooling the reaction mixture to 0 °C, methyl iodide (217 μL, 3.48 mmol) was added. The vial was tightly closed and the mixture was stirred at 50 °C for 30 min. After evaporating the solvent at reduced pressure, H<sub>2</sub>O was added and the aqueous phase was extracted four times with EtOAc. The combined organic layers were washed with H<sub>2</sub>O and NaCl saturated solution, dried over anhydrous Na<sub>2</sub>SO<sub>4</sub> and concentrated at reduced pressure, giving 290 mg of the product which was used in the following step without further purification (96% yield); <sup>1</sup>H NMR (300 MHz, CDCl<sub>3</sub>): δ 2.28 (s, 3H), 2.66 (s, 3H), 3.52 (s, 3H), 7.12 (dd, *J* = 5.2, 1.5 Hz, 1H), 7.22–7.24 (m, 1H), 8.44 ppm (d, *J* = 5.1 Hz, 1H); <sup>13</sup>C NMR (101 MHz, CDCl<sub>3</sub>): δ 13.7, 15.8, 32.3, 122.0, 123.5, 126.8, 138.5, 141.1, 145.5, 149.9, 152.0 ppm; MS-ESI *m/z*: [M + H]<sup>+</sup> calcd for C<sub>11</sub>H<sub>12</sub>ClN<sub>2</sub>S, 254.0; found, 254.0; HPLC (method 2): *t*<sub>R</sub> = 1.720 min.

**2-Chloro-4-(1-ethyl-4-methyl-2-(methylthio)-1H-imidazol-5-yl)pyridine (55)**. The title compound was synthesized following the same procedure of compound **54** starting from **52** (125 mg, 0.49 mmol), *t*-BuONa (47 mg, 0.49 mmol), and methyl iodide (90 μL, 1.44 mmol) giving 120 mg of the product, which was used in the following step without further purification (95% yield); <sup>1</sup>H NMR (300 MHz, CDCl<sub>3</sub>): δ 1.13 (t, *J* = 7.2 Hz, 3H), 2.15 (s, 3H), 2.57 (s, 3H), 3.85 (q, *J* = 7.2 Hz, 2H), 7.06 (dd, *J* = 5.1, 1.5 Hz, 1H), 7.13–7.18 (m, 1H), 8.35 ppm (d, *J* = 5.1, 0.5 Hz, 1H); <sup>13</sup>C NMR (75 MHz, CDCl<sub>3</sub>): δ 13.3, 15.5, 15.6, 39.7, 122.0, 123.5, 125.6, 138.3, 141.3, 144.4, 149.7, 151.8 ppm; MS-ESI *m/z*: [M + H]<sup>+</sup> calcd for C<sub>12</sub>H<sub>14</sub>ClN<sub>2</sub>S, 268.0; found, 268.0; HPLC (method 2): *t*<sub>R</sub> = 2.250 min.

**2-Chloro-4-(1-cyclopropyl-4-methyl-2-(methylthio)-1H-imidazol-5-yl)pyridine (56)**. The title compound was synthesized following the same procedure of compound **54** starting from **53** (210 mg, 0.74 mmol), *t*-BuONa (71.4 mg, 0.74 mmol), and methyl iodide (135 μL, 2.16 mmol) giving 200 mg of the product, which was used in the following step without further purification (95% yield); <sup>1</sup>H NMR (300 MHz, CDCl<sub>3</sub>): δ 0.59–0.71 (m, 2H), 0.93–1.03 (m, 2H), 2.27 (s, 3H), 2.67 (s, 3H), 3.03–3.14 (m, 1H), 7.19 (dd, *J* = 5.2, 1.5 Hz, 1H), 7.27–7.31 (m, 1H), 8.39 ppm (d, *J* = 5.1 Hz, 1H); <sup>13</sup>C NMR (75 MHz, CDCl<sub>3</sub>): δ 9.6, 13.9, 14.6, 26.1, 121.7, 123.1, 126.9, 138.1, 141.3, 148.3, 149.3, 151.5 ppm; MS-ESI *m/z*: [M + H]<sup>+</sup> calcd for C<sub>13</sub>H<sub>14</sub>ClN<sub>2</sub>S, 280.1; found, 280.0; HPLC (method 2): *t*<sub>R</sub> = 2.763 min.

**4-(1,4-Dimethyl-2-(methylthio)-1H-imidazol-5-yl)-N-(4-morpholinophenyl)pyridin-2-amine (57)**. In an argon-flushed pressure tube, compound **54** (100 mg, 0.39 mmol), 4-morpholinophenylamine (105.3 mg, 0.59 mmol), Pd<sub>2</sub>(dba)<sub>3</sub> (36.1 mg, 0.04 mmol), 2-dicyclohexylphosphino-2',4',6'-trisopropylbiphenyl (XPhos) (37.18 mg, 0.08 mmol), and Cs<sub>2</sub>CO<sub>3</sub>

(770.2 mg, 2.36 mmol) were suspended in dry 1,4-dioxane, and after closing the vial tightly, the mixture was stirred at 100 °C for 36 h. The solvent was evaporated at reduced pressure and after that NH<sub>4</sub>Cl saturated solution was added to the residue and the aqueous phase was extracted five times with EtOAc. The combined organic layers were washed twice with H<sub>2</sub>O and NaCl saturated solution, dried over anhydrous Na<sub>2</sub>SO<sub>4</sub> and concentrated at reduced pressure. Finally, the residue was purified twice by flash column chromatography (SiO<sub>2</sub>, DCM/EtOH 95:05 to 90:10) and (SiO<sub>2</sub>, DCM/EtOH 97:03) giving 30 mg of the desired product (20% yield); <sup>1</sup>H NMR (300 MHz, CDCl<sub>3</sub>): δ 2.23 (s, 3H), 2.62 (s, 3H), 3.07–3.23 (m, 4H), 3.46 (s, 3H), 3.83–3.94 (m, 4H), 6.52–6.62 (m, 2H), 6.72 (br s, 1H), 6.92 (d, *J* = 8.3 Hz, 2H), 7.24 (d, *J* = 8.4 Hz, 2H), 8.19 ppm (d, *J* = 5.1 Hz, 1H); <sup>13</sup>C NMR (101 MHz, CDCl<sub>3</sub>): δ 13.7, 15.9, 32.2, 49.6, 66.8, 107.2, 114.1, 116.7, 124.2, 128.4, 131.6, 137.5, 140.4, 144.3, 146.7, 148.5, 157.1 ppm; MS-ESI *m/z*: [M + H]<sup>+</sup> calcd for C<sub>21</sub>H<sub>22</sub>N<sub>2</sub>O<sub>2</sub>S, 396.2; found, 396.5; *m/z*: [M – H]<sup>–</sup> calcd for C<sub>21</sub>H<sub>22</sub>N<sub>2</sub>O<sub>2</sub>S, 394.2; found, 394.3; HPLC (method 2): *t*<sub>R</sub> = 2.116 min (99.3%).

**4-(1-Ethyl-4-methyl-2-(methylthio)-1H-imidazol-5-yl)-N-(4-morpholinophenyl)pyridin-2-amine (58)**. Under an argon atmosphere, 4-morpholinophenylamine (98.8 mg, 0.55 mmol), Pd<sub>2</sub>(dba)<sub>3</sub> (16.94 mg, 0.02 mmol), XPhos (17.64 mg, 0.04 mmol), and Cs<sub>2</sub>CO<sub>3</sub> (365 mg, 1.12 mmol) were placed and after that compound **55** (100 mg, 0.37 mmol) previously dissolved in 5 mL of dry 1,4-dioxane was added and the reaction mixture was stirred at 100 °C for 18 h. The solvent was evaporated at reduced pressure and after that NH<sub>4</sub>Cl saturated solution was added to the residue and the aqueous phase was extracted three times with EtOAc. The combined organic layers were washed with H<sub>2</sub>O and NaCl saturated solution, dried over anhydrous Na<sub>2</sub>SO<sub>4</sub> and concentrated at reduced pressure. Finally, the residue was purified by flash column chromatography (SiO<sub>2</sub>, DCM/EtOH 100:0 to 95:05) giving 30 mg of the desired product (20% yield); <sup>1</sup>H NMR (300 MHz, CDCl<sub>3</sub>): δ 1.16 (t, *J* = 7.1 Hz, 3H), 2.20 (s, 3H), 2.63 (s, 3H), 3.05–3.22 (m, 4H), 3.73–3.99 (m, 6H), 6.49–6.64 (m, 2H), 6.81–7.03 (m, 3H), 7.24 (d, *J* = 8.7 Hz, 2H), 8.19 ppm (d, *J* = 5.0 Hz, 1H); <sup>13</sup>C NMR (101 MHz, CDCl<sub>3</sub>): δ 13.5, 15.8, 16.1, 39.8, 49.8, 66.9, 107.2, 114.6, 116.8, 124.0, 127.9, 132.3, 137.2, 140.3, 143.0, 148.3, 148.4, 157.7 ppm; MS-ESI *m/z*: [M + H]<sup>+</sup> calcd for C<sub>22</sub>H<sub>22</sub>N<sub>2</sub>O<sub>2</sub>S, 410.2; found, 410.1; *m/z*: [M – H]<sup>–</sup> calcd for C<sub>22</sub>H<sub>22</sub>N<sub>2</sub>O<sub>2</sub>S, 408.2; found, 408.1; HPLC (method 2): *t*<sub>R</sub> = 2.427 min (98.0%).

**4-(1-Cyclopropyl-4-methyl-2-(methylthio)-1H-imidazol-5-yl)-N-(4-morpholinophenyl)pyridin-2-amine (59)**. The title compound was synthesized following the same procedure used for the preparation of compound **58** starting from **56** (150 mg, 0.53 mmol), 4-morpholinophenylamine (141.7 mg, 0.79 mmol), Pd<sub>2</sub>(dba)<sub>3</sub> (24.7 mg, 0.03 mmol), XPhos (25.2 mg, 0.05 mmol), and Cs<sub>2</sub>CO<sub>3</sub> (524 mg, 1.61 mmol). Purification by flash column chromatography (SiO<sub>2</sub>, DCM/EtOH 100:0 to 95:05) afforded 86 mg of the desired product (40% yield); <sup>1</sup>H NMR (300 MHz, CDCl<sub>3</sub>): δ 0.63–0.72 (m, 2H), 0.87–0.97 (m, 2H), 2.22 (s, 3H), 2.65 (s, 3H), 2.91–3.02 (m, 1H), 3.09–3.19 (m, 4H), 3.80–3.93 (m, 4H), 6.63 (br s, 1H), 6.66 (d, *J* = 5.1 Hz, 1H), 6.81 (br s, 1H), 6.91 (d, *J* = 8.9 Hz, 2H), 7.24 (d, *J* = 8.9 Hz, 2H), 8.16 ppm (d, *J* = 5.1 Hz, 1H); <sup>13</sup>C NMR (101 MHz, CDCl<sub>3</sub>): δ 9.4, 13.8, 14.7, 26.1, 49.7, 66.8, 107.0, 114.3, 116.7, 124.0, 128.6, 132.0, 137.0, 140.7, 146.4,



147.1, 148.3, 156.9 ppm; MS-ESI  $m/z$ :  $[M + H]^+$  calcd for  $C_{23}H_{27}N_2OS$ , 422.2; found, 422.0;  $m/z$ :  $[M - H]^-$  calcd for  $C_{23}H_{27}N_2OS$ , 420.2; found, 420.1; HPLC (method 2):  $t_R$  = 2.989 min (98.0%).

**2-Bromo-4-(1-(4-fluorophenyl)-1H-imidazol-5-yl)pyridine (64).** 2-Bromoisoicotinaldehyde (**60**, 300 mg, 1.61 mmol), 4-fluoroaniline (179 mg, 1.61 mmol), and AcOH (160  $\mu$ L), were dissolved in EtOH and the reaction mixture was stirred at reflux temperature for 2 h. After cooling to rt, the solvent was evaporated at reduced pressure and the residue was resuspended in a mixture 2:1 of MeOH and 1,2-dimethoxyethane (8 mL) and transferred into a three-neck round-bottom flask under an argon atmosphere. TOSMIC (471.5 mg, 2.41 mmol) and  $K_2CO_3$  (445 mg, 3.22 mmol) were added and the mixture was stirred at reflux temperature for 3 h. The mixture was cooled at rt and the solvent was evaporated at reduced pressure. The residue was suspended in DCM and the organic layer was washed three times with  $H_2O$  and one time with NaCl saturated solution. The organic phase was dried over anhydrous  $Na_2SO_4$  and evaporated at reduced pressure. Finally, the residue was purified by flash column chromatography (SiO<sub>2</sub>, DCM to DCM/EtOH 95:05) yielding 360 mg of the desired compound (70% yield);  $^1H$  NMR (400 MHz, DMSO- $d_6$ ):  $\delta$  7.03 (d,  $J$  = 4.3 Hz, 1H), 7.30–7.50 (m, 5H), 7.69 (br s, 1H), 8.08 (br s, 1H), 8.24 ppm (d,  $J$  = 4.3 Hz, 1H);  $^{13}C$  NMR (101 MHz, DMSO- $d_6$ ):  $\delta$  116.6 (d,  $J$  = 22.7 Hz), 120.5, 124.6, 128.3 (d,  $J$  = 8.8 Hz), 128.4, 131.9, 132.1 (d,  $J$  = 2.9 Hz), 139.5, 141.7, 142.0, 150.3, 161.8 ppm (d,  $J$  = 246.6 Hz); MS-ESI  $m/z$ :  $[M + H]^+$  calcd for  $C_{14}H_{10}BrFN_2$ , 318.0; found, 317.8; HPLC (method 1):  $t_R$  = 5.51 min.

**2-Chloro-4-(1-methyl-1H-imidazol-5-yl)pyridine (65).** Tetrakis(triphenylphosphine)palladium (367 mg, 0.317 mmol) was dissolved in dimethylformamide (DMF) (50 mL) and after that 5-bromo-1-methyl-1H-imidazole (**62**) (2.04 g, 12.7 mmol), (2-chloropyridin-4-yl)boronic acid (**63**) (1.0 g, 6.35 mmol),  $Ca_2CO_3$  (4.13 g, 12.7 mmol), and  $H_2O$  (228 mg, 12.7 mmol) were added and the reaction mixture was stirred at 60 °C for 24 h. The mixture was poured in  $H_2O$  and the aqueous phase was extracted five times with EtOAc. The combined organic layers were washed with NaCl saturated solution, dried over anhydrous  $Na_2SO_4$ , and concentrated at reduced pressure. The residue obtained was purified by flash column chromatography (SiO<sub>2</sub>, DCM/EtOH 95:05 to 90:10), affording 160 mg of the desired product (13% yield);  $^1H$  NMR (250 MHz,  $CDCl_3$ ):  $\delta$  3.79 (s, 3H), 7.27 (dd,  $J$  = 5.2, 1.6 Hz, 2H), 7.34 (br s, 1H), 7.38 (dd,  $J$  = 1.6, 0.6 Hz, 1H), 7.60 (br s, 1H), 8.43 ppm (dd,  $J$  = 5.2, 0.6 Hz, 1H); MS-ESI  $m/z$ :  $[M + H]^+$  calcd for  $C_9H_{10}BrN_2$ , 194.0; found, 194.0; HPLC (method 2):  $t_R$  = 1.162 min.

**4-(1-(4-Fluorophenyl)-1H-imidazol-5-yl)-N-(4-morpholinophenyl)pyridin-2-amine (66).** Under an argon atmosphere, compound **64** (200 mg, 0.62 mmol), 4-morpholinoaniline (134.5 mg, 0.75 mmol),  $t$ -BuONa (83.8 mg, 0.87 mmol),  $Pd_2(dba)_3$  (20 mg, 0.02 mmol), and 2,2'-bis(diphenylphosphino)-1,1'-binaphthyl (BINAP) (30 mg, 0.02 mmol) were dissolved in dry toluene (15 mL) and the reaction mixture was then stirred for 3 h at 80 °C. After removing the solvent at reduced pressure, the residue was suspended in  $H_2O$  and the aqueous phase was extracted with EtOAc. The combined organic layers were then dried over anhydrous  $Na_2SO_4$  and concentrated at reduced pressure. Finally, the residue was purified by flash column chromatography (DCM/MeOH 100:0 to 95:05), affording 62 mg of the product (24%

yield);  $^1H$  NMR (400 MHz, DMSO- $d_6$ ):  $\delta$  3.01 (s, 4H), 3.73 (s, 4H), 6.41–6.44 (m, 2H), 6.80–6.82 (m, 2H), 7.22–7.24 (m, 2H), 7.37–7.42 (m, 5H), 7.99 (s, 2H), 8.70 ppm (s, 1H);  $^{13}C$  NMR (101 MHz, DMSO- $d_6$ ):  $\delta$  49.3, 66.2, 106.3, 111.8, 115.8, 116.6 (d,  $J$  = 22.0 Hz), 127.4 (d,  $J$  = 9.0 Hz), 129.9, 132.5, 133.5, 137.3, 140.8, 146.0, 147.9, 156.6, 161.6 ppm (d,  $J$  = 244.0 Hz); FAB-MS  $m/z$ :  $[M]$  calcd for  $C_{26}H_{22}FN_4O$ , 415.2; found, 415.3; HPLC (method 1):  $t_R$  = 5.08 min (100%).

**4-(1-Methyl-1H-imidazol-5-yl)-N-(4-morpholinophenyl)pyridin-2-amine (67).** The title compound was synthesized according to general procedure A starting from **65** (140 mg, 0.72 mmol) and 4-morpholinoaniline (192.5 mg, 1.08 mmol). Purification by flash column chromatography (SiO<sub>2</sub>, DCM/EtOH 100:0 to 90:10) afforded 50 mg of the desired compound (35% yield);  $^1H$  NMR (250 MHz, DMSO- $d_6$ ):  $\delta$  2.97–3.07 (m, 4H), 3.69–3.79 (m, 7H), 6.78–6.85 (m, 2H), 6.89 (m,  $J$  = 9.0 Hz, 2H), 7.22 (d,  $J$  = 1.2 Hz, 1H), 7.52 (m,  $J$  = 9.0 Hz, 2H), 7.76 (br s, 1H), 8.11 (d,  $J$  = 5.1 Hz, 1H), 8.85 ppm (br s, 1H);  $^{13}C$  NMR (101 MHz, DMSO- $d_6$ ):  $\delta$  32.9, 49.4, 66.2, 106.9, 111.7, 115.9, 119.9, 128.9, 130.7, 134.0, 137.8, 141.1, 145.8, 147.8, 156.8 ppm; MS-ESI  $m/z$ :  $[M + H]^+$  calcd for  $C_{19}H_{21}N_5O$ , 336.2; found, 336.3;  $m/z$ :  $[M - H]^-$  calcd for  $C_{19}H_{21}N_5O$ , 334.2; found, 334.3; HPLC (method 1):  $t_R$  = 2.048 min (100%).

**2-Chloro-4-(1H-imidazol-2-yl)pyridine (69).** To a solution of 2-chloroisonicotinonitrile (**68**) (2.0 g, 14.44 mmol) in MeOH (8 mL), a 30% solution of NaOMe in MeOH (260  $\mu$ L, 1.44 mmol) was added and the reaction mixture was stirred at 40 °C for 1 h. After that both 2,2-dimethoxyethan-1-amine (1.56 mL, 14.44 mmol) and AcOH (1.56 mL, 27.22 mmol) were added dropwise and the mixture was stirred at reflux temperature for 30 min. After cooling to rt, the mixture was diluted with MeOH (8 mL) and then 6 N HCl solution (7.2 mL, 43.2 mmol) was added and the mixture was stirred at reflux temperature for 18 h. The solvent was evaporated at reduced pressure and after that a 10% solution of  $K_2CO_3$  was added to the residue until reaching pH = 10. The precipitate obtained was filtered off and washed with  $H_2O$ , affording 2.01 g of the product which was used for the following step without further purification (77% yield);  $^1H$  NMR (400 MHz, DMSO- $d_6$ ):  $\delta$  7.30 (br s, 2H), 7.78–7.91 (m, 1H), 7.95 (br s, 1H), 8.36–8.49 (m, 1H), 13.03 ppm (br s, 1H);  $^{13}C$  NMR (101 MHz, DMSO- $d_6$ ):  $\delta$  118.1, 118.6, 124.8, 140.7, 141.9, 150.5, 151.1 ppm; MS-ESI  $m/z$ :  $[M + H]^+$  calcd for  $C_8H_6ClN_2$ , 180.0; found, 179.8;  $m/z$ :  $[M - H]^-$  calcd for  $C_8H_6ClN_2$ , 178.0; found, 177.8; HPLC (method 1):  $t_R$  = 2.346 min.

**2-Chloro-4-(1-methyl-1H-imidazol-2-yl)pyridine (70).** Under an argon atmosphere, compound **69** (1.72 g, 9.61 mmol) was dissolved in dry DMF (20 mL) and after cooling the reaction mixture to 0 °C, NaH (231 mg, 9.61 mmol) was added and the mixture was stirred at 0 °C for 15 min. After that methyl iodide (1.61 mL, 25.6 mmol) was added dropwise and the reaction mixture was let to heat to rt and stirred for 90 min. The mixture was poured in  $H_2O$  and the aqueous phase was extracted three times with DCM. The combined organic layers were dried over anhydrous  $Na_2SO_4$  and the solvent was evaporated at reduced pressure. Finally, the residue was treated with a mixture of  $n$ -hexane/EtOAc 40:1 and the solid obtained was filtered off and dried in vacuo, affording 793 mg of the product which was used for the following step without further purification (43% yield);  $^1H$  NMR (400 MHz, DMSO- $d_6$ ):  $\delta$  3.82–3.93 (m, 3H), 7.09 (br s, 1H), 7.40 (br s, 1H), 7.71–

7.78 (m, 1H), 7.80 (br s, 1H), 8.40–8.53 ppm (m, 1H);  $^{13}\text{C}$  NMR (101 MHz, DMSO- $d_6$ ):  $\delta$  34.8, 121.0, 121.6, 125.8, 128.7, 140.9, 142.3, 150.1, 150.8 ppm; MS-ESI  $m/z$ :  $[\text{M} + \text{H}]^+$  calcd for  $\text{C}_{19}\text{H}_{16}\text{ClN}_5$ , 194.0; found, 193.8; HPLC (method 1):  $t_R = 1.161$  min.

**4-(1-Methyl-1H-imidazol-2-yl)-N-(4-morpholinophenyl)pyridin-2-amine (71).** The title compound was synthesized according to general procedure A starting from **70** (150 mg, 0.77 mmol) and 4-morpholinopyridin-2-amine (205 mg, 1.15 mmol). Purification by flash column chromatography ( $\text{SiO}_2$ , DCM/EtOH 95:05) afforded 100 mg of the desired compound (39% yield);  $^1\text{H}$  NMR (400 MHz, DMSO- $d_6$ ):  $\delta$  2.93–3.09 (m, 4H), 3.66–3.77 (m, 4H), 3.81 (s, 3H), 6.90 (d,  $J = 8.3$  Hz, 2H), 6.95–7.04 (m, 2H), 7.09 (s, 1H), 7.31 (s, 1H), 7.52 (d,  $J = 8.1$  Hz, 2H), 8.15 (d,  $J = 4.8$  Hz, 1H), 8.89 ppm (br s, 1H);  $^{13}\text{C}$  NMR (101 MHz, DMSO- $d_6$ ):  $\delta$  34.6, 49.4, 66.1, 107.8, 111.9, 115.9, 120.0, 124.5, 127.9, 133.9, 138.5, 144.3, 145.8, 147.6, 156.7 ppm; FAB-MS  $m/z$ :  $[\text{M}]^+$  calcd for  $\text{C}_{19}\text{H}_{21}\text{N}_5\text{O}$ , 335.2; found, 335.3; HPLC (method 1):  $t_R = 2.359$  min (100%).

**2-Bromo-1-(4-fluorophenyl)-2-(2-fluoropyridin-4-yl)ethan-1-one (73).**<sup>51</sup> Compound **72**<sup>19</sup> (1.0 g, 4.29 mmol) was dissolved in 30% HBr in AcOH (6 mL). After cooling the reaction mixture to 0 °C,  $\text{Br}_2$  (220  $\mu\text{L}$ , 4.29 mmol) was added dropwise and the reaction mixture was heated for 6 h at 40 °C. After evaporating the solvent at reduced pressure,  $\text{H}_2\text{O}$  was added and the pH was adjusted to 8 using  $\text{NH}_4\text{OH}$  solution. The water layer was then extracted three times by DCM and the combined organic layers were dried over anhydrous  $\text{Na}_2\text{SO}_4$  and concentrated at reduced pressure. Finally, the residue was purified by flash column chromatography ( $\text{SiO}_2$ , *n*-hexane/EtOAc 7:3), affording 1.0 g of the desired compound (75% yield). Analytical data were in agreement with the reported ones.<sup>51</sup>

**4-(4-Fluorophenyl)-5-(2-fluoropyridin-4-yl)-N-methylthiazol-2-amine (74).** Compound **73** (513 mg, 1.64 mmol) and *N*-methylthiourea (148 mg, 1.64 mmol) were dissolved in EtOH and the reaction mixture was stirred at reflux temperature for 1 h. After cooling to rt, the solvent was evaporated at reduced pressure and then  $\text{H}_2\text{O}$  was added. The solution was alkalinized to pH = 8 and then extracted three times with DCM. The combined organic layers were dried over anhydrous  $\text{Na}_2\text{SO}_4$ , concentrated at reduced pressure, and the residue was purified by flash column chromatography ( $\text{SiO}_2$ , DCM/EtOH 95:05), obtaining 495 mg of the desired compound (99% yield);  $^1\text{H}$  NMR (250 MHz, DMSO- $d_6$ ):  $\delta$  2.89 (d,  $J = 4.6$  Hz, 3H), 6.77 (br s, 1H), 6.93–7.02 (m, 1H), 7.14–7.29 (m, 2H), 7.40–7.52 (m, 2H), 8.04 (d,  $J = 5.4$  Hz, 1H), 8.10 ppm (q,  $J = 4.8$  Hz, 1H);  $^{13}\text{C}$  NMR (101 MHz, DMSO- $d_6$ ):  $\delta$  30.8, 106.8 (d,  $J = 39.5$  Hz), 114.2 (d,  $J = 3.7$  Hz), 115.4 (d,  $J = 21.2$  Hz), 120.4 (d,  $J = 3.7$  Hz), 130.9 (d,  $J = 8.1$  Hz), 131.4 (d,  $J = 3.7$  Hz), 145.9 (d,  $J = 8.8$  Hz), 147.6 (d,  $J = 16.1$  Hz), 149.2, 162.0 (d,  $J = 245.9$  Hz), 163.4 (d,  $J = 234.2$  Hz), 168.3 ppm; MS-ESI  $m/z$ :  $[\text{M} + \text{H}]^+$  calcd for  $\text{C}_{12}\text{H}_{11}\text{F}_2\text{N}_3\text{S}$ , 304.3; found, 304.1;  $m/z$ :  $[\text{M} - \text{H}]^+$  calcd for  $\text{C}_{12}\text{H}_{11}\text{F}_2\text{N}_3\text{S}$ , 302.3; found, 302.1; HPLC (method 2):  $t_R = 7.123$  min.

**4-(4-Fluorophenyl)-N-methyl-5-(2-((4-morpholinophenyl)amino)pyridin-4-yl)thiazol-2-amine (75).** The title compound was synthesized according to general procedure A starting from **74** (200 mg, 0.66 mmol) and 4-morpholinopyridin-2-amine (176.4 mg, 0.99 mmol). Purification by flash column chromatography ( $\text{SiO}_2$ , DCM/EtOH 97:03 to

90:10) afforded 143 mg of the desired compound (47% yield);  $^1\text{H}$  NMR (250 MHz, DMSO- $d_6$ ):  $\delta$  2.87 (d,  $J = 4.9$  Hz, 3H), 2.94–3.07 (m, 4H), 3.64–3.82 (m, 4H), 6.37 (dd,  $J = 5.4, 1.7$  Hz, 1H), 6.54 (d,  $J = 1.0$  Hz, 1H), 6.82 (m,  $J = 9.0$  Hz, 2H), 7.12–7.25 (m, 2H), 7.27–7.38 (m, 2H), 7.42–7.55 (m, 2H), 7.85 (q,  $J = 4.6$  Hz, 1H), 7.93 (d,  $J = 5.4$  Hz, 1H), 8.69 ppm (s, 1H);  $^{13}\text{C}$  NMR (101 MHz, DMSO- $d_6$ ):  $\delta$  30.7, 49.3, 66.1, 107.6, 112.7, 115.2 (d,  $J = 21.2$  Hz), 115.8, 116.3, 120.0, 130.8 (d,  $J = 8.1$  Hz), 131.8 (d,  $J = 2.9$  Hz), 133.7, 141.0, 145.8, 146.7, 147.8, 156.7, 161.7 (d,  $J = 244.4$  Hz), 167.3 ppm; MS-ESI  $m/z$ :  $[\text{M} + \text{H}]^+$  calcd for  $\text{C}_{22}\text{H}_{24}\text{FN}_5\text{OS}$ , 462.2; found, 462.1;  $m/z$ :  $[\text{M} - \text{H}]^+$  calcd for  $\text{C}_{22}\text{H}_{24}\text{FN}_5\text{OS}$ , 460.2; found, 460.1; HPLC (method 2):  $t_R = 8.518$  min (98.2%).

**2-Bromo-1-(2-chloropyridin-4-yl)propan-1-one (76).** 1-(2-Chloropyridin-4-yl)propan-1-one (**22**) (3.0 g, 17.68 mmol) was dissolved in a 30% solution of HBr in AcOH (20 mL), and after cooling the mixture to 0 °C, bromine (900  $\mu\text{L}$ , 17.68 mmol) was added and the reaction mixture was stirred at 45 °C for 2 h and then heated to 75 °C and stirred for additional 2 h. After evaporating the solvent at reduced pressure,  $\text{H}_2\text{O}$  was added and the pH was adjusted to 9 using  $\text{NH}_4\text{OH}$  solution. The aqueous phase was extracted three times with DCM and the combined organic layers were washed with  $\text{H}_2\text{O}$ , dried over anhydrous  $\text{Na}_2\text{SO}_4$ , and concentrated at reduced pressure. Finally, the residue was purified by flash column chromatography (*n*-hexane/EtOAc 90:10 to 80:20), affording 2.3 g of the desired product (52% yield);  $^1\text{H}$  NMR (300 MHz,  $\text{CDCl}_3$ ):  $\delta$  1.85 (d,  $J = 6.6$  Hz, 3H), 5.07 (q,  $J = 6.6$  Hz, 1H), 7.64 (dd,  $J = 5.1, 1.5$  Hz, 1H), 7.76 (dd,  $J = 1.4, 0.7$  Hz, 1H), 8.53 ppm (dd,  $J = 5.1, 0.7$  Hz, 1H);  $^{13}\text{C}$  NMR (75 MHz,  $\text{CDCl}_3$ ):  $\delta$  19.5, 41.2, 120.4, 123.0, 143.2, 150.9, 152.9, 191.2 ppm; MS-ESI  $m/z$ :  $[\text{M} + \text{H}]^+$  calcd for  $\text{C}_8\text{H}_7\text{BrClNO}$ , 247.9; found, 248.0;  $m/z$ :  $[\text{M} + \text{MeOH}]^+$  calcd for  $\text{C}_9\text{H}_8\text{BrClNO}$ , 279.9; found, 280.0; HPLC (method 2):  $t_R = 5.761$  min.

**4-(2-Chloropyridin-4-yl)-N,5-dimethylthiazol-2-amine (77).** Compound **76** (1.0 g, 4.0 mmol) and *N*-methylthiourea (362.7 mg, 4.0 mmol) were dissolved in EtOH (20 mL) and the reaction mixture was stirred at reflux temperature for 1 h. The solvent was evaporated at reduced pressure and after that the residue was suspended in  $\text{H}_2\text{O}$  and the pH was adjusted to 8 using  $\text{NH}_4\text{OH}$  solution. The resulting suspension was extracted three times with DCM and the combined organic layers were washed with  $\text{H}_2\text{O}$  and NaCl saturated solution, dried over anhydrous  $\text{Na}_2\text{SO}_4$ , and concentrated at reduced pressure. Finally, the residue was purified by flash column chromatography ( $\text{SiO}_2$ , DCM/EtOH 95:05) giving 510 mg of the desired product (53% yield);  $^1\text{H}$  NMR (250 MHz, DMSO- $d_6$ ):  $\delta$  2.43 (s, 3H), 2.83 (d,  $J = 4.9$  Hz, 3H), 7.47 (q,  $J = 4.9$  Hz, 1H), 7.61 (dd,  $J = 5.1, 1.5$  Hz, 1H), 7.64–7.66 (m, 1H), 8.40 ppm (dd,  $J = 5.1, 0.7$  Hz, 1H);  $^{13}\text{C}$  NMR (101 MHz, DMSO- $d_6$ ):  $\delta$  12.2, 30.5, 120.4, 121.2, 121.8, 141.0, 145.7, 149.8, 150.6, 165.5 ppm; MS-ESI  $m/z$ :  $[\text{M} + \text{H}]^+$  calcd for  $\text{C}_{10}\text{H}_{10}\text{ClN}_3\text{S}$ , 240.0; found, 239.9; HPLC (method 2):  $t_R = 9.091$  min.

**N,5-Dimethyl-4-(2-((4-morpholinophenyl)amino)pyridin-4-yl)thiazol-2-amine (78).** The title compound was synthesized according to general procedure A starting from **77** (150 mg, 0.62 mmol) and 4-morpholinopyridin-2-amine (165.8 mg, 0.93 mmol). Purification by flash column chromatography ( $\text{SiO}_2$ , DCM/EtOH 95:05) afforded 42 mg of the desired compound (17% yield);  $^1\text{H}$  NMR (250 MHz, DMSO- $d_6$ ):  $\delta$  2.40 (s, 3H), 2.82 (d,  $J = 4.9$  Hz, 3H), 2.95–3.07 (m, 4H), 3.67–3.80 (m, 4H), 6.81–6.93 (m, 3H), 7.01 (br s, 1H), 7.34 (q,  $J = 4.6$  Hz,



<sup>1</sup>H), 7.46–7.58 (m, 2H), 8.07 (d, *J* = 5.4 Hz, 1H), 8.78 ppm (s, 1H); <sup>13</sup>C NMR (101 MHz, DMSO-*d*<sub>6</sub>): δ 12.3, 30.6, 49.5, 66.2, 108.2, 112.6, 115.9, 117.3, 119.7, 134.4, 143.3, 143.3, 145.5, 147.2, 156.6, 165.4 ppm; MS-ESI *m/z*: [M + H]<sup>+</sup> calcd for C<sub>20</sub>H<sub>23</sub>N<sub>3</sub>O<sub>5</sub>, 382.2; found, 382.2; *m/z*: [M - H]<sup>-</sup> calcd for C<sub>20</sub>H<sub>23</sub>N<sub>3</sub>O<sub>5</sub>, 380.2; found, 380.2; HPLC (method 2): *t*<sub>R</sub> = 5.343 (99.4%).

## ■ ASSOCIATED CONTENT

### Supporting Information

The Supporting Information is available free of charge on the ACS Publications website at DOI: 10.1021/acsomega.8b00668.

Detailed procedures for the preparation of intermediates 17a–I and 33–35; crystal structure of compound 49; melting curves and method description of the nanoDSF experiments; experimental procedures for the crystallization and structure determination of JNK3 in the complex with compounds 38, 44, and AMP-PCP; selectivity screening of 44; and in vitro metabolic stability study for compound 44 (PDF)  
SMILES strings of tested compounds (CSV)

### Accession Codes

The atomic coordinates and structure factors of complex structures containing compounds 38 and 44 and AMP-PCP were deposited in the Protein Data Bank (PDB) with the respective accession codes 6EMH, 6EKD, and 6EQ9, respectively. The authors will release the atomic coordinates and experimental data upon article publication.

## ■ AUTHOR INFORMATION

### Corresponding Author

\*E-mail: pierre.koch@uni-tuebingen.de. Phone: +49 7071 2974579 (P.K.).

### ORCID

Stefan A. Laufer: 0000-0001-6952-1486

Pierre Koch: 0000-0003-4620-4650

### Present Addresses

<sup>†</sup>Chemistry Department, Faculty of Science, Menofia University, Gamal Abdel-Nasser Street, 32511 Shebin El-Khaim, Menofia, Egypt.

<sup>‡</sup>Department of Applied Sciences, Chemistry Branch, University of Technology-Baghdad, Sinaa' Street, 10066, Baghdad, Iraq.

### Notes

The authors declare no competing financial interest.

## ■ ACKNOWLEDGMENTS

The authors gratefully acknowledge Katharina Bauer, Jens Strobach, and Daniela Müller for the biological assays of the synthesized compounds. Moreover, we thank Philipp Krause, Urs Haun, and Raphael Ceamanos-Matilla for their support in the synthesis of some of the presented derivatives. Finally, we are grateful to Dr. Georg Zocher for his support with diffraction data processing and analysis; Dr. Tobias Pflüger (NanoTemper Technologies, Munich) for his assistance with nanoDSF measurements and the beamline staff of Swiss Light Source (SLS, Villigen, Switzerland) for assistance with crystallographic data collection.

## ■ ABBREVIATIONS

MAPK, mitogen activated protein kinase; JNK, c-Jun N terminal kinase; TOSMIC, toluene sulfonylmethylisocyanide; HR, hydrophobic region; AMP-PCP, β,γ-methyleneadenosine-5'-triphosphate; nanoDSF, nano differential scanning fluorimetry; hERG, human-ether-à-go-go related gene; CYP450, cytochrome P450; TLC, thin layer chromatography; HPLC, high performance liquid chromatography; DAD, diode array detector; NMR, nuclear magnetic resonance; ESI-MS, electrospray ionization mass spectrometer

## ■ REFERENCES

- Margutti, S.; Laufer, S. A. Are MAP kinases drug targets? Yes, but difficult ones. *ChemMedChem* **2007**, *2*, 1116–1140.
- Barr, R. K.; Bogoyevitch, M. A. The c-Jun N-terminal protein kinase family of mitogen-activated protein kinases (JNK MAPKs). *Int. J. Biochem. Cell Biol.* **2001**, *33*, 1047–1063.
- Davis, R. J. Signal transduction by the JNK group of MAP kinases. *Cell* **2000**, *103*, 239–252.
- Bogoyevitch, M. A. The isoform-specific functions of the c-Jun N-terminal kinases (JNKs): differences revealed by gene targeting. *BioEssays* **2006**, *28*, 923–934.
- Graczyk, P. P. JNK inhibitors as anti-inflammatory and neuroprotective agents. *Future Med. Chem.* **2013**, *5*, 539–551.
- Resnick, L.; Fennell, M. Targeting JNK3 for the treatment of neurodegenerative disorders. *Drug Discovery Today* **2004**, *9*, 932–939.
- Manning, A. M.; Davis, R. J. Targeting JNK for therapeutic benefit: from junk to gold? *Nat. Rev. Drug Discovery* **2003**, *2*, 554–565.
- Elbelt, N. D.; Cantrell, M. A.; Van Den Berg, C. L. c-Jun N-Terminal Kinases Mediate a Wide Range of Targets in the Metastatic Cascade. *Genes Cancer* **2013**, *4*, 378–387.
- Wagner, E. F.; Nebreda, A. R. Signal integration by JNK and p38 MAPK pathways in cancer development. *Nat. Rev. Cancer* **2009**, *9*, 537–549.
- Gehring, M.; Muth, F.; Koch, P.; Laufer, S. A. c-JunN-terminal kinase inhibitors: a patent review (2010–2014). *Expert Opin. Ther. Pat.* **2015**, *25*, 849–872.
- Koch, P.; Gehring, M.; Laufer, S. A. Inhibitors of c-Jun N-terminal kinases: an update. *J. Med. Chem.* **2015**, *58*, 72–95.
- Siddiqui, M. A.; Reddy, P. A. Small Molecule JNK (c-Jun N-Terminal Kinase) Inhibitors. *J. Med. Chem.* **2010**, *53*, 3005–3012.
- Cuenda, A.; Rousseau, S. p38 MAP-kinases pathway regulation, function and role in human diseases. *Biochim. Biophys. Acta, Mol. Cell Res.* **2007**, *1773*, 1358–1375.
- Corrêa, S. A. L.; Eales, K. L. The Role of p38 MAPK and Its Substrates in Neuronal Plasticity and Neurodegenerative Disease. *J. Signal Transduction* **2012**, *2012*, 1.
- Kumar, S.; Boehm, J.; Lee, J. C. p38 MAP kinases: key signalling molecules as therapeutic targets for inflammatory diseases. *Nat. Rev. Drug Discovery* **2003**, *2*, 717–726.
- Muth, F.; Günther, M.; Bauer, S. M.; Döring, E.; Fischer, S.; Maier, J.; Drückes, P.; Köppler, J.; Trappe, J.; Rothbauer, U.; Koch, P.; Laufer, S. A. Tetra-Substituted Pyridinylimidazoles As Dual Inhibitors of p38α Mitogen-Activated Protein Kinase and c-Jun N-Terminal Kinase 3 for Potential Treatment of Neurodegenerative Diseases. *J. Med. Chem.* **2015**, *58*, 443–456.
- Genovese, M. C. Inhibition of p38: Has the fit lady sung? *Arthritis Rheum.* **2009**, *60*, 317–320.
- Koch, P.; Ansidei, F. 2-Alkylauranyl-4(5)-acyl-5(4)-hetero-arylimidazoles: An Overview on Synthetic Strategies and Biological Activity. *Arch. Pharm.* **2017**, *350*, 1700258.
- Ansidei, F.; Lange, A.; El-Gokha, A.; Boeckler, F. M.; Koch, P. Fluorescence polarization-based assays for detecting compounds binding to inactive c-Jun N-terminal kinase 3 and p38α mitogen-activated protein kinase. *Anal. Biochem.* **2016**, *503*, 28–40.

- (20) Ansideni, F.; Dammann, M.; Boeckler, F. M.; Koch, P. Fluorescence polarization-based competition binding assay for c-Jun N-terminal kinases 1 and 2. *Anal. Biochem.* **2017**, *532*, 26–28.
- (21) Muth, F.; El-Gokha, A.; Ansideni, F.; Eitel, M.; Döing, E.; Sievers-Engler, A.; Lange, A.; Boeckler, F. M.; Lämmerhofer, M.; Koch, P.; Laufer, S. A. Tri- and Tetrasubstituted Pyridinylimidazoles as Covalent Inhibitors of c-Jun N-Terminal Kinase 3. *J. Med. Chem.* **2017**, *60*, 594–607.
- (22) Marchwald, W. Ein Beitrag zur Kenntnis der Imidazole und der Constitution des Glyoxalins. *Ber. Dtsch. Chem. Ges.* **1892**, *25*, 2354–2373.
- (23) Laufer, S. A.; Wagner, G. K.; Kotschenreuther, D. A.; Albrecht, W. Novel substituted pyridinyl imidazoles as potent anticytokine agents with low activity against hepatic cytochrome P450 enzymes. *J. Med. Chem.* **2003**, *46*, 3230–3244.
- (24) Koch, P.; Laufer, S. Unexpected Reaction of 2-Alkylsulfanylimidazoles to Imidazol-2-ones: Pyridinylimidazol-2-ones as Novel Potent p38<sup>MAPK</sup> Mitogen-Activated Protein Kinase Inhibitors. *J. Med. Chem.* **2010**, *53*, 4798–4802.
- (25) Radziewski, B. Ueber Glyoxalin und seine Homologe. *Ber. Dtsch. Chem. Ges.* **1882**, *15*, 2706–2708.
- (26) Neber, P. W.; Friedlohstein, A. V. Über eine neue Art der Umlagerung von Oximen. *Justus Liebigs Ann. Chem.* **1926**, *449*, 109–134.
- (27) Xi, N.; Xu, S.; Cheng, Y.; Tasker, A. S.; Hungate, R. W.; Reider, P. J. Regio-controlled synthesis of N-substituted imidazoles. *Tetrahedron Lett.* **2005**, *46*, 7315–7319.
- (28) Ansideni, F.; Andreev, S.; Kuhn, A.; Albrecht, W.; Laufer, S.; Koch, P. A Diverse and Versatile Regioselective Synthesis of Tetrasubstituted Alkylsulfanylimidazoles as p38<sup>MAPK</sup> Mitogen-Activated Protein Kinase Inhibitors. *Molecules* **2018**, *23*, 221.
- (29) Van Leusen, A. M.; Wildeman, J.; Oldenziel, O. H. Chemistry of sulfonylethyl isocyanides. 12. Base-induced cycloaddition of sulfonylethyl isocyanides to carbon-nitrogen double bonds. Synthesis of 1,5-disubstituted and 1,4,5-trisubstituted imidazoles from aldimines and imidoyl chlorides. *J. Org. Chem.* **1977**, *42*, 1153–1159.
- (30) Miyaura, N.; Suzuki, A. Palladium-Catalyzed Cross-Coupling Reactions of Organoboron Compounds. *Chem. Rev.* **1995**, *95*, 2457–2483.
- (31) Voss, M. E.; Beer, C. M.; Mitchell, S. A.; Blomgren, P. A.; Zhachkin, P. E. A simple and convenient one-pot method for the preparation of heteroaryl-2-imidazoles from nitriles. *Tetrahedron* **2008**, *64*, 645–651.
- (32) Hantsch, A.; Weber, J. H. Ueber Verbindungen des Thiazols (Pyridins der Thiophenreihe). *Ber. Dtsch. Chem. Ges.* **1887**, *20*, 3118–3132.
- (33) Goettert, M.; Graeser, R.; Laufer, S. A. Optimization of a nonradioactive immunosorbent assay for p38<sup>MAPK</sup> mitogen-activated protein kinase activity. *Anal. Biochem.* **2010**, *406*, 233–234.
- (34) Goettert, M.; Luik, S.; Graeser, R.; Laufer, S. A. A direct ELISA assay for quantitative determination of the inhibitory potency of small molecule inhibitors for JNK3. *J. Pharm. Biomed. Anal.* **2011**, *55*, 236–240.
- (35) Sterling, T.; Irwin, J. J. ZINC 15 - Ligand Discovery for Everyone. *J. Chem. Inf. Model.* **2015**, *55*, 2324–2337.
- (36) He, Y.; Duckett, D.; Chen, W.; Ling, Y. Y.; Cameron, M. D.; Lin, L.; Ruiz, C. H.; LoGrasso, P. V.; Kamenecka, T. M.; Koenig, M. Synthesis and SAR of novel isoxazoles as potent c-Jun N-terminal kinase (JNK) inhibitors. *Bioorg. Med. Chem. Lett.* **2014**, *24*, 161–164.
- (37) Scapin, G.; Patel, S. B.; Lisnock, J. M.; Becker, J. W.; LoGrasso, P. V. The Structure of JNK3 in Complex with Small Molecule Inhibitors. *Chem. Biol.* **2003**, *10*, 705–712.
- (38) Thaher, B. A.; Koch, P.; Schattel, V.; Laufer, S. Role of the Hydrogen Bonding Heteroatom-Lys53 Interaction between the p38<sup>MAPK</sup> Mitogen-Activated Protein (MAP) Kinase and Pyridinyl-Substituted 5-Membered Heterocyclic Ring Inhibitors. *J. Med. Chem.* **2009**, *52*, 2613–2617.
- (39) Wagner, G. K.; Kotschenreuther, D.; Zimmermann, W.; Laufer, S. A. Identification of Regioisomers in a Series of N-Substituted Pyridin-4-yl Imidazole Derivatives by Regioselective Synthesis, GC/MS, and 1H NMR. *J. Org. Chem.* **2003**, *68*, 4527–4530.
- (40) Toledo, L. M.; Lydon, N. B.; Elbaum, D. The structure-based design of ATP-site directed protein kinase inhibitors. *Curr. Med. Chem.* **1999**, *6*, 773–805.
- (41) Kamenecka, T.; Habel, J.; Duckett, D.; Chen, W.; Ling, Y. Y.; Frackowiak, B.; Jiang, R.; Shin, Y.; Song, X.; LoGrasso, P. Structure-activity relationships and X-ray structures describing the selectivity of aminopyrazole inhibitors for c-Jun N-terminal kinase 3 (JNK3) over p38. *J. Biol. Chem.* **2009**, *284*, 12853–12861.
- (42) Probst, G. D.; Bowers, S.; Sealy, J. M.; Truong, A. P.; Hom, R. K.; Galemmo, R. A.; Konradi, A. W.; Sham, H. L.; Quinicy, D. A.; Pan, H.; Yao, N.; Lin, M.; Tóth, G.; Artis, D. R.; Zmolek, W.; Wong, K.; Qin, A.; Lorentzen, C.; Nakamura, D. F.; Quinn, K. P.; Sauer, J. M.; Powell, K.; Ruslim, L.; Wright, S.; Chereasa, D.; Ren, Z.; Anderson, J. P.; Bard, F.; Yednock, T. A.; Griswold-Prenner, I. Highly selective c-Jun N-terminal kinase (JNK) 2 and 3 inhibitors with in vitro CNS-like pharmacokinetic properties prevent neurodegeneration. *Bioorg. Med. Chem. Lett.* **2011**, *21*, 315–319.
- (43) Swahn, B.-M.; Xue, Y.; Arzel, E.; Kallán, E.; Magnus, A.; Plobeck, N.; Viklund, J. Design and synthesis of 2'-amino-4,4'-bipyridines as selective inhibitors of c-Jun N-terminal kinase-3. *Bioorg. Med. Chem. Lett.* **2006**, *16*, 1397–1401.
- (44) Kamenecka, T.; Jiang, R.; Song, X.; Duckett, D.; Chen, W.; Ling, Y. Y.; Habel, J.; Laughlin, J. D.; Chambers, J.; Figueroa-Losada, M.; Cameron, M. D.; Lin, L.; Ruiz, C. H.; LoGrasso, P. V. Synthesis, Biological Evaluation, X-ray Structure, and Pharmacokinetics of Aminopyrimidine c-Jun N-terminal Kinase (JNK) Inhibitors. *J. Med. Chem.* **2010**, *53*, 419–431.
- (45) Laufer, S. A.; Hauser, D. R. J.; Domeyer, D. M.; Kinkel, K.; Liedtke, A. J. Design, synthesis, and biological evaluation of novel Tri- and tetrasubstituted imidazoles as highly potent and specific ATP-mimetic inhibitors of p38 MAP kinase: focus on optimized interactions with the enzyme's surface-exposed front region. *J. Med. Chem.* **2008**, *51*, 4122–4149.
- (46) Fricker, M.; LoGrasso, P.; Ellis, S.; Wilkie, N.; Hunt, P.; Pollack, S. J. Substituting c-Jun N-terminal kinase-3 (JNK3) ATP-binding site amino acid residues with their p38 counterparts affects binding of JNK- and p38-selective inhibitors. *Arch. Biochem. Biophys.* **2005**, *438*, 195–205.
- (47) Krenitsky, V. P.; Nadolny, L.; Delgado, M.; Ayala, L.; Clareen, S. S.; Hilgraf, R.; Albers, R.; Hegde, S.; D'Sidocky, N.; Sapienza, J.; Wright, J.; McCarrick, M.; Bahmanyar, S.; Chamberlain, P.; Deller, S. L.; Muir, J.; Giegel, D.; Xu, L.; Celeridad, M.; Lachowitz, J.; Bennett, B.; Moghaddam, M.; Khatsenko, O.; Katz, J.; Pan, R.; Bai, A.; Tang, Y.; Shirley, M. A.; Benish, B.; Bodine, T.; Blease, K.; Raymon, H.; Cathers, B. E.; Satoh, Y. Discovery of CC-930, an orally active anti-fibrotic JNK inhibitor. *Bioorg. Med. Chem. Lett.* **2012**, *22*, 1433–1438.
- (48) Heider, F.; Haun, U.; Döing, E.; Kudolo, M.; Sessler, C.; Albrecht, W.; Laufer, S.; Koch, P. From 2-Alkylsulfanylimidazoles to 2-Alkylimidazoles: An Approach towards Metabolically More Stable p38<sup>MAPK</sup> Kinase Inhibitors. *Molecules* **2017**, *22*, 1729.
- (49) Koch, P.; Bäuerlein, C.; Jank, H.; Laufer, S. Targeting the ribose and phosphate binding site of p38 mitogen-activated protein (MAP) kinase: Synthesis and biological testing of 2-alkylsulfanyl-, 4(5)-aryl-, 5(4)-heteroaryl-substituted imidazoles. *J. Med. Chem.* **2008**, *51*, 5630–5640.
- (50) Koch, P.; Jahns, H.; Schattel, V.; Goettert, M.; Laufer, S. Pyridinylquinoxalines and Pyridinylpyridopyrimidines as Lead Compounds for Novel p38<sup>MAPK</sup> Mitogen-Activated Protein Kinase Inhibitors. *J. Med. Chem.* **2010**, *53*, 1128–1137.
- (51) Revesz, L.; Blum, E.; De Padova, F. E.; Buhl, R.; Fefel, R.; Gram, H.; Haestand, P.; Manning, U.; Rucklin, G. Novel p38 inhibitors with potent oral efficacy in several models of rheumatoid arthritis. *Bioorg. Med. Chem. Lett.* **2004**, *14*, 3595–3599.

## Supporting Information

### Structural Optimization of a Pyridinylimidazole Scaffold: Shifting the Selectivity from p38 $\alpha$ Mitogen-Activated Protein Kinase to c-Jun N-terminal Kinase 3.

Francesco Ansideri,<sup>a</sup> Joana T. Macedo,<sup>b</sup> Michael Eitel,<sup>a</sup> Ahmed El-Gokha,<sup>a,c</sup> Dhafer S. Zinad,<sup>a,d</sup> Camilla Scarpellini,<sup>b</sup> Mark Kudolo,<sup>a</sup> Dieter Schollmeyer,<sup>e</sup> Frank M. Boeckler,<sup>a</sup> Bärbel S. Blaum,<sup>b</sup> Stefan A. Laufer<sup>a</sup> and Pierre Koch<sup>a,\*</sup>

<sup>a</sup>*Department of Pharmaceutical and Medicinal Chemistry, Institute of Pharmaceutical Sciences, Eberhard Karls Universität Tübingen, Auf der Morgenstelle 8, 72076 Tübingen, Germany;*

<sup>b</sup>*Interfaculty Institute of Biochemistry, Eberhard Karls Universität Tübingen, Hoppe-Seyler-Straße 4, 72076 Tübingen, Germany;*

<sup>c</sup>*current address: Chemistry Department, Faculty of Science, Menofia University, Gamal Abdel-Nasser Street, 32511 Shebin El-Khaim, Menofia, Egypt;*

<sup>d</sup>*current address: Department of Applied Sciences, Chemistry Branch, University of Technology-Baghdad, Sinaa' Street, 10066, Baghdad, Iraq;*

<sup>e</sup>*Department of Organic Chemistry, Johannes Gutenberg University Mainz, Duesbergweg 10-14, D-55099 Mainz, Germany.*

**Table of contents**

<b>Experimental procedures</b> .....	S3
<b>Structure determination of compound 49</b> .....	S24
Figure S1.....	S24
Table S1.....	S24
<b>Thermal shift assay by nanoDSF</b> .....	S26
Figure S2.....	S26
Experimental procedure.....	S26
<b>Structure determination of JNK3-38 and JNK3-44 complexes</b> .....	S28
Crystallization of JNK3 and the inhibitor complexes.....	S28
Data collection and structure determination.....	S28
Table S2.....	S29
Figure S3.....	S30
Figure S4.....	S31
Figure S5.....	S32
<b><i>In vitro</i> metabolic stability of compound 44</b> .....	S33
Figure S6.....	S33
Experimental procedure.....	S33
<b>Kinase selectivity screening</b> .....	S34
Table S2.....	S34
<b>References</b> .....	S36



## Experimental procedures

### General procedure for the synthesis of compounds 15a-1 (general procedure B)

In a 3 neck round-bottom flask under anhydrous conditions 2-chloro-4-methylpyridine (**9**) (1 eq) and the appropriate ethyl ester (1 eq) were dissolved in dry THF (2 mL). After cooling the reaction mixture to 0 °C, 2 M Sodium bis(trimethylsilyl)amide (NaHDMS) in dry THF (2.2 eq) was added dropwise and the mixture was stirred at 0 °C for 1.5 to 6 h. After adding H<sub>2</sub>O, the aqueous phase was extracted 3 times with DCM or EtOAc and washed with NaCl saturated solution. The combined organic layers were dried over anhydrous Na<sub>2</sub>SO<sub>4</sub> and the solvent was evaporated at reduced pressure. The obtained residue was employed for the next step without further purification or purified by flash column chromatography.

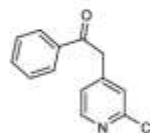
### General procedure for the synthesis of compounds 16a-1 (general procedure C)

Ethan-1-one intermediates **15a-1** (1 eq) and SeO<sub>2</sub> (1.1 eq) were suspended in 5-10 mL of glacial AcOH and the reaction mixture was stirred at 65 °C for 2 to 3 h. After cooling to rt, the formed solid residue of Se was removed by filtration and the filtrate was diluted with EtOAc and then washed with saturated NaHCO<sub>3</sub> solution for 4 times. Finally, the organic phase was washed with saturated NaCl solution, dried over anhydrous Na<sub>2</sub>SO<sub>4</sub> and concentrated at reduced pressure. The residue was purified by flash column chromatography.

### General procedure for the synthesis of compounds 17a-1 (general procedure D)

In a pressure vial ethane-1,2-dione derivatives **16a-1** (1 eq) and NH<sub>4</sub>OAc (10 eq) were suspended in 3 mL of glacial AcOH and after that a 37% aqueous solution of formaldehyde (1 eq) was added. The reaction vessel was heated in a CEM microwave reactor at 180 °C, with initial power of 200 W, for 2 to 5 min. The mixture was added dropwise to NH<sub>4</sub>OH concentrated solution at 0 °C. The suspension obtained was extracted 3 times with EtOAc and the combined organic layers were dried over anhydrous Na<sub>2</sub>SO<sub>4</sub> and concentrated at reduced pressure. The residue was purified by flash column chromatography.

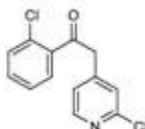
### 2-(2-Chloropyridin-4-yl)-1-phenylethan-1-one (**15a**)



The title compound was synthesized according to general procedure B starting from 2-chloropyridine (**9**) (1.0 g, 7.84 mmol), ethyl benzoate (1.17 g, 7.84 mmol) and 2 M NaHDMS in dry THF (8.62 mL, 17.25 mmol) (1.5 h). 1.82 g of product were obtained, which were employed for the following step without further purification (100% yield); <sup>1</sup>H NMR (300 MHz, DMSO-*d*<sub>6</sub>) δ = 4.56 (s, 2H), 7.33 (dd, *J*

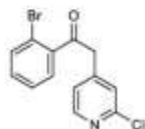
= 5.1, 1.4 Hz, 1H), 7.46 (br. s, 1H), 7.53 - 7.61 (m, 2H), 7.65 - 7.72 (m, 1H), 8.01 - 8.08 (m, 2H), 8.36 ppm (d,  $J = 5.0$  Hz, 1H);  $^{13}\text{C}$  NMR (101 MHz, DMSO- $d_6$ )  $\delta =$  ppm 43.5, 124.9, 125.7, 128.2, 128.8, 133.6, 136.1, 148.4, 149.4, 150.1, 195.9; MS-ESI:  $m/z$   $[\text{M}+\text{H}]^+$  calcd. for  $\text{C}_{13}\text{H}_{10}\text{ClNO}$ : 232.0, found: 232.0;  $m/z$   $[\text{M}-\text{H}]^-$  calcd. for  $\text{C}_{13}\text{H}_{10}\text{ClNO}$ : 230.0, found: 229.8; HPLC (method 2):  $t_{\text{R}} = 5.020$  min.

**1-(2-Chlorophenyl)-2-(2-chloropyridin-4-yl)ethan-1-one (15b)**



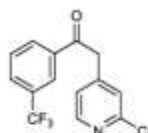
The title compound was synthesized according to general procedure B starting from 2-chloropicoline (**9**) (1.4 g, 10.83 mmol), ethyl 2-chlorobenzoate (2.0 g, 10.83 mmol) and 2 M NaHDMS in dry THF (11.9 mL, 23.8 mmol) (5 h). Purification by flash column chromatography ( $\text{SiO}_2$ ,  $n$ -hexane/EtOAc 90:10 to 80:20) afforded 1.96 g of the desired product (65% yield);  $^1\text{H}$  NMR (300 MHz,  $\text{CDCl}_3$ )  $\delta =$  4.28 (s, 2H), 7.15 (d,  $J = 5.04$  Hz, 1H), 7.28 (br. s, 1H, overlapping with the solvent peak), 7.32 - 7.50 (m, 4H), 8.36 ppm (d,  $J = 5.0$  Hz, 1H);  $^{13}\text{C}$  NMR (101 MHz,  $\text{CDCl}_3$ )  $\delta =$  48.0, 123.7, 125.4, 127.2, 129.3, 130.7, 131.1, 132.6, 138.4, 145.9, 149.6, 151.8, 198.1 ppm; MS-ESI:  $m/z$   $[\text{M}+\text{H}]^+$  calcd. for  $\text{C}_{13}\text{H}_9\text{Cl}_2\text{NO}$ : 266.0, found: 266.0;  $m/z$   $[\text{M}-\text{H}]^-$  calcd. for  $\text{C}_{13}\text{H}_9\text{Cl}_2\text{NO}$ : 264.0, found: 263.8; HPLC (method 2):  $t_{\text{R}} = 5.960$  min.

**1-(2-Bromophenyl)-2-(2-chloropyridin-4-yl)ethan-1-one (15c)**



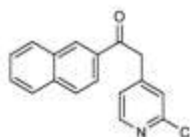
The title compound was synthesized according to general procedure B starting from 2-chloropicoline (**9**) (1.1 g, 8.73 mmol), ethyl 2-bromobenzoate (2.0 g, 8.73 mmol) and 2 M NaHDMS in dry THF (9.5 mL, 19.02 mmol) (1.5 h). Purification by flash column chromatography ( $\text{SiO}_2$ ,  $n$ -hexane/EtOAc 90:10 to 80:20) afforded 2.48 g of the desired product (92% yield);  $^1\text{H}$  NMR (300 MHz,  $\text{CDCl}_3$ )  $\delta =$  4.45 (s, 2H), 7.34 (d,  $J = 4.9$  Hz, 1H), 7.45 - 7.48 (m, 2H), 7.49 - 7.60 (m, 1H), 7.70 - 7.77 (m, 1H), 7.80 (dd,  $J = 5.9, 1.6$  Hz, 1H), 8.37 (d,  $J = 5.0$  Hz, 1H);  $^{13}\text{C}$  NMR (101 MHz,  $\text{CDCl}_3$ )  $\delta =$  48.0, 123.7, 125.4, 127.2, 129.3, 130.7, 131.1, 132.6, 138.4, 145.9, 149.6, 151.8, 198.1 ppm; MS-ESI:  $m/z$   $[\text{M}-\text{H}]^-$  calcd. for  $\text{C}_{13}\text{H}_9\text{BrClNO}$ : 308.0, found: 307.8; HPLC (method 2):  $t_{\text{R}} = 6.130$  min.

**2-(2-Chloropyridin-4-yl)-1-(3-(trifluoromethyl)phenyl)ethan-1-one (15d)**



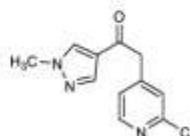
The title compound was synthesized according to general procedure B starting from 2-chloropicoline (**9**) (820 mg, 6.42 mmol), ethyl 3-(trifluoromethyl)benzoate (1.4 g, 6.42 mmol) and 2 M NaHDMS in dry THF (7.1 mL, 14.12 mmol) (3 h). 1.82 g of product were obtained, which were employed for the following step without further purification (81% yield);  $^1\text{H NMR}$  (300 MHz,  $\text{CDCl}_3$ )  $\delta$  = 4.33 (s, 2H), 7.14 (dd,  $J$  = 5.0, 1.5 Hz, 1H), 7.63 - 7.72 (m, 1H), 7.86 - 7.93 (m, 1H), 8.18 (d,  $J$  = 7.9 Hz, 1H), 8.25 (br. s, 1H), 8.38 ppm (dd,  $J$  = 5.0, 0.4 Hz, 1H);  $^{13}\text{C NMR}$  (101 MHz,  $\text{CDCl}_3$ )  $\delta$  = 44.4, 123.8 (q,  $J$  = 272.5 Hz), 124.0, 125.5 (q,  $J$  = 3.8 Hz), 125.7, 129.9, 130.5 (q,  $J$  = 3.5 Hz), 131.7, 132.0 (q,  $J$  = 32.7 Hz), 136.8, 146.1, 150.1, 152.3, 194.0 ppm; MS-ESI:  $m/z$   $[\text{M}+\text{H}]^+$  calcd. for  $\text{C}_{14}\text{H}_9\text{ClF}_3\text{NO}$ : 300.0, found: 300.0;  $m/z$   $[\text{M}-\text{H}]^-$  calcd. for  $\text{C}_{14}\text{H}_9\text{ClF}_3\text{NO}$ : 297.9, found: 263.8; HPLC (method 2):  $t_R$  = 7.240 min.

**2-(2-Chloropyridin-4-yl)-1-(naphthalen-2-yl)ethan-1-one (15e)**



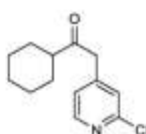
The title compound was synthesized according to general procedure B starting from 2-chloropicoline (**9**) (7.0 g, 54.8 mmol), ethyl 3-naphtoate (11.1 g, 54.8 mmol) and 2 M NaHDMS in dry THF (60 mL, 122 mmol) (1.5 h). After work up, the residue was washed with  $\text{Et}_2\text{O}$  and then filtered off, affording 11.5 g of the desired product (73% yield);  $^1\text{H NMR}$  (400 MHz,  $\text{DMSO}-d_6$ )  $\delta$  = 4.70 (s, 2H), 7.38 (d,  $J$  = 5.1 Hz, 1H), 7.51 (s, 1H), 7.62 - 7.74 (m, 2H), 7.98 - 8.09 (m, 3H), 8.17 (d,  $J$  = 8.1 Hz, 1H), 8.38 (d,  $J$  = 5.1 Hz, 1H), 8.81 ppm (s, 1H);  $^{13}\text{C NMR}$  (101 MHz,  $\text{DMSO}-d_6$ )  $\delta$  = 43.5, 123.6, 124.9, 125.7, 127.0, 127.7, 128.4, 128.8, 129.6, 130.3, 132.1, 133.4, 135.1, 148.5, 149.4, 150.1, 195.9 ppm; MS-ESI:  $m/z$   $[\text{M}-\text{H}]^-$  calcd. for  $\text{C}_{17}\text{H}_{12}\text{ClNO}$ : 280.1, found: 280.2; HPLC (method 2):  $t_R$  = 7.814 min.

**2-(2-Chloropyridin-4-yl)-1-(1-methyl-1H-pyrazol-4-yl)ethan-1-one (15f)**



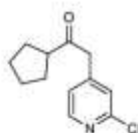
The title compound was synthesized according to general procedure B starting from 2-chloropicoline (**9**) (1.65 g, 12.97 mmol), ethyl 1-methyl-1*H*-pyrazole-4-carboxylate (2 g, 12.97 mmol) and 2 M NaHDMS in dry THF (13 mL, 25.94 mmol) (3 h). After work up, the residue was washed with Et<sub>2</sub>O and then filtered off, affording 1.2 g of the desired product (39% yield); <sup>1</sup>H NMR (250 MHz, DMSO-*d*<sub>6</sub>) δ = 3.89 (s, 3H), 4.22 (s, 2H), 7.31 (d, *J* = 4.9 Hz, 1H), 7.44 (s, 1H), 8.02 (s, 1H), 8.33 (d, *J* = 4.9 Hz, 1H), 8.49 ppm (s, 1H); <sup>13</sup>C NMR (101 MHz, DMSO-*d*<sub>6</sub>) δ = 44.8, 122.6, 124.5, 125.3, 134.2, 139.9, 148.1, 149.5, 150.1, 189.4 ppm; MS-ESI: *m/z* [M-H]<sup>-</sup> calcd. for C<sub>11</sub>H<sub>10</sub>ClN<sub>3</sub>O: 234., found: 234.2; HPLC (method 2): *t*<sub>R</sub> = 1.895 min.

#### 2-(2-Chloropyridin-4-yl)-1-cyclohexylethan-1-one (15g)

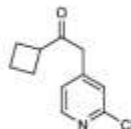


The title compound was synthesized according to general procedure B starting from 2-chloropicoline (**9**) (1.63 g, 12.8 mmol), ethyl cyclohexanecarboxylate (2.0 g, 12.8 mmol) and 2 M NaHDMS in dry THF (14.1 mL, 28.2 mmol) (2 h). Purification by flash column chromatography (SiO<sub>2</sub>, *n*-hexane/EtOAc 90:10 to 80:20) afforded 2.16 g of the desired product (71% yield); <sup>1</sup>H NMR (300 MHz, CDCl<sub>3</sub>) δ = 1.20 - 1.59 (m, 5H), 1.71 - 2.12 (m, 5H), 2.39 - 2.64 (m, 1H), 3.84 (s, 2H), 7.15 (dd, *J* = 5.0, 1.3 Hz, 1H), 7.27 (s, 1H), 8.41 ppm (d, *J* = 5.0 Hz, 1H); <sup>13</sup>C NMR (101 MHz, CDCl<sub>3</sub>) δ = 25.4, 25.6, 28.3, 45.9, 50.9, 123.6, 125.2, 146.5, 149.5, 151.7, 208.2 ppm; MS-ESI: *m/z* [M+H]<sup>+</sup> calcd. for C<sub>13</sub>H<sub>16</sub>ClNO: 238.1, found: 238.1; *m/z* [M-H]<sup>-</sup> calcd. for C<sub>13</sub>H<sub>16</sub>ClNO: 236.1, found: 235.9; HPLC (method 2): *t*<sub>R</sub> = 6.700 min.

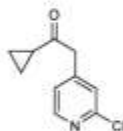
#### 2-(2-Chloropyridin-4-yl)-1-cyclopentylethan-1-one (15h)



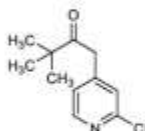
The title compound was synthesized according to general procedure B starting from 2-chloropicoline (**9**) (2.7 g, 21.1 mmol), ethyl cyclopentanecarboxylate (2.0 g, 21.1 mmol) and 2 M NaHDMS in dry THF (23.2 mL, 46.4 mmol) (3 h). Purification by flash column chromatography (SiO<sub>2</sub>, *n*-hexane/EtOAc 90:10 to 80:20) afforded 1.77 g of the desired product (38% yield); <sup>1</sup>H NMR (300 MHz, CDCl<sub>3</sub>) δ = 1.55 - 1.92 (m, 8H), 2.90 - 3.03 (m, 1H), 3.75 (s, 2H), 7.07 (dd, *J* = 5.0, 1.4 Hz, 1H), 7.19 (br. s, 1H), 8.32 ppm (d, *J* = 5.0 Hz, 1H); <sup>13</sup>C NMR (101 MHz, CDCl<sub>3</sub>) δ = 25.9, 28.9, 47.2, 51.6, 123.6, 125.2, 146.5, 149.5, 151.7, 207.5 ppm; MS-ESI: *m/z* [M+H]<sup>+</sup> calcd. for C<sub>12</sub>H<sub>14</sub>ClNO: 224.1, found: 224.0; *m/z* [M-H]<sup>-</sup> calcd. for C<sub>12</sub>H<sub>14</sub>ClNO: 222.1, found: 222.1; HPLC (method 2): *t*<sub>R</sub> = 5.530 min.

**2-(2-Chloropyridin-4-yl)-1-cyclobutylethan-1-one (15i)**

The title compound was synthesized according to general procedure B starting from 2-chloropicoline (**9**) (2.7 g, 21.1 mmol), ethyl cyclobutanecarboxylate (2.9 g, 21.1 mmol) and 2 M NaHDMS in dry THF (25.7 mL, 51.5 mmol) (3 h). Purification by flash column chromatography (SiO<sub>2</sub>, *n*-hex/EtOAc 95:05 to 80:20) afforded 1.22 g of the desired product (25% yield); <sup>1</sup>H NMR (300 MHz, CDCl<sub>3</sub>) δ = 1.78 - 2.02 (m, 2H), 2.10 - 2.30 (m, 4H), 3.28 - 3.39 (m, 1H), 3.63 (s, 1H), 7.04 (dd, *J* = 5.1, 1.4 Hz, 1H), 7.16 - 7.20 (m, 1H), 8.30 ppm (d, *J* = 5.0 Hz, 1H); <sup>13</sup>C NMR (100 MHz, CDCl<sub>3</sub>), δ = 17.6, 24.3, 45.5, 45.6, 123.6, 125.2, 146.3, 149.5, 151.7, 206.1 ppm; MS-ESI: *m/z* [M+H]<sup>+</sup> calcd. for C<sub>11</sub>H<sub>12</sub>ClNO: 210.1, found: 210.0; *m/z* [M-H]<sup>-</sup> calcd. for C<sub>11</sub>H<sub>12</sub>ClNO: 208.1, found: 207.8; HPLC (method 2): t<sub>R</sub> = 4.320 min.

**2-(2-Chloropyridin-4-yl)-1-cyclopropylethan-1-one (15j)**

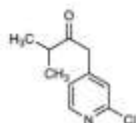
The title compound was synthesized according to general procedure B starting from 2-chloropicoline (**9**) (3.3 g, 26.28 mmol), ethyl cyclopropanecarboxylate (3 g, 26.28 mmol) and 2 M NaHDMS in dry THF (29 mL, 52.56 mmol) (3 h); Purification by flash column chromatography (SiO<sub>2</sub>, *n*-hexane/EtOAc 100:0 to 60:40) afforded 1.62 g of the desired product (32% yield); <sup>1</sup>H NMR (250 MHz, DMSO-*d*<sub>6</sub>) δ = 0.84 - 1.01 (m, 4H), 2.02 - 2.21 (m, 1H), 4.05 (s, 2H), 7.24 (dd, *J* = 5.0, 1.3 Hz, 1H), 7.38 (dd, *J* = 1.4, 0.7 Hz, 1H), 8.32 ppm (dd, *J* = 5.1, 0.7 Hz, 1H); <sup>13</sup>C NMR (101 MHz, DMSO-*d*<sub>6</sub>) δ = 10.5, 20.4, 47.3, 124.6, 125.3, 147.8, 149.4, 150.1, 205.8 ppm; MS-ESI: *m/z* [M-H]<sup>-</sup> calcd. for C<sub>10</sub>H<sub>10</sub>ClNO: 194.0, found: 194.2; HPLC (method 2): t<sub>R</sub> = 2.736 min.

**1-(2-Chloropyridin-4-yl)-3,3-dimethylbutan-2-one (15k)**

The title compound was synthesized according to general procedure B starting from 2-chloropicoline (**9**) (1.96 g, 15.36 mmol), ethyl pivalate (2 g, 15.36 mmol) and 2 M NaHDMS in dry THF (16.9 mL,

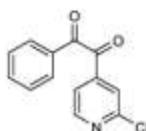
33.8 mmol) (**6h**); Purification by flash column chromatography (SiO<sub>2</sub>, *n*-hexane/EtOAc 90:10 to 80:20) afforded 2.9 g of the desired product (90% yield); <sup>1</sup>H NMR (300 MHz, CDCl<sub>3</sub>) δ = 1.19 (s, 9H), 2.02 (s, 2H), 7.02 (dd, *J* = 6.6, 3.8 Hz, 1H), 7.13 - 7.15 (m, 1H), 8.28 ppm (d, *J* = 5.0 Hz, 1H); <sup>13</sup>C NMR (101 MHz, CDCl<sub>3</sub>) δ = 26.1, 41.9, 44.8, 123.7, 125.3, 147.1, 149.3, 151.5, 210.3 ppm; MS-ESI: *m/z* [M+H]<sup>+</sup> calcd. for C<sub>11</sub>H<sub>14</sub>ClNO: 212.1, found: 212.2; *m/z* [M-H]<sup>-</sup> calcd. for C<sub>11</sub>H<sub>14</sub>ClNO: 210.1, found: 210.1; HPLC (method 2): t<sub>R</sub> = 4.870 min.

**1-(2-Chloropyridin-4-yl)-3-methylbutan-2-one (15l)**



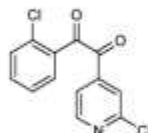
The title compound was synthesized according to general procedure B starting from 2-chloropicoline (**9**) (1.64 g, 12.91 mmol), ethyl isobutyrate (1.5 g, 12.91 mmol) and 2 M NaHDMS in dry THF (14.2 mL, 28.41 mmol) (**4h**); Purification by flash column chromatography (SiO<sub>2</sub>, *n*-hexane/EtOAc 90:10 to 80:20) afforded 2.8 g of the desired product (100% yield); <sup>1</sup>H NMR (300 MHz, CDCl<sub>3</sub>) δ = 1.15 (d, *J* = 6.9 Hz, 6H), 2.78 (sep, *J* = 6.9 Hz, 1H), 3.75 (s, 2H), 7.05 (dd, *J* = 6.4, 3.8 Hz, 1H), 7.18 - 7.20 (m, 1H), 8.32 ppm (d, *J* = 5.1 Hz, 1H); <sup>13</sup>C NMR (101 MHz, CDCl<sub>3</sub>) δ = 17.8, 41.0, 45.5, 123.4, 125.0, 146.2, 149.3, 151.5, 208.7 ppm; MS-ESI: *m/z* [M+H]<sup>+</sup> calcd. for C<sub>10</sub>H<sub>12</sub>ClNO: 198.1, found: 198.1; *m/z* [M-H]<sup>-</sup> calcd. for C<sub>10</sub>H<sub>12</sub>ClNO: 196.1, found: 195.9; HPLC (method 2): t<sub>R</sub> = 3.620 min.

**1-(2-Chloropyridin-4-yl)-2-phenylethane-1,2-dione (16a)**

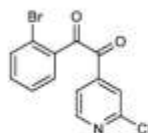


The title compound was synthesized according to general procedure C starting from **15a** (2.0 g, 8.63 mmol) and SeO<sub>2</sub> (1 g, 9.50 mmol) (**3h**); Purification by flash column chromatography (SiO<sub>2</sub>, *n*-hexane/EtOAc 90:10 to 80:20) afforded 948 mg of the desired product (45% yield); <sup>1</sup>H NMR (300 MHz, DMSO-*d*<sub>6</sub>) δ = 7.61 - 7.66 (m, 2H), 7.81 - 7.87 (m, 1H), 7.94 - 7.96 (m, 1H), 8.01 - 8.04 (m, 2H), 8.71 ppm (dd, *J* = 5.0 Hz, 0.5 Hz, 1H); <sup>13</sup>C NMR (100 MHz, DMSO-*d*<sub>6</sub>) δ = 122.0, 123.3, 129.4, 130.2, 131.8, 135.5, 141.9, 151.3, 151.5, 190.8, 191.3 ppm; MS-ESI: *m/z* [M+H]<sup>+</sup> calcd. for C<sub>13</sub>H<sub>8</sub>ClNO<sub>2</sub>: 246.0, found: 246.1; *m/z* [M-H]<sup>-</sup> calcd. for C<sub>13</sub>H<sub>8</sub>ClNO<sub>2</sub>: 244.0, found: 244.0; HPLC (method 2): t<sub>R</sub> = 5.790 min.

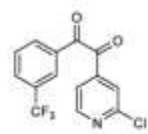


**1-(2-Chlorophenyl)-2-(2-chloropyridin-4-yl)ethane-1,2-dione (16b)**

The title compound was synthesized according to general procedure C starting from **15b** (1.85 g, 6.95 mmol) and SeO<sub>2</sub> (848 mg, 7.65 mmol) (**3h**); Purification by flash column chromatography (SiO<sub>2</sub>, *n*-hexane/EtOAc 90:10 to 80:20) afforded 592 mg of the desired product (30% yield); <sup>1</sup>H NMR (300 MHz, CDCl<sub>3</sub>) δ = 7.44 - 7.25 (m, 2H), 7.58 - 7.65 (m, 1H), 7.75 - 7.79 (dd, *J* = 5.0, 1.4 Hz, 1H), 7.83 - 7.93 (m, 2H), 8.66 ppm (d, *J* = 5.0 Hz, 1H); <sup>13</sup>C NMR (101 MHz, CDCl<sub>3</sub>) δ = 121.3, 123.8, 127.7, 130.4, 132.0, 133.2, 133.9, 135.2, 141.2, 151.0, 152.9, 188.9, 192.1 ppm; MS-ESI: *m/z* [M+MeOH]<sup>+</sup> calcd. for C<sub>13</sub>H<sub>7</sub>Cl<sub>2</sub>NO<sub>2</sub>: 312.0, found: 312.0; HPLC (method 2): *t*<sub>R</sub> = 6.690 min.

**1-(2-Bromophenyl)-2-(2-chloropyridin-4-yl)ethane-1,2-dione (16c)**

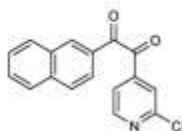
The title compound was synthesized according to general procedure C starting from **15c** (2.0 g, 6.44 mmol) and SeO<sub>2</sub> (786 mg, 7.08 mmol) (**3h**); Purification by flash column chromatography (SiO<sub>2</sub>, *n*-hexane/EtOAc 90:10 to 80:20) afforded 643 mg of the desired product (30% yield); <sup>1</sup>H NMR (300 MHz, DMSO-*d*<sub>6</sub>) δ = 7.64 - 7.74 (m, 2H), 7.80 - 7.92 (m, 2H), 7.97 (dd, *J* = 3.7, 1.3 Hz, 1H), 8.05 (br. s, 1H), 8.76 ppm (d, *J* = 5.0 Hz, 1H); <sup>13</sup>C NMR (101 MHz, DMSO-*d*<sub>6</sub>) δ = 121.4, 122.23, 123.5, 128.4, 132.5, 133.6, 134.5, 135.5, 141.5, 151.4, 151.6, 188.3, 191.8 ppm; MS-ESI: *m/z* [M+MeOH]<sup>+</sup> calcd. for C<sub>13</sub>H<sub>7</sub>BrClNO<sub>2</sub>: 355.9, found: 356.0; HPLC (method 2): *t*<sub>R</sub> = 6.650 min.

**1-(2-Chloropyridin-4-yl)-2-(3-(trifluoromethyl)phenyl)ethane-1,2-dione (16d)**

The title compound was synthesized according to general procedure C starting from **15d** (1.4 g, 4.67 mmol) and SeO<sub>2</sub> (570 mg, 5.14 mmol) (**3h**); Purification by flash column chromatography (SiO<sub>2</sub>, *n*-hexane/EtOAc 90:10 to 80:20) afforded 437 mg of the desired product (30% yield); <sup>1</sup>H NMR (300 MHz, CDCl<sub>3</sub>) δ = 7.69 - 7.78 (m, 2H), 7.86 (dd, *J* = 1.3, 0.8 Hz, 1H), 7.98 (d, *J* = 7.9 Hz, 1H), 8.19 (d, *J* = 7.8 Hz, 1H), 8.30 (br. s, 1H), 8.68 ppm (dd, *J* = 5.1, 0.7 Hz, 1H); <sup>13</sup>C NMR (101 MHz, CDCl<sub>3</sub>) δ = 121.0,

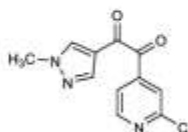
121.2 (q,  $J = 272.0$  Hz), 123.7, 126.8 (q,  $J = 3.7$  Hz), 129.9, 131.7 (q,  $J = 3.4$  Hz), 132.0 (q,  $J = 34.4$  Hz), 132.7, 133.3, 141.3, 151.2, 153.2, 189.7, 189.8 ppm; MS-ESI:  $m/z$   $[M+MeOH]^+$  calcd. for  $C_{14}H_7ClF_3NO_2$ : 346.0, found: 346.1; HPLC (method 2):  $t_R = 7.670$  min.

**1-(2-Chloropyridin-4-yl)-2-(naphthalen-2-yl)ethane-1,2-dione (16e)**



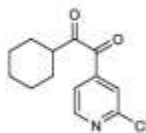
The title compound was synthesized according to general procedure C starting from **15e** (500 mg, 1.77 mmol) and  $SeO_2$  (216 mg, 1.95 mmol) (1.5 h); Purification by flash column chromatography ( $SiO_2$ , *n*-hexane/EtOAc 75:25) afforded 250 mg of the desired product (48% yield);  $^1H$  NMR (300 MHz,  $CDCl_3$ )  $\delta = 7.54 - 7.72$  (m, 2H), 7.75 (dd,  $J = 5.1, 1.4$  Hz, 1H), 7.84 - 8.03 (m, 4H), 8.08 (dd,  $J = 8.6, 1.7$  Hz, 1H), 8.42 (br. s, 1H), 8.63 ppm (dd,  $J = 5.0, 0.6$  Hz, 1H);  $^{13}C$  NMR (75 MHz,  $CDCl_3$ )  $\delta = 121.0, 123.5, 123.6, 127.4, 128.0, 129.3, 129.5, 130.0, 132.2, 134.0, 136.6, 141.7, 151.1, 153.0, 191.1, 191.7$  ppm; HPLC (method 2):  $t_R = 8.316$  min.

**1-(2-Chloropyridin-4-yl)-2-(1-methyl-1H-pyrazol-4-yl)ethane-1,2-dione (16f)**



The title compound was synthesized according to general procedure C starting from **15f** (974 mg, 4.13 mmol) and  $SeO_2$  (500 mg, 4.54 mmol) (1.5 h); Purification by flash column chromatography ( $SiO_2$ , *n*-hexane/EtOAc 50:50) afforded 362 mg of the desired product (35% yield);  $^1H$  NMR (300 MHz,  $CDCl_3$ )  $\delta = 3.98$  (s, 3H), 7.74-7.81 (m, 1H), 7.89 (br. s, 1H), 8.09 (br. s, 1H), 8.13 (s, 1H), 8.59 ppm (dd,  $J = 5.1, 0.6$  Hz, 1H);  $^{13}C$  NMR (75 MHz,  $CDCl_3$ )  $\delta = 39.5, 119.0, 121.5, 124.1, 135.4, 141.7, 142.2, 150.8, 152.7, 182.3, 189.0$  ppm.

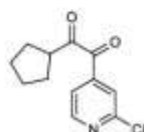
**1-(2-Chloropyridin-4-yl)-2-cyclohexylethane-1,2-dione (16g)**



The title compound was synthesized according to general procedure C starting from **15g** (2.0 g, 8.41 mmol) and  $SeO_2$  (1.2 g, 9.25 mmol) (2 h); Purification by flash column chromatography ( $SiO_2$ , *n*-hexane/EtOAc 90:10 to 80:20) afforded 820 mg of the desired product (38% yield);  $^1H$  NMR (300 MHz,

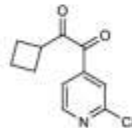
CDCl<sub>3</sub>)  $\delta$  = 1.12 - 1.48 (m, 5H), 1.68 - 1.95 (m, 5H), 3.10-3.23 (m, 1H), 7.68 (dd,  $J$  = 5.1, 1.4 Hz, 1H), 7.71 - 7.84 (m, 1H), 8.61 ppm (d,  $J$  = 5.1 Hz, 1H); <sup>13</sup>C NMR (101 MHz, CDCl<sub>3</sub>)  $\delta$  = 25.2, 25.6, 27.2, 45.3, 121.2, 123.8, 141.5, 150.9, 152.9, 190.1, 203.1 ppm; MS-ESI:  $m/z$  [M+H]<sup>+</sup> calcd for C<sub>13</sub>H<sub>14</sub>ClNO<sub>2</sub>: 252.1, found: 252.0;  $m/z$  [M-H]<sup>-</sup> calcd. for C<sub>13</sub>H<sub>14</sub>ClNO<sub>2</sub>: 250.1, found: 249.9; HPLC (method 2):  $t_R$  = 7.690 min.

**1-(2-Chloropyridin-4-yl)-2-cyclopentylethane-1,2-dione (16h)**

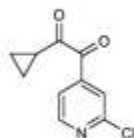


The title compound was synthesized according to general procedure C starting from **15h** (1.65 g, 7.37 mmol) and SeO<sub>2</sub> (900 mg, 8.11 mmol) (2 h); Purification by flash column chromatography (SiO<sub>2</sub>, *n*-hexane/EtOAc 90:10 to 80:20) afforded 834 mg of the desired product (48% yield); <sup>1</sup>H NMR (300 MHz, CDCl<sub>3</sub>)  $\delta$  = 1.59 - 1.99 (m, 8H), 3.57 - 3.77 (m, 1H), 7.72 (dd,  $J$  = 5.1, 1.4 Hz, 1H), 7.83 (s, 1H), 8.61 ppm (d,  $J$  = 5.0 Hz, 1H); <sup>13</sup>C NMR (101 MHz, CDCl<sub>3</sub>)  $\delta$  = 26.0, 28.2, 46.3, 121.3, 123.9, 141.6, 150.9, 152.8, 189.6, 202.1 ppm; MS-ESI:  $m/z$  [M-H]<sup>-</sup> calcd. for C<sub>12</sub>H<sub>12</sub>ClNO<sub>2</sub>: 236.1, found: 236.0; HPLC (method 2):  $t_R$  = 6.690 min.

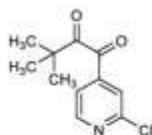
**1-(2-Chloropyridin-4-yl)-2-cyclobutylethane-1,2-dione (16i)**



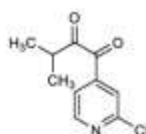
The title compound was synthesized according to general procedure C starting from **15i** (1.10 g, 5.24 mmol) and SeO<sub>2</sub> (640 mg, 5.77 mmol) (1.5 h); Purification by flash column chromatography (SiO<sub>2</sub>, *n*-hexane/EtOAc 90:10 to 80:20) afforded 605 mg of the desired product (52% yield); <sup>1</sup>H NMR (300 MHz, CDCl<sub>3</sub>)  $\delta$  = 1.90 - 2.20 (m, 2H), 2.26 - 2.43 (m, 4H), 3.92 - 4.04 (m, 1H), 7.76 (dd,  $J$  = 5.1, 1.4 Hz, 1H), 7.87 (br. s, 1H), 8.65 ppm (d,  $J$  = 5.0 Hz, 1H); <sup>13</sup>C NMR (101 MHz, CDCl<sub>3</sub>)  $\delta$  = 17.9, 23.8, 40.9, 121.1, 123.7, 141.2, 150.5, 152.5, 188.4, 199.7 ppm; MS-ESI:  $m/z$  [M+H]<sup>+</sup> calcd for C<sub>11</sub>H<sub>10</sub>ClNO<sub>2</sub>: 224.0, found: 224.1;  $m/z$  [M-H]<sup>-</sup> calcd. for C<sub>11</sub>H<sub>10</sub>ClNO<sub>2</sub>: 222.0, found: 222.0; HPLC (method 2):  $t_R$  = 5.560 min.

**1-(2-Chloropyridin-4-yl)-2-cyclopropylethane-1,2-dione (16j)**

The title compound was synthesized according to general procedure C starting from **15j** (1.0 g, 5.11 mmol) and SeO<sub>2</sub> (620 mg, 5.62 mmol) (1.5 h); Purification by flash column chromatography (SiO<sub>2</sub>, *n*-hexane/EtOAc 75:25) afforded 690 mg of the desired product (64% yield); <sup>1</sup>H NMR (300 MHz, CDCl<sub>3</sub>) δ = 1.20 - 1.40 (m, 4H), 2.64 - 2.77 (m, 1H), 7.77 (dd, *J* = 5.1, 1.4 Hz, 1H), 7.85 - 7.93 (m, 1H), 8.60 ppm (dd, *J* = 5.1, 0.6 Hz, 1H); <sup>13</sup>C NMR (75 MHz, CDCl<sub>3</sub>) δ = 14.2, 17.7, 121.7, 124.3, 141.3, 150.8, 152.7, 187.9, 199.3 ppm; HPLC (method 2): *t*<sub>R</sub> = 3.488 min.

**1-(2-Chloropyridin-4-yl)-3,3-dimethylbutane-1,2-dione (16k)**

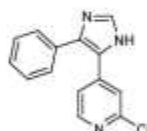
The title compound was synthesized according to general procedure C starting from **15k** (2.6 g, 12.28 mmol) and SeO<sub>2</sub> (1.5 g, 13.51 mmol) (5 h); Purification by flash column chromatography (SiO<sub>2</sub>, *n*-hexane/EtOAc 90:10 to 80:20) afforded 1.28 g of the desired product (46% yield); <sup>1</sup>H NMR (300 MHz, CDCl<sub>3</sub>) δ = 1.31 (s, 9H), 7.55 (dd, *J* = 5.0, 1.4 Hz, 1H), 7.65 - 7.69 (m, 1H), 8.61 ppm (d, *J* = 5.0 Hz, 1H); <sup>13</sup>C NMR (101 MHz, CDCl<sub>3</sub>) δ = 25.9, 42.8, 120.7, 123.2, 141.7, 151.1, 153.0, 191.9, 207.9 ppm; MS-ESI: *m/z* [M+H]<sup>+</sup> calcd. for C<sub>11</sub>H<sub>12</sub>ClNO<sub>2</sub>: 226.1, found: 226.1; *m/z* [M-H]<sup>-</sup> calcd. for C<sub>11</sub>H<sub>12</sub>ClNO<sub>2</sub>: 224.1, found: 223.9; HPLC (method 2): *t*<sub>R</sub> = 7.920 min.

**1-(2-Chloropyridin-4-yl)-3-methylbutane-1,2-dione (16l)**

The title compound was synthesized according to general procedure C starting from **15l** (2.3 g, 11.64 mmol) and SeO<sub>2</sub> (1.4 g, 12.80 mmol) (5 h); Purification by flash column chromatography (SiO<sub>2</sub>, *n*-hexane/EtOAc 90:10 to 80:20) afforded 854 mg of the desired product (35% yield); <sup>1</sup>H NMR (300 MHz, CDCl<sub>3</sub>) δ = 1.21 (d, *J* = 6.9 Hz, 6H), 3.43 (sep, *J* = 6.9 Hz, 1H), 7.70 (dd, *J* = 5.1, 1.4 Hz, 1H), 7.80-7.83 (dd, *J* = 1.3 Hz, 0.8 Hz, 1H), 8.62 ppm (dd, *J* = 5.0 Hz, 0.7 Hz, 1H); <sup>13</sup>C NMR (101 MHz, CDCl<sub>3</sub>) δ = 16.8, 35.9, 121.2, 123.8, 141.5, 150.9, 152.9, 189.8, 203.6 ppm; MS-ESI: *m/z* [M+H]<sup>+</sup> calcd. for

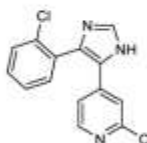
$C_{10}H_{10}ClNO_2$ : 212.0, found: 212.1;  $m/z$  [M-H]<sup>-</sup> calcd. for  $C_{10}H_{10}ClNO_2$ : 210.0, found: 210.0; HPLC (method 2):  $t_R$  = 5.050 min.

**2-Chloro-4-(4-phenyl-1H-imidazol-5-yl)pyridine (17a)**



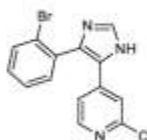
The title compound was synthesized according to general procedure D starting from **16a** (840 mg, 3.41 mmol),  $NH_4OAc$  (2.6 g, 34.1 mmol), and formaldehyde 37% aqueous solution (277  $\mu$ L, 3.41 mmol) (2 min); Purification by flash column chromatography ( $SiO_2$ , DCM/EtOH 90:10) afforded 349 mg of the desired product (36% yield);  $^1H$  NMR (300 MHz,  $DMSO-d_6$ )  $\delta$  = 7.41 (d,  $J$  = 5.0 Hz, 1H), 7.45 - 7.52 (m, 6H), 7.90 (br. s, 1H), 8.24 (d,  $J$  = 5.1 Hz, 1H), 12.81 ppm (br. s, 1H);  $^{13}C$  NMR (101 MHz,  $DMSO-d_6$ )  $\delta$  = 119.5, 120.0, 128.6, 128.9, 130.3, 130.4, 131.7, 136.5, 146.0, 149.7, 150.6, 150.6 ppm; MS-ESI:  $m/z$  [M+H]<sup>+</sup> calcd. for  $C_{14}H_{10}ClN_3$ : 256.1, found: 256.0;  $m/z$  [M-H]<sup>-</sup> calcd. for  $C_{14}H_{10}ClN_3$ : 254.1, found: 253.8; HPLC (method 2):  $t_R$  = 4.270 min.

**2-Chloro-4-(4-(2-chlorophenyl)-1H-imidazol-5-yl)pyridine (17b)**



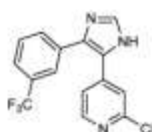
The title compound was synthesized according to general procedure D starting from **16b** (500 mg, 1.78 mmol),  $NH_4OAc$  (1.37 g, 17.8 mmol), and formaldehyde 37% aqueous solution (145  $\mu$ L, 1.78 mmol) (3 min); Purification by flash column chromatography ( $SiO_2$ , DCM/EtOH 97:03 to 90:10) afforded 293 mg of the desired product (57% yield);  $^1H$  NMR (300 MHz,  $DMSO-d_6$ )  $\delta$  = 7.20 (br. s, 1H), 7.35 (br. s, 1H), 7.45 - 7.72 (m, 4H), 7.96 (br. s, 1H), 8.15 - 8.28 (m, 1H), 12.92 ppm (br. s, 1H); MS-ESI:  $m/z$  [M+H]<sup>+</sup> calcd. for  $C_{14}H_9Cl_2N_3$ : 290.0, found: 290.0;  $m/z$  [M-H]<sup>-</sup> calcd. for  $C_{14}H_9Cl_2N_3$ : 288.0, found: 287.8; HPLC (method 2):  $t_R$  = 4.880 min.

**4-(4-(2-Bromophenyl)-1H-imidazol-5-yl)-2-chloropyridine (17c)**



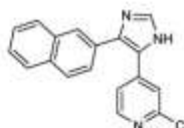
The title compound was synthesized according to general procedure D starting from **16c** (541 mg, 1.67 mmol),  $\text{NH}_4\text{OAc}$  (1.28 g, 16.7 mmol), and formaldehyde 37% aqueous solution (136  $\mu\text{L}$ , 1.67 mmol) (3 min); Purification by flash column chromatography ( $\text{SiO}_2$ , DCM/EtOH 97:03 to 90:10) afforded 392 mg of the desired product (70% yield);  $^1\text{H}$  NMR (300 MHz,  $\text{DMSO-}d_6$ )  $\delta$  = 7.10 - 7.65 (m, 5H), 7.82 - 7.95 (m, 2H), 8.21 (br. s, 1H), 12.85 ppm (br. s, 1H);  $^{13}\text{C}$  NMR (101 MHz,  $\text{DMSO-}d_6$ )  $\delta$  = 118.4, 118.9, 124.0, 128.3, 128.9, 131.5, 131.9, 132.46, 132.53, 133.1, 136.5, 145.5, 149.6, 150.7 ppm; MS-ESI:  $m/z$   $[\text{M}+\text{H}]^+$  calcd. for  $\text{C}_{14}\text{H}_9\text{BrClN}_3$ : 334.0, found: 334.0;  $m/z$   $[\text{M}-\text{H}]^-$  calcd. for  $\text{C}_{14}\text{H}_9\text{BrClN}_3$ : 332.0, found: 331.8; HPLC (method 2):  $t_R$  = 5.070 min.

**2-Chloro-4-(4-(3-(trifluoromethyl)phenyl)-1H-imidazol-5-yl)pyridine (17d)**



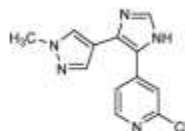
The title compound was synthesized according to general procedure D starting from **16d** (437 mg, 1.39 mmol),  $\text{NH}_4\text{OAc}$  (1.07 g, 13.9 mmol), and formaldehyde 37% aqueous solution (113  $\mu\text{L}$ , 1.39 mmol) (2 min); Purification by flash column chromatography ( $\text{SiO}_2$ , DCM/EtOH 90:10) afforded 175 mg of the desired product (39% yield);  $^1\text{H}$  NMR (300 MHz,  $\text{CDCl}_3$ )  $\delta$  = 7.32 (dd,  $J$  = 5.2, 1.5 Hz, 1H), 7.51 - 7.74 (m, 4H), 7.76 (br. s, 1H), 8.08 (br. s, 1H), 8.30 ppm (d,  $J$  = 5.2 Hz, 1H);  $^{13}\text{C}$  NMR (101 MHz,  $\text{CDCl}_3$ )  $\delta$  = 119.9, 121.6, 123.4 (q,  $J$  = 272.5 Hz), 124.9 (q,  $J$  = 3.7 Hz), 125.5 (q,  $J$  = 3.7 Hz), 129.5, 130.1, 131.0, 131.3, 131.4 (q,  $J$  = 32.9 Hz), 131.5, 136.1, 142.9, 149.4, 151.8 ppm; MS-ESI:  $m/z$   $[\text{M}+\text{H}]^+$  calcd. for  $\text{C}_{15}\text{H}_9\text{ClF}_3\text{N}_3$ : 324.0, found: 323.9;  $m/z$   $[\text{M}-\text{H}]^-$  calcd. for  $\text{C}_{15}\text{H}_9\text{ClF}_3\text{N}_3$ : 322.0, found: 321.8; HPLC (method 2):  $t_R$  = 6.960 min.

**2-Chloro-4-(4-(naphthalen-2-yl)-1H-imidazol-5-yl)pyridine (17e)**

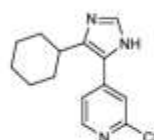


The title compound was synthesized according to general procedure D starting from **16e** (250 mg, 0.84 mmol),  $\text{NH}_4\text{OAc}$  (651 mg, 8.45 mmol), and formaldehyde 37% aqueous solution (69  $\mu\text{L}$ , 0.84 mmol) (5 min); Purification by flash column chromatography ( $\text{SiO}_2$ , DCM/EtOH 95:05) afforded 125 mg of the desired product (48% yield);  $^1\text{H}$  NMR (400 MHz,  $\text{DMSO-}d_6$ )  $\delta$  = 7.41 (d,  $J$  = 4.5 Hz, 1H), 7.50 - 7.64 (m, 4H), 7.89 - 8.05 (m, 4H), 8.08 (s, 1H), 8.17 - 8.30 (m, 1H), 12.96 ppm (br. s., 1H); MS-ESI:  $m/z$   $[\text{M}+\text{H}]^+$  calcd. for  $\text{C}_{18}\text{H}_{12}\text{ClN}_3$ : 306.1, found: 306.4;  $m/z$   $[\text{M}-\text{H}]^-$  calcd. for  $\text{C}_{18}\text{H}_{12}\text{ClN}_3$ : 304.1, found: 304.4; HPLC (method 2):  $t_R$  = 7.144 min.

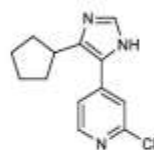


**2-Chloro-4-(4-(1-methyl-1H-pyrazol-4-yl)-1H-imidazol-5-yl)pyridine (17f)**

The title compound was synthesized according to general procedure D starting from **16f** (362 mg, 1.45 mmol), NH<sub>4</sub>OAc (1.12 g, 14.5 mmol), and formaldehyde 37% aqueous solution (118  $\mu$ L, 1.45 mmol) (5 min); Purification by flash column chromatography (SiO<sub>2</sub>, DCM/EtOH 95:05) afforded 140 mg of the desired product (37% yield); <sup>1</sup>H NMR (250 MHz, DMSO-*d*<sub>6</sub>)  $\delta$  = 3.91 (s, 3H), 7.46 - 7.60 (m, 1 H), 7.64 (br. s, 2H), 7.83 (br. s, 1H), 7.99 (br. s, 1H), 8.27 (d, *J* = 5.1 Hz, 1H), 12.59 ppm (br. s., 1H); <sup>13</sup>C NMR (101 MHz, DMSO-*d*<sub>6</sub>)  $\delta$  = 38.7, 110.4, 119.1, 119.6, 122.6, 130.0, 131.6, 136.2, 138.1, 146.2, 149.8, 150.7 ppm; MS-ESI: *m/z* [M+H]<sup>+</sup> calcd. for C<sub>12</sub>H<sub>10</sub>ClN<sub>5</sub>: 260.1, found: 260.0; *m/z* [M-H]<sup>-</sup> calcd. for C<sub>12</sub>H<sub>10</sub>ClN<sub>5</sub>: 258.1, found: 258.0; HPLC (method 2): *t*<sub>R</sub> = 1.584 min.

**2-Chloro-4-(4-cyclohexyl-1H-imidazol-5-yl)pyridine (17g)**

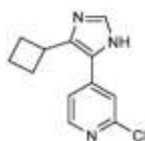
The title compound was synthesized according to general procedure D starting from **16g** (700 mg, 2.78 mmol), NH<sub>4</sub>OAc (2.14 g, 27.8 mmol), and formaldehyde 37% aqueous solution (226  $\mu$ L, 2.78 mmol) (3 min); Purification by flash column chromatography (SiO<sub>2</sub>, DCM/EtOH 97:03 to 90:10) afforded 269 mg of the desired product (37% yield); <sup>1</sup>H NMR (300 MHz, DMSO-*d*<sub>6</sub>)  $\delta$  = 1.20 - 1.60 (m, 5H), 1.65 - 1.82 (m, 5H), 2.94 - 3.07 (m, 1H), 7.54 (d, *J* = 4.5 Hz, 1H), 7.60 (br. s, 1H), 7.69 (br. s, 1H), 8.34 (d, *J* = 5.0 Hz, 1H), 12.28 ppm (br. s, 1H); <sup>13</sup>C NMR (101 MHz, DMSO-*d*<sub>6</sub>)  $\delta$  = 25.4, 25.9, 32.1, 34.7, 119.5, 120.0, 130.5, 135.3, 136.1, 146.6, 149.9, 150.8 ppm; MS-ESI: *m/z* [M+H]<sup>+</sup> calcd. for C<sub>14</sub>H<sub>16</sub>ClN<sub>5</sub>: 262.1, found: 262.1; *m/z* [M-H]<sup>-</sup> calcd. for C<sub>14</sub>H<sub>16</sub>ClN<sub>5</sub>: 260.1, found: 259.9; HPLC (method 2): *t*<sub>R</sub> = 5.050 min.

**2-Chloro-4-(4-cyclopentyl-1H-imidazol-5-yl)pyridine (17h)**

The title compound was synthesized according to general procedure D starting from **16h** (700 mg, 2.94 mmol), NH<sub>4</sub>OAc (2.24 g, 29.4 mmol), and formaldehyde 37% aqueous solution (239  $\mu$ L, 2.94 mmol) (3 min); Purification by flash column chromatography (SiO<sub>2</sub>, DCM/EtOH 97:03 to 90:10) afforded 326

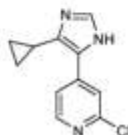
mg of the desired product (45% yield);  $^1\text{H}$  NMR (300 MHz,  $\text{DMSO-}d_6$ )  $\delta$  = 1.64 - 1.80 (m, 4H), 1.95 - 2.10 (m, 2H), 3.40-3.47 (m, 1H), 7.58 (d,  $J$  = 5.0 Hz, 1H), 7.62 (br. s, 1H), 7.70 (s, 1H), 8.33 (d,  $J$  = 5.1 Hz, 1H), 12.27 ppm (br. s, 1H);  $^{13}\text{C}$  NMR (101 MHz,  $\text{DMSO-}d_6$ )  $\delta$  = 24.8, 32.6, 35.7, 119.6, 119.9, 131.2, 134.3, 135.3, 146.3, 149.7, 150.5 ppm; MS-ESE:  $m/z$   $[\text{M}+\text{H}]^+$  calcd. for  $\text{C}_{13}\text{H}_{14}\text{ClN}_3$ : 248.1, found: 247.9;  $m/z$   $[\text{M}-\text{H}]^-$  calcd. for  $\text{C}_{13}\text{H}_{14}\text{ClN}_3$ : 246.1, found: 245.8; HPLC (method 2):  $t_R$  = 3.270 min.

**2-Chloro-4-(4-cyclobutyl-1H-imidazol-5-yl)pyridine (17i)**

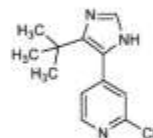


The title compound was synthesized according to general procedure D starting from **16i** (500 mg, 2.24 mmol),  $\text{NH}_4\text{OAc}$  (1.71 g, 22.4 mmol), and formaldehyde 37% aqueous solution (181  $\mu\text{L}$ , 2.24 mmol) (3 min); Purification by flash column chromatography ( $\text{SiO}_2$ ,  $\text{DCM}/\text{EtOH}$  97:03 to 90:10) afforded 255 mg of the desired product (49% yield);  $^1\text{H}$  NMR (300 MHz,  $\text{DMSO-}d_6$ )  $\delta$  = 0.98 - 1.17 (m, 2H), 1.35 - 1.70 (m, 4H), 2.95 - 3.10 (m, 1H), 6.50 - 7.00 (m, 3H), 7.40 - 7.60 (m, 1H), 11.35 - 11.85 ppm (m, 1H);  $^{13}\text{C}$  NMR (101 MHz,  $\text{DMSO-}d_6$ )  $\delta$  = 17.4, 28.2, 30.8, 119.2, 119.5, 130.4, 134.5, 135.4, 145.6, 149.6, 150.5 ppm; MS-ESE:  $m/z$   $[\text{M}+\text{H}]^+$  calcd. for  $\text{C}_{12}\text{H}_{12}\text{ClN}_3$ : 234.1, found: 234.0;  $m/z$   $[\text{M}-\text{H}]^-$  calcd. for  $\text{C}_{12}\text{H}_{12}\text{ClN}_3$ : 232.1, found: 231.8; HPLC (method 2):  $t_R$  = 2.750 min.

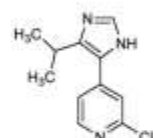
**2-Chloro-4-(4-cyclopropyl-1H-imidazol-5-yl)pyridine (17j)**



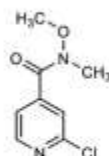
The title compound was synthesized according to general procedure D starting from **16j** (500 mg, 2.38 mmol),  $\text{NH}_4\text{OAc}$  (1.83 g, 23.8 mmol), and formaldehyde 37% aqueous solution (194  $\mu\text{L}$ , 2.38 mmol) (5 min); Purification by flash column chromatography ( $\text{SiO}_2$ ,  $\text{DCM}/\text{EtOH}$  95:05) afforded 350 mg of the desired product (67% yield);  $^1\text{H}$  NMR (250 MHz,  $\text{DMSO-}d_6$ )  $\delta$  = 0.68 - 0.82 (m, 2H), 0.93 - 1.11 (m, 2H), 2.03 - 2.20 (m, 1H), 7.64 (s, 1H), 7.79 (br. s., 2H), 8.27 - 8.42 (m, 1H), 12.23 ppm (br. s., 1H);  $^{13}\text{C}$  NMR (101 MHz,  $\text{DMSO-}d_6$ )  $\delta$  = 6.8, 7.3, 119.0, 119.3, 132.5, 132.7, 134.6, 146.1, 149.8, 150.7 ppm; MS-ESI:  $m/z$   $[\text{M}+\text{H}]^+$  calcd. for  $\text{C}_{11}\text{H}_{10}\text{ClN}_3$ : 220.1, found: 220.2;  $m/z$   $[\text{M}-\text{H}]^-$  calcd. for  $\text{C}_{11}\text{H}_{10}\text{ClN}_3$ : 218.2, found: 304.4; HPLC (method 2):  $t_R$  = 1.760 min.

**4-(4-(*Tert*-butyl)-1*H*-imidazol-5-yl)-2-chloropyridine (17k)**

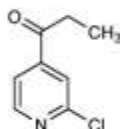
The title compound was synthesized according to general procedure D starting from **16k** (1.1 g, 4.89 mmol), NH<sub>4</sub>OAc (3.77 g, 48.9 mmol), and formaldehyde 37% aqueous solution (397  $\mu$ L, 4.89 mmol) (5 min); Purification by flash column chromatography (SiO<sub>2</sub>, DCM/EtOH 97:03 to 90:10) afforded 283 mg of the desired product (24% yield); <sup>1</sup>H NMR (300 MHz, DMSO-*d*<sub>6</sub>)  $\delta$  = 1.26 (s, 9H), 7.44 (dd, *J* = 5.1, 1.2 Hz, 1H), 7.47 (br. s, 1H), 7.63 (s, 1H), 8.37 (d, *J* = 4.9 Hz, 1H), 12.04 ppm (br. s., 1H); <sup>13</sup>C NMR (101 MHz, DMSO-*d*<sub>6</sub>)  $\delta$  = 30.6, 31.2, 124.2, 124.5, 131.7, 134.3, 136.6, 149.0, 149.3, 149.8 ppm; MS-ESI: *m/z* [M+H]<sup>+</sup> calcd. for C<sub>12</sub>H<sub>14</sub>ClN<sub>3</sub>; 236.1, found: 236.2; *m/z* [M-H]<sup>-</sup> calcd. for C<sub>12</sub>H<sub>14</sub>ClN<sub>3</sub>; 234.1, found: 234.0; HPLC (method 2): *t*<sub>R</sub> = 2.470 min.

**2-Chloro-4-(4-isopropyl-1*H*-imidazol-5-yl)pyridine (17l)**

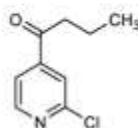
The title compound was synthesized according to general procedure D starting from **16l** (750 mg, 4.89 mmol), NH<sub>4</sub>OAc (2.74 g, 35.5 mmol), and formaldehyde 37% aqueous solution (289  $\mu$ L, 3.55 mmol) (3 min); Purification by flash column chromatography (SiO<sub>2</sub>, DCM/EtOH 97:03 to 90:10) afforded 135 mg of the desired product (17% yield); <sup>1</sup>H NMR (300 MHz, CDCl<sub>3</sub>)  $\delta$  = 1.35 (d, *J* = 7.0 Hz, 6H), 3.44 (sep, *J* = 7.0 Hz, 1H), 7.51 (dd, *J* = 5.2, 1.5 Hz, 1H), 7.56 - 7.65 (m, 1H), 7.69 (s, 1H), 8.36 ppm (d, *J* = 5.2 Hz, 1H); <sup>13</sup>C NMR (100 MHz, DMSO-*d*<sub>6</sub>)  $\delta$  = 21.9, 24.6, 119.4, 119.8, 129.9, 135.1, 136.6, 146.3, 149.6, 150.5 ppm; MS-ESI: *m/z* [M+H]<sup>+</sup> calcd. for C<sub>11</sub>H<sub>12</sub>ClN<sub>3</sub>; 222.1, found: 222.2; *m/z* [M-H]<sup>-</sup> calcd. for C<sub>11</sub>H<sub>12</sub>ClN<sub>3</sub>; 220.1, found: 220.0; HPLC (method 2): *t*<sub>R</sub> = 2.080 min.

**2-Chloro-*N*-methoxy-*N*-methylisonicotinamide (20)<sup>1</sup>**

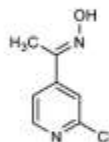
The title compound was synthesized as previously reported<sup>1</sup> and the analytical data were in agreement with the reported ones.

**1-(2-Chloropyridin-4-yl)propan-1-one (22)**

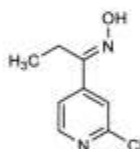
A solution of Weinreb amide **20** (10 g 49.84 mmol) in dry THF (60 mL) was cooled to  $-10\text{ }^{\circ}\text{C}$  and after that a 2M solution of ethylmagnesium bromide in dry THF (15.6 mL, 64.8 mmol), previously diluted with 30 mL of dry THF, was added dropwise. After completion of the addition the reaction mixture was stirred at the same temperature for 3 h. After letting the mixture heat to rt, 200 mL of  $\text{NH}_4\text{Cl}$  saturated solution were added and the mixture was stirred for 10 min. The 2 phases formed were separated and the aqueous phase was further extracted 3 times with EtOAc. The combined organic layers were dried over anhydrous  $\text{Na}_2\text{SO}_4$  and concentrated at reduced pressure. Finally, the residue was purified by flash column chromatography ( $\text{SiO}_2$ , *n*-hexane/EtOAc 85:15 to 70:30) affording 5.82 g of the desired compound (69% yield);  $^1\text{H}$  NMR (300 MHz,  $\text{CDCl}_3$ )  $\delta$  = 1.24 (t,  $J$  = 7.2 Hz, 3H), 2.99 (q,  $J$  = 7.2 Hz, 2H), 7.66 (dd,  $J$  = 5.0, 1.5 Hz, 1H), 7.76 (dd,  $J$  = 1.4, 0.7 Hz, 1H), 8.57 ppm (dd,  $J$  = 5.1, 0.7 Hz, 1H);  $^{13}\text{C}$  NMR (75 MHz,  $\text{CDCl}_3$ )  $\delta$  = 7.6, 32.4, 119.8, 122.3, 145.5, 150.8, 152.8, 198.5 ppm; HPLC (method 2):  $t_R$  = 3.651 min.

**1-(2-Chloropyridin-4-yl)butan-1-one (23)**

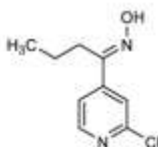
Under Argon atmosphere, Mg turnings (5.5 g, 100 mmol) were suspended in dry THF (40 mL) and subsequently 1-bromopropane (6.15 g, 50 mmol) was added and the mixture was stirred at rt for 60 min. The residual Mg was let decanting and the surmatant was added dropwise to a solution of compound **20** (5.0 g, 25 mmol) in dry THF (20 mL) under Argon atmosphere, previously cooled at  $-10\text{ }^{\circ}\text{C}$  and the mixture was stirred at the same t for 3 h. After heating to rt,  $\text{NH}_4\text{Cl}$  saturated solution (100 mL) was added to the reaction. The 2 phases formed were separated and the aqueous phase was further extracted for 2 times with EtOAc. The combined organic layers were then dried over anhydrous  $\text{Na}_2\text{SO}_4$  and the solvent was evaporated at reduced pressure. Finally, the residue was purified by flash column chromatography ( $\text{SiO}_2$ , *n*-hexane/EtOAc 8:2 to 7:3) affording 3.4 g of the desired compound (75%);  $^1\text{H}$  NMR (300 MHz,  $\text{CDCl}_3$ )  $\delta$  = 0.99 (t,  $J$  = 7.4 Hz, 3H), 1.65 - 1.88 (m, 2H), 2.92 (t,  $J$  = 7.2 Hz, 2H), 7.64 (dd,  $J$  = 5.1, 1.4 Hz, 1H), 7.68 - 7.79 (m, 1H), 8.54 ppm (dd,  $J$  = 5.1, 0.5 Hz, 1H);  $^{13}\text{C}$  NMR (101 MHz,  $\text{CDCl}_3$ )  $\delta$  = 13.6, 17.1, 40.9, 119.8, 122.3, 145.8, 150.8, 152.9, 198.1 ppm; MS-ESI:  $m/z$  [ $\text{M}+\text{H}$ ] $^+$  calcd. for  $\text{C}_9\text{H}_{10}\text{ClNO}$ : 184.0, found: 184.0;  $m/z$  [ $\text{M}-\text{H}$ ] calcd. for  $\text{C}_8\text{H}_9\text{ClNO}$ : 182.0, found: 181.9; HPLC (method 2):  $t_R$  = 3.390 min.

**1-(2-Chloropyridin-4-yl)ethan-1-one oxime (24)**

To a solution of hydroxylamine hydrochloride (1.61 g, 23.14 mmol) in a mixture of H<sub>2</sub>O/MeOH (50 mL, 1:1), 5 mL of 20% NaOH solution were added. After cooling the reaction mixture at 0 °C, 4-acetyl-2-chloropyridine (**21**, 3.0 g, 19.28 mmol) was added in one portion and the reaction mixture was stirred for 2 h at the same temperature. The obtained precipitate was filtered off, washed with cold H<sub>2</sub>O and dried, affording 2.96 g of the desired compound which was used for the following step without further purification (90% yield); <sup>1</sup>H NMR (400 MHz, DMSO-*d*<sub>6</sub>) δ = 2.15 (s, 3H), 7.63 (d, *J* = 5.1 Hz, 1H), 7.65 (s, 1H), 8.40 (d, *J* = 5.3 Hz, 1H), 11.93 ppm (s, 1H); <sup>13</sup>C NMR (101 MHz, DMSO-*d*<sub>6</sub>) δ = 10.9, 119.2, 120.2, 147.6, 150.0, 150.8, 150.9; MS-FAB: *m/z* [M+H]<sup>+</sup> calcd. for C<sub>9</sub>H<sub>10</sub>ClNO: 171.0, found: 171.1; HPLC (method 1): *t*<sub>R</sub> = 3.690 min.

**1-(2-Chloropyridin-4-yl)ethan-1-one oxime (25)<sup>2</sup>**

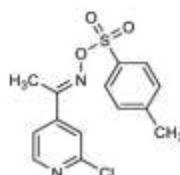
The title compound was synthesized as previously reported and analytical data were in agreement with the reported ones.<sup>2</sup>

**1-(2-Chloropyridin-4-yl)butan-1-one oxime (26)**

Compound **23** (3.38 g, 18.43 mmol) was dissolved in MeOH (20 mL) and, after cooling the reaction to 0 °C, a mixture of hydroxylamine hydrochloride (1.41 g, 20.27 mmol) in H<sub>2</sub>O (10 mL) and 20% NaOH (10 mL) was added dropwise and the reaction mixture was letting slowly heating to rt and stirred for 1 h. After removing the MeOH at reduced pressure, H<sub>2</sub>O was added, and the aqueous phase was extracted 3 times with EtOAc. The combined organic layers were dried over anhydrous Na<sub>2</sub>SO<sub>4</sub> and concentrated at reduced pressure. Finally, the residue was purified by flash column chromatography (SiO<sub>2</sub>, *n*-hexane/EtOAc 80:20) affording 3.1 g of the desired product (85% yield); <sup>1</sup>H NMR (300 MHz, CDCl<sub>3</sub>)

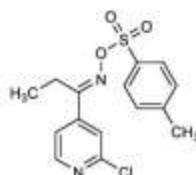
$\delta$  = 0.99 (t,  $J$  = 7.4 Hz, 3H), 1.50 - 1.67 (m, 2H), 2.66 - 2.82 (m, 2H), 7.46 (dd,  $J$  = 5.3, 1.6 Hz, 1H), 7.56 (dd,  $J$  = 1.5, 0.6 Hz, 1H), 8.40 (dd,  $J$  = 5.3, 0.6 Hz, 1H), 9.70 ppm (br. s., 1H);  $^{13}\text{C}$  NMR (101 MHz,  $\text{CDCl}_3$ )  $\delta$  = 14.1, 19.6, 27.2, 119.3, 121.3, 146.8, 149.7, 152.0, 156.5 ppm; MS-ESI:  $m/z$   $[\text{M}+\text{H}]^+$  calcd. for  $\text{C}_9\text{H}_{11}\text{ClN}_2\text{O}$ : 199.1, found: 199.1;  $m/z$   $[\text{M}-\text{H}]^-$  calcd. for  $\text{C}_9\text{H}_{11}\text{ClN}_2\text{O}$ : 197.1, found: 196.9; HPLC (method 2):  $t_{\text{R}}$  = 5.451 min.

**1-(2-Chloropyridin-4-yl)ethan-1-one *O*-tosyl oxime (27)**



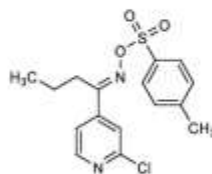
To a solution of 1-(2-chloropyridin-4-yl)ethan-1-one oxime (**24**, 2.94 g, 17.23 mmol) in dry pyridine (15 mL) *p*-toluenesulfonyl chloride (3.94 g, 48.28 mmol) was added and the mixture was stirred at rt for 24 h. 100 mL of ice-cold  $\text{H}_2\text{O}$  were added and the mixture was stirred for 3 h. Finally the precipitate formed was filtered off, washed with cold  $\text{H}_2\text{O}$  and dried, obtaining 4.11 g of the desired product (74% yield);  $^1\text{H}$  NMR (400 MHz,  $\text{DMSO}-d_6$ )  $\delta$  = 2.35 (s, 3H), 2.41 (s, 3H), 7.50 (d,  $J$  = 7.8 Hz, 2H), 7.57 (d,  $J$  = 5.3 Hz, 1H), 7.66 (s, 1H), 7.92 (d,  $J$  = 7.8 Hz, 2H), 8.50 (d,  $J$  = 5.1 Hz, 1H);  $^{13}\text{C}$  NMR (400 MHz,  $\text{DMSO}-d_6$ )  $\delta$  = 13.7, 21.1, 120.1, 121.7, 128.5, 130.1, 131.5, 144.1, 145.8, 150.6, 151.0, 162.1; MS-FAB:  $m/z$   $[\text{M}+\text{H}]^+$  calcd. for  $\text{C}_{14}\text{H}_{13}\text{ClN}_2\text{O}_3\text{S}$ : 325.1, found: 325.1; HPLC (method 1):  $t_{\text{R}}$  = 6.930 min.

**1-(2-Chloropyridin-4-yl)propan-1-one *O*-tosyl oxime (28)<sup>2</sup>**



The title compound was synthesized as previously reported and analytical data were in agreement with the published ones.<sup>2</sup>

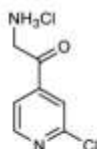
**1-(2-Chloropyridin-4-yl)butan-1-one *O*-tosyl oxime (29)**





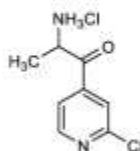
To a solution of 1-(2-chloropyridin-4-yl)butan-1-one oxime (**26**, 3.09 g, 15.58 mmol) in dry pyridine (20 mL) *p*-toluenesulfonyl chloride (4.45 g, 23.38 mmol) was added and the mixture was stirred at rt for 48 h. 100 mL H<sub>2</sub>O were added and the aqueous phase was extracted 3 times with EtOAc. The combined organic layers were dried over anhydrous Na<sub>2</sub>SO<sub>4</sub> and the solvent was evaporated at reduced pressure, affording 4.4 g of the desired product which was used for the following step without further purification (80% yield); <sup>1</sup>H NMR (300 MHz, DMSO-*d*<sub>6</sub>) δ = 0.80 (t, *J* = 7.4 Hz, 3H), 1.30 - 1.47 (m, 2H), 2.40 (s, 3H), 2.75 - 2.87 (m, 2H), 7.45 - 7.53 (m, 2H), 7.56 (dd, *J* = 5.2, 1.5 Hz, 1H), 7.62 - 7.67 (m, 1H), 7.85 - 7.95 (m, 2H), 8.50 ppm (dd, *J* = 5.2, 0.5 Hz, 1H); <sup>13</sup>C NMR (75 MHz, DMSO-*d*<sub>6</sub>) δ = 13.4, 19.2, 21.1, 28.4, 120.6, 121.8, 128.5, 130.1, 131.4, 143.3, 145.8, 150.8, 151.2, 165.3 ppm; HPLC (method 2): *t*<sub>R</sub> = 8.430 min.

#### 2-Amino-1-(2-chloropyridin-4-yl)ethan-1-one hydrochloride (**30**)



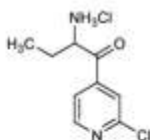
Under Argon atmosphere potassium (241 mg, 6.16 mmol) was added portionwise to 20 mL of absolute EtOH. After complete dissolution the reaction mixture was cooled to 0 °C and a solution of 1-(2-chloropyridin-4-yl)ethan-1-one *O*-tosyl oxime (**27**, 2 g, 6.16 mmol) in absolute EtOH (100 mL) was slowly added dropwise. After completion of the addition the reaction mixture was stirred for 1 h at rt and after that 150 mL of dry Et<sub>2</sub>O were added and the mixture was stirred at rt for 16 h. The white precipitate formed was filtered and washed twice with 50 mL Et<sub>2</sub>O. HCl was bubbled in the combined organic layer and the white precipitate formed was filtered off, washed with Et<sub>2</sub>O and dried. The solid obtained was dissolved in concentrated HCl (25 mL) and stirred at 55 °C for 50 h. After concentrating the mixture at reduced pressure warm MeOH was added and the product was then precipitated by adding Et<sub>2</sub>O. The red solid formed was finally filtered off and dried giving 210 mg which were use in the following step without further purification (17% yield); <sup>13</sup>C NMR (101 MHz, DMSO-*d*<sub>6</sub>) δ = 45.4, 120.6, 122.3, 143.1, 151.4, 151.5, 192.1 ppm; MS-FAB: *m/z* [M+H]<sup>+</sup> calcd. for C<sub>7</sub>H<sub>6</sub>Cl<sub>2</sub>N<sub>2</sub>O: 171.0, found: 171.1; HPLC (method 2): *t*<sub>R</sub> = 1.145 min.

#### 2-Amino-1-(2-chloropyridin-4-yl)propan-1-one hydrochloride (**31**)



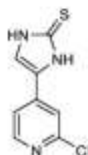
Under Argon atmosphere potassium (1.18 g, 30.14 mmol) was added portionwise to 50 mL of absolute EtOH. After complete dissolution the reaction mixture was cooled to 0 °C and a solution of 1-(2-chloropyridin-4-yl)propan-1-one *O*-tosyl oxime (**28**, 10.21 g, 30.14 mmol) in absolute EtOH (200 mL) was added dropwise. After completion of the addition the reaction mixture was stirred for 1 h at 0 °C and after that 100 mL of dry Et<sub>2</sub>O were added and the mixture was stirred at rt for 16 h. The white precipitate formed was filtered and the filtrate was concentrated at reduced pressure. The oily residue obtained was dissolved in concentrated HCl (30 mL) and stirred at 55 °C for 1 h. Finally, after evaporating the solvent at reduced pressure, the residue was treated with acetone and the white precipitate formed was filtered off and washed with cold acetone, giving 3.34 g of the desired compound as a hydrochloride salt (50% yield); HPLC (method 2): *t<sub>R</sub>* = 1.258 min.

**2-Amino-1-(2-chloropyridin-4-yl)butan-1-one hydrochloride (32)**

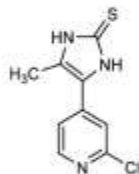


The title compound was synthesized following the same procedure as compound **31** starting from potassium (718 mg, 18.37 mmol) and 1-(2-chloropyridin-4-yl)butan-1-one *O*-tosyl oxime (**29**, 4.32 g, 12.25 mmol) affording 1.7 g of the desired product as a hydrochloride salt which was directly used for the following step (60% yield).

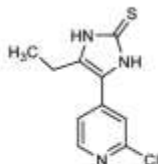
**4-(2-Chloropyridin-4-yl)-1,3-dihydro-2H-imidazole-2-thione (33)**



Compound **30** (3.54 g, 17.1 mmol) was dissolved in MeOH (90 mL) and after that KSCN (8.25 g, 84.9 mmol) was added. The reaction mixture was heated to reflux temperature and stirred for 4 h. The yellow precipitate formed was filtered off, washed with H<sub>2</sub>O and dried *in vacuo* obtaining 1.51 g of the desired product which was used for the following step without further purification (43% yield); <sup>1</sup>H NMR (400 MHz, DMSO-*d*<sub>6</sub>) δ = 7.66 (d, *J* = 5.1 Hz, 1H), 7.83 (s, 1H), 7.87 (s, 1H) 8.36 (d, 5.3 Hz, 1H), 12.51 (s, 1H), 13.82 ppm (s, 1H); <sup>13</sup>C NMR (101 MHz, DMSO-*d*<sub>6</sub>) δ = 117.0, 117.3, 117.7, 125.3, 138.6, 150.3, 151.2, 163.5 ppm; MS-FAB: *m/z* [M+H]<sup>+</sup> calcd. for C<sub>8</sub>H<sub>6</sub>ClN<sub>3</sub>S: 212.0, found: 212.2; HPLC (method 2): *t<sub>R</sub>* = 2.270 min.

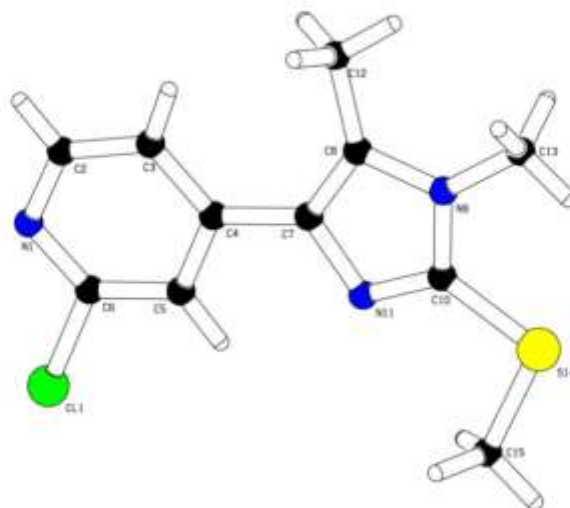
**4-(2-Chloropyridin-4-yl)-5-methyl-1,3-dihydro-2H-imidazole-2-thione (34)<sup>2</sup>**

Compound **31** (5.5 g, 21.36 mmol) was dissolved in MeOH (50 mL) and after that KSCN (6.23 g, 97.18 mmol) was added. The reaction mixture was heated to reflux temperature and stirred for 3 h. After cooling down, the white precipitate formed was filtered off, washed with cold MeOH and cold H<sub>2</sub>O and dried, obtaining 3.42 g of the desired compound (71% yield); Analytical data were in agreement with the previously reported ones.<sup>2</sup>

**4-(2-Chloropyridin-4-yl)-5-ethyl-1,3-dihydro-2H-imidazole-2-thione (35)**

The title compound was synthesized following the same procedure as compound **34** starting from **32** (1.65 g, 6.08 mmol) and KSCN (1.77 g, 18.23 mmol), giving 850 mg of the desired product (60% yield); <sup>1</sup>H NMR (300 MHz, DMSO-*d*<sub>6</sub>)  $\delta$  = 1.17 (t, *J* = 7.5 Hz, 3H), 2.66 (q, *J* = 7.5 Hz, 2H), 7.44 (dd, *J* = 5.4, 1.6 Hz, 1H), 7.51 - 7.60 (m, 1H), 8.38 (dd, *J* = 5.4, 0.4 Hz, 1H), 12.35 - 12.51 ppm (m, 2H); <sup>13</sup>C NMR (101 MHz, DMSO-*d*<sub>6</sub>)  $\delta$  = 13.0, 17.9, 118.8, 119.4, 119.7, 132.4, 139.1, 150.2, 151.1, 161.8 ppm; MS-ESI: *m/z* [M-H] calcd for C<sub>10</sub>H<sub>10</sub>ClN<sub>3</sub>S: 238.0, found: 237.9; HPLC (method 2): *t*<sub>R</sub>=2.698 min.

## Structure determination of compound 49



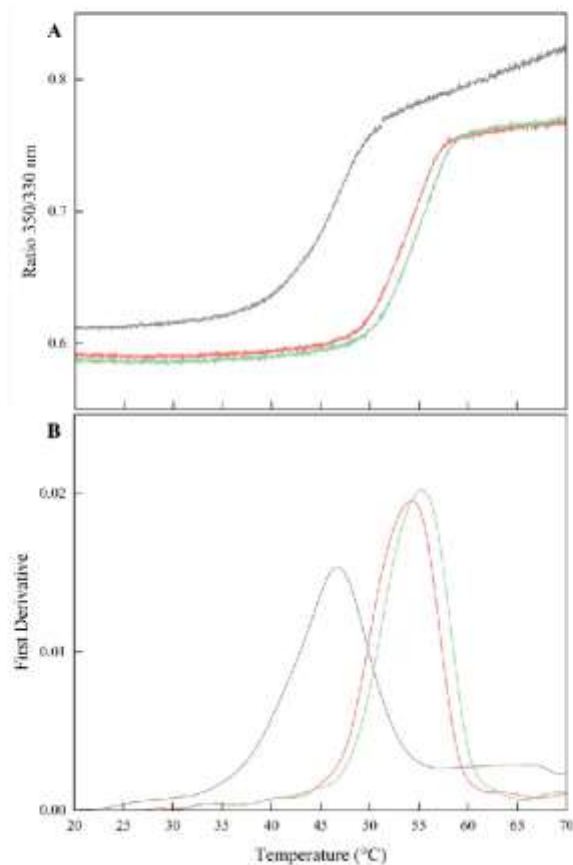
**Figure S1.** Crystal structure of compound 49. The structure confirms the substitution of the imidazole-N atom distal from the pyridine ring. Diffraction data were collected at 193 K with a STOE IPDS-2T diffractometer with Mo K $\alpha$  radiation. Data processing was performed using the STOE-software. The structure was solved using Direct methods (SIR-2004) and refined with SHELXL-2014. Data for atomic coordinates, thermal parameters and reflections can be obtained from the Cambridge Crystallographic Data Centre under the CCDC Nr. 1824231.

**Table S1.** Data collection and refinement statistics

Data collection	
Space group	P-1 (triclinic Nr.2)
Cell dimensions	determinate from 5730 reflections with $2.7^\circ < \theta < 28.2^\circ$
$a, b, c$ (Å)	8.2302(8), 8.2302(8), 9.1962(9)
$\alpha, \beta, \gamma$ (°)	100.036(7), 98.894(8), 111.423(7)
$V$ (Å <sup>3</sup> ), $z$	586.65(9), 2
Crystal size (mm <sup>3</sup> )	0.04 x 0.16 x 0.24 (colorless plate)
Range of Measurement	$2^\circ \leq \theta \leq 28^\circ$ , $-10 \leq h \leq 10$ $-11 \leq k \leq 11$ $-12 \leq l \leq 12$
No. of reflections:	
Measured	6001
Unique	2814 ( $R_{int} = 0.0482$ )
Observed ( $ F_o /o(F) > 4.0$ )	1976

**Table S1.** continued

<b>Refinement</b>	
Nr. of parameters	148
wR2	0.1069
R1(observed), R(all)	0.0391, 0.0612
Goodness of Fit	0.971
Max. deviation of parameters	0.001 * e.s.d.
Max. Peak final diff. Fourier synthesis ( $e \text{ \AA}^{-3}$ )	0.22, -0.25

**Thermal shift assay by nanoDSF**

**Figure S2.** Effects of ligand binding on JNK3 thermal stability determined by nanoDSF. a) Intrinsic fluorescence intensity ratio of tryptophans and tyrosines (350/330 nm) plotted as a function of temperature; b) First derivative analysis used to deduce the melting temperature ( $T_m$ ). The gray curve corresponds to JNK3, whereas the light red and light green curves correspond to the JNK3-**38** and JNK3-**44** complexes, respectively.

**Experimental procedure**

Samples were prepared using the protein buffer 50 mM HEPES pH 7, 100 mM NaCl, 2 mM MgCl<sub>2</sub>, 10 mM β-mercaptoethanol. Compounds **38** and **44** (stock concentration of 10 mM in DMSO) were diluted in protein buffer to 100 μM and then added to the protein sample. The final protein and inhibitor



concentrations were 5  $\mu\text{M}$  and 50  $\mu\text{M}$ , respectively. 10  $\mu\text{L}$  of each sample were loaded into capillary glass tubes and measured in triplicates in a single nanoDSF experiment using a Prometheus NT.48 instrument (NanoTemper Technologies, Munich). All loaded capillaries were heated from 20  $^{\circ}\text{C}$  to 70  $^{\circ}\text{C}$  with a rate of 1  $^{\circ}\text{C}/\text{min}$ . Changes in the intrinsic fluorescence of tryptophans and tyrosines were monitored as the ratio of the emission at the wavelengths of 350 and 330 nm as a function of temperature. First derivative analysis of the resulting melting curves allowed the determination of the melting temperature ( $T_m$ ).

## Structure determination of JNK3 in complex with compounds 38 and 44

### Crystallization of JNK3 and the inhibitor complexes

JNK3 crystals were obtained by adapting the experimental procedure described by Lange *et al.*<sup>3</sup> Pure protein in 50 mM HEPES pH 7, 100 mM NaCl, 2 mM MgCl<sub>2</sub>, 10 mM β-mercaptoethanol buffer was initially mixed with 1 mM AMP-PCP (β,γ-Methyleneadenosine 5'-triphosphate disodium salt from Sigma-Aldrich), 0.4 mM Zwittergent 3-14 (Calbiochem) and 10% ethylene glycol and incubated on ice for 30 min. Crystals were grown at 20 °C using the sitting drop vapor diffusion method in a reservoir solution of 0.1 M Bis-Tris pH 5.5, 0.2 M NaCl and 29% (v/v) polyethylene glycol 3350. To improve the crystal quality, a final JNK3 concentration of 2.5 mg/mL was used together with microseeding. After one week, AMP-PCP containing crystals were incubated with the inhibitors over 36 h by gradually exchanging the crystal drop solution with reservoir solution supplemented with 10 mM of compounds 38 or 44. The crystals were then stepwise cryo-protected by incubation in reservoir solution containing 10 mM of the respective compound and 15% (v/v) glycerol and flash frozen in liquid nitrogen prior to synchrotron data collection. For structural comparison, crystals containing AMP-PCP were also cryo-protected with 15% (v/v) glycerol and flash frozen for data collection.

### Data collection and structure determination

Diffraction data were collected at 100 K and a wavelength of 1 Å at the Swiss Light Source (PSI, Villigen, Switzerland) beamline X06DA using the Pilatus 2M-F detector. Data processing was performed using the XDS-software<sup>4</sup> and initial phases were obtained by molecular replacement using MOLREP<sup>5</sup> and a search model derived from a reported complex structure (PDB ID 4X21)<sup>3</sup>. The individual JNK3 complexes belonged to different space groups, which resulted in a different number of copies of ligand-bound JNK3 in the individual crystal asymmetric units. For JNK3 bound to compound 38 and AMP-PCP, chain A was used for further structural analysis, due to the lower overall B-factors and the high structural similarity to the other copies (Figure S4 for JNK3-38 superposed copies). All ligands could be placed unambiguously in the difference electron density map in all JNK3 chains. Structural refinement was carried out by alternating cycles of model building in Coot<sup>6</sup> and restrained reciprocal refinement including transition-libration-screw (TLS) parameterization in REFMAC5<sup>7</sup>. After the final refinement step, ligand molecules were removed from the model and an unbiased difference omit map was produced in PHENIX<sup>8</sup> using simulated annealing. Data collection and refinement statistics were obtained (Table S2) and the simulated annealing omit difference maps were calculated (Figure S5). Structural figures were prepared using PyMOL (The PyMOL Molecular Graphics System, Version 1.8.4.1 Schrödinger, LLC).

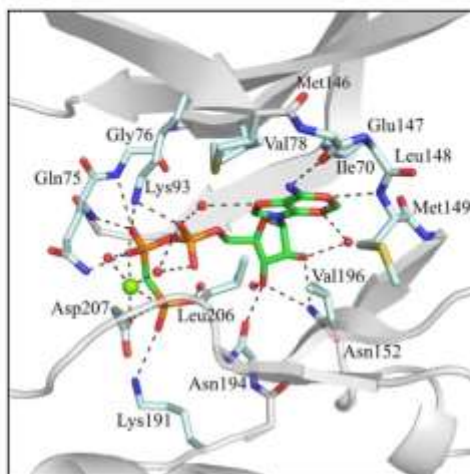
**Table S2.** Data collection and refinement statistics.

	JNK3-AMP-PCP	JNK3-38	JNK3-44
PDB ID	6EQ9	6EMH	6EKD
<b>Data collection*</b>			
Space group	P2 <sub>1</sub> 2 <sub>1</sub> 2	P2 <sub>1</sub> 2 <sub>1</sub> 2 <sub>1</sub>	C222 <sub>1</sub>
Cell dimensions			
<i>a, b, c</i> (Å)	156.73, 110.49, 43.95	88.56, 114.26, 157.8	81.51, 124.82, 68.89
$\alpha, \beta, \gamma$ (°)	90, 90, 90	90, 90, 90	90, 90, 90
JNK3 monomer/ASU	2	4	1
Resolution (Å)	47.23-1.83 (1.94-1.83)	48.01-1.76 (1.81-1.76)	48.49-2.10 (2.15-2.10)
Measured reflections	784898 (108776)	4164005 (296660)	540357 (39002)
Unique reflections	68590 (10906)	157963 (11494)	20913 (1538)
Completeness (%)	98.8 (95.9)	99.9 (98.9)	100 (99.9)
Redundancy	11.4 (9.97)	26.4 (25.8)	25.8 (25.4)
CC1/2 (%)	99.9 (66.2)	100 (63.2)	100 (55.6)
<i>I</i> / $\sigma$ ( <i>I</i> )	18.1 (1.63)	22.98 (1.4)	26.4 (1.61)
Wilson <i>B</i> -factor (Å <sup>2</sup> )	29.75	30.84	43.79
<b>Refinement</b>			
Resolution (Å)	47.23-1.83	48.01-1.76	48.49-2.10
<i>R</i> <sub>int</sub> / <i>R</i> <sub>free</sub>	20.62/25.18	21.81/26.85 <sup>**</sup>	20.56/25.90
Number of atoms			
Protein chain a/b/c/d	2812/2606	2826/2826/2700/2665	2558
Water	391	861	104
Ligand <sup>***</sup>	62	100	27
<i>B</i> -factors (Å <sup>2</sup> )			
Protein chain a/b/c/d	34.68/39.57	38.5/40.7/44.2/46.4	52.55
Water	41.26	43.6	48.46
Ligand <sup>***</sup>	47.85	37.7	46.48
R.m.s. deviations			
Bond lengths (Å)	0.015	0.014	0.015
Bond angles (°)	1.439	1.515	1.513

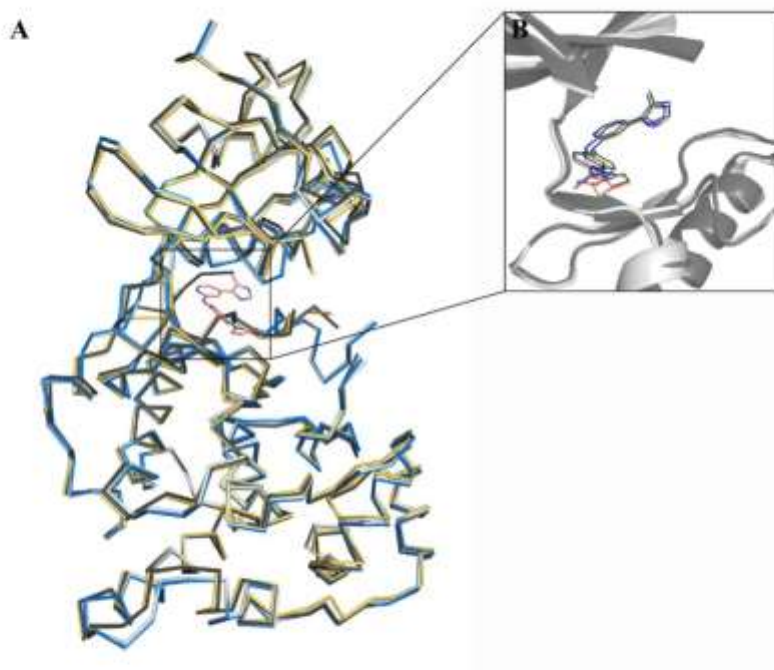
\*Values in parentheses correspond to the highest resolution shell.

\*\*Pseudo translational symmetry is present.

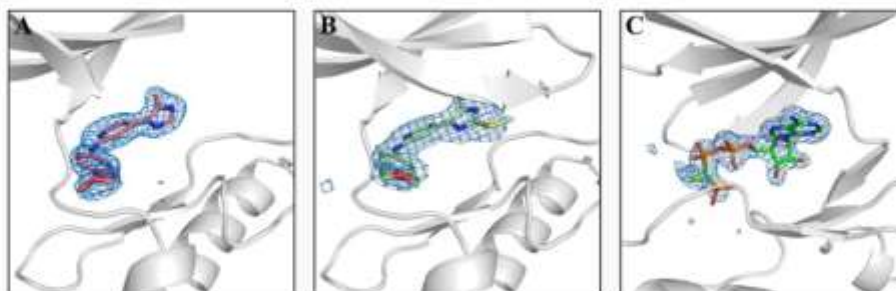
\*\*\*AMP-PCP and compounds **38** and **44**.



**Figure S3.** Binding mode of the non-hydrolyzable ATP analogue, AMP-PCP, to JNK3. For clarity, only the chain A present in the crystal asymmetric unit is shown. AMP-PCP is shown in stick display with the adenine and ribose groups highlighted in green and the three phosphate groups in orange. Amino acids contributing to key interactions are shown as sticks in light blue and are labeled. A magnesium ion interacting with the AMP-PCP molecule is displayed as a green sphere, H<sub>2</sub>O molecules are shown as red spheres, and hydrogen bonds as black dashed lines. The structure of unphosphorylated JNK3 in complex with an ATP analogue was first reported in 1998<sup>9</sup>, and the structure reported here in complex with AMP-PCP is substantially identical, with an overall RMSD of 0.853 Å.

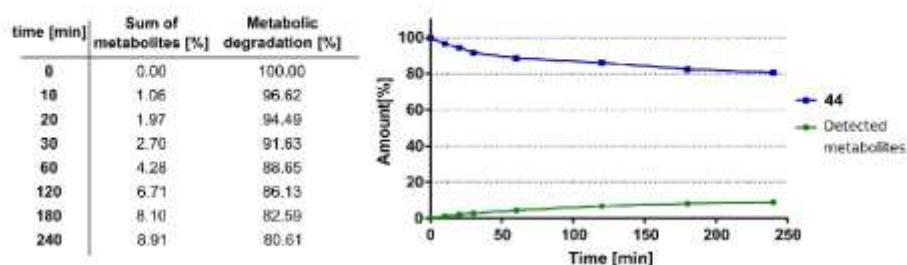


**Figure S4.** Overlay of the four JNK3-38 copies present in the crystal asymmetric unit. Superposition of the copies was performed using the “align” function in PyMOL; a) Overview of the four protein chains shown in ribbon display (A: light gray, B: blue, C: dark gray and D: yellow) and the compound bound to chain A (light red); b) Close-up view of the binding pocket of chains A (light grey) and C (dark grey) and superposition of the four compounds bound to each copy in the asymmetric unit. Compounds are shown in the same colors as the protein chains displayed in a). Orientation and placement of all compounds is almost identical.



**Figure S5.** Binding of compounds **38** and **44** and AMP-PCP to JNK3. Simulated annealing omit difference electron density maps were counteracted at  $3.0 \sigma$  and are displayed within a radius of  $5 \text{ \AA}$  around the ligand; a) compound **38** bound to chain A of the crystal asymmetric unit; b) Compound **44**; c) AMP-PCP bound to chain A of the crystal asymmetric unit.



***In vitro* metabolic stability of compound 44**

**Figure S6.** Results of metabolic stability assay; A) table reporting percentage of residual compound and formed metabolites at different time points; B) plot of obtained results;

**Experimental procedure**

Pooled adult male and female human liver microsomes (HLMs) were purchased from Merck (Schneidldorf, Germany). The incubations of HLMs were performed in the presence of an NADPH-regenerating system consisting of 5 mM glucose-6-phosphate, 5 U/mL glucose-6-phosphate dehydrogenase, 1 mM NADP<sup>+</sup>, and 4 mM MgCl<sub>2</sub>-hexahydrate. All solutions were made in 0.1 M Tris buffer (pH 7.4 at 37 °C). After addition of the HLMs to the NADPH-regenerating system the mix was pre-incubated at 37 °C for 5 min and 750 rpm in a shaker. The final concentration of microsomal protein content was 1 mg/mL. Compound **44** was pre-incubated separately under the same conditions.

The reaction was started by adding compound **44** to the NADPH-regenerating system and the incubation mix was subsequently split into 50 µL aliquots. The incubations were stopped at selected time points (0, 10, 20, 30, 60, 120, 180, 240 min) by the addition of 100 µL ice-cold acetonitrile spiked with internal standard with a concentration of 33 µM. After vortexing, the samples were centrifuged (19800 rcf at 4 °C, 20 min) and the supernatant was subjected to LC-MS analysis. In order to ensure that the decrease of compound concentration was exclusively due to metabolic degradation heat inactivated HLMs were used as control. All incubations were conducted in triplicates. None of the incubations exceeded the limit of 1% organic solvent.

**Kinase selectivity screening of 44.**

Compound **44** was tested at Cerep, Eurofins (Celle L'Evescault, France) in the ExpresS Diversity Kinase Panel against 45 selected human kinases at a concentration of 10  $\mu$ M.

**Table S3.** Inhibition of selected kinases (n=2).

#	kinase name	kinase family <sup>a</sup>	mean inhibition (%)
1	Abl	TK	19.3
2	Akt1 (PKBalpha)	AGC	-2.9
3	Aurora-A	other	40.6
4	CaMK2alpha	CAMK	-5.7
5	CDK1	CAMGC	62.0
6	CDK2	CAMGC	66.4
7	CHK1	CAMK	12.4
8	CHK2	CAMK	-5.4
9	c-Raf (Raf-1)	TKL	64.1
10	EGFR	TK	56.6
11	EPHA2	TK	17.1
12	EPHA3	TK	-6.3
13	EphB4	TK	18.2
14	ERK2 (MAPK1)	CMGC	5.3
15	FGFR	TK	26.2
16	FGFR2	TK	44.9
17	FGFR3	TK	70.4
18	GSK3beta	CMGC	5.7
19	HGK (MAP4K4)	STE	77.9
20	IKKalpha	Other	48.8
21	IR	RTK	-1.8
22	IRAK4	TKL	45.8
23	JAK3	TK	65.5
24	JNK1	CMGC	88.6
25	KDR (VEGFR2)	TK	95.1

Table S3. continued.

#	Kinase Name	kinase family*	mean inhibition (%)
26	LCK	TK	15.8
27	MAPKAPK2	CAMK	-1.9
28	MARK1	CAMK	20.1
29	Met	TK	28.2
30	MNK2	CAMK	94.9
31	NEK2	Other	20.0
32	PAK2	STE	1.4
33	PAK4	STE	-3.9
34	PDK1	AGC	41.3
35	PIM2	CAMK	-4.8
36	PKA	AGC	5.0
37	PKCbeta	AGC	1.3
38	PLK1	Other	6.3
39	ROCK1	AGC	-4.2
40	SAPK2A (p38alpha)	CMGC	11.4
41	SGK1	AGC	34.8
42	SIK	CAMK	21.6
43	SRC	TK	12.5
44	TAO2	STE	2.1
45	TRKA	TK	10.1

\*AGC: containing PKA, PKG and PKC families; CAMK: calcium/calmoduline-dependent protein kinases; CK1: casein kinase 1-like; CMGC: containing CDK, MAPK, GSK3 and CLK families; TK: tyrosine kinase; TKL: tyrosine kinase-like; STE: homologs of yeast sterile 7, sterile 11, sterile 20 kinases.

## References

1. Ansideri, F.; Andreev, S.; Kuhn, A.; Albrecht, W.; Laufer, S. A.; Koch, P. A Diverse and Versatile Regiospecific Synthesis of Tetrasubstituted Alkylsulfanylimidazoles as p38alpha Mitogen-Activated Protein Kinase Inhibitors. *Molecules* **2018**, *23*, 221.
2. Muth, F.; El-Gokha, A.; Ansideri, F.; Eitel, M.; Döring, E.; Sievers-Engler, A.; Lange, A.; Boeckler, F. M.; Lämmerhofer, M.; Koch, P.; Laufer, S. A. Tri- and Tetrasubstituted Pyridinylimidazoles as Covalent Inhibitors of c-Jun N-Terminal Kinase 3. *J. Med. Chem.* **2017**, *60*, 594-607.
3. Lange, A.; Günther, M.; Michael Büttner, F.; Zimmermann, M. O.; Heidrich, J.; Hennig, S.; Zahn, S.; Schall, C.; Sievers-Engler, A.; Ansideri, F.; Koch, P.; Lämmerhofer, M.; Stehle, T.; Laufer, S. A.; Boeckler, F. M. Targeting the Gatekeeper MET146 of C-Jun N-Terminal Kinase 3 Induces a Bivalent Halogen/Chalcogen Bond. *J. Am. Chem. Soc.* **2015**, *137*, 14640-52.
4. Kabsch, W. Xds. *Acta Crystallogr., Sect. D: Biol. Crystallogr.* **2010**, *66*, 125-132.
5. Vagin, A.; Teplyakov, A. MOLREP: an automated program for molecular replacement. *J. Applied Crystallogr.* **1997**, *30*, 1022-1025.
6. Emsley, P.; Cowtan, K. Coot: model-building tools for molecular graphics. *Acta Crystallogr., Sect. D: Biol. Crystallogr.* **2004**, *60*, 2126-2132.
7. Murshudov, G. N.; Skubak, P.; Lebedev, A. A.; Pannu, N. S.; Steiner, R. A.; Nicholls, R. A.; Winn, M. D.; Long, F.; Vagin, A. A. REFMAC5 for the refinement of macromolecular crystal structures. *Acta Crystallogr., Sect. D: Biol. Crystallogr.* **2011**, *67*, 355-367.
8. Adams, P. D.; Afonine, P. V.; Bunkoczi, G.; Chen, V. B.; Davis, I. W.; Echols, N.; Headd, J. J.; Hung, L. W.; Kapral, G. J.; Grosse-Kunstleve, R. W.; McCoy, A. J.; Moriarty, N. W.; Oeffner, R.; Read, R. J.; Richardson, D. C.; Richardson, J. S.; Terwilliger, T. C.; Zwart, P. H. PHENIX: a comprehensive Python-based system for macromolecular structure solution. *Acta Crystallogr., Sect. D: Biol. Crystallogr.* **2010**, *66*, 213-221.
9. Xie, X. L.; Gu, Y.; Fox, T.; Coll, J. T.; Fleming, M. A.; Markland, W.; Caron, P. R.; Wilson, K. P.; Su, M. S. S. Crystal structure of JNK3: a kinase implicated in neuronal apoptosis. *Struct. Fold. Des.* **1998**, *6*, 983-991.

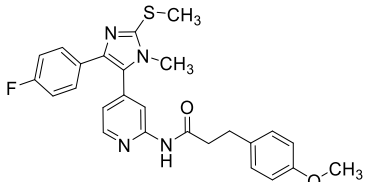
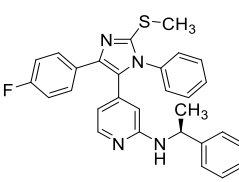
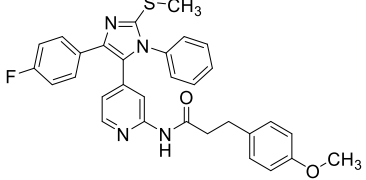


# List of synthesized compounds

Cpd ID	Structure	Cpd ID	Structure
PIT 0105001		PIT 0105009	
PIT 0105002		PIT 0105010	
PIT 0105003		PIT 0105011	
PIT 0105004		PIT 0105012	
PIT 0105005		PIT 0105013	
PIT 0105006		PIT 0105014	
PIT 0105007		PIT 0105015	
PIT 0105008		PIT 0105016	

Cpd ID	Structure	Cpd ID	Structure
PIT 0105017		PIT 0105025	
PIT 0105018		PIT 0105026	
PIT 0105019		PIT 0105027	
PIT 0105020		PIT 0105028	
PIT 0105021		PIT 0105029	
PIT 0105022		PIT 0105030	
PIT 0105023		PIT 0105031	
PIT 0105024		PIT 0105032	



Cpd ID	Structure	Cpd ID	Structure
PIT 0105033		PIT 0105035	
PIT 0105034		PIT 0105036	